

GDANSK UNIVERSITY OF TECHNOLOGY
FACULTY OF OCEAN ENGINEERING AND SHIP TECHNOLOGY
SECTION OF TRANSPORT TECHNICAL MEANS
OF TRANSPORT COMMITTEE OF POLISH ACADEMY OF SCIENCES
UTILITY FOUNDATIONS SECTION
OF MECHANICAL ENGINEERING COMMITTEE OF POLISH ACADEMY OF SCIENCE

ISSN 1231 – 3998
ISBN 83 – 900666 – 2 – 9

Journal of

POLISH CIMAC

ENERGETIC ASPECTS

Vol. 7

No. 1

Gdansk, 2012

Science publication of Editorial Advisory Board of POLISH CIMAC

Editorial Advisory Board

J. Girtler (President) - *Gdansk University of Technology*
L. Piaseczny (Vice President) - *Naval Academy of Gdynia*
A. Adamkiewicz - *Maritime Academy of Szczecin*
J. Adamczyk - *University of Mining and Metallurgy of Krakow*
J. Blachnio - *Air Force Institute of Technology*
C. Behrendt - *Maritime Academy of Szczecin*
P. Bielawski - *Maritime Academy of Szczecin*
T. Chmielniak - *Silesian Technical University*
R. Cwilewicz - *Maritime Academy of Gdynia*
T. Dąbrowski - *WAT Military University of Technology*
Z. Domachowski - *Gdansk University of Technology*
C. Dymarski - *Gdansk University of Technology*
M. Dzida - *Gdansk University of Technology*
J. Gardulski - *Silesian University of Technology*
J. Gronowicz - *Maritime University of Szczecin*
V. Hlavna - *University of Žilina, Slovak Republic*
M. Idzior - *Poznan University of Technology*
A. Iskra - *Poznan University of Technology*
A. Jankowski - *President of KONES*
J. Jaźwiński - *Air Force Institute of Technology*
R. Jedliński - *Bydgoszcz University of Technology and Agriculture*
J. Kiciński - *President of SEF MEC PAS, member of MEC*
O. Klyus - *Maritime Academy of Szczecin*
Z. Korczewski - *Gdansk University of Technology*
K. Kosowski - *Gdansk University of Technology*
L. Ignatiewicz Kowalczyk - *Baltic State Maritime Academy in Kaliningrad*
J. Lewitowicz - *Air Force Institute of Technology*
K. Lejda - *Rzeszow University of Technology*

J. Macek - *Czech Technical University in Prague*
Z. Matuszak - *Maritime Academy of Szczecin*
J. Merksiz - *Poznan University of Technology*
R. Michalski - *Olsztyn Warmia-Mazurian University*
A. Niewczas - *Lublin University of Technology*
Y. Ohta - *Nagoya Institute of Technology*
M. Orkisz - *Rzeszow University of Technology*
S. Radkowski - *President of the Board of PTDT*
Y. Sato - *National Traffic Safety and Environment Laboratory, Japan*
M. Sobieszkański - *Bielsko-Biala Technology-Humanistic Academy*
A. Soudarev - *Russian Academy of Engineering Sciences*
Z. Stelmasiak - *Bielsko-Biala Technology-Humanistic Academy*
Z. Smalko - *Warsaw University of Technology*
M. Ślęzak - *Ministry of Scientific Research and Information Technology*
W. Tarelko - *Maritime Academy of Gdynia*
W. Wasilewicz Szczagin - *Kaliningrad State Technology Institute*
F. Tomaszewski - *Poznan University of Technology*
J. Wajand - *Lodz University of Technology*
W. Wawrzyński - *Warsaw University of Technology*
E. Wiederuh - *Fachhochschule Giessen Friedberg*
M. Wyszynski - *The University of Birmingham, United Kingdom*
S. Żmudzki - *West Pomeranian University of Technology in Szczecin*
B. Żółtowski - *Bydgoszcz University of Technology and Life Sciences*
J. Żurek - *Air Force Institute of Technology*

Editorial Office:

GDANSK UNIVERSITY OF TECHNOLOGY
Faculty of Ocean Engineering and Ship Technology
Department of Ship Power Plants
G. Narutowicza 11/12 80-233 GDANSK POLAND
tel. +48 58 347 29 73, e – mail: sek4oce@pg.gda.pl

www.polishcimac.pl

This journal is devoted to designing of diesel engines, gas turbines and ships' power transmission systems containing these engines and also machines and other appliances necessary to keep these engines in movement with special regard to their energetic and pro-ecological properties and also their durability, reliability, diagnostics and safety of their work and operation of diesel engines, gas turbines and also machines and other appliances necessary to keep these engines in movement with special regard to their energetic and pro-ecological properties, their durability, reliability, diagnostics and safety of their work, and, above all, rational (and optimal) control of the processes of their operation and specially rational service works (including control and diagnosing systems), analysing of properties and treatment of liquid fuels and lubricating oils, etc.

All papers have been reviewed

@Copyright by Faculty of Ocean Engineering and Ship Technology Gdansk University of Technology

All rights reserved

ISSN 1231 – 3998

ISBN 83 – 900666 – 2 – 9

Printed in Poland

CONTENTS

| | |
|---|-----|
| Adamkiewicz A., Drzewieniecki J.: OPERATIONAL EVALUATION OF PISTON RING WEAR IN LARGE MARINE DIESEL ENGINES | 9 |
| Bocheński D.: SELECTION OF DRIVE ENGINES FOR DREDGE PUMPS | 19 |
| Burdzik R., Czech P., Konieczny Ł., Wojnar G.: ANALYSIS OF DIRECTIONAL DISTRIBUTION OF VIBRATIONS GENERATED BY THE COMBUSTION ENGINE | 27 |
| Burdzik R., Fabiś P., Czech P., Konieczny Ł.: STATISTICAL ANALYSIS OF MAXIMUM POWER OF CHOSEN DIESEL ENGINES | 33 |
| Bzura P.: FAILURE MODEL OF MAIN ELEMENTS OF THE SHIP ENGINE CRANKSHAFT-PISTON ASSEMBLY | 39 |
| Dymarski C., Dymarski P.: DESIGN SOLUTION AND SELECTED RESEARCH RESULTS OF THE SEA-WAVE ENERGY CONVERTER | 45 |
| Girtler J.: THE ISSUES OF QUANTUM IN EMPIRICAL RESEARCH ON MACHINES AND OTHER POWER SYSTEMS | 57 |
| Górski Z., Giernalczyk M.: STATISTIC DETERMINATION OF MAIN PROPULSION POWER AND TOTAL POWER OF ONBOARD ELECTRIC POWER STATION ON ANCHOR HANDLING TUG SUPPLY VESSELS AHTS SERVICING OIL RIGS | 67 |
| Herdzik J.: POWER PLANTS MAIN SWITCHBOARDS CONFIGURATION OF MULTI-MODE SHIPS | 73 |
| Krajniuk A., Klyus O.: COMPRESSOR OF CASCADE EXCHANGE BY PRESSURE | 81 |
| Krajniuk A., Klyus O.: THE CASCADE EXCHANGER AND NEW PRINCIPLES OF THE ORGANIZATION OF WORKING PROCESS OF THE GAS-TURBINE ENGINE | 87 |
| Korczewski Z.: THE CONCEPTION OF ENERGETIC INVESTIGATIONS OF THE MULTISYMPPTOM FATIGUE OF THE SIMPLE MECHANICAL SYSTEMS' CONSTRUCTIONAL MATERIALS | 99 |
| Kowalski J.: LABORATORY STUDY ON INFLUENCE OF THE EXHAUST DUCT THROTTLING ON EXHAUST GAS COMPOSITION IN MARINE FOUR-STROKE DIESEL ENGINE | 109 |
| Krakovski R.: CONTROL ALGORITHM ENGINE COOLING SYSTEM WITH INCREASED COOLANT TEMPERATURE | 117 |
| Krakovski R.: THE INFLUENCE OF THE REGULATION METHOD OF COOLING PUMP PERFORMANCE, AT HEAT TRANSFER INTENSITY IN THE PRESSURE COOLING SYSTEM | 125 |
| Krzyżanowski J.: INFLUENCE OF THE CRUISING SPEED OF A SHIP ON EXHAUST GAS BOILER EFFICACY | 133 |

| | |
|--|-----|
| Labuda W., Charachalis A.: THE ANALYSIS OF GEOMETRIC STRUCTURE OF THE PINS IN MARINE ANGULAR MOMENTUM PUMPS SHAFTS THAT UNDERWENT FINISH TREATMENT | 141 |
| Lejda K., Zielińska E.: TAXONOMIC ASSESSMENT OF THE ENVIRONMENTAL PROBLEMS OF MOTOR TRANSPORT FACILITIES BASED ON THE EXAMPLE OF GENERATED WASTE | 149 |
| Michalski R.: THE ANALYSIS OF THE DESIGN LIMITATIONS OF THE SELECTED THERMODYNAMIC PARAMETERS OF THE WORKING MEDIA IN THE MARINE WASTE ENERGY RECOVERY SYSTEMS | 159 |
| Mroziński S., Skocki R.: INFLUENCE OF TEMPERATURE AND TOTAL STRAIN ON THE FATIGUE DAMAGE OF CAST STEEL | 167 |
| Murawski L.: SOME ASPECTS OF TORSIONAL VIBRATION ANALYSIS METHODS OF MARINE POWER TRANSMISSION SYSTEMS | 175 |
| Nanowski D.: GAS PLANT OF ETHYLENE GAS CARRIER AND A TWO STAGES COMPRESSION OPTIMIZATION OF ETHYLENE AS A CARGO BASED ON THERMODYNAMIC ANALYSIS | 183 |
| Rostek E., Biernat K.: LIQUID BIOFUELS OF THE FIRST AND SECOND GENERATION – THE METHOD OF PREPARATION AND APPLICATION | 191 |
| Rudnicki J.: EVALUATION OF COMPRESSION REALIZATION IN DIESEL ENGINE BASED ON PERFORMANCE INDICATOR CHANGES | 201 |
| Rudź K.: MODEL OF SEAWATER POLLUTED BY OIL-IN-WATER EMULSION AS A RESPONSE TO THE INCREASING SHIPPING ACTIVITIES | 209 |
| Serdecki W.: ANALYSIS OF RING PRESSURE DISTRIBUTION ON A DEFORMED CYLINDER FACE | 219 |
| Szelangiewicz T., Żelazny K.: INCREASING SHIP PROPULSION EFFICIENCY AS AN ALTERNATIVE TO HELP REDUCE FUEL CONSUMPTION AND CO2 EMISSION - Part I | 227 |
| Szelangiewicz T., Żelazny K.: INCREASING SHIP PROPULSION EFFICIENCY AS AN ALTERNATIVE TO HELP REDUCE FUEL CONSUMPTION AND CO2 EMISSION - Part II | 235 |
| Tarełko W.: INSTALLATION VESSELS OF OFFSHORE WIND FARMS AND THEIR TAKE-OFF SYSTEMS | 245 |
| Valishin A., Adamkiewicz A.: SIMULATION OF VIBRATIONS OF MACHINE ELEMENTS ON THE EXAMPLE OF VIBRATIONS OF MARINE DIESEL CYLINDER LINERS | 257 |
| Varbanets R.A., Karianskiy S.A. Karianskiy: ANALYSE OF MARINE DIESEL ENGINE PERFORMANCE | 269 |
| Wawrzyniak S.: ENHANCING HEAT EXCHANGE IN FORCED CONVECTION WITH VARIABLE AIR FLOW DIRECTION | 277 |
| Wygonik P.: INFLUENCE OF BASIC TURBOFAN ENGINE PARAMETERS ON MULTIPURPOSE AIRCRAFT MANEUVERS INDEXES | 285 |
| Zadrag R., Zellma M.: THE USAGE OF MULTI-EQUATION MODELS IN THE ANALYSIS OF DYNAMIC PROCESS IN MARINE DIESEL ENGINE RESEARCH | 295 |

| | |
|--|-----|
| Zeńczak W.: THE SELECTED METHODS OF UTILISING THE WIND POWER AS THE AUXILIARY SOURCE OF ENERGY ON DIESEL ENGINE POWERED SHIPS | 305 |
| Żółtowski B., Stanowski P.: THE ETHANOL THE SUPPLEMENTARY FUEL OF THE COMBUSTION ENGINE | 315 |



OPERATIONAL EVALUATION OF PISTON RING WEAR IN LARGE MARINE DIESEL ENGINES

**Andrzej Adamkiewicz
Jan Drzewieniecki**

Maritime University of Szczecin
Department of Condition Monitoring & Maintenance of Machinery
ul. Podgórna 52/53, 70-205 Szczecin
tel.: +48 91 4338123, fax: +48 91 4318542
e-mail: a.adamkiewicz@am.szczecin.pl, j.drzewieniecki@am.szczecin.pl

Abstract

This article presents operational evaluation of piston ring wear in large marine diesel engines based on inspection through cylinder liner scavenge ports. It contains a description of verification methods of piston rings based on visual inspections, clearance measurement of piston rings in piston grooves and piston rings gap measurement. Moreover, it is indicated that piston ring gap measurements can lead to an evaluation of piston ring wear and by calculating into running hours can be treated as a reference parameter at next inspections and a parameter determining wear trends. Furthermore, application of chromium layers on working surfaces of piston rings enforces the need to control chromium layer wear by measuring the layer thickness by induction and eddy current methods. Concluding, the authors discussed constructional – operational methods of improvement between tribological pair – liner and piston rings in working conditions.

Keywords: large marine diesel engines, tribological pair, wear, piston rings, chromium layer, piston gap

1. Introduction

Global economy crisis and continuous growth of fuel prices have forced ship owners to look for drastic reduction of operation costs. It can be achieved by ship's speed reduction to Economical or Slow Steaming Speed. However, the reduction in ship's speed and thus the reduction of the engine load leads to the possibility of various operational difficulties which can include, among others increased wear of cylinder liners and piston rings.

Piston rings in large marine diesel engines rated 6000 kW by cylinder are under significant mechanical and thermal loads as an effect of action of mass (inertial) forces and combustion pressure changes. Besides, due to engine operation, reduction of cylinder oil feed rate in relation to load and extension of maintenance periods for piston's overhauling, the technical condition, correct fitting to liner's circumference and existence of chromium layer on working surfaces increasing resistance for abrasion and thermal resistance, are the significant factors in safe and economical operation of diesel engines and have decisive influence on their reliability.

Therefore, operational evaluation of wear and technical condition in tribological pair cylinder liner - piston rings is a highly important factor in maintaining proper maintenance schedule. Due to

the size of the problem authors limited this issue to operational evaluation of wear and technical condition of piston rings.

2. Visual evaluation of piston ring wear and condition through scavenge ports

The first and primary step in assessment of piston ring wear and condition is a visual inspection through scavenge ports in which the following issues are evaluated:

- amount of deposits on the top of the piston crown and skirt;
- elasticity of piston rings (if not broken) and their contact with the liner (there is no blow-by);
- movement of piston rings into the grooves on the motion TDC-BDC;
- condition of working surfaces, fig. 1.

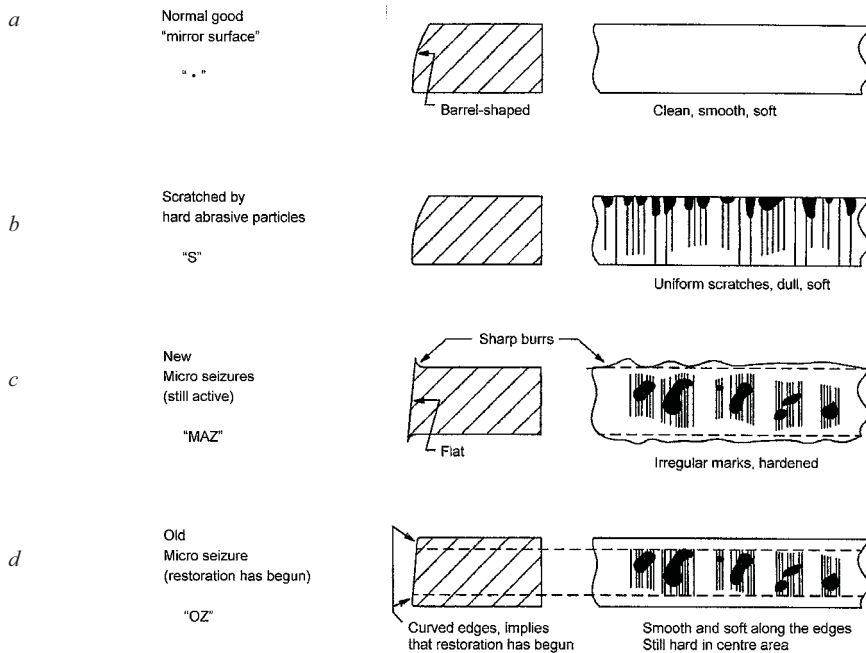


Fig. 1 Inspection through scavenge ports: Instruction for evaluation of piston rings [1]

Running surface of piston rings is the indicator of the cylinder condition in general. "Polished mirror surface", smooth, clean and without scratches is a normal good running condition, fig. 1a & 2a. Piston rings surfaces with vertically scratches caused by sharp, hard abrasive particles that have the source in fuel oil, e.g. catalyst particles and in air e.g. sand, are presented in fig 1b. These hard grains wear down the surface by continuous ploughing and scratching. With higher levels of abrasive wear, the surface displays vertical scratches, the size of which depends on the dimensions of the particles involved. These particles can also affect the sides of the rings as they jam in the ring groove, thereby causing "pitting" of the surface. When particles pass down the ring pack, via the ring joint gaps, they will cause a "sand blasting" effect on the upper edge of the ring below, which protrudes from the piston ring groove and "the trumpet-shape" scratches on run-in surface. In this situation, fuel oil and turbocharger intake filter have to be maintained clean and piston rings condition has to be monitored with temporary increased cylinder oil feed rate.

Corrosive wear on piston rings and cylinder liners is caused by chemical attack on the metallic surface caused by sulfuric acid formed through a chemical reaction in the combustion chamber. Alkaline lubricating oils make it possible to keep the corrosive wear within tolerable limits,

despite the use of heavy fuel oil. Observations of corrosive attacks on piston ring running surfaces are very rare, as there is a continuous abrasive polish, which is normally more severe than the corrosion.

Micro-seizures (new – still active, fig. 1c and old – restoration has begun, fig.1d) and mild adhesive wear is the "normal" wear that takes place mostly at the top dead center where the oil film is not sufficiently thick to completely separate the piston ring from the liner surface. Severe adhesive wear or scuffing takes place when the temperature, the sliding speed or the load exceeds a critical value. This usually starts at a very small part of the contact surface but spreads rapidly due to the significant deterioration of the surface. The friction is so intense that the surface is melted and forms the so-called "white layers", which are very hard and brittle. When they crack, small, hard particles flake off and plough the surface, producing the typical scuffing appearance, fig. 4a & d. If it covers $\frac{1}{4}$ circumference of piston ring, it should be replaced.

The presence of combustion deposits (carbon) is the results of gases blow-by through piston rings caused by loss of seal due to excessive ring breakage, lost of piston ring movement – sticking/ sluggish in groove, fig. 2b or due to broken piston ring, fig. 3a. However, a partially broken piston ring, fig. 3b can still hold the seal. In the mentioned circumstances, piston rings should be replaced at the earliest opportunity.

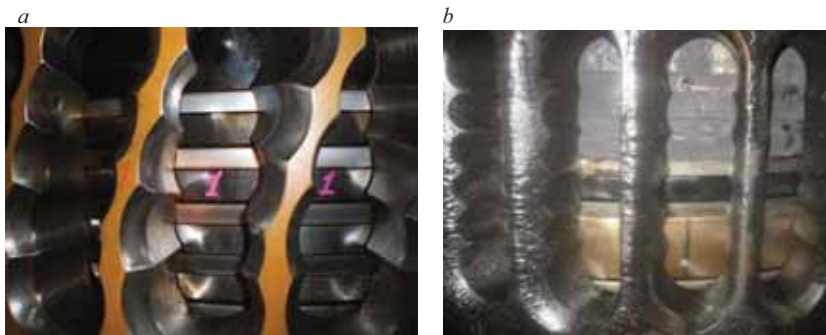


*Fig. 2 Piston rings inspection through scavenge ports:
a – perfect condition 384 running hours Mitsubishi 7UEC85LII, b – blow-by through piston rings no. 1 & 2 which have stuck into ring groove, gas seal is completely broken, Hitachi B&W 6S80MC-C*

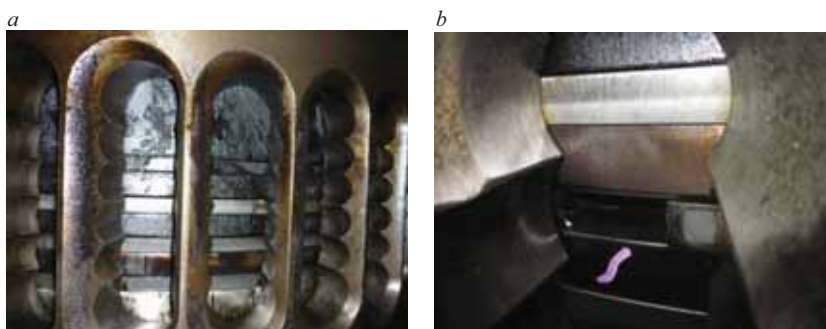


*Fig. 3 Piston rings inspection through scavenge ports:
a – broken piston ring opposite ring gap Mitsui 7S80MC, b – broken off part of piston ring near gap Mitsubishi 7UEC85LII*

The Chrome-ceramic coating is a lifetime coating [2]. However, the actual wear depends on piston running conditions. A partially worn CC-coating does not necessarily mean that the piston ring has to be changed immediately. If the remaining chrome layer is intact, it is still fit for continued

service. Obviously the scuffing resistance of the ring will decrease accordingly. If the chrome layer is damaged i.e. pieces of coating broken out, or patches of coating peeling off, the ring should be replaced at the earliest opportunity, fig. 4b & c.

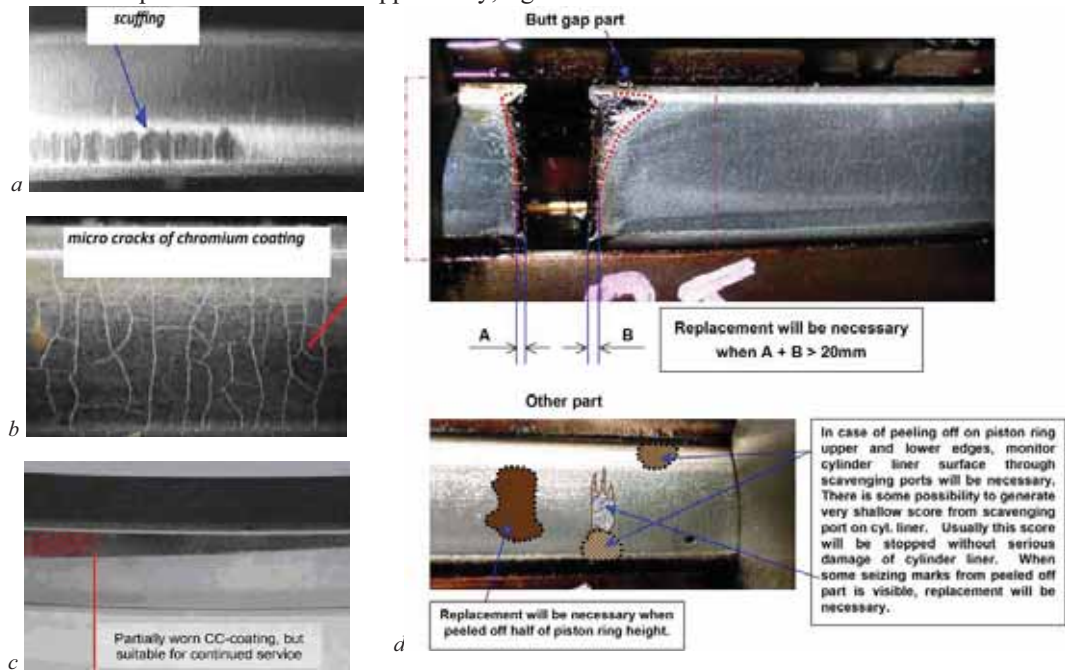


Fig. 4 Examples of piston rings wear [2]

2. Estimation of piston ring wear amount by piston ring gap measurement

During inspection through scavenge ports the following wear amount measurements of piston rings can be carried out:

- measurement of radial wear in piston ring carried out by the measurement of piston ring gap;
- measurement of axial wear in piston ring carried out by clearance measurement of piston rings in piston grooves.

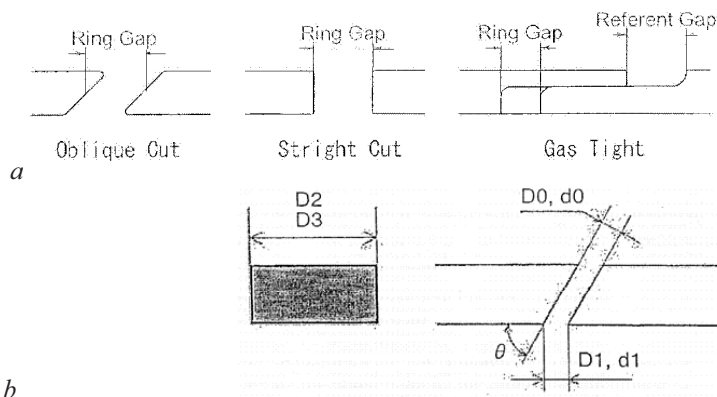


Fig. 6 Measurement of piston ring gap: a – types of piston ring gaps, b – piston ring gap dimensions [4]

To measure the piston ring wear amount, it is customary to remove a piston ring and measure its width by using a gauge. This is costly and time consuming because of the necessity of piston withdrawal. Therefore, a method in which the wear amount can be estimated indirectly by ring gap length is applied hereinafter, fig. 6. However, the diameter near liner ports is a mere assumption, which may cause wide variation of the estimated wear amount, so this method should be regarded as just a rough criterion of the necessity of ring replacement.

With the piston brought near the bottom dead center using the turning gear, the ring gap length (t) is measured through the liner ports. For the cylinder liner diameter near ports (d) the diameter measured last or the initial diameter near ports shown in the shop test result should be used. By substituting these data in the equation (1) the estimated piston ring wear amount (h) is calculated.

$$h = \frac{t - (t_o + \pi(d - D))}{2\pi} \quad (1)$$

where:

- h: estimated piston ring (radial) wear amount (mm)
- t: ring gap length measured (mm)
- t_o: initial ring gap length (specification in manual, e.g. in Tab. 1) (mm)
- d: liner diameter (near scavenge ports) (mm)
- D: liner diameter (nominal size) (mm)

Table 1: Data of initial ring gap lengths and allowable wear amount for new piston rings

| Engine Type | Cyl. Liner Dia. Nominal [mm] | Initial ring gap length t _o [mm] | Ring width b [mm] | Allowable wear amount [mm] |
|-----------------|------------------------------|---|-------------------|----------------------------|
| Wärtsilä RTA 84 | 840 | 6.18 | 26.5 +/- 0.2 | 5.3 |
| B&W MC-C 80 | 800 | 9.4 | 25.2 | 4.2 |
| UEC 85LS II | 850 | 7.0 | 27.2 | 4.7 |

Piston ring wear amount (h) can be also calculated using the calculating chart, fig. 7 that allows to check wear limits for the measured gap.

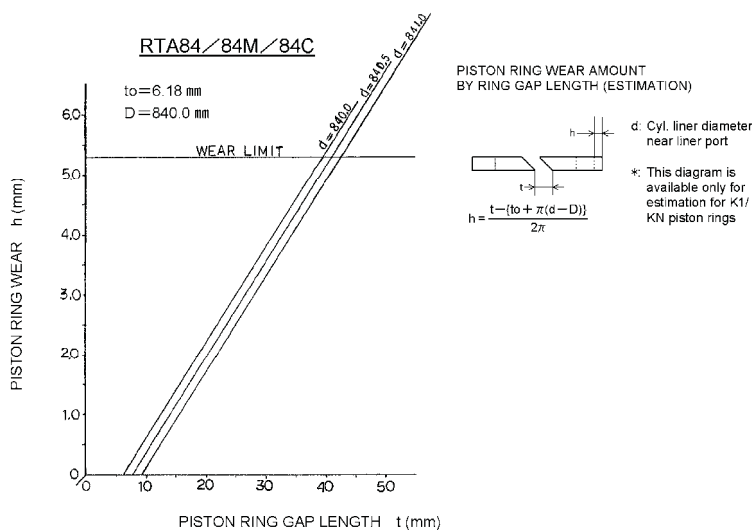


Fig. 7 Calculating chart for piston rings wear and gap measurement [6]

A piston ring gap can be obtained by the so called “finger prints” and measured with a ruler, or measured with special vernier calipers [5].

Another measurement of piston rings (radial) wear amount is carried out by measuring groove depth in piston relief groove rings (CL ring) carried out with special vernier calipers, fig. 9b. Usually, CL piston rings are applied on top piston rings and their presence confirms the usefulness to further operation.

In the next step, the obtained results of the piston ring gap are entered into tables with formulas to calculate overall wear and wear rate per running hours, fig 8.

| Vessel | | ORIENTAL JADE | | Engine Type | | MHI 7UEC85LII | |
|---------------------|-----------|---------------|-----------|---------------------|-------|---------------|--|
| No | 54 | Reported | 11-mar-11 | At Port | Yosu | | |
| Measured Date Fresh | 05-may-11 | Previous | 11-mar-11 | Total Working Hours | 10639 | | |

| Cyl. No. | 1 | 2 | 3 | 4 | 5 | 6 | 7 | 8 | 9 | 10 |
|----------------|-----------|--------|--------|--------|--------|--------|--------|--------|---|----|
| Top | clearance | 16,220 | 16,230 | 17,960 | 14,150 | 10,740 | 7,000 | 12,520 | | |
| | wear | 1,308 | 1,469 | 1,744 | 1,138 | 0,595 | 0,000 | 0,879 | | |
| | wear rate | 0,123 | 0,136 | 0,164 | 0,107 | 0,056 | 0,000 | 0,083 | | |
| 2nd | clearance | 9,120 | 8,600 | 7,760 | 7,900 | 6,660 | 8,160 | | | |
| | wear | | 0,337 | 0,255 | 0,121 | 0,143 | -0,054 | 0,185 | | |
| | wear rate | | 0,032 | 0,024 | 0,011 | 0,013 | -0,005 | 0,017 | | |
| 3rd | clearance | 8,460 | 9,160 | | 7,690 | 6,770 | 8,130 | | | |
| | wear | | 0,231 | 0,342 | | 0,110 | -0,037 | 0,180 | | |
| | wear rate | | 0,022 | 0,032 | | 0,010 | -0,003 | 0,017 | | |
| 4th | clearance | 9,580 | | 10,940 | | | | 8,820 | | |
| | wear | 0,411 | | 0,627 | | | | 0,290 | | |
| | wear rate | 0,039 | | 0,059 | | | | 0,027 | | |
| Ring Condition | 1. Top | 1 | 1 | 1 | 1 | 1 | 1 | 1 | | |
| | 2. Break | 2 | 2 | 2 | 2 | 2 | 2 | 2 | | |
| | 3. Dry | 3 | 3 | 3 | 3 | 3 | 3 | 3 | | |
| | 4. Seal | 4 | 4 | 4 | 4 | 4 | 4 | 4 | | |

| CYLINDER OIL | |
|----------------|---------------------|
| BRAND | Shell Axelia Oil 50 |
| INJECTION RATE | 1,08 gph |

| | |
|-------------------------|----|
| Engine Room Temperature | 32 |
| Liner Temperature | 70 |

Original Size
B = 16.9 mm
T = 27.2 mm
Limit 22.5 mm

Wear = $\frac{1 - 10}{2}$
1: Measured value (mm)
10 = 7.00 mm (initial value)

* Subject the result of measurement at least once in 1000 running hours.

Fig. 8 Piston rings gap measurement report for Mitsubishi 7UEC85LII

Measuring of piston rings (axial) wear amount is carried out by clearance measurement of piston rings in piston grooves by utilization of special vernier calipers or feeler gauges. Next, the results are subject to analyses by comparing to previously obtained results and calculating wear rate per 1000 running hour at the reference groove depth of 2mm, fig. 9.

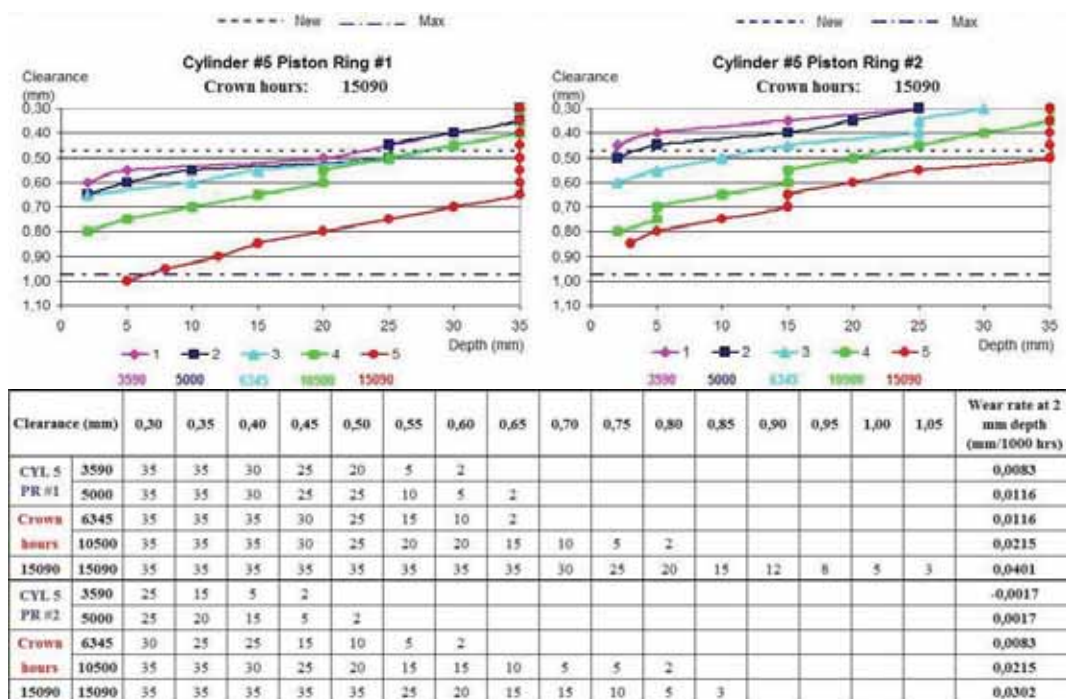


Fig. 9 The part of cylinder condition report – groove profile for HHI MAN B&W 6S90MC-C

3. Alternative Methods of Piston Ring Wear Amount

Other methods of assessing the condition and wear of piston rings rely on measurement of run-in coating on their surfaces, fig. 10 & 11. The following coatings are presently applied on piston rings in large marine diesel engines:

- top coating (outer layers) for initial run-in property and high scuff resistance, soft plasma thermal sprayed coating of graphite, Cu or Sn to reduce the run in period at initial running. After app. 500 hours this coating is being worn out and it can be evaluated visually;
- undercoating to increase wear resistance, plasma thermal sprayed coating of Mo/ NiCr/ Cr-C – wear-resistant coating that can be measured by lepto-scopes with utilization of electro-magnetic (induction) methods of layers measurement on ferrous base.

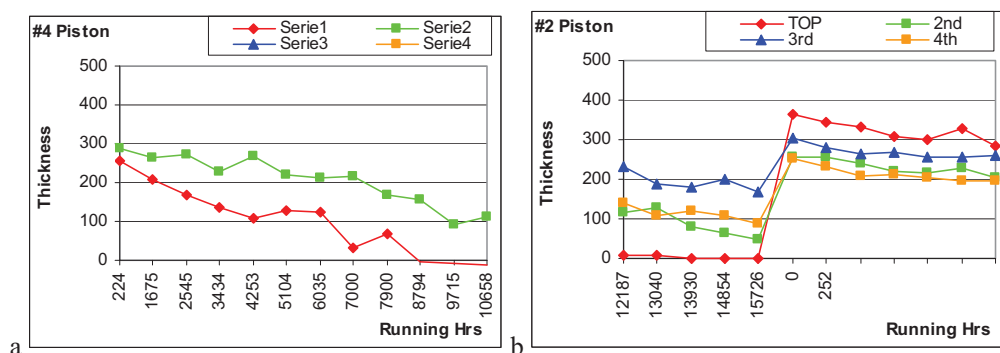


Fig. 10 Chromium layer measurement: a – Mitsubishi 7UEC85LII, b – Mitsui B&W 7S80MC-C

The wear-resistant coating loses its thickness together with the number of hours worked out by the piston rings. The results of such measurements for Mitsubishi, Mitsui B&W and Wartsila engines are presented in fig. 10 and 11. The measurements for Mitsui B&W engine (fig. 10b) were taken before and after dry docking when all piston rings were replaced.

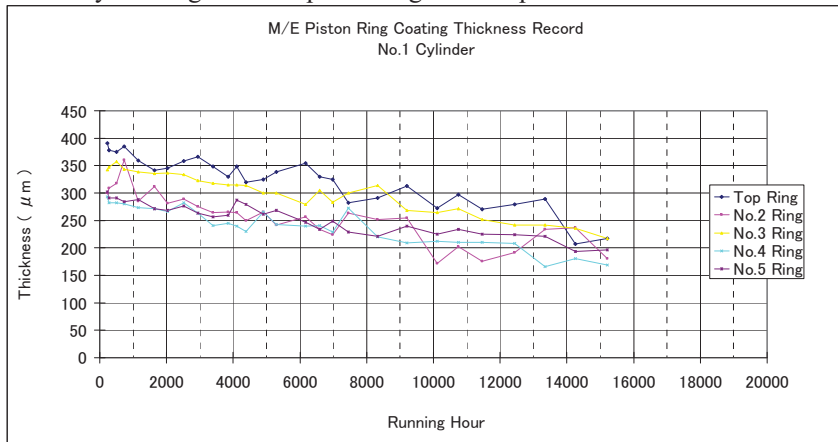


Fig. 11 Chromium layer measurement: Wartsila 7RTA84T

Conclusions

Contemporary requirements of main engine condition maintenance lead to the need to prolong the periods of its satisfactory operation between shipyard overhauls. The basis to perform main overhauls are the trends in changes of the measured operational and condition parameters of main engines. In such a case the role of periodical inspections, in which the measurement of piston ring gaps and ring wear amount take place, increases in importance. Visual evaluation through scavenge ports is sufficient for the purpose of decision making referring to the need of shipyard overhaul. This decision depends on the following:

- wear of piston rings (increased gap clearance, achieved limits in dimensions of relief grooves CL - Groove);
- achieving maximum clearance in the piston ring groove;
- cracked, broken or "stuck" ring;
- loss of seal tightness rings - "blow-by";
- active, deep scoring - abrasive wear on working surfaces, piston rings on the surface of the circuit more than a quarter of the ring;
- total loss of chromium layer;
- loss of material of size greater than half the height of the piston ring.

Based on authors' practical experience with operation of large marine diesel engines, the following the constructional – operational methods of improvement in working condition between tribological pair – liner and piston rings have been mentioned as a countermeasure plans against ring/ liner inconvenience and its safety and economical aims [3, 7, 8]:

- applying gas control rings as top rings (controlled pressure relief ring – CPR ring) – reduced variations in gas leakage from the ring gap and gas seal property in long time use in accordance with increase wear of ring or liner;
- applying as top rings relief groove ring – CL ring, to improve the thermal deformation of ring ends, gas seal performance;
- applying oval rings – reduction in local gas leakage from around the ring gap;
- applying of run-in coating – improved cooling effects from the liner that act on the ring at initial running-in period;

- applying of undercoating to increase wear resistance (chromium coating ring CCRing);
- piston cleaning/ anti-polishing rings – PC and APR rings;
- increased jacket cooling water temperature (80-85°C) – reduction of corrosive wear;
- liner insulation – insulated water cooling channels inside cylinder liner;
- increased chromium layer in piston ring grooves;
- adding lubricating groove to liner (multi level lubrication) – reduction of wear caused by poorly permeated cylinder oil;
- applying electronically controlled cylinder oil feed rate (MAN B&W Alpha Lubrication System, Wärtsilä RPLS: Retrofit Pulse Lubrication System, Mitsubishi SIP System);
- honing of cylinder liner to remove the hard layer on the running surface and to create a good surface profile with oil pockets and roughness
- installing pre-catcher guide plate for water mist catcher to increase total efficiency in separation of condensed water droplets are generated in hot and high humidity areas.

Analyzing constructional and operational solutions used by engine's manufacturers in order to increase durability and resistance to wear of engine components it can be observed that they seek similar directions, deal with the same issues and the differences between them are negligible. However, a common denominator for the benefits arising from their use, which include:

- reduced wear of engine components, in particular the piston rings and the cylinder liner;
- reduced cylinder oil feed rate and consequently reduction in consumption;
- extended Time Between Overhauls - TBO.

Investment costs are quickly offset during operation and changes to existing structures do not require complex operations. In addition, all new engines are built based on these solutions.

Summarize the mentioned in this article issues it can be stated that the present economical situation in shipping industry can meet operational requirements including extension of time between overhauls under the following conditions:

- application of new constructional and operational solutions to reduce wear of piston rings and the use of an electronically controlled engine cylinder liner lubrication;
- performing a complete inspection involving not only visual methods but also a comprehensive measurement, archiving and identification of wear trends;
- maintaining properly functioning fuel and air exchange systems.

REFERENCES:

- [1] Mitsui MAN B&W: *MC-C Engines, Instruction Book, Volume 1, Operation and Data*. Mitsui Engineering & Shipbuilding Co. Ltd. 2010.
- [2] Wärtsilä: *Daros Chromium-Ceramic Piston Rings*. Technical Information to all Owners/ Operators of Sulzer RTA and RT-flex Engines. Service Bulletin RTA-65, Winterthur, Wärtsilä Switzerland Ltd. 25.09.2003.
- [3] Mitsui B&W: *Improvement of Cylinder Condition*. Mitsui Circular Note No.162, Mitsui Engineering & Shipbuilding Co. Ltd. June 2003.
- [4] Hitachi B&W: *Simple Way to Measure Wear Amount of Oblique Cut Piston Ring*. HZSD-B0507, Hitachi MAN B&W Diesel Service Data. 12.12.2005.
- [5] Mitsui MAN B&W: *Piston Inspection Gauge*. Mitsui Engineering Co. Ltd. 2010.
- [6] DU-Sulzer: *Simple Estimation of Piston Ring Wear Amount*. Service Information, DUQ1-006E. Diesel United Sulzer Ltd. 05.06.1990.
- [7] Moser M., Schnellmann L., Werner T.: *Sulzer TriboPack: Service Experience Report*. Wärtsilä Corporation. Zürich, May 2003.
- [8] Mitsui OSK Lines: *Specification of Counter Measures Related to Ring/ Liner on Ships with UEC85LSII Mitsubishi Engines*. Mitsubishi Circular Note No. WMS-9634E, Marine Diesel Engine Department, Mitsubishi Heavy Industries Co. Ltd. Oct. 2011.



SELECTION OF DRIVE ENGINES FOR DREDGE PUMPS

Damian Bocheński

Gdańsk University of Technology
Ul. Narutowicza 11/12, 80-952 Gdańsk, Poland
Tel.: +48 58 3472773, fax: +48 58 3472430
e-mail: daboch@pg.gda.pl

Abstract

This paper presents the principles of selecting drive engines for dredge pumps, formulated by this author. In order to formulate them influence of drive engines on dredge pump characteristics and dredger effectiveness, have been analyzed. Also, an analysis of results of the author's operational investigations concerning energy consumption and parameters of excavated soil transport on board dredgers has been performed.

Keywords: *dredgers, dredge pumps, drive pump*

1. Introduction

The problem of selection of dredge pumps is widely described in the literature [2,7,9, 10,11]. It is different case with selection of drive engines for such pumps. The influence of drive engines on characteristics of dredge pumps is already described in [7,9,10], but recommendations as to their selection are still lacking.

The dredge pumps, in contrast to typical pumps, operate in the systems in which water- soil mixture is forced through. The mixture is characterized by different density and granulation of soil grains that greatly affects characteristics of both pumps and piping. The most important feature of working conditions of dredge pumps is a wide range of pipeline length (e.g. for medium – size cutter suction dredger its pipeline length may be contained in the range from a few hundred to several thousand meters). Power of dredge pumps depends on their function and design assumptions and first of all on dredger's size. It is contained in the wide range from several hundred kW to even a dozen or so thousand kW [1,2,7,9].

Power of dredge pumps and their working conditions show that the problem of correct selection of their drive engines is very important. The selection principles for drive engines should take into account: assumptions as to dredger's capacity as well as changeability of operational parameters which characterize operation of a dredging installation in question.

This paper is an attempt to formulating the selection principles for drive engines of dredge pumps, which take into account the above specified factors.

2. Design capacity of dredger

In owners design assumptions the so called design capacity of a dredger is usually specified. In the case of the dredgers fitted with dredge pump (pumps) the capacity is dependent

on possible mining the soil by loosening devices (dredging wheels, cutterheads, excavating dragheads etc) and possible soil transporting by the dredge pump. In the case of pumping the soil the design capacity of dredger decreases along with increasing the pipeline length that results from limitations of the selected engine – pump.

For driving the dredge pumps combustion engines and electric motors are used. Type and size of drive engine seriously affects pump characteristics; therefore we have to speak then about characteristics of the entire engine-pump system. The permissible operational area of diesel engine is limited by the maximum torque line and the limitation resulting from engine – turbo-compressor interaction as well as the maximum rotational speed line (i.e. characteristics of rotational speed governor). In Fig. 1a is presented the permissible operational area of the diesel engine, and in Fig. 1b – the characteristics of the diesel engine – dredge pump [7,9].

The characteristics of electric motor – dredge pump system is somewhat different. It results from that the permissible operational area of electric motor is limited in the range of higher values of rotational speed by maximum power line and the line of maximum torque - in the range of lower values of rotational speed [7,9,10].

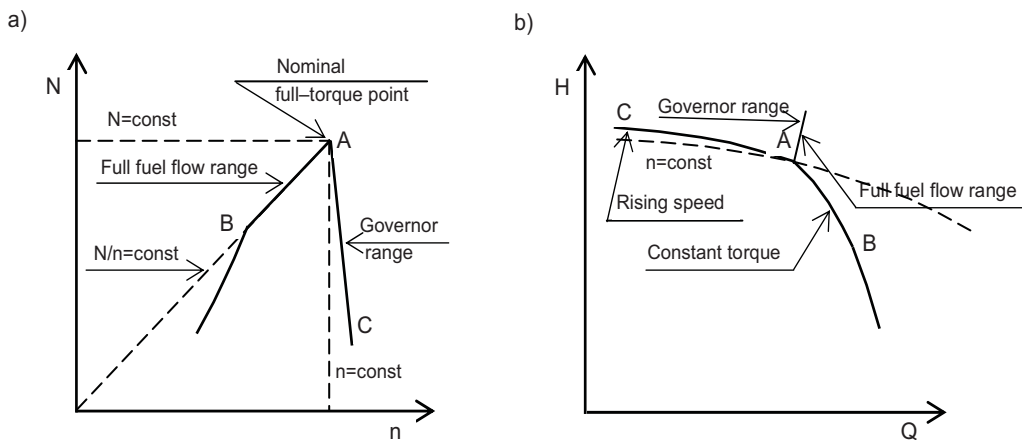


Fig. 1. Limitations imposed on characteristics of dredge pump driven by diesel engine ; a) permissible operational area of diesel engine, b) characteristics of diesel engine – dredge pump

The influence of the selected pump driving engine on the dredger design capacity is exemplified by IHC 175-37,5-75 pump. The rated parameters of the pump are: $H_w = 590 \text{ kPa}$, $Q_w = 2,3 \text{ m}^3 / \text{s}$ at $n = 320 \text{ rpm}$ - where: H_w - the dredge pump lifting height determined for water, Q_w - the dredge pump volumetric rate of delivery determined for water.

The characteristics of the pump and pipeline are determined for medium-cohesive, grainy soil (medium grainy sand of 0,2 mm mean diameter grains and 1950 kg/m^3 density in its deposition site). To determine the pipeline characteristics the dredging depth $z = 10 \text{ m}$ was assumed. And, 1300 kg/m^3 density was assumed for the water-soil mixture. The determined characteristics are presented in Fig. 2. The range of the dredge pump operation ($Q_{\min} - Q_{\max}$) was determined by calculating: the critical speed associated with sedimentation of the winning on the piping bottom ($Q_{\min} = 1,5 \text{ m}^3/\text{s}$), as well as the disposed pump suction head ($Q_{\max} = 2,5 \text{ m}^3/\text{s}$). The diesel engine drive was assumed. Three values of pump drive power were proposed as follows (pump shaft power): $N_1 = 1460 \text{ kW}$ (Line 1 is that of constant torque value of $M_1 = N_1/\omega$, where ω – pump angular speed), $N_2 = 1840 \text{ kW}$ (Line 2 is that of constant torque value of $M_2 = N_2/\omega$), $N_3 = 2180 \text{ kW}$ (Line 3 is that of constant torque value of $M_3 = N_3/\omega$). For the values dredger design capacity characteristics were determined (Fig.3).

From the characteristics presented in Fig. 3 results that drive engine of a lower output will cause, at a given range of pipeline length, the decreasing of the design capacity of the dredger. In the considered case the engine of 1840 kW power output (line 2) will cause the decrease of the dredger design capacity at the pipeline length range of 700÷1300 m, and the engine of 1460 kW power output (line 1) – at the pipeline length range of 500÷1500 m.

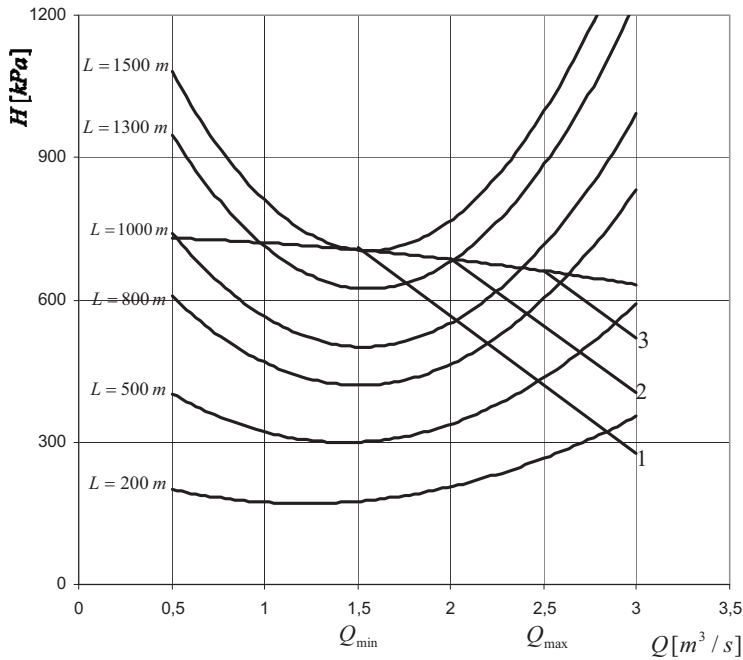


Fig. 2. Interaction between the drive engine - IHC 175-37,5-75 pump system and the pipe lines of different length values ; 1- the system with 1460 kW engine, 2- the system with 1840 kW engine, 3- the system with 2180 kW engine

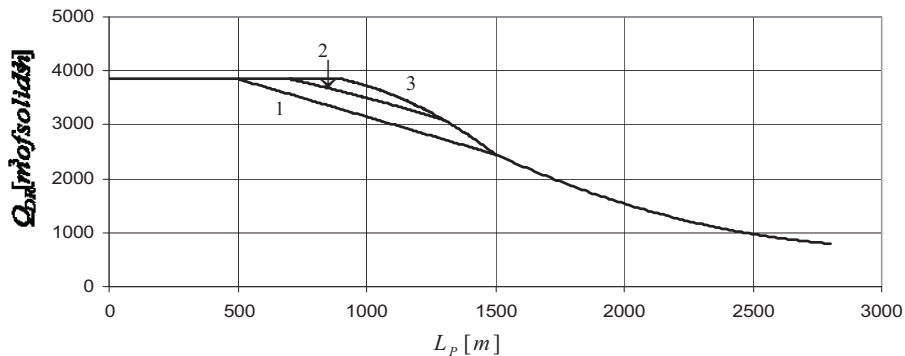


Fig. 3. Characteristics of dredger design capacity for three drive power values for IHC 175-37,5-75 pump

3. Operational parameters of dredge installation fitted with dredge pump

The results of operational investigations carried out by this author [3,4,5], dealing with capacity of dredgers have shown important differences between real capacities of dredgers and assumed design ones. The operational capacities of cutter suction dredgers amount to about 50-

60% of their maximum design capacities [4] that obviously resulted in respectively lower loads exerted onto dredge pumps.

Below, in Tab. 1 are collected the basic rated parameters of the dredge pumps installed on the investigated dredgers as well as the parameters of operational load distributions for the pumps, namely: the average values and standard deviations (N_{DP}^{av} , σ_{DP}), the relative loads \bar{N}_{DP}^{av} as well as the values of the coefficient $N_{DP}^{max} / N_{DP}^{nom}$ defined as the ratio of maximum operational power of pump and its rated power.

All the results deal with the case of pumping-over the mixtures of water and medium-cohesive grainy soils.

Tab. 1

The basic rated parameters of the dredge pumps installed on the investigated dredgers as well as the parameters of operational load distributions for the pumps

| Dredger | Basic rated parameters of the dredge pumps | | | Parameters of operational load distributions for the pumps | | | |
|-------------|--|-------------------|----------------|--|---------------------|---------------|-------------------------------------|
| | P_{DP}^w | Q_{DP}^w | N_{DP}^{eff} | N_{DP}^{av} | \bar{N}_{DP}^{av} | σ_{DP} | $\frac{N_{DP}^{max}}{N_{DP}^{nom}}$ |
| | kPa | m ³ /s | kW | kW | - | kW | |
| TSHD 300 | 370 | 0,55 | 203,5 | 216,5 | 0,666 | 29,6 | 0,894 |
| TSHD 400 | 490 | 0,5 | 245 | 189,4 | 0,451 | 20,9 | 0,597 |
| TSHD 1600-1 | 385 | 1,6 | 2×616 | 832,9 | 0,757 | 101,4 | 0,956 |
| TSHD 1600-2 | 385 | 1,6 | 2×616 | 828,3 | 0,753 | 90,9 | 0,923 |
| TSHD 7200 | 430 | 3,0 | 2×1290 | 1815,9 | 0,769 | 178,4 | |
| TSHD 9900 | 560 | 3,0 | 2×1680 | 2194,5 | 0,708 | 240,6 | 0,894 |
| TSHD 13700 | 1240 | 4,1 | 5084 | 3861,9 | 0,434 | | |
| CSD 1600 | 600 | 1,0 | 600 | 544,1 | 0,544 | 114,1 | 0,865 |
| CSD 1500 | 530 | 0,95 | 503,5 | 433,9 | 0,517 | 50,4 | 0,685 |
| UB 750 | 1160 | 1,75 | 2×2030 | 1204,5 | 0,371 | 300,3 | 0,668 |
| UB 500 | 440 | 0,7 | 308 | 240,5 | 0,445 | 29,5 | 0,574 |
| BLD 325 | 410 | 0,4 | 164 | 158,4 | 0,634 | 27,1 | 0,884 |

P_{DP}^w - rated dredge pump pressure for water pumping conditions,

Q_{DP}^w - rated dredge pump capacity for water pumping conditions,

N_{DP}^{eff} - effective dredge pump power for water pumping conditions.

The performed calculations of the load distribution parameters of dredge pumps during pumping-over the water-soil mixture showed that for particular dredgers the relative mean loads were contained within the interval of 0,371÷0,769. It manifests that operational conditions of dredgers are very different and they depart from those assumed nominal (design ones). The calculated values of the variation coefficient of pump load distribution $v_{DP} = \sigma_{DP} / N_{DP}^{av}$ are contained within the interval of 0,1÷0,25, where the lower values dealt with suction hopper dredgers and the higher values - with suction-cutter and silting-up ones [3]. The magnitude of the coefficient suggests that pump load variability is relatively high. It results from variability of pipeline length. As results from the performed investigations the maximum pipeline length L_{pipe}^{max} amounted on average to $4,46L_{pipe}^{min}$ (where: L_{pipe}^{min} – minimum pipeline length). It's interesting that maximum values of pipeline length amounted to only 70-80% of those specified in the design assumptions [3].

The data presented in the above attached table were used for elaboration of the method for determining operational load distributions of dredge pumps [6]. The following relations were examined:

$$\left. \begin{aligned} N_{DP}^{av} &= f(N_{DP}^{eff})^{nom} \\ \sigma_{DP} &= f(N_{DP}^{eff})^{nom} \end{aligned} \right\} \quad (1)$$

The calculation results are given in Tab. 2. The relationships presented in the table are statistically significant. The permissible intervals of independent variables for the equations given in Tab. 2 result from the data contained in Tab. 1.

Tab. 2

Linear regression equations which determine mean loads of dredge pumps

| Relations | Statistical evaluation | | | | |
|--|------------------------|----------|------|----------|-----|
| | R | σ | t | t_{kr} | m |
| $N_{DP}^{av} = 0,712 \cdot (N_{DP}^{eff}) + 2,43$ | 0,993 | 136,7 | 26,6 | 2,23 | 12 |
| $\sigma_{DP} = 0,076 \cdot (N_{DP}^{eff}) + 22,01$ | 0,868 | 49,5 | 5,24 | 2,23 | 12 |

where: R - the coefficient of correlation, σ - the standard deviation, t - the value of the test t-Student, m - the sample number.

4. Formulation of principles for selection of drive engines of dredge pumps

The above presented data were used to formulate principles for selection drive engines of dredge pumps. The general conclusion drawn from Ch. 3 is that drive engine for dredge pump should not be selected for the conditions of maximum pipeline length and design values of water- soil mixture density. As it will lead to selection of an engine of a high power output which will not be practically utilized during dredger operation.

This author has proposed to make use of the results of the above presented operational investigations. On the basis of the data contained in Tab. 2, predicted loads for pumps in operation can be determined; the loads should be then transformed into drive engine loads with taking into account the reduction gear efficiency η_{DP}^{TM} :

$$\left. \begin{aligned} N_{DE}^{av} &= \frac{(N_{DP}^{av})}{\eta_{DP}^{TM}} \\ \sigma_{DE} &= \frac{\sigma_{DP}}{\eta_{DP}^{TM}} \end{aligned} \right\} \quad (2)$$

where: N_{DE}^{av} - the mean values of loads of drive engines, σ_{DE} - the standard deviation of load distribution of drive engines.

In the case of one - engine propulsion system, value of the design (computational) rated power output of drive engine can be determined from the following relationship [3]:

$$(N_{DE}^{nom})^{design} = \frac{N_{SG}^{av}}{(\bar{N}_{DE}^{av})^{design}} \quad (3)$$

The value $(N_{DE}^{nom})^{design}$ in Eq. (3) is determined on the basis of operational values of \bar{N}_{DE}^{av} for the investigated dredge pumps (Tab.1) with accounting for values of the ratio $N_{DE}^{max} / N_{DE}^{nom}$ and assuming an appropriate value of the drive engine power margin ΔN_{DE} . Value of the margin depends on operational conditions and character of load changeability of power consumers driven by the engine in question. For pumps of a low changeability of instantaneous loads the margin may be assumed on the level of $\Delta N_{DE} = (10 \div 15)\% N_{DE}^{nom}$ [8]. Taking this into account one should assume the value of $(\bar{N}_{DE}^{av})^{design} = 0,6 \div 0,65$ for cutter suction dredgers and silting-up ones, and $(\bar{N}_{DE}^{av})^{design} = 0,65 \div 0,7$ for trailing suction hopper dredgers.

The other way of determining the value of design rated power output of main engine is to use the following relation:

$$(N_{DE}^{nom})^{design} = (N_{DE}^{av} + \beta_{DE} \cdot \sigma_{DE}) + \Delta N_{DE} \quad (4)$$

where: β_{DE} - the relative maximum load range coefficient; by assuming $\beta = 3$ it is possible to estimate maximum load value with the probability of 0,997;

So selected drive engine for dredge pump ensures that it will operate with the highest operational efficiency. Obviously, it is possible to assume other parameters of predicted load distribution for dredge pump than those determined on the basis of Tab. 2.

Coming back to the example presented in Ch. 2 and applying the above given recommendations concerning selection of pump drive engine we obtain the following values of design rated power output of drive engine for IHC 175-37,5-75 pump :

- $(N_{DE}^{nom})^{design} = 1490 \div 1635 \text{ kW}$ - acc. Eq. (3);
- $(N_{DE}^{nom})^{design} = 1495 \div 1565 \text{ kW}$ - acc. Eq. (4).

On this basis we are able to select a diesel engine of power output value contained within the above specified intervals, e.g. 8L20Wartsila diesel engine of 1600 kW rated power output and 1000 rpm rotational speed, as well as an appropriate reduction gear of the ratio $n_1/n_2=1000/320$.

Examining Fig. 2 we can observe that the selected engine will impose limitations onto pump characteristics, between the lines 1 and 2. The design capacity of the dredger will be also placed between the lines 1 and 2 (Fig. 3).

References

- [1] Bocheński D., Kubiak A.: Wybrane problemy eksploatacji pomp gruntowych na pogłębiarkach. /Materiały/ XXI Sympozjum Siłowni Okrętowych SymSO 2000', Gdańsk 2000
- [2] Bocheński D., Kubiak A.: Analiza i ocena warunków pracy pomp gruntowych na pogłębiarkach ssących nasiębiernych. Międzynarodowa XIX Sesja Naukowa Okrętowców NT. TECHNIKA MORSKA NA PROGU XXI WIEKU. Materiały konferencyjne, vol.2, Szczecin-Dziwnówek 4-6.V.2000r, 35-43
- [3] Bocheński D. (Kierownik projektu) i in.: Badania identyfikacyjne energochłonności i parametrów urabiania oraz transportu urobku na wybranych pogłębiarkach i refulerach. Raport końcowy projektu badawczego KBN nr 9T12C01718. Prace badawcze WOio PG nr 8/2002/PB, Gdańsk 2002
- [4] Bocheński D.: Porównanie wydajności pogłębiarek wieloczerpakowych i frezujących ssących. W: [Mat] XXVIII Sympozjum Siłowni Okrętowych 2007. Akademia Morska, Gdynia 2007
- [5] Bocheński D.: Operational loads of dredge pumps in their basic service on selected types of dredgers. Journal of Polish CIMAC, Energetic aspects vol. 2, no 2, Gdańsk 2008
- [6] Bocheński D.: Determination of operational load parameters of dredge pumps under dredging operations. Journal of Polish CIMAC, Energetic aspects vol. 2, no 2, Gdańsk 2009
- [7] de Bree S. E. M.: Centrifugal dredge pumps. Ports & Dredging 77-89, IHC Holland 1973-76
- [8] Jędral W.: Pompy wirowe. Wydawnictwo Naukowe PWN, Warszawa 2001
- [9] Vlasblom J. W.: Dredge pumps. Lecture notes, TUDelft 2002
- [10] Vlasblom J. W.: Designing dredging equipment. Lecture notes, TUDelft 2003-05

[11] Welte A.: Nassbaggertechnik. Institut für Maschinenwesen in Baubetrieb, Universität Fridericiana, Karlsruhe 1993



ANALYSIS OF DIRECTIONAL DISTRIBUTION OF VIBRATIONS GENERATED BY THE COMBUSTION ENGINE

Rafał Burdzik, Piotr Czech, Łukasz Konieczny, Grzegorz Wojnar

Silesian University of Technology
ul. Krasińskiego 8, 40-019 Katowice, Poland
tel.: +48 32 6034166, fax: +48 32 6034118
e-mail: rafal.burdzik@polsl.pl

Abstract

The article provides a discussion on the studies and analysis of directional distribution of vibrations generated by the combustion engine. The engine is one of the sources of the vibrations in vehicles. The analysis of the vibration propagation from source should take into account the directions of the propagation and the dynamics of the vibration. The experiment was conducted on the vehicles combustion engine and the orthogonal axes vibrations were measured. Analysis of the results allows comparing the values and frequencies of the vibration propagation.

Keywords: engine vibration, directional distribution of the vibration

1. Introduction

Road surface roughness often acts as a major source that excites the vibration of the vehicle running on the ground through the tire/wheel assembly and the suspension system [9,10]. There are many of different vibration sources in vehicles as well. One of those is motor-car engine. The engine vibrations are strongly random processes because there are many of different source of vibration in engine. They can have different mechanism of generation and different values and frequencies of vibration. The engine block mainly is characterised by the low coefficient of dumping. The vibrations of low and medium frequencies up to a few kHz are only slightly absorbed. Higher vibration absorbing effects appear only for frequencies of 10 kHz or more [6]. Those parameters are determined by materials used in engine construction. There are a lot of novel materials used in engine with modern production technologies. Thus the optimal material parameters can be obtained [3,7].

Vibration processes in combustion engine are unwanted effects but at the same time they can be very useful. There are many publications on application of vibration signal in diagnostic [1,2,4,5,6,8]. This paper takes into account influence of the vibration as the detrimental effect on the safety and comfort in mean of transport. The human response to vibration is depending on the values, frequencies and directions. Perceptibility of the same frequencies and values of vibration in exposure in different directions can be diametrically different.

2. Engine as the source of vibration

The suspension system is very important for reduction of vibration transfer to car body. Before

attempting to reduce the vibration levels in a machines or structure of the vehicles by increasing its damping, every effort should be made to reduce the vibration excitation at its source. Motor engine should be considered as one of the vibration generators. Rotating machinery such as motors can generate disturbing forces at several different frequencies such as the rotating speed and blade passing frequency. Reciprocating machinery such as compressors and engines can rarely be perfectly balanced, and an exciting force is produced at the rotating speed and at harmonics. There are two basic types of structural vibration: steady-state vibration caused by continually running machines such as engines, air-conditioning plants and generators either within the structure or situated in a neighbouring structure, and transient vibration caused by a short-duration disturbance such as a lorry or train passing over an expansion joint in a road or over a bridge.

Consider the vibroacoustics analysis of an internal combustion engine one should take into account the fact, that a high level of nominal vibrations is generated, resulting from the target function realisation. Internal combustion engine is an object under the influence of internal and external inputs. Among them there are mainly: burning pressure, the movement of the piston-crank mechanism, inputs from the timing gear system, inputs resulting from the work of the fittings of the engine, inputs transmitted from the motor-car body and the drive transmission system. One of the most important inputs during the work of the piston-crank mechanism are the impacts of the piston by the change of its work direction [4].

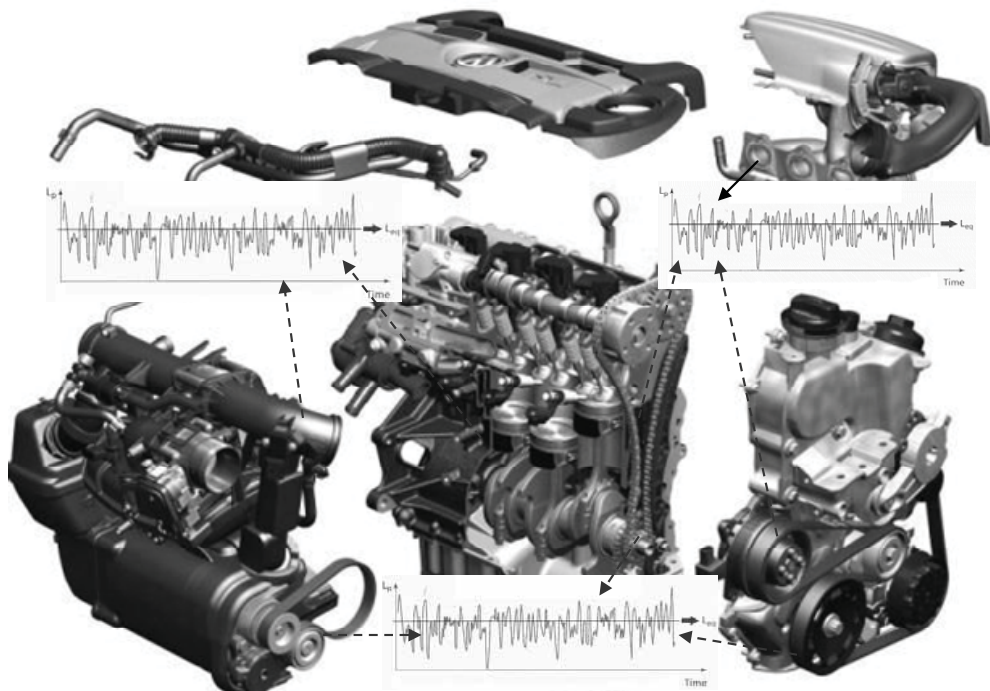


Fig. 1. Motor engine as the vibration generator

3. Research

The research goal was analysis of directional distribution of vibrations generated by the combustion engine. The acceleration of vibration sensors type ADXL were used. The ADXL are

complete acceleration measurement systems on a single, monolithic IC. It was used the dual-axis accelerometer. The acceleration converters are characterised by big direction selectivity, the proper sensor placement enables the spatial selection of the diagnostic signal. The studies were block of the combustion engine. Under the studies in question, active experiments were undertaken featuring measurements of vibration accelerations in a three directions. It were recorded the vibration in three orthogonal axes (X,Y,Z). The position and directions of measurements has been depicted in Fig. 2.

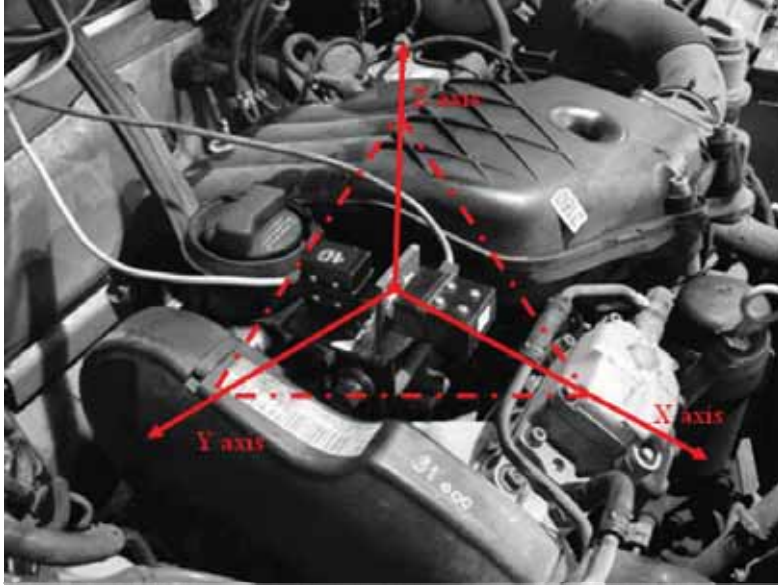


Fig. 2. Measurement of vibration of combustion engine in 3 directions

The recorded signals for idle gear of engine load have been depicted in Fig. 3-5.

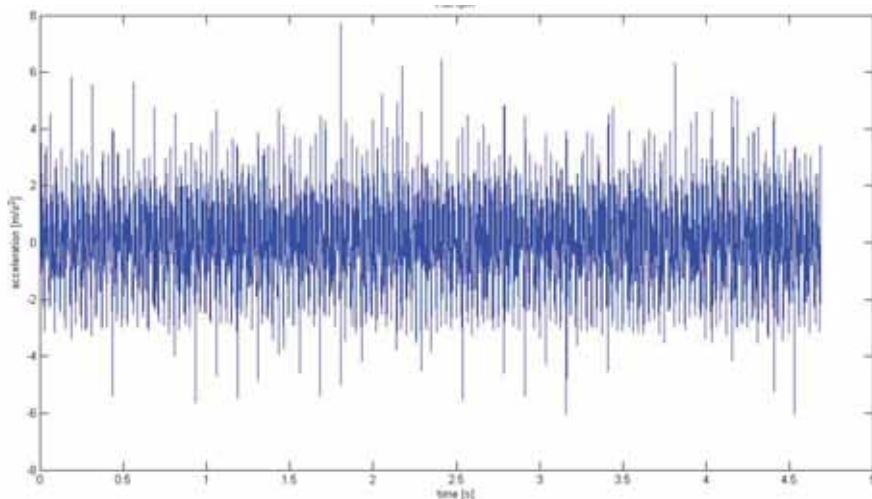


Fig. 3. Vibration signal recorded in X axis

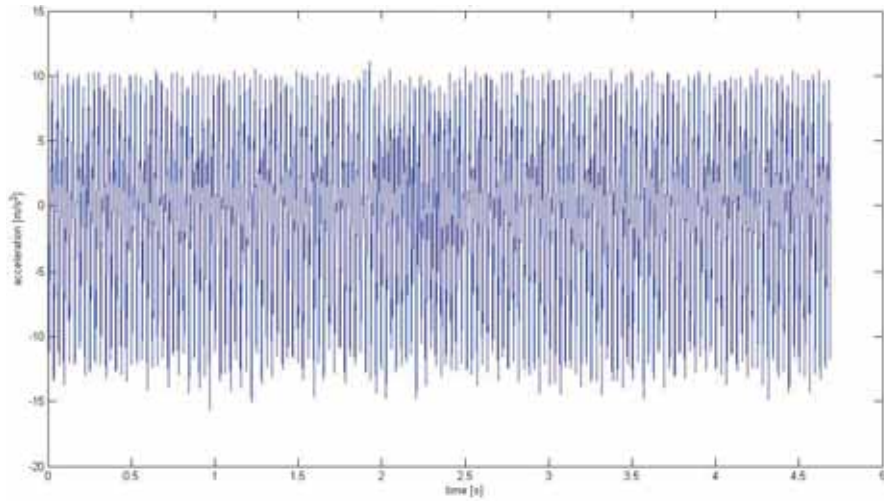


Fig. 4. Vibration signal recorded in Y axis

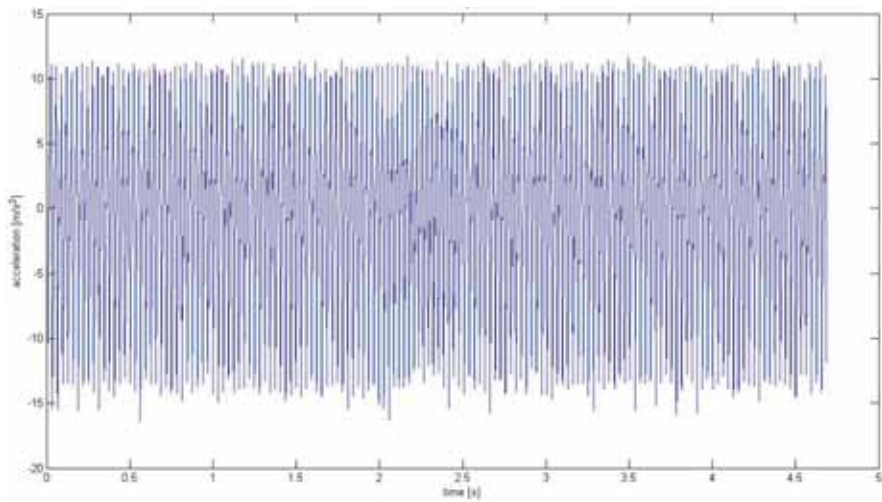


Fig. 5. Vibration signal recorded in Z axis

Based on the analysis of the acceleration of vibration in time dimension it can be assumed that the vibrations acceleration in vertical direction (Z axis) are the larger value of amplitude. The longitudinal vibrations (X axis) have smallest amplitudes. For the analysis the dynamics of the vibration in directions the spectrum of the signal can be very helpful. The Fast Fourier Transformations (FFT) of the recorded signals were done. The results of the FFT for signals in 3 directions have been depicted in Fig. 6-8.

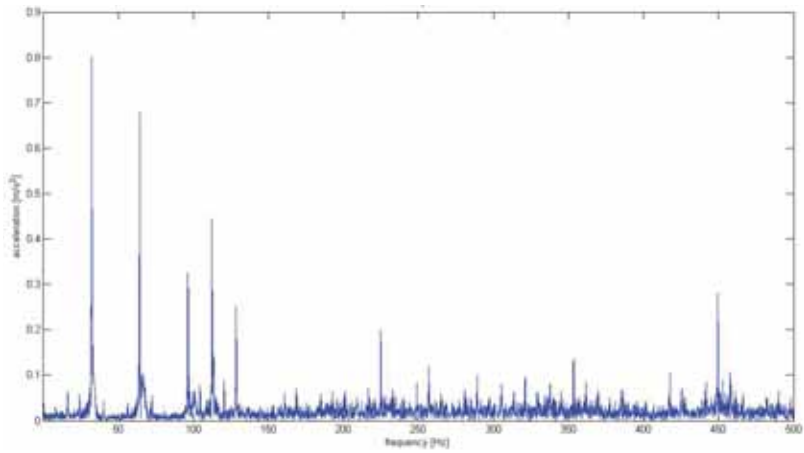


Fig. 6. Spectrum of the vibration signal recorded in X axis

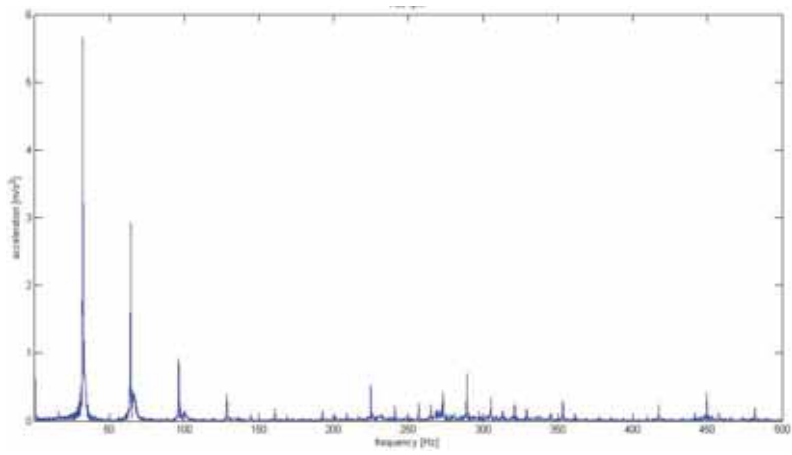


Fig. 7. Spectrum of the vibration signal recorded in Y axis

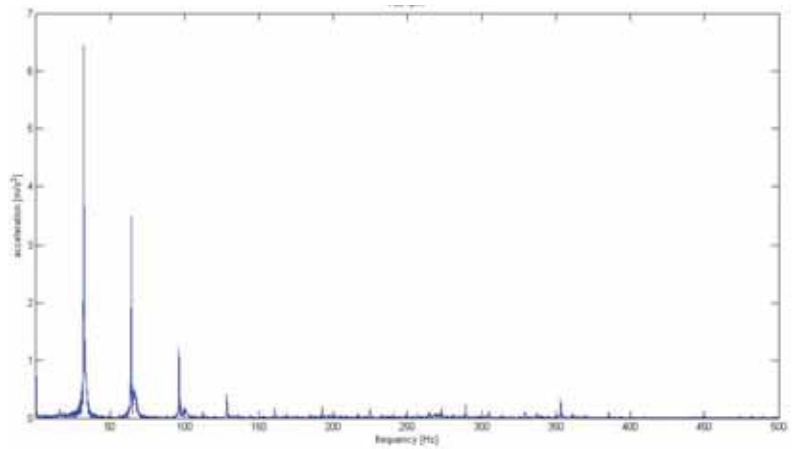


Fig. 8. Spectrum of the vibration signal recorded in Z axis

4. Conclusion

In the spectrum of the signals the characteristics frequencies can be identifying. The ca. 32 Hz frequency is correlated with rotation velocity of the idle gear of the engine. The vertical vibrations have the largest amplitude but the signal is most stationary. The frequencies not correlated with rotation velocity of the idle gear of the engine (1-3 harmonics) are very low energy. The horizontal vibration have more frequencies, especially in the spectrum of the X axis vibration can be identified many of different frequencies. The directional distribution of vibration can be resulted from the elements and systems of the suspension and the mounting of engine. It can be resulted of the unbalance of the rotating elements of the engine or other defects.

The received signal is strongly interfered by various vibration sources and that is why there is a necessity to use advanced methods of signal selection and observation in time-frequency domains.

References

- [1] Burdzik, R., *The research of vibration of vehicle floor panel*, Silesian University of Technology Scientific Papers, s. Transport 67, pp. 23-30, Gliwice: Silesian University of Technology Academic Press, 2010.
- [2] Burdzik, R., Stanik, Z., Warczek J., *Method of assessing the impact of material properties on the propagation of vibrations excited with a single force impulse*, Archives of Materials and Metallurgy vol. 57 issue 2, pp. 409-416, 2012.
- [3] Burdzik, R., Węgrzyn, T., *Effect of Mn and Mo on the quality of welding trucks steel supporting structures*, Journal of Achievements in Materials and Manufacturing Engineering JAMME, 43(1), pp. 276-279, 2010.
- [4] Czech, P., Łazarz, B., Madej, H., Wojnar, G., *Vibration diagnosis of car motor engines*, Acta Tech. t. 3 fasc. 1, pp. 37-42, Corviniensis - Bull. Eng. 2010.
- [5] Jamro, E., Wielgosz, M., Bieniasz, S., Cioch, W., *FPGA – ARM heterogeneous system for high speed signal analysis*, Solid State Phenomena, vol. 180, pp. 207—213, 2012.
- [6] Madej H., *Wykorzystanie analizy modalnej w diagnostyce WA silników spalinowych*, Zeszyty Naukowe Politechniki Śląskiej, s. Transport, z. 63, pp.61-68, Gliwice 2006.
- [7] Oleksiak, B., Siwiec, G., Blacha, A., Lipart, J., *Influence of iron on the surface tension of copper*, Archives of Materials Science and Engineering 44 (1), pp. 39-42, 2010.
- [8] Piecha, J., Węgrzyn, T. Ed., *Transactions on Transport Systems, Telematics and Safety*, [in:] Burdzik, R., *Research of the vibration in 3 axes of car body for different idle gear rotational speed*, pp. 203-214, Gliwice: Silesian University of Technology Academic Press, 2011.
- [9] Wong, J.Y., *Theory of ground vehicle*, 3rd Edition, Wiley, USA, NewYork 2001.
- [10] Xua, Y.L., Guo, W.H., *Effects of bridge motion and crosswind on ride comfort of road vehicles*, Journal of Wind Engineering and Industrial Aerodynamics 92, 2004.



STATISTICAL ANALYSIS OF MAXIMUM POWER OF CHOSEN ENGINES

Łukasz Konieczny, Rafał Burdzik, Paweł Fabiś, Piotr Czech

Silesian University of Technology
ul. Krasińskiego 8, 40-019 Katowice, Poland
tel.: +48 32 6034166, fax: +48 32 6034118
e-mail: lukasz.konieczny@polsl.pl

Abstract

Testing of production quality and control of assembly operation requires test of each engine. The paper presents results of statistical analysis of maximum power for chosen engines. There were tested 40 the same type engines in engine test house.

Keywords: engine, maximum power, statistical analysis

1. Introduction

In order to unify methods of measuring engine power produced within the European Union and to prevent technical barriers to trade, the European Council introduced the EWG type-approval procedures [2,3,4]. Directive related to research engines determines what documentation that must be submitted to the authorities. It also defines "netto power", the "maximum netto power," "standard equipment ". This document includes also accurate measurements of power, torque, engine speed, fuel consumption, inlet air temperature to the engine, barometric pressure, exhaust manifold pressure, pressure in the exhaust pipe of the vehicle. There are also listed the components that are necessary to conduct a reliable test.

All these ensure the quality of manufactured engines. Nominal parameter values that characterize the type of engine as the power and maximum torque are given as a specific value. This is a generalization because the actual values of both maximum power and torque are within specified tolerances.

Typical parameters of the engine are used for the monitoring system. The authors conducted some research on vibroacoustics signals application for monitoring the engine [5,9].

2. Types of engine tests

Testing of production quality and control of assembly operation requires test of each engine Presented results of engine testing apply to company (name couldn't be presented) where are tested all produced engines in engine test house, checking the assembly operation for 100% producing population. Moreover this company had special engine test house for characteristics test, COP (Conformance of Production), LOK (Lubrication Oil Consumption), durability test, and other tests to be commissioned by the company or on client's request [1,6,7,8].

Every engine, which is taken off the line is sent to a separate stand of the so-called subassembly. There passes the leak test, which consists of introducing air under pressure into the cooling system, then the pressure measurement is made. In this stand, the engine is flooded with oil, coolant and fuel. The so-called cold test is made. It involves the simulation of engine work by turning the crankshaft. This process is designed to distribute the fuel, oil and coolant throughout the system, as well as validation of the submission an assembly of crankshaft, pistons and connecting rods .

Hot tests are made on the working engine (a few minutes). Nearly 90% of the engines are tested for short time while the remaining 10% are tested longer (the longest tests are designed for prototype engines). The main task of this type of testing is to validate the correctness of the assembly and operation of the engine. Sealing elements are controlled, and the visible water or oil leaks are being checked.

It is only when the engine passes through a hot test can be taken to another test that is made for a randomly selected engines. The frequency of these tests is changed depending on the number of engines produced.

During the hot test are checked and recorded: numbers: the engine and its model, etc., oil pressure and fuel injection temperature for a selected speed, idle speed, engine management system diagnostics, automatic assessment of the turbocharger noise, vibration, beating the flywheel and crankshaft pulley, exhaust fumes, leaking coolant, oil, fuel, unusual noises).

Characteristics test - during the test, speed range is tested and on its basic a characteristic of the engine (power and torque) is formed. It is also verified: fuel flow, torque, maximum power, smoke, characteristics of the controller, specific fuel consumption, oil pressure, the maximum exhaust temperature, boost pressure.

COP test (Conformance of Production) is carried out based on customer requirements. Preparation is the same as for the characteristics test. The first step is the automatic warm-up, which is used to determine the required parameters of the engine (coolant temperature, air pressure and exhaust gas). Then characteristics test is made. The next step is a few hours test of engine operation at given parameters with variable load, then re-test characterization is carried out with the assessment that is reported to the client.

Test LOC Lubrication Oil Consumption test is performed during by tens of hours the test duration is a few hours. During this test, every 30 minutes are monitored and recorded torque, fuel flow, the cooling temperature at the inlet and outlet, the oil parameters (temperature and pressure), exhaust temperature, exhaust pressure, boost pressure. The test is made at a constant speed. The purpose of this test is to measure the oil consumption. Oil consumption is evaluated by the ratio of oil used during the test to the duration of the entire test.

Durability test continues until about tens of hours. The engine is prepared identically to the characteristics test. The first step is the automatic warm-up, which is to identify all the engine parameters (temperature, etc.). After this test, the engine is disassembled into pieces, with a precise measurement of torque on each connection. These parts are to be reviewed. There is checked the wearing of all components. After that the engine is assembled and re-passes the characteristics test.

3. Engine parameters

Figure 1 presents a sample graph of the torque and power from the diesel engine. The maximum power output value is determined for the assumed speed (which in this case is 4500 rpm). Similarly, the torque value is determined for a speed of 2300 rpm.

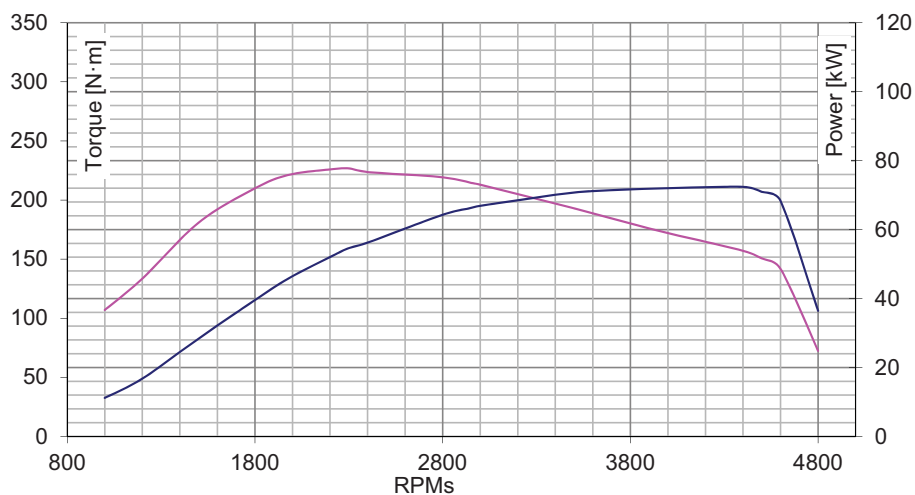


Fig.1. Power and torque characteristic for Diesel engine :pink line-torque; blue line-power

4. Statistical analysis

Table 1 presents the results of measurements of maximum power for a sample size of 40 engines.

Tab.1 Results of measurement

| Maximum Power | | Maximum Power | |
|---------------|-------|---------------|-------|
| No. | kW | No. | kW |
| 1 | 73,84 | 21 | 73,36 |
| 2 | 73,32 | 22 | 73,22 |
| 3 | 73,39 | 23 | 73,91 |
| 4 | 74,37 | 24 | 71,61 |
| 5 | 73,32 | 25 | 72,22 |
| 6 | 71,51 | 26 | 71,67 |
| 7 | 73,08 | 27 | 72,94 |
| 8 | 73,43 | 28 | 71,94 |
| 9 | 70,21 | 29 | 73,52 |
| 10 | 71,94 | 30 | 72,64 |
| 11 | 71,91 | 31 | 71,91 |
| 12 | 72,01 | 32 | 71,72 |
| 13 | 72,76 | 33 | 73,08 |
| 14 | 72,68 | 34 | 72,64 |
| 15 | 70,92 | 35 | 73,53 |
| 16 | 72,36 | 36 | 73,14 |
| 17 | 71,54 | 37 | 69,92 |
| 18 | 71,78 | 38 | 73,86 |
| 19 | 71,93 | 39 | 72,21 |
| 20 | 72,85 | 40 | 72,4 |

The statistical analyzes were made in Statistica. In order to conduct a statistical test procedure the distribution of the data in Table 1 was grouped into six classes (fig. 2). Due to the similar values of mean, median and dominants it was hypothesized that the normal distribution describes the values of maximum engine power.

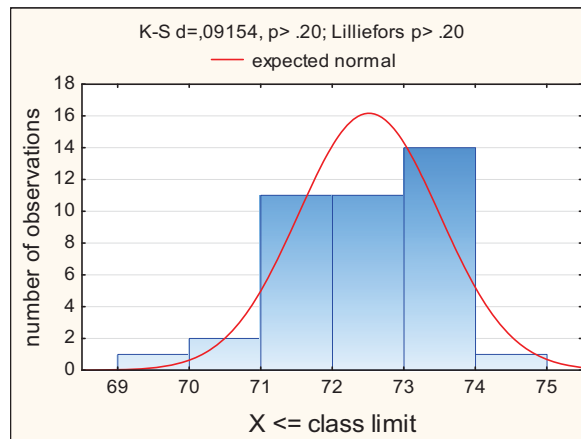


Fig.2. Maximum power grouped in classes

Figure 3 presents the median, lower and upper quartile of maximum power. Median and average values are similar and provide a symmetrical distribution. It also confirms the low value of the kurtosis.

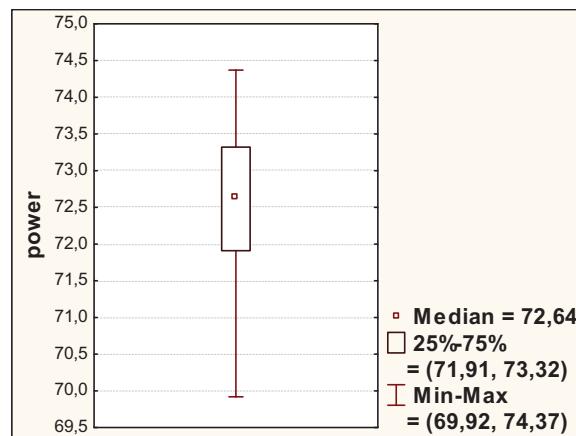


Fig.3. Median, lower and upper quartile

N = 40,000000
 % valid=100,000000
 mean= 72,514750
 confidence interval -95,000%= 72,199031
 confidence interval 95,000= 72,830469
 Median = 72,640000
 Sum=2900,590000
 Minimum= 69,920000
 Maximum= 74,370000
 lower quartile 71,910000
 upper quartile 73,320000

Percentile 10,00000= 71,525000
 Percentile 90,00000= 73,685000
 range= 4,450000
 quartile range = 1,410000
 variation= 0,974544
 standard deviation= 0,987190
 confidence interval of standard deviation. -
 95,000%= 0,808667
 confidence interval of standard deviation
 +95,000%= 1,267587
 kurtosis= 0,277375

The next figure (4) shows the empirical distribution function for the cumulative value of the maximum engine power with the curve representing the normal distribution and confidence intervals.

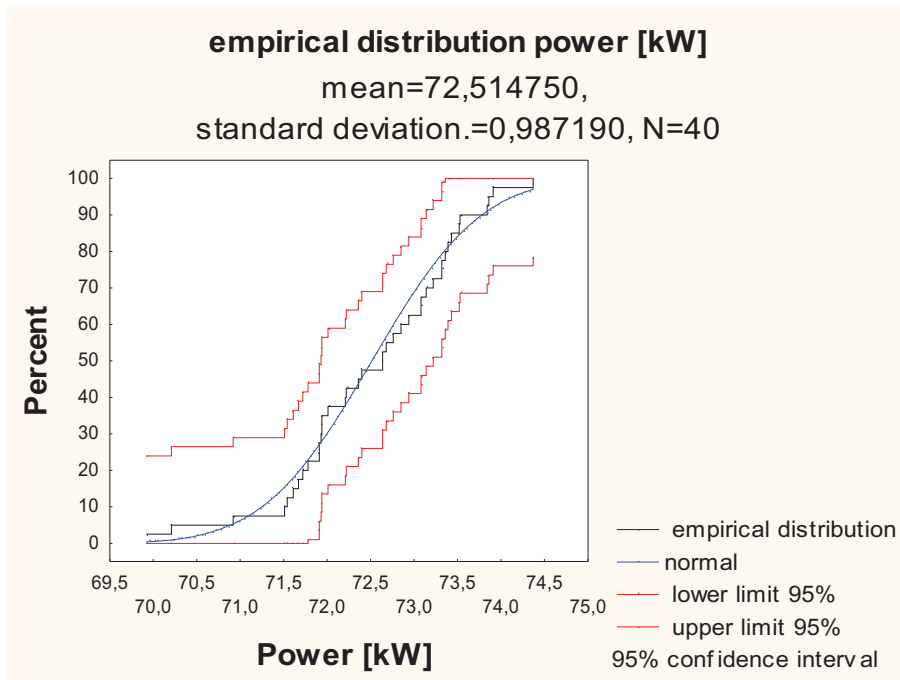


Fig.4. Empirical distribution

5. Summary

Presented results of statistical analyses show the extent of the real values for the analysed maximum power Diesel engines. Narrow range of the standard deviation of the order of 1 kW proves the high quality of our engines. The mean value is lower by 1.5 kW from the nominal value. It is worth to give by the nominal value with tolerance limits allowable by manufacturer of engines.

References

- [1] Luft S., *Pojazdy samochodowe. Podstawy budowy silników*, Wydawnictwo Komunikacji i Łączności, Warszawa 2003.
- [2] *Dyrektywa 80/1269/EWG W sprawie zbliżania ustawodawstwa Państw Członkowskich dotyczących mocy silników pojazdów silnikowych.*
- [3] *Dyrektywa 98/69/EC dla wszystkich pojazdów.*
- [4] *Dyrektywa 2007/715/EC dla lekkich samochodów osobowych.*
- [5] Burdzik, R., Konieczny, Ł., *Wpływ wybranych uszkodzeń silnika pojazdu samochodowego na poziom generowanego hałasu*, VII Sympozjum Naukowo-Techniczne „Silniki spalinowe w zastosowaniach wojskowych”, Czernica 17-20 października 2010.

- [6] Ferguson C., R., Kirkpatrick A., T.: Internal Combustion Engines. John Wiley & Sons, INC, 2001.
- [7] Heywood J., B.: Internal Combustion engine fundamentals. 1988,
- [8] Kin Wong P., Mou Tam L., Li K.: Automotive engine power performance tuning under numerical and nominal data. Control Engineering Practice 20 (2012) 300–314
- [9] Konieczny, Ł., Burdzik, R., *Research into noise emissions by a car combustion engine exhaust system*, Zeszyty Naukowe Akademii Marynarki Wojennej rok LII NR 1 (184), pp. 7-12, 2011.



FAILURE MODEL OF MAIN ELEMENTS OF THE SHIP ENGINE CRANKSHAFT-PISTON ASSEMBLY

Piotr Bzura

Gdansk University of Technology
ul. Narutowicza 11/12, 80-950 Gdańsk, Poland
tel. +48 58 3472573
e-mail: pbzura@pg.gda.pl

Abstract

The paper presents a failure model of main elements of the crankshaft-piston assembly, based on failures of crankshaft-piston assembly and timing gear system of the Sulzer RD engines, retrieved from the equipment reliability data of selected ships.

Keywords: reliability, durability, failures

1. Introduction

Reliability and durability of piston engines used on ships is an immensely important problem as the engines are objects of a very complex structure operating in difficult marine conditions. Therefore, extensive engine failures can cause ship disasters. Those failures are of a random event character. The available world statistics give only information on damage caused by the disasters and not the failure event data, although such information could be obtained from properly lined diagnostic parameter measurements. Such measurement lines have already been developed and used in diagnostic systems, e.g. by the big ship engine producers – German-Danish MAN Diesel and Finnish-Swiss Wärtsilä companies. Those companies have developed such diagnostic systems as CoCoS (MAN Diesel) and CBM (Wärtsilä) [10,11,15,16].

In Poland [5], in the years 1972-1977 more than 96000 data were collected on failures and inefficiency of selected engines (e.g. 58 Sulzer RD engines) installed on 105 ships owned by the Polish Ocean Lines and Polish Steamship Company. From those data indices were calculated allowing to detect weak points of the engines.

2. Analysis of failures

Mechanisms of the marine engine failures in operation can be different but are always connected with forcing factors, e.g. load force and torque, vibration, temperature changes etc.

In references [1,8], failure is defined as an event whose occurrence causes the element to cease (totally or partly) performing its functions.

The Sulzer RD engine crankshaft-piston assembly and timing gear system consist of many elements, so failure of one element need not cause inefficiency of the whole respective assembly. One of the results of an element failure in a complex system may be deterioration of the properties

of other elements. This can lead to a “failure avalanche”. The second result may be deterioration of the technical condition of another element, which can lead to shorter life of the remaining system elements.

In references [1,7] a classification of failures is used depending on the extension of their effects (Table 1).

Table 1. Classification of failures [1,7]

| Failure form | Immediate cause | Typical symptoms |
|---|--|--|
| Wear of surface layer | Wear due to sliding friction, contact loads and thermal wear | Change of dimensions, shape and surface smoothness, increased clearances, contacts, motion discontinuity, change of trajectory |
| Fracture, break or cracks of elements | Insufficient tensile, fatigue or impact strength | Loss of coherence, loss of functional properties, inefficiency of the whole assembly, loss of rigidity |
| Plastic strain, deformation of elements | Exceeded admissible loads | Change of shape or form, local indentation, elongation |
| Deregulations | Variable loads, vibrations | Slackened connections, knocks, loss of functional properties |
| Leakage | Immediate or variable loads, sliding friction wear, ageing | Loss of liquid or gas medium, loss of functional properties |
| Burnings | Excessive thermal loads | System inefficiency, loss of functional properties |
| Fouling, choking | Chemical and physical phenomena | System inefficiency, worsening of work parameters |
| Other | Ageing of elements, erosion, corrosion, scale, destroyed protective coatings | Change of colour, smoothness and lustre, unesthetic appearance |

Failure investigations consist, among other actions, in collecting information on operation of the crankshaft-piston assembly and timing gear system by means of questionnaires and processing the information in the SONUS system [6]. The following indices have been adopted for reliability estimation:

- SCPU – mean time to failure, in hours;
- INU – standardized per 1000 hours index of the reparable equipment failure development speed;
- CZU – index of the equipment reparable failure structure.

Various engine systems were subjected to failure analysis and results are presented in tables. For instance, an analysis is shown of the Sulzer RD engine type crankshaft-piston assembly and timing gear system failures in the years 1972-1974 (Table 2) [12,13,14] and the subsystem failures that occurred in 1974 are listed (Table 3) [14].

Table 2. Failure indices and form of the RD type engine crankshaft-piston assembly and timing gear system failures [12,13,14]

| Year | Number of failures, by failure form | | | | | | | | | | | | | | | | | SCPU | INU | CZU | |
|------|-------------------------------------|----------------|----------------|----------------|----------------|----------------|----------------|----------------|----------------|-----------------|-----------------|-----------------|-----------------|-----------------|-----------------|-----------------|-----------------|------|-------|--------|------|
| | U ₁ | U ₂ | U ₃ | U ₄ | U ₅ | U ₆ | U ₇ | U ₈ | U ₉ | U ₁₀ | U ₁₁ | U ₁₂ | U ₁₃ | U ₁₄ | U ₁₅ | U ₁₆ | U ₁₇ | | | | Σ |
| 1972 | 34 | 106 | 13 | 283 | 6 | 8 | - | 10 | - | - | - | 2 | - | - | - | - | 13 | 475 | 11398 | 0,0877 | 0,42 |
| 1973 | 37 | 105 | 13 | 500 | 20 | 4 | - | 50 | - | - | 1 | - | 6 | 1 | - | - | 17 | 754 | 10371 | 0,0964 | 0,42 |
| 1974 | 99 | 192 | 71 | 1348 | 36 | 7 | 4 | 101 | 1 | - | 12 | - | 15 | 10 | 3 | 1 | 11 | 1911 | 12741 | 0,0784 | 0,54 |

Table 3. Failure indices and form of the RD type engine crankshaft-piston assembly and timing gear system failures in 1974 [14]

| Specification | Number of failures, by failure form | | | | | | | | | | | | | | | | | SCPU | INU | CZU | |
|-----------------------------|-------------------------------------|----------------|----------------|----------------|----------------|----------------|----------------|----------------|----------------|-----------------|-----------------|-----------------|-----------------|-----------------|-----------------|-----------------|-----------------|------|-------|--------|------|
| | U ₁ | U ₂ | U ₃ | U ₄ | U ₅ | U ₆ | U ₇ | U ₈ | U ₉ | U ₁₀ | U ₁₁ | U ₁₂ | U ₁₃ | U ₁₄ | U ₁₅ | U ₁₆ | U ₁₇ | | | | Σ |
| Piston with rings | 8 | 65 | 41 | 319 | 5 | 6 | 4 | 30 | - | 8 | 3 | - | 12 | 8 | 3 | - | 7 | 507 | 8959 | 0,1116 | 0,27 |
| Piston rod with crosshead | 11 | 69 | 1 | 33 | 13 | - | - | 2 | - | 2 | - | - | - | 2 | - | - | 4 | 136 | 15781 | 0,0633 | 0,07 |
| Piston rod packing, sealing | | | 7 | 6 | - | - | 1 | 32 | 1 | - | - | - | - | - | - | - | - | 445 | 14461 | 0,0691 | 0,23 |
| Connecting rod | - | - | - | 6 | - | - | - | - | - | - | - | - | - | - | - | - | - | 6 | 13000 | 0,0769 | - |
| Crankshaft | - | - | - | 4 | - | - | - | - | - | - | - | - | - | - | - | - | - | 4 | 39063 | 0,0255 | - |
| Camshaft, fuel cams | 14 | 7 | - | 75 | 8 | - | - | - | - | - | - | - | - | - | - | 1 | - | 105 | 17621 | 0,0567 | 0,05 |
| Timing gear mechanism | - | - | - | 2 | - | - | - | - | - | - | - | - | - | - | - | - | - | 2 | 10498 | 0,0952 | - |
| Exhaust valves | 57 | 45 | 28 | 450 | 8 | - | 3 | 37 | - | - | 9 | - | 3 | - | - | - | - | 640 | 12381 | 0,0807 | 0,33 |
| Valve adjustment mechanism | 2 | - | - | 61 | 2 | 1 | - | - | - | - | - | - | - | - | - | - | - | 66 | 18101 | 0,0552 | 0,03 |

Where: U₁ – strain, U₂ – crack, U₃ – fracture, break, U₄ – wear, U₅ – seizure, U₆ – slackening, contact, U₇ – melting, U₈ – leakage, U₉ – fouling, U₁₀ – choking, U₁₁ – overheating, U₁₂ – corrosion, U₁₃ – burning, U₁₄ – ageing, U₁₅ – erosion, U₁₆ – scale, U₁₇ – other.

It can be estimated from the failures (Table 2) that most of the 17 forms of failure were caused by linear wear (friction, adhesion, corrosion) or volumetric wear (e.g. cracks). In the Sulzer RD engine crankshaft-piston assembly and timing gear system they made up: in 1972 - 60%, in 1973 - 66%, in 1974 - 71% of all failures. Additionally, from the share in the CZU overall failure structure: 1972 - 0.42; 1973 - 0.42; 1974 - 0.54 the increasing number of failures with increasing engine age can be seen. Therefore, Table 3 presents failures occurred in 1974.

Cracks, fractures and breaks, which may lead even to engine stoppage, took the second place in the registered failure forms. Table 3 shows that these type of failures occur most often in the piston-rings subsystem (21%) and the piston rod-crosshead subsystem (51%). Such subsystem failures require comprehensive analysis of the failure event causes as well as laboratory examinations in order to verify the operational experience conclusions.

3. Model of the piston-rings and piston rod-crosshead subsystem failures

Analysis of the Sulzer RD engine crankshaft-piston assembly and timing gear system failures indicates that subsystems requiring the most thorough examination are piston with rings and piston rod with crosshead – parts of the crankshaft-piston assembly. The two subsystems are considered operational when respective characteristics of the subsystem component elements are contained within limits defined by their work character. When one of the work characteristics [2,3,4,5,9] (e.g. working medium parameters) exceeds the admissible limits and for instance the crosshead bearing begins to work defectively, then it is treated as inefficiency.

The work characteristic of any main element of the crankshaft-piston assembly (Fig.1) gets monotonically worse under the impairing relaxation stimuli. It may be assumed that the subsystem inefficiency occurs when one of its elements exceeds the admissible limits given in the specification. The element trouble-free operation time “T” is counted until the moment when the work characteristic exceeds the assumed limit value. Fig.1 presents also a situation when single stimuli of a determined value occur at randomly selected moments. After “r” such occurrences the element as a whole appears nonoperational (inefficient). Action of a single stimulus appears as stepwise decrease of the element efficiency by a certain value “y” [2,3].

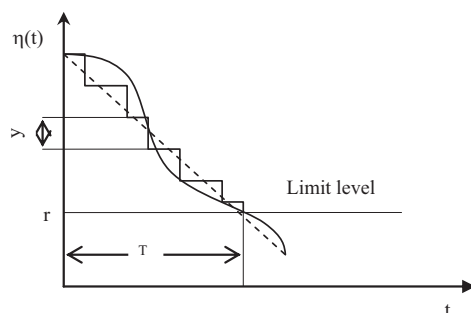


Fig. 1. Action of impairing relaxation stimuli: $\eta(t)$ – operating characteristic of a crankshaft-piston element; t – time; T – trouble-free operation time, element durability; r – number of stimuli necessary to cause element inefficiency; y – stepwise wear

The failure model may be considered useful when it describes a stable (or normal) period of the impairing stimulus action. Then the probability of an increase of the number of failures

in the time interval from "t" to "t+Δt" does not depend on the number of such increases in the time interval from 0 to t.

It may be concluded from the results of failures of the piston with rings and piston rod with crosshead assemblies that usefulness of the presented wear model may be accepted and that the wear model is well described by the gamma distribution [2,4,5,9]. Then the value of the subsystem trouble-free operation probability for time t can be determined in a simple way from the nomogram presented in Fig.2 [3].

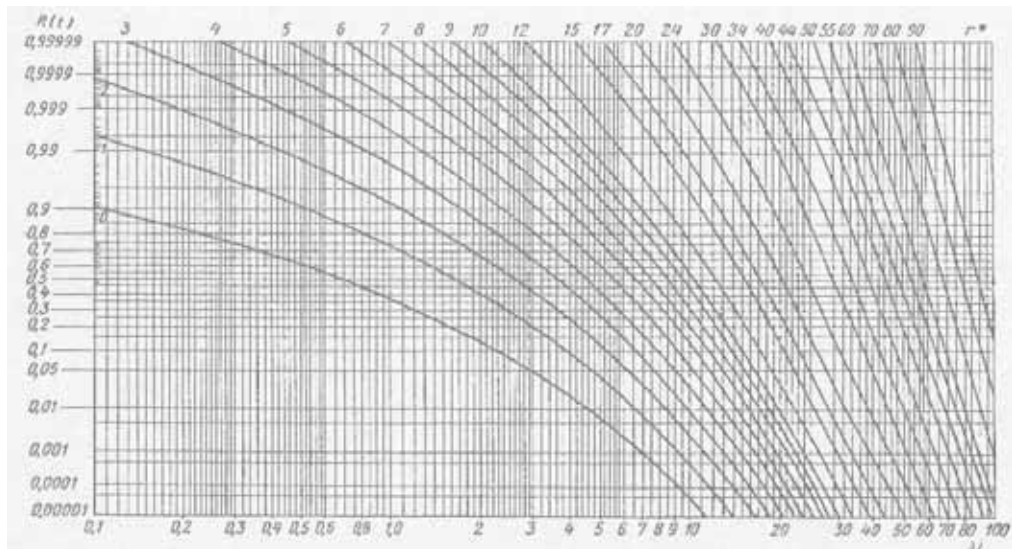


Fig.2. Nomogram for reliability $R(t)=P(T>t)$ determination in accordance with the gamma distribution: $r^*=r-1$ [3]

The above presented considerations allow to estimate the probability values of trouble-free operation of the piston with rings and piston rod with crosshead assemblies. From data given in Table 3 the λ (i.e. the failure intensity) and r (i.e. the number of stimuli necessary for inefficiency to occur) parameters can be estimated [2]. Probabilities of trouble-free operation during $t_1 = 1$ year (8760 h) and $t_2 = 3$ years (26280 h) determined by means of the nomogram in Fig.2 are presented in Table 4.

Table 4. Probabilities of trouble-free operation

| Subsystem | $P(T>8760h)$ | $P(T>26280h)$ |
|---------------------------|--------------|---------------|
| Piston with rings | 0,7 | 0,2 |
| Piston rod with crosshead | 0,9 | 0,5 |

Conclusions regarding the failures indicate that the most important elements are piston with rings.

4. Conclusions

1. The analysis of failures and the constructed wear model have shown that the main elements (piston and rings) belonging to the crankshaft-piston assembly should be investigated in the laboratory conditions by the accelerated wear methods in order to determine the causes of crack, fracture or break.

2. The reliability investigation statistical data are useful for increasing the reliability level of the crankshaft-piston assembly and timing gear system elements in the design and manufacture phase.

Bibliography

- [1] Adamkiewicz W., Hempel L., Podsiadło A., Śliwiński R., *Badania i ocena niezawodności maszyn w systemie transportowym*, Wydawnictwo Komunikacji i Łączności, Warszawa 1983
- [2] Bzura P., *Reliability Model of Slide Bearings With Particular Attention Given To Lubricating Oil*, Journal of Polish Cimac (Vol.6, No.2, pp.41-44), Gdańsk, 2011
- [3] Gercbach I.B., Kordonowski CH.B., *Modele niezawodnościowe obiektów technicznych*, Wydawnictwo naukowo-techniczne, Warszawa 1968
- [4] Girtler J., *Modele matematyczne w badaniach niezawodności silników o zapłonie samoczynnym*, Szczecin-Kopenhaga 1998
- [5] Grabski F., Jaźwiński J., *Metody Bayesowskie w niezawodności i diagnostyce*, Wydawnictwo Komunikacji i Łączności, Warszawa 2001
- [6] Grzywaczewski Z., *Niezawodność statku*, Wydawnictwo Przemysłu Maszynowego WEMA, Warszawa 1988
- [7] Hebda M., Mazur T., Pelc H., *Teoria eksploatacji pojazdów*, Wydawnictwo Komunikacji i Łączności, Warszawa 1978
- [8] Lewitowicz J., *Podstawy eksploatacji statków powietrznych.T.1., Systemy eksploatacji statków powietrznych* Wyd. ITWL, Warszawa 2001
- [9] Lewitowicz J., Kustron K., *Podstawy eksploatacji statków powietrznych.T.2., Własności i właściwości eksploatacyjne statków powietrznych*, Wyd. ITWL, Warszawa 2003
- [10] *CoCoS-Demo*, CD. MAN B&W Diesel A/S, Kopenhaga 2001
- [11] *Condition Based Maintenance*. Wärtsilä Corporation, Waasa 200
- [12] *Obsługa Banku Niezawodności Wyposażenia Okrętowego. Syntetyczne dane o niezawodności wyposażenia wybranych statków PLO i PŻM w 1972 roku*, Wydawnictwo Instytutu Morskiego 1974
- [13] *Obsługa Banku Niezawodności Wyposażenia Okrętowego. Syntetyczne dane o niezawodności wyposażenia wybranych statków PLO i PŻM w 1973 roku*, Wydawnictwo Instytutu Morskiego 1975
- [14] *Obsługa Banku Niezawodności Wyposażenia Okrętowego. Syntetyczne dane o niezawodności wyposażenia wybranych statków PLO i PŻM w 1974 roku*, Wydawnictwo Instytutu Morskiego 1975
- [15] *SIPWA-TP - Piston ring wear*. Wärtsilä Corporation, Waasa 2004.
- [16] *Sulzer RT - flex, Engine Selection and Project Manual*. Wärtsilä Corporation, Helsinki 2004.



DESIGN SOLUTION AND SELECTED RESEARCH RESULTS OF THE SEA-WAVE ENERGY CONVERTER

Czesław Dymarski

*Gdansk University of Technology
ul. Narutowicza 11/12; 80-233 Gdansk, Poland
Tel.: +48 58 3471608
e-mail: cpdymars@pg.gda.pl*

Paweł Dymarski

*Gdansk University of Technology
ul. Narutowicza 11/12; 80-233 Gdansk, Poland
Tel.: +48 58 3472397
e-mail: pawdymar@pg.gda.pl*

Abstract

The paper presents a novel device, a special buoy, for capturing the energy of sea-waves and the design of its model for conducting test in a towing-tank. The paper also presents the research program and general analyses on selecting the turbine and hull form, systems of anchoring and propulsion. In addition, it includes some chosen results of model tests and numerical calculations. Model of the buoy at the scale of 1:5 was tested in the towing tank for some range of wave height and its frequency and for two value of column length, a few states of ballast and tension of the anchor ropes. Numerical calculations were conducted for the same conditions and additionally for several anchor systems as well.

Keywords: *sea- wave energy, wave power device, hydrodynamics model tests*

1. Introduction

Presently over 80% of world production of electric power comes from fuel power station. In view of forecasted farthest increment of request for this kind of energy and shrinking stocks of traditional fuels and threat of adverse climatic changes evoked of their intensive expenditure there is urgent requirement of new finding and improvement of existing methods of utilization of renewable energy sources.

Energy of sea and ocean wave is one of such renewable source. There is enormous energy potential, but diffused on big surface and because of it practically not exploited until now. It is valued for European Union, modestly counting, on 120 – 190 TWh/year for opened reservoirs and additional 34 – 46 TWh/year for coastal zone [1]. Average Atlantic wave bears on meter of width about 70 kW. Somewhat Baltic waves bear less. According to estimates of Marine Institute in Gdansk these capabilities are considerably smaller for polish coastal zone and they amount to 3 – 5 kW /m [5].

Problems of capturing of sea-wave energy are new relatively and investigated during last some tens years mainly by scientific and research centres of seaside highly economically

developed countries only. However, it is necessary to note, that last time interest grows this topic fastly. Along with growing request for renewable energy and development of new technology perfecting of existing and working out of new methods of capturing of sea-wave energies are processed. Designing of the objects for commercial use of this kind of energy requires exact researching and knowledge and solutions of many difficult problems [7], [8]. Especially it concerns such problems as hydrodynamics of wavy motion and, in case of floating object, its movement trajectory on wave also so, in order to convert this changeable and spread over sea-wave energy to electric power most effectively.

Mentioned problems have been captivated in topic of research in the Faculty of Ocean Engineering and Ship Technology of Gdansk University of Technology [2,3,4]. From about three years there are conducted research project which title is: Experimental and numerical research of the buoy for capturing of the sea-waves energy. The paper presents an original method of winning of sea-wave energy by means of rolling buoy and it's construction solution based on the general concept contained in the patent of Mr. Sławomir Klukowski [6], and also some chosen results of model research and numeric calculations.

2. Design requirements assumptions

Prior to starting to design any novel structure, especially one mean to work under marine conditions, it is necessary to conduct analysis of the forecasted atmospheric and sea conditions which may occur during operation with emphasis on extreme weather scenarios. Such analysis allows for assessing the character and value of acting loads, as well as of the various hazards and technical problems, allowing for greater accuracy in establishing technical requirements assumptions of the structure and its equipment.

In case of the presented power buoy it was decided that the prototype would be meant to operate on the Baltic Sea in the Polish coastal zone at the depth of about 20 meters. It was also determined that the design and construction of the prototype should be proceeded by model based research in a towing-tank. The decision was made to build at least two models of the buoy at the scale of 1:5. The scale was selected based on the possibility of conducting research tests of the models on the large towing-tank located in the Ship Design and Research Centre in Gdansk, where it is possible to create model conditions close to those found at sea. This fact has significant impact on generalizing the measurement results and employing them for the verification of calculations. The towing-tank has the dimensions of $L \times B \times H = 260 \times 12 \times 6$ m and is equipped with a wave generator, as well as a towing carriage with measuring equipment. The tank allows for conducting tests for a wide range conditions with waves up to 0.7 m in height and 14 m in length for regular wave and even greater height for irregular waves. The large towing-tank dimensions significantly decrease the influence of wall deflection and creation of a shallow-water wave, allowing for conducting longer measuring sessions.

Taking into account the above factors, the following general model buoy design requirements were set:

- transverse buoy hull dimensions – 2.0 to 2.5 m;
- total draught of turbine column – up to 3.5 m;

3. Construction solutions

There were prepared two designs of the buoy models which differed mostly in the shape of the hull, power transmission system, the type of power generator and the buoy anchoring system.

The first designed solution of the model buoy, which more precise description is presented in the paper [3], is shown in fig. 1.

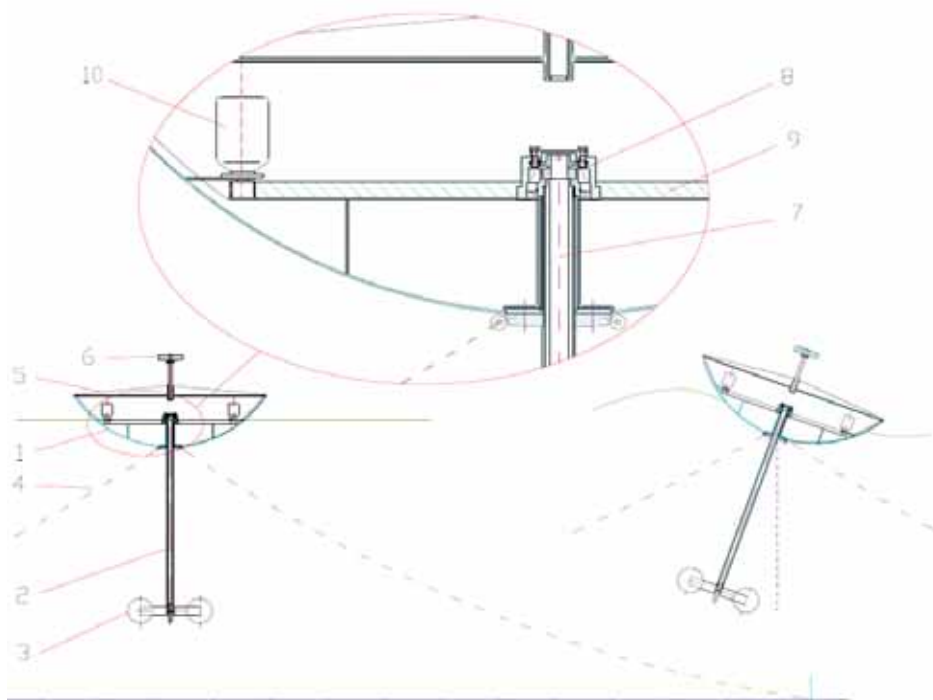


Fig. 1. Conceptual design of the buoy model for towing-tank tests: 1 – buoy body, 2 – column in form of tube, 3 – turbine, 4 – anchoring chain or line, 5 – buoy body cover, 6 – slidable weight for controlling buoy's centre of gravity, 7 – shaft, 8 – unidirectional clutch with bearing system, 9 – main gear, 10 – generator.

The second variant of the buoy was created at a later date following a more extensive theoretical analysis of the behavior of objects at the top of a wave, as well as after taking into account realistic technical and financial capabilities of the research. In comparison to the previous solution a number of significant changes were introduced. The axially symmetrical hull shape was abandoned in favor of form somewhat similar to “Salter’s duck” with a markedly elongated front and cylindrical rear part, as can be seen in Fig. 3. It was decided that such a shape allows for better use of waves’ kinetic and potential energy. This stems from the fact that the significant power of the hydrostatic lift of the water below acting on the elongated bow part of the hull should increase the angle of buoy’s deflection. In addition, after the crest of the wave passes the bow part above the water surface will increase the torque of the returning motion due to the longer arm of its centre of gravity in relation to the axis of the roll.

Assumed following general model buoy geometric parameters:

- transverse buoy hull dimensions – $L \times B = 2,03 \text{ m} \times 2,0 \text{ m}$;
- draught of the turbine: - variant 1 – $T1 = 2,3 \text{ m}$; - variant 2 – $T2 = 3,1 \text{ m}$;
- nominal displacement: - variant 1 – $D1 = 0,67 \text{ m}^3$; - variant 2 – $D2 = 6,9 \text{ m}^3$;

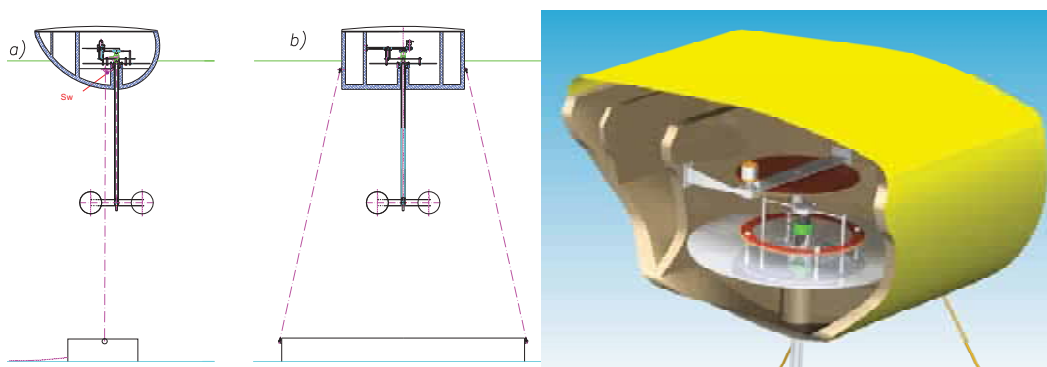


Fig. 2. Construction solution of the buoy: a) – longitudinal section, b) – cross section and on left side – 3 D longitudinal section

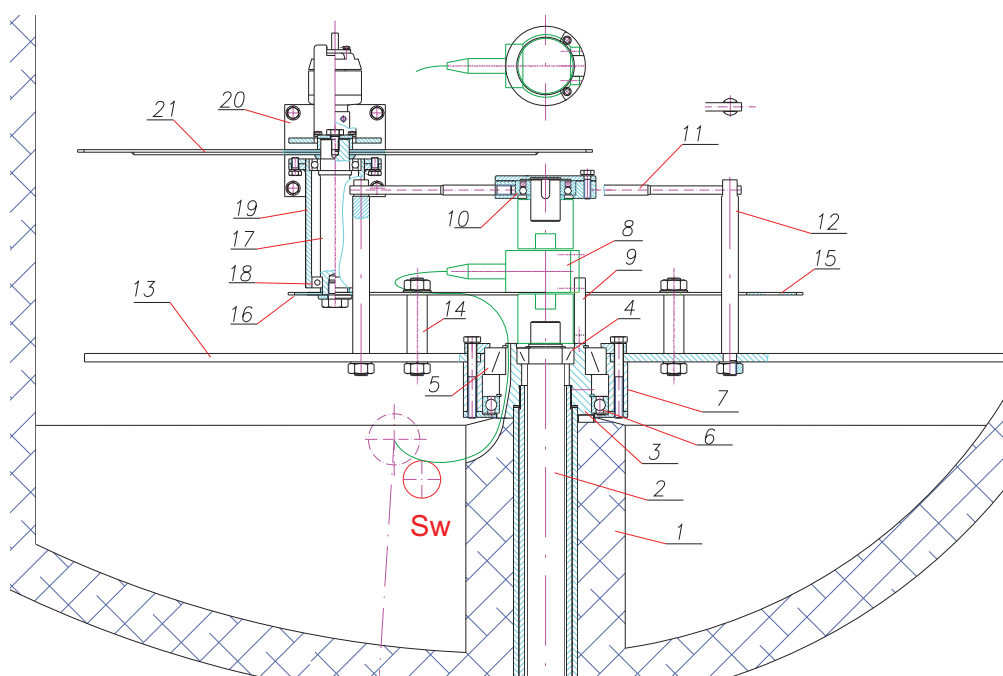


Fig. 3. Power transmission from the turbine shaft to the generator. Nomenclature: 1 – buoy hull, 2 – turbine shaft, 3 – head of column, 4, 5 – tapered roller bearings, 6 – roll bearing, 7 – hub of flywheel, 8 – torque meter, 9 – bracket, 10 – unidirectional clutch, 11 – casing of the clutch with two horizontal rods, 12 – vertical rods, 13 – flywheel, 14 – bolts, 15, 16 – 1st stage chain pulley, 17 – upper shaft journal, 18 – roll bearing, 19 – sleeve, 20 – transmission casing, 21 – 2nd stage chain pulley transmitting power to located above generator

The shaft 1 is placed inside the column on roller bearings. Turbine is attached to the lower end of the shaft. Blades of the turbine are semi-spherical in shape. This shape ensures turbine spin in only one direction independently of any lateral motion of the turbine. Number and diameter of the blades and diameter of their localization was established after model tests of turbines in towing-tank with different number and configuration of the blades. The mentioned parameters are following:

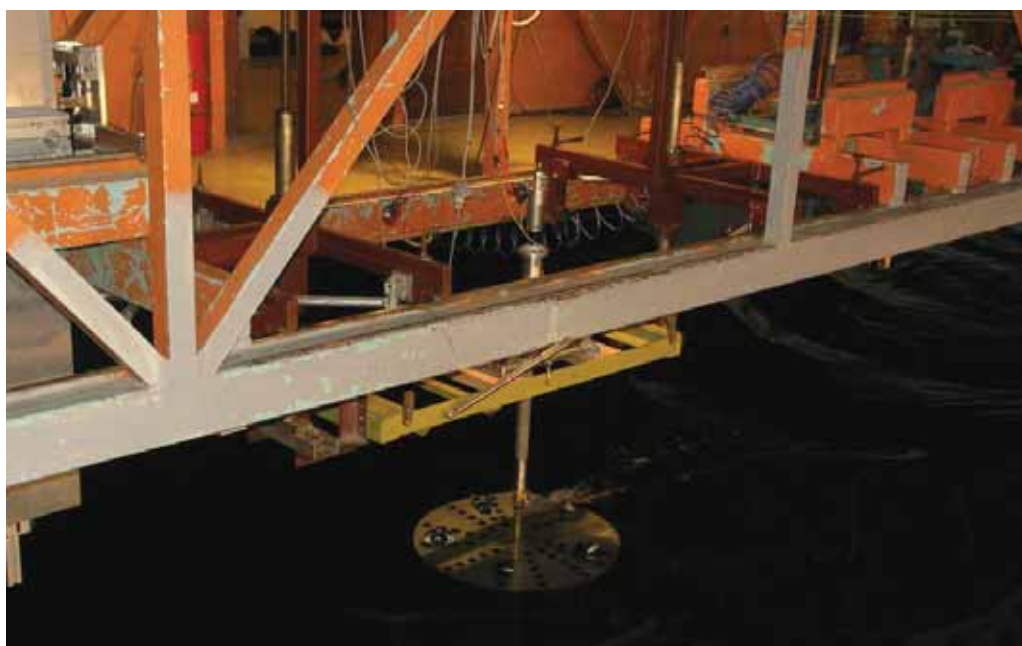


Fig. 4. Photographs of the turbine model tests in the towing tank

- number of blades – $N_{\text{cup}} = 3$
- diameter of blade – $D_{\text{cup}} = 0,36 \text{ m}$
- diameter of turbine – $D_T = 1,08 \text{ m}$

The new buoy hull also required changes to the anchoring system. Two anchoring strands were attached to the flat sidewalls of the hull. Proper selection of the attachment point of the anchoring strands was of high importance. In opinion of the authors' of this paper the attachment point should be located somewhat in front of and at the same time above the buoy's uplift centre. Such location is characterized by a very favorable course of the righting moment in the function of the buoy's angle of deflection. This moment is very small for low deflection angles due to the short arm of the force acting in the anchoring strand and does not interfere with hull's deflection. It increases to large values with high deflection angles, as a result of the uplift center and roll axis shifting away from the point of anchoring strand attachment, which to some degree protects the buoy from turning over and facilitates its returning motion.

The lower ends of anchoring strands are attached to a sinker resting on the bottom which in turn is connected by a separate strand to the bottom anchoring element. The sinker has the form of a box filled with heavy elements. The width of the sinker is substantially larger than the buoy width which protects the turbine from catching onto the anchoring strands during its rolling atop waves. The weight of the sinker in the water is appropriately smaller than total hull displacement, so that in the event of a very high wave the buoy would remain on the surface lifting only the sinker. The length of the anchoring strands was set as the approximate straight line distance between the points of their attachment to the buoy and the sinker. This means that in a certain foreseen range of wave height, the buoy not being able to float freely on the water surface will as the waves swell increase its draught. In doing so it will create increasingly large resistance, taking on growing amounts of wave energy which will manifest itself in increased amplitude of its roll which translates into greater efficiency.

4. The buoy model tests

The buoy model presented above was tested in the towing-tank. The apparatus installed on the model allowed measuring and recording the following parameters:

- linear acceleration in three directions,
- buoy rolling angles,
- heaving height,
- torque on turbine shaft,
- rotation speed and current parameters of the generator.

The measuring system allows for collecting data with constant rotation speed and variable torque or with constant torque and variable rotation speed of the generator.

The prepared program encompassed the following research tasks:

- Establishing favorable shape of the buoy hull depending on the chosen variant of defined or undefined wave direction.
- Preparing efficient anchoring system for both of the above mentioned variants of wave motion.
- Establishing the impact of the location of buoy's centre of gravity and moment of inertia on its rolling characteristic and power generation efficiency.
- Investigating the impact of the moment of inertia of the rotating elements of the system transmitting power from the turbine to the generator, as well as the influence of the gyroscope effect on the effectiveness and parameter stability of the generated electrical power..
- Setting outermost wave parameters:
 - the minimum necessary for starting the process of power generation,
 - the maximum where danger of mechanical or electrical damage appears - if possible to obtain in the towing-tank.
- Setting the general efficiency characteristic of generating power as function of wave parameters.
- Preparing a mathematical model and calculating program for simulating operation of the power buoy.

Verification of calculation results with data obtained during the model-based research phase.

Two photographs of the model buoy are presented in Fig.5 below - before launching in the towing-tank and during tests in regular wave conditions.



Fig. 5. Photographs of the power buoy model - on the left during preparation for launching, on the right during tests in the towing tank

The first series of model tests was conducted for the buoy with short column. Depth of dip of the turbine was 2,3 m. There were measured angles and displacements of the buoy' hull as

well as rotary speed and torque of the turbine's shaft for assumed ranges of wave height $H_{wM} = 0,35 - 0,5\text{m}$ and it's frequencies $f_M = 0,3 - 0,44\text{ Hz}$. Obtained power and angles of pitch of the buoy for two values of wave height converted on real parameters are presented in fig. 6a and fig. 7a.

Remaining model tests were carried for the buoy with the column extended about 0,8 m. Extension of the column has caused change of mass and dips of draught of the hull about 0,006 m, and consequently displacement in bottom direction of a mass centre of the buoy and change of moment of inertia in respect to pitch movement. After measurements conducted in the same way as in first series the tests were repeated for boosted mass of ballast in the hull about 100 kg, what caused increase draught of the buoy about far 0,032 m and next - for eased anchor ropes about 0,08 m.

Results of this series of the tests are show in fig. 6b and fig. 7b. It is possible to see distinct influence of increase of the column length as well as moment of inertia of the buoy pitch movement on displacement of extremes of pitch angle and power in direction of lower values of wave frequencies

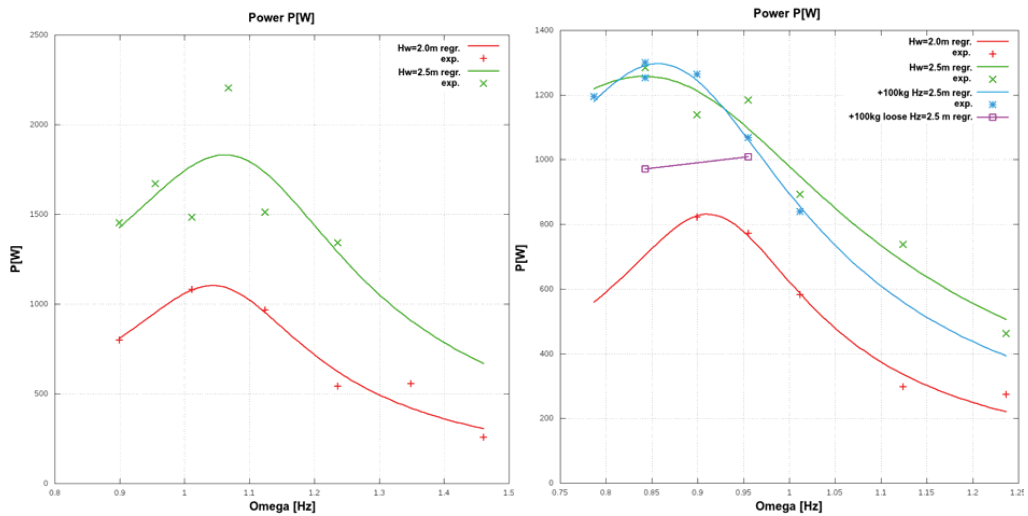


Fig. 6. Power of the buoy: a) – with short column, b) – with long column

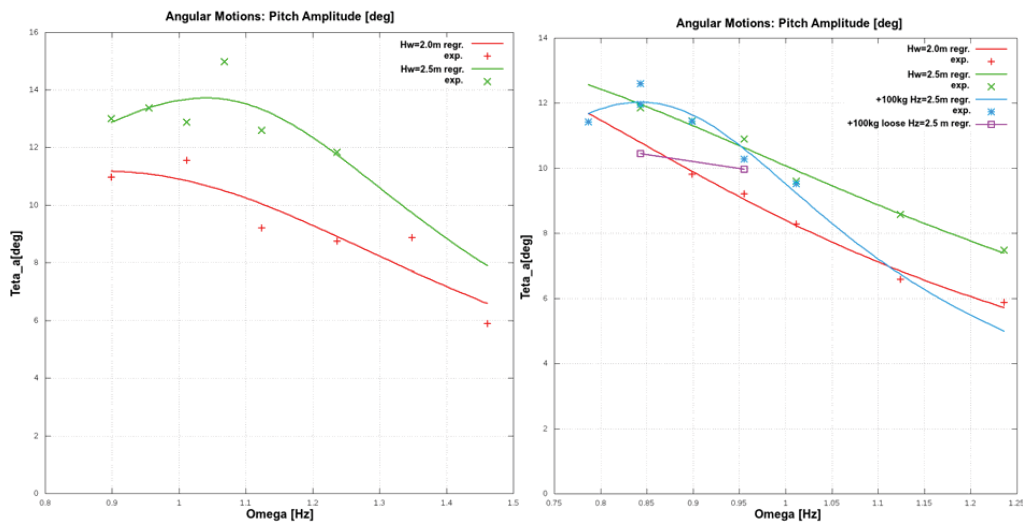


Fig. 7. Pitch of the buoy: a) – with short column, b) – with long column

There is visible also an advantageous influence increased rigidity of the anchoring system on efficiency of tested device's action. It should be mentioned that received results considerably differ from expected, especially in value of power. These values are smaller than in case of buoy with short column. Reason of this could be for example some technical fault committed during exchange of the column on longest one or any error in measurements. Because of high cost of the model tests and limited financial means on this purpose the tests could not be repeated. Further research of the buoy for different anchoring systems and geometric parameters were conducted with use of numerical simulations only.

5. Numerical simulation

Theoretical model has been developed based on rigid body motion in six degrees of freedom. Forces and moments acting on the buoy are caused by hydrodynamic external reactions according to wave, anchoring system and gravitation. Hydrostatic forces are calculated by integrating the static pressure of the submerged area of hull surface of the buoy. Buoy hull is modelled using quadrilateral panels. During calculation of the hydrostatic forces, acting on the panel, it is checked by algorithm whether the panel is fully immersed. If the panel is immersed partly, the force is calculated only for the wetted area. Hydrodynamic reaction is a sum of two components of frictional resistance and pressure resistance. The resistance of appendages is calculated based on its drag coefficient.

In the presented method water wave motion is modelled using a linear theory of waves. In addition, corrections have been introduced taking into account the impact of the free surface deformation on the value of hydrostatic pressure. Hydrodynamic pressure is calculated from the Bernoulli equation. Impacts, related to the presence of water added masses, is modelled using a simplified method based on the strip theory. Buoy hull is divided into strips with a specified thickness. Each section is associated a mass of water which causes hydrodynamic reaction during accelerated motion. Mass of water around frame depends on its shape and direction of motion.

To calculate the total hydrodynamic reactions the buoy acceleration ought to be known. The acceleration, in turn, depend on the sum of the forces acting on the hull. Therefore, calculation of the forces due to added masses should be done by successive approximations.

The first version of anchoring system of the buoy consist of two main ropes and two auxiliary lines. Main ropes are (almost) vertical. The ropes are strained to increase draft of the buoy. Auxiliary lines are horizontal, their role is to prevent yawing. The stiffness of vertical ropes is high to prevent heave motions. However horizontal lines are flabby, in order to minimize yawing without reducing pitching. The sketch of the anchoring system is presented at Fig. 8.

The buoy turbine is moving progressive (due to pitch motion) and rotating. Hydrodynamic reaction on rotor is calculated as the sum of forces induced on canopies and additional elements to which the canopies are attached. Hydrodynamic reaction induced on singular (isolated) canopy were calculated after defining and evaluation of the characteristics of drag and lift coefficients using RANSE-CFD method. The total torque of the turbine is the difference between hydrodynamic interactions and torque response to the generator. Torque

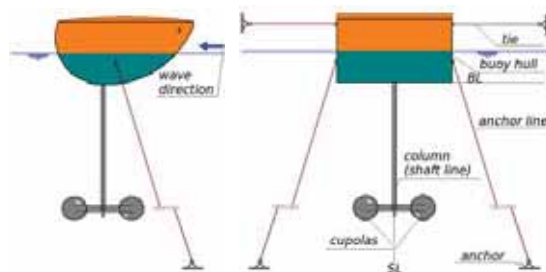


Fig. 8. Sketch of the modelled anchoring system

on the generator is a function of turbine rotational speed. In this model, we have assumed that this is a linear function.

Below some results of chosen examples of numerical calculations for a two variants of the buoy's anchoring systems are presented. The calculations were conducted for following common parameters according to fig. 9:

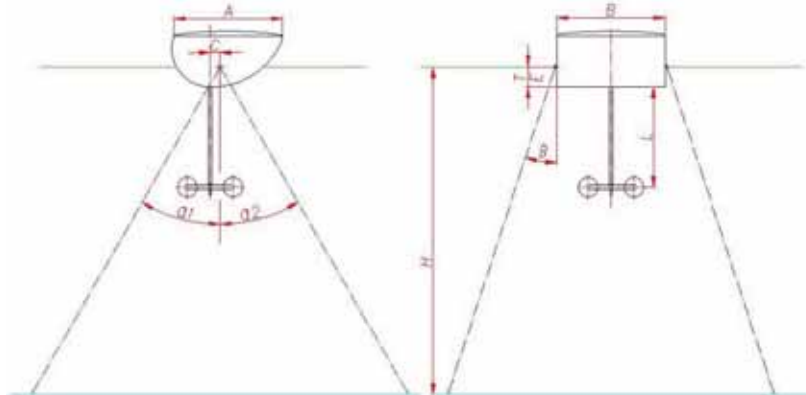


Fig. 9. View of the anchored system of the buoy with shown basic geometrical parameters

- $A = 2,0 \text{ m}$; $B = 2,0 \text{ m}$; $C = 0,162 \text{ m}$; $L = 1,84 \text{ m}$; $E = 0,370 \text{ m}$; $H = 6,0 \text{ m}$; α_1 ; α_2 ; $b = 18^\circ$
- $T_0 = E = 0,320 \text{ m}$ – draught of the buoy's hull before tensioning of the anchor wire;
- $T_k = 0,370 \text{ m}$ – draught of the buoy's hull after tensioning of the anchor wire;
- $d = 0,005 \text{ m}$ diameter of the anchor wire;
- $H_w = 0,4 \text{ m}$ – height of wave;

Variant 1 of the anchoring system shown in fig. 2 is the same which was tested in the towing tank. It contains only two anchor wires which, in an end view, in calm water look like vertical line. It means $\alpha_1 = \alpha_2 = 0^\circ$. Captured power, pitch, horizontal and vertical displacement of the buoy calculated for real scale for the same range of the wave angular speed are presented in fig. 10, 11, 12 and 13.

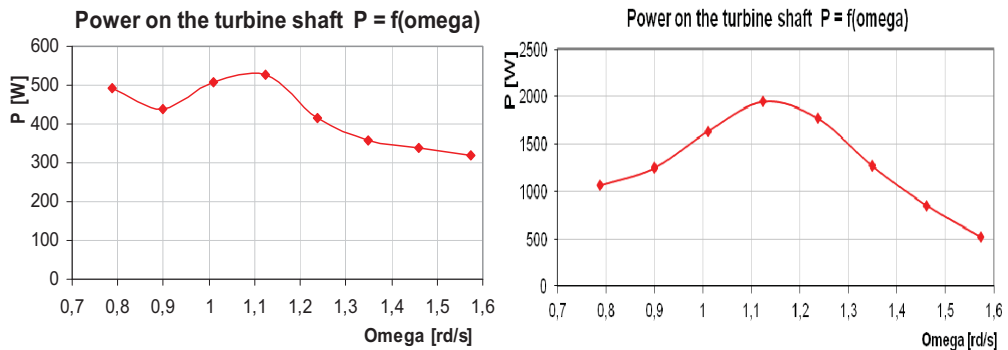


Fig. 10. Power on the turbine shaft calculated for the buoy with a short column ($L = 1,84 \text{ m}$) on left side and with a long column ($L = 2,64 \text{ m}$) on right side.

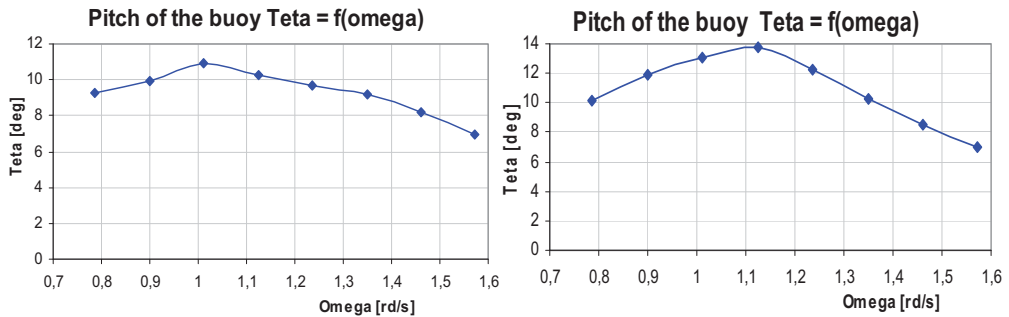


Fig. 11. Calculated pitch of the the buoy: with the short – on the left and long column on the right side.

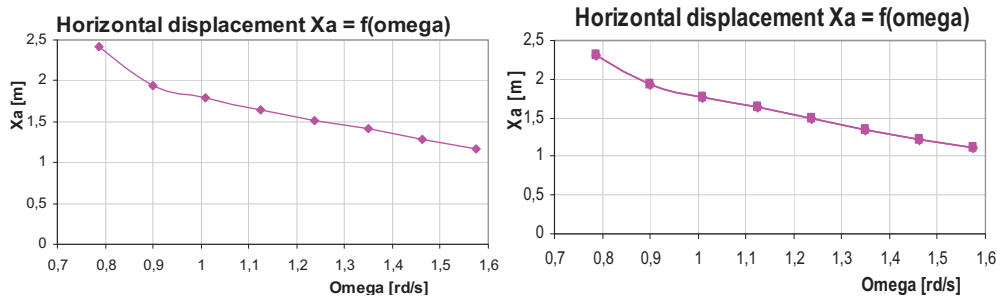


Fig. 12. Calculated pitch of the the buoy: with the short – on the left and long column on the right side.

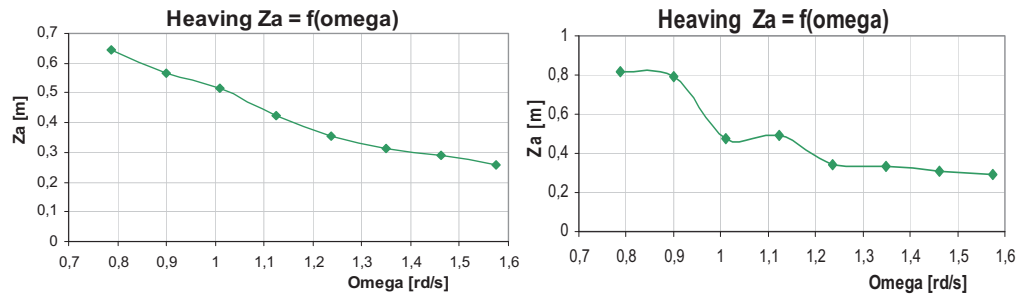


Fig. 13. Calculated heaving of the the buoy: with the short – on the left and long column on the right side.

Comparing the results of model tests shown in Figure 6 with the results of calculations presented in Fig. 10, one can see significant differences in the values. In autor's opinion the results of model tests of the buoy with the short column are the most reliable. It means that theoretical model of calculations gives understated results of captured power by more than half. So it can be concluded that shown below values of calculated power under the real conditions will be more than twice bigger.

Variant 2 of the anchoring system is shown in fig. 9. It consists of four anchor wires, which position are defined by dimensions C,E, H and angles α_1 and α_2 . Values of the rest mentioned geometrical parameters are the same as in variant 1. It is possible to create some variation of the system depending on the values of angles α_1 and α_2 . Figures 14 ÷ 16 present power, torque and rotary speed on the turbine shaft in function of the wave angular velocity of the sea-wave, calculated for four different configurations of anchoring system. These anchoring configurations differ only by values of angles α_1 and α_2 . Presented results are calculated for buoy with long column and 2m of wave height.

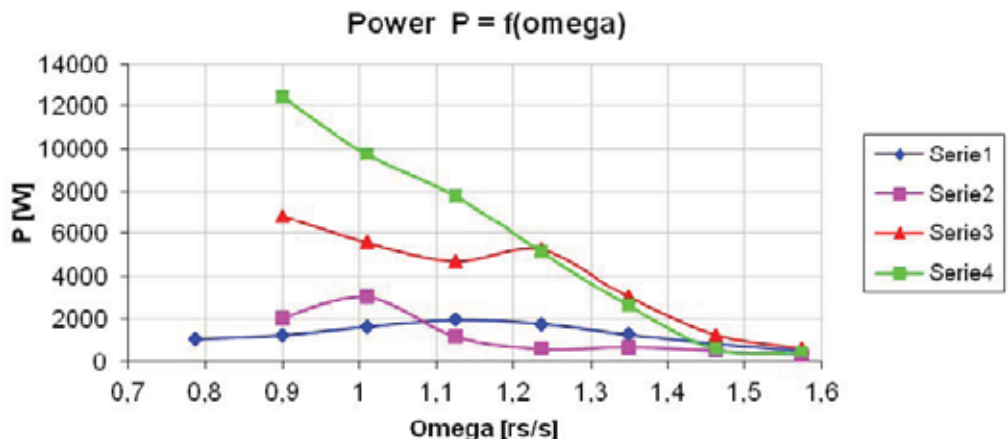


Fig. 14. Power on the turbine shaft calculated for the buoy with a long column:
 Serie 1 - $\alpha_1 = \alpha_2 = 0^\circ$; serie2 - $\alpha_1 = \alpha_2 = 15^\circ$; serie 3 - $\alpha_1 = \alpha_2 = 30^\circ$; serie 4 - $\alpha_1 = 15^\circ$; $\alpha_2 = 45^\circ$

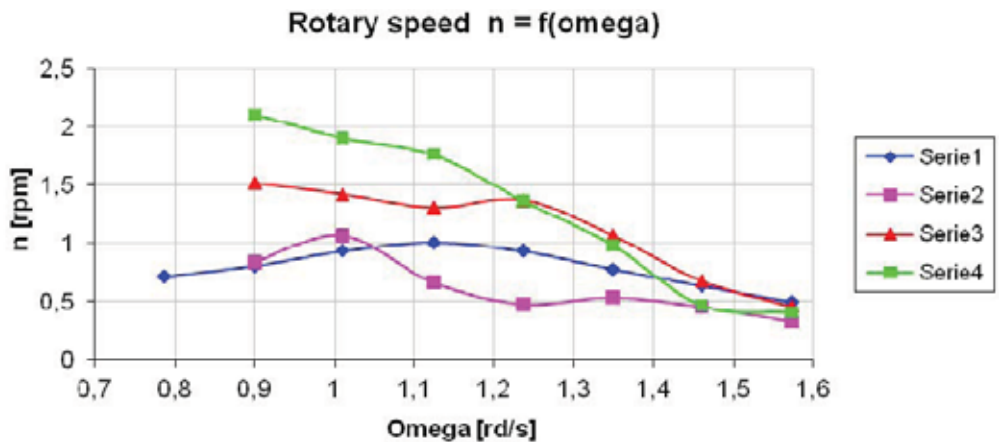


Fig. 15. Rotary speed of the turbine calculated for the buoy with a long column:
 Serie 1 - $\alpha_1 = \alpha_2 = 0^\circ$; serie2 - $\alpha_1 = \alpha_2 = 15^\circ$; serie 3 - $\alpha_1 = \alpha_2 = 30^\circ$; serie 4 - $\alpha_1 = 15^\circ$; $\alpha_2 = 45^\circ$

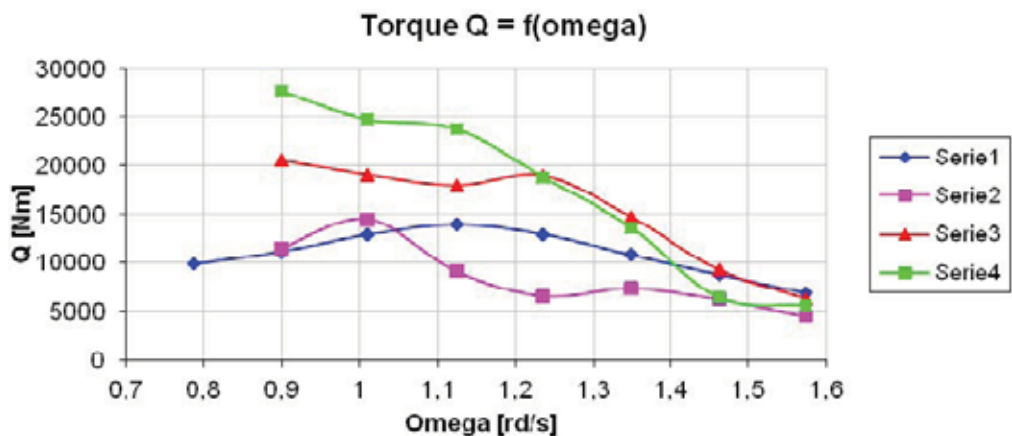


Fig. 16. Torque on the turbine shaft calculated for the buoy with a long column:
 Serie 1 - $\alpha_1 = \alpha_2 = 0^\circ$; serie2 - $\alpha_1 = \alpha_2 = 15^\circ$; serie 3 - $\alpha_1 = \alpha_2 = 30^\circ$; serie 4 - $\alpha_1 = 15^\circ$; $\alpha_2 = 45^\circ$

6. Conclusions

The design solution of the device for capturing the sea-wave energy as well as the model tests in the towing tank and numerical simulations presented in the paper are the first stage of this subject study, which started over two years ago at the Faculty of Ocean Engineering and Ship Technology of the Gdansk University of Technology. Even if these studies are not completed yet it allowed to determine the impact of various structural and geometrical parameters on the quality and effectiveness of device. Right now we can say, that as expected, one of the most important is the anchor buoy system. The system applied to the model tests was not the most preferred, but was a compromise between the desirable and feasible in the existing technical conditions of the towing tank. With the developed method of calculation it was possible to perform simulations of the device for several variants of this system. Selected results of these simulations are shown in Figures 10 - 15 and they indicate that by changing the anchoring system several times more power from the same device operating in the same sea conditions may be received.

When submitting the paper for publication there are conducted further simulations of the device operating, for determining the influence of other geometrical parameters and the buoy hull shape. We hope that the results of these studies are interesting enough that they were suitable for further publication.

Acknowledgment

The research presented in this paper has been conducted with the support of the Research Grant no. N N511 367 537 of the Polish Ministry of Science and Higher Education

References

- [1] Bernhoff H., Sjøstedt E., Leijon M.: Wave energy resources in sheltered sea areas: A case study of the Baltic Sea. The Fifth European Wave Energy Conference, 17-20 September 2003, In Cork, Ireland.
- [2] Dymarski P., Dymarski Cz.: *Numerical simulation of energy buoy motion in wave*. IV International Conference on Computational Methods In Marine Engineering IMARINE 2011 Lisbon, Portugal, 28 – 30 September 2011.
- [3] Dymarski C. Dymarski P. Litwin W.: *Novel Design of an Ocean Wave Power Device*; KEY ENGINEERING MATERIALS 2012 s. 206-215.
- [4] Dymarski Cz., Dymarski P.: *Device to capturing of the sea waves energy using a propeller with a self-adjusting turbine blades*. Patent application No P 394958. Poland, 2011.
- [5] GLOBEnergia 2/2008 Renewable Energy Sources – bimonthly. Publication of Maritime Institute in Gdańsk.
- [6] Klukowski S.: *Dispositif pour collecter l'énergie de la houle (Converter for Sea Wave Power Extraction)*. Patent application in France - Paris No 08/00951. 22/02/2008 (INPI - Institut National de la Propriete Industrielle).
- [7] Ocean of Energy. *European Ocean Energy Roadmap 2010-2050*. European Ocean Energy Association.
- [8] Price A.: *New Perspectives on Wave Energy Converter Control*. A thesis submitted for the degree of Doctor of Philosophy. The University of Edinburgh. March 2009.



THE ISSUES OF QUANTUM IN EMPIRICAL RESEARCH ON MACHINES AND OTHER POWER SYSTEMS

Jerzy Girtler

*Technical University of Gdańsk
Faculty of Ocean Engineering and Ship Technology
Department of Marine and Land Power Plants
tel. (+48 58) 347-24-30; fax (+48 58) 347-19-81
e-mail: jgirtl@pg.gda.pl*

Abstract

The paper provides justification for that the scientific research on empirical systems, particularly machines as well as other power systems, should take into account randomness and unpredictability of events which exist in their operation. The reference is made to achievements of the quantum mechanics, pointing the emerging postulate that the quantities called complementary have an important property consisting in that simultaneous and accurate measurement of their values is impossible. It has been shown herein that from the quantum mechanics it follows that by repeating empirical researches, whether they are observations, experiences or experiments, we cannot expect the same results, but we can expect the same frequency of acquiring the individual results. This indicates that acquirement of a particular research result is a random event. Additionally, the attention is paid that discovery in science, of the principle of ambiguous causality has led to oppugning the former belief of existence of unequivocal determinism (i.e. unequivocal effect from each cause) and adopting the ambiguous determinism that is determinism resulting from the probabilistic laws of the quantum mechanics, which allows (as known) the existence of choice.

Considering the achievements of the quantum mechanics as well as the empirical research results acquired in the phase of operation of machines and other power systems, it has been proposed to take the achievements into account for the empirical research.

Keywords: *decision, diagnostics, probability, reliability, diagnosing system*

1. Introduction

During operation of any machine, as well as any other power system, regardless of the type of the applied measuring system, the information on energy properties is obtained as a result of initiating and sustaining the operating process that leads to the performance of measurement. This process is [2, 5, 6] a two-dimensional stochastic process $\{D(t, \mathcal{G}): t \geq 0, \mathcal{G} \geq 0\}$, which is composed of the process $\{B(t): t \geq 0\}$ of operating the measuring devices and the process $\{C(\mathcal{G}): \mathcal{G} \geq 0\}$ of acquiring information by the devices, which is the result of measurement.

Publications referring to metrology [eg. 18, 19] say that the measurement means an action where it can be stated that at a given time and under defined conditions and by using defined methods and the related measuring devices, a determined measured quantity (w) is a value from the numerical interval $[a, b]$, i.e. that

$$a \leq w \leq b \quad (1)$$

where

$b - a = 2\varepsilon$, where 2ε - threshold.

The process $\{B(t): t \geq 0\}$ is a process that results from use of measuring devices when a tested machine (or other power system) is under operation performing a specific task, thus, is a process considered in a long time, which may but do not have to involve the following:

- repeated or various momentary measurements leading to obtaining the momentary values (x_i, t_i) , $i = 1, 2, \dots, n$ as well as
- elaborated results of the tests and developed reasoning that results from them.

This process has a significant impact on reliability of the results of empirical studies [7, 8, 9, 17, 23]. However, the process $\{C(\mathcal{G}): \mathcal{G} \geq 0\}$ is a process connected with performing measurements of physical quantities (energy parameters of machines) and with conducting a reasoning (inductive, deductive) at a defined time called a short time, so at operating (working) time of measuring devices, within which the final information (diagnosis) on energy state of the machine is obtained. Thus, the process $\{C(\mathcal{G}): \mathcal{G} \geq 0\}$ is made by the following realizations: diagnostic testing which consists in measuring a physical quantity characterizing the machine and reasoning which leads to development of a diagnosis on energy state of the tested machine (power system). Thus, an output of completion of the process $\{C(\mathcal{G}): \mathcal{G} \geq 0\}$ is a diagnosis, whose the reliability is the greatest when the measuring devices worked reliably during the course of the process, and disturbances resulting from interaction of the environment were of small scale due to resistance of these devices to such disturbances.

However, each inference about energy state of a machine is characterized by uncertainty because some mistakes can (and generally do) happen while making measurements.

Each measurement is performed with a defined accuracy which depends on the applied measuring methods and measuring devices (means), and testing conditions and qualifications of the staff doing the measurements. Thus, it arises a problem of existing inaccuracy in each measurement. This inaccuracy results from both: errors of the applied methods and measuring devices as well as changes in properties (characteristics) of the tested machine, proceeding while making the measurements. The cause of the inaccuracy is mainly a limited resolution of the measuring devices (which results from their threshold, randomness of the studied phenomena) and such errors as: quantization error, aperture error and sampling time error in case of using a digital signal for measuring [18]. Thus, the empirical studies of each machine or other power system involve measurement uncertainty which should be explained at least to the extend to be able to determine the main cause, i.e. whether the inaccuracy is mainly the result of [18, 19]:

- errors of measuring methods and measuring devices which, as known, depend largely on accuracy, sensitivity of measuring transducers or sensors, inaccuracy of the devices, which is defined by the inaccuracy class, as well as on stability and reliability of measuring devices – or
- changes in the characteristics of the machine while making measurements.

A correct explanation for the reasons of these inaccuracies in measurements is necessary to be able to estimate rightly the inaccuracies of the machine properties (power systems) and to make the right choice of proportion between the inaccuracy in measuring devices and the current inaccuracy in the properties of a machine as well as other power systems. The difficulty in determining the measurement uncertainty connected with the properties of the measuring methods and measuring devices, and the properties of diagnosed machines (and other power systems) is the quantum nature of their changes that causes randomness and unpredictability of events in empirical research. Therefore, it is necessary to consider this issue.

2. Randomness and unpredictability of events in empirical research

The measurement technique is dominated by a deterministic approach to identification of energy state of machines, however, more and more often the probabilistic aspects of empirical studies are noticed [6, 13, 16, 22, 23]. This is due to the traditional perception of the changes in energy state of machines and other power systems, which assumes that randomness and unpredictability in empirical research when making the measurements can be, in general, omitted. For this reason, an analysis of results is limited to the use of the classic account of errors and sometimes this account of errors is omitted without thorough justification of its uselessness for empirical research. One of the important reasons for this approach in diagnostics of machines was the fact that from the early years of the twentieth century, in science, there was in force a deterministic theory for describing phenomena, events and processes, finally developed by marquis Pierre Simon de Laplace. In the theory, P.S. de Laplace made an assumption that there were similar laws in both the macro- and micro-world, according to which all the changes proceed. In compliance with these laws every phenomenon occurs, lasts and disappears, all events (facts) proceed and any processes are realized. Following this theory, the entire universe is completely determined in both macro-and micro-scales. This vision of changes proceeding in space and time, was the basis for development of the science of those days, also the basic methodological assumption of physicists, until the early twentieth century. This view has led to development of the mechanics known today as classical (i.e. non-quantum, before quantum). Also it caused an emergence of belief that the laws of motion and any other changes can be expressed in the form of differential equations that have unequivocal solutions. This determinism is expressed in

- the principles formulated by Isaac Newton, describing the laws of nature,
- partial differential equation proposed by Erwin Schrödinger (1926), whose the solution is the wave function determining the quantum state of a micro-particle at any time in deterministic aspect,
- Albert Einstein's equation regarding the photoelectric effect as well as in the equation which describes, also in the deterministic aspect, the relationship between energy, mass and its velocity.

These equations are not only deterministic, but also reversible over time [14, 20]. It turned out, however, that despite the efforts of many mathematicians, they did not succeed to prove the existence of uniqueness of the solutions to differential equations. This situation caused an eagerness to seek a probabilistic concept for interpretation of the reality. An example for this can be a probabilistic interpretation of the wave function obtained from the said Schrödinger's wave equation, which was proposed by Max Born (in 1926), who could not accept the fact that this function represented the "real" electron wave, even though other physicists accepted this equation as a tool for solving the problems of the quantum mechanics. In this interpretation the wave function (Ψ) is such a product with values which are complex numbers [4, 11], that $|\Psi|^2$ is a measure of the probability of finding a micro-particle in a given space area (point). That means that you cannot be sure where such a micro-particle as an electron is located, but you can calculate the probability that it finds itself in a given point in space, if the aforementioned wave function is known. This corresponded to Niels Bohr's believes, who accepted the partial and wave theoretical models of existence of micro-particles. Also he believed that it was impossible to predict a specific outcome of empirical studies, and it was only possible to calculate the probability that the outcome of e.g. the given experiment would be such this and no other. But the final blow to the deterministic theory of P.S. de Laplace was done by Werner Heisenberg's uncertainty principle (1926), which together with the Max Planck's quantum hypothesis (1900), explaining the essence of the radiation of hot bodies, became one of the fundamental elements (achievements) of the quantum mechanics. This theory is nowadays the basis of the modern science and technology. It

was established in the twenties of the last century by Werner Heisenberg, Erwin Schrödinger, Paul Dirac, and also Wolfgang Pauli, Niels Bohr. Albert Einstein and Richard Feynman (creator of nanotechnology, considered by physicists as a genius No. 2 after A. Einstein) made their contributions to this theory, too. Its rules explain functioning of e.g. transistors and integrated circuits, thus one of the most important components of electronic devices, without which there are no modern measuring instruments. These rules apply to modern chemistry (quantum chemistry), cryophysics (quantum liquid) and biology. Among the physical sciences only the theory of gravitation and cosmology are not yet fully agreed with the quantum mechanics [12]. However, it should be expected that one day this will happen. The general theory of relativity describes well the observations because in ordinary conditions there exist weak gravitational fields. However, from the singularity theorems it follows that the gravitational field is very strong in at least two situations: in the area of black holes and during the Big Bang, as well as just afterwards [12]. In the fields of this kind, the quantum effects cannot be omitted [12, 20]. Therefore, it can be expected that the classical theory of relativity should fall due to the mentioned space-time singularities. Currently, the efforts are focused on developing a quantum theory of gravity. The classical (non-quantum) mechanics fell down because it assumed that the atoms should be brought to the state of infinite density. According to the assumptions of the theory, a hot body should radiate electromagnetic waves with the same intensity at all wave frequencies. This would mean that the inference that the total energy emitted by the body is infinite, is true. This inference is, however, wrong and that is why Max Planck formulated the hypothesis saying that electromagnetic waves cannot be emitted at any free rate, but only in specific portions which he called the quanta (hence the name of quantum hypothesis).

Moreover, from the quantum mechanics it follows that such physical quantities as energy, angular momentum (rotational momentum) can change only in steps. It also results that the quantities called complementary have an important property which consists in that impossible is simultaneous and accurate measurement of their values. For instance, the more accurate measurement of the micro-particle position we get, the less precisely its momentum, and thus - its velocity, is determined. This proceeds in compliance with the mentioned Heisenberg's uncertainty principle which determines the degree of inaccuracy in the measurements of the basic physical quantities (position and momentum of a particle, and also energy and time) and this has nothing in common with the accuracy of the measuring methods nor the accuracy of the measuring devices (instruments) [4, 11, 12]. From this it follows that in the micro-world it is not possible to predict accurately the future position of the particle being smaller than the atom, which is important for example for controlling the electron beam in a cathode ray tube. Thus, it is justifiable that the models of the atom, first by Joseph John Thompson, then by Lord Ernest Rutherford and N. Bohr (though the Bohr's model explained quite well the structure of the simplest atom, a hydrogen atom) have been replaced by a model of the atom based on the quantum mechanics. In this model, the electrons in atoms do not move on any specific orbits, but in so-called the orbitals considered as the areas of space around the nucleus, where the probability of existence of (finding) an electron at a given time has a strictly defined value. As proposed by Richard Feynman it is assumed that a particle does not move on one track, but on all the possible trajectories (available orbits) [1, 12]. The available orbits called the orbitals of the electrons in atoms, are understood as the areas of space around the nucleus where an electron can appear at a defined time, with a determined probability [1].

Transferring these findings into the field of macro scale research, it can be assumed that from W. Heisenberg's uncertainty principle it results that by repeating empirical research, regardless of whether they are observations, experiences or experiments, you cannot expect the same results. Thus, the question arises: how different can the results be expected? The answer is as follows: this depends on the taken testing method, accuracy of the used measuring instruments, conditions of the tests, and possibility of their repeatability, experience of the person conducting the tests, the

number of performed measurements, duration of the tests, etc. This means that by repeating the empirical tests, especially experiments, under given conditions, we should always expect different results. This indicates that acquirement of a specific test result is a random event. Thus, the measured values must be considered as random variables. Of course, if the variability of results is small, it can be omitted, but in any such case the reasonability for such proceeding must be justified. The most important phases of empirical research include performance of measurements [3, 6, 13, 16, 22, 23]. Each measurement has got a feature that the acquired measurement results (values of physical quantities) involve the said uncertainty and errors arising from the existence of different disturbances. It must, therefore, be assumed that the randomness of each measurement result is its integral attribute.

Thus, the quantum mechanics based on W. Heisenberg's uncertainty principle, introduces the unavoidable randomness and unpredictability into the science and practice.

More general uncertainty than the said uncertainty principle is introduced by a phenomenon known as deterministic chaos [21]. This phenomenon can be observed if the studied model is a system of differential equations, especially nonlinear equations of the second, third and fourth order. It is known that the solution to a deterministic system of differential equations takes the form of very complicated oscillations, of which the cause is not a large number of degrees of freedom or local disturbances, but the increasing instability dependent on the precision in determining the initial state which depends on the initial conditions connected with time and also on the coefficients of the time-dependent equations. The deterministic chaos is closely related to occurrence of so-called attractors that are usually non-periodic trajectories attracting other trajectories from their environment [1, 21]. Detection of the attractors enables better prediction of appearing random events. Thus, making an allegation that the empirical system develops chaotically may simplify the study of its evolution. This means that chaos is not always a negative phenomenon. Adding the noise with random properties to the non-disturbed empirical system, can lead to statistical stabilization or periodicity in the evolution of the system. This requires a new approach to the relationships existing among deterministic and statistical and probabilistic methods for empirical studies on machines and other power systems.

Another source of chaos may be inaccuracy in defining the parameters in the model. This fact is connected with the phenomenon of bifurcation (splitting into real test results acquired when testing the empirical systems and the expected (supposed) ones).

Discovery of the principle of ambiguous causality in science has led to oppugning the old belief of unequivocal determinism (i.e., unequivocal effect from a cause) and adopting an ambiguous determinism that is determinism resulting from the probabilistic laws of the quantum mechanics, which allows (as known) the existence of choice.

From the presented considerations it results that by organizing and conducting empirical tests of machines and other power systems, the attention should include the following laws (rules) of:

- ambiguous causality, i.e. existence of randomness of events (including the event which is a diagnose about a machine's state), and therefore, it is necessary to recognize at least the ambiguous determinism,
- uncertainty formulated by W. Heisenberg,

and also such facts as:

- existence of general randomness of nature as its indispensable feature, resulting from its infinite complexity,
- existence of deterministic chaos resulting from the so-called sensitivity of models of empirical systems, especially machines, to their initial state,
- limited (always) accuracy of measuring methods and measuring devices, thus also of the measurements performed with these devices,
- inaccuracy of the machine being an empirical system,

- unreliability of the measuring systems (instruments) adopted to perform the measurements and thus to identify the energy state of the machines.

The measurements refer to specific test procedures during which when implemented there can be made many mistakes as a consequence of:

- performance of empirical tests in highly disturbing conditions,
- improper performance of measurements and calculation of errors (e.g. not taking into account the quantization error and aperture error, and time sampling error), because of using the measuring devices with insufficient (inadequate) accuracy and/or omitting some measurements,
- wrong recording the results of measurements being properly performed and signaled by measuring devices,
- incorrect interpretation of measurement results at the stage of their acquisition and subsequent inferences about the state (energy, technical) of the machine due to inaccurate (incorrect) readings of indications by gauges (measuring devices) and adoption of inaccurate data processing algorithms,
- improper identification of machine's energy state, even though proper performance of measurements and disposal of the correct results from empirical tests.

This all makes that in empirical research where measuring methods and measuring devices are applied, there exists a problem of measurement uncertainty that results from changes in properties of the machine being an object of empirical studies, which takes place when performing the measurements, as well as from errors of the measuring methods and measuring means [12, 13]. Consequently, uncertainty arises which has to be explained in the research. The explanation should include at least a formulation of the main cause for this uncertainty, mainly whether it is the result of:

- changes in properties of the machine being an object of empirical research, which proceed at the time of measurements, or
- errors of the measuring methods and measuring devices (instruments, means).

Therefore, for this type of studies, it is important [19]:

- 1) to estimate the value of uncertainty for the object of empirical studies which is the machine,
- 2) to estimate the value of uncertainty for the measuring technique (measuring methods and measuring devices),
- 3) to select appropriate proportion between the uncertainty of measuring technique and the existing uncertainty of the studied object (machine).

In this situation, elaboration of a specific information (diagnosis) on the energy state of the machine or any other power system, requires application of the mathematical statistics, calculus of probability and stochastic processes.

3. Indications for quantum aspects of empirical studies on machines and other power systems


During empirical studies of machines and other power systems there exists a research situation that causes randomness and unpredictability of the recorded events. Therefore, [5, 7, 9, 10, 13, 16, 18, 19, 22, 23]:

- for empirical studies of machines and other power systems there is a degree of uncertainty in the test results, connected with all the examined phenomena and events involving wear, damage, generation of energy signals, etc.),
- it is not possible to predict precisely the changes in technical and energy characteristics of machines and other power systems under operation,

- there are changes in state of machines and other power systems (being the objects of empirical studies) when making measurements, as well as errors of the applied measuring methods and measuring devices,
- negligible variability can be determined as a result of application of the calculus of errors that does not lead to defining a real value,
- significant variability requires an application of the statistical estimation,
- real value (correct value) is an abstract term,
- it is necessary to assume that the value of the arithmetic mean, obtained from the measurements, is different than the real value of the measured physical quantity,
- one cannot expect the same results, but can expect the same frequency of obtaining the given result.

The considerations demonstrate that in empirical studies of machines and other power systems an uncertainty arises in the results acquired during performance of measurements. Therefore, a necessity occurs to identify the reasons of the uncertainty in the results. The most important reasons for the uncertainty in the results include among others [4, 8, 9, 10]:

- quantum changes in the properties of machines and other power systems (their energy and wear), that lead to quantum dissipation of their energy

$$E_{max} = E_1 \rightarrow E_2 \rightarrow \dots \rightarrow E_{n-2} \rightarrow E_{n-1} \rightarrow E_n = E_{min} \quad (2)$$


where:

E_i ($i = 1, 2, \dots, n$) – energies determined due to recording by the measuring system the subsequent drops in energy (E) of the machine (mechanism) in a form of portions (quanta) e ;
 E_{max} – maximum energy that can be generated by a machine (mechanism) at the time of correct operation, possible to be recorded by the measuring system, E_{min} – minimal energy that can be generated by a machine (mechanism) at the time of failure (recording this energy by the measuring system does not have to be possible),

- quantum symptom of changes in physical quantities which characterize: the flow of heat or electricity, energy radiation in the form of a stream of particles or electromagnetic waves, radioactive decay, etc.,
- in metrology, the term of “quantum of time” was implemented instead of the term of “time”,
- digital signal is a quantized and sampled quantity involving errors of quantization and aperture and the error of the sampling time,
- a set of tensions generated by the analog-to-digital transducer is discrete, the successive voltage values differ by the quantum “ q ”,
- there are programs used for generating the reference voltage (U_w), named „quantum by quantum programs”, which in the successive „ i ” steps generate the voltage $U_w = i \cdot q$, q – value of the voltage quantum,
- frequency is quantized by nature over time,
- essence of the measurement $a \leq w \leq b \rightarrow b - a = 2\varepsilon$ is quantized,
- measured values are random variables,
- conditions that cause variability of measures are variable,
- there is uncertainty of the applied measuring methods and measuring instruments,
- time of measuring is different due to the need of repeating the measurements,
- there are different experiences of the persons performing the measurements,

- there is uncertainty of the properties in the power systems being the objects of studies,
- recording the momentary values is a stochastic process,
- ambiguous causality implies ambiguous determinism, that is determinism resulting from the probabilistic laws of the quantum mechanics,

The considerations present that changes in energy state of machines and other power systems will have a quantum nature. These changes considered during operation of the systems will be realizations that can be regarded as continuous-time discrete-state stochastic processes. An exemplary realization of such a process depicting changes in dissipated (dissipation) energy of any marine power system is shown in Fig. 1.

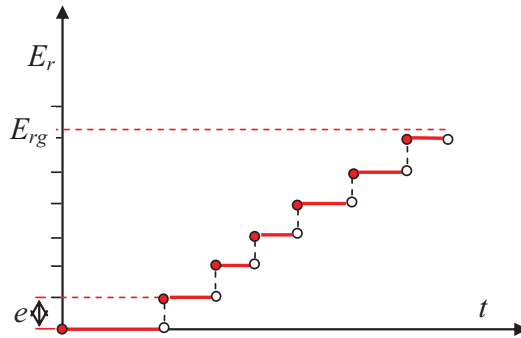


Fig. 1. Interpretation of the process of accumulating dissipated energy E_r for a machine (power system): e – portion of energy (quantum), by which the energy E_r decreases, E_{rg} – boundary dissipation energy

The presented research situation shows that the empirical studies on machines and other power systems have to include uncertainty of test results. This is necessary, because it means that such studies require determining the consequences of the uncertainty. Thus, while performing empirical tests of machines and other power systems it is worth to keep in mind the achievements of the quantum mechanics.

The general premises that induce to take advantage of the achievements of the quantum mechanics for empirical studies on mechanisms in a machine and other power systems can include the following [3, 4, 11, 15]:

- 1) the quantum theory is considered to be one of the most perfect theories being applied for various domains of physics,
- 2) no incompatibility has been noted between the quantum theory and the results of empirical studies in the areas of knowledge wherever used,
- 3) the quantum mechanics tends to describe the relationships among macroscopic phenomena, events and processes, that have been initiated by micro-objects,
- 4) a knowledge of surveying, which like the quantum mechanics uses quanta for the measured values, is applied for empirical studies,
- 5) properties of the power systems are expressed by physical quantities of a random nature.

Therefore, due to the existing randomness and unpredictability of events, including acquiring the same momentary values of different physical quantities, the test results obtained from empirical studies of machines and other power systems must be considered in the probabilistic approach by using the calculus of probability theory, mathematical statistics and the theory of stochastic processes. A deterministic approach can be applied for analysis of the test results for the mentioned empirical systems only in cases justified by the assumed purpose of the studies. However, this approach have to be precisely argued by providing adequate explanation for its

validity by employing the methods of inductive reasoning, deductive reasoning and reasoning by analogy.

4. Summary – remarks and conclusions

The empirical studies of machines and other power systems have to take into account the randomness and unpredictability of events which exist in their operation. The operating practice of the machines and other systems as well as the quantum mechanics show that by repeating empirical tests, regardless of whether they are observations, experiences, or experiments, we cannot expect the same results, but can expect the same frequency of acquiring the particular results. It means that that acquirement of a specific test result (measurement result) is a random event. This shows the need of regarding in this type of research the calculus of probability, mathematical statistics and the theory of the stochastic processes.

The principle of ambiguous causality has to be considered in the empirical studies of machines and other systems, which means the need of assuming the ambiguous determinism, so determinism resulting from probabilistic laws of the quantum mechanics, allowing (as known) existence of choice.

References

1. Aczel A.D.: *Prawdopodobieństwo = 1*. Zysk i S-ka Wydawnictwo s.c., Poznań 1997. Tytuł oryginału: Probability 1. Why There Must Be Intelligent Life in The Universe.
2. Benjamin J. R., Cornell C. A.: *Probability, Statistics, and Decision for Civil Engineers*. Copyright 1970 by McGraw-Hill, Inc. Wyd. polskie: *Rachunek prawdopodobieństwa, statystyka matematyczna i teoria decyzji dla inżynierów*. WNT, Warszawa 1977.
3. Będkowski L.: *Elementy diagnostyki technicznej*. Wydanie 2, WAT, Warszawa 1992.
4. Birula I., Cieplak M., Kamiński J.: *Teoria kwantów. Mechanika falowa*. Wydawnictwo Naukowe PWN, Warszawa 2001.
5. Girtler J.: *Sterowanie procesem eksploatacji okrętowych silników spalinowych na podstawie diagnostycznego modelu decyzyjnego*. Monografia. Zeszyty naukowe AMW, Gdynia 1989 nr 100A.
6. Girtler J.: *Diagnostyka jako warunek sterowania eksploatacją okrętowych silników spalinowych*. Studia Nr 28. WSM, Szczecin 1997.
7. Girtler J.: *Probabilistic measures of a diagnosis' likelihood about the technical state of transport means*. Archives of Transport. Polish Academy of Sciences. Committee of Transport. Quartelly. Vol. 11, iss. 3-4, Warsaw 1999, p.33-42.
8. Girtler J.: *Zastosowanie wiarygodności diagnozy do podejmowania decyzji w procesie eksploatacji urządzeń*. Materiały V Krajowej Konferencji DIAG'2003 nt. „Diagnostyka techniczna urządzeń i systemów”. Wydział Elektroniki Wojskowej Akademii Technicznej, Warszawa – Ustroń, s.100-109.
9. Girtler J.: *Probabilistyczne miary wiarygodności diagnozy o stanie technicznym maszyn i innych urządzeń*. Materiały XXXI Ogólnopolskiego Sympozjum DIAGNOSTYKA MASZYN, s. 24 (streszczenie), referat na CD-R.
10. Girtler J.: *Conception of valuation of combustion engine operation*. Journal of KONES. Powertrain and Transport. Editorial Office Institute of Aeronautics BK, Warsaw 2008, pp. 89-96.
11. Gribbin J.: *W poszukiwaniu kota Schrödingera*. Zysk i S-ka Wydawnictwo s.c., Poznań 1997. Tytuł oryginału: In Search of Schrödinger's Cat. Quantum Physics Reality.

12. Hawking S.W.: *Krótką historia czasu. Od wielkiego wybuchu do czarnych dziur*. Wydawnictwa ALFA, Warszawa 1990. Tytuł oryginału: A Brief History of Time: From the Bing Bang to Black Holes.
13. Michalski R.: *Diagnostyka Maszyn Roboczych*. Wyd. ITE, Radom 2004.
14. Moskowitsa M.: *Czy nauka jest dobra*. Wydawnictwo CiS, Warszawa 1997. Tytuł oryginału: Science and Society. The John C. Polanyi Nobel Laureates Lectures.
15. Nalewajski R.F.: *Podstawy i metody chemii kwantowej*. Wydawnictwo Naukowe PWN, Warszawa.
16. Niziński S.: *Elementy diagnostyki obiektów technicznych*. Wyd. UW-M, Olsztyn 2001.
17. Pabis S.: *Metodologia i metody nauk empirycznych*. PWN, Warszawa 1985.
18. Piotrowski J.: *Podstawy miernictwa*. WNT, Warszawa 2002.
19. Polański Z.: *Planowanie doświadczeń w technice*. PWN, Warszawa 1984.
20. Schutz B.F.: *Wstęp do ogólnej teorii względności*. Wydawnictwo Naukowe PWN, Warszawa 2002.
21. Tempczyk M.: *Teoria chaosu dla odważnych*. Wydawnictwo Naukowe PWN, Warszawa 2002.
22. Żółtowski B.: *Podstawy diagnostyki maszyn*. Wyd. ATR, Bydgoszcz 1996.
23. *Inżynieria diagnostyki Maszyn*. Praca zbiorowa po redakcją B. Żółtowskiego i C. Cempla. PTDT. Wyd. ITE, Warszawa, Bydgoszcz, Radom 2004.



STATISTIC DETERMINATION OF MAIN PROPULSION POWER AND TOTAL POWER OF ONBOARD ELECTRIC POWER STATION ON ANCHOR HANDLING TUG SUPPLY VESSELS AHTS SERVICING OIL RIGS

Zygmunt Górski , Mariusz Giernalczyk

*Katedra Siłowni Okrętowych
Akademia Morska w Gdyni, ul. Morska 83, 81-225 Gdynia, Poland
Tel.: +48 58 6901324, +48 58 6901307
e-mail: zyga@am.gdynia.pl , magier@am.gdynia.pl*

Abstract

The paper presents statistic method of preliminary determination of main propulsion power and total power of onboard electric power station for AHTS (Anchor Handling Tug Supply Vessel) type ships servicing oil rigs. At the beginning a characteristic and classification of AHTS vessels was presented. Also analysis of AHTS main propulsion plants and onboard electric power station was executed. Conventional and diesel-electric propulsion plants were taken into consideration as well as propulsion plants equipped with fixed pitch and controllable pitch propellers. Statistic methods elaborated in Marine Power Plants Department of Gdynia Maritime University make possible in quick and simple way to determine parameters of ship energetic system. Good accuracy of methods is confirmed by coefficients of regression determination and coefficients of correlation. Statistic methods also make possible to forecast the development trends in energetic systems construction of ships, which can be built in the future. Elaborated dependencies of main propulsion power and total power of onboard electric power station are not universal and should be determined separately for every type of ships. In this paper results concerning AHTS tugs servicing oil rigs are presented.

Keywords: oil rig service tug AHTS, main propulsion power, electrical power, statistics

1. Introduction

Tug boats are seagoing vessels designed for towing marine objects not equipped with propulsion plant, assisting seagoing vessels during berthing and leaving harbours, assisting vessels during manoeuvres, towing and protecting defected ships, participating in rescue operations etc. Tug boats are commonly driven by diesel engines. Usually the tug boat is equipped with high power engines (from a few to a dozen or so thousand kW) incommensurate with tug boat dimension. It makes possible to achieve very high towing force (from a dozen to even above hundred tons). A serious development of tug boats group has been observed in last years. New types of tugs were constructed according to new tasks often very specialized, for example AHTS (*Anchor Handling Tug Supply*) vessels used for oil rigs maintenance. Objects of analysis are AHTS vessels used for oil rigs servicing. These vessels

are fitted for operation at open sea mainly for oil rigs general service. However their versatility make possible also other marine objects service and assistance. The main task of AHTS vessels is oil rigs and other marine objects high accuracy anchor handling (about a few meters). Oil rigs can be fitted with 4 to 12 anchors. AHTS vessels are equipped with two main winches – towing and anchor handling as well as a number of smaller winches and auxiliary capstans. The majority of these vessels are also equipped with dynamic positioning system DP, which makes possible precise approach to objects and keeping a long stay at one position. Many of them are additionally equipped with special deck and engine equipment for example heavy cranes for heavy constructions handling, flat cargo deck, helicopter landing platform, deep water robots, high capacity firefighting pumps, cargo tanks etc. This equipment can perform many additional tasks as follows:

- firefighting,
- heavy objects transport,
- supply of oil rigs and other objects with solid materials (e.g. cement, special mud used as lubricant in drilling works etc.),
- supply with liquid or gas stock (oil, fuel, fresh water, liquid chemicals etc.).

Supplied materials are carried on deck in containers, on pallets, in baskets, in potable tanks and in bulk, whereas oil, fuel, cement, water, drilling mud etc. are carried in built in tanks.

AHTS vessels are usually equipped with multi-engine conventional diesel and diesel-electric propulsion plants. In conventional diesel propulsion the main engine power is delivered to propeller and often also to shaft generators and firefighting pumps.

All AHTS vessels are fed with diesel oil so there the steam is not used and boiler rooms are not installed. Some heaters used on AHTS are electrical type.

2. Analysis of AHTS vessels energetic systems

The target of this research is analysis of main propulsion plants and onboard electric power stations of AHTS vessels servicing oil rigs and elaboration of formulas describing dependencies of main propulsion power and onboard electric power station on basic dimensions of vessel by using statistic methods.

To fulfil these requirements the “reference list” of 28 of AHTS vessels was prepared where basic construction parameters were listed. From construction parameters these ones were analysed which are logically and functionally tight with energy demand for ship main propulsion and ship electric network.

The executed analysis of “reference list” shows that basic construction parameters of AHTS vessels are:

- overall length 65 ÷ 85 m,
- breadth 14 ÷ 18 m,
- draught 4,5 ÷ 7 m,
- bollard pull 100÷200 tons,
- designed towing winch pull usually is two times higher than bollard pull and amounts 150÷500 tons,
- maximum sailing speed when at sea 13÷17 knots,

- main propulsion usually consists of two powerful medium speed diesel engines 2000÷5000 kW each; on the largest 4÷6 medium speed diesel engines are installed; engines drive propellers via reduction gear or operate in diesel-electric system,
- AHTS vessels usually are driven by two controllable pitch propellers (sometimes fixed pitch propellers) working in Kort nozzle,
- due to high power anchor handling winches AHTS vessels are equipped with high power onboard electric power stations; usually they consist of two shaft generators 1500÷2500 kW each and additionally 1÷3 diesel generators 200÷800 kW each; if shaft generators are not installed there are 2÷3 diesel generators; each AHTS vessel is equipped with emergency diesel generator, which is used as port generator when berthing,
- when diesel-electric propulsion system is used 4÷6 main diesel generators are installed 2000÷3000 kW each and one auxiliary generator about 400 kW; each diesel-electric propulsion driven AHTS is equipped with emergency generator about 175 kW.



Fig. 1. AHTS vessel CBO Chiara sailing at sea

Typical AHTS vessel CBO CHIARA is shown in figure 1 [9]. The vessel overall length is 80 m, breadth 18 m, draught 6,6 m, sailing speed at open sea 13 knots. The vessel is equipped with two medium speed diesel engines driving two controllable pitch propellers working in nozzles, two shaft generators 1200 kW each, two diesel generators 350 kW each, one harbour/emergency diesel generator 120 kW, two firefighting pumps capacity 3600 m³/h each. Dynamic positioning system DP consists of one bow thruster, one rudder propeller and two stern thrusters shown in fig. 2.

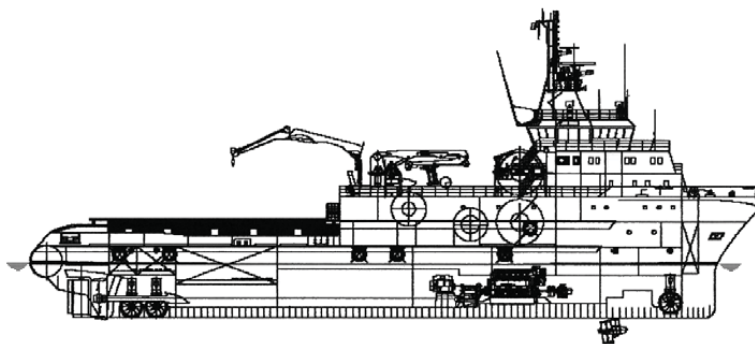


Fig. 2. Longitudinal section of AHTS vessel CBO Chiara.

3. Analysis and determination of main propulsion power

One of the basic parameters of AHTS vessel is bollard pull. During the analysis of AHTS vessels construction it was confirmed that main propulsion power N_w [kW] is the function of bollard pull U [tons] as well as product of hull main dimensions $L*B*T$ [m³]. Analysis were executed according to linear regression pattern using least squares method. Results are shown in figure 3. High values of regression determination coefficient and correlation coefficient are to be noticed.

As a result of calculations the following formula was obtained:

$$N_w = 751,9 + 36,15 \cdot U \text{ [kW]} \quad (1)$$

$$r^2 = 0,6908, \quad r = 0,8311$$

where: N_w [kW] – main propulsion power,
 U [ton] – bollard pull.

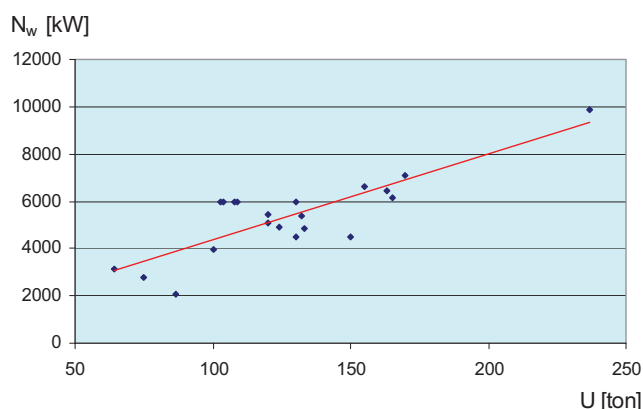


Fig. 3. Linear regression of dependency of main propulsion power on bollard pull $N_w = f(U)$ for AHTS vessels

The second part of analysis was executed to determine dependency of main propulsion power on hull main dimensions. Also in this case analysis were executed according to linear regression pattern using least squares method. Results are shown in figure 4. Also here high values of regression determination coefficient and correlation coefficient are to be noticed.

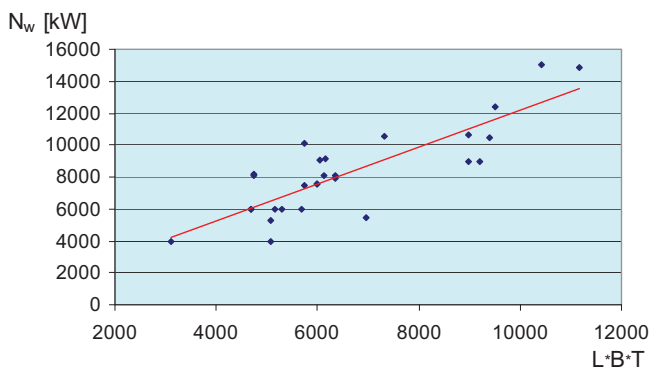


Fig. 4. Linear regression of dependency of main propulsion power on hull main dimensions $N_w = f(L*B*T)$ for AHTS vessels

During calculations the following formula was obtained:

$$N_w = 611,5 + 1,161 \cdot (L \cdot B \cdot T) \text{ [kW]} \quad (2)$$

$$r^2 = 0,7026, \quad r = 0,8382$$

where: N_w [kW] – main propulsion power,
 L [m] – overall ship length,
 B [m] – ship breadth,
 T [m] – draft.

4. Analysis and determination of onboard electric power station

During the determination of electric power demand for AHTS vessels it was assumed that total power of electric generators (total power of onboard electric power station) is linear function of hull main dimensions. Thus analysis were executed according to linear regression pattern using least squares method. 23 vessels from reference list were taken into consideration. The following formula was obtained as a result of calculations:

$$\Sigma N_{el} = -2189 + 0,839 \cdot (L \cdot B \cdot T) \text{ [kW]} \quad (3)$$

$$r^2 = 0,7393, \quad r = 0,8598$$

where: ΣN_{el} [kW] – total electric power of generators,
 L [m] – overall ship length,
 B [m] – ship breadth,
 T [m] – draft.

Graphical solution of formula (3) is shown in figure 5. High values of regression determination coefficient and correlation coefficient confirm good accuracy of formula (3) and its usability in preliminary calculation of onboard power station.

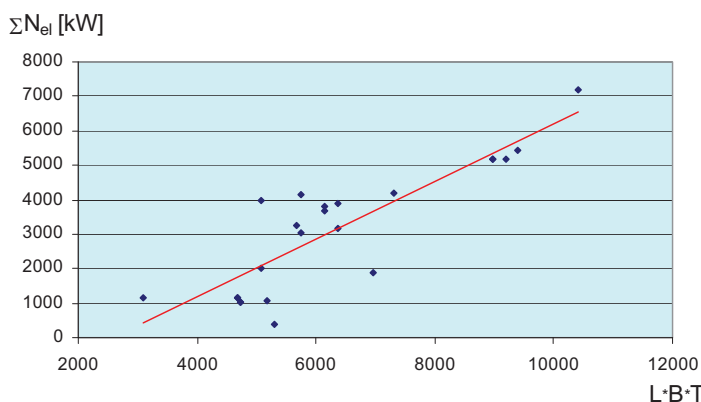


Fig. 5. Linear regression of dependency of onboard electric power station on hull main dimensions
 $\Sigma N_{el} = f(L \cdot B \cdot T)$ for AHTS vessels

The electric power described by formula (3) does not consist emergency generator. All AHTS vessels are equipped with emergency generator 65÷150 kW frequently used as harbour generator during vessel berthing.

5. Conclusions

Last years due to development of offshore oil industry the demand for AHTS vessels increases. These vessels are also built in Polish shipyards mainly in Remontowa Shipbuilding S.A. Gdańsk.

Contemporary AHTS vessels are examples of vessels equipped with complicated energetic systems including main propulsion and onboard electric power station. Main propulsion engines and electric power generators have incommensurable high power in relation to hull main dimensions. That is why formulas concerning other ship types can not be adopted. In contrary to other ship types in case of AHTS vessel the relation between main propulsion power and ship sailing speed was not observed. It is the result of situation that many additional machines besides thrusters are driven by main engines e.g. shaft generators, winches, dynamic positioning devices, pumps etc. During the operation near oil rig at vessel stay full power of main engines is supplied to these machines.

With reference to onboard electric power station it is not possible to state that total electric power depends on main propulsion power. It is the result of supply of bow and stern thrusters, winches, cranes and many other electric energy large consumers. Main engines also drive many machines, which are not driven by electric motors.

6. References

- [1]. Balcerski A., Bocheński D.: *Układy technologiczne i energetyczne jednostek oceanotechnicznych*. Politechnika Gdańska. Gdańsk 1998.
- [2]. Draper N.R., Smith H.: *Analiza regresji stosowana*. Warszawa 1973.
- [3]. Giernalczyk M., Górski Z.: *Method for the Determination of energy demands for main propulsion and onboard electric power for modern harbor tug boats by means of statistics*. Journal of Kones Powertrain and Transport, European Science Society of Powertrain and Transport Publication, Vol. 19, No. 1, page 147 – 154, Warsaw 2012.
- [4]. Giernalczyk M., Górski Z., Kowalczyk B.: *Estimation method of ship main propulsion power, onboard power station electric power and boilers capacity by means of statistics*. Journal of Polish Cimac, Energetic aspects, Vol. 5, No. 1, page 33 – 42, Gdańsk 2010.
- [5]. Hewlett Packard : HP-65 Stat Pac 1, Cupertino, California, March 1976.
- [6]. Michalski R.: *Ship propulsion plants. Preliminary calculations*. Szczecin Technical University. Szczecin (1997).
- [7]. *Unification of ship engine room. Part V. Ship power plant*. Study of Ship Techniques Centre (CTO). Gdańsk 1978.
- [8]. Urbański P.: *Gospodarka energetyczna na statkach*. Wydawnictwo Morskie. Gdańsk 1978.
- [9]. www.estaleiroalianca.com.br



POWER PLANTS MAIN SWITCHBOARDS CONFIGURATION OF MULTI-MODE SHIPS

Jerzy Herdzik

Gdynia Maritime University
ul. Morska 81/87, 81-225 Gdynia, Poland
tel.: +48 58 6901430, fax: +48 58 6901399
e-mail: georgher@am.gdynia.pl

Abstract

It was presented the main switchboards' configurations of multi-mode ship power plants. It has dominated diesel-electric propulsion systems. The development of main switchboards has an aim the increasing of power system reliability from main engines, through generators and electrical network to electric motors of main propulsion and dynamic positioning thrusters. This is a way of increasing redundancy and reliability of propulsion system. The superior aim is the fulfillment of DP class 2 and DP class 3 dynamic positioning requirements.

Keywords: multi-mode ship, main switchboard, configuration, propulsion system, diesel-electric propulsion

1. Introduction

All ships ought to have minimum two electric generators driven by two independent engines. One of them has been reserved generator and one has covered the maximum demand for electric energy in the all exploitation conditions. Often it would be met more complicated electric network. In that case the main switchboard may be made in different configurations. The solution of switchboard configuration may influence on many other power elements.

The distribution system is the vital link connecting the generators that produce electric power to the equipment that uses it. It transmits electric power from the power source to the power user. The distribution system also protects (by means of circuit breakers and fuses) itself, and its generators from damage that might otherwise be caused by faults in the system or connected equipment.

The simple switchboard configuration is presented on Fig.1.

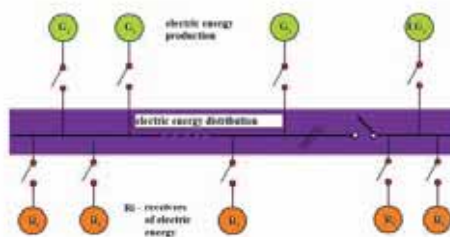


Fig.1. An example of simple switchboard configuration with parallel work of generators

There are three auxiliary and one emergency generators. During parallel work of auxiliary generators the overloading or other failures may result in the domino effect. The trip-out of one generator working on electric network may cause the overloading of the other generators, following the trip-out of next generator and black-out in all electric network. This is a dangerous situation for ship safety. For this reason an emergency generator is installed on ships. It gives the electric energy in time maximum 30 seconds after black-out but supplies only receivers from the emergency switchboard. It allows to recover the electric energy in main switchboard. It allows to recover the electric energy in main switchboard.

2. The development of ship main switchboards

A main switchboards (MSB) is a switchboard directly supplied by the main source of electrical power or power transformer and intended to distribute electrical energy to the unit's services or switchboards not being directly supplied by the main source of power will be considered as main switchboards when this is found relevant from a system and operational point of view [2,4].

The electric energy distribution system can be divided into *feeder side* and the *load side*. The feeders are the generators, the loads are various ship's consumers.

Due to reliability of supplying in electric energy and an avoidance of fully black-out it may be met more complicated configurations of main switchboards (Fig.2). In normal condition the all bus-ties are in closed position. In a necessary it may work on electric network more than one auxiliary generator. It needs the parallel work of them. In case of necessity the bus bus-ties may stay in opened position and each the auxiliary generator works only on a part of receivers (consumers). In this situation only partially black-out might occur.

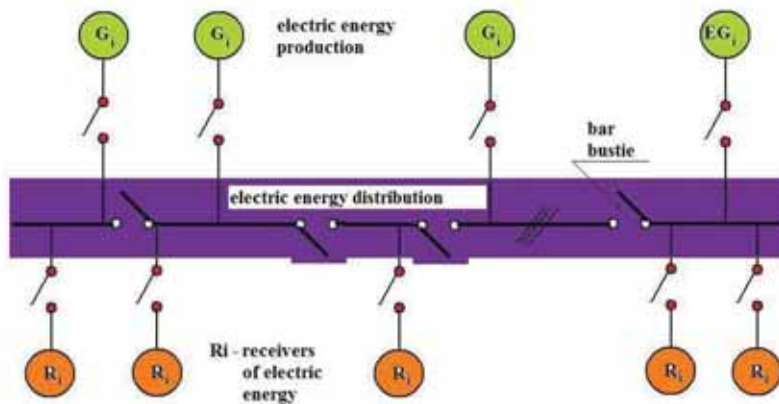


Fig.2. Main switchboard configuration with parallel or independent work of generators

The configuration presented on Fig.2 gives only a few possibilities of generators work on electric network. The partially black-out might occur and in that case it is impossible to supply the chosen section of receivers from the other generator. This is a serious imperfection. On ships with dynamic positioning DP class 2 it is used as requisite the ring switchboard configuration like presented on Fig.3. Due to ring (possible two smaller rings on Fig.3) there are possible configuration where all consumers may be supplied when a section of bars in the switchboard is out of order (a failure or other system faults). The failure of any single circuit or bus-bar section shall not endanger for the services necessary for the offshore unit's manoeuvrability. For DP class 2 it is accepted that the bus-bar sections are arranged in one switchboard. The bus-bar control and protection system shall be designed to work both open and closed bus-tie breakers [5].

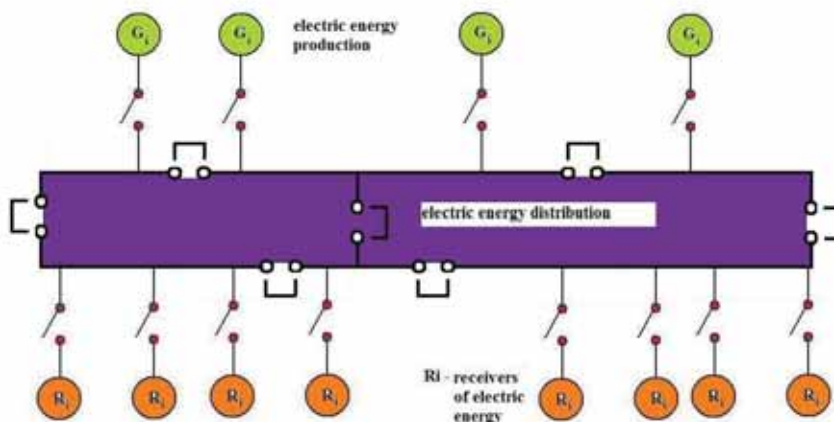


Fig.3. An example of the ring configuration of main switchboard

In DP class 2 or above, any single failure must not render the system inoperable. The philosophy is applied throughout the vessel design including the switchboards, propulsion and power generation. On ships with DP class 3 it is required that each bus-bar section is isolated from other by watertight A-60 partitions. There shall be a bus-tie breaker on each side of this partition [1,5]. Class 3 of DP provides triple redundancy in terms equipment failure and must also remain operable in case of fire and flooding. The vessel with minimum two engine rooms has A60 bulkhead separation. The power and propulsion system must be design such that adequate power and thrust is available even under failure conditions [4,5,6]. An example of switchboard configuration for DP class 3 was presented on Fig.4.

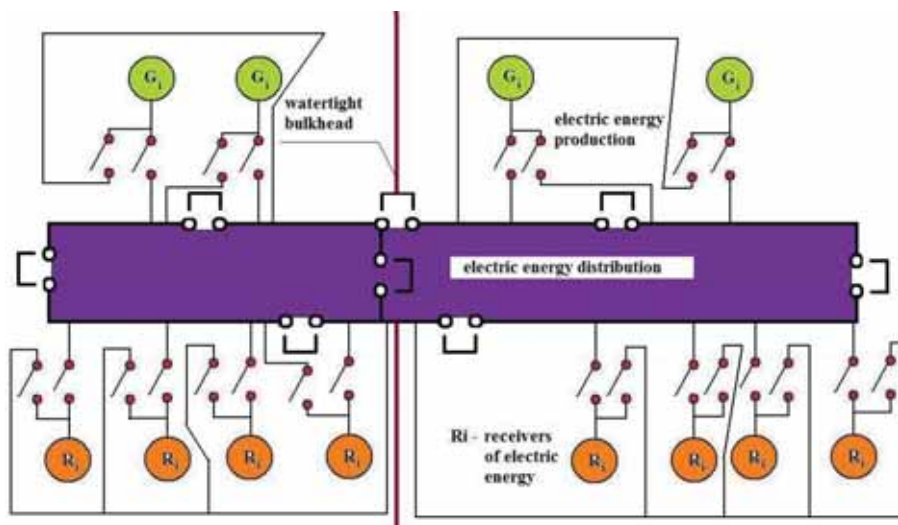


Fig.4. An example of the ring configuration of main switchboard with watertight bulkhead for ships with DP3

An example of existing ship mv. Solitaire with two separated engine rooms, eight main generators, eight thrusters and switchboard configuration is presented on Fig.5. This is ship with DP class 3 for pipe-laying.

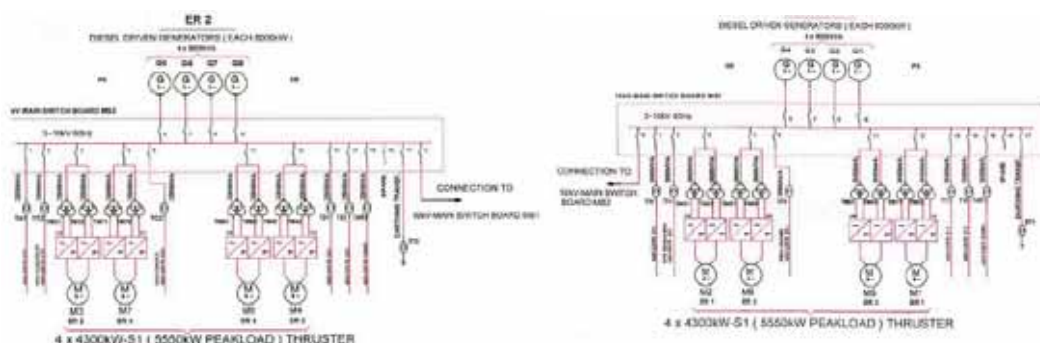


Fig. 5. Power system configuration with two engine rooms of mv. Solitaire [7]

The thrusters driven by electric motors have each nominal power of 4300 kW, but in a necessary the power may increase to 5550 kW, of course with load limiting time up to 5 minutes for that thruster. It was used a synchroconverter with parameters: current strength AC 1225 A, voltage 2×1454 V and frequency 35 Hz, 520 RPM of thruster propeller.

3. Control arrangement

Engine control power is typically 24V DC. It may be derived from a DC power supply (battery backup, UPS, voltage converter). Switchboard control supplies 24V DC and sometimes other DC power. The engine control and safety system should have separate power supplies. It ought to be from separate sources, sometimes may accept separate fuses from the same distribution. The normal source of supply should be the main power system.

Electrical protection schemes are designed to prevent the uncontrolled release of energy associated with power system faults, thus protecting life and limiting damage to equipment [1,3]. For DP vessels with DP class 2 and 3 the power system protection scheme must also ensure continuity of supply to essential consumers such as thrusters and other auxiliary systems. The primary protection function is over current protection, which is intended to prevent excessively high currents causing cables to catch fire.

The overall electrical protection scheme can be divided into three following sections:

- generator protection;
- bus-bar protection;
- feeder protection.

Due to costs many ship-owners try to resign with the bus-bar protection. This fault has very small probability of event but gives very serious damage and/or fire if occurs. Bus-bar protection is designed to isolate the effects of short circuits and earth faults acting directly to bus-bars or their connections. Bus-bar protection can take the following forms, depending on the number of bus sections that have to be protected:

- over current protection;
- differential protection;
- directional over current protection;
- optical arc detection;
- pressure detection;
- earth fault protection.

When electric propulsion is utilised (popular solution on multi-mode vessels), the electric power generation and distribution system shall be equipped with an automatic control system having at least the following functions [1]:

- ensure adequate power for safe manoeuvring is available at all times;
- ensure even load sharing between on-line generators (to protect over load);
- execute load tripping and/or load reduction when the power plant is overloaded;
- execute that adequate power for safe manoeuvring is available also if one running generator is tripped (for example: by way of tripping of non-essential consumers);
- control the maximum propulsion motor output;
- if the automatic system fails, in that case that is no start or stop of generators shall occur as an effect of a failure, so no changes in available power shall occur.

4. Control power arrangement

The power management systems (PMS) or energy management systems (EMS) are used to avoid the ship's electric network before the partially or fully black-outs. These systems are still developed and fulfill more functions.

A power system is in a fault if any of its critical parameters are out of tolerance for more than an acceptable time period, also during expected power system transients. The parameters which must remain within tolerance include: voltage, current, frequency, levels of harmonic distortion, line current balance, phase voltage balance.

The basic faults conditions on three phase system are [1,3]:

- short circuit – on one or more phases;
- open circuit – on one or more conductors;
- earth fault;
- over/under frequency;
- over/under voltage;
- over load – rating of engine exceeded;
- over current – rating of alternator, bus-bar, cables, motors, transformer or other consumer exceeded;
- severe active power sharing imbalance;
- severe reactive power sharing imbalance;
- excessive regeneration of power;
- severe waveform distortion;
- loss of synchronization or crash synchronization.

On Fig.6 is presented typical control power arrangement with separate sources of supply: DCA and DCB. If the emergency distribution is from UPS – the UPS battery endurance should be a minimum of 30 minutes. On Fig.6 all engines (generators) on one bus share a control power supply.

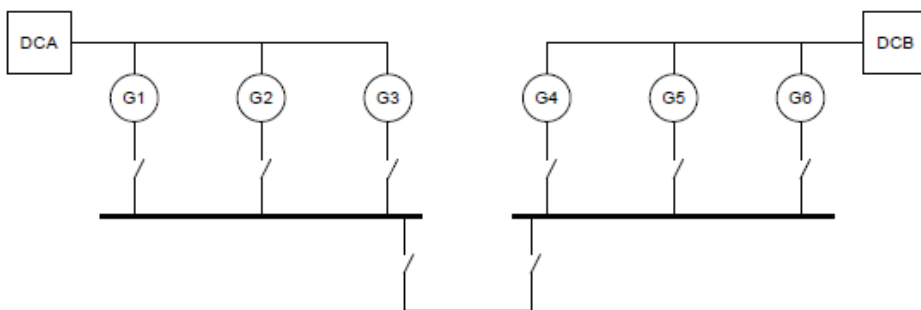


Fig.6. Typical control power arrangement [1]

Losing multiple generators as the result of a single failure (causing black-out) is extremely destructive and dangerous to the power system. On Fig.7 was shown the alternators with permanent magnet generator system. There is only one source of control power but each generator is independent of the external control power source.

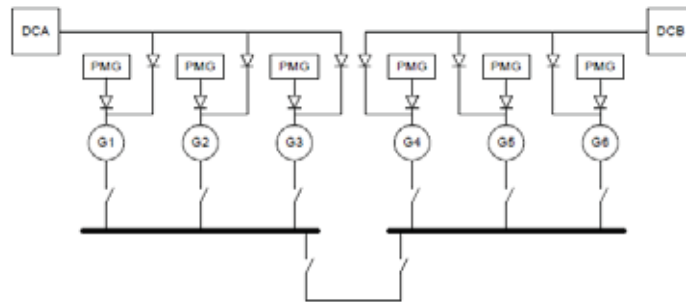


Fig. 7. Engine control power with permanent magnet generator (PMG) backup [1]

These solutions are unsatisfactory for power system of multi-mode and electric propulsion ships. Alternatively each generator can be supplied from its own power system (Fig.8).

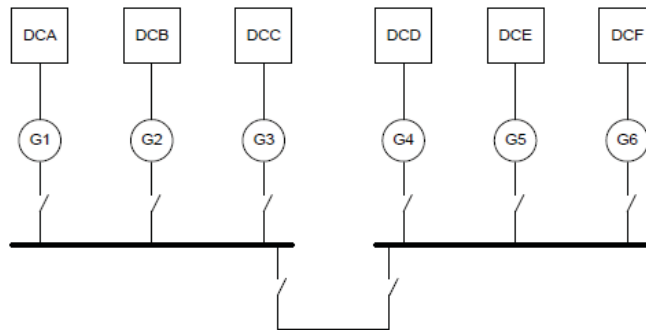


Fig.8. Independent engine control supplies [1]

The redundancy concept of using only two control supplies is presented on Fig.9 with diode isolated system. It is not recommended for multi-mode vessels due to a voltage dip associated a fault in one control power system shall be seen by all control systems. It is not recommended as a way of improving reliability too.

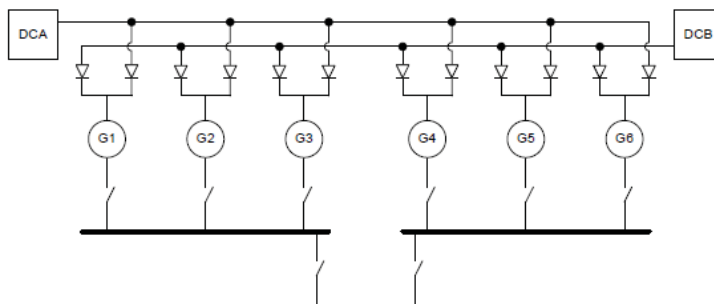


Fig.9. Diode isolated dual supplies [1]

If the voltage dip ride through is insufficient then all running engines may malfunction. The second problem is dependent on the selectivity of the fuses at the generator and power supplies to ensure a fault in one engine supply does not blow the main fuses at each DC supply output.

5. Basic requirements of the generators control

A typical malfunction generator protection relay is shown in Tab.1. and on the other way the requiring generator protective functions for ships with DP systems.

Tab. 1. Generator protective functions [1](X – yes, N – no) [1]

| Function | Generator trip | Quick trip of bus-tie | Excitation trip | Start all generators | Generator lockout | Alarm |
|------------------------------|----------------|-----------------------|-----------------|----------------------|-------------------|-------|
| Phase current differential | X | N | X | N | X | N |
| Negative current sequence | X | X | N | X | N | X |
| Under voltage | X | X | N | X | N | X |
| Over voltage | X | X | X | N | N | X |
| Reactive power | X | N | N | X | N | X |
| Phase reversal | X | N | N | N | N | N |
| Under frequency | X | X | N | N | N | X |
| Loss of excitation | X | N | N | N | N | N |
| Reverse power | X | N | N | X | N | X |
| Phase over current | X | N | N | N | N | N |
| Over frequency | X | X | X | N | N | X |
| IAS/PMS E-stop | X | N | X | N | X | X |
| IAS PMS CB open | X | N | N | N | N | X |
| High set over current | N | X | N | N | N | N |
| Trip coil monitor | N | N | N | X | N | X |
| VT fuse failure | N | N | N | X | N | X |
| Diode failure | N | N | N | X | N | X |
| Generator winding high temp. | N | N | N | X | N | X |
| Generator bearing high temp. | N | N | N | N | N | X |
| Field current | N | N | N | X | N | X |
| Relay fault | N | N | N | X | N | N |
| ESD emergency shut down | X | N | N | N | X | X |
| Earth fault | X | X | N | X | N | X |

IAS – Integrated Automation System

The rules and requirements of classification societies for ships with DP systems are similar. Presented in Tab.1. generator protective functions are implemented as a standard.

6. Accumulators of energy

The main reason of black-outs is overloading when the accessible power from working generators is less than the power demand from consumers. The possibility of accumulating energy in AC network is limited. The UPS battery endurance should be a minimum of 30 minutes but only for control power.

A global and marine industry exists for Uninterruptible Power Supply (UPS) systems. It was needed a source of high energy in the emergency situations: inefficiency, failure, peak of power demand, etc. For multi-mode vessels the needed energy storage is about 100-250 kWh with possibility of feeding during 1-2 minutes with the power up to 5 MW. This is a challenge for energy storage devices. It was presented in the Tab.2 the storage devices and theirs basic parameters. In marine appliances only the first three would be taken into consideration but only flywheels are the best for high cyclic and high power applications.

Tab.2. Energy storage devices and basic parameters [8]

| type | storage mechanism | common duration | cycles |
|--------------|-------------------|--------------------|------------------|
| capacitor | electrical charge | seconds or minutes | 100,000's |
| flywheel | kinetic energy | seconds or minutes | 1000's-100,000's |
| battery | electro-chemical | minutes or hours | 100's-1000's |
| pumped hydro | potential energy | hours | 1000's |
| thermal | ice, molten salts | hours | 1000's |

A large number of applications (ship power plant as well) exist that collectively can be categorized under “peak power support”. For example, drilling vessels and drilling platforms maintain a number of diesel engines as D-E systems to meet the peak power needs. The generators working parallel loads the engines at idles or at low capacity factor due to irregular power demands of drilling units and/or DP operations. A flywheel system could augment the capacity of the diesel generators, making possible to meet the peak power demand requirements with smaller number of working gensets. In that case it will be the ability to reduce needed investment cost due to application of smaller total number of installed gensets. The added value of that application may derive from reduced wear and tear on generating equipment and reduced air emissions, especially important on ECA areas (mandated air pollution limits or taxes).

The dimensions of 100 kWh ARPA-E flywheel and mass (about fifteen tons) are convenient for marine appliances (omitting small ships below 60 m of length). The Beacon POWER proposition was given to naval ships with smaller units. The biggest one is a flywheel of 10MW power with the energy storage of 27.8 kWh.

7. Final remarks

The development of main switchboards configuration and marine power plant protection have been made in recent years. The greatest improvement has come in the form of protection systems for example able to identify which generator is responsible for causing a severe active or reactive imbalance. The system faults in functions of generator protective system are common in multi-mode vessels. In fact the incorrect response of traditional generator protection is usually responsible for causing the black-out. The protection system are now available from several sources.

Now new functions of advanced generator protection (AGP) system are coming into use like: core protection functions, predecessors of modern AGP and two basic principles of operation: voting system and conformance to predicted generator behavior [1].

References:

- [1] *A Guide to DP Electrical Power and Control Systems*, IMCA M206, 2010, www.imca-int.com.
- [2] *Naval Ships' Technical Manual, Electric Power Distribution Systems*, S9086-KY-STM-010/CH-320R2, revision 2, 1998.
- [3] Radan, D., *Integrated Control of Marine Electrical Power Systems*, Norwegian University of Science and Technology, ISBN 978-82-471-6647-5, 2008.
- [4] *Electrical Installations*, Offshore Standard DNV-OS-D201, DNV 2011.
- [5] *Dynamic Positioning Systems*, Rules for Classification of Ships, part 6, chapter 7, DNV, 2011.
- [6] *Ships Electrical Standards*, Revision 02, Transport Canada, 2008.
- [7] *Pipelaying Vessel “Solitaire”, Electrical Propulsion System 10kV Supply and Distribution System*, SAM Electronics GmbH, Hamburg, 2011.
- [8] Lazarewicz M., *Joint ARPA-E/ASD(R&E) Workshop Energy Storage*, Beacon Power Corporation, 2011.



COMPRESSOR OF CASCADE EXCHANGE BY PRESSURE

Aleksander Krajniuk¹, Oleh Klyus²

¹East-Ukrainian National University named after V. Dal, Molodyozhny block, 20a, Lugansk,
91034, Ukraine,

e-mail: ljagar@rambler.ru

Maritime University of Szczecin, str. Waly Chrobrego 1-2, 70-500 Szczecin, Poland

e-mail: olegklus@o2.pl

Abstract

A new method of organization of working cycle of device of direct transformation of heat in the located work of compression of air, based on principle of cascade exchange by pressure, is exposed; the results of pre-selection of basic dimensional and structural parameters of thermal compressor of cascade exchange by pressure are adduced; some special features of its working process are considered; main directions of perfection of working cycle of thermal compressors of cascade exchange of pressure are shown.

Key words: compressor, cascade exchange

1. Introduction

Development of pneumatic transport of granular freights and technological pneumatic sets of road-building and special machinery supposes the reduction of manufacturing cost of the compressed air. Air injection by expensive and complex on design piston or vane-type compressors particularly with self-contained, for example, diesel drive is characterized by high power expenditures. The efficiency of compressor with a diesel engine taking into account the losses of transformation of initial thermal energy into mechanical one in a diesel and mechanical energy in the located work of compression of air does not exceed the values of 0,2 0,21 in the best specimens.

2. The feature of the cascade pressure exchangers

Considerable reserve of reduction of power expenditures of production of the compressed air and simplification of design of supercharger associates with the use of devices of direct transformation of thermal energy in the compressed air on the base of cascade pressure exchange (CPE). The sets realizing the cascade compression are a new variety of pressure exchangers, in particular applied in the systems of supercharging of internal combustion engines. Compression of air in CPE as well as in wave pressure exchanger of the known supercharging system of «Comprex» is carried out as a result of direct contact with compressing gases, however with the substantial distinction of organization of working process. Principle of the action of CPE is described in works [1, 2, 3].

Typical construction of exchanger (fig. 1.) is the rotor with longitudinal head-exchanging cells, revolved in stator. Mass-changing channels as well as the window of admission and rejection of compressing gas are located in one of end face covers of stator (A), but the window of admission and rejection of compressed gas are located in other of end face covers (B). The rotor is driven to the rotation with rotational speed of $2000 \dots 3000 \text{ min}^{-1}$ by means of an electric motor or other drive of small power.

The still pictures of basic units of one of the CPE construction are shown on the fig. 2.

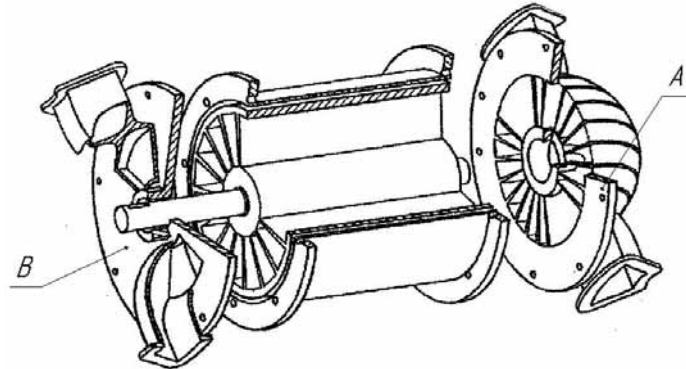


Fig. 1. Principal view of cascade pressure exchanger (CPE)



Fig. 2. Basic elements of construction of the experimental model of the CPE:

a – stator; b – rotor; c – body; d – end face cover from the side of admission and rejection of compressing gas

The high efficiency of the CPE is confirmed by the stand tests on the base of the engine 6FSch12/14. So, at the parameters of the compressing gas $T_{g1}=800 \text{ K}$, $P_{g1}=0,25 \text{ MPa}$ the efficiency of pilot plant of the CPE achieves 0,84 and on the mode of $T_{g1}=850 \text{ K}$, $P_{g1}=0,25 \text{ MPa}$ – 0,86.

Power perfection of working process of cascade exchanger is realized in the considerable exceeding of expense of the compressed air of relatively compressing medium, and the temperature of the medium is higher, the in a greater degree.

3. Application of the cascade pressure exchangers in compressors of heat compression

The noted property of cascade exchangers is fixed in the basis of creation of compressor of direct transformation of thermal energy in the located work of the compressed air. A part of the forced air is discharged to the user in the simplest chart of the thermal compressor, and other part of air is heated in the source of admission of heat and is directed in the window of admission of high

pressure of exchanger, where is used as a compressing medium. Unique simplicity and rather high efficiency of single-stage thermal compressor stipulate attractiveness of its application in the systems of air supply with maximal pressure of supercharging to 0,4...0,5 MPa depending on the maximal temperature of the working cycle T_z .

Substantially high pressure head and power efficiency has been realized by the double-stage compressor of cascade exchange by pressure. The chart of the modernized compressor of the CPE thermal compressor with the intermediate cooling and preliminary heating of the compressed air and compressing medium is shown on the fig. 3.

Pumping of air in the given device is carried out as a result of successive compression of cold air and thermal expansion of hot air in aggregates of the CPE of the first and second stages. Thus, the relations of degrees of compression of air in the first and second stages π_I , π_{II} are not arbitrary, as, from one side, it is subordinate to the condition of balance of charges of working mediums in the lines of high pressure of the first stage and low pressure of the second stage, with other side – to the condition of providing of blowing out and ousting of working medium in the cells of both CPE rotors in the indicated lines.

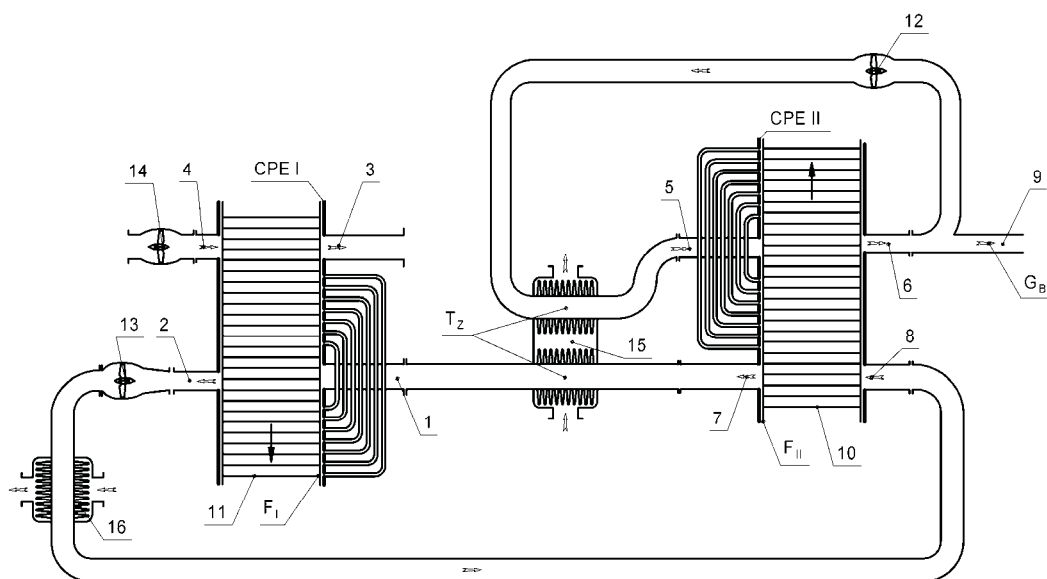


Fig. 3. Flow diagram of the double-stage thermal compressor of the CPE

1, 2, 5, 6 – windows of admission and removal of high pressure (AHP and RHP) according to CPEI and CPEII;

3, 4, 7, 8 – windows of removal and admission of low pressure (RLP and ALP) accordingly CPE I and the CPE II;

9 – branch pipe of the compressed air bleed-off; 10 – rotor of the CPE II; 11 – rotor of the CPE I; 12 – positive-displacement fan of the second stage; 13 – positive-displacement fan of the first stage; 14 – scavenger fan; 15 – heater; 16 – cooler

In such a case the relations π_I and π_{II} depend on total pressure head of the thermal compressor π_K and maximal temperature of the working cycle T_z .

Gas dynamic analysis of double-stage thermal compressor of the cascade change of pressure is enough labor-consuming in spite of the structural simplicity of device of the CPE thermal

compressor. The analysis includes the search of the modes of joint operations of CPE aggregates of the first and second stages. Therefore the pre-selection of basic dimensional parameters of elements of the system,

meeting the condition of realization of the productivity of compressor, must precede to the more precise computation of working cycle of the CPE thermal compressor.

The results of calculations of dimensional relations of frontal sizes of rotors of exchangers of the first and second stages are below brought on the example of compressor by the productivity $G_b = 0,1$ kg/sec with different total pressure head π_k , with the maximal temperature T_z of the cycle and differential pressures created by the scavenger fan ΔP_B .

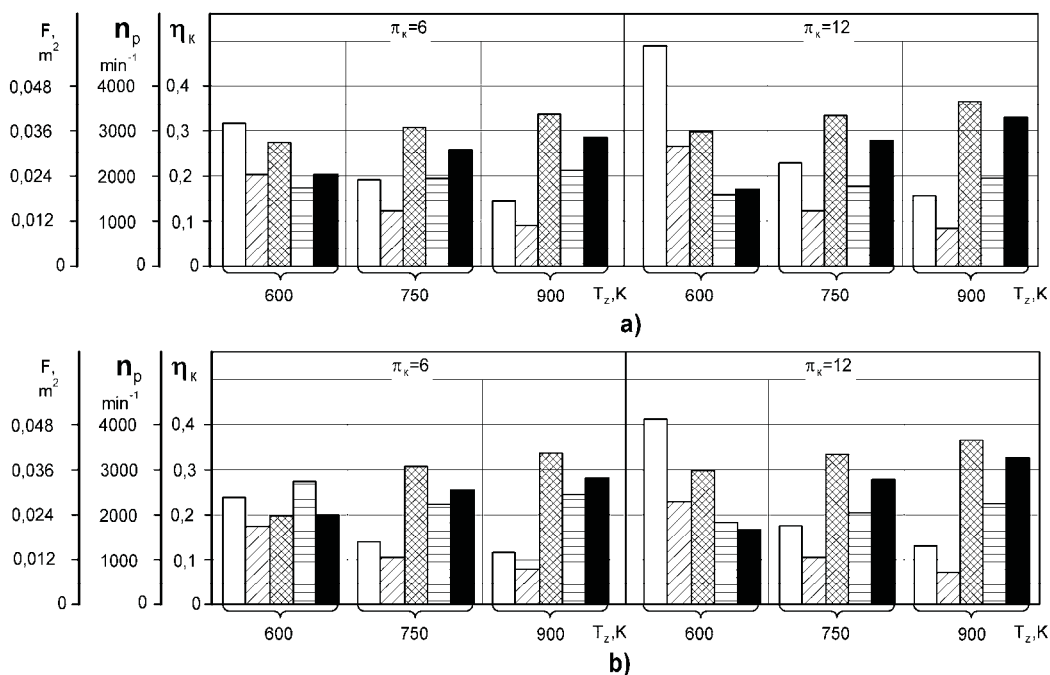


Fig. 4. Combination of structural and regime parameters of the CPE compressor by productivity $G_b=0,1$ kg/sec for different conditions of its work.

a – at pressure head of scavenger fans of the first and second stages $\Delta P_{BI}=\Delta P_{BII}=15$ kPa;

b – at pressure head of scavenger fan of the first and second stages $\Delta P_{BI}=\Delta P_{BII}=20$ kPa;

F_{PI} - channel part area of the CPEI rotor; F_{PII} - channel part area of the CPEII, n_I - rotational speed of the CPEI rotor, n_{II} - rotational speed of the CPEII rotor, η_c - power efficiency of the compressor,

The principal method of reduction oft overall sizes of the CPE thermal compressor is an increase of the pressure head of scavenger and positive-displacement fans 14, 13, 12 (see the Fig. 3.).Main purpose of these fans is the- realization of circulation of working mediums in the contours of low and high pressure of both exchangers. As seen from .the histograms resulted on a fig.4, even the insignificant rise of pressure head of scavenger fans allows considerably to decrease the channel part areas (F_{PI} and F_{PII}) of

rotors of both CPE. At the same time, rise of ΔP_{BI} and ΔP_{BII} is accompanied by the increase of consumptions of mechanical energy on the drive of fans. Thus, the pressure differentials created by circulation fans, are essentially the key parameters of varying at the search of the trade-off between sizes and efficiency of the. thermal compressor.

It should be noted, however, that since some moment relying on a general dimensionality and feature of structural execution of compressor, further reduction of ΔP_{BI} and ΔP_{BII} is not accompanied by the rise of η_c because of strengthening of losses through the end face interfaces of rotors in view of the increase of sizes of the lasts.

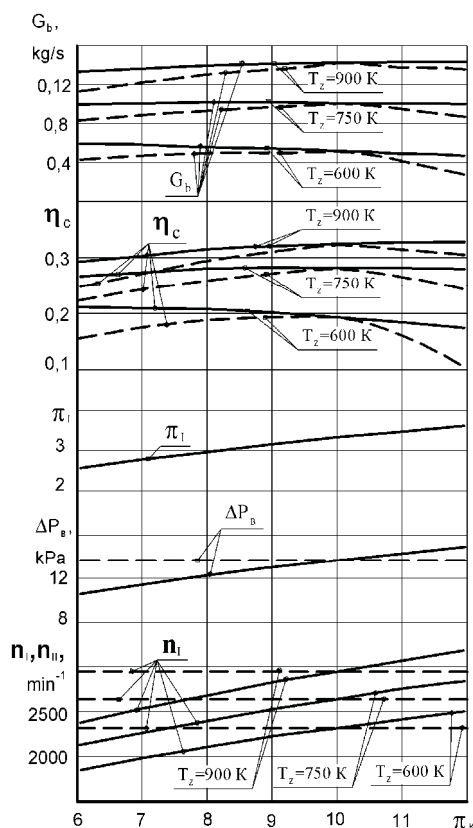


Fig. 5. Load characteristic of the CPE double-stage compressor:

— — without regulation;
 — — with regulation of rotational speed n_{PI} of the CPE rotor and pressure head ΔP_{BI} of scavenger fan of the first stage

The maximal temperature T_z of the cycle exerts highly noticeable influence on the indexes of working process. The T_z increase is not only the instrumental in the substantial increase of efficiency but also provides the lowering of frontal dimensions of the exchangers of both stages. Thus the T_z influencing on η_c , does increase as far as the rise of general compressor pressure head π_K . In its turn, the lowering of sizes of the exchangers at the T_z rise is related to reduction of relative expenditure of compressing medium on the compression of the compressed air.

At the temperature $T_z=900K$ on the mode $\pi_K=12$, the calculation value of efficiency η_c , makes 0,32. In the real cycle of the pilot plant of thermal compressor, created in the laboratory of the DVS of EUNU named after V.Dahl, an index of efficiency $\eta_c=0,28$ is attained already on the stage of preliminary tests. Possibility to carry out the working cycle of the CPE with $T_z=900K$ is conditioned by the cyclic cooling of the rotors of the CPE in the process of the periodic filling of pressure head-changing cells of the CPE rotor by an air charge. The level of power efficiency

realized by the thermal compressor is unattainable on today , even in the theoretical cycle for the off-line units of transformation of thermal energy in the located work of compression of air, as far as the authors know.

The positive feature of working cycle of the double-stage thermal compressor with the intermediate cooling of the compressed air and intermediate heating of the compressing medium consists in the declivity of its hydraulic characteristic (fig. 5.).

Thus in the case of the simultaneous regulating of rotational speeds n_{PI} and n_{PII} of the CPE and pressure head ΔP_{BI} of scavenger fan depending on total pressure head π_k of the compressor, the expenditure G_k of the forced air and compressor efficiency η_c are subject to the insignificant influencing of hydraulic resistance of user in the range of the operating modes of work of the set, saving substantial dependence only on the maximal temperature T_z of the cycle.

And finally, it is impossible not to note the failure-free operation of the CPE set exposed in the process of tests of the pilot construction of compressor and row of pre-production models of the aggregates of the CPE. It is due to the absence of mechanical displacers, discretely controlled gas-distributing organs, as well as because of relatively low rotational speed of the CPE rotor.

4. Conclusions

High power efficiency and propitious hydraulic characteristic of discharge under pressure of the CPE double-stage thermal compressor in combination with reliability of its construction exposes prospects of its application as an aggregate of air supply of wide class of thermal power plants.

The principal reserve of the further increase of the compressor efficiency consist in the rise of maximal temperature T_z of the cycle by means of application of new high-temperature materials (for example, carbon-fibrous polymers) for manufacture of channel running elements of device, and also due to reduction of losses of working medium through the end interfaces of co-rotors.

References

- [1] Ключ О.В., Крайнюк А. И., Алексеев С. В. The principle organization of work process unit of cascade compression and its application// scientific journals Maritime University of Szczecin. Szczecin. – 2008 – 14(86). –С. 25-29.
- [2] Крайнюк А. И., Алексеев С. В., Брянцев М. А. Особенности рабочего процесса каскадного обменника давления// Вісн. Східноукр. нац. ун-ту імені Володимира Даля.- Луганськ.- 2005.- № 8(90).- С. 176-179.
- [3] Расчет и выбор основных параметров каскадного обменника давления/ А.И.Крайнюк, А.А.Крайнюк, С.В.Алексеев, М.А.Брянцев// Двигатели внутреннего сгорания: Научно-технический журнал. Харьков: НТУ “ХПИ”.- 2007.- №1.- С. 57-62.



THE CASCADE EXCHANGER AND NEW PRINCIPLES OF THE ORGANIZATION OF WORKING PROCESS OF THE GAS-TURBINE ENGINE

Aleksander Krajniuk¹, Oleh Klyus²

¹East-Ukrainian National University named after V. Dal, Molodyozhny block, 20a, Lugansk, 91034, Ukraine,

e-mail: ljagar@rambler.ru

Maritime University of Szczecin, str. Waly Chrobrego 1-2, 70-500 Szczecin, Poland

e-mail: olegklus@o2.pl

Abstract

Main trends of perfection of gas-turbine engines (GTE) by application of principles of the cascade pressure exchange (CPE) for air compression in the working cycle of gas-turbine plant have been analyzed. The results of computational investigation of four variants of the GTE working process organization on the basis of the two-staged compression assembly with intermediate cooling and heating of air-gas medium have been adduced. Possibility and reserve of raise of power efficiency of GTE with the CPE at the expense of increase in the maximum temperature of the cycle and recuperation of the residual heat of compressing gases have been shown.

Key words: gas-turbine engines, cascade pressure exchange, thermal compressor, working cycle, temperature, power efficiency, performance, load characteristic

1. Introduction

The basic obstruction of gas-turbine engines (GTE) wide integration in ground transport is high sensitivity to change of almost all operating conditions of the plant that is peculiar to blade machines. It is resulted in a decline of traction and economic characteristics even at an insignificant deviation of regimes of its work from the nominal. Acceleration characteristics and fuel economy at idle stroke are especially unsatisfactory for variable service conditions of the GTE. The turbine-driven units have the restricted resource and demand high level of maintenance in view of a high rotational speed of the rotor. Insignificant unbalance of rotors, for example, caused by pollution or blade breakage, generates an extreme reinforcement of vibrating and dynamic loads.

Despite high thermal efficiency of theoretical cycle, in practice the possibility of raise of power efficiency of the GTE (by increase in the maximum temperature of the cycle) is restricted by thermo-strength properties of materials applied in turbine construction. One of known directions of possible increase in the relation of boundary temperatures of a cycle at restriction of temperature of gases in front of the turbine is connected with the use of wave rotors as topping stage for gas turbine [1, 2, 3, 4, 5, 6].

The idea of using wave-rotor topping cycle has been first proposed by Claude Seippel of Brown Boveri Company (BBC) in Switzerland in 1942 [7, 8]. Now BBC is Asea Brown Boveri (ABB) and its pressure wave supercharger termed as the Comprex has been used commercially for passenger car and heavy diesel engines [9, 10, 11, 12, 13].

The general advantage of using a wave rotor consists in possible increase in thermodynamic efficiency of the cycle by raise of its maximum temperature at restriction of temperature of gases in front of the turbine.

At the same time, use of wave rotor in the capacity of top stage of the gas-turbine engine does not eliminate, and in some cases aggravates the main deficiency of the gas-turbine engine – unsatisfactory efficiency on transitive and partial regimes. Strongly expressed wave character of exchange processes in wave rotor predetermines the sensitivity of its consumed characteristics to thermodynamic parameters of working mediums in gas-distributing windows and to rotor rotational speed. The deviation of operating mode of the GTE from design conditions is accompanied by a sharp decline of parameters of wave rotor work as owing to both an error signal of the moments of connection of cells to gas-distributing windows, and owing to increase in incompleteness of displacement of compressed air in the combustion chamber [14].

Considerable jump in performance and operating characteristics of transport gas turbine engine can be achieved by applying the principles of the cascade exchange of pressure for realization of compression of gas-air working mediums in the running cycle of the plant. The units realizing such compression are the cascade pressures exchangers (CPE). They represent new generation of exchangers of pressure with mainly static character of interacting of the compressing and compressed mediums [15, 16].

Power effectiveness of the CPE working cycle is realized in considerable excess of the consumption of compressed air concerning the compressing medium, in the greater degree, the higher temperature of the last (see fig. 3). Noted property of "charge multiplication» opens a prospect of creation of basic new installations of heat transforming multipurpose machines on the CPE baseline, such as : thermal compressors [17], gas-turbine engines, air refrigerating machines [18, 19], gas generators [20], and supercharging systems of high forcing Internal Combustion Engines (ICE) also [21, 22].

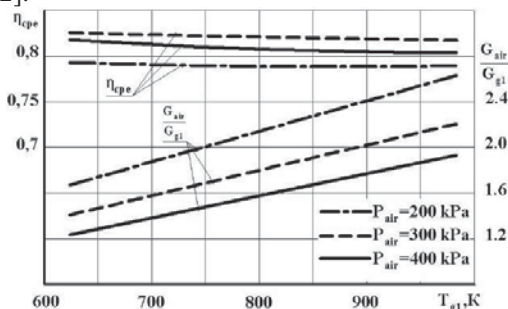


Fig.3. Effect of temperature of the compressing medium T_{g1} on the efficiency η_{cpe} and the ratio of consumptions of the compressed and compressing medium G_{air}/G_{g1} in the CPE

In the paper main trends of development of transport GTE on the basis of units of the cascade-recuperative compression of working mediums are analyzed.

2. Use of principles of the cascade exchange by pressure in systems of compression of air

In the elementary circuit design of the thermal compressor (fig.4,a) on the basis of the cascade pressure exchanger 1, the input window of a high pressure 2 is connected with the outlet window of a high pressure 3 by means of the channel 4 with the source of heat supply 5 (internal combustion or an external heat supply) placed in the channel 4. The connecting pipe 6 of compressed air outlet to a user is connected to the channel 4 between the window 3 and heat supply 5. The part of air discharged under pressure by the exchanger 1 through a connecting pipe 6 is taken away to the user, another part through the channel 4 goes to the heat supply 5 where it is heated, and further is brought to the window 2 in the capacity of compressing medium.

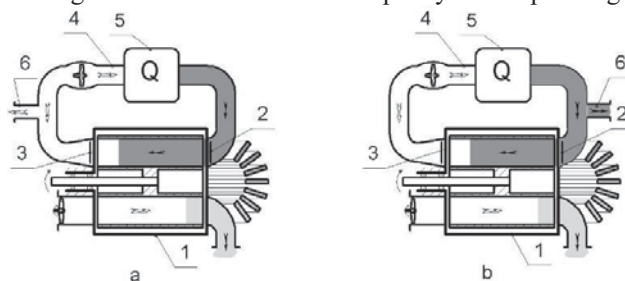


Fig.4. Principal schemes of the thermal compressor (a) and the gas generator (b)

The overall performance of the thermal compressor is evaluated by power efficiency (η_k) according to expression: $\eta_k = (G \cdot H)/Q$, where G – the compressed air charge; H – adiabatic heat drop; Q – the supplied heat.

From the point of view of transformation of the primary thermal energy, the experimentally confirmed values η_k of the thermal compressor efficiency are highly enough. On regimes of $T_z = 1000 \dots 1100$ K for $\pi_k = 3.9 \dots 4.2$ $\eta_k = 0.2 \dots 0.215$. The pressure head of the thermal compressor depends on the relative charge of compressed air \bar{G}_{out} . \bar{G}_{out} represents the ratio of the consumption of air which has been taken away to the user to mass carrying capacity of the rotor. The maximum degree of raise of pressure π_k and optimum value of \bar{G}_{out} by criterion of power inputs increases considerably with raise of the maximum temperature T_z of the cycle. Unique simplicity of the one-stage thermal compressor stipulates attractiveness of its application in systems of air supply with the maximum discharge pressure up to 0.4... 0.5. The design of the thermal compressor is easily converted to the gas generator by connection of the connecting pipe of the working medium outlet to the channel 4 between the heat supply 5 and the window 2 of the compressing medium input (see fig.4,b). The characteristics of productivity of the gas generator are analogous to parameters of the thermal compressor, but have higher values of power efficiency.

Higher pressure head and power efficiency is realized by the two-staged thermal compressor of the CPE with intermediate cooling of compressed air and heating of the compressing medium (fig. 5) [11].

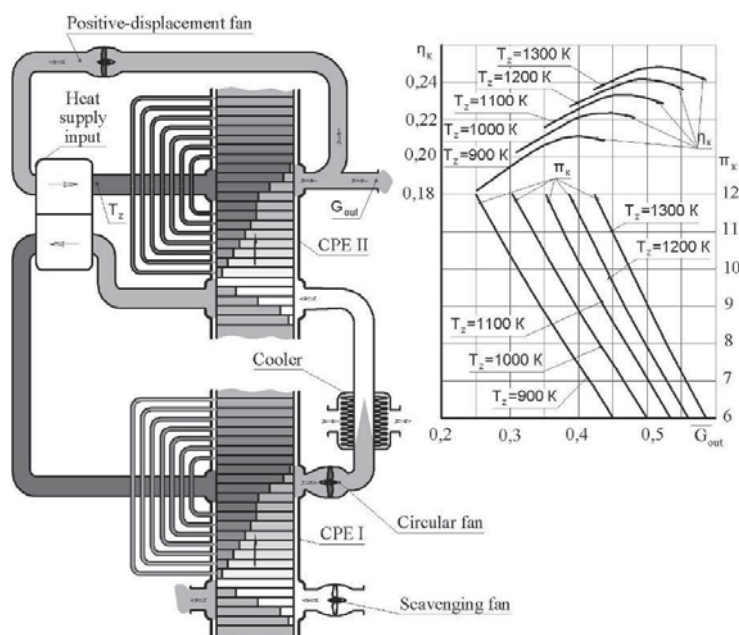


Fig.5. The principal scheme and indexes of operation of two-staged thermal compressor the CPE

Application of the CPE units in the capacity of compressor stage of the GTE allows to carry out working medium compression mainly at the expense of direct transformation of brought heat as a result of internal redistribution of an indicator work of the cascade power interchange with insignificant derivation of mechanical energy from the power take-off shaft. And due to it the power turbine of the gas-turbine engine of the cascade pressure exchange (GTE - CPE) has several times smaller sizes concerning the turbine of the baseline GTE of equivalent power.

3. Parameters of gas turbine engines with the compressor stage of the cascade type

There is a large variety of possible schemes of designs of GTE plants of the cascade pressure exchange. In this work four variants of the GTE working process organization on the basis of the two-staged compressor of the CPE with intermediate cooling of compressed air and reheating of expanding gases are analyzed. (Fig. 6, 7, 8, 9).

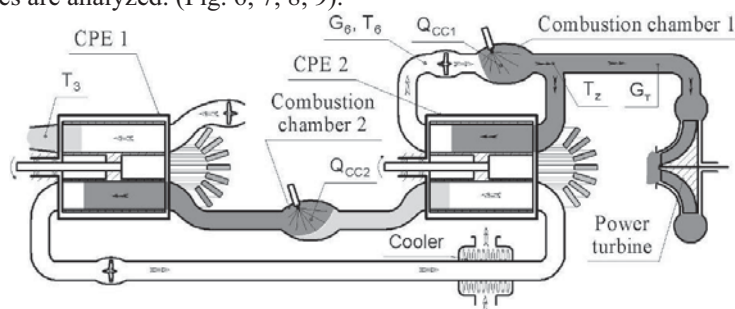


Fig.6. Circuit design of the GTE with two stage cascade pressure unit

In the circuit design on fig. 6 (variant I) two stage cascade pressure unit with direct flow of working mediums is used in the capacity of the gas generators directly connected to the power turbine. The circuit design on fig. 7 (variant II) differs from the circuit design of variant I by the presence of a regenerator of the residual heat of the compressing gases leaving the first stage of cascade pressure unit. In the circuit design on fig. 8 (variant III) two stage cascade pressure unit is used in the capacity of a source of the compressed air which is discharged under pressure in the power turbine after heating in the regenerator by the residual heat of compressing gases. In the circuit design on fig. 9 (variant IV) the mixture of the air and gas flows which are discharged under pressure by two stage cascade pressure unit is used in the capacity of working medium of the power turbine.

The results of calculation determination of effective indexes of these variants of the GTE - CPE with various parameters of working process are completed in tab. 1, 2, 3, 4. According to circuit designs on fig. 6,7,8,9 the designations are specified: η_{GTE} , N_{GTE} - overall efficiency and power of engine correspondingly; $\pi_{k\Sigma}$, π_{k1} , π_{k2} — degrees of raise of pressure, the general in two-units of the CPE, in units of the CPE of 1st and 2nd stages correspondingly; Q_{CC1} , Q_{CC2} , Q_{reg} – power of thermal flows in the high pressure combustion chamber, in the intermediate pressure combustion chamber, in the regenerator of heat of the burnt (exhaust) gases correspondingly; G_6 and T_6 - accordingly the air charge (consumption) and air temperature through the window of high pressure of the CPE of 2nd stage; G_T - the consumption of gases through the power turbine; T_z — the maximum temperature of the cycle; T_T - working medium temperature in front of the power turbine; T_3 - temperature of compressing gases on the outlet from the second stage.

At calculation of performance of the GTE - CPE the turbine politropic efficiency is taken equal 0.81. 3% pressure drop is assumed in combustion chamber also (combustion pressure ratio $\pi_{comb}=0.97$). Geometrical sizes of the CPE units of both stages are invariable for various variants of circuit designs and conditions of the working processes organization of the GTE with the CPE. (outer diameters of rotors are accordingly 200 and 160 mm). The methodology of performance calculation is similar to the one introduced in the works [13] with some modifications.

Table 1 Parameters of working process and performance of the GTE by the variant I of circuit design (fig.6)

| η_{GTE} | N_{GTE} , kW | $\pi_{k\Sigma}$ | π_{k1} | π_{k2} | Q_{CC1} , kJ/sec | Q_{CC2} , kJ/sec | Q_{reg} , kJ/sec | G_T , kg/sec | G_6 , kg/sec | T_T , K | T_6 , K | T_3 , K |
|--------------|-------------------|-----------------|------------|------------|-----------------------|-----------------------|-----------------------|-------------------|-------------------|--------------|--------------|--------------|
| $T_z=900K$ | | | | | | | | | | | | |
| 0.233 | 46.2 | 6 | 2.63 | 2.28 | 149 | 30.3 | 0 | 0.160 | 0.3 | 900 | 406 | 666 |
| 0.253 | 48.8 | 8 | 3.01 | 2.65 | 142 | 36.4 | 0 | 0.150 | 0.3 | 900 | 430 | 639 |
| 0.262 | 49.7 | 10 | 3.35 | 2.98 | 136 | 42.6 | 0 | 0.143 | 0.3 | 900 | 449 | 618 |
| 0.265 | 49.9 | 12 | 3.66 | 3.28 | 131 | 46.3 | 0 | 0.136 | 0.3 | 900 | 466 | 602 |
| $1100K$ | | | | | | | | | | | | |
| 0.256 | 64.8 | 6 | 2.62 | 2.29 | 209 | 30.2 | 0 | 0.185 | 0.3 | 1100 | 407 | 816 |
| 0.279 | 69.5 | 8 | 3.00 | 2.66 | 202 | 36.3 | 0 | 0.178 | 0.3 | 1100 | 431 | 782 |
| 0.292 | 72.1 | 10 | 3.34 | 2.99 | 196 | 42.6 | 0 | 0.171 | 0.3 | 1100 | 450 | 756 |
| 0.299 | 73.5 | 12 | 3.65 | 3.28 | 191 | 46.3 | 0 | 0.166 | 0.3 | 1100 | 466 | 736 |

Advantages of a recuperative cycle are manifested in the greater degree, the higher the maximum temperature of cycle T_z and the lower the general compression ratio $\pi_{k\Sigma}$. So, at parameters $T_z=1000\text{K}$, $\pi_{k\Sigma}=6$ the regeneration provides a raise η_{GTE} at 19% (from 0.256 to 0.304), while at parameters $T_z=800\text{K}$, $\pi_{k\Sigma}=12$ raise η_{GTE} makes 7 % at the expense of regeneration (with 0.234 to 0.251). At the same time, at choice of the GTE – CPE rational parameters we need to have in view the following regularities of working process:

1. Modular power increases with raise of $\pi_{k\Sigma}$ the GTE – CPE at the expense of increase in quantity of heat of an intermediate stage brought in the intermediate combustor, despite decrease of quantity of the heat brought in the top stage combustor;

2. The value $\pi_{k\Sigma}$, optimum by criterion of power inputs, depends on the maximum temperature of the cycle T_z . With raise of T_z an extreme overall efficiency is displaced in a direction of great values of $\pi_{k\Sigma}$, and at $T_z > 950\text{K}$ is in area of $\pi_{k\Sigma} > 12$. We notice that implementation of cycles with $\pi_{k\Sigma} > 12$ is interfaced to constructive complication of the GTE because of negative effect of leaks in rotors of the CPE and necessity of application of the multistage turbine.

3. For fixed values of T_z , the extreme overall efficiency of the GTE with regeneration (fig. 7) corresponds to smaller values of $\pi_{k\Sigma}$ relatively to the GTE - CPE without regeneration (fig. 8).

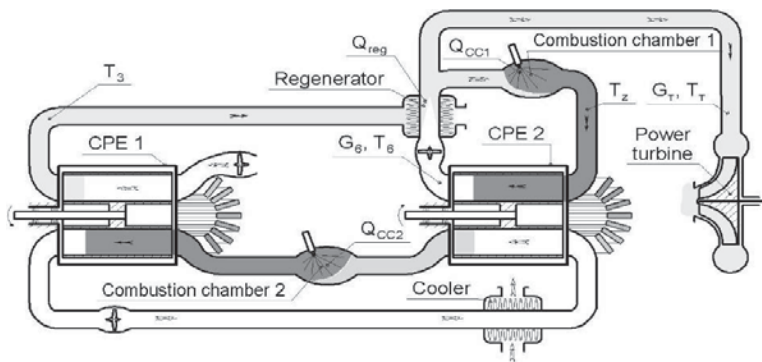


Fig.8. Circuit design of the GTE with two stage cascade pressure unit and with air power turbine

Table 3 Parameters of working process and performance of the GTE by the variant III of circuit design (fig. 8)

| η_{GTE} | η_{GTE} | $N_{\text{GTE}}, \text{kW}$ | $\pi_{k\Sigma}$ | π_{k1} | π_{k2} | $Q_{\text{CC1}}, \text{kJ/sec}$ | $Q_{\text{CC2}}, \text{kJ/sec}$ | $Q_{\text{reg}}, \text{kJ/sec}$ | $G_t, \text{kg/sec}$ | $G_6, \text{kg/sec}$ | T_t, K | T_6, K |
|----------------------|---------------------|-----------------------------|-----------------|------------|------------|---------------------------------|---------------------------------|---------------------------------|----------------------|----------------------|-----------------|-----------------|
| $T_z=900 \text{ K}$ | | | | | | | | | | | | |
| 0.248 | 25.9 | 6 | 2.63 | 2.28 | 56.0 | 30.3 | 29.4 | 0.160 | 0.3 | 503 | 406 | 666 |
| 0.255 | 27.8 | 8 | 3.01 | 2.65 | 58.1 | 36.4 | 25.1 | 0.150 | 0.3 | 513 | 430 | 639 |
| 0.251 | 28.8 | 10 | 3.35 | 2.98 | 60.1 | 41.6 | 21.4 | 0.143 | 0.3 | 520 | 449 | 618 |
| 0.243 | 29.1 | 12 | 3.66 | 3.28 | 61.9 | 46.3 | 17.9 | 0.136 | 0.3 | 525 | 466 | 602 |
| $T_z=1100 \text{ K}$ | | | | | | | | | | | | |
| 0.294 | 31.7 | 6 | 2.62 | 2.29 | 65.6 | 30.2 | 37.8 | 0.185 | 0.3 | 532 | 407 | 816 |
| 0.305 | 34.9 | 8 | 3.00 | 2.66 | 68.2 | 36.3 | 34.6 | 0.178 | 0.3 | 545 | 431 | 782 |
| 0.305 | 36.8 | 10 | 3.34 | 2.99 | 70.5 | 41.6 | 31.7 | 0.171 | 0.3 | 555 | 450 | 756 |
| 0.300 | 38.1 | 12 | 3.65 | 3.28 | 72.6 | 46.3 | 29.1 | 0.166 | 0.3 | 563 | 466 | 736 |
| $T_z=1300 \text{ K}$ | | | | | | | | | | | | |
| 0.320 | 36.1 | 6 | 2.60 | 2.30 | 73.1 | 30.1 | 43.6 | 0.203 | 0.3 | 552 | 407 | 965 |
| 0.334 | 40.2 | 8 | 2.99 | 2.67 | 76.2 | 36.3 | 41.1 | 0.196 | 0.3 | 567 | 431 | 925 |

Table 4 Parameters of working process and performance of the GTE by the variant IV of circuit design (fig. 9)

| η_{GT} E | η_{GT} TE | N_{GT} E, K W | $\pi_{k\Sigma}$ | π_{k1} | π_{k2} | Q_{CC} 1, kJ/s ec | Q_{CC} 2, kJ/s ec | Q_{reg} , kJ/s ec | G_{T_2} , kg/s ec | G_6 , kg/se c | T_{T_2} , K | T_3 K |
|------------------|-------------------|--------------------------|-----------------|------------|------------|------------------------------|------------------------------|---------------------------|---------------------------|-----------------------|------------------|------------|
| $T_z=1100$ K | | | | | | | | | | | | |
| 0.3 01 | 53. 0 | 6 | 2.6 2 | 2.2 9 | 13 4 | 30.2 | 37.8 | 0.18 5 | 0.3 | 900 | 40 7 | 816 |
| 0.3 21 | 56. 9 | 8 | 3.0 0 | 2.6 6 | 13 2 | 36.3 | 34.6 | 0.17 8 | 0.3 | 900 | 43 1 | 782 |
| 0.3 28 | 59. 0 | 10 | 3.3 4 | 2.9 9 | 13 0 | 41.6 | 31.7 | 0.17 1 | 0.3 | 900 | 45 0 | 756 |
| 0.3 30 | 60. 1 | 12 | 3.6 5 | 3.2 8 | 12 9 | 46.3 | 29.1 | 0.16 6 | 0.3 | 900 | 46 6 | 736 |
| $T_z=1300$ K | | | | | | | | | | | | |
| 0.3 12 | 57. 3 | 6 | 2.6 1 | 2.3 0 | 14 4 | 30.2 | 43.6 | 0.20 3 | 0.3 | 900 | 407 | 965 |
| 0.3 34 | 62. 1 | 8 | 2.9 9 | 2.6 7 | 14 2 | 36.3 | 41.1 | 0.19 6 | 0.3 | 900 | 431 | 925 |
| 0.3 44 | 65. 0 | 10 | 3.3 4 | 3.0 0 | 14 0 | 41.6 | 38.9 | 0.19 1 | 0.3 | 900 | 450 | 894 |
| 0.3 48 | 66. 8 | 12 | 3.6 5 | 3.2 9 | 14 0 | 46.3 | 36.9 | 0.18 6 | 0.3 | 900 | 466 | 870 |
| $T_z=1300$ K | | | | | | | | | | | | |
| 0.31 2 | 70. 1 | 6 | 2.6 0 | 2.3 0 | 18 5 | 30.1 | 43.6 | 0.20 3 | 0.3 | 110 0 | 407 | 965 |
| 0.33 7 | 75. 9 | 8 | 2.9 9 | 2.6 7 | 18 1 | 36.3 | 41.1 | 0.19 6 | 0.3 | 110 0 | 431 | 925 |
| 0.35 0 | 79. 4 | 10 | 3.3 4 | 3.0 0 | 17 9 | 41.6 | 38.9 | 0.19 1 | 0.3 | 110 0 | 450 | 894 |
| 0.35 6 | 81. 6 | 12 | 3.6 5 | 3.2 9 | 17 7 | 46.3 | 36.9 | 0.18 6 | 0.3 | 110 0 | 467 | 870 |

Forcing of the GTE - CPE working cycle on T_z with simultaneous optimization of temperature of air-gas medium in front of the power turbine allows to realize the highest power and economical parameters of the plant. So, at $T_{T_2}=900$ K raise of the maximum temperature T_z from 900K (tab. 3) to 1100K (tab. 4) promotes increasing η_{GTE} on 11.8 % (with 0.295 to 0.33) and to raise N_{GTE} on 20% (with 49.9 to 60kW), and at raise of T_z from 900K to 1300K the rise of η_{GTE} and N_{GTE} accordingly makes 18 % and 33 %. On regime of $T_z=1300$ K, $\pi_{k\Sigma}=12$, $T_{T_2}=1100$ K the GTE - CPE overall efficiency with mixing the gas and air flows in front of the power turbine attains the value 0.356.

4. Conclusions

Thermodynamic efficiency of the GTE - CPE is based on higher efficiency of transformations of heat in the combustion chamber to energy of compressed air concerning the working process of the classical GTE where air compression is carried out in the conditional turbo-compressor which

is consisting of the vane compressor and part of the power turbine equivalent on power. In analyzed GTE - CPE installations rather insignificant power of an external source is spent for the drive of both CPE. The work of compression of air is carried out at the expense of internal redistribution of energy of gas flows in the flowing elements of the CPE units. Only the part of gas from the combustion chamber goes to the power turbine which, as a result, has essentially smaller sizes and developed power at equivalent power of the GTE. With decrease of the charge of gases (G_{out}) through the turbine the absolute power losses are reduced in it, therefore, imperfection of working process of the turbine including, on off-design conditions influences the GTE overall efficiency to the lesser degree. And, at last, noted above the insensibility of the working cycle of the CPE to incompleteness of displacement of compressed air from rotor cells at a deviation of its rotational speed and thermodynamic variables of working mediums from design values stipulates essential expansion of field of effective work of the GTE with the CPE.

Application of principles of the cascade compression of air-gas medium in the gas-turbine engine working cycle allows to improve significantly the traction and economic characteristics of the GTE and opens a prospect of wider application of the GTE in the capacity of ground transport power plants

References

- [1] Mathis. G. P. Wave enhanced Gas Turbine Engine Cycles: Cornell University, Ithaca,/ Mathis. G. P., M. S. thesis, New York-1991.
- [2] Wilson J. Jet engine Performance Enhancement Through Use of a Wave-Rotor Topping Cycle / Wilson J., Paxson D. E., NASSA, - 1993. TM-4486.
- [3] Paxson D. E. A Numerical of the Startup Transient in Wave Rotor: ASME J. Gas Turbines Power 119(3) / Paxson D. E., 1997. pp. 676-682
- [4] Akbari P. Performanse investigation of small gas turbine engines topped with wave rotors: Conference and exhibit / Akbari P., Muller N. Huntsville Allabama 2003. AIAA2003-4414.
- [5] Akbari P. Performance Enhancement of Microturbine Engines Topped With Wave Rotors: ASME J. Eng. Gas Turbines Power, 128(1)/ Akbari P., Nalim M. R., Muller N, 2006, pp. 190-202.
- [6] Akbari P. A. Review of Wave Rotor Technology and its Application: ASME O. Eng. Gas Turbines Power, 128(10) / Akbari P. A. Nalim M. R., Muller N, 2006, pp. 717-734.
- [7] Meyer A. Recent Developments in Gas Turbines: Journal of Mechanical Engineerring, 69, №4 / Meyer A., 1947. pp. 273-277.
- [8] Weber H. E. Shock Wave Engine Design: John Wiley and Sons / Weber H. E. New York. 1995
- [9] Mayer A. Extruded Ceramic – A New Technologjy for the Comprex Rotor: SAE Paper 890452 / Mayer A., Oda J., Kato K., Haase W., Fried R. 1989
- [10] Zehnder G. The Free Running Comprex: SAE Paper 890452 / Zehnder G., Meyer A., Mathews L. 1989.
- [11] Benini E. Centrifugal Compressor of A 100KW Microturbine: Part 1-Experimental and Numerical Investigation on Overall Performanse” ASME Paper GT2003-38152 / Benini E., Toffolo A., Lazzaretto A. 2003.
- [12] Rogers C. Some Effects of Size on the Performance of Small Gas Turbine: ASME Paper GT2003-38027 / Rogers C. 2003.
- [13] Welch G. E. Overview of Wave-Rotor Technology for Gas Turbine Engine Topping Cycles: Novel Aero Propulsion Systems International Symposium, The Institution of mechanical Engineers / London - 2000, pp. 2-17.
- [14] Krajniuk A.I., Storcheous J.V., 2000. Systems of gas-dynamic supercharging. – Publ. EUSU. Lugansk., 2004, 224 p.
- [15] Klyus O.V., Krajniuk A.I., Alekseev S.V., 2008. The principle organization of work process unit of cascade compression and its application// Scientific journals Maritime University of Szczecin, Szczecin – 2008. №14(86). –P. 25-29.

- [16] Krajniuk A.I., Alekseev S.V., Brjantsev M. A., 2005. Features of working process of a cascade exchanger of pressure // Publ. EUSU. Lugansk. - 2005. - № 8 (90). - p. 176-179.
- [17] Krajniuk A.I., 2009. Thermal compressor of cascade exchange by pressure: Silesian university of technology publication faculty of transport. I International Scientific Conference. Transport problems, Katowice-Kroczyce, 17-19. 2009 p.186-191.
- [18] Krajniuk A.I., Krajniuk A.A., 2008. New principle of the organization of working process of central airs of air railway and sea transports// Silesian university of technology publication faculty of transport. VIII Scientific Conference telematics, logistics and transport safety. Katowice-Cieszyn. 2008. p.64-68
- [19] Brjantsev M. A, Krajnjuk A.A., 2008, "Use of principles of a cascade exchange by pressure in a running cycle of gas refrigerators", Internal combustion engines//Scientifically - the technical journal. Kharkov, CTU «HPI».-. № 1.p.-57-61
- [20] Krajniuk A.I., 2010. New schemes and principles of the organization of working processes of heat power cars // Publ. EUSU. Lugansk, № 7(125). Part.2. – 2010. p.-197-200
- [21] Krajniuk A.I., Alekseev S.V., Brjantsev M. A., Krajniuk A.A. 2008. System of forced aspiration transport ECI with a cascade exchanger of pressure// Publ. EUSU. Lugansk, № 5(120). Part.2. – 2008. p.-200-208
- [22] Krajnjuk A. I., 2010, "Development of supercharging systems of internal combustion engines with the cascade pressure exchanger" TEKA Kom. Mot. i Energ. Roln. – OL PAN, Lublin 2010, 10A, 303-310



THE CONCEPTION OF ENERGETIC INVESTIGATIONS OF THE MULTISYMPOTOM FATIGUE OF THE SIMPLE MECHANICAL SYSTEMS' CONSTRUCTIONAL MATERIALS

Zbigniew Korczewski

*Gdansk University of Technology, Poland
Faculty of Ocean Engineering and Ship Technology
Department of Marine and Land Power Plants
11/12 Narutowicza Str. 80–233 Gdańsk, tel/fax: (58) 347 21 81,
e-mail: z.korczewski@gmail.com*

Abstract

The article presents the basic assumptions of the research project aimed, as the main scientific purpose, an identification of the slow-changeable energy processes surrounding the high-cycle fatigue of constructional materials within the plain mechanical system, especially the marine one, for diagnostic purposes. There is foreseen an application of alternative diagnostic methods based on energetic observations of the multi-symptom, continuous and irreversible alterations of the fatigue state within the material and construction of the elements transmitting the stream of mechanical energy from the propulsion engine to the propeller. Such methods will represent an essential supplement of already existing diagnosing systems of marine engines as well as marine propulsions. Only then an implementation of the condition based maintenance within the marine propulsion operation can be seen fit to approve.

Second part of the paper demonstrates the results of preliminary experimental investigations conducted on the Schenck fatigue machine. The machine has been especially adapted for the purposes of the planned energy research and equipped with measuring apparatus of vibration, acoustic emission and thermal emission.

Keywords: mechanical system, high-cycle fatigue, diagnostics.

1. Introduction

Within the period of intensive works engaged upon the improvement of reliability, durability and economy of marine combustion engines' action, a problem of the effective diagnostic methods gets the more and more larger meaning - especially, because last several years there was observed getting off the engines' planned maintenance operation instead of their operation according to the actual technical state (MAN Diesel&Turbo - „CoCoS-EDS - Computer Controlled Surveillance - Engine Diagnostic System", Wärtsilä - „CBM - Condition-Based Maintenance", General Electric - „ICAS - Integrated Condition Assessment System"). This is a desirable activity especially in case of the unforeseen damage inputs the large hazard degree. It also concerns fatigue damages within the engine's mechanical system and its driving line where possibilities of early recognizing the diagnostic symptoms are extremely limited because of the very little supervisory susceptibility.

Hence, despite hearing more and more often about implementation into operation system a so-called complex (defined in such a way with a decidedly excessive, exaggeratedly manner),

multisymptom diagnostic systems of the marine engines they still involve the working spaces mainly or the fuel fed systems eventually. Furthermore, a key diagnostic problem concerning an evaluation of the fatigue state of the elements within the engine's mechanical system (and within the whole propulsion system) still remains unsolved. These elements being exposed to cyclic, changeable loads undergo fatigue failures (cracks) [Hebda and Wachal, 1999]. This kind of failure seems to be foreseeable which results from a clear interdependence between the failure formation's intensity and the engine's worktime. Additionally, a dispersion of the occurring failures is contained in the narrow time interval - Fig. 1. However numerous deviations from this rule occur. They result

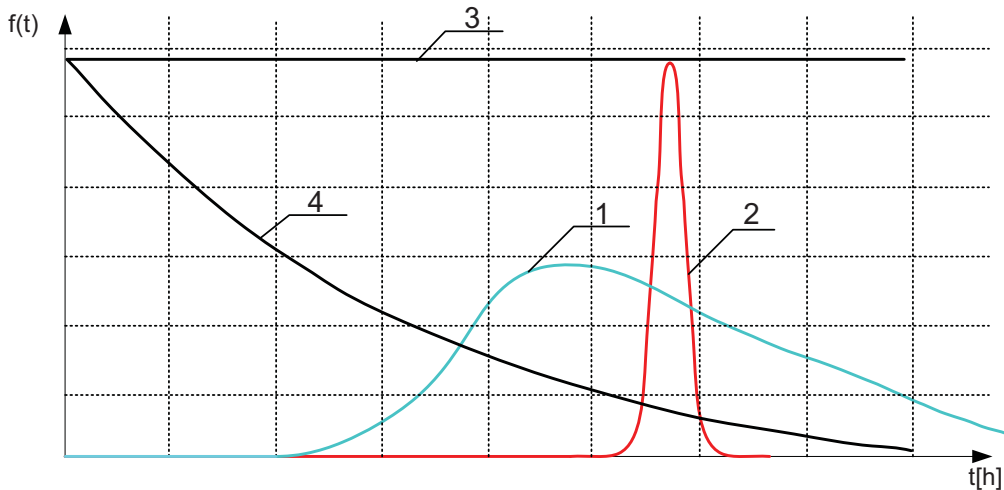


Fig. 1. Characteristic time courses of a probability density function of the worktime up to the failure for the marine combustion engines basic functional systems [Czajgucki, 1984].
1 – thermal-flow system (working spaces), 2 – mechanical system, 3 i 4 – control system.

most often from the post technological lattice defects within the constructional material, and also, what happens more often, from the long-lasting usage of the ship's propulsion system in conditions of a stability loss within the mechanical system and consequently, the resonance vibrations [Cudny, 1976; Drganantchev, 2000; Korczewski and Rudnicki, 2012].

Then, the occurring maximum amplitudes of changeable internal tensions cause a considerable limitation of the load alterations cycles' number, at which the elements transmitting a torque from the engine to the propeller undergo the accelerated fatigue wear and tear, up to the irreversible damages (cracks, deterioration of the constructional material's mechanical properties etc.) - Fig. 2. What is interesting, the fatigue state, in a sense of dislocations within the lattice, caused by amplitudes of the cyclically changeable tensions, is "memorized" by the constructional material and in spite of removal of the primary reasons extorting vibrations a spontaneous restoration of the primary mechanical properties does not follow. On the contrary, a fatigue weakening constructional structure becomes more sensitive to strenuous load alterations because the initial Wöhler curve moves in the direction of more and more lower values of the transferred tensions as well as the smaller cycle number at which a fatigue cracks initiation follows, and so the smaller fatigue durability.

The problem of fatigue consequences of vibrations, as an energy "microdynamic" phenomena (quickchangeable), occurring within the material microstructure related to one cycle of the changeable load, has been represented in numerous publications within the range of the Materials' Strength for many years now [Kocańda and Szala, 1997; Kaleta, 1998; Boroński and Szala, 2008; Maciejewski et al., 2003]. However, there is still noticeable the lack of bibliographic

positions presenting this issue in an aspect of identification of the "macrodynamic" processes (slowchangeable), describing the material behavior in a macroscopic scale, during a continuous, transient flow of the mechanical energy flux (along with the energy's dissipation and accumulation) from the engine to the propeller.

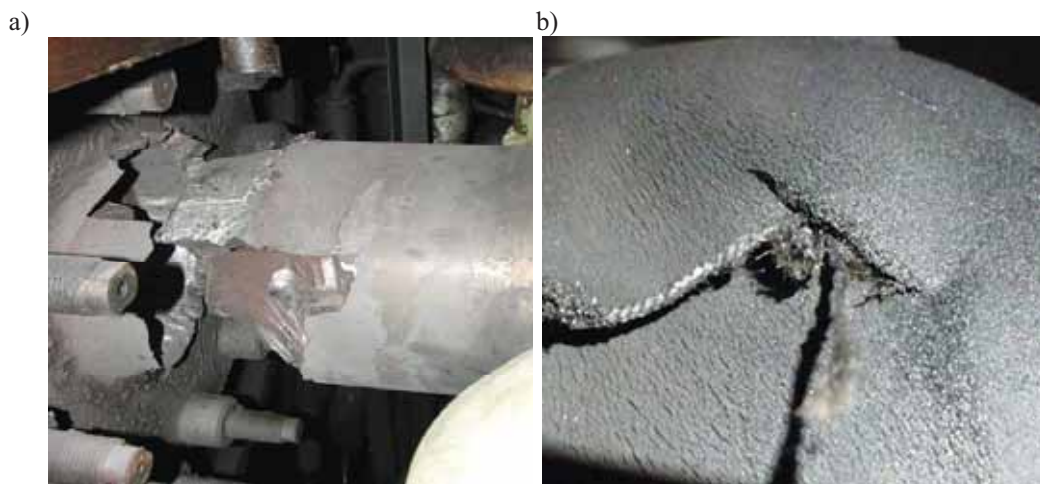


Fig. 2. Fatigue failures of the shaftings' elements within the marine propulsion unit:

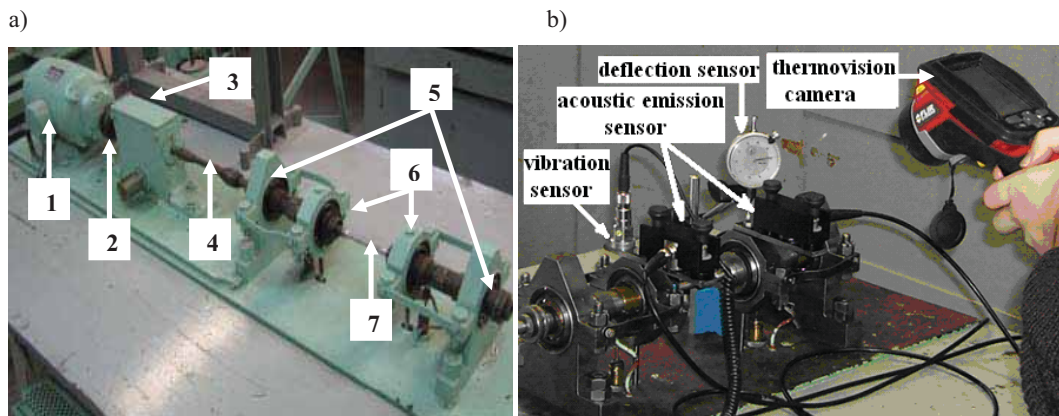
- a) broken propeller shaft of the marine propulsion unit as a consequence of the structural material's high-cycle fatigue (mechanical), b) rubber flexible element of the Vulkan RATO coupling along with fatigue wear traces [Korczewski, 2008].

In an ideal marine propulsion unit the whole energy delivered to the propulsion engine is transformed into the effective, basic rotational motion of the propulsive line's mechanical system. As the result of the progressive technical state degradation of the line's constructional elements accompanying motions are generated additionally. They are undesirable from the efficiency viewpoint of energy transformation and transmission processes within the whole propulsion unit. Moreover they represent a reason for the kinetic energy's dissipation of the masses within the rotational motion as well as the internal energy's accumulation within the constructional materials. After crossing the critical values of these energies the fatigue damage follows. Its course is characterized with residual energy processes: vibroacoustic and thermal that induce the observable diagnostic symptoms of technical state alterations.

Therefore, how to estimate quantitatively a current fatigue state of the constructional material of elements transmitting a torque within a simple mechanical unit of the marine propulsion system in operation condition? More and more perfect measuring apparatus unlocks completely new horizons in this regard. Its application in diagnostic investigations enables the user to observe precisely the course of residual energy processes within the mechanical unit. It aims to evaluate the measures' patterns (estimators) of diagnostic signals (vibration, acoustic and radiant emission) for the given high-cycle fatigue of the constructional elements' material. Consequently, this is also possible to evaluate a diagnostic inference method about the technical state of the simple mechanical units within the marine propulsion systems, and not only, in their operation conditions. This is the main aim which shone the Author of the present article during planning the investigative project.

2. Research test stand

In the first stage of diagnostic investigations of the real marine propulsion mechanical arrangements at high-cycle fatigue conditions it was necessary to build, in a certain scale, a physical model of the simplified mechanical system. The model preserving essential dynamic features of the real object enables an observation of the realized energy processes' course. There were good reasons for the decision to apply Schenck fatigue machine to this aim. The Schenck machine is mainly designed to evaluate the fatigue boundary of the constructional materials at the double-sided bending - Fig. 3a. During the standard fatigue test a standardized sample of the constructional material is subject to the clear bending-torsion moment of the constant value, on its whole length. It means, that the same fatigue stress exists in its every section. In this way, by relating the conditions of the laboratory fatigue test to the real running conditions of the marine propulsion unit shafts misalignment or deflection might be simulated. Such undesirable malfunctions take the effect on the growing trust forces in bearings and therefore a growth of the mechanical losses moment for overcoming friction forces within the mechanical system takes place. The alterations of the driveline's rotational speed represent an observable result of the unestablished balance of the system's mechanical energy. Transverse vibrations generated in the bearing nodes, acoustic emission of disappearing springy waves as well as thermal emission (infra-red radiation) of the system's elements accumulating the internal energy, increasing as a result of the work executed over the system stand for the additional consequences of the sample's enforced springy and plastic deformations. A manner of the measuring apparatus sensors' assembly on the test stand is shown in Fig. 3b.



Rys. 3. Schenck fatigue-testing machine designed to exam a fatigue boundary of the constructional materials at the double-sided bending

1 – propulsion engine (shunt direct-current motor), 2 – silent-block flexible disk coupling (pins along with rubber pads), 3 – rev-counter worm gear (transmission ratio 1:100), 4 – spring-actuated flexible coupling, 5 – immovable rolling bearing (ball bearing), 6 – self-aligning rolling bearing (ball bearing), 7 – sample under investigation.

During a fatigue test completion there are registered diagnostic signals reflecting energy consequences of the progressive degradation process of the sample's structure material which is subject to rotatory bending, in successive stages of the fatigue process: from an appearing the first slips in grains, across an initiation and development of the mikro- and macro-cracks, until to the total fatigue destruction. A flow of energy streams within of the considered mechanical system illustrates Fig. 4.

After starting-up a propulsion engine and getting-out the mechanical system from the standstill to the settled rotational speed 2000 rev/min the sample's loading with the bending moment follows. The sample's cyclic sinusoidal load induces cyclic fatigue deformations and stresses in it. An initial growth and subsequent fall of the system's rotational speed, as a measure of appropriate alterations of the accumulated kinetic energy of the masses in rotatory motion, represents, among other things, their observable diagnostic symptoms - Fig. 5.

An initial growth of the system's rotational speed might be explained with the transitional, intensive reinforcement of the sample's material structure in the result of slips' incubation in some grains of the lattice that are unfavorably-oriented in relation to the load direction. Then an equally intensive decrease of the sample's deflection might be observed. In the next phases of the process a thereafter, moderated reinforcement of the sample's material follows. It results from the plastic deformations extorting the evolution of the lattice's defects along with the mutual blocking dislocations that are moving in different, intersecting slips' planes. Then the sample's deflection is also equally moderate. A continuous growth of temperature and trust forces in bearings causes the anti-torque's growth in the mechanical unit's rotational motion, i.e. the propulsion engine's load torque (shunt direct-current motor).

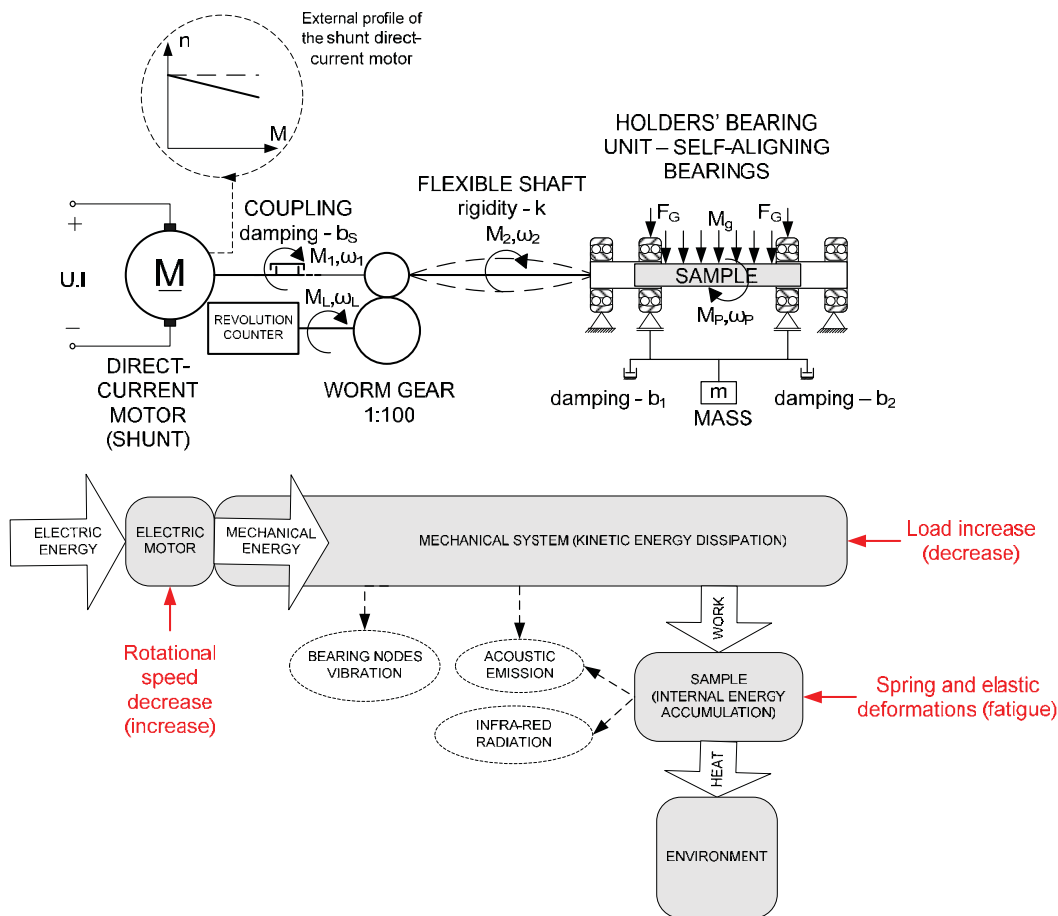


Fig. 4. Mechanical system of the Schenck fatigue-testing machine along with a flow of energy streams

According to the right of angular momentum alterations for the considered propulsion unit a kinetic energy dissipation in its mechanical system and decrease in rotational speed follows. In case of a shunt direct-current motor for the reduced rotational speed, at unchanged magnetical stream, responds the smaller counter-electromotive force which counteracts against the voltage. In such a situation the larger current flows through the engine's armature enlarging a turning moment generated in the engine. The unsteady process will be lasted till the balance between breaking torque from the mechanical system (moment of mechanical losses) and the engine's propulsion torque. Considering this process in an aspect of electric energy transformation into mechanical one what is worked out in the propulsion engine it goes without saying that the more is the load torque the more is the current's amount consumed by the propulsion engine from the electric net (the larger feed electric energy stream to the engine).

An alteration of the temperature field in a deformed material as well as the permanent growth the sample's averaged temperature stands for the thermal consequence of the mechanical fatigue. Observable distribution temperature alterations on the sample's surface (learning on the infra-red radiation detection) represent, on a macroscopic level, the adequate diagnostic symptom of microscopic phenomena setting within the material's crystalline structure. The phenomena are mainly associated with the dislocations' movement as well as their interaction (an influence of the point defects is negligible small) [Boroński and Szala, 2008]. According to the first law of thermodynamics an alteration of the internal energy amount that is accumulated during the fatigue test realization is calculated as a sum of the heat flux emitted to surroundings and the power needed on the sample's material deformation handiwork. Taking into considerations energy hypotheses of the fatigue damages, presented in publications of scientific teams directed by S. Kocańda and J. Szala as well as J. Kaleta a constructional element undergoes the fatigue destruction, when a total internal energy accumulated in its material reaches the critical value [Kocańda and Szala, 1997; Kaleta, 1998].

A measurement and analysis of the vibration generated by the mechanical system's bearing nodes stands for the particularly complex metrological aspect of the high-cycle fatigue process's energy consequences in the conditions of growing lattice's defects of the material sample. This is also very complex to investigate impulses of disappearing springy waves of the acoustic emission that are locally freed, from the intermolecular bonds' energy release. What, in turn, is caused by the lattice's deformations and its defects' displacements (pointwise and linear). Then, the root-mean-square value (rms value) of the registered amplitude spectrum constitutes the basic diagnostic parameter, as a measure of dissipated kinetic energy of the mechanical system in rotational motion devoted to the vibration and acoustic emission enforcing. Within L. Rogera publications presenting the comparative analyses of both the methods in an aspect of the fatigue cracks identification of the rolling bearings you can find unequivocal conclusions confirming a decidedly larger efficiency of observation of the acoustic emission phenomenon, which is more tender and unambiguous in the material defects evaluation [Roger, 1979 and 2001].

Because of the continuous alterations of the lattice structure as well as temperatures of the getting warm material sample follow the suitable alterations of the natural vibration frequency follow. This frequency gets smaller along with the sample temperature, as a result of the material stiffness's decrease (a value of the material's longitudinal modulus of elasticity gets smaller). It results, from the conducted calculations, that in a range of the material temperature's changeability of the sample and bearing nodes, the natural vibration frequencies change in the range of a dozen or so, or even tens percentage during realization of the accelerated fatigue test. It can lead to the considerable "wander" of resonance frequencies. Hence, a frequency analysis of the registered amplitude spectrum does not bring in essential diagnostic information.

The representative time courses of the observed control parameters registered during the pilot fatigue test execution on the Schenck test stand were introduced in Fig. 5.

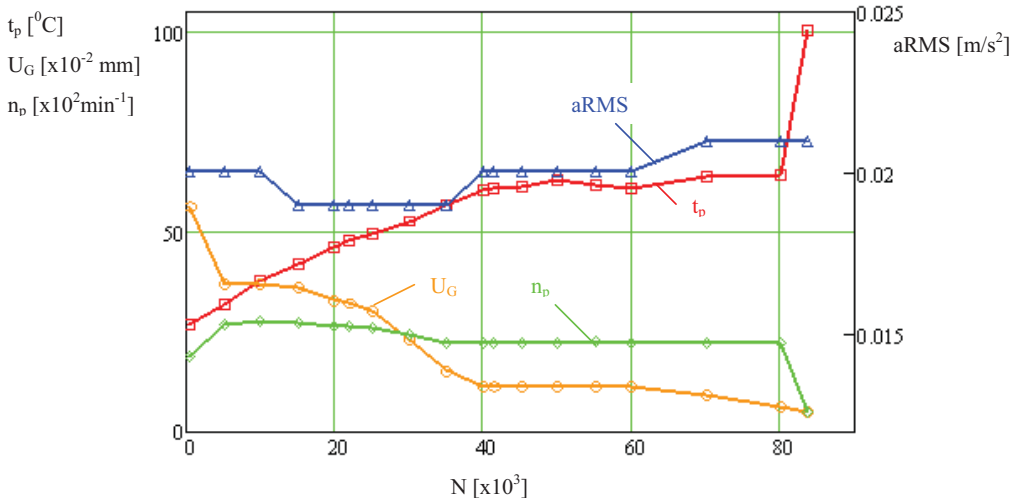


Fig. 5. Time courses of the observed control parameters registered during the pilot fatigue test execution on the stainless-steel sample (unalloyed, fine-grained, weldable steel of S355N type)

t_p – sample's temperature, n_p – sample's rotational speed, U_G – sample's deflection, a – vibration acceleration, a_{RMS} – root-mean-square value of the vibration acceleration, N – cycle number.

3. Physical model of energy processes

A creation of the adequate mathematical model represents one of key execution conditions for a quantitative evaluation of the energy consequences of the sample constructional material's high-cycle fatigue making up the mechanical system's element. Only a set of the differential non - linear equations of partial derivatives delivers the precise movement description of such a system [Cannon, 1973; Cichy, 2001]. The influences of accidental factors were omitted within the elementary, necessitating approach to the issue of modelling processes. Moreover, the physical model of analysed energy processes, possessing the essential dynamic features characterizing an energy streams' flow in unsteady states, was maximally simplified (idealized). Assuming, that the state parameters of dynamic processes change only in relation to the time and that they do not alter their values in relation to the position, the simplest, zero-dimensional model (of the concentrated parameters) was accepted in the initial stage of investigations. It was adjusted, that the zero-dimensional model fulfils the assumed particularity requirements of the real object functioning's mathematical description (a fatigue machine of the Schenck product), for the established modelling purposes - a creation of the diagnostic simulation model of the plain mechanical system. It was additionally adjusted, that a period of the neck creation in the sample, while the spatial stresses state begins affecting, will be neglected.

With regard to the extensiveness and complexity of the energy processes mathematical modelling of the considered mechanical system in unsteady states, the worked out physical model was limited only to the simplified flow of input and output signals among dynamic modules during the fatigue test realization - Fig. 6. Such a model stands for an introduction to the further, wider issue analysis.

4. Conclusions and final remarks

The conception introduced within this scientific study concerns a diagnostic application of the energy investigations of the slow-changeable unsteady processes that go with the high-cycle fatigue of materials and constructions of the plain mechanical systems. It represents for an introduction to elaborate a diagnostic method of their technical state evaluation in real operating conditions. There is foreseen, that the method will supplement a lacking link of the existing diagnosing systems of the marine engines and propulsions.

The presented physical model of the energy processes worked out within the Schenck fatigue machine stands for an initial stage of these processes' mathematical modeling for the qualitative and quantitative identification of the developing fatigue defects' impact on time courses of the observed unsteady process's state variables.

References

- [1] Boroński D., Szala J.: Ocena stanu zmęczenia materiału w diagnostyce maszyn i urządzeń. Biblioteka Problemów Eksploatacji, Bydgoszcz 2008.
- [2] Cannon R.H.: Dynamika układów fizycznych. WNT, Warszawa 1973.
- [3] Cichy M.: Modelowanie systemów energetycznych. Wydawnictwo PG, Gdańsk 2001.
- [4] Cudny K. Linie wałów okrętowych. Wydawnictwo Morskie, Gdańsk 1976.
- [5] Czajgucki J.Z.: Niezawodność spalinowych siłowni okrętowych. Wydawnictwo Morskie, Gdańsk 1984.
- [6] Dragantchev H.: Control and Diagnostics of Ship Shafting. Proceedings of the IMAM 2000, Ischia, April 2-6, 2000, Session L, 115-122.
- [7] Hebda M., Wachal A.: Trybologia. WNT Warszawa 1999.
- [8] Kaleta J.: Doświadczalne podstawy formułowania energetycznych hipotez zmęzeniowych. Oficyna Wydawnicza Politechniki Wrocławskiej. Wrocław 1998.
- [9] Kocańda S., Szala J.: Podstawy obliczeń zmęzeniowych. PWN Warszawa 1997.
- [10] Korczewski Z., Rudnicki J.: Stability evaluation of the marine propulsion unit's mechanical system by means of vibration measurements and their analysis. 5th International Conference, Maritime Transport 2012, Barcelona, 27-29 June 2012.
- [11] Maciejewski Ł., Myszka W., Ziętek G.: Zmęzeniowe hipotezy energetyczne dla obciążeń pseudolosowych: symulacja i eksperyment. II Sympozjum Mechaniki Zniszczenia Materiałów i Konstrukcji. Augustów, 4-7 czerwca 2003.
- [12] Roger L.M.: The application of vibration analysis and acoustic emission source location to on-line condition monitoring of antifriction bearings. Tribology International, 1979, p. 51-59.
- [13] Roger L.M.: Structural and engineering monitoring by acoustic emission methods – fundamentals and applications. Lloyd's Register Technical Investigation Department. UK 2001.



LABORATORY STUDY ON INFLUENCE OF THE EXHAUST DUCT THROTTLING ON EXHAUST GAS COMPOSITION IN MARINE FOUR-STROKE DIESEL ENGINE

Jerzy Kowalski

Gdynia Maritime University
Department of Engineering Sciences
Morska Street 81-87, 81-225 Gdynia, Poland
tel.: +48 58 6901434, fax: +48 58 6901399
e-mail: jerzy95@am.gdynia.pl

Abstract

Presented paper shows results of laboratory tests on the relationship between the throttling of a cross area of an exhaust outlet duct and the composition of exhaust gas from the marine engine. The object of research is a laboratory four-stroke diesel engine, worked with a load from 50kW to 250kW at a constant speed equal 750rpm. During the laboratory tests over 50 parameters were measured of the engine with technical condition recognized as a "working properly" and with simulated the exhaust outlet duct throttling. The simulation consisted of changing the angle of the barrier mounted in the exhaust duct after the turbine, limiting duct cross-sectional area. Results of laboratory research confirm that the best indicator of the throttling of the exhaust gas duct among considered thermodynamic parameters of the engine is pressure of exhaust gas after turbine. Unfortunately mentioned pressure is usually very little and for this reason technically difficult to measure during on-board operation. In the case of measuring the composition of exhaust gas, the throttling of the exhaust gas duct causes visible changes of the oxygen and carbon oxide quantity in the exhaust gas. Other measured gaseous components changed not significant during the throttling of the exhaust gas. The conclusion is that the results of measurements of the composition of exhaust gas may contain valuable diagnostic information about the technical condition of the exhaust gas duct of the marine engine.

Keywords: marine diesel engine, exhaust gas composition, toxic emission, laboratory investigation, exhaust gas duct throttling

1. Introduction

Diesel four-stroke engines used in marine applications must complying requirements of economic operation and environmental regulations. Necessary for this purpose is the preparation and delivery to the engine cylinders homogeneous combustible mixture in the whole engine load. Operation of the engine causes, in time, the deterioration of its work efficiency, due to various kinds of disability. These failures result in deterioration of the combustion process in engine cylinders. The effect of this situation is increased fuel consumption and changes in exhaust gas composition emitted from the marine engine [1 – 3]. Due to not effective combustion process of mixture in cylinders the composition of exhaust gas is changed [4 – 7].

The fuel dose injected to the engine cylinder is fragmented and evaporated. After mixing the evaporated fuel with air the combustion process is started. Burning process causes changes in the air-fuel mixture with rotation of the crankshaft, the engine load and speed, and the technical condition of engine components and systems. Solid particles contained in the air and soot from the

exhaust gas can cause damage to the turbine blades, the exhaust gas duct and other components of the engine charging system. This causes the exhaust gas duct throttling and changes in the parameters of the combustion process. The effect of these may be change composition of exhaust gas also.

The paper presents results of experimental studies on the effects of the throttling the cross area of the engine exhaust gas duct on the composition of exhaust gas.

2. Laboratory stand

The object of study is 3-cylinder, four-stroke, laboratory engine type AL25/30 Cegielski-Sulzer manufacturer, installed in the Laboratory of Internal Combustion Engines in Gdynia Maritime University. This engine is loaded with generator, electrically connected to the water resistance and supercharged by VTR 160 Brown-Boveri turbocharger. During tests the engine was fuelled by diesel oil and worked at a constant speed, equal to 750rpm. There were measured 56 parameters of the laboratory stand including the engine load and speed, parameters of the turbocharger, systems of cooling, fuelling, lubricating, and air exchange. The composition of exhaust gas was also recorded using electrochemical gas analyser. Pressure, temperature and humidity of air were recorded by laboratory equipment also. All mentioned results were recorded with a sampling time of 1 second. Injection pressures and pressures of combustion in all cylinders of the engine were also collected. Scheme of the laboratory stand is presented in Fig.1 and the engine parameters are presented in Tab.1.

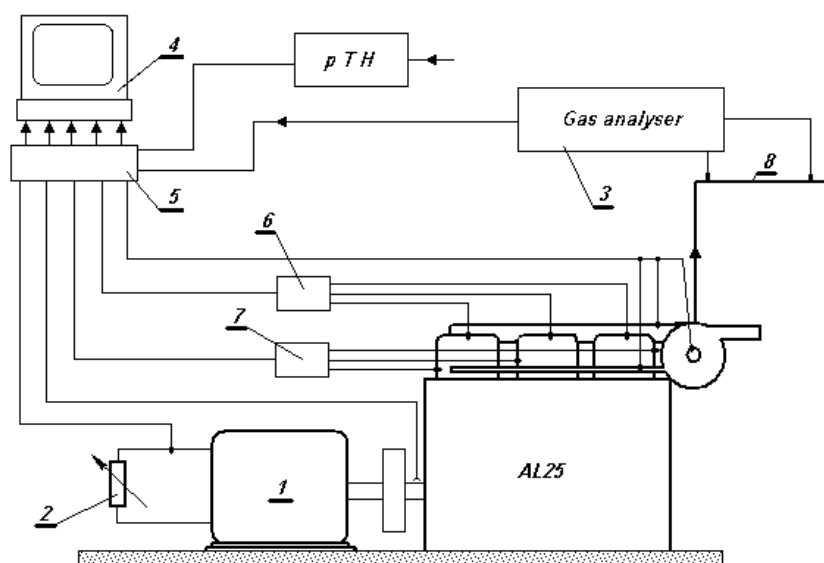


Fig.1. Laboratory stand scheme. 1 – generator, 2 – water resistance, 3 – gas analyser, 4 – computer, 5 – A/C converter, 6 – combustion pressure indicator, 7 – injection pressure indicator, 8 – exhaust gas duct

Tab.1. Parameters of the AL25/30 engine

| Parameter | Value | Unit |
|-------------------|-------|------|
| Max Power | 250 | kW |
| Rotational speed | 750 | rpm |
| Bore diameter | 250 | mm |
| Piston stroke | 300 | mm |
| Compression ratio | 12,7 | – |

During each start of observation, the engine was loaded to maximum load equal 250kW, and after stabilizing temperature of exhaust gas after the turbine, engine operating parameters were recorded for 3 to 5 minutes. After this the load of the engine was decreased by 10kW and after stabilizing temperature of exhaust gas after the turbine, engine operating parameters were recorded again. Observation was continued with loads up to 50kW. The engine did not work with a load of 190kW due to resonance vibrations.

3. Results and discussion

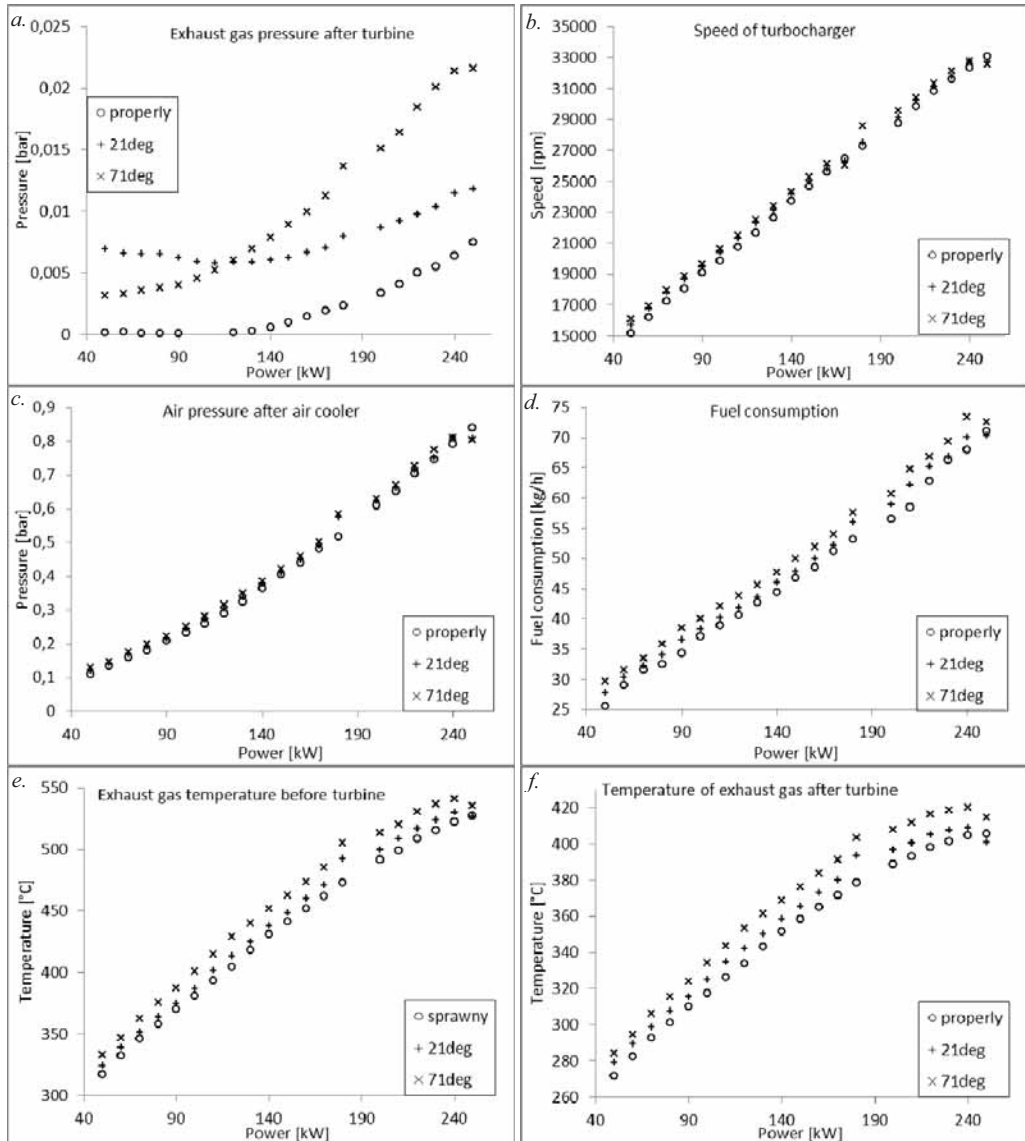


Fig.2. Thermodynamic changes during the throttling of the exhaust duct: a. Exhaust gas pressure after turbine, b. Speed of turbocharger, c. Air pressure after air cooler, d. Fuel consumption, e. Exhaust gas temperature before turbine, f. Temperature of exhaust gas after turbine

Presented laboratory study consists of 3 stages:

- first stage consists of 4 observations during operation of the engine assumed as “working properly”,
- second stage consists of 3 observations during operation of the engine with the throttling of the cross area of the exhaust gas duct by changing the barrier angle mounted in the exhaust gas duct after the turbine by 21 degrees,
- third stage consists of 3 observations during operation of the engine with the throttling of the cross area of the exhaust gas duct by changing the barrier angle mounted in the exhaust gas duct after the turbine by 71 degrees.

Scheme of the throttling of the cross area of the exhaust gas duct is presented in Fig. 2.

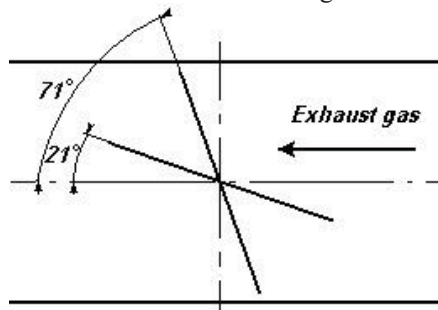


Fig.3. Scheme of the throttling of the cross area of the exhaust gas duct

Presented results are average values for individual engine loads and observations.

3.1 Thermodynamic changes

The throttling of the cross area of the exhaust gas duct decreases pressure of exhaust gas after turbine and increases its temperature before and after turbine. Fig.2a shows visible changes of exhaust gas pressure. According to results presented in Fig.2e and Fig.2f temperature of exhaust gas before and after turbine increases average of 2% for the throttling with angle 21deg. and 5% for the throttling with angle 71deg. Changes in temperature and pressure of exhaust gas are so insignificant that there do not affect the speed of turbocharger. Mentioned speed is presented in Fig.2b. Lack of changes in speed of turbocharger takes effect no changes in pressure of air, delivered to the engine. Pressure of air after air cooler is presented in Fig.2c. Abnormalities in the combustion process causes growth of fuel consumption. Figure 2d shows measured fuel consumption for all considered states of the engine. The throttling of the exhaust gas duct by change of the barrier angle by 21deg. causes average increase of fuel consumption by 3,7% and 8,2% for changing the barrier angle by 71deg respectively. It should be noted that the fuel consumption is very important parameter from an economic point of view but in a practical marine applications very difficult to measure.

Assuming the measuring thermodynamic parameters are not enough to indicate abnormal throttling of the exhaust gas duct. According to presented results best indicator of the throttling of the exhaust gas duct among considered thermodynamic parameters of the engine is pressure of exhaust gas after turbine. Unfortunately mentioned pressure is usually very little and for this reason technically difficult to measure during on-board operation.

3.2 Exhaust gas composition changes

Figure 4a presents oxygen mole fraction in exhaust gas. According to presented results increasing the throttling of the exhaust gas duct decreases mole fraction of oxygen in exhaust gas.

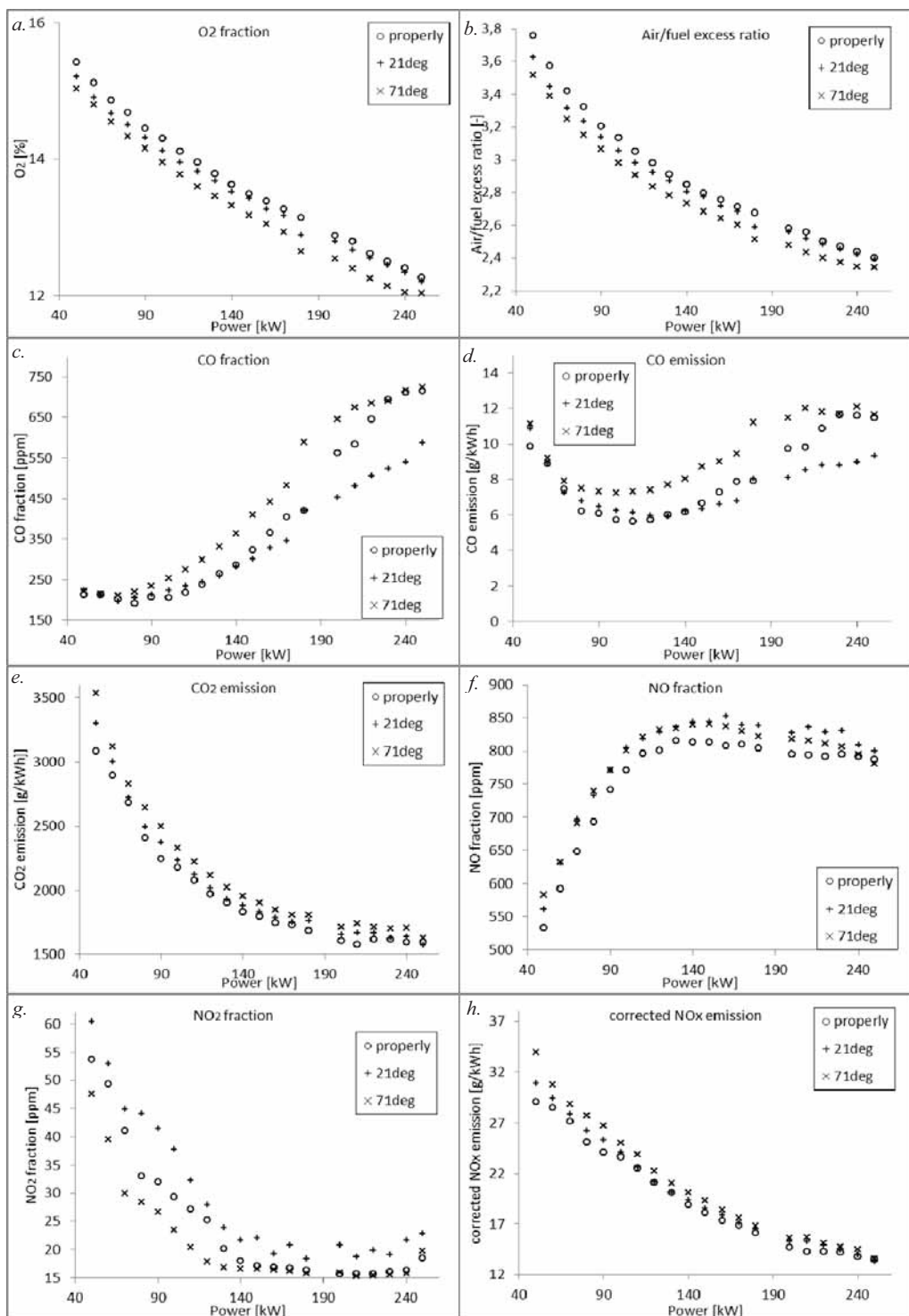


Fig.4. Exhaust gas composition: a. Oxygen fraction, b. Air-fuel excess ratio, c. Carbon oxide fraction, d. Carbon oxide emission, e. Carbon dioxide emission, f. Nitric oxide fraction, g. Nitric dioxide fraction, h. Corrected nitric oxides emission

It means that though not changed pressure of air after air cooler (Fig.2c) and turbocharger speed (Fig.2b) the quantity of air delivered to the engine decrease. The reason of this situation is increasing temperature of air. Simultaneously with this phenomenon the quantity of delivered fuel is increase. The effect of this is combustion richest mixtures in cylinders. The confirmation of this state of affairs is decreasing of air-fuel excess ratio. Figure 4b presents dependences between calculated air-fuel excess ratio and the load of the engine in the different throttling of the exhaust gas duct.

The air-fuel excess ratio was calculated according to the following dependence:

$$\lambda = \frac{21\%O_2}{21\%O_2 - U_{O_2}}, \quad (1)$$

where:

- λ – air-fuel excess ratio [-],
- $21\%O_2$ – mole fraction of oxygen in air,
- U_{O_2} – mole fraction of oxygen in exhaust gas.

Similarly to earlier presented results the air-fuel excess ratio decreases average by 1,8% for the 21deg. angle of barrier in the exhaust gas duct. The 71deg. angle of barrier in the exhaust gas duct causes decreasing of the air-fuel excess ratio average by 4,5%. The effect of the throttling is more apparent in high load conditions. Decreasing among of air delivered to engine cylinders causes the combustion process of a mixture consisting of more fuel. This situation promotes extension of the combustion process in time [8]. The effect of this is increasing the exhaust gas temperature after and before the turbine (Fig.2e and Fig.2f).

As mentioned earlier during the throttling of the cross section area of the exhaust gas duct the richest mixture is combusted in engine cylinders. This phenomenon takes effect of deteriorations in the combustion process and changes with carbon oxide fractions in exhaust gas. Figure 4c shows dependences between the mole fraction of carbon oxide in exhaust gas and load of the engine and the throttling of the exhaust gas duct. The exhaust gas duct throttling causes increasing of mole fraction of carbon oxide in low loads of the engine. The maximum load of the engine decreases of mentioned mole fraction. The effect of decreasing of carbon oxide mole fraction is most visible during the little throttling. It means that the efficiency of the combustion process is changed with the load of the engine [9]. Figure 4d presents a level of carbon oxide emission from the engine for all considered loads of the engine and all considered states of malfunctions. Levels of emission of all mentioned chemical compounds of exhaust gas are calculated according to ISO 8178 standard regulations [10]. According to presented results the low throttling of the exhaust gas duct take effect low increase of carbon oxide emission in low loads of the engine. Average increase is 4,5%. Working the engine in loads from 140kW to 250kW decreases the carbon oxide emission level average by 14%. It should be noted that the throttling of the exhaust gas duct takes effect of changing the shape of both the carbon oxide mole fraction and the emission from the engine according to results from the “worked properly” engine. It means that the high throttling of the exhaust gas duct causes increasing of the carbon oxide emission level average for 5,1% for very low and very high loads of the engine and average for 26% for loads of the engine between 80kW and 210kW.

Increasing the dose of fuel delivered to the combustion process increases carbon dioxide fraction in exhaust gas [9]. Decreasing of the engine load and increasing of the throttling of the exhaust gas duct increase the carbon dioxide emission from the engine. Fig.4e presents the calculated emission level of carbon dioxide from engine. According to presented dependences the low exhaust gas duct throttling increases the level of carbon dioxide emission average by 3% in all considered loads of the engine. More appearance effects are in the higher throttling conditions.

The high throttling causes increasing of the carbon dioxide emission level average by 7%. Obtained results are compatible with results of increasing fuel consumptions (Fig.2d).

Figures 4f and 4g present dependence of the engine load on the mole fractions of nitric oxide and nitric dioxide in exhaust gas respectively. Low load of the engine take effect minimal fraction of nitric oxide and maximum fraction of nitric dioxide. During increasing load of the engine nitric dioxide mole fraction decreases but nitric oxide mole fraction increases. The relation between nitric oxides and nitric dioxides is like 8 to 1 in low loads of the engine and increases to 1 to 40 for high loads of the engine. Obtained results are qualitatively consistent with other results [6]. According to presented dependences the 21deg. throttling of the exhaust gas duct increases both the nitric oxide and nitric dioxide mole fraction in exhaust gas. Observed average increasing is 4,3% for nitric oxide and 21,4% for nitric dioxide respectively. The 71deg. throttling of the exhaust gas duct take different effect. During the high throttling nitric oxide increases average by 4% (similar to the 21seg. throttling) but at the same time mole fraction of nitric dioxide decreases in exhaust gas by 10% average for all considered loads of the engine. The explanation of this phenomenon is great changes in the combustion process. It's possible that changes of the throttling of the exhaust gas duct causes changing in chemical reactions during the combustion process. It should be noted that mole fractions of chemical compounds in exhaust gas not depends on an exhaust gas flow rate.

Fig.4h shows dependences between a corrected nitric oxides emission and the load of the engine and the throttling of the exhaust gas duct. The nitric oxides emission, calculated from a sum of nitric oxide and nitric dioxide mole fractions, depends not only on parameters of the working engine but on parameters of surrounded the engine air. Mentioned parameters are temperature, pressure and humidity of air. According to ISO 8178 standard regulations measured parameters of air for the nitric oxides correction are:

- pressure – 101,3kPa,
- temperature – 25°C,
- humidity – 10,71g_{H2O}/kg of air.

According to mentioned European Standard all emissions of nitric oxides from diesel engines measured in other air conditions must be corrected to standard parameters by using the correction formulas. The dependencies from Fig.4h show that, despite results presented in the Fig.4f and Fig.4g, increase the throttling of the exhaust gas duct increases the emission level of nitric oxides for all considered loads of the engine. Increasing of the load of the engine decreases the level of corrected nitric oxides emission. Changes of the nitric oxides emission with the throttling of the exhaust gas duct are little visible. For the 21deg. throttling the average increase of the nitric oxides emission is 2,7% and for the 71deg.% throttling the nitric oxides emission increases average by 6,7%.

Presented results show that the throttling of the exhaust gas duct causes visible changes of the oxygen and carbon oxide quantity in exhaust gas. Other measured gaseous components changed not significant during the throttling of the exhaust gas.

4. Conclusions

The paper presents results of laboratory tests carried out on the four-stroke diesel engine for marine applications. The study consisted in determining the impact of the throttling of the exhaust gas duct on the engine operating parameters including the composition of exhaust gas. The obtained results allow concluding that the measuring thermodynamic parameters are not enough to indicate the abnormal throttling of the exhaust gas duct. According to presented results best indicator of the throttling of the exhaust gas duct among considered thermodynamic parameters of

the engine is pressure of exhaust gas after turbine. Unfortunately mentioned pressure is usually very little and for this reason technically difficult to measure during on-board operation.

Presented results of exhaust gas composition show that the throttling of the exhaust gas duct causes visible changes of the oxygen and carbon oxide quantity in exhaust gas. Other measured gaseous components changed not significant during the throttling of exhaust gas.

Obtained results allow concluding that the composition of exhaust gas can give with its image important diagnostic signals about the technical condition of the engine exhaust gas duct.

Acknowledgments

The project was supported by the National Science Centre in Poland, granted on the basis of decision No. DEC-2011/01/D/ST8/07142

References

- [1] Kowalski J., *Laboratory study on influence of air duct throttling on exhaust gas composition in marine four-stroke diesel engine*, Journal of Kones Powertrain and Transport, Vol. 19, No 1, pp. 191 – 198, Warsaw 2012.
- [2] Kowalski J., *Wpływ wybranych niesprawności układu paliwowego na skład emitowanych spalin z czterosuwowego silnika okrętowego*, Zeszyty Naukowe Nr. 178A AMW w Gdyni, Wydawnictwo AMW w Gdyni, str. 133 – 138, Gdynia 2009.
- [3] Kowalski J., *Wpływ wybranych niesprawności układu doładowania na skład emitowanych spalin z czterosuwowego silnika okrętowego*, Zeszyty Naukowe Nr. 178A AMW w Gdyni, Wydawnictwo AMW w Gdyni, str. 139 – 144, Gdynia 2009.
- [4] Hountalas D.T., Kouremenos A.D., *Development and application of a fully automatic troubleshooting method for large marine diesel engines*, Applied Thermal Engineering, Vol. 19, pp. 299-324, Elsevier 1999.
- [5] Hountalas D.T., *Prediction of marine diesel engine performance under fault conditions*, Applied Thermal Engineering, Vol. 20, pp. 1753-1783, Elsevier 2000.
- [6] Kuo K.k., *Principles of combustion*, Willey & Sons Inc., New Jersey 2005.
- [7] Poinot T., Veynante D., *Theoretical and numerical combustion*, Edwards 2005.
- [8] Kluj S., *Diagnostyka urządzeń okrętowych*, Studium Doskonalenia Kadr S. C. WSM, Gdynia 1995.
- [9] Heywood J. B., *Internal Combustion Engine Fundamentals*, McGraw-Hill 1988.
- [10] ISO 8178 - *Reciprocating internal combustion engines*.



CONTROL ALGORITHM ENGINE COOLING SYSTEM WITH INCREASED COOLANT TEMPERATURE

Rafał Krakowski

Faculty of Marine Engineering
ul. Morska 83, 81-225 Gdynia, Poland
tel.: +48 58 6901398
e-mail: r.krakowski@am.gdynia.pl

Abstract

The article presents the test stand dedicated to research the cooling system of elevated coolant temperature. The test stand was developed in the software simulation AmeSim and the corresponding model was built. The temperature of this liquid was increased to the temperature of boiling water, as a basic compound of the cooling liquid. This system was designed for the four cylinder diesel engine 4CT90 with indirect fuel injection system. Intensity of the cooling, protected against too higher pressure, were changed by switching short and large liquid circulation and one or two fans of the cooler. Overpressure inside the cooling system was limited to 0,2 MPa, the temperature inside the cooling system was increased to 125°C. It was shown that it is possible to maintain the assumed constant pressure in the system and obtain at the elevated temperature of the liquid, leading to increased economic efficiency of the engine. The control algorithm to use of specific control procedures of cooling intensity in the pressure cooling system was developed. In the software simulation and the model stand liquid temperature and pressure course in selected points of system were determined. The characteristics obtained in the simulation software, and the model stand were designated using the developed algorithm. The software simulation was used electronic controls, while the model stand manually was controlled.

Keywords: : algorithm, combustion engines, cooling systems, higher coolant temperature, simulation

1. Introduction

Internal combustion engines, which are characterized by low efficiency, are still commonly used for vehicle propulsion. Work is currently underway on the introduction of hybrid vehicles, but due to technical difficulties, their use is still the matter of the future. Therefore, research on the development of internal combustion engines in the direction of increasing efficiency and reducing toxic exhaust are still being carried [7].

In the piston internal combustion engines, the most popular means of cooling is the cooling liquid, which provides a more uniform temperature around the combustion chamber than direct cooling air. In case of exceeding the boiling point must be a corresponding increase of pressure [3 - 5].

Efficiency of liquid cooling systems can be improved by use of electronic control unit, as well as less intense cooling of the engine and thus reduction the heat loss [2].

2. Test stands for testing the cooling system at elevated coolant temperature

In AMESIM software was developed the model stand scheme expressed with the help of

flowcharts and was performed calculations and simulations showing the courses of pressure and temperature for the assumed parameters of pressure [8]. The model of the cooling system was made on the basis of test stand solutions designed and built using the original components of diesel engine 4CT90 (Fig. 1). The primary source of heat of the test stand are three heating elements with different electrical power adjacent to the walls of each cylinder.

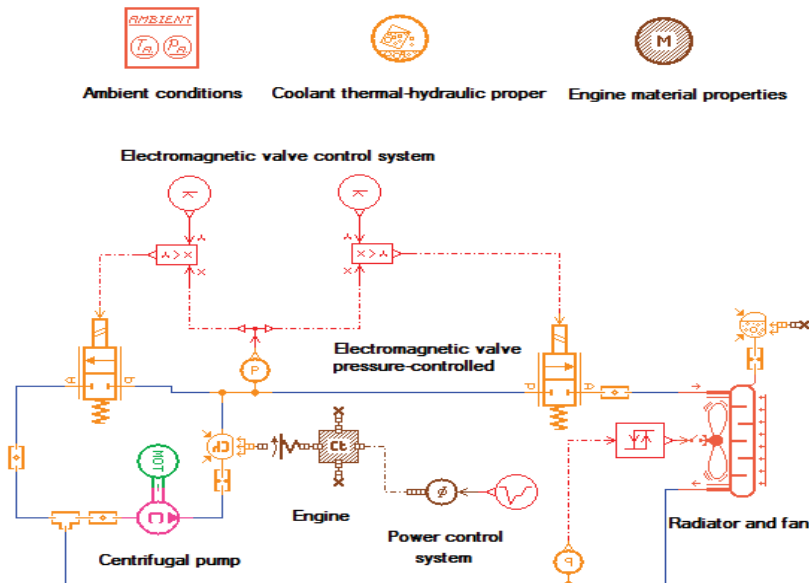


Fig. 1. Model stand scheme of cooling system developed in AMESIM software

In the presented model are elements which represent the engine block along with the system responsible for removing heat from the walls and transferring it to the coolant. The control system, through the change of power of heating, enables regulation of heat which is discharged by the cooling system. Electrically driven centrifugal pump with adjustable speed was used. Because of that, cooling intensity was not related to the assumed engine speed. The flow of liquid between the short and large circulation was controlled by pressure regulated solenoid valves. In order to perform the calculation of the cooling circuit parameters (temperature and pressure of liquid, coolant pump flow, operational characteristics of pumps and valves), was necessary to introduce a large amount of data including, first of all, the liquid properties, material properties of the engine, environment parameters, the volume of liquid in a small and a large circulation, the mass of the engine, etc. Detailed information was introduced according to the requirements of the program.

The experimental stand was built using original elements and units of the 4CT90 engine (Fig. 2a). Thermal energy of combustion process was simulated by units of electric immersion heaters, installed in every cylinder, fed from the electric network (Fig. 2b). Immersion heaters had a length of the stroke of the piston and were divided into three segments with different power: the highest of any segment of the heater power had 2,5 kW, central one had 1,5 kW, and the lowest one had a power of 1 kW. The test stand was equipped with thermoelements located in the engine block and the head, as well as into thermoelements placed in the system of heat exchange with the environment.

Two cooling fans placed in the channels with the sensors to enable measurement of the temperature and the rate of air flow. Channels of cooling liquid during measurements were shielded with foam reducing losses of the heat. The centrifugal water pump was driven with the electric motor, which the rotation speed was controlled with the programmed inverter what

enabled to control intensity of cooling by changing the coolant flow rate [4, 7]. Flow of liquid between the short and large circulation, was controlled by solenoid valves. The pressure in the system was measured with the electric manometer.

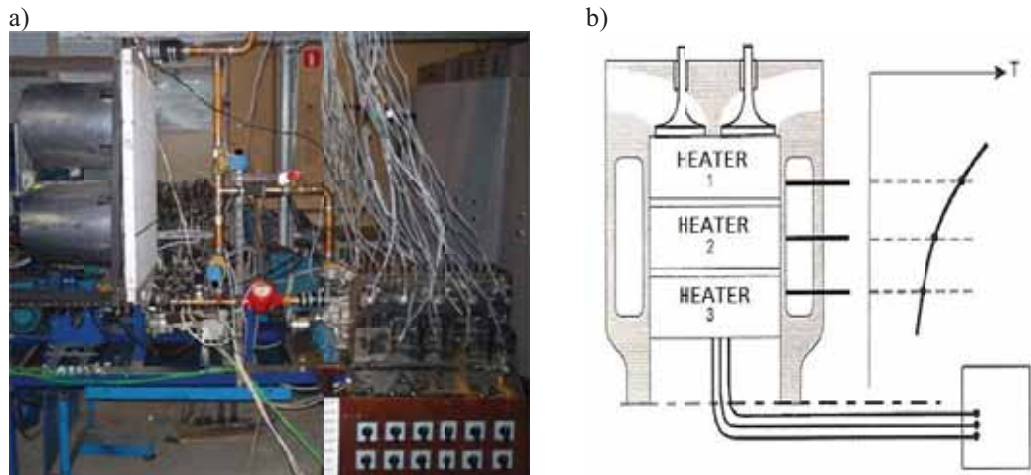


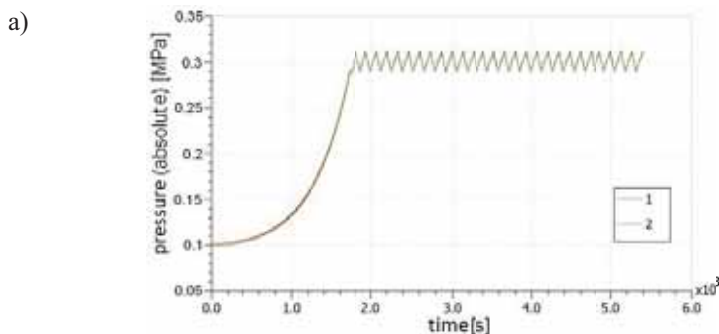
Fig. 2. The experimental research stand for cooling systems investigation: a) stand view, b) the heaters placement inside the engine cylinders [6]

3. Characteristics performed in the software simulation and on the model stand

3.1. Results of the simulation in AmeSim software

Simulations were performed for overpressure of 0,2 MPa at 80% of the filling with coolant at a total volume of 11 dm³.

As a result of the simulation characteristics of the liquid temperature course before and after the cooler and the output from the engine, and the liquid pressure course in the short and full circulation were determined.



For about 27 minutes followed the gentle increase overpressure of 0,2 MPa. After this time, it was necessary to maintain pressure on the average value of 0,2 MPa within 0,19 ÷ 0,21 MPa by changing the intensity of cooling (Fig. 3a).

At 80% of the coolant filling level, the temperature at the exit of the engine increased to 125°C, while at the exit of the radiator temperatures ranged 97°C ÷ 120°C (Fig. 3b). Courses characteristics due to switch between short and large circuits, the speed of the water pump and

turn on and off the fan or fans, the pressure course was characterized by a relatively high homogeneity and stability throughout the heating cycle lasting about 100 minutes.

b)

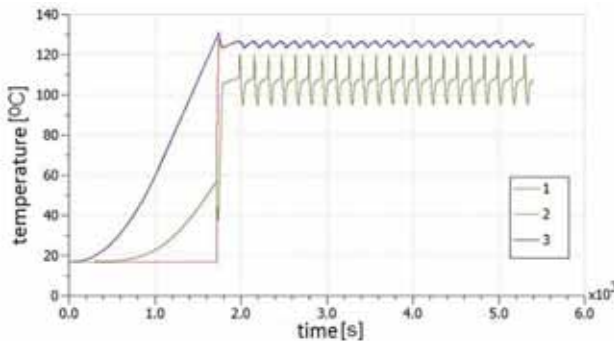


Fig. 3. Courses characteristics at the overpressure of 0,2 MPa and 80% of the coolant filling level: a) pressure: 1 - short circuit, 2 - large circuit, b) temperature: 1 - entrance to the radiator, 2 - out of the radiator, 3 - out of the cylinder block

3.2. Results on the model stand

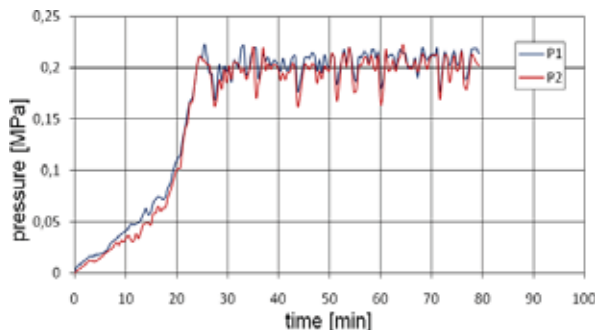
Experimental research was carried out on a model of diesel engine 4CT90 at the overpressure of 0,2 MPa and 80% filling of liquid system. The courses characteristics of coolants temperature before and after the radiator and the output from the engine, moreover the courses characteristics of coolants pressure in the small and large circulation were made.

The cooling system was heated up in the small system about 24 minutes when the pressure in the system received established value, the system switched from small to large circulation, resulting in pressure reduced to about 0,17 MPa, and its value ranged $0,17 \div 0,22$ MPa (Fig. 4a). The temperature dropped about 10°C , but it was possible to achieve maximum value at 120°C (Fig. 4b).

Analyzing graphs of the simulation and experimental research, it is noted that the results are very similar, which indicates that the properly constructed simulation model mimics the action of the corresponding experimental engine cooling system. The characteristics show some differences, which may also derive from the fact that the mathematical model used an electronic control of all processes, whereas in studies of actual control takes place by hand.

As in the case of simulation characteristics courses result coming from switching between the short and full circulation, change the water pump speed, and turn on and off the fan or fans.

a)



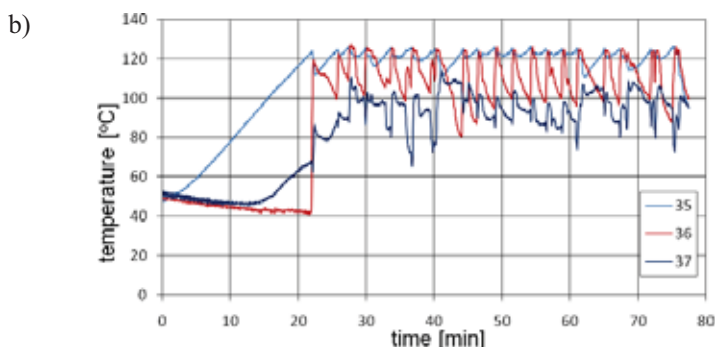


Fig. 4. Courses characteristics at the pressure of 0,2 MPa and 80% of the filling with coolant: a) pressure: P1 - small circuit, P2 - large circuit, b) temperature: 35 - out of the cylinder block, 36 - entrance to the radiator, 37 - out of the radiator

4. The working algorithm of the pressure cooling system

Cooling intensity at the model stand was controlled manually. Based on experience gained during this control, the algorithm was developed which enables the construction of the automatic control of cooling system [1].

Given control algorithm ensures the maintenance of assumed pressure, resulting in a rise in temperature. In a logical and efficient use of the individual controls on the engine cooling intensity, depending on the needs of the moment.

The algorithm assumes gradual of the various methods of changes in cooling intensity in the system until the moment when at all operating levels of cooling system, the pressure reaches a critical value in large circulation (Fig. 5).

When power is turned on the cooling liquid flows in the short circuit, after reaching assumed pressure, the system switches to a large circuit.

When the pressure drops below a set, the system switches back to the small circulation. When the system operates on the large circulation, the pressure control is done by increasing or decreasing the speed of the coolant pump.

Another level of control the intensity of cooling is switching on and off one or two fans. Despite work of two fans at the same time, still will be a further increase in pressure to achieve the critical pressure, the control system will give a signal to the decrease in load until the engine stops completely (in this case the electric heaters will be turned off).

The algorithm assumes a step regulation of the pump speed in order to simplify the algorithm. Modulating control (smooth) inverter operation is also possible, but requires the use of the controller with the possibility of analyzing the analog signal. If you need an easy way, by multiplying the number of blocks increase the speed of decision-making or to build a pump control algorithm continuously with appropriate parameters.

Marked pressure parameters can be determined depending on the physical properties of the system and therefore the algorithm is not given a specific value. These values can be stored in a separate table without having to type them into the algorithm.

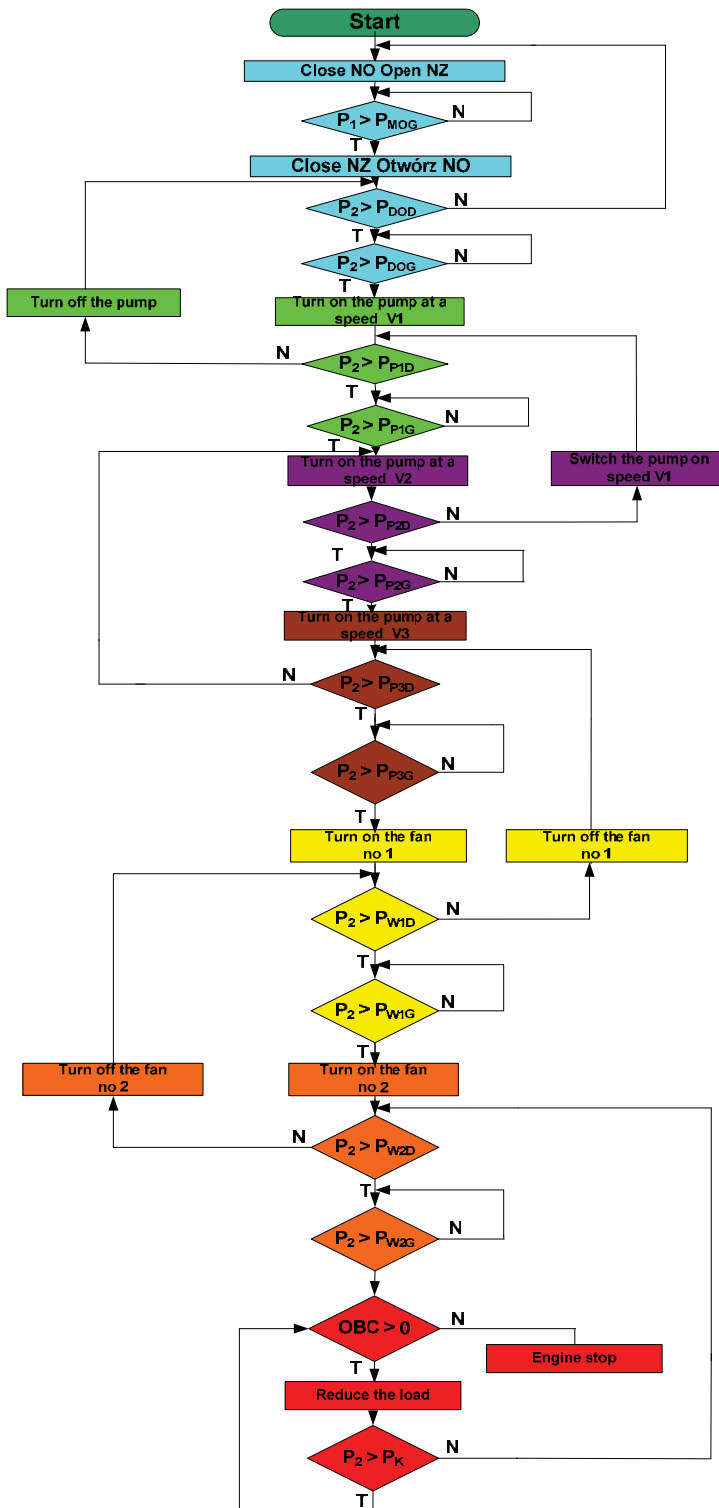


Fig. 5. The algorithm controls the cooling intensity

Tab. 1. Description of signs used in the algorithm

| No. | DESIGNATION | DESCRIPTION |
|-----|--------------|---|
| 1 | Blue color | The algorithm applies to control solenoid valves (switching between circuits, large and short) |
| 2 | Green color | The algorithm applies to the pump regulation at a speed of V_1 and open valve of the large circuit |
| 3 | Purple color | The algorithm applies to the pump regulation at a speed of V_2 and open valve of the large circuit |
| 4 | Brown color | The algorithm applies to the pump regulation at a speed of V_3 and open valve of the large circuit |
| 5 | Yellow color | The algorithm applies to the fan control No 1 with working pump on high speed and open valve of the large circuit |
| 6 | Orange color | The algorithm applies to the fan control No 2 with working pump and fan No 1 and open open valve of the large circuit |
| 7 | Red color | The algorithm applies to the system critical pressure control |
| 8 | P_1, P_2 | Pressures measured in the short (P_1) and large (P_2) system |
| 9 | P_{MOG} | Established upper value of the pressure maintained in the short system |
| 10 | P_{DOD} | Established lower value of the pressure maintained in the large system |
| 11 | P_{DOG} | Established upper value of the pressure maintained in the large system |
| 12 | P_{PID} | Established lower value of the pressure maintained in the large system at V_1 speed pump |
| 13 | P_{PIG} | Established upper value of the pressure maintained in the large system at V_1 speed pump |
| 14 | P_{P2D} | Established lower value of the pressure maintained in the large system at V_2 speed pump |
| 15 | P_{P2G} | Established upper value of the pressure maintained in the large system at V_2 speed pump |
| 16 | P_{P3D} | Established lower value of the pressure maintained in the large system at V_3 speed pump |
| 17 | P_{P3G} | Established upper value of the pressure maintained in the large system at V_3 speed pump |
| 18 | P_{W1D} | Established lower value of the pressure maintained in the large system with working fan No 1 |
| 19 | P_{W1G} | Established upper value of the pressure maintained in the large system with working fan No 1 |

| No. | DESIGNATION | DESCRIPTION |
|-----|----------------|---|
| 20 | P_{W2D} | Established lower value of the pressure maintained in the large system with working fan No 2 |
| 21 | P_{W2G} | Established upper value of the pressure maintained in the large system with working fan No 2 |
| 22 | NO | Normally open valve |
| 23 | NZ | Normally closed valve |
| 24 | V_1 :- V_3 | The pump speed |
| 25 | P_K | The critical pressure above which should reduce the load on the engine or turn off the engine |
| 26 | OBC | Engine load |

5. Conclusions

As a result of simulation studies was found that temperatures can be maintained at nearly constant level in the block and head, and at the entrance and exit of the engine in this field of research. This means that one can control the system so it is possible to maintain the pressure and temperature at a given level and within acceptable limits.

During the studies the algorithm, which will allow to construct the automatic control of cooling system was developed. The algorithm ensures the sustaining of assumed pressure, resulting in a rise in temperature. In a logical and efficient use of the individual controls on the engine cooling intensity, depending on the needs of the moment.

The algorithm assumes gradual of the various methods of changes in cooling intensity in the system until the moment when at all operating levels of cooling system, the pressure reaches a critical value in the large circulation.

Adopting developed control algorithm of cooling intensity requires designing and building from scratch some bands of the pressure cooling system, for a very difficult and sometimes impossible task was to find existing standard components to the target system (eg pumps, flow meters, solenoid valves with adjustable bandwidth etc.).

References

- [1] Banachowski L., Diks K., W. Rytter W., *Algorytmy i struktury danych*, WNT, Warszawa 2006.
- [2] Kneba Z., *Kompleksowy model nowej generacji układu chłodzenia silnika spalinowego. Silniki spalinowe*, SC1/2007.
- [3] Luft S., *Podstawy budowy silników*. WKŁ, Warszawa 2006.
- [4] Ogrodzki, A., *Chłodzenie trakcyjnych silników spalinowych*, WKŁ, Warszawa 1974.
- [5] Walentyłowicz J., *Chłodzenie tłokowych silników spalinowych*, WPT nr 12/1996.
- [6] Walentyłowicz J., Kałdoński T., Szczęch L., Karczewski M., Rajewski M.: *Układ chłodzenia tłokowego silnika spalinowego o podwyższonej temperaturze płynu chłodzącego*. Raport z realizacji projektu PBG 457/01, WAT, Warszawa 2003.
- [7] Walentyłowicz, J., Krakowski, R., *Modeling of the higher pressure cooling system for transport vehicles engines*, TRANSPORT PROBLEMS, Vol. 5, No 4, 2010.
- [8] www.amesim.com.



THE INFLUENCE OF THE REGULATION METHOD OF COOLING PUMP PERFORMANCE, AT HEAT TRANSFER INTENSITY IN THE PRESSURE COOLING SYSTEM

Rafał Krakowski

Faculty of Marine Engineering
ul. Morska 83, 81-225 Gdynia, Poland
tel.: +48 58 6901398
e-mail: r.krakowski@am.gdynia.pl

Abstract

This paper presents a model test stand for testing the cooling system with increased coolant temperature. On the model stand, as a result of the research, determined the characteristics of temperature and pressure courses coolant. The study was preceded by the determination of the intensity of the liquid flowing out of the engine block and flowing through the radiator as a function of the opening of the valve throttling the flow of liquid and as a function of speed water pump. An adjustable valve was located in the water outlet duct of the engine. During the test the cooling system was filled with coolant at 90%. After preliminary studies, the degree of filling of the liquid was found to be optimal, because the greater the amount of water in the system observed difficulties in obtaining elevated temperature, whereas at lower amounts of liquid vortex centrifugal pump had problems with the rib. Then, the characteristics of the two ways of controlling the pump capacity were made, ie by throttling the discharge and change in speed. The characteristics indicate that the first way to adjustment of the pump flow rate and thus cooling intensity was less effective, because a small amount of throttling was not affect the change. The second way to adjustment of the liquid flow rate with changes in the speed of the water pump was more efficient, because it was easier to maintain the pressure established in the cooling system.

Keywords: internal combustion engines, cooling system, model research, pump capacity

1. Introduction

Piston internal combustion engines are still widely used for the propulsion of vehicles and work on their development are carried out, inter alia, to increase their efficiency. It is now widely used method of cooling is liquid cooling.

One way to improve the efficiency of the currently used internal combustion engines is a more accurate control of individual motor units, reducing heat loss resulting from the cooling and heat escaping from the exhaust (turbine drive air compressor) [5, 7].

So far, the known ways of reducing the loss of cooling and radiation was the use shielding of the engine and the so-called adiabatyization, the shielding walls of the combustion chamber with ceramic liners. So far, this is the way expensive, and used in piston engines are unreliable and ineffective [1, 3]. In the case of direct engine cooling air, which allows the maximum increase in temperature of the engine components, there are also problems of uniform cooling of the individual cylinders of the engine and the head of a wide range of engine speed and engine load

For this reason, the most popular and widely used method of cooling is the cooling liquid, which provides a more uniform temperature around the combustion chamber, although the

properties of the water is limited by the maximum temperature of the coolant.

Efficiency of liquid cooling systems as a comprehensive unit of energy management in vehicles, can be improved by the electronic control unit work, as well as the less intense cooling of the engine and thus reducing heat loss [2, 4].

The aim of this study was to determine the effect of adjustment performance of cooling water pump on the intensity of the heat transfer in the pressure cooling system.

2. The research object

The model test stand was built using original components and assemblies, where are used the cylinder block and head diesel engine 4CT90 (Fig. 1).

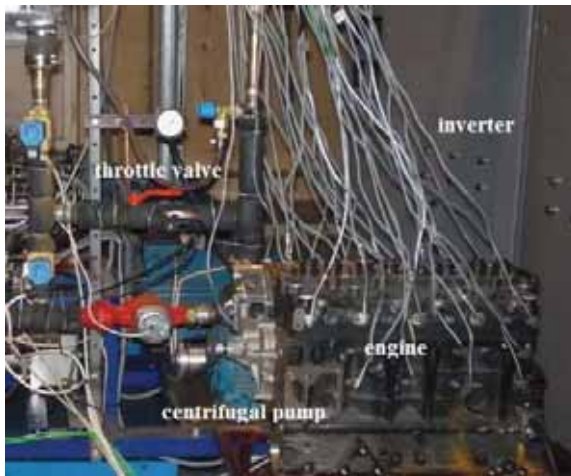


Fig. 1. The stand to research the influence of the regulation method of cooling pump performance



Fig. 2. View of the radial centrifugal coolant pump of the engine 4CT90

The cooling system was designed to operate with increased internal pressure, and consisted of the following components:

- radiator with two fans,
- flowmeter for measuring the flow of water in the system,
- unit thermocouples inside the block and cylinder head,
- water pump drive unit,
- engine block heaters,
- gauges to measure the pressure inside the system.

Inside each cylinder was placed heaters of different power. The test stand was equipped with a thermocouples located in the engine block and head, as well as the thermocouples placed in the heat exchange system with the environment. Thermocouples were connected to the computer temperature meter with three analog-to-digital measurement cards APCI-3200. Two fans provided in the channels with sensors to enable measurement of the temperature and air velocity. Water centrifugal pump was driven by an electric motor whose rotational speed was controlled in a programmed inverter, allowing control of cooling intensity by changing the coolant flow rate [6, 8]. The flow of liquid between large and small circuits was controlled by solenoid valves.

Electronic manometer with pressure transducer A-10 Danfoss and needle manometer the extent of 0,147 MPa were used to measure the pressure in the cooling system. Electronic pressure transducers connected to the measurement cards with special software that allows the configuration and execution of measurement.

3. The results of the cooling system as a model stand

Research of the effect of adjustment performance of cooling water pump on the intensity of the heat transfer was preceded by determining the intensity of the liquid flowing out of the engine block and flowing through the radiator as a function of the opening of the throttle valve and fluid flow as a function of speed water pump. As a measure of valve opening the number of valve rotation was assumed from the fully open position to the closed valve position. The total adjustment range was 6 rotation dial valve. Changes in flow rate as a function of the number of the valve revolutions and rotational speed of the water pump shown in Fig. 3

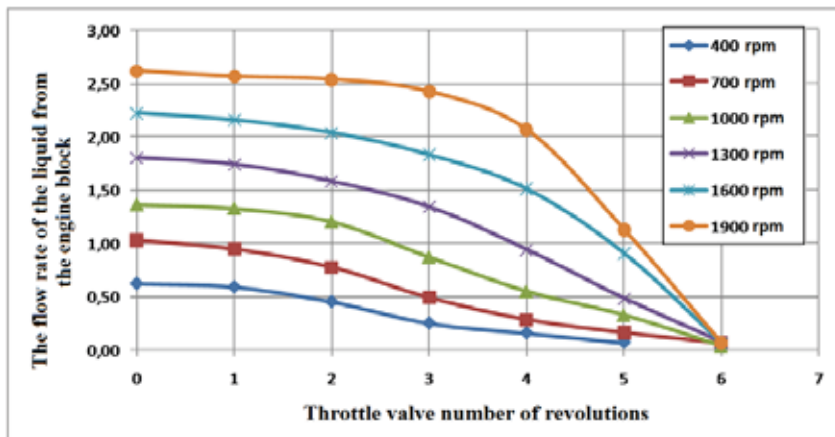


Fig. 3. The effect of the number of valve revolutions on the flow rate of coolant from the engine block at different speeds of the liquid pump

During the first cycle tests were performed with capacity control coolant flow by means of the throttle valve setting. The impact of this control method on the ability to maintain and stability of the pressure in the cooling system and its effect on the control of the intensity of cooling was checked. The water pump speed was set to $n = 500$ rev/min and was maintained at a constant level throughout the test. The valve at the water outlet from the engine engine was set in six positions, including a fully open position.

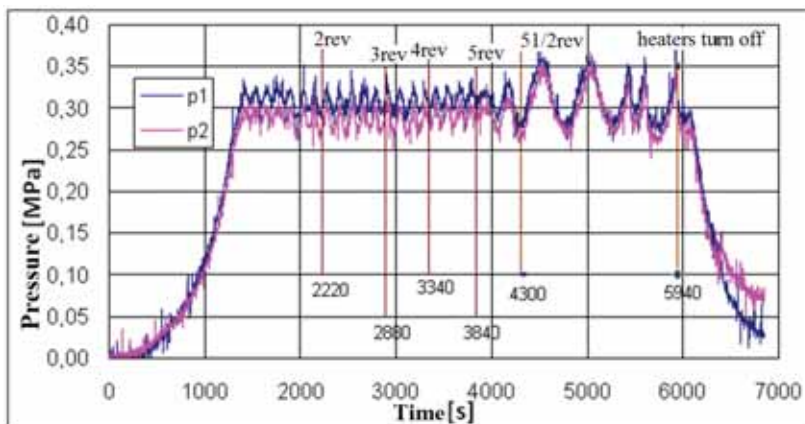


Fig. 4. Overpressure courses in the cooling system at 90% of the system filling in the coolant with flow control by a valve: p1 - overpressure at the outlet from the engine, p2- overpressure behind the radiator (the upper description - tap number of revolutions, the description of the bottom - time throttling settings)

After the warm-up and fully open the water valve, control the intensity of cooling takes place by switching on and off one or two fans at the same time so that the overpressure in the large circulation was about 0,3 MPa. In this way, you could keep the overpressure established between 0,28 ÷ 0,31 MPa (Fig. 4). In the figure, courses pressure of transducer placed at the liquid outlet from the engine P1 and behind the radiator P2.

After warming up the system and reducing the flow of coolant to the fourth rotation tap water valve, throttling growth generally did not affect the overpressure courses in the system (Fig. 4). Fluid overpressure behind the engine block was slightly higher than the overpressure behind the radiator. At the the liquid flow fans were switched on at the same time for several seconds at about 2 minutes regardless of throttling the flow of liquid, and the temperature inside the fan channels changed in the range 30 ÷ 58°C (Fig. 5). The air temperature was below in the channel of the lower fan.

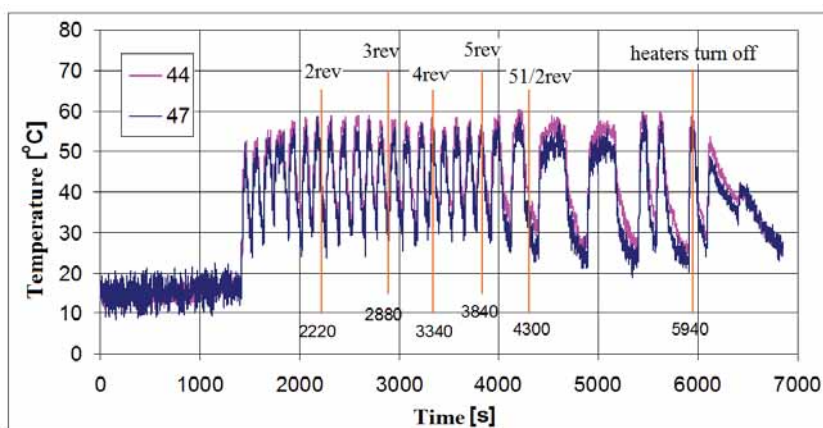


Fig. 5. Temperature courses in the fans channel at 90% of the system filling in the coolant with flow control by a valve: 44 - top fan, 47 - bottom fan
(the upper description - tap number of revolutions, the description of the bottom - time throttling settings)

Try to turn on individual fans reduced the response time of the system and cause an excessive increase in overpressure in the cooling system. The difference between the temperature of the liquid at the inlet and outlet of the radiator was on average about 15 ÷ 20°C (Fig. 6). Coolant temperature changes in the engine block were smaller, and their amplitude changes in the range of valve opening was about 5°C near the inlet to the engine block (head before 1 cylinder) and head on the other side of the engine block (head behind 4 cylinder). Temperature of the liquid for the fourth cylinder was about 5°C higher than that of the head from the side of the coolant flow (Fig. 7).

Reducing the liquid flow of 5 (3840 seconds) and 5,5 rotation of tap valve (4300 seconds) resulted in an excessive throttling of the flow and as a result it was necessary to extend the cooling time of the liquid in the radiator to reduce the pressure, as shown in temperature courses in the fans channels (Fig. 5). Temperature of the cooling liquid behind the cooler in period of cooling was much lower and reached values of about 75°C at 5 rotations of valve, and spin of the valve of 5,5 rotation even reached 55°C (Fig. 6).

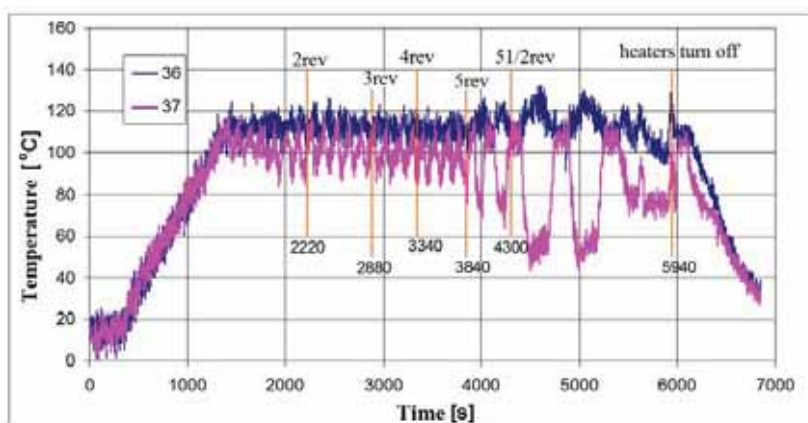


Fig. 6. Temperature courses in the cooling system at 90 % of the system filling in the coolant with flow control by a valve: 36 – flow of the liquid to the cooler, 37 – outflow of the liquid from the cooler (the upper description - tap number of revolutions, the description of the bottom - time throttling settings)

Moreover, with such a large flow throttling was difficult to obtain reproducible courses pressure and temperature, as can be seen between 4000 and 6000 second of measurement. Range overpressure changes in the cooling system increased significantly and overpressure changed in the range 0,26 ÷ 0,37 MPa (Fig. 4), and temperature changes in the cylinder head ranged from 110°C to nearly 130°C (Fig. 7).

The characteristics that were presented to show that method of adjustment the coolant flow by throttling valve located in the the water outlet channel of the engine, and thus the intensity of the cooling is not efficient, because small changes of throttle do not affect the changes in operating parameters of the system, while at increased throttling is overcool of the liquid in the radiator and a growing range of overpressure changes.

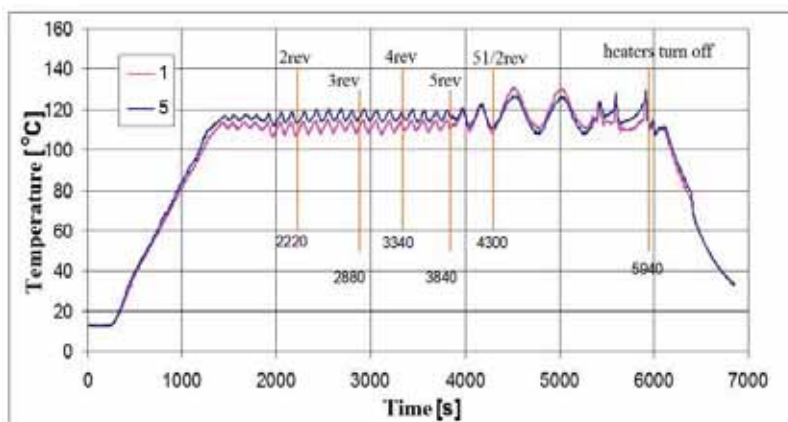


Fig. 7. Temperature courses in the cooling system at 90 % of the system filling in the coolant with flow control by a valve: 1 – engine head before 1 cylinder, 5 – engine head behind 4 cylinder (the upper description - tap number of revolutions, the description of the bottom - time throttling settings)

The second way to control the flow of liquid through the cooling system was control by changing the flow rotation speed of the water pump. The rotational speed of the electric motor which drives the pump was varied from 200 to 800 rev/min, the ratio of $i = 2,4$ gave the change of speed of the pump impeller 480 to 1920 rev/min.

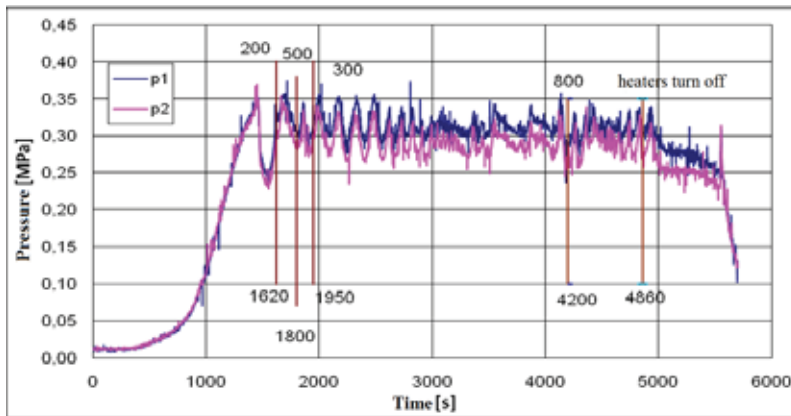


Fig. 8. Overpressure courses in the cooling system at 90% of the system filling in the coolant with speed control of the water pump: p1 – overpressure at the outlet from the engine, p2- overpressure behind the radiator

(the upper description – pump engine speed, the description of the bottom – rotation speed change time)

Figure 8 shows characteristic of the overpressure course which changed initially between $0,25 \div 0,35$ MPa, and then between $0,27 \div 0,32$ MPa. In Figure 9 it can be seen also the appearance of spontaneous circulation in the cooling system water after about 1000 seconds. When the water pump is turned off, it was caused by a phenomenon called thermosyphon, which is caused by a tilted heated water, due to its lower density and fall of cold water. After reaching the assumed overpressure (0,35 MPa) launched successively lower and upper fan.

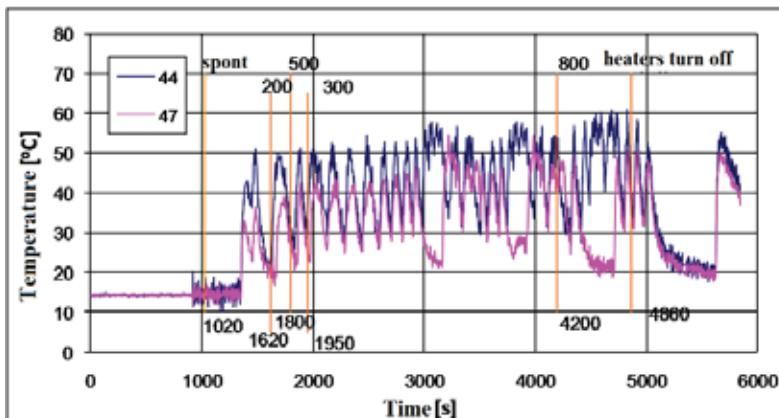


Fig. 9. Temperature courses in the fans channel at 90% of the system filling in the coolant with speed control of the water pump: 44 – upper fan, 47 – lower fan

(the upper description – pump engine speed, the description of the bottom – rotation speed change time)

The next level of intensity of the cooling when the operating fan was not able to maintain the established pressure, was to start the engine of the water pump, initially at a speed of 200 rev/min (pump speed was $n_p = 480$ rev/min), and then the speed was increased to $n = 500$ rev/min ($n_p = 1200$ rev/min) and after some time, pump engine speed reduced to $n = 300$ rev/min ($n_p = 720$ rev/min). In about 4200 seconds to maintain established overpressure require increased engine speed drive the water pump to $n = 800$ rev/min ($n_p = 1920$ to rev/min).

Adjusting with variable speed water pump was more effective than control performance by throttling the discharge, because it was easier to maintain established overpressure. System quickly reacted to changes in pump speed, temperature and pressure courses were generally characterized

by greater uniformity. In paragraphs 44 and 47 has changed nature of the courses between 3000 and 4000s and 4200 and 4800 s, because intensity control was tested with a single cooling fan to maintain a temperature of the coolant escaping from the radiator to the highest possible level. During this time, the work change or one fan, or two at a time. In the 4000 second worked two fans, but despite this it was necessary to increase the pump motor speed to 800 rev/min to maintain the established overpressure in the cooling system. Next cooling intensity control was done by means of fans. Temperature of the air flowing through the radiator changed within $23 \div 50^{\circ}\text{C}$ (T44 and T47), and at the end of the cycle, the temperature in the upper fan channel even temporarily increased to 60°C (Fig. 9).

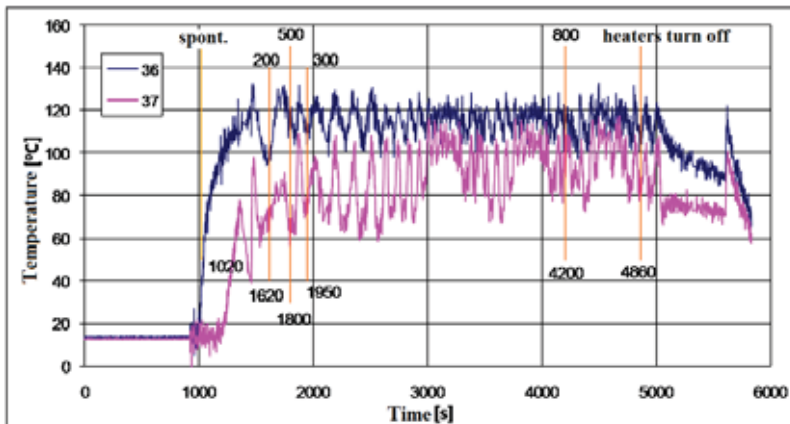


Fig. 10. Temperature courses in the cooling system at 90% of the system filling in the coolant with speed control of the water pump: 36 – flow of the liquid to the cooler, 37 – outflow of the liquid from the cooler
(the upper description – pump engine speed, the description of the bottom – rotation speed change time)

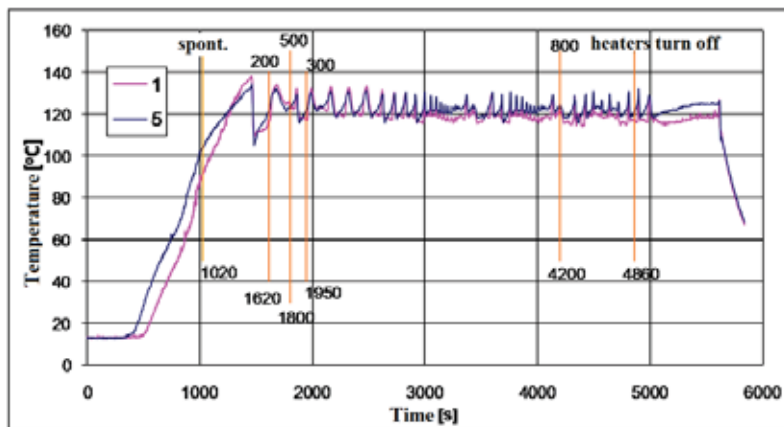


Fig. 11. Temperature courses in the cooling system at 90% of the system filling in the coolant with speed control of the water pump: 1 – engine head before 1 cylinder, 5 – engine head behind 4 cylinder
(the upper description – pump engine speed, the description of the bottom – rotation speed change time)

The temperature of the coolant flowing to the radiator (T36) changed within the limits of $110 \div 130^{\circ}\text{C}$ throughout the study period, while the temperature of the coolant flowing (T37) from the radiator was lower and was at the level of 70 to 105°C and increased up to 112°C (Fig. 10). Courses temperature in the cylinder head are characterized by relatively high uniformity, and the temperature measured in the head at point T1 and T5 varied in the range $120 \div 130^{\circ}\text{C}$ (Fig. 11).

The characteristics show that the method of adjustment by changing the intensity of the cooling speed, and thus the water pump flow rate, it is much more effective way to maintain required pressure and temperature. Courses of both temperature and pressure, as compared to the intensity of the throttle, are more uniform, and moreover is relatively easy to control the intensity of the cooling system.

4. Conclusions

During the test the cooling system was filled with coolant at 90%. The degree of filling of the liquid was recognized for the optimum preliminary studies because the greater amount of water in the system to cause difficulties in obtaining high temperatures, but with a smaller amount of liquid vortex centrifugal pump had problems with the rib.

During the study checked two ways to adjust the pump capacity, ie, by throttling the discharge and change of speed. The first way of pump flow control, and thus the intensity of the cooling is not efficient. Small throttling does not affect the change. Large throttling of flow causes significant the disorder, and work of water pump, similar to those that occur during the filling of a small liquid.

The second way to control the flow of liquid by means the pump speed changes of water is more effective than the control efficiency by throttling of the discharge. It is easier to maintain the pressure established. In addition, system more responsive to changes in pump speed, causing a corresponding change in the liquid flow rate. Therefore, the control flow by changing the speed of rotation was used in further studies.

References

- [1] Kawamura H., *Development of the ceramic adiabatic engine having 68% thermal efficiency*, ASME 2000 FALL TECHNICAL CONFERENCE, Peoria 2000.
- [2] Kneba Z., *Kompleksowy model nowej generacji układu chłodzenia silnika spalinowego*, Silniki Spalinowe, SC1/2007, R. 46.
- [3] Komo R., Bryzik W., *Adiabatic turbocompound diesel engine*, Paper D4.5 CIMAC CONGRES, Paryż 1983.
- [4] Krakowski R., *Wpływ podwyższonej temperatury płynu chłodzącego na zwiększenie ekonomiczności pracy tłokowego silnika spalinowego*, Zeszyty Naukowe Akademii Morskiej w Gdyni, 2011, nr 68.
- [5] Luft S., *Podstawy budowy silników*, WKŁ, Warszawa 2006.
- [6] Walentynowicz J., *Stanowisko testowe do badania układów chłodzenia silników spalinowych*, Journal of KONES, Vol. 14, 2007, No 4.
- [7] Walentynowicz J., *Wyznaczanie bilansu cieplnego silnika spalinowego o zapłonie samoczynnym*, Biuletyn WAT, 2006, nr 2.
- [11] Walentynowicz J., Krakowski R., *Decreasing of thermal energy loses in piston combustion engines*, RSM "System Level Thermal Management for Enhanced Platform Mobility" NATO RTO AVT – 178, Bucharest 4-7.10.2010.



INFLUENCE OF THE CRUISING SPEED OF A SHIP ON EXHAUST GAS BOILER EFFICACY

Jacek Krzyżanowski

Gdynia Maritime University
ul. Morska 83, 81-225 Gdynia, Poland
tel. +48 58 6901371
e-mail: jacekk@am.gdynia.pl

Abstract

The paper presents simulation calculations for a ship's power transmission system and the associated exhaust gas boiler with the aim of assessing the boiler's efficacy. Increasing prices of marine fuels force ship owners to limit the cruising speed of ships. This has negative impact on the operation of an exhaust gas boiler powered with exhaust fumes from the main engine. The boiler's capacity decreases, seriously limiting the tasks ascribed to vapour. Simulation calculations were conducted for the most typical system used on sea ships, i.e. a multi-turn engine and the associated exhaust gas boiler which generates saturated vapour. Adopting several values of ship cruising speed, which were smaller than the nominal speed, was a starting point for the calculations. Main engine powers were calculated with partial loads. Next, relevant values of excess air number were assigned to those powers and classic combustion calculations were conducted with the use of stoichiometric combustion equations. For assumed fumes temperatures in front of and behind the boiler drops in fumes enthalpy were noted. It enabled to calculate the values of heat fluxes released by the fumes in the boiler. After adopting relevant vapour parameters boiler capacities were evaluated as appropriate. Results of those calculations are shown in tables and on the graphs. The summary of the paper includes conclusions and suggestions which may be helpful as far as designing waste heat recovery systems is concerned.

Keywords: thermodynamics, heat transfer, marine power plants, marine steam boilers, marine diesel engines

1. Introduction

In recent years a systematic, or at times even a sudden, increase of marine fuels has been observed. With varying intensity, this phenomenon occurred before as "fuel crises" in the years 1973, 1979 and a number of subsequent years. It was characteristic that when fuel prices increased, ship owners resorted to recovery systems to increase power plant's efficiency and thus reduce the consumption of ever more expensive fuel. Over time, more and more advanced, and hence more expensive, deep waste heat recovery systems were introduced. Amortization period for such systems is calculated not in months but in years, sometimes even many years. The systems have been developing mainly towards recovering waste heat generated by fumes from the main engine.

The recent fuel crisis in the first decade of the 21st century caused unprecedented reaction among the majority of ship owners. Expensive deep waste heat recovery systems were replaced by another method of reducing operating costs, that is reducing the cruising speeds of ships. In effect, efficiency of all waste heat recovery systems has deteriorated, and in some cases the systems have been fully or partly exempt from operation.

Exhaust gas boilers are being matched with an engine operating at a nominal load or with any partial load as indicated by the ship owner [1,2].

Below, simulation calculations are presented, which were made for the assumed main engine cooperating with the most typical exhaust gas boiler, i.e. the boiler generating saturated vapour for heating and technological purposes. Those calculations are based on the assumption that the boiler was matched with the nominal load of the main engine to ensure the nominal speed of the ship. Subsequent calculation points reflect decreasing cruising speeds, and thus a decreasing power of the main engine.

2. Combustion calculations

Calculations were made for engine 8S50MC by MAN Diesel & Turbo. It is a dual stroke, crosshead, supercharged engine operating at low-speed, with the following technical parameters [6]:

- number of cylinders.....8,
- nominal power.....11,140 kW,
- nominal rotational speed.....127 rpm

The engine, coupled with a screw by a shaft line, constitutes a direct power transmission system. An assumption was made that while working at a nominal power and nominal rotational speed the engine powers the ship at a speed of 20 knots.

Simulation calculations were made for the following six cruising speeds of the ship: 20 k, 19 k, 18 k, 17 k, 16 k, 15 k. It was assumed that when the ship's speed is being gradually decreased, sailing conditions remain the same, which means that all the time the power screw is operating at a fixed value of advance coefficient. Therefore, the ship's forward speed is proportional to the screw's rotational speed. It was assumed that the power developed by the engine is proportional to the rotational speed of the engine (screw) to the third power. Table 1 shows relevant powers for adopted cruising speeds.

Tab.1. Relationship between power of the main engine and the ship's speed

| No. | V [k] | N [kW] | N [%] |
|-----|-------|--------|-------|
| 1 | 20 | 11,140 | 100 |
| 2 | 19 | 9,551 | 85,7 |
| 3 | 18 | 8,121 | 72,9 |
| 4 | 17 | 6,840 | 61,4 |
| 5 | 16 | 5,703 | 51,2 |
| 6 | 15 | 4,678 | 42 |

where:

No. – ordinal number,

V – ship's speed,

N – engine's power.

For combustion calculations, heavy fuel with the following working composition was used (mass contents): C=85.44%; H=10.85%; O=0.39%; S=1.18%; N=1.14%; W=1.00%.

where:

C – coal content,

H – hydrogen content,

O – oxygen content,

S – sulphur content,

N – nitrogen content,

W – humidity content.

When calculating fumes enthalpy, a change in the excess air number λ , which occurs when the engine load is changed, was taken into account. Experimental data obtained in the combustion engine laboratory in the Department of Maritime Power Plants in the Gdynia Maritime University were used. The relationship shown in Figure 1 was created based on the balance of carbon dioxide contained in fumes.

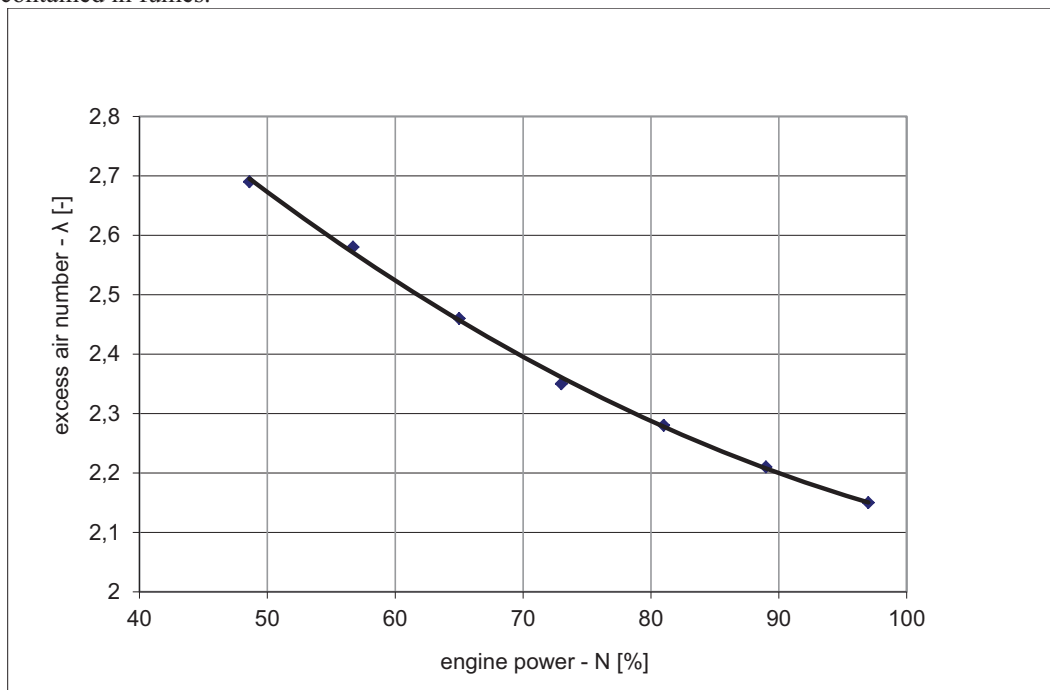


Fig. 1. Relationship between excess air and engine power

For further calculations, it was assumed that the nature of excess air number λ changes is as shown in Figure 1. Relevant values λ were calculated based on the experimental data approximating equation. λ values reflecting relevant cruising speeds of the ship were show in Table 2.

Tab.2. Relationship between excess air number λ and the ship's speed

| No. | V [k] | λ |
|-----|-------|-----------|
| 1 | 20 | 2,11 |
| 2 | 19 | 2,22 |
| 3 | 18 | 2,35 |
| 4 | 17 | 2,49 |
| 5 | 16 | 2,64 |
| 6 | 15 | 2,80 |

To calculate the values of heat fluxes allowing for utilization, fumes enthalpy graphs in the function of fumes temperature were developed for six λ values as specified in Table 2. Fumes enthalpy was calculated based on equation (1) [3].

$$I = V_{CO_2}i_{CO_2} + V_{SO_2}i_{SO_2} + V_{N_2}i_{N_2} + V_{O_2}i_{O_2} + V_{H_2O}i_{H_2O} \text{ [kJ/kg fuel]}, \quad (1)$$

where:

I [kJ/kg fuel] – fumes enthalpy produced by using up one kilogram of fuel,

V [Nm³/kg fuel] – volume of one fumes component,

i [kJ/Nm³] – enthalpy of a given fumes component.

Volume of each fumes component was calculated based on stoichiometric combustion equation. Results of fumes enthalpy calculations in the function of fumes temperature for six different values of excess air number are shown in Figure 2.

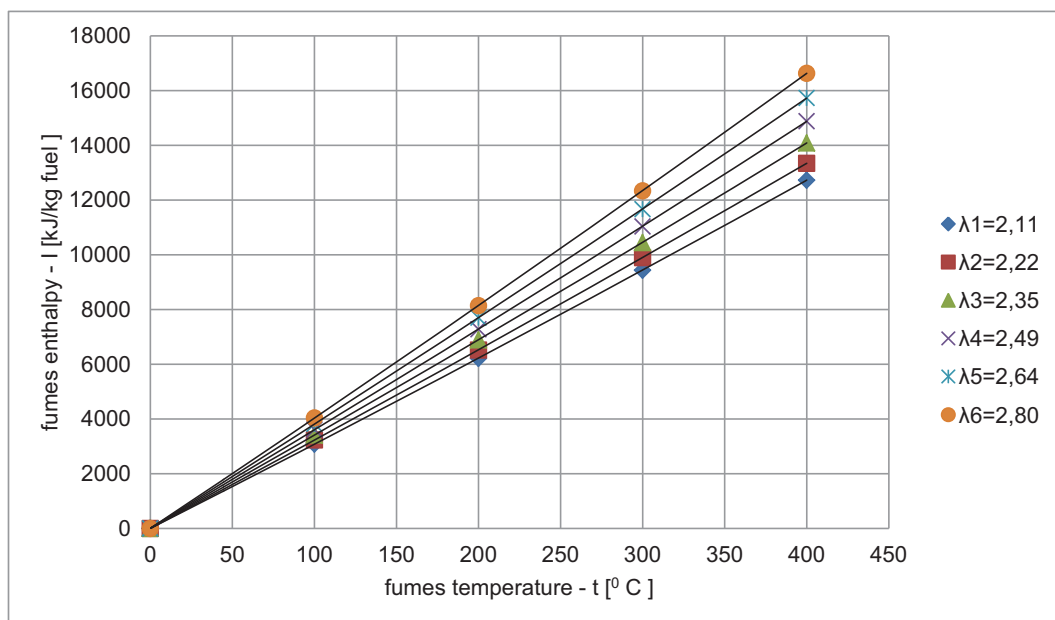


Fig. 2. Relationship between fumes enthalpy and fumes temperature for selected values of excess air number

3. Heat transfer calculations

Engine specifications provided by manufacturers and numerous performance measurements [5] made on ships point out that within the 50% - 100% range of engine load changes fumes temperature behind the turbocharger is very stable. Based on specifications of a given engine [6] the adopted value of fumes temperature behind the turbocharger was $t_s=230$ °C. The same temperature was adopted for further calculations as temperature at the front of the boiler.

It was assumed that the boiler produces saturated vapour with working pressure $p_r=0.7$ MPa. This pressure corresponds to the temperature saturated vapour $t_n=170$ °C. It was assumed that the minimum temperature discrepancy between heat transferring factors (pinch point) is 10 °C. Thus, temperature of exhaust fumes released by the boiler (behind the last heating surface) is $t_{wyl}=180$ °C. Decrease in the fumes temperature in the boiler is: $\Delta t_{sp} = t_s - t_{wyl} = 230 - 180 = 50$ °C.

On the $I = f(t)$ graph relevant values of fumes enthalpy were read for temperatures t_s i t_{wyl} . Table 3 shows relevant values of fumes enthalpy and discrepancies for individual values of excess air number.

Tab.3. Fumes enthalpy for fumes temperatures in the front of and behind the boiler, with different values of excess air number λ

| No. | λ | I_s [kJ/kg fuel] | I_{wy1} [kJ/kg fuel] | ΔI [kJ/kg fuel] |
|-----|-----------|-----------------------|---------------------------|----------------------------|
| 1 | 2.11 | 7,180 | 5,588 | 1,591 |
| 2 | 2.22 | 7,532 | 5,862 | 1,670 |
| 3 | 2.35 | 7,957 | 6,194 | 1,763 |
| 4 | 2.49 | 8,404 | 6,542 | 1,861 |
| 5 | 2.64 | 8,885 | 6,918 | 1,967 |
| 6 | 2.80 | 9,401 | 7,319 | 2,081 |

where:

I_s – fumes enthalpy in front of the boiler,

I_{wy1} – fumes enthalpy behind the boiler,

ΔI – difference between fumes enthalpy in front of and behind the boiler.

The next stage of calculations is to calculate fuel consumption with relevant forward speeds. Unit fuel consumption was adopted based on specifications [6]. Relevant values of fuel consumption are shown in Table 4.

Tab.4. Fuel consumption for individual cruising speeds

| No. | V [k] | g_e [g/kWh] | B[kg/h] | B_s [kg/s] |
|-----|-------|---------------|---------|--------------|
| 1 | 20 | 171 | 1,956 | 0,5433 |
| 2 | 19 | 170 | 1,666 | 0,4627 |
| 3 | 18 | 169 | 1,409 | 0,3913 |
| 4 | 17 | 170 | 1,194 | 0,3316 |
| 5 | 16 | 171 | 1,001 | 0,2780 |
| 6 | 15 | 172 | 702 | 0,1950 |

where:

g_e – unit fuel consumption,

B – fuel consumption per hour,

B_s – fuel consumption per second.

Heat flux released by fumes in exhaust gas boiler was calculated based on equation (2).

$$Q_{sp} = B_s \Delta I \text{ [kW]} \quad (2)$$

where:

Q_{sp} – heat flux released by fumes in the exhaust gas boiler.

Relevant values of heat fluxes Q_{sp} are show in Table 5.

Tab.5.Heat fluxes released by fumes in the boiler at individual cruising speeds

| No. | V [k] | Q _{sp} [kW] |
|-----|-------|----------------------|
| 1 | 20 | 864 |
| 2 | 19 | 772 |
| 3 | 18 | 689 |
| 4 | 17 | 617 |
| 5 | 16 | 546 |
| 6 | 15 | 405 |

Heat received by water in the boiler reduced by losses of heat released to atmosphere. That loss is accounted for by heat keeping coefficient ϕ . The adopted value was $\phi=0,9$. Therefore, fluxes of heat intercepted by water Q_w may be calculated based on equation (3).

$$Q_w = \phi Q_{sp} \text{ [kW]} \quad (3)$$

Relevant values of heat fluxes Q_w are show in Table 6.

Tab.6. Fluxes of heat intercepted by water at individual cruising speeds

| No. | V [k] | Q _w [kW] |
|-----|-------|---------------------|
| 1 | 20 | 855 |
| 2 | 19 | 764 |
| 3 | 18 | 682 |
| 4 | 17 | 610 |
| 5 | 16 | 540 |
| 6 | 15 | 401 |

The boiler's capacity, with relevant heat fluxes Q_w may be calculated based on equation (4).

$$D = \frac{Q_w}{i_p - i_{wz}} \text{ [kg/s]} \quad (4)$$

where:

D [kg/s] – boiler's capacity per second.

i_p [kJ/kg] – vapour enthalpy,

i_{wz} [kJ/kg] – enthalpy of the water powering the boiler.

The boiler's capacities for relevant cruising speeds are shown in Table 7.

Tab.7. Boiler's capacity at individual cruising speeds.

| No. | V [k] | D[kg/s] | D _h [kg/h] |
|-----|-------|---------|-----------------------|
| 1 | 20 | 0.350 | 1,264 |
| 2 | 19 | 0.313 | 1,130 |
| 3 | 18 | 0.280 | 1,080 |
| 4 | 17 | 0.250 | 902 |
| 5 | 16 | 0.221 | 789 |
| 6 | 15 | 0.164 | 593 |

where:

$D_h[\text{kg/h}]$ – hourly capacity.

Capacity per second, taken directly from equation (4) is provided here, along with the so called hourly capacity, in other words capacity provided by the manufacturer in specifications. The results are shown in tables and on the graph in Figure 3. The graphic representation of data involves only hourly capacity, which is often used to show boiler performance.

Relationship between the boiler's capacity and the cruising speed is shown in Figure 3.

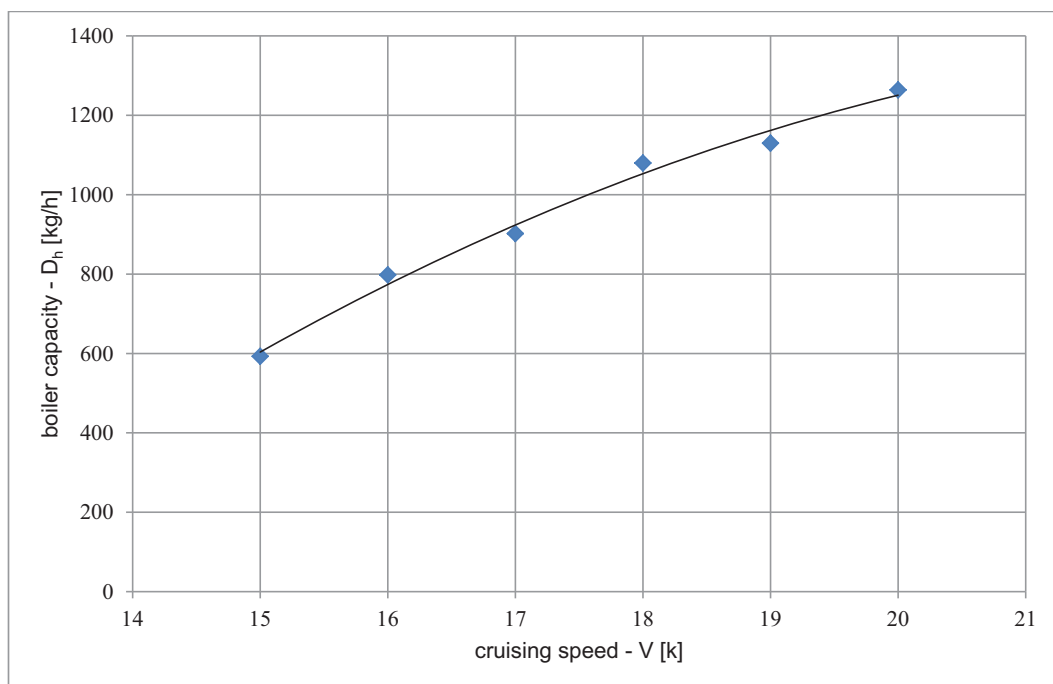


Fig.3. Relationship between boiler's capacity and cruising speed

4. Summary

Results of simulation calculations point out that even the slightest decrease in cruising speed leads to significant decrease in the boiler's capacity. So, reducing the speed by 5 knots, from 20 to 15, i.e. by 25%, causes a drop in the boiler's capacity by as much as 53%.

Such a serious drop in vapour production may be associated with the necessity to launch a fired boiler. This is a completely normal procedure during manoeuvres, river or canal crossing, or in other situations where the time is limited, which may be encountered by a sea ship. Nevertheless, during long-term sea or ocean cruises, such a situation may be considered pathological.

A power plant designed for a contemporary sea ship equipped in waste heat recovery system should account for emergency situations when sometimes even for long periods of time a ship will be cruising at lower speeds than the nominal speed. To maintain the appropriate efficiency of waste energy recovery processes, possibilities of heat recovery from other sources, e.g. by cooling powering air, should be considered. Such solutions may be autonomous or may be closely connected with a classic exhaust gas boiler, ensuring production of required amount of vapour on a ship.

References

- [1] Charchalis, A., Krefft, J., *Analiza bilansu pary uzyskiwanej w kotle utylizacyjnym na etapie projektu wstępnego*, Zeszyty Naukowe Akademii Marynarki Wojennej, pp. 43-48, Rok XLX, Nr 178A, Gdynia 2009.
- [2] Górski, Z., Perepeczko, A., *Okrętowe kotły parowe*, Fundacja Rozwoju Wyższej Szkoły Morskiej w Gdyni, Gdynia 2002.
- [3] Kowalski, A., Krzyżanowski, J., *Teoria okrętowych kotłów parowych*, Gdynia 1993.
- [4] Krzyżanowski, J., *Analiza możliwości wytwarzania pary grzewczej kosztem ciepła powietrza doladującego z okrętowych silników średnioobrotowych*, Zeszyty Naukowe Akademii Marynarki Wojennej, pp. 157-162, Rok XLX, Nr 178A, Gdynia 2009.
- [5] Warmiński, T., *Projekt kotła utylizacyjnego współpracującego z silnikiem Sulzer 6RTA58*, praca magisterska napisana pod kierunkiem J. Krzyżanowskiego, Gdynia 1994.
- [6] *S50MC Mk6 Project Guide Two-stroke Engines*, 4th Edition September 1997.



THE ANALYSIS OF GEOMETRIC STRUCTURE OF THE PINS IN MARINE ANGULAR MOMENTUM PUMPS SHAFTS THAT UNDERWENT FINISH TREATMENT

Wojciech Labuda, Adam Charchalis

Gdynia Maritime University, The Faculty of Marine Engineering

ul.Morska 81-87, 81-225 Gdynia

Tel: +48586901549, fax: +48586901399

e-mail: wlabuda@am.gdynia.pl, achar@am.gdynia.pl

Abstract

Angular momentum pumps are very often applied onboard ships. These pumps are used in cooling circuits of medium and high power engines, power plant boilers and in bilge, ballast and fire installations. Very extensive use of angular momentum pumps on board is connected with their numerous advantages. During operation the wear of marine hull, the rotor and shaft seals takes place. The research attempts to increase the service life of shafts. The article presents the research results referring to the analysis of the influence of finish treatment (lathing, grinding and burnishing) on the geometric structure of the surface of steel applied to marine pump shafts. The research was performed on a roller of 40 mm in diameter made of X5CrNi18-10 (AISI 304 L) stainless steel. The lathing process was carried out by means of a WNMG WF 080408 Sandvik Coromant cutting tool with replaceable inserts. The grinding process was performed by grinding attachment for lathes. The 1 - 80x10x32 - 99C 80-N V grinding wheel was used for the process. The process of burnishing was done by SRMD burnisher by Yamato. In addition, the influence of the burnisher passes number on the geometric structure of the surface properties was determined. The paper will present the results of research related to roughness parameters, material ratio and surface waviness.

Keywords: angular momentum pump, stainless steel, burnishing, surface layers, surface geometric structure.

1. Introduction

Centrifugal angular momentum pumps are utilized in the cooling system of high and medium speed engines, for supplying boilers, in bilge systems, ballast systems and in fire fighting installations. During their service the pump body, rotor, sealing and shaft wear out. The research works made efforts to improve the shafts service durability and was based on carrying out tests for contact fatigue, friction wear and electrochemical corrosion. Due to hard service conditions marine pumps working in sea water environment are made of corrosion resistant materials. In spite of the fact that pump shafts are made of an expensive material, it is not possible to avoid service damage. This damage includes cracking, plastic deformation, excessive wear of pins in places of mounting rotor discs and sealing chokes, corrosive wear, friction wear, erosive wear and splineways knock outs. During service experience the most common problem that is observed is excessive wear of pins causing their diameter decrease as well as exceeding the permissible shape deviations in place of chokes mounting.

Technology used in the production process has a vital influence on the reliability and service life of machine parts. The final formation of surface layer, that is the dimensions and service

properties, is achieved during finish treatment of a given element. The fundamental aim of burnishing is to reach suitable properties of a surface layer which will considerably affect the machine parts durability. The burnishing technology allows to eliminate traditional finish machining such as: grinding, super finishing, honing and polishing. Therefore the final formation of dimensions and service properties by means of burnishing becomes a chipless and dustless treatment which qualifies burnishing for ecological treatment method. In industrial environment this process is carried out on universal machine tools as well as on CNC but belongs to plastic tooling. Burnishing process enables surface working at high dimensional precision (accuracy class 7 and 6) which gives the following advantages [8, 9]:

- ability to achieve high smoothness ($R_a = 0.32 - 0.04 \mu\text{m}$) of the surface and high bearing surface of roughness profile (90%),
- increasing the surface hardness,
- increasing resistance to surface as well as volumetric fatigue,
- increasing resistance to abrasive and mashing wear,
- lack of abrasive grain, chips, sharp and hard built-up edge fragments on burnished surface,
- possibility of using burnish tools on universal lathes (the concept of one stand working),
- eliminating or limiting the time consuming operations such as: honing, lapping, grinding and polishing,
- ability to eliminate heat treatment in specific cases,
- high process efficiency (one working transition of a tool) and reduction of production costs,
- high durability of burnishers,
- decreasing the expenses related to machine parts production.

The main limitation of burnishing is the material condition. Burnished objects must be made of materials enabling their tooling at ambient temperature, and in case of steel burnishing tools - they must have a limited hardness. The above mentioned criteria have different meanings for particular burnishing methods. Other limitation results from OUPN system (working tool, fixture, object, tool) and its rigidity which should be the highest as it determines the measurement accuracy of the object toolled.

Many scientific centres all over the world deal with burnishing treatment, and the research programs comprise, among others, matters related with burnishing of cast iron, some heat resisting alloys and stainless steels, copper and aluminium alloy, titanium and its alloys, composite and intermetallic coatings [4, 5, 10,] and padded coatings as well as parts produced by sintering metal powders.

The surface layer of material is specifically subjected to various degradable factors. However it is not possible to avoid adverse phenomena of surface degradation during working conditions as well as corrosive influence of work environment. Therefore the aim of the paper is to obtain proper technological quality and suitable service properties of angular momentum pump shaft pins applied in sea water systems in marine engines. Within the research, the optimization of burnishing technological parameters was carried out and the influence of the number of burnishing tool passes on the hardness and stereometric parameters of angular momentum pump shaft pins was defined [1, 2, 3, 6, 7]. Therefore burnishing should be performed on account of the minimization of R_a surface roughness factor as well as maximization of S_u surface layer relative hardness level. The article will present the results of the research on roughness parameters, surface waviness, material ratio and frequency profile.

2. Samples preparation

Finish tooling of shafts pins was carried out on a CDS 6250 BX-1000 universal centre lathe.

Shafts pins ϕ 40 mm in diameter and made of X5CrNi18-10 stainless steel were machined. The process of finish lathing was conducted by a knife with replaceable plates WNMG 080408 WF type (super finishing plates) by Sandvik Coromant (Fig. 1). Owing to appropriate geometry of a corner the Wiper plates ensure high efficiency of finish lathing. The possibility of applying two times more feed does not change the quality of the surface obtained in relation to traditional plates. During the process of lathing the following machining parameters were applied: machining speed $V_c=112$ m/min, feed $f=0.27$ mm/obr, machining depth $a_p=0.5$ mm. In order to perform finish lathing, a Wiper knife was also utilized. During the operation, the machining parameters were the same as for roughing, only feed was decreased and was equal to $f=0.13$ mm/rev.



Fig.1. General view of OUPN tooling system (machine, grip, object, tool) - finish lathing

The grinding process was performed by grinding attachment for lathes (Fig.2). The 1 - 80x10x32 - 99C 80-N V grinding wheel was used for the process. The process was carried out at the following grinding parameters: shaft speed $n=80$ rev/min, feed $f=0.08$ mm/rev, grinding depth $a_p=0.05$ mm and the pressure of 0.8 MPa which allowed to reach the grinding wheel speed of 8000 rev/min.



Fig. 2. General view of OUPN tooling system (machine, grip, object, tool) – grinding.

The process of burnishing (Fig. 3) was conducted by SRMD one roll burnish by Yamato (Fig. 4). The technological process parameters applied for surface plastic treatment are shown in Table 1. The influence of the number of burnishing passes on surface roughness was determined within the research. A shaft journal after three applications of burnishing tool was used for the test experiment, with the technological parameters included in Table 1.



Fig. 3. General view of OUPN tooling system (machine, grip, object, tool): burnishing



Fig. 4. Burnishing tool

Table 1. Technological parameters of burnishing process

| Parameter | | Values |
|--------------------------|----------|--------|
| Burnishing force - F | [kN] | 1.1 |
| Burnishing speed – V_n | [m/min] | 35 |
| Feed - f | [mm/rev] | 0.13 |

3. Research methodology

The surface roughness was measured by HOMMEL TESTER T 1000 profile meter. The measuring length of test sample amounted to 4.8 mm, while the sampling length was 0.08 mm. The evaluation of surface geometric structure was conducted on the basis of the commonly used parameters for surface roughness, waviness and material ratio : R_a , R_q , R_z , R_t , W_t , W_z , W_a , M_{r1} , M_{r2} , R_{pk} , R_{vk} , R_k [11, 12, 13].

4. Research results

The application of the unchanged technological parameters of the preliminary machining

treatment led to the achievement of diversified results of roughness tests of the examined shafts. The value of the mean arithmetic roughness profile deflection in the optimization analysis ranged from 0.5 to 1.18 μm . The mean value of the R_a roughness coefficient reached 0.83 μm . The tables show the exemplary profile (Fig.5) as well as material ratio (Fig.6) for the shaft surface, whose value of R_a parameter amounted to 0.83 μm . The results of the basic statistic analysis were shown in Table 2.

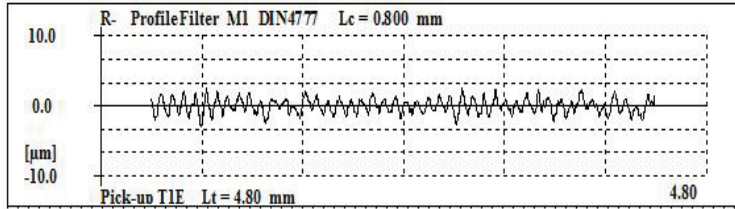


Fig. 5. Exemplary shaft surface profile after preliminary lathing

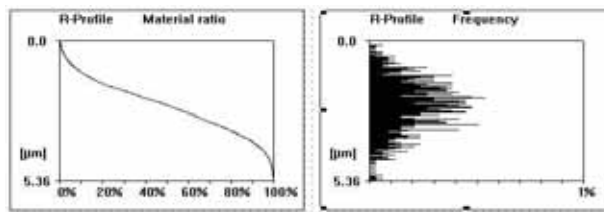


Fig 6. Exemplary material ratio curves and frequency profile after preliminary lathing

Tab. 2. The basic results of R_a parameter statistic analysis (number of measurements 48)

| Mean | Median | Minimum | Maximum | Stan.Deflection | Stan. Error |
|------|--------|---------|---------|-----------------|-------------|
| 0.83 | 0.79 | 0.50 | 1.18 | 0.14 | 0.02 |

Shaft pins underwent traditional finish lathing after preliminary machining. The results obtained from the surface geometric structure measurements were presented in the tables below. The roughness measurements results for the marine pumps shaft pins finish machining were given in Table 3, the material ratio measurements results in Table 4, whereas surface waviness results in Table 5.

Tab. 3. The mean values of surface roughness parameters for finish treatment

| Parameter | R_a [μm] | R_q [μm] | R_t [μm] | R_z [μm] |
|--------------------|-------------------------|-------------------------|-------------------------|-------------------------|
| Grinding | 0.28 | 0.36 | 2.66 | 2.07 |
| Finish lathing | 0.35 | 0.42 | 2.47 | 2.03 |
| Burnishing | 0.07 | 0.09 | 0.85 | 0.59 |
| 3 burnisher passes | 0.06 | 0.09 | 0.95 | 0.53 |

Tab. 4. The mean values of material ratio parameters for finish treatment

| Parameter | M_{r1} [%] | M_{r2} [%] | 100%- M_{r2} | R_{pk} [μm] | R_{vk} [μm] | R_k [μm] |
|--------------------|--------------|--------------|----------------|----------------------------|----------------------------|-------------------------|
| Grinding | 9.03 | 86.63 | 13.37 | 0.34 | 0.46 | 0.86 |
| Finish lathing | 6.47 | 87.73 | 12.27 | 0.25 | 0.49 | 1.17 |
| Burnishing | 7.6 | 90.1 | 9.9 | 0.09 | 0.14 | 0.24 |
| 3 burnisher passes | 8.2 | 87.6 | 12.4 | 0.08 | 0.13 | 0.21 |

Tab. 5. The mean values of surface waviness parameters for finish treatment

| Parameter | W_t [μm] | W_a [μm] | W_z [μm] |
|--------------------|-------------------------|-------------------------|-------------------------|
| Grinding | 0.93 | 0.14 | 0.65 |
| Finish lathing | 1.58 | 0.31 | 1.26 |
| Burnishing | 0.42 | 0.08 | 0.25 |
| 3 burnisher passes | 0.45 | 0.08 | 0.26 |

The shaft pins surface that underwent burnishing are characterized by really favourable roughness parameters. It signifies honing of surface roughness peaks by burnishing tool and reaching a surface of a relatively low surface roughness. The process of finish grinding and lathing allowed to obtain surfaces of a definitely worse surface compared to plastic treatment application. The values of the main parameters that were found were three or even four times higher than after burnishing.

Low values of R_k and big differences in M_{r1} and M_{r2} values make it possible to conclude that the surfaces show high load, resistance to mashing as well as resistance to abrasive fatigue. The mean values of the material ratio parameter curve for burnishing are characterized by several times lower R_{pk} , R_{vk} and R_k parameters values when compared with traditional finish treatment. The same situation occurred for surface waviness parameters. Therefore the surface after burnishing and consequently after plastic deformation of surface peaks reaching low surface roughness should be characterized by higher resistance to tribologic wear. Moreover it should also show higher resistance to electrochemical corrosion and contact fatigue.

Figures 7, 8, 9, 10 presents exemplary profiles for shaft pins, whereas Figure 11 presents material ratio curves as well as frequency profiles of the results shown in the tables above.

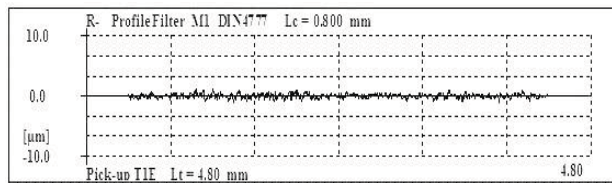


Fig. 7. Exemplary shaft surface profile after grinding

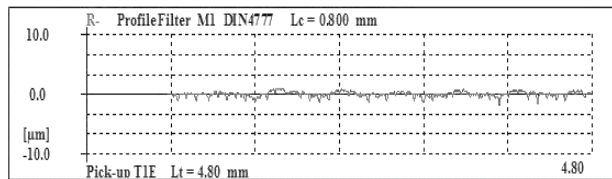


Fig. 8. Exemplary shaft surface profile after finishing lathing

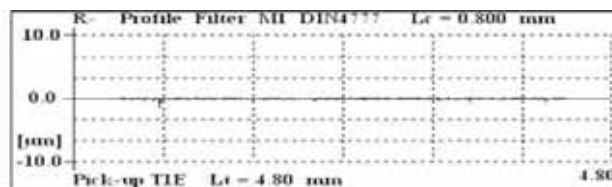


Fig. 9. Exemplary shaft surface profile after burnishing

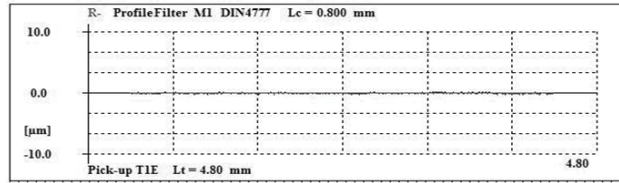


Fig. 10. Exemplary shaft surface profile after 3 passes of burnisher tool

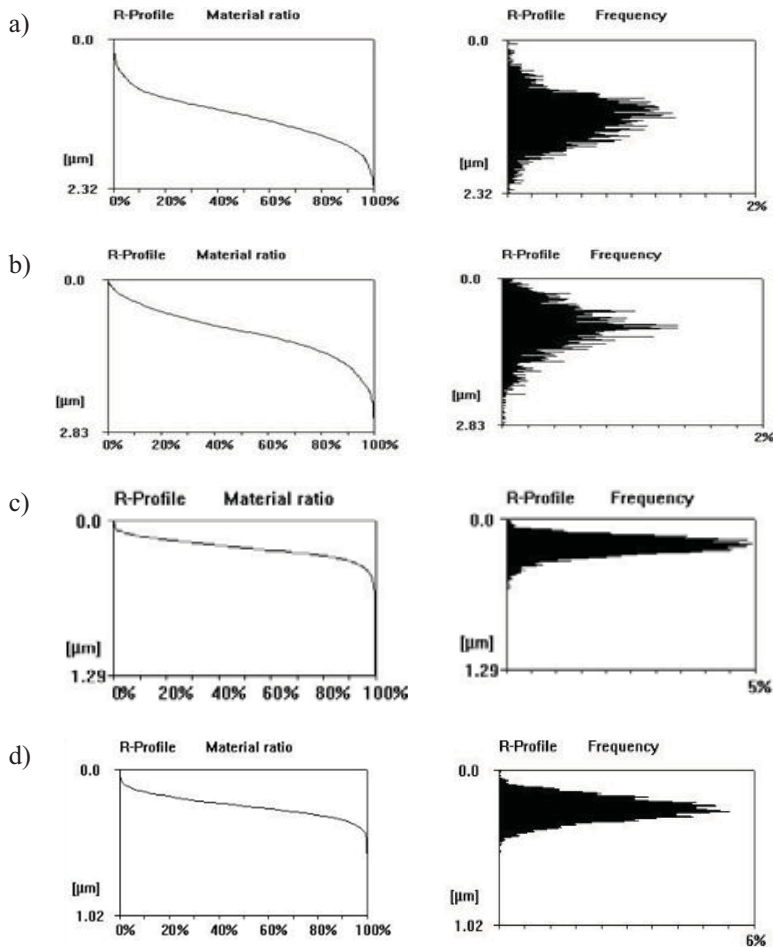


Fig. 11. Exemplary material ratio curves and frequency profile after:
a) grinding b) finishing lathing, c) burnishing d) after 3 passes of burnisher tool

5. Conclusions

The analysis of the results obtained in the research proved that the burnishing process allows to achieve surface geometric structure with more favourable parameters of roughness, material ratio and surface waviness than after traditional finish treatment of shaft pins. Subjecting marine pumps

shaft pins to burnishing process made it possible to produce surface which should show higher resistance to tribological wear, electrochemical corrosion as well as contact fatigue.

6. Literature:

- [1] Charchalis, A., Starosta, R., Labuda, W., *Multi-criteria optimalization of steel burnishing parameters applied to marine pumps shaft pins*, Journal of KONES Powertrain and Transport, Vol. 17/ No. 3, pp. 55 – 62, Jurata 2010.
- [2] Charchalis, A., Starosta, R., Labuda, W., *Estimation of the influence of burnishing tool passes number on ships pumps shafts surface layers strengthening and roughness changes*, Journal of KONES Powertrain and Transport, Vol. 16/ No. 4, pp. 43 – 50, Zakopane 2009.
- [3] Charchalis, A., Starosta, R., Labuda, W., *The influence of burnishing parameters on the roughness, plastic strain and shape deviations of marine pumps crankshaft pins in fresh water installations*; Journal of KONBiN, , No 1-2 (9,10), pp. 57 -66, Warszawa 2009.
- [4] Dyl, T., Skoblik, R., Starosta, R., *The Effect of the Ceramic Dispersion on the Nickel Matrix Composite Coating Properties after Plastic Working*, Solid State Phenomena, Vol. 147-149, pp. 813-818, Switzerland 2009.
- [5] Dyl, T., Starosta, R., Skoblik, R., *The effect of the unit pressure on the NiAl and Ni₃Al intermetallic coatings selection parameters after plastic working*, Solid State Phenomena, Vol. 165, pp. 19-24, Switzerland 2010.
- [6] Labuda, W., Starosta, R., *Estimation of the influence of burnishing parameters on X5CrNi18-10 steel*, Solid State Phenomena , Trans Tech Publication, Vol. 165, pp 300 – 305, Switzerland 2010.
- [7] Labuda, W., Starosta, R., Dyl, T., *Estimation of the influence of burnishing parameters on steel X5CrNi1810 surface layers strengthening and roughness changes*, Journal of KONES Powertrain and Transport, Vol. 15/ No. 3, pp. 259 – 267, Warszawa 2008.
- [8] Przybylski, W., *Współczesne problemy w technologii obróbki przez nagniatanie*, Wydawnictwa Politechniki Gdańskiej, Gdańsk 2005.
- [9] Przybylski, W., *Współczesne problemy w technologii obróbki przez nagniatanie. Tom 2*, Wydawnictwa Politechniki Gdańskiej, Gdańsk 2008.
- [10] Starosta, R., *The influence of plastic strain on the corrosive properties of plasma sprayed intermetallic NiAl and Ni₃Al coatings*, Solid State Phenomena, Vol. 165, pp. 165-177, Switzerland 2010.
- [11] PN-EN ISO 13565-1: 1999, *Struktura geometryczna powierzchni: metoda profilowa, powierzchnie o warstwowych właściwościach funkcjonalnych. Filtrowanie i ogólne warunki pomiaru*.
- [12] PN-EN ISO 13565-2: 1999, *Struktura geometryczna powierzchni: metoda profilowa, powierzchnie o warstwowych właściwościach funkcjonalnych. Opis wysokości za pomocą linearyzacji krzywej udziału materiałowego*;
- [13] PN-EN ISO 13565-3: 1999, *Struktura geometryczna powierzchni: metoda profilowa, powierzchnie o warstwowych właściwościach funkcjonalnych. Opis wysokości za pomocą dystrybuanty krzywej udziału materiałowego*.



TAXONOMIC ASSESSMENT OF THE ENVIRONMENTAL PROBLEMS OF MOTOR TRANSPORT FACILITIES BASED ON THE EXAMPLE OF GENERATED WASTE

Kazimierz Lejda, Edyta Zielińska

Rzeszow University of Technology
Al. Powstańców Warszawy 6, 35-959 Rzeszów, Poland
tel./fax: +48 17 854 31 12, e-mail: klejda@prz.edu.pl

Abstract

Environmentally conscious activities performed in, among other things, motor transport facilities are of considerable importance for the environmental protection. Unfortunately, the analysis of the situation confirms that environmental protection in this kind of facilities is put at the bottom of the agenda. The economic effect of the sale of services, backed up with the expenditure on marketing and oriented to the maximization of profits and not to the environmental protection still prevails. This paper discusses the choice of an environmental strategy for motor transport facilities using a taxonomic method. It provides the purpose for using this method to assess environmental issues and describes its determinants. Basic taxonomic equations and an algorithm for the calculations are also presented. The taxonomic method is characterized on the example of harmfulness of generated waste. The paper presents the calculation results and their interpretation in respect of the choice of a suitable technology to be applied. The data pertaining to the nuisance from generated waste were collected from 15 companies offering motor transport services. In order to ensure credible results, we adopted the data for defined parameters collected during consultation meetings with the technical inspectors of the companies under study and with the employees assigned to specific jobs.

Keywords: ecology, managing environmental problems, motor transport, technical facilities, taxonomic method

1. Introduction

The development of motor transport and its consequence in the form of the growing number of vehicles used as well as easy access to such transport means cause considerable risks to this sector of economy. The main motor transport problems would include the environmental damage and the lack of technical facilities functioning appropriately in terms of inspections, repairs and diagnostic testing [8].

The solution of the most essential motor transport problems in Poland depends on quick investment and organizational decisions aimed at making the Polish transport system equal to the logistic systems used in EU countries.

The issues addressed in this article include a proposal of a logistic system strategy for motor transport facilities with respect to waste management by using a taxonomic method [1,6]. The taxonomic method enables comparison and choice of the most favourable solutions from among the considered technologies that are described by various parameters and units of measure. The ordering of technologies as factors according to defined criteria is closely related to systematics, on the basis of which the taxonomy functions.

2. Basic equations used in the taxonomic method and the algorithm for the calculations

The taxonomic method relates to theoretical principles, procedures and rules of classifying technical objects from an analytical perspective. The method allows for graphic presentation of an affinity between the operations based on the example of selected logistic management strategies that are considered in comparison with the distance within a multidimensional metric space. For the purpose of this paper, each coordinate means a specific parameter assigned to a strategy for managing environmental parameters. Dendrites for the selected parameter group are depicted in graphic form to enable search for the smallest average difference between these parameters. This method is used to search for a so called effective parameter group based on specific assumptions [2,3].

The parameters for a specific environmental management technology for motor transport facilities are physical and chemical quantities. In the taxonomic model, it is necessary to normalize parameters so that they take non-dimensional values. During the normalization it is important not to disrupt the correlations in particular technologies. Another important problem is the so called correspondence between parameters. It is important to make such limitations where all the covariance matrices of the technologies in question are identical.

The modelling algorithm for logistic processes in motor transport facilities can be presented in the following order [4,6]:

- 1) The vector for the management of environmental problems, comprised of n elements, has the following form:

$$x(t) = \begin{bmatrix} x_1(t) \\ x_n(t) \end{bmatrix} \quad (1)$$

The above relationship is a time function but not in an evident way because each of the subsequent stages of the logistic process is a function of logistic indices for the management of environmental problems (eg WN_1, \dots, WN_n). So, this can be written as follows:

$$x(WN_1, \dots, WN_n) = \begin{bmatrix} x_1(WN_1, \dots, WN_n) \\ x_n(WN_1, \dots, WN_n) \end{bmatrix} \quad (2)$$

There are as many indices for the management of environmental problems as the system elements. They are chosen from among the system indices $WN_1 - WN_n$, defined separately for each element. Each of the WN_i indices can take various values within a definite time period $(0, T)$ and can influence the management procedure x_i as well as other procedures.

- 2) It is possible to digitize the time within the bracket of $(0, T)$ by dividing the period into K short lengths of time, Δt long each:

$$\Delta t = \frac{T}{K} \quad (3)$$

Determining the value of the i -th index for the management of environmental problems with k_i , the equation (2) can be at k -th time written as follows:

$$x(k_1, \dots, k_n) = \begin{bmatrix} x_1(k_1, \dots, k_n) \\ x_n(k_1, \dots, k_n) \end{bmatrix} \quad (4)$$

This equation presents the dependence of the vector for the logistics of the management of environmental problems from the digitized system indices.

- 3) Given the values of the system indices at times k ($k = 1, \dots, K$) it is possible to determine the value of the vector for the logistic system by using for this purpose a multidimensional discrete-time nonlinear model:

$$\left[\frac{x_1(k_1 + 1, \dots, k_n)}{x_n(k_1, \dots, k_n + 1)} \right] = F \left\{ \frac{x_1(k_1, \dots, k_n)}{x_n(k_1, \dots, k_n)} \right\} k_1, \dots, k_n = 1, \dots, K \quad (5)$$

where: F - vector function with independent variable being a vector for the logistic system.

- 4) The equation (5) can be written in a way that enables iterative determination of the vector for the logistic system.

$$\left[\frac{x_1(k_1 + 1, \dots, k_n)}{x_n(k_1, \dots, k_n + 1)} \right] = F \left[\frac{f_1[x_1(k_1, \dots, k_n), \dots, x_n(k_1, \dots, k_n)]}{f_n[x_1(k_1, \dots, k_n), \dots, x_n(k_1, \dots, k_n)]} \right] \quad (6)$$

where: f_1, \dots, f_n - functions describing the correlation between logistic procedures.

- 5) The logistic system vectors defined in the above way can be analysed by determining the spatial positions of the coordinates (the indices for the logistics of the management of environmental problems) in relation to the other, and thus determining the place in the entire sample. This in turn gives the ability to order and classify them. The indices for the management logistics are expressed in various units and cannot be added up directly. In this case one can use the method for relative mean differences expressed by the below formula:

$$R_{1,2} = \sum_{j=1}^{j=n} \left| \frac{WN_{1j} - WN_{2j}}{WN_{srj}} \right| \quad (7)$$

where:

$R_{1,2}$ - sum of the differences between the technologies,

WN_{1j} - value of the index for the logistics of the management of environmental problems of characteristic j of technology **1**,

WN_{2j} - value of the index for the logistics of the management of environmental problems of characteristic j of technology **2**,

WN_{srj} - mean value of the index for the logistics of the management of environmental problems of characteristic j .

- 6) The logistic system technologies can be ordered by dendrite method. The dendrite of the smallest differences between the indices for the logistics of the management of environmental problems, obtained as result of such ordering, graphically depicts the system clusters.
- 7) Given the sums of the differences between the indices for the management logistics, it is possible to construct a metric square matrix (by Czekanowski's method) that allows for verification of the dendrite ordering:

$$R = \begin{vmatrix} R_{11} & R_{12} & R_{13} & \dots & R_{1m} \\ R_{21} & R_{22} & R_{23} & \dots & R_{2m} \\ R_{31} & R_{32} & R_{33} & \dots & R_{3m} \\ \dots & \dots & \dots & \dots & \dots \\ R_{n1} & R_{n2} & R_{n3} & \dots & R_{nm} \end{vmatrix} \quad (8)$$

3. Taxonomic analysis of harmfulness of generated waste

As mentioned in the introduction to this paper, environmental problems related to the waste generated in motor transport facilities were assessed using the taxonomic method. The method allows for dendrite ordering that is better to reproduce the positions of the examined factors in the multidimensional parameter space, as opposed to all kinds of optimization method that allow for only linear ordering of selected indices [5].

For the taxonomic assessment of environmental threats resulting from the waste generated in motor transport facilities, their general harmfulness to the environment was chosen. The data pertaining to the nuisance from generated waste were collected from 15 companies, with the range of 0 or 1 (0 - least nuisance, 1- biggest nuisance) adopted. All the selected companies offer motor transport services. And all the motor transport companies under study are called “technologies” because, when making their documents and materials on generated waste available to us, some of them did not give their consent to their names and affiliations to be disclosed. The data adopted for the defined parameters were repeatedly consulted with the companies’ technical inspectors and employees assigned to specific jobs to ensure that credible results are obtained [6,7].

The choice of the most favourable variant in respect of the adopted comparison criteria necessary to carry out an analysis by taxonomic method required three additional parameters correlated with environmental issues in those companies (i.e. model parameters) to be defined. Our in-depth analysis has allowed us to define the following: CO₂ emissions to the environment (WP1), total amount of waste material (WP2), and power demand in respect of environmentally friendly works (WP4). The fourth model parameter is the general harmfulness of generated waste (WP3). Table 1 includes the model parameters selected for calculations and their corresponding units of measure.

Tab. 1. Parameters for the environmental assessment of the technical facilities, chosen for the analysis

| No | PARAMETER SYMBOL | PARAMETER TYPE | MEASUREMENT UNIT |
|----|------------------|---|------------------|
| 1. | P1 | Emission of carbon dioxide (CO ₂) to atmosphere | [kg/rok] |
| 2. | P2 | Total quantity of material waste | [kg/rok] |
| 3. | P3 | General “harmfulness” of generated waste (in terms of toxicity) | [0-1]* |
| 4. | P4 | Energy demand with reference to pro-ecological projects | [kWh/m-c] |

* 0 - lowest, 1 - highest

3.1. Study results

The results obtained by taxonomic method have been additionally verified in this paper by Czekanowski’s matrices. In the case of similarity of the results it can be concluded that the procedure adopted for the calculations was correct. The order of the connected points and the values of the mean differences between those points matter greatly when drawing the conclusions. The closeness and the clustering of specified technologies show that the parameter concerned is similar, which allows selection of an optimal quantity.

The research results have been collated in tables and presented graphically in the form of dendrites and Czekanowski’s matrices, including:

- table 2 - collation of the analysed parameters for all the companies under study,
- table 3 - parameter values determined by taxonomic method for the least troublesome waste with respect to environmental protection, in 5 of the companies under study,
- table 4 - mean differences between the technologies under study (according to table 3),
- table 5 - Czekanowski’s diagonal matrix (verification: Fig. 1),
- table 6 - parameter values determined by taxonomic method for moderately troublesome waste with respect to environmental protection, in 5 of the companies under study,
- table 7 - mean differences between the technologies under study (according to table 6),
- table 8 - Czekanowski’s diagonal matrix (verification: Fig. 2),
- table 9 - parameter values determined by taxonomic method for the most troublesome waste with respect to environmental protection, in 5 of the companies under study,
- table 10 - mean differences between the technologies under study (according to table 9),
- table 11 - Czekanowski’s diagonal matrix (verification: Fig. 3),

- Fig. 1 - dendritic differentiation of the technologies according to harmfulness of the waste for the 5 lowest values,
- Fig. 2 - dendritic differentiation of the technologies according to harmfulness of the waste for the 5 medium values,
- Fig. 3 - dendritic differentiation of the technologies according to harmfulness of the waste for the 5 highest values.

Tab. 2. Analysed parameters for the 15 companies under research (including the model parameters)

| Parameters Technology | P1 | P2 | P3 | P4 |
|--------------------------|-------|---------|------|-------|
| 1 | 929 | 58 518 | 0,35 | 800 |
| 2 | 1 328 | 63 372 | 0,72 | 900 |
| 3 | 1 679 | 55 846 | 0,27 | 950 |
| 4 | 1 000 | 31 982 | 0,26 | 600 |
| 5 | 2 647 | 113 516 | 0,13 | 975 |
| 6 | 1 221 | 48 288 | 0,49 | 740 |
| 7 | 3 017 | 106 424 | 0,31 | 250 |
| 8 | 1 921 | 84 961 | 0,87 | 1000 |
| 9 | 1 395 | 62 282 | 0,59 | 430 |
| 10 | 896 | 55 423 | 0,70 | 740 |
| 11 | 1 093 | 63 230 | 0,18 | 800 |
| 12 | 4 329 | 161 326 | 0,19 | 940 |
| 13 | 2 247 | 57 013 | 0,64 | 800 |
| 14 | 1 444 | 65 510 | 0,25 | 850 |
| 15 | 2 309 | 124 893 | 0,13 | 900 |
| WP1 | 672 | 41 568 | 1 | 555 |
| WP2 | 750 | 23 987 | 1 | 450 |
| WP3 | 1 441 | 63 721 | 1 | 750 |
| WP4 | 2 262 | 79 818 | 1 | 187,5 |

Tab. 3. List of parameters according to harmfulness of the waste for the 5 lowest values from among the companies under study

| Parameters Technology | P1 | P2 | P3 | P4 |
|--------------------------|-------|--------|------|------|
| 8 | 1 921 | 84 961 | 0,87 | 1000 |
| 2 | 1 328 | 63 372 | 0,72 | 900 |
| 10 | 896 | 55 423 | 0,70 | 740 |
| 13 | 2 247 | 57 013 | 0,64 | 800 |
| 9 | 1 395 | 62 282 | 0,59 | 430 |
| WP1 | 672 | 41 568 | 1,00 | 555 |
| WP2 | 750 | 23 987 | 1,00 | 450 |
| WP3 | 1 441 | 63 721 | 1,00 | 750 |
| WP4 | 2 262 | 79 818 | 1,00 | 188 |

Tab. 4. Mean differences between the technologies under study (according to table 3)

| Technology | 8 | 2 | 10 | 13 | 9 | WP1 | WP2 | WP3 | WP4 |
|------------|---------|---------|---------|---------|---------|---------|---------|---------|---------|
| 8 | | 2146,98 | 2885,16 | 2694,37 | 2244,01 | 4220,54 | 5896,81 | 2060,95 | 1091,67 |
| 2 | 2146,98 | | 836,40 | 931,81 | 542,67 | 2127,11 | 3803,37 | 357,72 | 1812,33 |

| | | | | | | | | | |
|-----|---------|---------|---------|---------|---------|---------|---------|---------|---------|
| 10 | 2885,16 | 836,40 | | 615,15 | 1044,95 | 1342,40 | 3019,58 | 893,54 | 2626,04 |
| 13 | 2694,37 | 931,81 | 615,15 | | 900,94 | 1623,59 | 3238,84 | 802,90 | 2539,55 |
| 9 | 2244,01 | 542,67 | 1044,95 | 900,94 | | 2121,03 | 3682,79 | 550,84 | 1883,30 |
| WP1 | 4220,54 | 2127,11 | 1342,40 | 1623,59 | 2121,03 | | 1689,32 | 2163,82 | 3809,71 |
| WP2 | 5896,81 | 3803,37 | 3019,58 | 3238,84 | 3682,79 | 1689,32 | | 3837,11 | 5411,25 |
| WP3 | 2060,95 | 357,72 | 893,54 | 802,90 | 550,84 | 2163,82 | 3837,11 | | 2001,91 |
| WP4 | 1091,67 | 1812,33 | 2626,04 | 2539,55 | 1883,30 | 3809,71 | 5411,25 | 2001,91 | |

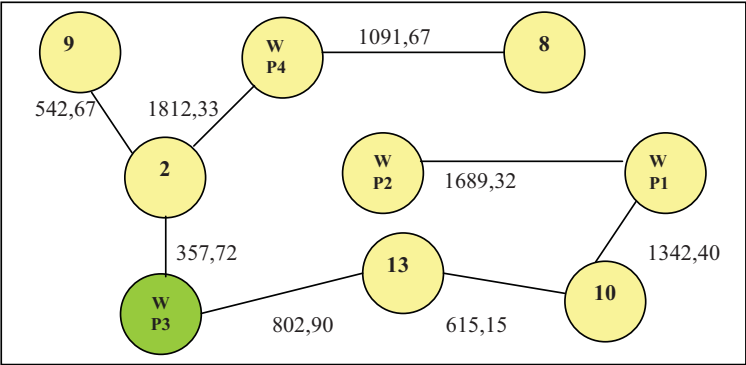


Fig. 1. Dendritic differentiation of the technologies according to harmfulness of the waste for the 5 lowest values

Tab. 5. Czekanowski's diagonal matrix (dendrite verification according to Fig. 1)

| Name | 1 | 2 | 3 | 4 | 5 | 6 | 7 | 8 | 9 |
|-------|---|---|---|---|---|---|---|---|---|
| 1 8 | ● | • | • | • | • | | | • | • |
| 2 2 | | ● | • | • | • | • | | • | • |
| 3 10 | | | ● | • | • | • | • | • | • |
| 4 13 | | | | ● | • | • | • | • | • |
| 5 9 | | | | | ● | • | • | • | • |
| 6 WP1 | | | | | | ● | • | • | • |
| 7 WP2 | | | | | | | ● | • | • |
| 8 WP3 | | | | | | | | ● | • |
| 9 WP4 | | | | | | | | | ● |

●

0 - 8594

•

8595 - 19954

•

19955 - 24835

•

> 24835

Tab. 6. Parameters according to harmfulness of the waste for the 5 medium values from among the companies under study

| Parameters Technology | P1 | P2 | P3 | P4 |
|-----------------------|-------|---------|------|-----|
| 6 | 1 221 | 48 288 | 0,49 | 740 |
| 1 | 929 | 58 518 | 0,35 | 800 |
| 7 | 3 017 | 106 424 | 0,31 | 250 |
| 3 | 1 679 | 55 846 | 0,27 | 950 |
| 4 | 1 000 | 31 982 | 0,26 | 600 |
| WP1 | 672 | 41 568 | 1,00 | 555 |
| WP2 | 750 | 23 987 | 1,00 | 450 |
| WP3 | 1 441 | 63 721 | 1,00 | 750 |
| WP4 | 2 262 | 79 818 | 1,00 | 188 |

Tab. 7. Mean differences between the technologies under study (according to table 6)

| Technology | 6 | 1 | 7 | 3 | 4 | WP1 | WP2 | WP3 | WP4 |
|------------|---------|---------|---------|---------|---------|---------|---------|---------|---------|
| 6 | | 1319,63 | 5704,15 | 1195,88 | 1572,25 | 970,27 | 2352,95 | 1677,59 | 3221,37 |
| 1 | 1319,63 | | 4774,70 | 819,90 | 2548,44 | 1707,93 | 3320,58 | 1080,33 | 2371,91 |
| 7 | 5704,15 | 4774,70 | | 5034,81 | 7215,07 | 6315,27 | 7981,52 | 4214,46 | 2577,86 |
| 3 | 1195,88 | 819,90 | 5034,81 | | 2358,06 | 1568,22 | 3105,89 | 989,99 | 2590,46 |
| 4 | 1572,25 | 2548,44 | 7215,07 | 2358,06 | | 1009,37 | 783,42 | 3058,33 | 4645,56 |
| WP1 | 970,27 | 1707,93 | 6315,27 | 1568,22 | 1009,37 | | 1689,32 | 2163,82 | 3809,71 |
| WP2 | 2352,95 | 3320,58 | 7981,52 | 3105,89 | 783,42 | 1689,32 | | 3837,11 | 5411,25 |
| WP3 | 1677,59 | 1080,33 | 4214,46 | 989,99 | 3058,33 | 2163,82 | 3837,11 | | 2001,91 |
| WP4 | 3221,37 | 2371,91 | 2577,86 | 2590,46 | 4645,56 | 3809,71 | 5411,25 | 2001,91 | |

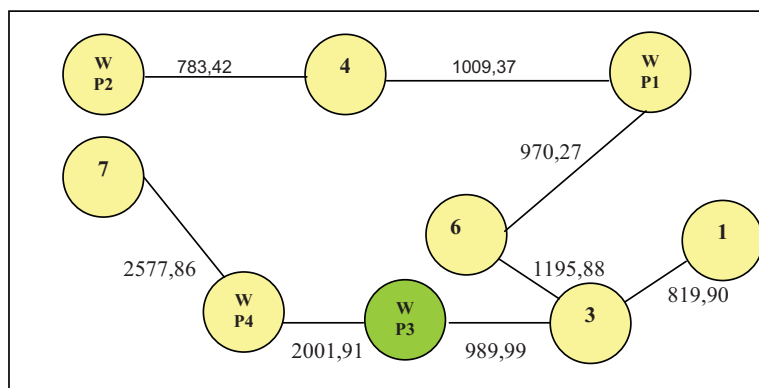


Fig. 2. Dendritic differentiation of technologies according to harmfulness of the waste for the 5 medium values

Tab. 8. Czekanowski's diagonal matrix (verification: Fig. 2)

| Name | 1 | 2 | 3 | 4 | 5 | 6 | 7 | 8 | 9 |
|-------|---|---|---|---|---|---|---|---|---|
| 1 6 | ● | ● | ● | ● | ● | ● | ● | ● | ● |
| 2 1 | ● | ● | ● | ● | ● | ● | ● | ● | ● |
| 3 7 | ● | ● | ● | ● | ● | ● | ● | ● | ● |
| 4 3 | ● | ● | ● | ● | ● | ● | ● | ● | ● |
| 5 4 | ● | ● | ● | ● | ● | ● | ● | ● | ● |
| 6 WP1 | ● | ● | ● | ● | ● | ● | ● | ● | ● |
| 7 WP2 | ● | ● | ● | ● | ● | ● | ● | ● | ● |
| 8 WP3 | ● | ● | ● | ● | ● | ● | ● | ● | ● |
| 9 WP4 | ● | ● | ● | ● | ● | ● | ● | ● | ● |

● 0 - 13134

● 13135 - 24835

● 24836 - 36624

● > 36624

Tab. 9. Parameters according to harmfulness of the waste for the 5 highest values

| Parameters Technology | P2 | P13 | P14 | P21 |
|-----------------------|-------|---------|------|-----|
| 14 | 1 444 | 65 510 | 0,25 | 850 |
| 12 | 4 329 | 161 326 | 0,19 | 940 |
| 11 | 1 093 | 63 230 | 0,18 | 800 |
| 15 | 2 309 | 124 893 | 0,13 | 900 |
| 5 | 2 647 | 113 516 | 0,13 | 975 |
| WP1 | 672 | 41 568 | 1,00 | 555 |
| WP2 | 750 | 23 987 | 1,00 | 450 |
| WP3 | 1 441 | 63 721 | 1,00 | 750 |
| WP4 | 2 262 | 79 818 | 1,00 | 188 |

Tab. 10. Mean differences between the technologies under study (according to table 9)

| Technology | 14 | 12 | 11 | 15 | 5 | WP1 | WP12 | WP3 | WP4 |
|------------|---------|----------|---------|---------|---------|----------|----------|---------|---------|
| 14 | | 9277,03 | 1264,60 | 5865,67 | 5021,38 | 2335,36 | 4011,45 | 745,66 | 1824,96 |
| 12 | 9277,03 | | 9510,66 | 3703,76 | 4645,04 | 11609,48 | 13285,65 | 9450,61 | 7901,15 |
| 11 | 1264,60 | 9510,66 | | 5941,20 | 4989,51 | 2251,43 | 3776,22 | 912,86 | 1757,25 |
| 15 | 5865,67 | 3703,76 | 5941,20 | | 2029,78 | 8037,54 | 9714,72 | 5919,93 | 4383,47 |
| 5 | 5021,38 | 4645,04 | 4989,51 | 2029,78 | | 7041,35 | 8650,23 | 5360,95 | 3710,97 |
| WP1 | 2335,36 | 11609,48 | 2251,43 | 8037,54 | 7041,35 | | 1689,32 | 2163,82 | 3809,71 |
| WP2 | 4011,45 | 13285,65 | 3776,22 | 9714,72 | 8650,23 | 1689,32 | | 3837,11 | 5411,25 |
| WP3 | 745,66 | 9450,61 | 912,86 | 5919,93 | 5360,95 | 2163,82 | 3837,11 | | 2001,91 |
| WP4 | 1824,96 | 7901,15 | 1757,25 | 4383,47 | 3710,97 | 3809,71 | 5411,25 | 2001,91 | |

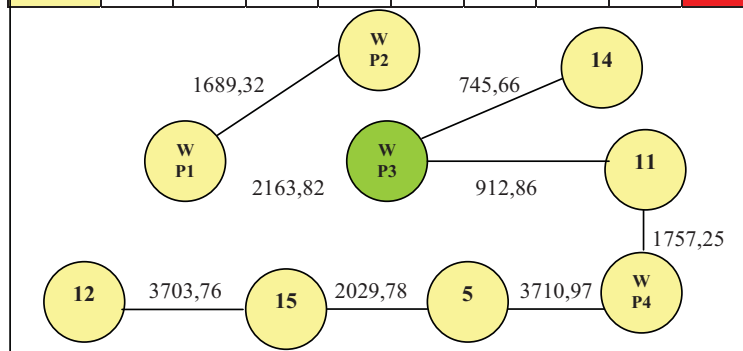


Fig. 3. Dendritic differentiation of technologies according to harmfulness of the waste for the 5 highest values

Tab. 11. Czekanowski's diagonal matrix (verification: Fig. 3)

| Name | 1 | 2 | 3 | 4 | 5 | 6 | 7 | 8 | 9 |
|-------|---|---|---|---|---|---|---|---|---|
| 1 14 | | ● | ● | • | • | • | • | • | • |
| 2 12 | | | ● | • | • | | | | • |
| 3 11 | | ● | | ● | • | • | • | • | • |
| 4 15 | | • | • | | ● | • | • | • | • |
| 5 5 | | • | • | • | | ● | • | • | • |
| 6 WP1 | | • | • | • | • | | ● | • | • |
| 7 WP2 | | • | • | | | • | | ● | • |
| 8 WP3 | | ● | ● | • | • | • | • | | • |
| 9 WP4 | | • | • | • | • | • | • | • | |

● 0 - 20466

• 45945 - 69072

◐ 20467 - 45944

◑ > 69072

4. Conclusions

Ordering of environmentally conscious technologies by taxonomic method in a motor transport facility is an effective way of finding an appropriate solution. The taxonomic method can also be used to effectively choose a logistic system for environmental threats occurring in a motor transport facility. Czekanowski's matrices can be employed to additionally verify the differentiation results for environmentally conscious technologies and logistic systems.

The evaluation of the results treated in this paper allows for their interpretation with respect to the usefulness of the technologies in question. The list covering the harmfulness of the waste for the group of 5 companies characterized by the slightest impact on the environment shows that the company behind the number 2 is in the most favourable situation in this respect. Moreover, taxonomic differentiation allows us to state that technology no. 2 is also in a favourable situation with respect to power consumption (the model technology WP4 is also close to technology no. 8).

The same dendrite also reveals that the desirable technology can be company no. 13 which is close to WP3 in the taxonomic space.

In the group of companies ordered according to the mean harmfulness of the waste, the technology behind no. 3 has the lowest value which means that it is in the most favourable situation in terms of its impact on the environment. Technology no. 6 is close to the model technology WP1 which is not insignificant on account of CO₂ emissions (the greenhouse effect). This is revealed by dendritic differentiation of the technologies and confirmed by Czekanowski's diagram.

In the group of 5 companies that are the most troublesome to the environment in terms of harmfulness of the waste they generate the best technologies are numbered 11 and 14. Technology no. 14 that is closest to the model value WP3 in the taxonomic space is characterized by the lowest value of parameter P3 in this group of companies. Dendrite ordering is verified by Czekanowski's diagonal matrix which shows similar results.

References

- [1] Chaciński, J., Jędrzejewski, Z., *Zaplecze techniczne transportu samochodowego*, Wyd. Komunikacji i Łączności, p. 423, Warszawa 1982.
- [2] Matusek, M., Bartnicki, M., *Metoda porównań międzyzakładowych z wykorzystaniem metod taksonomicznych*, Zeszyty Nauk. PŚI, Nr 1597, pp. 45-53, Gliwice 2003.
- [3] Młoda, A., *Analiza taksonomiczna w statystyce regionalnej*, Wyd. DIFIN, p. 262, Warszawa 2006.
- [4] Stolarski, B., *Metody taksonomiczne w technologii samochodów*, Wyd. Politechniki Krakowskiej, p.117, Kraków 1990.
- [5] Zielińska, E., *Możliwość wykorzystania metody taksonomicznej do opracowania modelu zarządzania ekologicznego w zapleczu technicznych środków transportu*, Materiały Międzynarodowej Konferencji Naukowej SAKON'06 nt. „Metody obliczeniowe i badawcze w rozwoju pojazdów samochodowych i maszyn roboczych samojezdnych; Zarządzanie i marketing w motoryzacji, pp. 263-268”, Rzeszów-Przeclaw 2006.
- [6] Zielińska, E., *Logistyka zaplecza technicznych środków transportu samochodowego w aspekcie problemów ekologicznych*, Rozprawa doktorska, Uniwersytet Przyrodniczy w Lublinie, p. 170, Lublin 2008.
- [7] Zielińska, E., Lejda, K., *Wykorzystanie metody taksonomicznej do oceny problemów ekologicznych w zapleczu technicznym transportu*, Czasopismo Logistyka N° 1/2009 - wersja elektroniczna – CD.
- [8] Zielińska, E., Lejda, K., *Ecological problems of transport vehicle*, Polish Academy of Sciences – Branch in Lublin, TEKA, Vol. X, pp. 548-556, Lublin 2010.



THE ANALYSIS OF THE DESIGN LIMITATIONS OF THE SELECTED THERMODYNAMIC PARAMETERS OF THE WORKING MEDIA IN THE MARINE WASTE ENERGY RECOVERY SYSTEMS

Ryszard Michalski

West Pomeranian University of Technology in Szczecin
71-065 Szczecin, 41 Piastów Ave,
tel.: +48 91-449 49 41
e-mail: rysard.michalski@zut.edu.pl

Abstract

The waste energy utilisation degree in the marine Diesel power plants grows as the exhaust gas boiler exhaust gas temperature decreases. The limitation in this case is not only a likelihood of sulphur corrosion occurrence in the boiler and exhaust gas ducts, but also the obtainment of too little, or altogether negative values of so called pinch point.

The article presents the analysis of the limitations related with the pinch point and minimum boiler exhaust gas temperature which are possible for the acceptance at the stage of the preliminary design in terms of the system correct operation and its energetic effectiveness. The possible negative results of the exhaust gas boiler exhaust gas temperature reduction and the methods to prevent the results have been presented. In the effect of conducting the calculations for the selected thermodynamic parameters of a model waste energy recovery system there has been presented the graphic course of the changes in the achieved power of the steam turbine generator and the pinch point in exhaust gas boiler in relation to the boiler exhaust gas temperature, the generated steam pressure, recovery system feedwater temperature and the main engine exhaust gas temperature. The data presented in the article are but of general nature and reflect the relations between the selected thermodynamic parameters that characterise the model of the waste energy recovery system in the marine Diesel power plant.

Keywords: *marine power plants, waste energy recovery systems, design limitations*

1. Introduction

The obtainment of the high energetic effectiveness ratios on the Diesel powered ships [also referred to as the ‘motor ships’] is possible owing, inter alia, to the application of the complex waste energy recovery systems. One of the methods to make it possible to improve the effectiveness of the use of this energy is the application of the possibly low temperature of the exhaust gas boiler outlet exhaust gas that characterises the waste energy deep recovery systems. It is universally assumed that the limit values of this temperature result chiefly from the level of water dew point temperature of the exhaust gas directed to the exhaust gas boiler and the heat transfer surface in the boiler possible to be accepted from the economic point of view. However it should also be noticed that there are some other limitations resulting from the physical phenomena occurring in the exhaust gas boilers which are present during the operation of the waste heat recovery systems. The tendency of the boiler heating surface to get contaminated is, among others,

of significant importance. This phenomenon in the exhaust gas boilers is related with the adherence of the soot particles contained in the exhaust gas to the heating surface. The dominating mechanisms during this process are the inertial collision of those particles with the heat transfer surface and their tearing away as well as thermophoresis (Soret effect), resulting from the difference in the temperatures between the heating surface and the exhaust gas [9]. The inertial collisions of the solid particles form the prevailing mechanism for the particles exceeding 10 μm [9]. The presence of the asphaltenes in fuel significantly increases the contents of those particles in the exhaust gas. It should be noted that the effect of the thermophoresis decreases as the heat transfer surface in the boiler grows [2, 3]. The other unfavourable phenomenon is the generation of the sulphur trioxide in the exhaust gas in the effect of the reaction occurring both in high and low temperatures.

The sulphur oxide and water content in the exhaust gas significantly influences the value of the dew point temperature for the water in exhaust gas. This temperature is related with the water dew point temperature decreased by the value related with partial pressure values of acid and water. The adequate formulae to allow to determine this temperature have already been elaborated within the 1950's of XX century [7]. On account of relatively high general air excess factor in Diesel engines the water dew point temperature in the exhaust gas is relatively low. For the air temperature of 45°C and RH 100% the water dew point temperature amounts to approximately 48°C [3, 4]. The higher the fuel sulphur content, the higher exhaust gas water dew point temperature [8, 11, 12]. The presence of the sulphur oxides in the exhaust gas causes the generation of the sulphuric acid and thus the sulphur corrosion of the boiler elements and exhaust gas ducts. The remaining acid becomes isolated by condensation on the boiler heat transfer surface, if this has the lower temperature than the exhaust gas water dew point temperature. In case of the majority of the exhaust gas boilers the temperature of the heat transfer surface external walls is slightly higher than the temperature of the medium flowing inside the piping due to the high heat transfer coefficient at the side of this medium. Thus the temperature of the heat transfer surface in the boiler – instead of the temperature of the exhaust gas itself – is the decisive factor for the acid condensation and the corrosion intensity. The high-concentration acid gets deposited on cool surface just below the exhaust gas dew point temperature [7] and is not as aggressive to the steel as a diluted acid which occurs at the water dew point temperature [2, 7]. Therefore the exhaust gas boiler is supplied with water of adequately high temperature, exceeding the temperature of the condensate supplied by the recovery system feedwater pump.

It is worth emphasising that the exclusive application of the natural and forced LNG evaporation product as the fuel is characterised by low emission of the harmful engine exhaust gas (according to Wärtsilä the reduction is as big as the tenfold in relation to the emission of the harmful exhaust gas emitted by slow-speed Diesel engines supplied with liquid fuel [5]). It should be noted that the application of the natural gas as the fuel, particularly in the marine Diesel and gas turbine power plants, provides large potential for the heat recovery from the engine exhaust gas [4]. However, a limitation in this case might be the significantly large heat transfer surface in the boiler and the value of the minimum difference in the temperature of the exhaust gas and saturated steam (ΔT_{min}) in the exhaust gas boiler referred to as the “pinch point”. The need to maintain the positive value of this parameter may influence significantly the limitations in relation to the apparently big possibilities of the usage of the exhaust gas heat by way of lowering its temperature at the outlet from the exhaust gas boiler.

2. The Specification of the Object of the Analysis

The object of the analysis are the selected working parameters of a model recovery system of the heat contained in the ship's main engine exhaust gas. The schematic diagram of the system is presented in figure 1. The figure 2 shows the course of the changes in the working media

temperatures – exhaust gas and water as well as steam in the exhaust gas boiler. The table 1 shows, on the other hand, the basic input data for the calculations of the thermodynamic parameters of the analysed system. The calculations have been conducted, inter alia, basing on the method determined in [6].

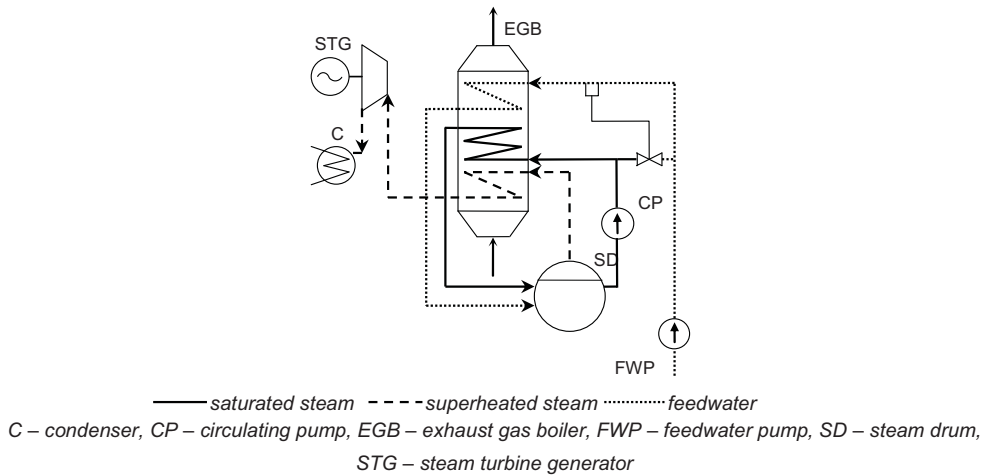


Fig 1. The simplified schematic diagram of the outlet exhaust gas heat recovery system

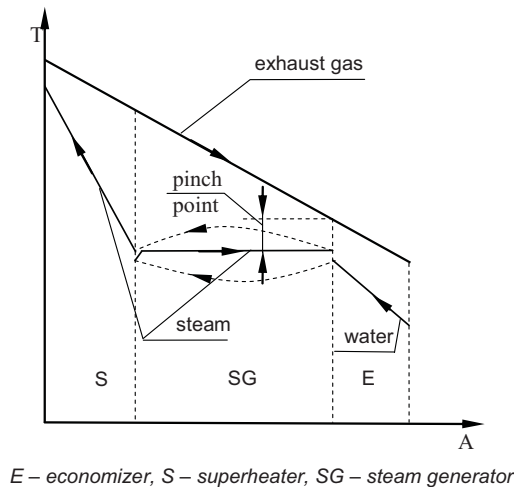


Fig 2. The courses of the changes of the thermodynamic parameters in exhaust gas boiler

Tab. 1. Calculation Input Data

| | | |
|--|-------|--------|
| Main engine exhaust gas stream | 20,28 | kg/s |
| The specific heat capacity of exhaust gas | 1,069 | kJ/kgK |
| Exhaust gas temperature after main engine | 275 | °C |
| Exhaust gas temperature after exhaust gas boiler | 180 | °C |
| Exhaust gas temperature drop after main engine | 5 | °C |
| Exhaust gas boiler efficiency | 0,98 | - |
| Steam turbine generator efficiency | 0,675 | - |
| Steam consumption coefficient for the needs of steam turbine generator | 0,07 | - |
| Recovery system feedwater temperature | 60 | °C |

| | | |
|---|-------|-----|
| Generated steam pressure | 0,7 | MPa |
| Steam pressure drop before steam turbine generator | 0,015 | MPa |
| Steam temperature drop before steam turbine generator | 2 | °C |
| Steam pressure in condenser | 0,005 | MPa |
| Heat flux for heating purposes | 600 | kW |

The research covered the influence of the changes of the exhaust gas temperature after exhaust gas boiler, the pressure of the generated steam in the exhaust gas boiler, the temperature of the recovery system feedwater and the temperature of the main engine exhaust gas on the value of the power output of the steam turbine generator and the value of pinch point in the boiler. The values of the remaining parameters shown in table 1 have been meanwhile maintained.

The analysis did not include, inter alia, the change of the steam turbine generator efficiency ensuing from the change of its power output and the steam parameters at the turbine inlet and outlet. The inclusion of this value does in fact influence the value of the turbine generator power output whereas it does not have any influence on the value of the pinch point in boiler which has been the basic object of the conducted analysis. The research has not covered either the influence of the thermodynamic parameters on the size of the heat transfer surface in the boiler and condenser and operation parameters of the other auxiliary equipment of the waste energy recovery system.

3. The Analysis Results Specification

The graphic results of the analysis conducted are shown in figures No 3 to 10. The increase of the temperature of the exhaust gas leaving the exhaust gas boiler leads to decrease in the power output of the steam turbine generator which is the evident effect of the reduced amount of the heat recovered in the exhaust gas boiler. This is shown in figure 3. The assumption of the low value of this temperature allows to achieve the bigger power output of the steam turbine generator, but it is also likely to cause that the pinch point value shall become negative. As shown in figure 4, for the set of the data determined in table 1, the zero value of the pinch point has been reached at the exhaust gas temperature of approximately 143°C. Below this value ΔT_{\min} shall be already negative. Thus the excessive reduction of the temperature of the exhaust gas at the exhaust gas boiler outlet, even if the exhaust gas water dew point temperature is not exceeded, may turn unacceptable from the technical point of view.

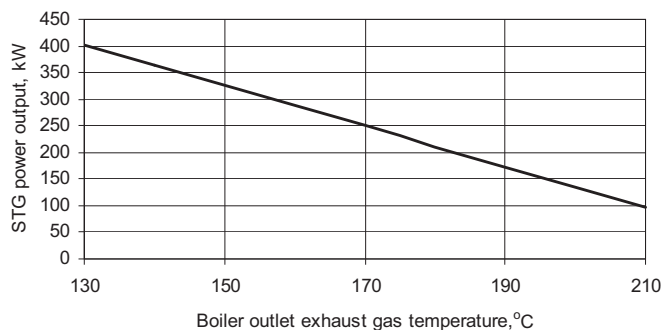


Fig 3. The relation of the STG power output and the temperature of the of the exhaust gas at the boiler outlet

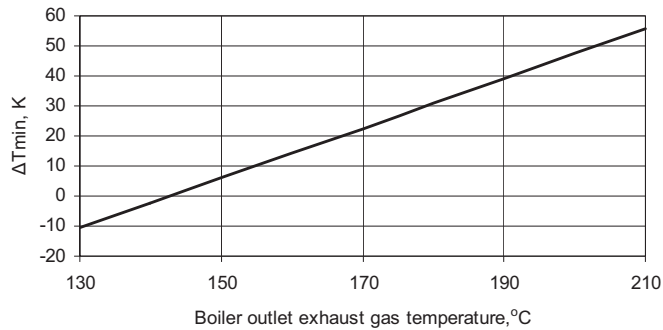


Fig 4. The relation of the boiler minimum temperature and the boiler outlet exhaust gas temperature

The course of the value ΔT_{\min} is also influenced by the pressure of the steam generated in the boiler. The increase of the steam pressure favourably influences the steam turbine generator power output (provided that the constant *effective efficiency* is assumed), because this increases the efficiency of Clausius-Rankine cycle. This is shown in figure 5. However, with the steam high pressure values the value of ΔT_{\min} decreases, which is shown in figure 6. Thus the assumption of the high steam pressures with the simultaneous reduction of the exhaust gas at the exhaust gas boiler outlet is likely to accelerate significantly the moment of reaching too low values of pinch point.

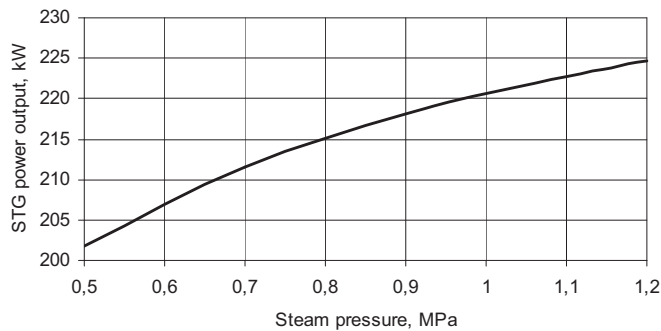


Fig 5. The relation of the steam turbine generator power output and the steam pressure

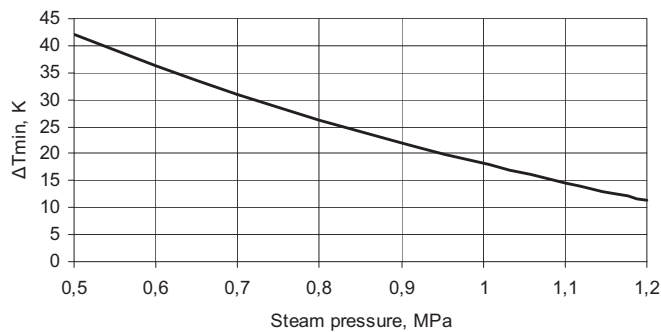


Fig 6. The relation of the minimum temperature in the boiler and steam pressure

A significant parameter influencing both the reached power output of the steam turbine generator and the pinch point value is the temperature of the feedwater supplied by pump to the recovery system. Its value results from the balance of the condensate mass stream and the heat of the heating steam condensate returning from the heaters and the condensate mass and the heat of the turbine outlet steam condensate. The bigger steam turbine generator power output corresponds to the higher temperature of this water (figure 7).

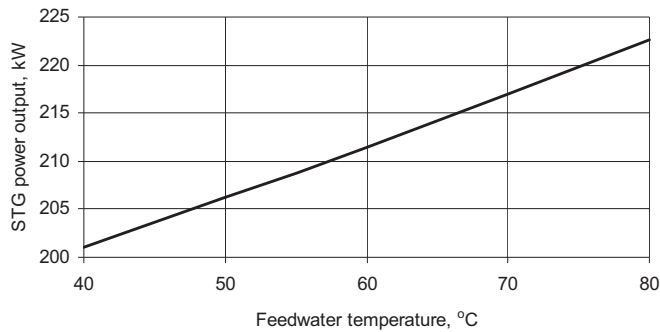


Fig 7. The relation of steam turbine generator power output and the recovery system feedwater temperature

As shown in figure 8 the pinch point value decreases however as the recovery system feedwater temperature grows. From this point of view it becomes favourable to reduce the steam pressure in condenser owing to which the steam condensation temperature in the condenser is reduced which in turn leads to reduction of the recovery system feedwater temperature. While striving to maintain the possibly high energetic effectiveness of the recovery system, this temperature might be increased within certain limits by the application, inter alia, of the complex recovery of the engine waste energy where the heat contained in engine charging air or the remaining waste heat of low energetic potential are used [1].

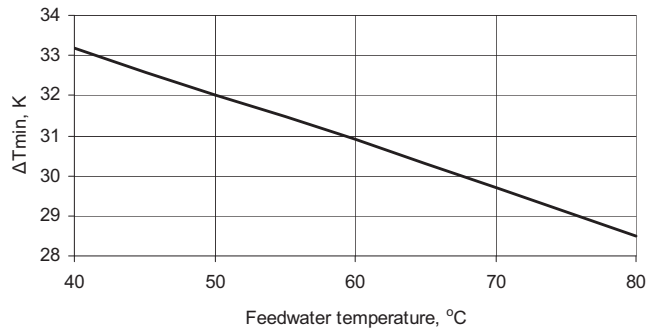


Fig 8. The relation of the boiler minimum temperature and the recovery system feedwater temperature

The exhaust gas temperature after main engine, thus the temperature of the exhaust gas at the inlet to the exhaust gas boiler, has the similar influence on both the steam turbine generator power output and the value of the pinch point. The courses of the changes of these parameters are shown in figures 9 and 10, respectively. They reflect the increase of their value accompanying the increase of the temperature of the exhaust gas after main engine. The outlet exhaust gas temperature of the engine assumed as the main propulsion, however, depends on its characteristics/specification data and may only constitute a constant input value for the calculations.

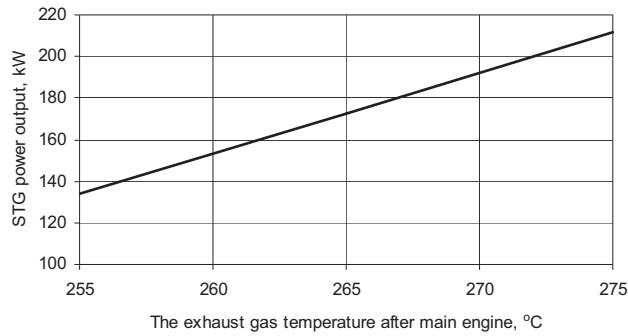


Fig 9. The relation of the steam turbine generator power output and the main engine exhaust gas temperature

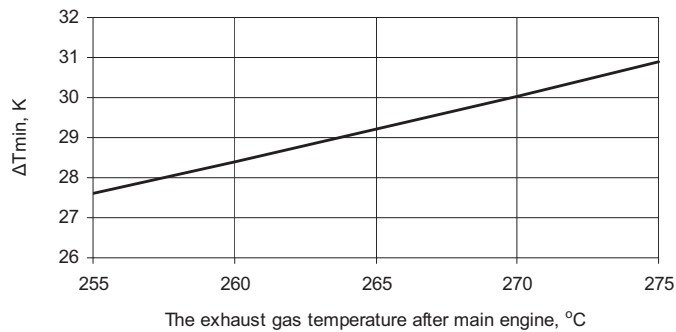


Fig 10. The relation of the boiler minimum temperature and the temperature of the main engine exhaust gas

4. Conclusions

While striving to improve the ship's energetic effectiveness one should tend to adopt the marine power plant arrangements characterised, inter alia, by the high degree of the utilisation of the chemical energy contained in the fuel burnt. This can be achieved, apart from the improvement of the primary engine efficiency, by way of the complex and deep recovery of the waste energy.

The waste energy utilisation degree grows as the exhaust gas boiler outlet exhaust gas temperature decreases. The limitation in this case is not only the likelihood of the occurrence of the sulphur corrosion in the boiler and exhaust gas ducts, but also the obtainment of too low or just altogether negative values of so called pinch point value.

Several other parameters also influence the pinch point value. They include, among others, the generated steam pressure or the recovery system feedwater temperature whose higher values allow to increase the theoretical efficiency of the steam cycle, however, at the same time causing the reduction of the pinch point value.

The data presented in the article are but of general nature and reflect the relations between the selected thermodynamic parameters that characterise the model of the waste energy recovery system in the marine Diesel power plant.

References

- [1] Adamkiewicz, Andrzej, Michalski, Ryszard, Zeńczak, Wojciech, *Wybrane problemy technologii konwersji energii w okrętowych systemach energetycznych*, KAPRINT, Lublin 2012.
- [2] Condra, Thomas, *Low Temperature Exhaust Gas Heat Recovery*, 17 th International Congress on Combustion Engines, D-82, Warszawa 1987.
- [3] Condra, Thomas, *Research into Low Temperature Exhaust Gas Heat Recovery*, MER, No 6, 1988, pp 19-21.
- [4] Głomski, Paweł, Michalski, Ryszard, *Selected Problems of Boil-Off Gas Utilization on LNG Carriers*, Journal of Polish CIMAC, 2011, Vol 6, No1, pp.141-148.
- [5] Laurilehto, M., *Propulsion systems for future LNG carriers*, <http://www.wartsila.com>.
- [6] Michalski, Ryszard, *Siłownie okrętowe*, Politechnika Szczecińska, Szczecin 1997.
- [7] Müller, P, *Beitrag zur Frage des Einflusses der Schwefelsäure auf die Rauchgas-Taupunkttemperatur*, Chemie-Ing. Techn., 1959/Nr5, pp.345-351.
- [8] Perepeczko, Andrzej, *Okrętowe kotły parowe*, Wydawnictwo Morskie, Gdańsk 1979.
- [9] Rosner, D. E., *Rational Engineering Correlations of Diffusional and Inertial Particle Deposition Behaviour in Non-Isothermal Forced Convection Environments*, Fouling of Heat Exchanger Surfaces Conference, White Haven, 1982, pp. 235-256.
- [10] Sneller, Slavko, *The "Cold Corrosion" Limits of Marine Exhaust-Gas Boiler*, IX Symposium on Theory and Practica of Shipbuilding. In memorien prof. Leopold Sorta, pp. 192-200, Dubrownik 1990.
- [11] Soot Deposits and Fires in Exhaust Gas Boiler, MAN&Diesel A/S, Copenhagen, Denmark, 2004.
- [12] Urbański, Przemysław, *Spalinowe Siłownie Okrętowe*, Politechnika Gdańska, Gdańsk 1968.



INFLUENCE OF TEMPERATURE AND TOTAL STRAIN ON THE FATIGUE DAMAGE OF CAST STEEL

Stanisław MROZIŃSKI¹, Radosław SKOCKI²

^{1,2} *University of Technology and Life Sciences in Bydgoszcz, Faculty of Mechanical Engineering, Al. Prof. S. Kaliskiego 7, 85-789 Bydgoszcz,
tel.: 48 52 340-82-64, fax: 48 52 340-82-71, e-mail: stanislaw.mrozinski@utp.edu.pl*

Abstract

The paper presents test results of the course of fatigue damage of the GX12CrMoVNbN9 in conditions of the constant-amplitude loadings. As the parameter of fatigue damage there was assumed the change of mechanical properties which was determined in various stages of fatigue life. Three stages with a different rate of growth of the fatigue damage parameter were distinguished in the course of fatigue damage. It was stated that the critical value for the fatigue damage parameter depends on the level of loading and temperature.

Keywords: *cyclic properties, fatigue life, fatigue damage, martensitic cast steel*

1. Introduction

Description of the course of fatigue damage cumulation and decrease of the mechanical properties of structural materials caused by the cyclic loading makes an essential engineering problem for many years [1, 2]. Studies on fatigue damages development were always connected to the searching for applicable measure of the fatigue damage. Various methods were used (direct and indirect): optical, changes of the electric or magnetic field, temperature, acoustic emission, mechanical properties, etc. [3, 4, 5, 6]. Mentioned methods are not for all-purposes and they are chosen dependently of the character of the fatigue damage development.

In this paper the change of the material reaction to the cyclic loadings was assumed as the fatigue damage parameter. This paper attempts to verify the methods for measuring fatigue damage parameter under low cycle fatigue (LCF) conditions.

LCF tests can be carried out under controlled loading or strain. Under controlled loading testing machine keeps the amplitude of the loading constant ($\sigma_a = \text{const}$). During the tests changes in the total strain (ε_{ac}) or plastic strain (ε_{ap}) may occur. It may be caused due to the fatigue damage. During the tests under controlled strain the amplitude of total strain ($\varepsilon_{ac} = \text{const}$) or plastic strain ($\varepsilon_{ap} = \text{const}$) is kept constant which afterwards may result in changes of the amplitude of the loading (σ_a).

In Fig. 1 there is presented a scheme of possible changes of control parameters of the testing machine and measured parameters for the mentioned tests.

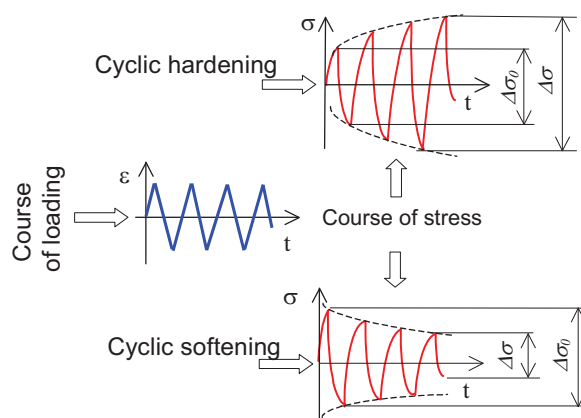


Fig. 1. Controlled parameters of testing machine and measured values

During LCF tests softening or hardening of material often takes places, followed by so called stabilization. Changes of the analysed hysteresis loop parameters after the stabilization can be ascribed to the progressive process of the fatigue damage.

Damage parameter can be defined in various ways [7, 8, 9]. In case of loading control ($\sigma_a = \text{const}$) the damage parameter D_σ may be described as follows:

$$D_\sigma = 1 - \frac{\Delta \varepsilon_0}{\Delta \varepsilon} \quad (1)$$

where: $\Delta \varepsilon_0$ – the range of total strain during the stabilization period

$\Delta \varepsilon$ – the range of total strain during the damage period

Whereas for the tests with the total strain control ($\varepsilon_{ac} = \text{const}$) the damage parameter D_σ may be described as follows:

$$D_\varepsilon = 1 - \frac{\Delta \sigma_0}{\Delta \sigma} \quad (2)$$

where: $\Delta \sigma_0$ – the range of stress during the stabilization period,

$\Delta \sigma$ – the range of stress for the damage period,

The aim of this work is the analysis of the influence of the temperature and level of total strain on the critical value of the damage parameter and its course during loadings.

2. Description of tests

Specimens for the tests were made of GX12CrMoVNB9-1 martensitic cast steel. The shape and dimensions of the specimens were in agreement with the standard [12] PN-84/H-04334. Chemical composition of the cast steel is collected in table 1.

Tab. 1. Chemical composition [%]

| C | Mn | Si | P | S | Cr | Mo | V | Nb | N |
|------|------|------|-------|-------|------|------|------|------|------|
| 0.12 | 0.47 | 0.31 | 0.014 | 0.004 | 8.22 | 0.90 | 0.12 | 0.07 | 0.04 |


At first static tensile tests were carried out in order to determine levels of total strain for the fatigue tests. There were used specimens for the fatigue tests. The specimens underwent increasing loading with the rate of machine piston displacement speed of 0.05 mm/s. Specimen's elongation was measured by a 12.5 mm gauge length axial extensometer with measuring range of 3.75 mm which was fixed to the specimen. The static tensile tests were carried out under temperatures of 20, 400, 600°C. Strength properties are collected in table 2.

Tab. 2. Strength parameters of cast steel for the three temperatures

| Parameter | Temperature, °C | | |
|-----------------|-----------------|--------|--------|
| | 20 | 400 | 600 |
| R_e , MPa | 503 | 418 | 303 |
| R_m , MPa | 663 | 535 | 338 |
| $El_{12.5}$, % | 36.3 | 38 | 63.5 |
| A , % | 63.4 | 71 | 87.3 |
| E , MPa | 206870 | 180234 | 150120 |

After analysing static tensile tests five levels of total strain ε_{ac} were accepted in low cycle tests according to table. 3.

Tab. 3. Parameters of loading programs

| Course of loading | Parameters |
|---|----------------------------|
|  | $\varepsilon_{ac1}=0,25\%$ |
| | $\varepsilon_{ac2}=0,3\%$ |
| | $\varepsilon_{ac3}=0,35\%$ |
| | $\varepsilon_{ac4}=0,5\%$ |
| | $\varepsilon_{ac5}=0,6\%$ |
| | $f=0,2\text{ Hz}$ |

Tests consisted in cyclically loading specimens until the specimens break. Procedure of measuring strain employed for LCF tests was the same as for static tensile test. Test temperature of 20°C and frequency of 0.2 Hz were employed. Accepted sampling frequency of force signal and strain signal allowed to describe loading cycles with set of 200 points. As the end criterion of the fatigue test, the deformation of hysteresis loop (during semi cycle of compression) is accepted. During the tests momentary values of loading force and strain for selected loading cycles were recorded.

3. Test results and discussion

Recorded momentary values of the loading force and strain for loading cycles allowed to plot the hysteresis loop in stress σ - strain ε coordinate system. Stresses in the specimen under tensile loading were calculated by dividing momentary value of loading force by cross-sectional area before the specimen was loaded. Exemplary hysteresis loops for the two levels of total strain ($\varepsilon_{ac}=0,25\%$ and $\varepsilon_{ac}=0,6\%$) obtained for the two levels of temperature ($T=20^\circ\text{C}$ and $T=600^\circ\text{C}$) were shown in Fig 2 and 3.

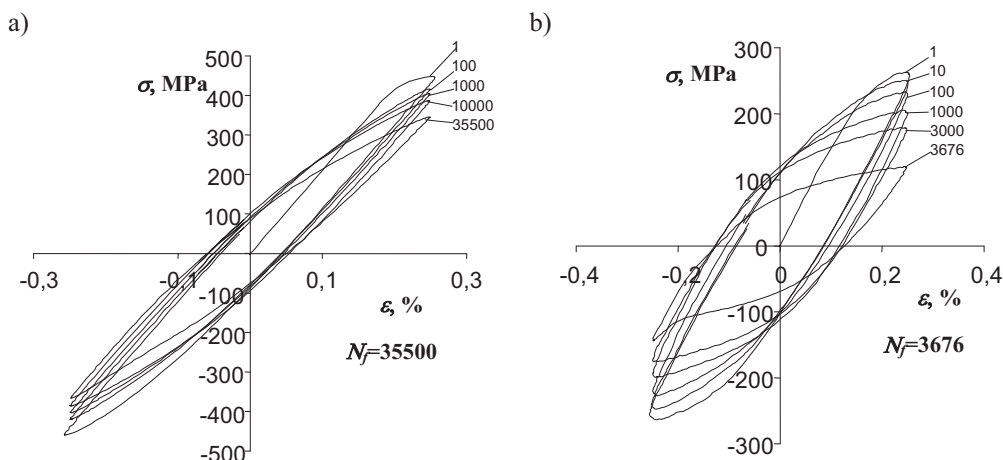


Fig. 2. Hysteresis loops for the level of total strain of $\varepsilon_{ac}=0,25\%$: a) $T=20\text{ }^{\circ}\text{C}$, b) $T=600\text{ }^{\circ}\text{C}$

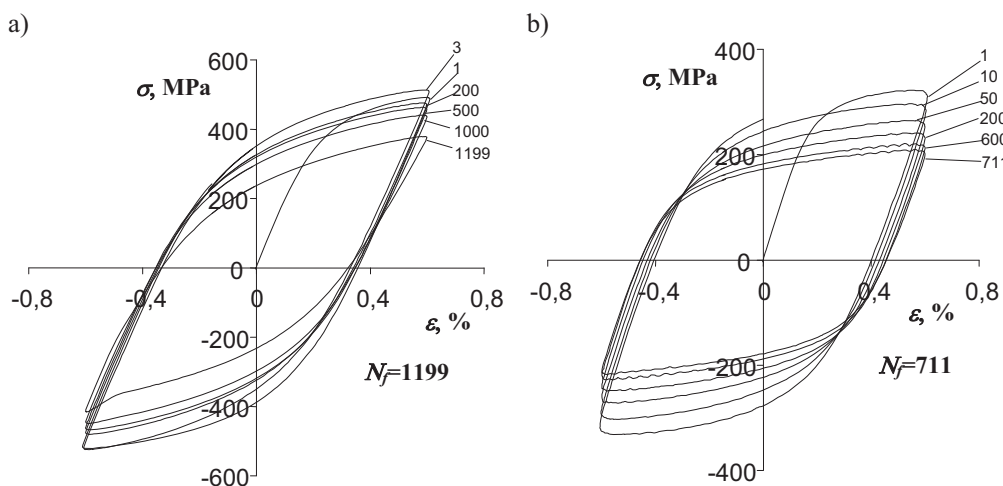


Fig. 3. Hysteresis loops for the level of total strain of $\varepsilon_{ac}=0,6\%$: a) $T=20\text{ }^{\circ}\text{C}$, b) $T=600\text{ }^{\circ}\text{C}$

On the basis of analysis of hysteresis loop shape it can be stated that tested material cyclically softens. With increasing of the number of cycles the range of stress decreases $\Delta\sigma$ and the range of plastic strain $\Delta\varepsilon_{ap}$ increases. The above changes were observed at room temperature and at elevated temperatures. In order to illustrate the changes of the mentioned parameters there were shown exemplary courses of changes of the range of stress $\Delta\sigma$ in the function of number of loading cycles obtained for the two temperatures (Fig. 4).

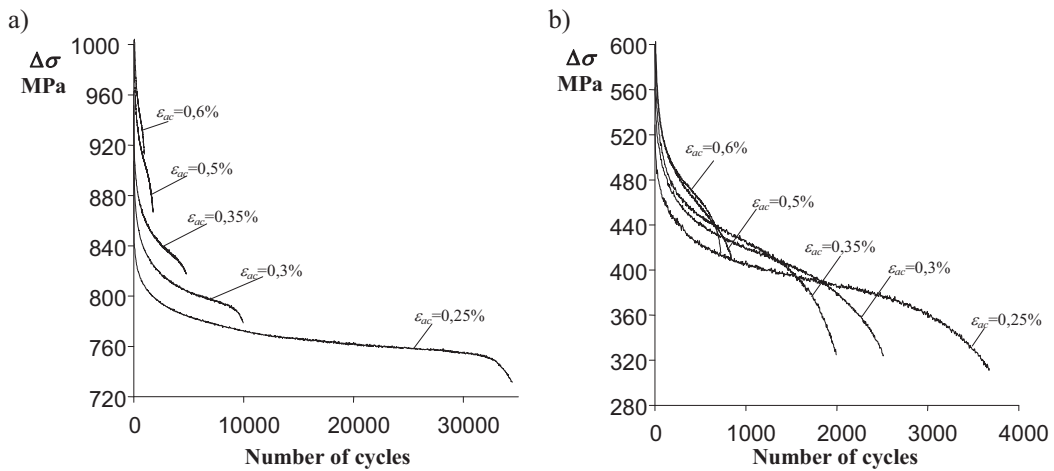


Fig. 4. Changes of stress $\Delta\sigma$ in the function of loading cycles: a) $T=20^\circ\text{C}$, b) $T=600^\circ\text{C}$

On the basis of the performed curves it can be stated that during LCF tests there was lack of the stabilization period. In the courses of $\Delta\sigma$ three distinctive stages can be drawn with various intensity of softening. These stages were widely described in the work [10, 11].

Values of the range of stress $\Delta\sigma$ from different period of fatigue life were employed to calculate the damage parameter D_σ . Due to lack of the stabilization period, the value of $\Delta\sigma_0$ determined in equation (2) was assumed from the first loading cycle.

Exemplary results of changes of the damage parameters D_σ in the function of cycles obtained for the five levels of total strain at temperature of 20 and 600 °C were shown in Fig. 5.

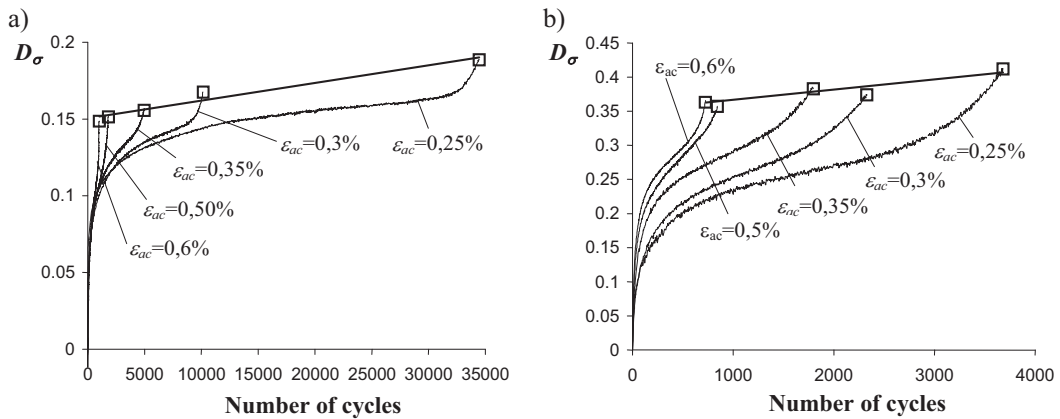


Fig. 5. Changes of damage parameter D_σ in the function of number of cycles: a) $T=20^\circ\text{C}$, b) $T=600^\circ\text{C}$

After comparative analysis of curves of damage parameter D_σ it can be stated that their course depends on the level of total strain. On the diagrams of this parameter three characteristic stages can be distinguished. The stage of quick growth of the damage parameter (stage A), steady growth (stage B) and once again quick growth (stage C). These stages occurred for all levels of total strain. The largest rate of growth of D_σ occurred in the stage A. The rate of growth of D_σ in this stage is influenced by the level of total strain ϵ_{ac} and temperature of the tests. In order to evaluate the influence of the temperature on the changes of the D_σ parameter in Fig. 6 there was shown

exemplary courses of this parameter for the three levels of total strain and three temperatures (20, 400, 600 °C).

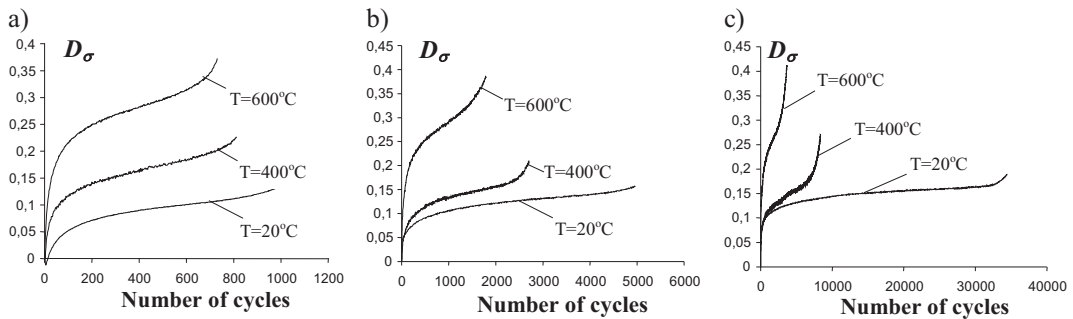


Fig. 6. Influence of the temperature on the damage parameter D_σ : a) $\varepsilon_{ac}=0,25\%$, b) $\varepsilon_{ac}=0,35\%$, c) $\varepsilon_{ac}=0,6\%$

According to the diagrams in Fig 5 and 6 it can be stated that the value of the D_σ parameter at the moment when damage of specimen occurs is not constant. The value is influenced by the level of total strain and temperature of the tests. In Fig. 7. there were presented diagrams which illustrate the influence of the level of total strain and temperature on the critical value of the damage parameter D_σ .

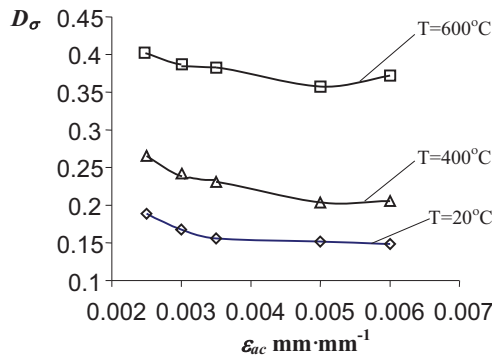


Fig.7. Influence of total strain and temperature on critical value of damage parameter D_σ

On the basis of performed curves it can be stated that the critical value of the damage parameter decreases with the increase of total strain ε_{ac} . Decrease in the damage parameter with the increase of the total strain is not large and equals from 11% for the temperature of $T=20^\circ\text{C}$ to about 14% at the temperature of $T=600^\circ\text{C}$. The temperature of tests is very important. The lowest values of the D_σ parameter occurs at the room temperature ($T=20^\circ\text{C}$). The highest values occurs at the temperature of $T=600^\circ\text{C}$. The critical value of the D_σ at the temperature of $T=600^\circ\text{C}$ is almost 2 times higher than its values at the temperature of $T=20^\circ\text{C}$.

4. Conclusions

Tested material softens during LCF with no significant stabilization period. Lack of this period makes difficult an analysis of the D_σ damage parameter during LCF test as its value covers the changes of properties caused by the softening of material and also course of the damage. In order

to formulate applicable conclusions it is necessary to perform tests with using another parameters of hysteresis loop which would be insensitive on changes of cyclic properties e.g. plastic strain energy ΔW_{pl} . It was shown in the work [10, 11].

The course of D_σ damage parameter is influenced by the level of total strain and temperature of test. On the basis of analysis of diagrams with damage parameter in the function of loading cycles three characteristic stages can be determined with various rate of growth of the damage parameter. Critical value of this parameter when the material breaks is not a constant value and it depends on the test temperature and slightly on the level of total strain.

Minor influence of the level of total strain on the critical value of the damage parameter confirms the reports in the literature, where this parameter is considered to be in use in scientific research or in engineering to control the level of damage of technical object. A drawback of the method of measuring the level of damage is a destructive character of the tests which has to be performed in order to obtain the information about momentary values of the damage parameter.

References

- [1] Chakraborti, P.C.; Mitra, M.K., *Room temperature low cycle fatigue behaviour of two high strength lamellar duplex ferrite–martensite (DFM) steels*. International Journal of Fatigue, Volume: 27, Issue: 5, 2005, pp. 511-518.
- [2] Collins J.A., *Failure of Materials In Mechanical Design. Analysis, Prediction, Prevention*. John Wiley & Sons, New York 1993.
- [3] Fatemi A., Yang L., *Cumulative Fatigue Damage and Life Prediction Theories: A Survey of the State of the Art for Homogeneous Materials*. International Journal of Fatigue 20(1), 1998, pp. 9-34,
- [4] Lemaitre J., *A Course on Damage Mechanics*, Springer Verlag, 1996.
- [5] Kukla D., Dietrich L., Ciesielski M., *Ocena stopnia uszkodzenia eksploatacyjnego materiału rurociągu parowego na podstawie analizy zmian właściwości zmęczeniowych i mikrostruktury*. VI Międzynarodowe Sympozjum Mechaniki Materiałów i Konstrukcji, Augustów, 2011.
- [6] Socha G., *Prediction of the fatigue life on the basis of damage progress rate curves*. International Journal of Fatigue. Vol. 26, No 4. 2004, pp. 339-347.
- [7] Kurzydłowski J., Sychalski W. oraz inni., *Research on possibilities of application of non-destructive testing in degradation evaluation of materials used in infrastructure working under the influence of aggressive hydrogen environment*. 3rd International Conference on Environmental degradation of Engineering Materials. Gdańsk Jastrzębia Góra, 2007.
- [8] Cheng Y. S, Huang Y., *Measurement of Continuous Damage Parameter*, Engineering Fracture Mechanics, Vol 31(6), 1988, pp. 985-992,
- [9] Piechnik S., Pachla H., *Law of Continuous damage Parameter for Non-Ageing Materials*, Engineering Fracture Mechanics, Vol. 12, 1979, pp. 199-209.
- [10] Mroziński S., Skocki R., *Wrażliwość parametrów pętli histerezy na zmiany właściwości cyklicznych*. XXIV Sympozjum Zmęczenia i Mechaniki Pęknięcia, Bydgoszcz –Pieczyska 2012, pp. 105-106.
- [11] Mroziński S., *Stabilizacja własności cyklicznych metali i jej wpływ na trwałość zmęczeniową*. Wydawnictwo Uczelniane Uniwersytetu Technologiczno-Przyrodniczego, Rozprawy Nr 128, Bydgoszcz, 2008.
- [12] PN-84/H-04334 Badania niskocyklowego zmęczenia metali.

The paper was financed from MNiSW funds for the education in 2011-2013 years as a research project no. 1215/B/T02/2011/40.



SOME ASPECTS OF TORSIONAL VIBRATION ANALYSIS METHODS OF MARINE POWER TRANSMISSION SYSTEMS

Lech Murawski

Gdynia Maritime University
ul. Morska 81-87, 81-225 Gdynia, Poland
tel.: +4858 6901 480, fax: +4858 690 13 99
email: lemur@wm.am.gdynia.pl

Abstract

In the paper, the torsional vibrations of marine power transmission system's nonlinear method have been presented. Short presentation of marine propulsion system evolution (and its influence on ship's vibration level) in the last 30 years was included in the introduction. Some aspects of the modeling method of the elements of propulsion system have been shown. Comparison between one-degree model and 3-D Finite Element Method model was discussed. Short description of advantages and disadvantages of the undercritical and overcritical propulsion system was presented. Modeling method of propeller's mass characteristics and damping recalculation method have been shown as an example. Specialised software, for the marine power transmission system torsional vibration's analysis, made by the author, has been performed as an iterative process. Also example of torsional vibration analysis, for tanker ship, was presented in the paper. A discussion about calculation results was included in the final part of the paper. Overcritical power transmission system is better for typical ship (with slow-speed main engine and directly driven propeller).

Keywords: torsional vibration, marine propulsion system, FEM procedure, damping, added water mass

1. Introduction

Two-stroke, slow speed main engines are mostly installed on merchant ship since the late 70-ties (oil crisis). The engines are connected to a directly driven propeller by a relatively short shaft line. A typical marine propulsion system is presented on Fig. 1.

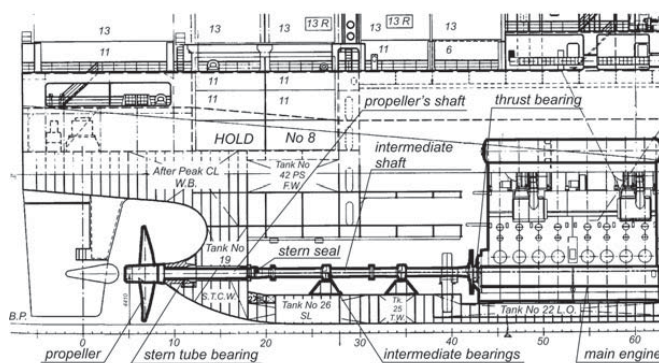


Fig. 1. Typical power transmission system

In the same time, the power from one engine's cylinder has been increased. Therefore engines have less cylinders and the engine room is shortened (cargo space is larger). Described type of propulsion system has a lot of advantages (e.g. efficiency) but is a source of relatively high vibrations level. Vibrations may have dangerous influence on crew comfort and ship's equipments strength and then on the ship safety.

The ability to predict a propulsion system operating parameters by numerical analysis is very important. During the design process all changes are possible and cheap, but when the ship is built they become nearly impossible. One of the most important parameter is torsional vibrations of the power transmission system. Torsional vibrations of the marine power transmission system are usually the most dangerous for the shaft line and the crankshaft [3].

Torsional vibrations are the result of the pulsing torque of the reciprocating combustion engine as well as reciprocating propeller's power output, and the torsional elasticity of the power transmission system. All system components like the crankshaft, intermediate shaft, propeller shaft and optional couplings and gears have to transmit the static and additionally dynamic torque. Research methods of torsional vibrations have been developed since the 1950s [9, 10]. Despite so intense research, still several elements needs to be investigated; for instance: propeller damping, cylinder damping, moment of inertia of propeller's added water mass, and characteristics of specific shaft line elements like dampers, gears, elastic clutch. All those elements may have nonlinear characteristics. On the other hand, torsional vibrations are one of the main source of coupled longitudinal vibrations and dynamic excitations (on the thrust bearing) of the ship hull and deckhouse.

2. Modeling method

For calculation purposes, the reciprocating and rotating masses of the engine including the crankshaft, the intermediate shaft(s), the propeller shaft and the propeller are, modeled as a system of rotating masses (inertias) interconnected by the torsional spring. An example of model for torsional vibration analysis, of propulsion system with 6th cylinder main engine is shown on Fig. 2. A power transmission system's model with one degree of freedom in each node is used. In general, the multi-node, unbounded vibration form is interesting. There is no problem with any boundary conditions. Therefore, more detailed model of the power transmission system is not required in typical analysis. For instance, detailed FEM model of the crankshaft (see Fig. 3) is used, by the author, only for determining coupling effects between torsional and longitudinal vibrations [7] or some special case of shaft line bending vibrations [8]. The gas pressure and mass forces of the engine act through the connecting rod mechanism on each crank, exciting torsional vibration in the system. Excitations have different frequencies therefore torsional frequencies are complex. The couplings influences on the torsional vibration as opposed to other vibration types are negligible. The torsional vibration is the source of longitudinal vibration excitations but not inversely.

The first question is where the main natural frequency of a system should be situated (obviously: away from the normal operating speed range). This can be achieved by changing the masses and/or the stiffness of the system so as to give a much higher, or much lower natural frequency, called undercritical or overcritical running, respectively. In the undercritical case one-node resonance vibration with the main critical order should occur about 35÷45% above the nominal engine speed. Such undercritical conditions can be realised by choosing a rigid shaft system, leading to a relatively high natural frequency. The characteristics of an undercritical propulsion system are normally: a relatively short shafting system, probably with no tuning wheel, a turning wheel with relatively low inertia and large diameters of shafting. The main advantage of undercritical propulsion is that the system does not have a barred speed range. But, the highest torsional stress level in the nominal main engine speed is a disadvantage. When running

undercritical, significant varying torque at nominal conditions of about 100÷150% of the mean torque is expected. This torque (propeller torsional amplitude) induces a significant varying propeller thrust. Changed propeller thrust might be a source of high level of longitudinal vibrations on the power transmission system and then double bottom and ship hull and deckhouse. For those reasons the undercritical propulsion system is quite rarely applied.

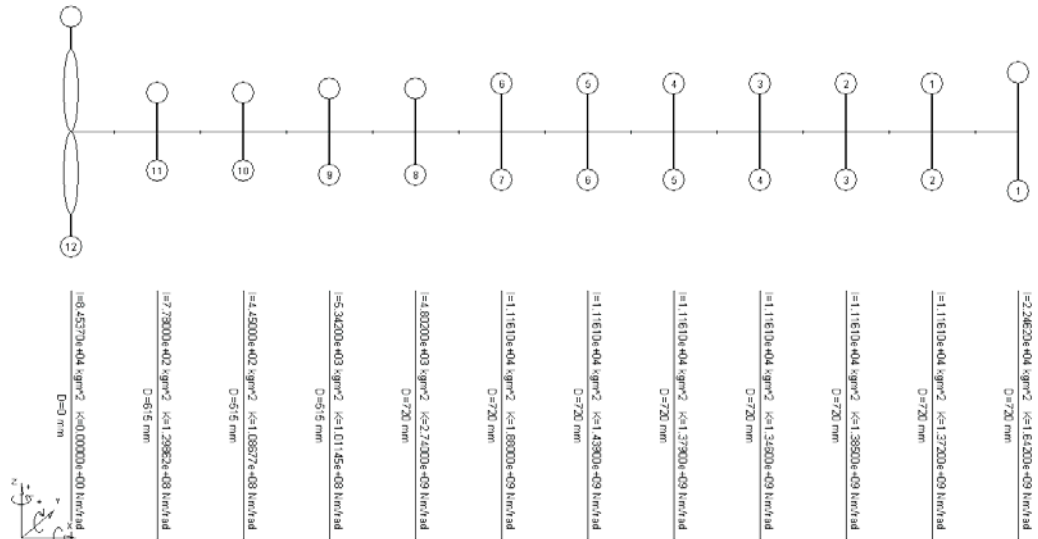


Fig. 2. Model of the power transmission system for the torsional vibration calculation

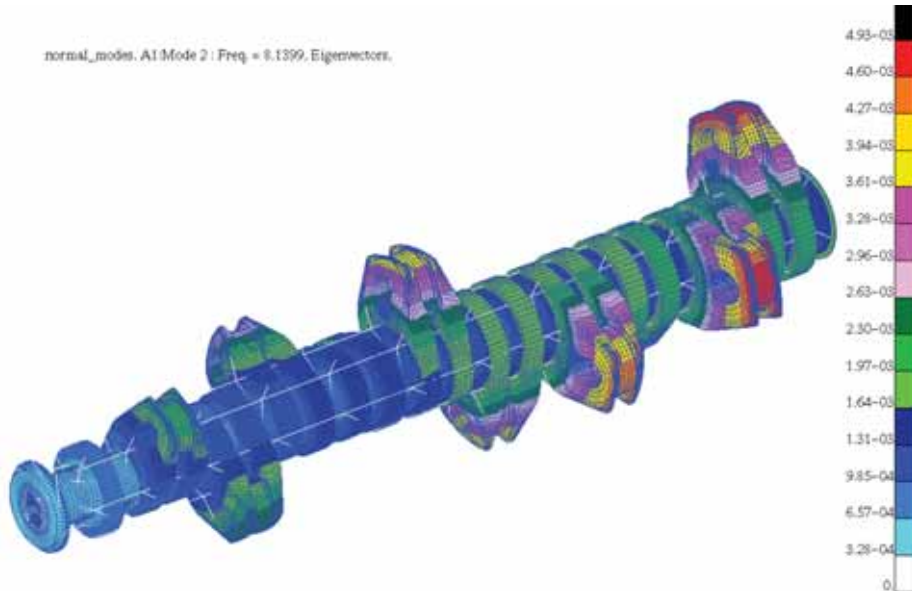


Fig. 3. Natural torsional vibrations of crankshaft of 10 K98 MC main engine

In the overcritical case one-node natural vibration frequency is placed about 30÷70% below the nominal engine speed. Such overcritical conditions can be realised by choosing an elastic shaft system, leading to a relatively low natural frequency. The characteristics of an undercritical propulsion system are a tuning wheel necessary on the crankshaft fore end, a turning wheel with relatively high inertia and shafts with relatively small diameters (requiring shafting material with a relatively high ultimate tensile strength). A barred speed range is expected in this propulsion system. Excessive torsional vibrations in overcritical conditions may have to be eliminated by the use of a torsional vibration damper. Overcritical layout is normally applied for engines with more than four cylinders.

Specialised software, for the marine power transmission system torsional vibration's calculations, has been made by the author. The algorithm is based on the Finite Element Method, written in Builder Borland C++. In each node only one, torsional degree of freedom is active. All characteristic matrixes (masses, dampings and stiffnesses) are related to a rotational degree of freedom. There are no geometrical stiffness matrix and gyroscopic effects. Some untypical algorithms are applied in the software; for instance elements, with nonlinear characteristics, depended on shafts rotational speed, like elastic coupler's stiff and damping characteristics, propeller and cylinder damping. Therefore the calculations have been performed as an iterative process.

There are several formulas describing propeller inertia of added water mass value [4]. The best one, in author opinion, has been derived on the basis of Parson's theory (the equation no. 1 and Tab. 1).

$$J_H = D^5 \rho \left[CJ_1 + CJ_2 \frac{A_e}{A_0} + CJ_3 \frac{P}{D} + CJ_4 \left(\frac{A_e}{A_0} \right)^2 + CJ_5 \left(\frac{P}{D} \right)^2 + CJ_6 \frac{A_e}{A_0} \frac{P}{D} \right], \quad (1)$$

where:

J_H – inertia of entrained water [kgm²],
 D – propeller diameter [m],
 ρ – specific mass of sea water (usually 1025 kg/m³),
 CJ_i – coefficients given in table 14,
 A_e/A_0 – expanded area blade ratio,
 P/D – propeller pitch ratio.

Tab. 1. Coefficients for propeller inertia of entrained water

| No. of blades | CJ_1 | CJ_2 | CJ_3 | CJ_4 | CJ_5 | CJ_6 |
|---------------|-----------|------------|------------|-----------|-----------|-----------|
| 4 | 3.0315E-3 | -8.0782E-3 | -4.0731E-3 | 3.4170E-3 | 4.3437E-4 | 9.9715E-3 |
| 5 | 2.7835E-3 | -7.1650E-3 | -3.7301E-3 | 3.0526E-3 | 4.6275E-4 | 8.5327E-3 |
| 6 | 2.3732E-3 | -6.2877E-3 | -3.0606E-3 | 2.7478E-3 | 2.9060E-4 | 7.3650E-3 |

Damping characteristics are the most difficult data to determine, when a reliable damping value is lacking. What is more, there are several different methods of characterising damping phenomena. A conversion method of different damping definitions is shown in Tab. 2. On the other hand damping has no real influence on natural frequencies. Forced vibration (especially in resonance range) is strongly depended on damping. Damping can be described by a vibration magnifier on the basis of measurements. These magnifiers may be used on a similar mechanism. In

the ship construction a typical vibration magnifier is between 20÷25. Some manufacturers (mostly engine factories) give us damping factors corresponding to their products.

Tab. 2. Conversion table of different damping values

| | c | ε | ψ | Q |
|---------------|--|--|---|---|
| c | 1 | $\frac{\varepsilon \cdot k}{\omega}$ | $\frac{\psi \cdot k}{2 \cdot \pi \cdot \omega}$ | $\frac{k}{\omega} \cdot \sqrt{\frac{1}{Q^2 - 1}}$ |
| ε | $\frac{c \cdot \omega}{k}$ | 1 | $\frac{\psi}{2 \cdot \pi}$ | $\sqrt{\frac{1}{Q^2 - 1}}$ |
| ψ | $\frac{2 \cdot \pi \cdot \omega \cdot c}{k}$ | $2 \cdot \pi \cdot \varepsilon$ | 1 | $\frac{2 \cdot \pi}{\sqrt{Q^2 - 1}}$ |
| Q | $\frac{\sqrt{k^2 + c^2 \cdot \omega^2}}{c \cdot \omega}$ | $\frac{\sqrt{1 + \varepsilon^2}}{\varepsilon}$ | $\frac{\sqrt{4 \cdot \pi^2 + \psi^2}}{\psi}$ | 1 |

where:

c – linear viscous damping [Nms/rad],
 ε – undimensioned damping factor,
 ψ – ratio of damping energy,
 Q – vibration magnifier,
 ω – phase velocity of vibration [rad/s],
 k – stiffness [Nm/rad].

Beside the engine cylinder's damping (received from the producers), usually only the propeller's dampings are significant. During torsional vibration analysis other dampings are negligible, except elastic couplings and torsional dampers, if applied. Some authors (the Archer theory) make the propeller's damping dependant on torque and revolutions. But more popular formulas, and better in author opinion, make the propeller's damping dependant on its geometry. An advanced formula has been worked out by H. Dien and H. Schwanecke [4] (equation no. 2).

$$c_p = \frac{\rho \cdot \omega}{\pi} \cdot D^5 \cdot \left(\frac{P}{D}\right)^2 \cdot \frac{A_e}{A_0} \cdot 0.0231 \text{ [Nms / rad]} \quad (2)$$

where:

D – propeller diameter [m],
 ρ – specific mass of sea water (usually 1025 kg/m3),
 ω – angular frequency [rad/s],
 A_e/A_0 – expanded area blade ratio,
 P/D – propeller pitch ratio.

3. Example of torsional vibration calculations

Analysis of the power transmission system torsional vibrations was performed by the author's specialised FEM software. Propulsion system of the tanker ship (245 m length, 104 000 DWT) was analysed. The propulsion system is based on a slow-speed, two-stroke, six-cylinder main engine: MAN B&W 6 S60 MC-C type. The engine main parameters are as follows: power – 13600 kW and nominal speed – 105 rpm. The propulsion system was equipped in five-blade propeller: diameter 7.2 m and mass in air – 28400 kg. Propulsion system has been designed as overcritical - main torsional resonance (43.8 rpm) is placed 58% below nominal main engine speed. The FEM model of the power transmission system is presented in fig. 2. The first five modes and frequencies of the natural vibrations were determined. One and two-node mode is presented on Fig. 4. In that case, only the first of the natural vibration mode (with one node in the intermediate shaft region) is significant. In the intermediate shaft region minimal torsional amplitudes and maximal torsional stresses are expected. Therefore, torsional vibrations verifying should be performed by strain/stress measurements (by strain gauges or optical FBG sensors). Torsional amplitudes measurement (laser method) is not good method in that case. Maximal torsional amplitudes are expected in propeller and crankshaft free-end.

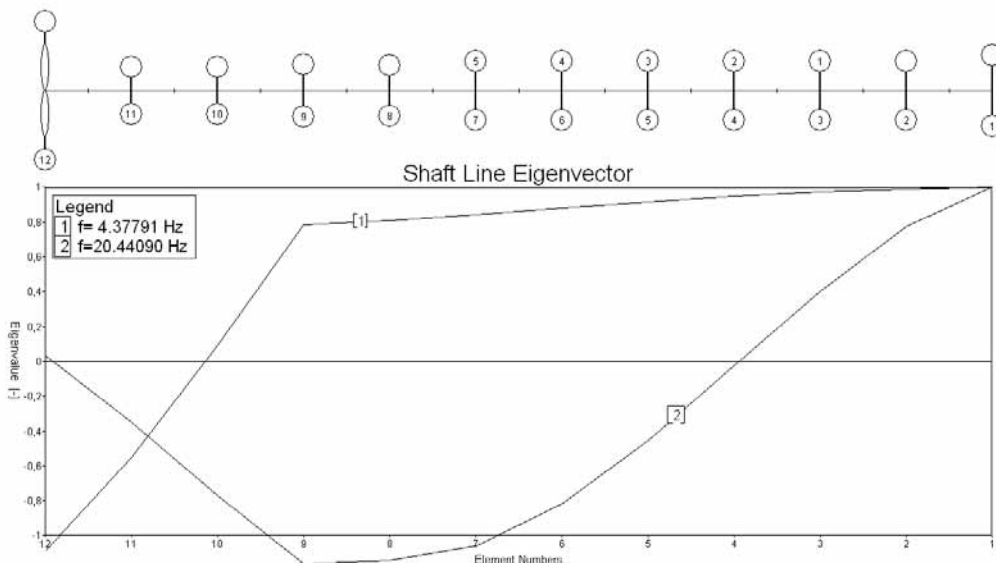


Fig. 4. Power transmission system's natural torsional vibrations

Torsional vibration amplitudes (comes from forced vibration analysis) of a propeller are presented on Fig. 5. The amplitudes are equal to 2.5° in torsional resonance region (43.8 rpm). The revolutions range between 33 and 55 rpm should be forbidden (barred speed range) for normal continuous work. Torsional vibration amplitudes in nominal main engine speed are very low; about 0.03° . In case of undercritical propulsion system amplitudes equal to 0.5° will be expected in the nominal revolutions. Therefore, overcritical power transmission system is better for analysed ship. For this engine type (two-stroke, six-cylinder) the most dangerous is the 6th harmonic component. But in some revolutions over components might be dominant. For instance 3rd stress harmonic component is the highest in the 87.5 rpm. Torsional stresses for all significant harmonic components are presented on Fig. 6. The diagram is prepared for intermediate shaft because the highest stress level. Similar figure for stresses expected in crankshaft is presented on Fig. 7.

Calculated torsional vibration stresses are located below permissible stress levels in whole range of main engine speed except barred speed range. Therefore the following limitation of the propulsion system is necessary: “a main engine speed range: 33-55 rpm has to be prohibited for continuous running in all conditions of operation; it is permitted to pass this range as quickly as possible”.

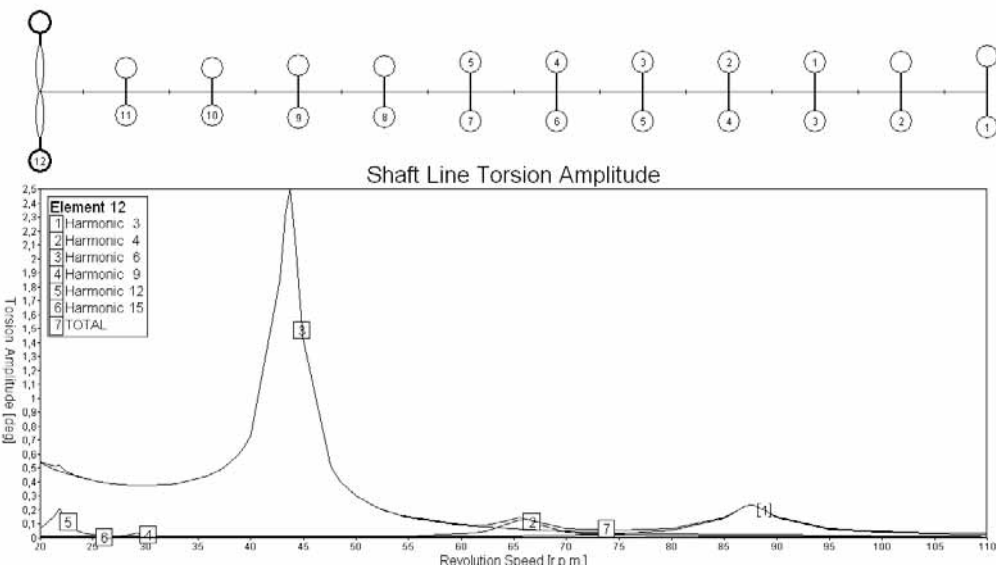


Fig. 5. Torsional vibrations amplitudes of a propeller

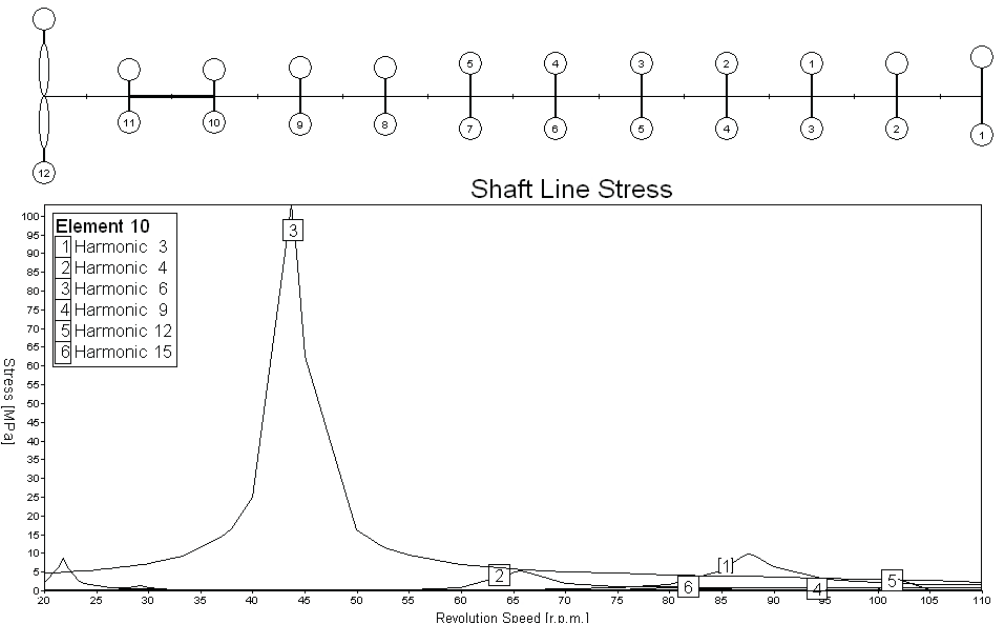


Fig. 6. Torsional vibrations stresses of an intermediate shaft

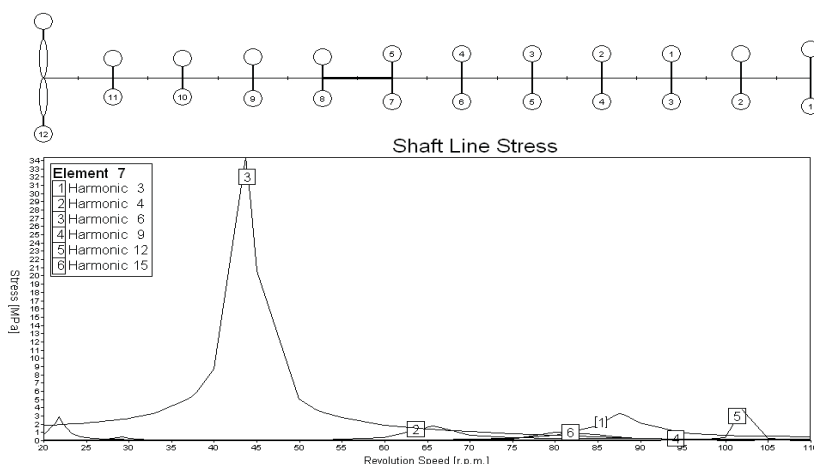


Fig. 7. Torsional vibrations stresses of a crankshaft

Similar calculations have to be performed for an engine with one cylinder misfiring [2, 5, 6]. Calculations were made for two conditions of main engine operation: cylinder no. 1 and no. 6 were not firing. After this analysis the next preliminary limitation is necessary: “a main engine speed reduction to 85 rpm is needed in the misfiring condition”. Confirmation of these limits has to be done by measurements during a ship sea trial.

The calculations presented above have been performed to verify the author’s algorithm. The results have been compared with the analogical calculations made by independent numerical programs [1] in an independent design office. The results conformity is very good – the differences were less than 1%.

References

- [1] Aarvik J. A.: *Software for shafting systems*. DNV Software News, No. 3, pp. 11, December 2005.
- [2] Chłopek Z., Piaseczny L.: *Irregularity of static working states of ship combustion piston engine*. Polish Maritime Research, No 2(48), Vol. 13, pp. 9÷14, April 2006.
- [3] Cudny K.: *Linie Wałów Okrętowych: Konstrukcje i Obliczenia*. Wydawnictwo Morskie, Gdańsk 1990.
- [4] Dien R., Schwanecke H.: *Die propellerbedingte wechselwirkung zwischen schiff und maschine - teil 2*. Motortechnische, vol. 34, pp. 45÷56, no 11, 1973.
- [5] Geveci M., Osburn A.W., Franchek M.A.: *An investigation of crankshaft oscillations for cylinder health diagnostics*. Mechanical Systems and Signal Processing, vol. 19, pp. 1107÷1134, September 2005.
- [6] Kosowski K.: *Some aspects of vibration control. Part I: Active and passive correction*. Polish Maritime Research, No 4(42), Vol. 11, pp. 22÷27, December 2004.
- [7] Murawski L.: *Axial vibrations of a propulsion system taking into account the couplings and the boundary conditions*. Journal of Marine Science and Technology, vol. 9, no. 4, pp. 171÷181, Tokyo 2004.
- [8] Murawski L.: *Shaft line whirling vibrations: effects of numerical assumptions on analysis results*. Marine Technology and SNAME News, vol. 42, no. 2, pp. 53÷61, April 2005.
- [9] Nestorides E. J.: *A Handbook on Torsional Vibration*. Cambridge University Press, 1958.
- [10] Wilson W. K.: *Practical Solution of Torsional Vibration Problems*. Chapman & Hall LTD, London 1963.



GAS PLANT OF ETHYLENE GAS CARRIER AND A TWO STAGES COMPRESSION OPTIMIZATION OF ETHYLENE AS A CARGO BASED ON THERMODYNAMIC ANALYSIS

Dariusz Nanowski

Gdynia Maritime University
ul. Morska 81-87, 81-226 Gdynia, Poland
tel.: +48 586901449
e-mail: dariuszn@am.gdynia.pl

Abstract

Ethylene as a cargo is more and more popular in maritime transport. Its temperature approx. -104°C during discharging requires sufficient efficiency of reliquefaction plant. Short description of that gas plant is shown including cascade system and processes are described. Based on Mollier diagram and ethylene mass flows, refrigeration capacity of the system is calculated when some changes in the cargo economizer are done. Some of these changes are carried out by crew members of gas carriers in order to reduce second stage discharge temperatures of reciprocating compressors. These losses of refrigeration efficiency are calculated to assess its influence on Ethylene temperature in the cargo tanks. On the other hand some assumptions are used to improve refrigeration capacity by Ethylene compression process.

Keywords: refrigeration cycle, reliquefaction plant, thermodynamic analysis, Ethylene gas carrier

1. Introduction

Ethylene is one of the primary petrochemical building blocks. It is used in the manufacture of polyethylene plastics, ethyl alcohol, polyvinyl chloride (PVC), antifreeze, polystyrene and polyester fibres. It is obtained by cracking either naphtha, ethane or LPG. About 85 million tonnes of ethylene is produced worldwide each year but, because most of this output is utilised close to the point of manufacture, only some 2.5 million tonnes is moved long distances by sea on semi-pressurised carriers [5].

Boiling point of Ethylene at atmospheric pressure is -103.8°C means that cooling processes are not belong to cryogenics e.g. below 111.1 K when at the same pressure Methane has boiling point [2]. However temperatures below -100°C achieved in Ethylene carriers cargo tanks require using cascade systems, because cooling down the cargo between -60°C till -100°C with multi-stages cycles is very difficult or even impossible [4]. Of course, Ethylene is not only one grade of cargo for these ships [6,7].

2. The gas plant of Ethylene carrier

General principles of cargo gas plant operation are being described by using as an example simplified layout of reliquefaction and cascade systems, whereas processes parameters are shown on Mollier diagrams [3]. The layout and parameters of processes of gas plant described

in this paper are taken from real ship, and are different from those one which can be found in some references [9].

Reliquefaction system with reciprocating compressor is shown on Fig. 1. The characteristic points of system and processes are marked by figures 1 to 10. The same figures denote thermodynamic processes drawn on Mollier diagram (Fig. 2). Values of the parameters are taken from compressor data sheet of real ship with Ethylene as a cargo [8]. When Ethylene vapour is sucked from the cargo tank by first stage of cargo compressor (point 1 – temperature $t_1 = -35^\circ\text{C}$), vapour has already left suction drum, where liquid phase could be separated from compressor suction line (to avoid liquid hammering). After discharging by interstage absolute pressure $p_2 = 5$ bar (point 2) and temperature $t_2 = 85^\circ\text{C}$, before compressing in the compressor second stage, vapour is cooled down by mixing with saturated vapour after its vaporization (from point 9 to 10) in the cargo economizer:

$$h_3 = (m_1 \cdot h_2 + m_2 \cdot h_{10}) / m_1 + m_2, \quad (1)$$

where:

m_1, m_2 – Ethylene vapour mass flows, kg/s,

h_1, h_3, h_{10} – specific enthalpy of Ethylene vapour, kJ/kg.

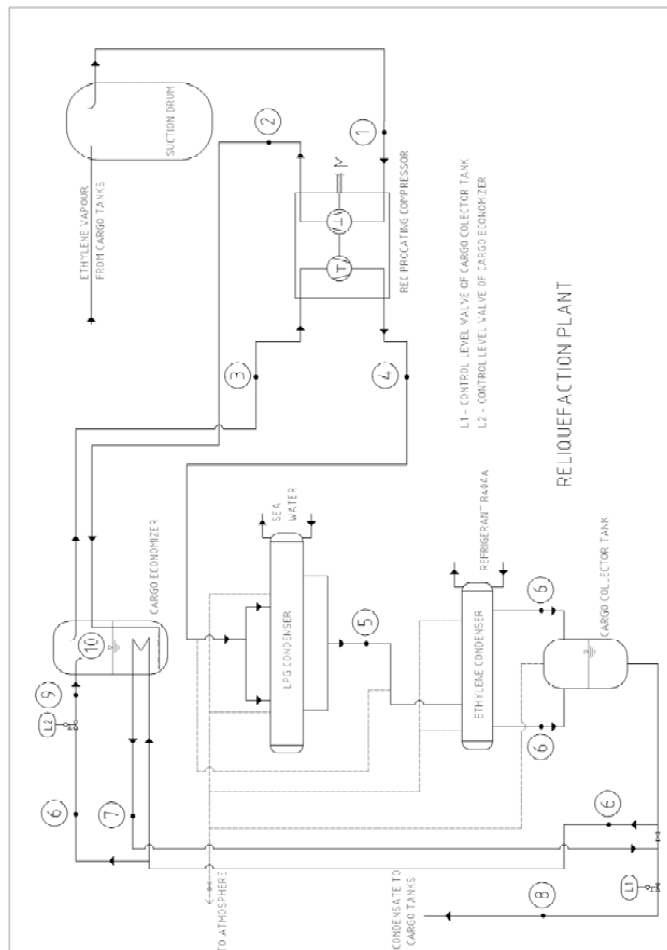


Fig. 1. Layout of reliquefaction plant

By this way vapour temperature in compressor second stage suction is decreased from t_2 to $t_3 = 50^\circ\text{C}$. Second stage compression increases vapour temperature up to $t_4 = 130^\circ\text{C}$, by pressure $p_4 = 18.5$ bar and Ethylene is directed to LPG condenser. There is no any Ethylene condensing process in this heat exchanger, but only cooling down of vapour from t_4 to temperature $t_5 = 30^\circ\text{C}$ by using sea water as a cooling medium. Condensing process 5-6 takes place in Ethylene condenser. In this heat exchanger are connected two systems: reliquefaction (Fig. 1) and refrigerant (Fig. 3), because Ethylene condensing process is carried out by vaporization of refrigerant R404A in Ethylene condenser, common heat exchanger of both systems: reliquefaction and refrigerant, as a one cascade system. By high gauge pressure $p_4 = 18.5$ bar is possible to condense Ethylene and cooling down to temperature $t_6 = -30^\circ\text{C}$ by means of R404 of which evaporating temperature is -40°C . In next step, flowing through the cargo economizer coil Ethylene condensate is subcooled in process 6-7 to temperature $t_7 = -63^\circ\text{C}$ with the use of Ethylene, which evaporates (process 9-10) by interstage pressure $p_2 = 5$ bar and temperature $t_9 = -72^\circ\text{C}$ in the cargo economizer.

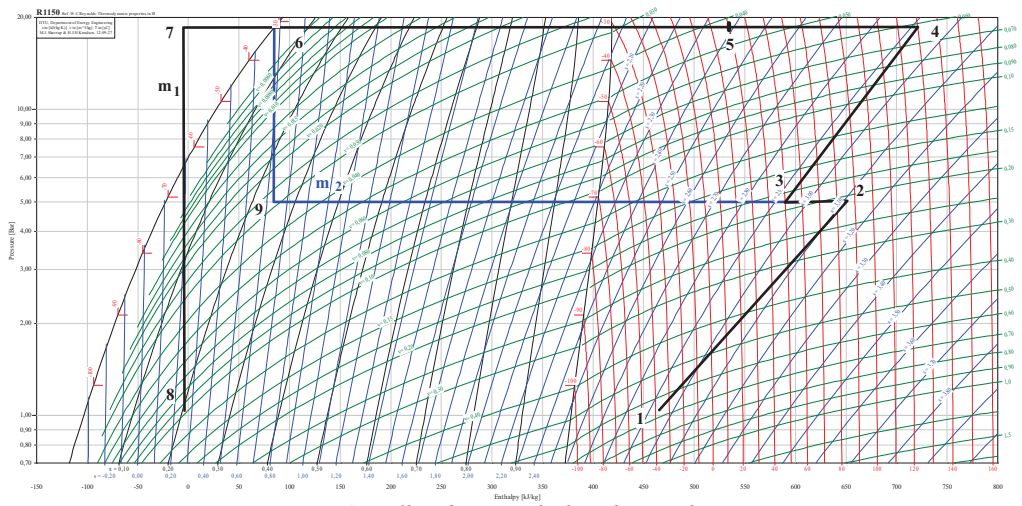


Fig. 2. Mollier diagram of reliquefaction plant

Total refrigeration capacity Q of Ethylene in the cargo tank is equal:

$$Q = m_1 \cdot (h_1 - h_8) \text{ [kW]}. \quad (2)$$

Subcooled in the cargo economizer Ethylene condensate is expanded to the cargo tank pressure where evaporates by temperature $t_8 = -103^\circ\text{C}$.

Second part of gas plant called **refrigerant system** is shown on Fig. 3 and its Mollier diagram on Fig. 4. General aim of using refrigerant system is to achieve temperature -40°C in the Ethylene condenser and enable condensing of Ethylene vapour. As a close system – refrigerant R 404A does not mix with cargo.

After vaporization in Ethylene condenser by temperature $t_7 = -40^\circ\text{C}$ and increasing temperature for superheat to $t_1 = 0^\circ\text{C}$ (Fig. 4), R404A is sucked by first stage of screw compressor. By interstage pressure, before second stage compression this flow of refrigerant connects with another after subcooling process in the refrigerant economizer according to equation:

$$m_1 \cdot h_2 + m_2 \cdot h_9 = (m_1 + m_2) \cdot h_3. \quad (3)$$

R404A vapour with parameters of point 3 is compressed in second stage (discharging parameters: temperature $t_4 = 80^\circ\text{C}$ and pressure $p_4 = 17\text{ bar}$) and through an oil separator directed to the refrigerant condenser, where cooled by sea water changes its phase into liquid (parameters of point 5).

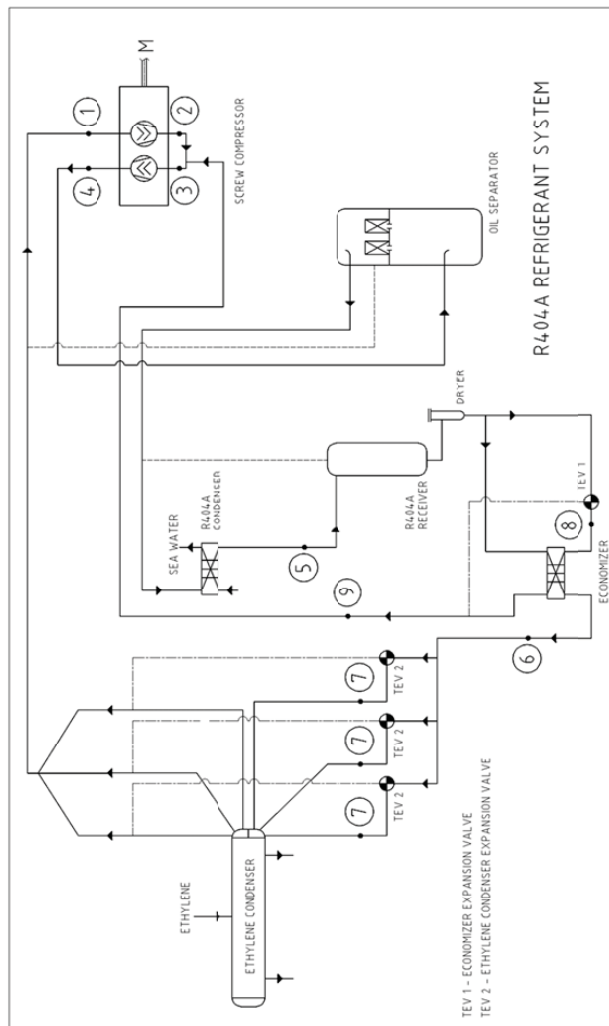


Fig. 3. Layout of refrigerant system

When compressor is loaded 85% or more, then the refrigerant economizer is used in the system and then it operates with increased refrigeration capacity. The refrigerant economizer enables to achieve subcooling of liquid R404A before thermostatic expansion valves (TEV) in isobaric process 5-6 (from temperature $t_5 = 40^\circ\text{C}$ to $t_6 = 20^\circ\text{C}$). Isenthalpic expansion of refrigerant 6-7 is carried out by means of three TEVs, which operate as a controllers for supplying R404A to Ethylene condenser.

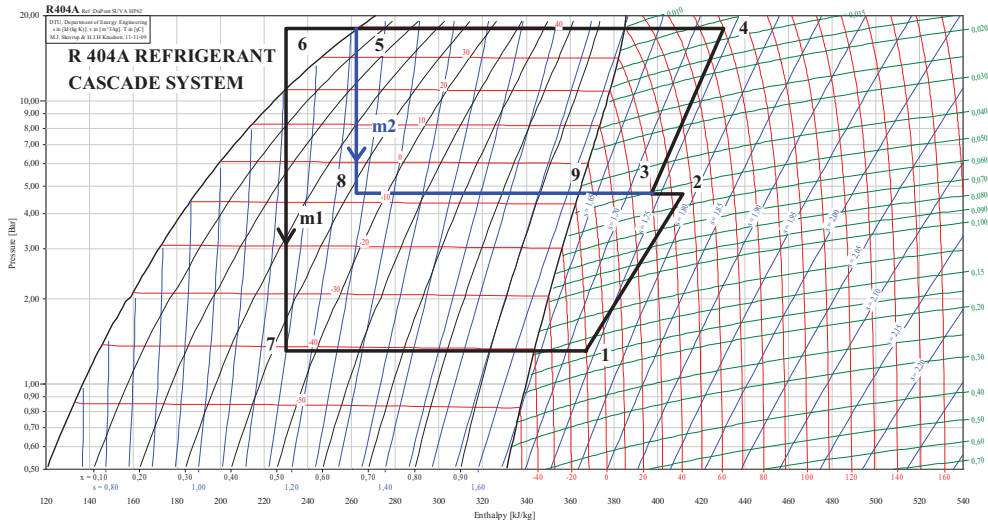


Fig. 4. Mollier diagram of refrigerant system

Above on Fig. 4 real parameters of refrigerant system are shown. In comparison with cycle shown on Fig. 2 it looks very similarly, but it has to be emphasized that increasing part of mass flow m_2 (Fig. 2) used to cool down Ethylene vapour from temperature t_2 to temperature t_3 (suction of second stage compression) decreases refrigeration capacity of reliquefaction plant, whereas increasing mass flow m_2 of refrigerant system increases refrigeration capacity of this system.

3. Optimization of Ethylene compression

Taking into account reciprocating compressor Sulzer- Burckhardt 2K160-2H with 580 rpm, it may be assumed that with 1.5 bar absolute pressure of Ethylene on first stage suction its suction volume is approx. 700m³/h. Specific volume of Ethylene under this pressure and temperature -35°C is $v_1 = 0.5 \text{ m}^3/\text{kg}$ (Fig. 5).

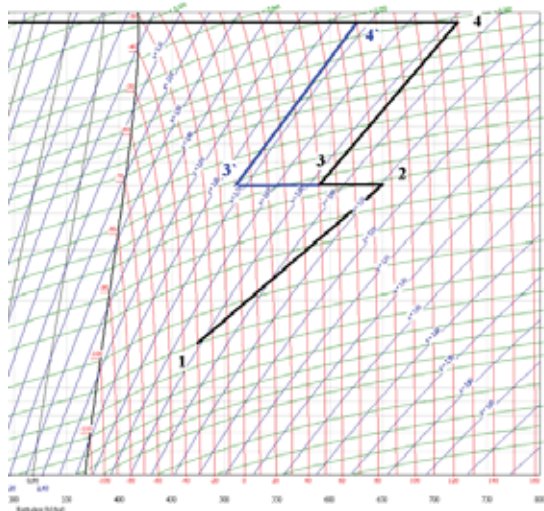


Fig. 5. Compression processes

It very easy to calculate [1] that mass flow m_1 (Fig. 2) of Ethylene is equal $m_1 = 0.4$ kg/s. It means that total refrigeration capacity of reliquefaction plant may be calculated according to equation (2), after finding enthalpies h_1 and h_8 on Mollier diagram (Fig. 3):

$$h_1 = 465 \text{ kJ/kg}$$

$$h_8 = -10 \text{ kJ/kg}$$

total refrigeration capacity is equal:

$$Q = m_1 * (h_1 - h_8) = 0.4 * (465 + 10) = 190 [\text{kW}]. \quad (4)$$

Part of mass flow m_2 is used to cool down Ethylene vapour after first stage e.g. from temperature t_2 to t_3 . By this process required refrigeration capacity Q_1 (Fig. 2, Fig. 5):

$$Q_1 = m_1 * (h_2 - h_3) = 0.4 * (650 - 590) = 24 [\text{kW}] \quad (5)$$

is excluded from total refrigeration capacity, only to reduce discharge temperature of the compressor second stage. At the ships temperature t_3 is reduced by crew member even to $t_3 = 0^\circ\text{C}$ (discharge $t_4 = 80^\circ\text{C}$), see point 3' on Fig. 5. Then enthalpy of point 3' is decreased to $h_{3'} = 510$ kJ/kg and necessary refrigeration capacity Q'_1 increases to value:

$$Q'_1 = m_1 * (h_2 - h_{3'}) = 0.4 * (650 - 510) = 56 [\text{kW}]. \quad (6)$$

To asses a part of mass flow m_2 , which is used to achieve this refrigeration capacity, this Q'_1 has to be used in equation (Fig. 2):

$$Q'_1 = m_2 * (h_3 - h_9),$$

(7)

$$m_2 = Q'_1 / (h_3 - h_9) = 56 / (510 - 80) = 0.13 [\text{kg/s}]. \quad (8)$$

It means that second stage of Sulzer-Burckhardt type 2K160-2H is loaded with 30% higher mass flow of Ethylene only for reducing second stage suction temperature t_3 . Of course the best way to achieve most efficiency cycle of reliquefaction plant is not use interstage cooler at all, as shown on Fig. 6.

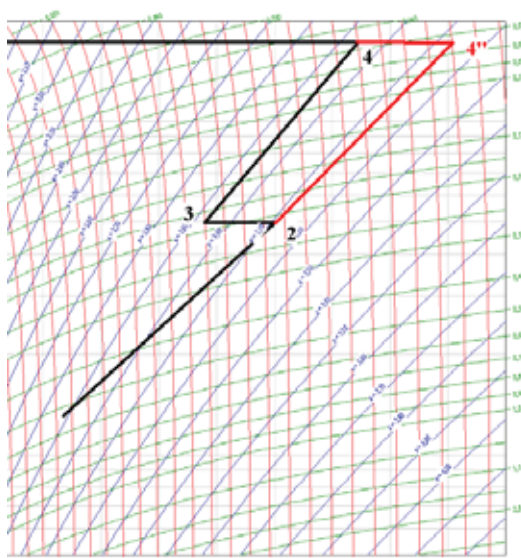


Fig. 6. Compression processes without intercooling

Process 2-4'' ensures the best efficiency of reliquefaction cycle from thermodynamic point of view (exergy!). Of course high discharge temperature $t_{4''}=170^{\circ}\text{C}$ causes some limitations regarding cargo or compressor.

Below is shown a list of typical cargoes carried by gas carriers with description of cycles which may be used in the reliquefaction plant:

- **Ammonia:** single stage, 2 stage NIC, 2 stage LSC;
- **isoButane:** single stage, 2 stage NIC;
- **Butadiene:** single stage, 2 stage NIC (included);
- **Butylene:** single stage NIC, 2 stage NIC (included);
- **n-Butane:** single stage (included), 2 stage NIC (included);
- **Propane:** single stage, 2 stage NIC, 2 stage LSC;
- **Commercial Propane** (2.5 mole% ethane): single stage, 2 stage NIC, 2 stage LSC;
- **Propylene:** single stage, 2 stage NIC, 2 stage LSC;
- **Vinyl Chloride Monomer** – single stage, 2 stage NIC;

where:

2 stage NIC – denotes 2 stage compression without using intercooler,

2 stage LSC – denotes 2 stage compression with liquid subcooling and using the cargo economizer as interstage cooler.

It should be noted, that LSC cycle is not used, if some another limitations do not appear. It has to be realized that cooling down $+80^{\circ}\text{C}$ hot Ethylene vapour in the interstage cooler by minus 70°C liquid is not efficient process from exergy point of view. Sea water temperature for cooling LPG condenser of reliquefaction plant, is also some condition, which allow for example by its low temperature to employ for VCM (Vinyl Chloride Monomer) single stage cycle with higher refrigeration capacity, instead of 2 stage cycle.

The last issue is volume efficiency of reciprocating cargo compressor. When pressure ratio between discharge and suction of the compressor exceeds 6, then 2 stage compression is recommended because of decreasing performance of compressor. It means that volume losses during compression are too high and less mass flow of cargo decreases total refrigeration capacity of the gas plant.

Conclusions

Unnecessary cooling down the cargo vapour in the interstage cooler always decreases refrigerant capacity of reliquefaction plant. During cargo gas plant operation second stage discharge temperature from thermodynamic point of view should be as high as possible. Ethylene example presented and calculated in this paper is based on real parameters taken from the ship during operation at sea. Calculations show that cooling down vapour in the interstage cooler and reduction second stage discharge temperature from 130°C to 80°C, increases loss of refrigeration capacity from 24kW (equation 5) to 56 kW (equation 6) e.g. from 13% to 30% of total reliquefaction plant refrigeration capacity.

Using the cargo economizer (Fig. 1) for decreasing compressor discharge temperature without reason, always causes either reduction of refrigeration capacity or increasing of fuel consumption for the compressor driving.

References

- [1] Bohdal, T., Charun, H., Czapp, M., *Urządzenia chłodnicze sprężarkowe parowe*, Wydawnictwo Naukowo-Techniczne, Warsaw 2003.
- [2] Chorowski, M., *Kriogenika podstawy i zastosowania*, I.P.P.U. Masta, Gdańsk 2007.
- [3] Coolpack 1.49 – IPU& Department of Mechanical Engineering Technical University of Denmark.
- [4] Królicki, Z., *Termodynamiczne podstawy obniżania temperatury*, Oficyna Wydawnicza Politechniki Wrocławskiej, Wrocław 2006.
- [5] McGuire and White, *Liquefied gas principles on ships and in terminals*, Witherby &Co, London 2000.
- [6] Nanowski, D., *Regulacja wydajności chłodniczej systemu etylenowego z kaskadą dla mieszaniny propan-etan cz.1*, Technika Chłodnicza i Klimatyzacyjna, № 9(187), 2011, pp.451-454.
- [7] Nanowski, D., *Regulacja wydajności chłodniczej systemu etylenowego z kaskadą dla mieszaniny propan-etan cz.2*, Technika Chłodnicza i Klimatyzacyjna, № 12(190), 2011, pp.574-575.
- [8] Nanowski, D., *Wybrane parametry procesów termodynamicznych rzeczywistego obiegu kaskadowego wykorzystywanego do morskiego transport etylenu*, Technika Chłodnicza i Klimatyzacyjna, № 4(194), 2012, pp.182-185.
- [9] Praca zbiorowa pod red. J.K. Włodarskiego, *Bezpieczeństwo transportu gazów skroplonych na zbiornikowcach*, Studium Doskonalenia Kadr Wyższej Szkoły Morskiej, Gdynia 1993.



LIQUID BIOFUELS OF THE FIRST AND SECOND GENERATION – THE METHOD OF PREPARATION AND APPLICATION

Ewa Rostek

*Motor Transport Institute, Centre of Materials Testing and Mechatronics
Jagiellońska Street 80, 03-301 Warsaw, POLAND
tel. +48 22 438 53 25, fax: +48 22 438 54 01
ewa.rostek@its.waw.pl*

Krzysztof Biernat

*Automotive Industry Institute, Department of Fuels and Renewable Energy
Jagiellońska Street 55, 03-301 Warsaw, POLAND
phone.: +48 22 7777 225, fax.: +48 22 7777 020
kbiernat@pimot.org.pl*

Abstract

Sustainable economic and industrial growth requires safe, sustainable energy resources. Unfortunately, first-generation biofuels are fuels produced from organic matter, which can also be used to produce food or feed. Only second-generation fuels are based on the need for sustainable development and are produced using processes such as pyrolysis, Fischer-Tropsch synthesis or hydrotreating. This paper presents the method for obtaining the first- and second-generation biofuels. Also discussed the possibility of their application.

Keywords: *biomass, liquid first- and second-generation biofuels, biodiesel, bioethanol, pyrolysis*

1. Introduction

Under the name of biofuels lie all fuels that are produced from biomass. As biomass and, in accordance with the applicable European Directive 2009/28/EC [4], it is biodegradable fraction of products, waste and residues of biological origin from agriculture, forestry and related industries, including fisheries and aquaculture, as well as the biodegradable fraction of industrial and urban areas. For the production of biofuels used primarily sugar beets, grains, corn, sugarcane, oilseeds such as rapeseed, palm or jatropha and straw and wood waste, sewage sludge, compost, garbage or food scraps. Biomass plant, from which biofuels are produced, is a storehouse of solar energy.

The use of biofuels is a way to reduce imports and consumption of fossil fuels and reduce carbon dioxide emissions into the atmosphere [8,15]. This is achieved through a closed loop cycle of carbon dioxide that is emitted during the combustion of biofuels, but also absorbed by plants during photosynthesis.

2. First-generation liquid biofuels

First-generation biofuels are fuels produced from organic matter that can be used also for

production of food or feed. First-generation biofuels are produced using conventional methods do not require large energy inputs (such as fermentation, esterification). The use of raw materials such as sugar cane, wheat or corn sugar beets, which can produce food for human and pet food makes its production competes with food production and do not always have enough material for both processes [10]. Tab. 1. shows the transformation of biomass into first-generation liquid fuels.

Tab. 1. The transformation of biomass into first-generation liquid fuels

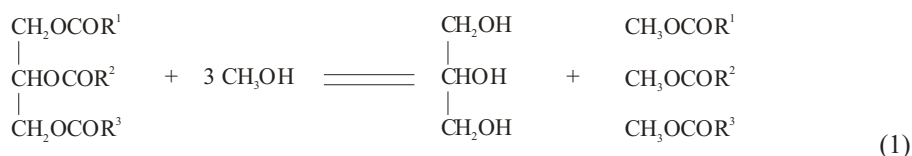
| conversion processes | BIOMASS | | |
|----------------------|------------------------------|--------------------|-------------------|
| | cold pressing and extraction | transestrification | enzyme hydrolysis |
| | | | fermentation |
| product | pure vegetable oils (PVO) | Biodiesel | Bioetanol |

2.1. Conversion processes for first-generation liquid biofuels

Biodiesel (rapeseed oil methyl esters (RME) or methyl esters (FAME) and ethyl (FAEE), higher fatty acids other oil crops) is obtained by cold-pressing process, the extraction and transestrification [12]. Esterification can be carried out in a homogeneous or heterogeneous phase. Raw materials for the transestrification of vegetable oils are homogeneous, used vegetable oils, fatty acids, animal fat and methanol or ethanol. The catalyst may be alkaline (sodium hydroxide, potassium hydroxide) or acid (sulfuric acid).

As a result of esterification of fatty acids are derived fatty acid methyl esters [12]. It was created in the process of the concentration of the glycerin can be sold as a technical glycerin (80%), which is widely used the pulp industry, the synthesis of dyes, nitroglycerin, dynamite, and also in pharmaceutical and food industries. The resulting fatty acid methyl esters are subjected to neutralization treatment and drainage. They can then be formulated into diesel or, after processing with special additives, used as a self-contained biofuel.

Esterification in a heterogeneous phase with a catalyst, which is zinc oxide on alumina allows to obtain fatty acid methyl esters of high purity and pharmaceutical grade glycerine. Esterification process is as follows:



The solid acid catalyzed biodiesel production by simultaneous esterification and transestrification of low quality oil containing high FFA (free fatty acid) was performed by Kulkarni et al. [9]. The reaction mechanism of simultaneous esterification and transestrification using Lewis acid takes place between free fatty acids (RCOOH) and methanol (CH₃OH) whereas transestrification takes place between triglyceride (RCOOR') (taken as representative of triglycerides in this case) and methanol adsorbed on acidic site of catalyst surface. The interaction of the carbonyl oxygen of FFA or monoglyceride with acidic site of the catalyst forms carbocation. The nucleophilic attack of alcohol to the carbocation produces a tetrahedral intermediate. During esterification the tetrahedral intermediate eliminates water molecule to form one mole of ester (RCOOCH₃). The transestrification mechanism can be extended to tri- and di-glyceride. It is well

known that transesterification is a stepwise reaction. In the reaction sequence the triglyceride is converted stepwise to di- and monoglyceride and finally glycerol. The tetrahedral intermediate formed during reaction eliminates di-, monoglyceride and glycerol when tri-, di- and monoglyceride come in contact with the acidic sites, respectively, to give one mole of ester (RCOOCH_3) in each step. In cases, esterification and transesterification produce methyl ester, the same final product. Also the catalyst is regenerated after the simultaneous esterification and transesterification reactions. Use of excess alcohol favors forward reaction and thus maximizes the ester yield [9].

The speed of the above reaction is dependent on process temperature, pH and substrate quality. The advantages of this type of fuel are very good lubricating properties and the lack of sulfur in the flue gas, and the disadvantages: the possibility of dissolving the seals and hoses made of certain types of rubber and plastic, not very good low temperature properties, and problems with the proper metering of fuel to the engine which is connected with the changing of some physical properties of esters with increasing temperature.

Bioethanol is ethanol derived from plant products containing sugar (sugar cane, wheat, sugar, fruit, juice, palm, etc.) or starch (wheat, barley, rice, corn, potatoes, cassava) can be used as fuel in specially adapted engines or the as an additive to gasoline [14]. Ethanol, $\text{CH}_3\text{CH}_2\text{OH}$ has in its structure, in addition to carbon and hydrogen, the oxygen atom, so that addition of ethanol to gasoline increases the octane of fuel and reduces the concentration of hydrocarbons and carbon monoxide in the exhaust.

Ethanol production relies mainly on the fermentation and distillation. Production of fuel in this way carries with it high costs of production. Reduce production costs can be achieved using other substrates such as cellulosic wastes (lignocellulosic) - fuel derived from this process is the second-generation biofuels.

Basically, for the production of ethanol by fermentation in anaerobic conditions, are used by enzymes produced in yeast. The enzymatic hydrolysis proceeds in two steps. Chemical structure of starch consists of long chain polymer of glucose. The macromolecular starch cannot be directly fermented to ethanol by conventional fermentation technology. The macromolecular structure first broke down in to simpler and smaller glucose. In this process, starch feedstocks are grounded and mixed with water to produce a mash typically contained 15–20 % starch. The mash is then cooked at or above its boiling point and treated subsequently with two enzyme preparation. The first enzyme hydrolyzes starch molecules to short chains to glucose. The first enzyme is amylase, amylase liberates "maltodextrin" ligosaccharides by liquefaction process. The dextrin and oligosaccharides are further hydrolyzed by enzyme such as pullulanase and glucoamylase in a process known as saccharification. Saccharification converts all dextrans to glucose, maltose and isomaltose. The mash is then cooled to 30 °C and yeast is added for fermentation [11].

For first-generation liquid biofuels are among the so-called PVO - pure vegetable oils - pure vegetable oils obtained from cold pressing process and the extraction of oilseeds. These oils can be used both as a food and fuel applied directly (without esterification) cannot be used in normal diesel engines. Their destiny is determined mainly by quality. Those with better quality are used for cooking. In most vegetable oils are used as an intermediate for the production of biodiesel.

3. Second-generation liquid biofuels

Raw first generation, which is produced biofuels compete with food, so the ideal solution is cellulosic products such as wood, straw, long grass or wood waste. Fuels produced from these raw materials are called second-generation biofuels [6, 22]. They can meet the demand for fuel in a fair and environmentally beneficial way. The advantage of second generation biofuels is the ability to use the whole plant (including stem, leaves and peels), and not just its parts (for example grains), as is the raw material first generation. Second-generation fuel can also produce, with plants of

which no part is edible, such as jatropha and switchgrass (a type of tall grass growing in South America), cereal grains contain very little, waste from wood processing and pulp of the fruit.

The main problem in the production of second generation biofuels are processes to break down the structure of lignocellulose and the release of simple sugars.

3.1. Conversion processes for second-generation liquid biofuels

Liquid biofuels from biomass can be obtained through thermochemical processing or by chemical treatment. Thermo-chemical treatment comprises thermal decomposition and chemical transformation of substrates by the action of the temperature in the presence of various concentrations of oxygen. The advantage of thermal treatment in relation to the chemical is able to convert all organic ingredients, not just the polysaccharides, as is the case with chemical treatment [6]. Tab. 2. shows the transformation of biomass into liquid biofuels second generation.

Tab. 2. The transformation of biomass into second-generation liquid biofuels

| | BIOMASS | | | | |
|-----------------------------|---------------------------------|-----------------|-----------|-------------------|-----------------------------|
| type of biomass | forest residue | lignocellulosic | | | vegetable oils, fatty acids |
| conversion processes | extraction of valuable chemical | gasification | pyrolysis | enzyme hydrolysis | hydrotreating |
| | | condensation | | fermentation | |
| | | | | distillation | |
| product | Bio-oil | FT-oil | Bio-oil | Bioetanol | Green diesel |

The physical transformation of raw materials into liquid biofuels include [14, 20]:

- mechanical extraction - crude vegetable oils are recovered from the oil seeds by applying a mechanical pressure using screw press (expeller). Screw press can be applied in two ways: prepressing and full pressing. In pre-pressing, only part of the oil is recovered and the partially de-oiled meal (cake with 18–20% oil) is further treated by solvent extraction. Combined pre-pressing and solvent extraction is commonly applied for oilseeds with high oil content (30–40%). Full pressing requires 95,000 kPa to squeeze out. as much oil as possible;

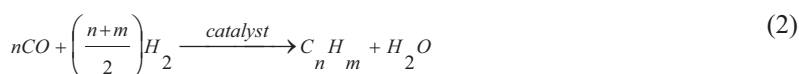
- briquetting of biomass - compaction of waste biomass from agricultural production or forestry residues takes place in closed chambers compression process combining crushing and maceration; Some time these two processes are combined, in pressing there is a close correlation of an increase in density with an increase in applied pressure in the early stage of compression, but the rate of increase in density fall rapidly as the density of pressed material approaches the density of water. There is no such close correlation of density change and degree of maceration, which may be chopping, grinding, and pulverizing. A coarse chopping of some materials may be as effective as ultrafine grinding.

- distillation - the most important method for extracting essential oil and relies on the evaporation of the more volatile constituents of a blend to separate them from the nonvolatile parts. Biomass is first crushed, then the distillation of essential oils evaporate and are condensed and condensed back into liquid.

Biomass can be converted into energy during the process of thermo-chemical or biological. Thermochemical processes include direct combustion, gasification, liquefaction and pyrolysis. Heating biomass in a lack of oxygen leads to the production of synthesis gas which consists primarily of hydrogen and carbon monoxide. This gas can either be burned directly or converted to other products of gas or liquid.

Direct combustion of biomass is to produce heat and leads to obtain carbon dioxide and water. Combustion of this should be done in well ventilated areas. Emissions of sulfur is in this case lower than for conventional fuels and combustion is at a level of 0.05 - 0.2% (m/m) [11].

Gasification of biomass is in the creation, in an atmosphere of oxygen, air or water vapor, the gas mixture (H_2 , CO, CO_2 , CH_4 and N_2) called synthesis gas or syngas and residual mineral in the form of ash. Gasification can be conducted in the presence of a catalyst at about 900 °C or without catalyst at a temperature of about 1300 °C. During the implementation process can also create by-products - tar. Syngas can be converted into electricity and heat or, using the Fischer-Tropsch process, to convert synthesis gas to aliphatic hydrocarbons and water [2]. The resulting product is free from sulfur and nitrogen. The FT reaction is given below:



where:

n average length of hydrocarbon chain
 m the number of hydrogen atom per carbon.

All the reactions are exothermic and the product is a mixture of different hydrocarbons in that paraffin and olefins are main parts. In FT one mole of CO reacts with two mole of H_2 in the presence of catalyst to form a hydrocarbon chain:



Depending on the process and especially the used catalyst in the FT process can get synthetic diesel oil (cobalt catalyst), synthetic gasoline (catalytic iron) and biomethanol (copper-zinc catalyst supported on alumina).

The pyrolysis is thermal degradation of biomass by heat in the absence of oxygen, which results in the production of charcoal (solid), bio-oil (liquid), and fuel gaseous products. Properties of the products depend upon temperature, process time, the atmosphere of the process as well as the characteristics of the material subjected to pyrolysis. During the process of biomass pyrolysis is a thermal conversion, in the absence of oxygen. Depending on the conditions of this process can be divided into conventional pyrolysis, fast and flash [13].

Conventional pyrolysis occurs under a slow heating rate (0.1–1 K/s) and residence time is 45–550 s and massive pieces of wood. In the first stage of biomass decomposition which occurs in between 550 and 950 K is called pre-pyrolysis. During this stage, some internal rearrangement such as water elimination, bond breakage, appearance of free radicals, formation of carbonyl, carboxyl and hydroperoxide group take place. The second stage of solid decomposition corresponds to the main pyrolysis process. It proceeds with a high rate and leads to the formation of pyrolysis products. During the third stage, the char decomposes at a very slow rate and it forms carbon rich solid residues.

In the process of fast pyrolysis of biomass, fine particles (<1 mm), low humidity are heated with a heating rate of 10 to 200 K/s to a temperature of 850 ÷ 1250 K. The duration of fast pyrolysis is 0.5 to 10 s. The result of this process is liquid product - Bio-oil with calorific value of

about 16 to 19 MJ / kg. Small amounts are also formed gas and charcoal, which are immediately burned and provide heat for the pyrolysis process.

Fast pyrolysis produced 60–75 % of Bio-oil, 15–25 % solid char and 10–20 % non-condensed gases depending upon feedstocks [18].

Bio-oil is a dark brown viscous, corrosive and sour liquid with a characteristic "smoky" smell, which can be used as fuel in furnaces, gas turbines and diesel engines. The Bio-oil includes, among other things: aliphatic alcohols/aldehydes, furans, benzene and pyrene derivatives, fatty acids and hydrocarbons of high molecular weight. These compounds can be extracted from Bio-oil by means of selective solvents.

Flash pyrolysis it differs strongly from that of conventional pyrolysis, which is performed slowly with massive pieces of wood. It occurs in the temperature range of 1050–1300 K, fast heating rate (>1000 K/s), short residence time (<0.5 s) and very fine particle (<0.2 mm). The conversion of biomass to crude oil can have an efficiency of up to 70 % for flash pyrolysis process. The so called bio-crude can be used in engines and turbines. Its use as feedstocks for refineries is also being considered [3].

Rich in isoparaffins "Green diesel" produced in the process of hydrotreating raw materials containing triglycerides and fatty acids in the presence of a cobalt-molybdenum or nickel-molybdenum. Isomerization resulting "Green diesel" has a composition similar to the composition of a typical diesel fuel, has a high cetane number, good low temperature properties and a sulfur content below 1 ppm. Compared to FAME's properties do not depend on the quality of raw and hydrogenated biodiesel is readily miscible with diesel [7].

Conversion of lignocellulosic biomass to ethanol is a more involved process than obtaining bioethanol from starch and consists of pretreatment, acid or enzymatic hydrolysis, fermentation and distillation.

Lignocellulosic biomass is mainly composed of cellulose (crystalline biopolymer of glucose), hemicelluloses (amorphous polymers of xylose and arabinose) and lignin or large poly-aromatic compounds. Enzymatic hydrolysis of cellulose is slower than the hydrolysis of starch due to the presence of bonds β -1,4-glucosidic linkages in the molecule of the biopolymer (starch present in the binding of α -1,4-glycosidic bonds).

The pretreatment processes separate xylose and lignin from the crystalline cellulose. The steam explosion process is an efficient pre-processing method for converting lignocellulosic biomass. In this process biomass sample is placed in a pressure vessel (i.e. digester) and vaporized using saturated steam for a short time at a temperature 473–543 K and high pressure 14–16 bar. The pressure in digester is then dropped quickly by opening the steam and the material is exposed to normal atmospheric pressure to cause explosion which disintegrate lignocellulosic biomass [19].

Steam explosion causes the hemicellulose and lignin from the wood to be decomposed and converted into low molecular weight fractions which can be easily extracted. Therefore most of the water soluble fraction of hemicellulose can be removed by water extraction. At the same time, a part of the low molecular weight fraction of lignin is also extracted. The xylose can be fermented to ethanol and the lignin can be further processed to produce other fuels. The crystalline cellulose remains solid after the pretreatment and later break down to glucose by enzymatic hydrolysis process. The glucose is further fermented to alcohol and the hemicellulose fraction is converted to xylose. The conversion of xylose to ethanol is a difficult process, therefore, pretreatment is necessary to reduce the crystallinity of cellulose to lessen the average polymerization of the cellulose and hemicellulose–lignin sheath that surround the cellulose and to increase available surface area for the enzyme to attack [19].

Ethanol can be blended with gasoline to produce an oxygenated fuel with lower hydrocarbon and greenhouse gas emissions, certain aldehydes are increased. Automobiles can be operated on ethanol/gasoline blends from 5% to 25% without any alterations in engine equipment's or setting.

The major engine operation issue with alcohol blended fuels is fuel quality, volatility, octane number, cold start, hot operation, and fuel consumption.

In order to extract bio-oil from oil seeds solvent extraction can be done (usually as the solvent used is hexane) followed by distillation. Extraction refers to a process in which the desired substance is selectively removed from the raw materials by allowing the desired substance to dissolve into the solvent, and subsequently recovering the substance from the solvent. To remove the particular substance from biomass, extraction and separation are both essential.

Typically biomass (wood, wheat straw, aromatic grasses, etc.) contains high volume of macromolecular compounds (polysaccharide, cellulose, hemicellulose, and lignin) called primary metabolite. The other low volume and high value biochemical molecules like terpenoids, waxes, resins, sterols, and alkaloids are known as secondary metabolites or extractive biomass. In the biorefinery process these chemicals are initially extracted from biomass by using solvent extraction or supercritical fluid extraction.

The extraction can also be performed using CO₂ or supercritical water. A supercritical fluid is defined as a substance that is at temperature and pressure conditions which are above its vapour liquid critical point (for water it is 644 K and 22 MPa; for CO₂ it is 304 K and 7.4 MPa) [16]. At supercritical conditions a fluid is neither liquid nor gas as it can not be made to boil by decreasing the pressure at constant temperature, and it would not condense by cooling at constant pressure.

Supercritical fluid processing of biomass to chemicals represents an alternative path to acid hydrolysis, enzymatic hydrolysis of cellulose to sugars. With acid hydrolysis acid recovery is a costly and polluting issue. Enzymatic saccharification needs pretreatment of lignocellulosic biomass. Supercritical water can quickly convert cellulose to sugar and convert biomass into a mixture of oils, organic acids, alcohol and methane. In supercritical and near critical state acid (H⁺) and base components (OH⁻) of water are separate and dissolve in the biomass. The dissolved supercritical water breaks the bonds of cellulose and hemicellulose rapidly to produce small sugar molecules, glucose, xylose and oligosaccharide [17].

4. Opportunities and plans to use liquid biofuels in the industry (including military)

In December 2009, AltAir Fuels entered into a memorandum of understanding with 14 commercial airlines (including Delta, United, US Airways, Mexicana airlines, Air Canada) for the purchase of up to 750 million gallons of sustainable jet fuel over a 10 year period. In the same year AIR FRANCE KLM Group, North Sea Group and Spring Associates, after test flight, create consortium - Sky Energy, which is responsible for the development of aviation biofuels. SkyRND (research and development) develops sustainable jet fuel for the global aviation market based on a unique low cost operating model. Sky Energy has a proven track record; it has so far supplied sustainable jet fuel to more than 15 airlines around the world on all continents apart from Africa.

The 2007 National Defense Authorization Act (NDAA 2007) required that U.S. Department of Defense produce or procure 25 percent of all energy from renewable sources by 2025 [21]. The military has in fact, moved beyond this type of broad mandate toward the creation of a new energy strategy with each service branch developing its own energy strategic plan. For example, the U.S. Air Force, the largest consumer of liquid fuels in the military, has a stated goal of acquiring half of its domestic aviation fuel from domestic, synthetic (i.e., non-petroleum) sources by 2016 [5]. U.S. Air Force also plans to test flying B-52 bomber and a transport C-17 Globemaster fed a mixture of kerosene and biofuel derived from FT synthesis (in the ratio 50:50).

The Navy (in US), which consumes daily approximately 80,000 barrels of oil at sea and 20,000 MWh of electricity on shore, has set a goal of making half of its bases net-zero energy facilities by 2020. By 2016, the U.S Navy also plans to sail the “Great Green Fleet,” a carrier strike group composed of nuclear ships, hybrid electric ships running on biofuels, and aircraft flying on biofuels [1].

In Poland the production of biofuels is mainly obtained FAME and Green diesel, which are then added to a mixture of diesel fuel.

5. Conclusions

National governments strongly support the development of refineries producing biofuels on a commercial scale. The European Union aims to meet the objectives set out in Decree 20/20/20, which is to increase energy efficiency by 20 percent, reduce greenhouse gas emissions by 20 percent and ensure that 20 percent of the total energy production will come from renewable sources by 2020. This opens up tremendous opportunities for the biofuel market. From the standpoint of limiting carbon dioxide emissions reduction is an important resource pool for biofuel production to areas where effective control is possible (i.e. the European Union countries), because otherwise the use of biofuels could lead to an increase in its emissions.

According to many analyzes of second-generation biofuels could soon completely replace the first-generation biofuels made from food materials. Before doing so, we need to address the problem of very high production costs of biomass. The solution may be optimization of processing technology of various raw materials for production of biofuels and more efficient use of by-products.

Increasingly popular to enjoy the start of the third generation biofuels based on algae derived, which are not only restrict the emission of greenhouse gases during combustion, but also allow the capture of CO₂ from coal particles, and even directly from the air, and thus contribute to further increase the reduction greenhouse gas emissions. However, while the algal culture is relatively easy to have the oil extracted from them difficult.

6. References

- [1] *A Navy Energy Vision for the 21st Century*, <http://greenfleet.dodlive.mil/files/2010/10/Navy-Energy-Vision-Oct-2010.pdf>, 2012.
- [2] Balat, M., *Sustainable transportation fuels from biomass materials*, Energy Education Science Technology, No 17, pp. 83-103, 2006.
- [3] Demirbas, A., *Green Energy and Technology – Biorefineries For Biomass Upgrading Facilities*, Springer-Verlag London Limited, 2010.
- [4] *Directive 2009/28/EC of The European Parliament and of The Council of 23 April 2009 on the promotion of the use of energy from renewable sources and amending and subsequently repealing Directives 2001/77/EC and 2003/30/EC*, 2009.
- [5] *F-22 Raptor flown on synthetic biofuel*, www.af.mil/news/story.asp?id=123248331, 2012.
- [6] Gomez, L.D., Clare, G.S., McQueen-Mason, J., *Sustainable liquid biofuels from biomass: the writing's on the walls*, No 178, pp. 433-85, New Phytol 2008.
- [7] Kalnes., T., Marker, T., Shonnard, D.R., *Green diesel: a second generation biofuels*, International Journal of Chemical Reactor Engineering, No 5, pp. 748-750, 2007.
- [8] Kamm, B., Gruber, R.P., Kamm, M., *Biorefinery industrial processes and products*, Ullmann's Encyclopedia of Industrial chemistry, Wiley-VCH Verlag GmbH&Co. KGaA, 2007.
- [9] Kulkurni, M., Gopinath, R., Meher, L.C., Dalai, A.K., *Solid acid catalyzed biodiesel production by simultaneous esterification and transesterification*, Green Chemistry, No 8, pp. 1056-62, 2006.
- [10] Laursen, W., *Students take a green initiative*, Chemical Engineering, pp. 32-34, 2006.
- [11] Lee, S., Speight, J.G., Loyalka S.K., *Handbook of alternative fuel technologies*, CRC Taylor and Francis Group, 2007.

- [12] Meher, L.C., Vidyasagar, D., Nail, S.N., *Technical aspects of biodiesel production by transesterification – a review*, Renewable Sustain Energy Reviews, No 10, pp. 248-68, 2006.
- [13] Mohan, D., Pitman, C.U., Steele, P.H., *Pyrolysis of wood/biomass for bio-oil: a critical review*, Energy Fuel, No 20, pp. 848-89, 2006.
- [14] Naik, S.N., Goud, V., Rout, P., Dalai, A.K., *Production of first and second generation biofuels: A comprehensive review*, Renewable and Sustainable Energy Reviews, No 14, pp. 578-597, 2010.
- [15] Osama, K., Carl, H.W., *Biomass Handbook*, Gordon Breach Science Publisher, 1989.
- [16] Saka, S., Ehara, K., Sakaguchi, S., Yoshida, K., *Useful products from lignocellulosics by supercritical water technologies*, Proceedings of The Second Joint International Conference on Sustainable Energy and Environment, pp. 485-489, 2006.
- [17] Sasaki, M., Kabyemela, B., Malaluan, et al., *Cellulose hydrolysis in subcritical and supercritical water*, Journal of Supercrit Fluid, No 13, pp. 261-268, 1998.
- [18] Shafizadeh, F., *Introduction to pyrolysis of biomass*, Journal of Analytical and Applied Pyrolysis, No 3, pp. 283-305, 1982.
- [19] Shelley, M.: *Alcoholic fuels*, CRC Taylor and Francis Group, 2006.
- [20] Stevens, C.V., Verhé, R., *Renewable bioresources scope and modification for non-food application*, John Wiley & Sons Ltd., England, 2004.
- [21] U.S. Congress. *National Defense Authorization Act for Fiscal Year 2007*, <http://www.govtrack.us/congress/bill.xpd?bill=s109-2507>, 2012.
- [22] Zabaniotou, A., Ioannidou, O., skoulou, V., *Rapeseed residues utilization for energy and 2nd generation biofuels*, Fuel, No 87, pp. 1492-1502, 2008.



EVALUATION OF COMPRESSION REALIZATION IN DIESEL ENGINE BASED ON PERFORMANCE INDICATOR CHANGES

Jacek Rudnicki

Gdansk University of Technology
ul. Narutowicza 11/12, 80-233 Gdańsk, Poland
tel.: +48 58 3472973, fax: +48 58 3471981
e-mail: jacekrud@pg.gda.pl

Abstract

In the article a method of evaluation of a diesel engine during the realization of processes of working circuit on the example of compression is described. The method is based on the use of the quantity called performance indicator in the description of the engine's work, which contains the information on the energy values, which may be disposed using the engine and the time at which it can be delivered. Theoretical information has been supplemented with information processed, in accordance with the proposed procedure, experimental results, which helped to illustrate the essence of this method.

Keywords: operation, working circuit, diesel engine

1. Introduction

An objective assessment of the reliability of any marine diesel engine forces the evaluative (quantitative) approach to this problem and the search for such measures, which are the most reliable in describing this feature of the engine.

On the other hand, the precise definition of the task except for the conditions of performance, requires specifying the duration as well. This issue is so important that the specific tasks in maritime transport is generally associated with the necessity of long-term operation of essential equipment of the vessel, especially its main drive.

Thus, it becomes particularly important, not only what the amount of energy which can be disposed using the main engine, but also the time in which it can be delivered.

Therefore, it is sensible to consider engine's operation (it's functional systems) in such an approach, so it could be described simultaneously by both energy and time.

Operation (D) in the time interval [0, t] can in this case be interpreted as a product of the physical quantity determined as the ratio of the time variable energy $E = f(\tau)$ τ and time:

$$D = \int_0^t E(\tau) d\tau \quad (1)$$

Method of processing of the engine in such a way as has been described inter alia in thesis referred to [1, 2, 4, 5, 6].

Because the concept of operation is also used e.g. in mechanics theory, to prevent the discussion, the D value described with general relation (1) it was decided to describe it as the performance indicator.

Description of the engine operation in the references above pertains to the time scale of the operation, which results from the fact that tasks duration in maritime transport can reach very high values and hence the value of the definite integral (1), which, for the assumptions taken is a measure of the engine operation, will also be very high.

Thesis [6] was, therefore, an attempt to answer the question, if one can “move” the considered performance assessment in a micro scale, that is to reduce the considered time - up to a maximum execution time of a single working circuit of the engine. This study is presented to verify and expand the considerations presented there and analyzes based on the results of experimental tests on in laboratory conditions with diesel engine.

2. The description of the test bench and measurement equipment

The study was carried out on a laboratory engine „Farymann Diesel” type D. It is a single cylinder diesel engine, four-stroke, naturally aspirated, fuel-injected into the pre-swirl of the combustion chamber, cooled by evaporation.

Tab. 1 Basic information about Farymann Diesel type D engine

| | |
|---------------------|---------------------|
| Rated power | 6 kW |
| Bore | 100 mm |
| Nominal speed | 1500 rpm |
| Displacement volume | 765 cm ³ |
| Compression ratio | 22 |

The engine has a manual start and decompression valve for easy starting a cold engine. It also has a casting ignition paper screwed in the cylinder head. Threaded hole of the paper cast ignition has scored thread M14x1, 25 which was used to install the valve cylinder pressure.

a)



b)

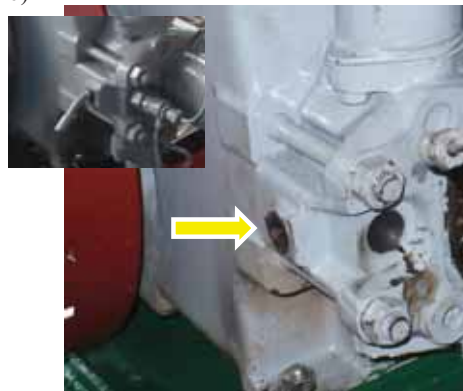


Fig. 2 View Farymann Diesel engine type D (a) and slot indicator assembly (b) at the ignition paper holder

For the measurement of pressures inside the cylinder electronic indicator PREMETS, XL version was used (http://www.lemag.de/premet_c.0.html).

Tab. 2 Basic information about electronic indicator PREMET C XL

| | |
|--|-----------------|
| Ignition pressure range | 0 – 25 MPa |
| Speed range | 40 – 1800 rpm |
| Max. number of cylinders | 20 |
| Max. number of measurements/cylinder | 30 |
| Manufactured according to ISO 9001 | |
| Compensation of temperature | |
| PC connection | USB |
| Stainless steel housing with isolated thermogrip | |
| High resolution colour display | |
| Accuracy | better than 1,6 |

a)



b)



Fig. 2 Indicator valve installed in a place of holder of ignition paper (a) an electronic indicator PREMET C on a laboratory stand (b)

The set of experimental results, which were used to verify the theoretical considerations contained in [6] has been accumulated during the 1.5 years of the use of the engine, in which the engine worked for about 50 hours. During this time were no operator action taken affecting the condition of the piston - cylinder unit, which has a decisive influence on the process of compression in the engine.

From this set of results containing approximately 60 indications, 4 samples were selected on the following assumptions:

- the identity of the measurement conditions (load and engine speed)
- subsequent spacing of the indicated time, the results of which were taken into account - at least 10 hours of operation,
- due to the fact that at the test bench there is no possibility of compression pressure measurement, the end of the compression was believed to be the position of the piston 10 ° before TDC (the angle of injection timing for the engine to be tested is about 8.5 before TDC).

Sample results (for readability of the graph, only the first and last indications) for the chosen subset are shown in Figure 3.

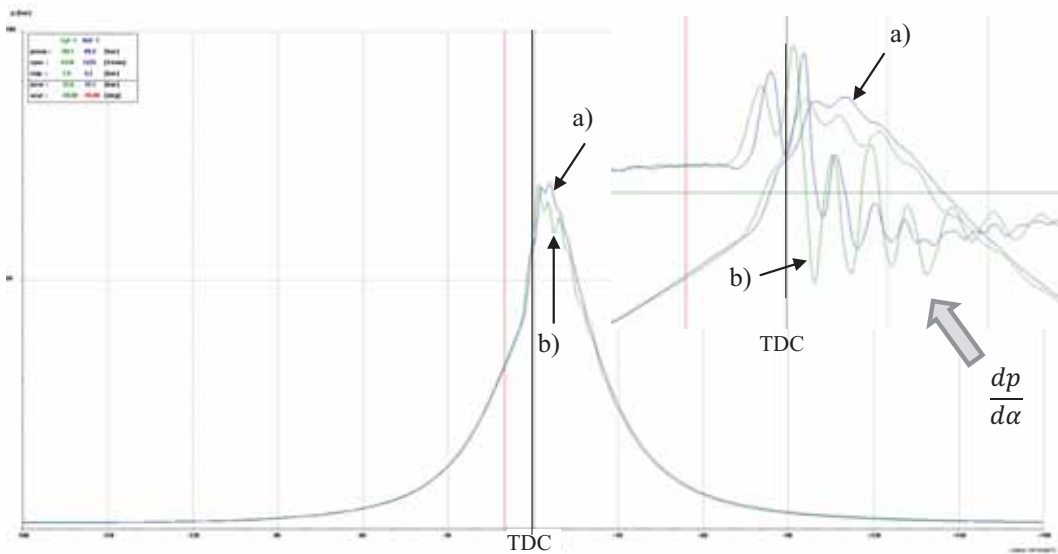


Fig.3 Results engine indications, dated. 26.05.2011 r - (a) and 31.08.2012 - (b); TDC – top dead center of the piston

As you can see in the charts compression differ practically unnoticed. You might also notice quite a significant difference in the combustion duration and the fact of more hard work after that engine use - higher value $\frac{dp}{d\alpha}$.

3. Evaluation of the implementation process of compression using pressure measurements inside the cylinder and index of operation

Indicator charts and analysis play a crucial role in assessing the operation of the engines during the operation. Indicated above, further discussed inter alia in the above-cited works a quantitative assessment of the engine using the operation ratio $D(t)$ provides the possibility of another processing the results obtained during indication.

Strictly limiting to the analysis of this compression process requires:

- changes in the upper limit of integration in equation (1) for the duration of the concerned process – t_{com} ,
- a decision which the volume associated with the course of the compression process can be regarded as time-variable power according to equation (1).

The first of the problems described above, of course, does not present any difficulty because of making the assumption of shut-off fuel inflow to the cylinder concerned, in the general case this duration, is a duration of a stroke and is expressed in the formula:

$$t_{1str} = \frac{1}{2} \cdot t_{1obr} = \frac{1}{2 \cdot n} \quad (2)$$

where:

- t_{1str} – duration of one stroke [s],
- t_{1obr} – duration of one crankshaft rotation [s],
- n – frequency of crankshaft rotation [s^{-1}].

In the absence of possibility to turn combustion in the cylinder off and create the contractual end of compression for a given value of the angle of the crankshaft position (in this study endcom $\alpha_{endcom} = 10^\circ$ of crankshaft rotation before TDC) relationship (2) is modified as follows:

$$t_{1com} = \frac{1}{2} \cdot t_{1obr} = \frac{1}{2 \cdot n} \cdot \left(1 - \frac{\alpha_{endcom}}{180} \right) \quad (3)$$

where:

α_{endcom} – angle of a contractual end of compression process (expressed in [° owk] before TDC),

The issue of selecting a quantity that corresponds to the time – variable energy may cause some doubts, because the very concept of energy, as the scalar size describing the state of the system creates a fairly wide range of interpretation. Considered the context of earlier results pressures inside the cylinder and opportunities they are presented in the coordinate system p - V (volume - pressure), it seems appropriate for the processing of work (a form of energy transfer) as the search value.

Limiting ourselves to the concept of absolute work [3] and assuming the contractual principle that the work done by the working medium is positive, and the work associated with environmental impacts in the factor - a negative sign, during the compression process engine performance can be determined by solving the following equations:

- operation indicator considered for the entire stroke - no fuel combustion in the cylinder:

$$D_{CS} = \int_0^{t_{1str}} L(\tau) dt = \int_0^{t_{1str}} \left(\int_{V_1}^{V_2} p(V) dV \right) dt \quad [J \cdot s], \quad (4)$$

where:

V_1 – workspace volume corresponding to $t = 0$ (Total volume of the workspace),

V_2 – workspace volume corresponding to $t \leq t_{1com}$ (compression chamber volume),

or:

- operation indicator considered as a function of time (index value until time t) – time interval $[0, t_{1com}]$ (if there is a possibility of turning off the combustion in the cylinder $t_{1com} = t_{1str}$)

$$D_{CS}(t) = \int_0^{t \leq t_{1com}} L(\tau) dt = \int_0^{t \leq t_{1com}} \left(\int_{V_1}^{V_t} p(V) dV \right) dt \quad [J \cdot s], \quad (5)$$

where:

t_{1com} – contractual time of a completion of the compression (for a given value of the angle position of the crankshaft α_{endcom}),

V_t – workspace volume corresponding to $t \leq t_{1com}$.

Interpretation of the operation indicator D presented above for the compression process as a value – D_{CS} and $D_{CS}(t)$ can be the basis of the evaluation of operation circuit in the engine.

Using equations (4) and (5) an evaluation of the compression process can be carried out by:

- comparative analysis of the set values of performance indicators - D_{CS} and $D_{CS}(t)$, of the reference of a new engine capable of technical efficiency and full fitness
- in case of lack of data mentioned above, eg. in reference to theoretical (izentrop pV^k - idem) realization of the process. Such an index can be defined as follows (limiting to equation (5)):

$$\psi(t) = \frac{D_{CS}(t)}{D'_{CS}(t)} = \frac{\int_0^{t \leq t_{com}} \left(\int_{V_1}^{V_t} p(V) dV \right) dt}{\int_0^{t \leq t_{com}} \left(\int_{V_1}^{V_t} p_1 \cdot \left(\frac{V_t}{V_1} \right)^\kappa dV \right) dt} \quad [-], \quad (6)$$

where:

$\psi(t)$ – engine performance evaluation index during the compression process (as a function of time)

$D_{CS}(t)$ – operations indicator during the compression in real engine,

$D'_{CS}(t)$ – operations indicator during the compression in realization of theoretical circuit

p_1 – pressure at the beginning of compression stroke

V_1 – workspace volume corresponding to $t = 0$

V_t – workspace volume corresponding to $t \leq t_{com}$

κ – izentrop index

4. The results and analysis

On the basis of the results, the analysis of the engine was carried out as outlined in section 3 of this thesis (for the considered data of indicated and accepted the contractual end of the compression process $t_{com} = 0,0944$ s).

The result is:

- value of $D'_{CS}(t)$ index calculated for the compression process carried out according to the isentropic equation pV^κ - idem,
- values of operation indexes $D_{iCS}(t)$ calculated as in equation (5) for analyzes set of indications ($i=1,2 \dots, 4$) Results were presented in figure 4 and due to poor readability in the time interval referring to the whole process, in the figure 5 - magnified.

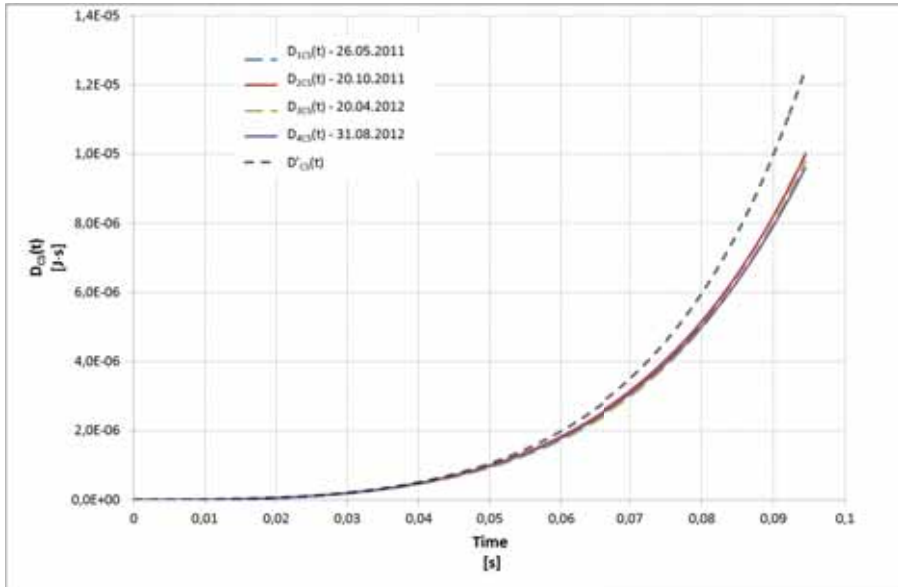


Fig.4 Values of operation indexes $D_{iCS}(t)$

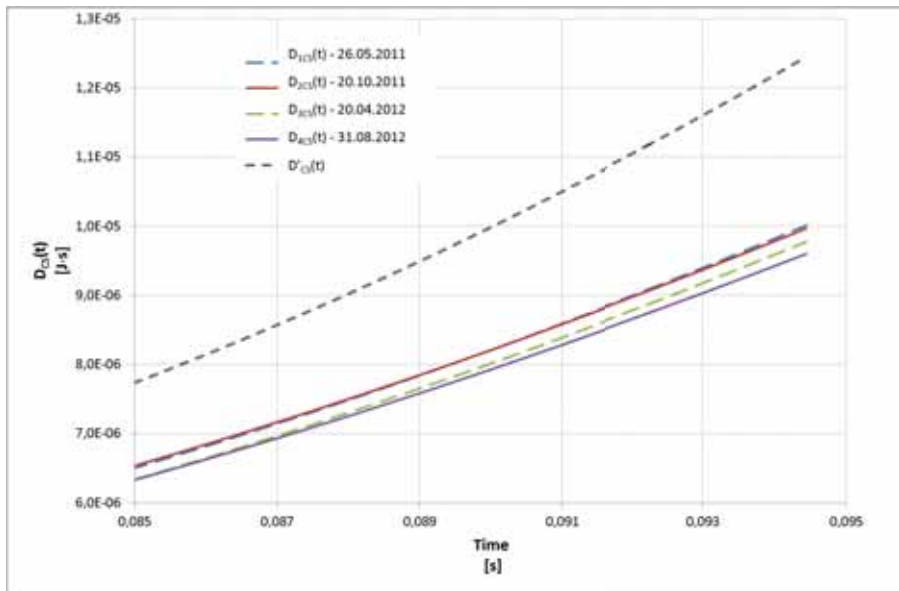


Fig.4 Values of operation indexes $D_{iCS}(t)$ (zoomed part of the plot)

- assessment indexes values $\psi_i(t)$ calculated according to equation (6) to concerned set of results of indication ($i = 1, 2 \dots, 4$). The results are shown in Figure 6 (due to low readability of the graph in the time interval relating to the duration of the whole process - only magnified fragment).

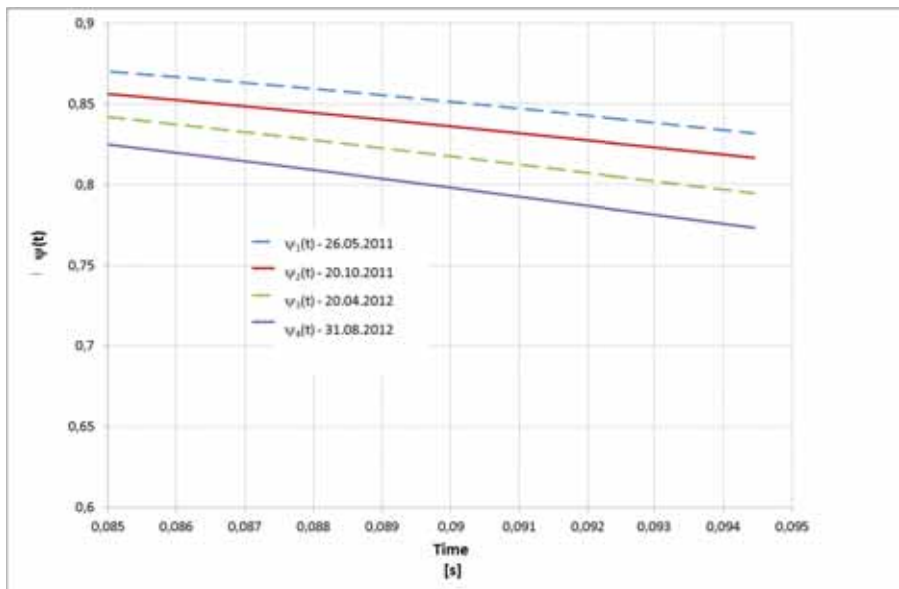


Fig. 5 Values of assessment indexes $\psi_i(t)$

The analysis of the data presented in Figure 4 - 6 gives rise to the following conclusions:

- evaluation of the compression process using a defined relationship (6) evaluation index $\psi(t)$ is possible - for the progressive degradation of engine condition, the value of the

rate is lower, which is consistent with the assumptions taken into account in the definition and nature of the real processes occurring in the engine,

- changes of value of the index $\psi(t)$ with the progressive wear engine are more pronounced, and therefore more easily to notice than, for example to register the change in compression
- determination of the intensity of changes in ratio $\psi(t)$ may result in defining the quantity describing the real engine reliability in terms of the implementation of the compression process - but this requires further study, a longer period of use [4].

5. Summary

The presented method appears to be an acceptable addition to the methods of assessment the quality of execution of a working circuit of the diesel engine used so far. The possible utility of course requires further theoretical studies and field tests. Due to the fact that marine engines indication is widespread and routine testing, access to the results of such tests is relatively easy, and thus is conducive to the development the assessment tools of the method.

The main advantage of this method is correlation of the assessment of the work and the time at which the task is performed - in this case the engine operating circuit.

Not without significance is also the fact that all the necessary calculations are relatively simple and can be made on the basis of the indicator diagram alone. The development of modern electronic indicators, so-called pressure analyzers allows for seamless implementation of these calculations in the software environment of the device.

The practical utility of the results can now be questionable - but further empirical research can lead to practical application of the proposed method for evaluation of such engines.

References

- [1] Girtler J., Kuzmider S., Plewiński L., *Valuation Method for Operation of Crankshaft-Piston Assembly in Combustion Engines in Energy Approach*, Journal of Polish CIMAC, Vol. 6, No 1, Gdańsk 2011.
- [2] Girtler J., *A Method for Evaluating the Performance of a Marine Piston Internal Combustion Engine Used As the Main Engine on a Ship During Its Voyage in Different Sailing Conditions*, Polish Maritime Research, No 4(67), Vol. 17, Gdańsk 2010.
- [3] Ochęduszek S., *Termodynamika stosowana*, WNT, Warszawa 1970.
- [4] Rudnicki J., *Działanie systemu energetycznego w ujęciu wartościującym z uwzględnieniem jego struktury niezawodnościowej oraz stopnia zużycia potencjału użytkowego. Praca wykonana w ramach projektu finansowanego przez MNiSW Nr N509 045 31/3500. Projekt badawczy pt., „Kształtowanie bezpieczeństwa działania systemów energetycznych środków transportowych na przykładzie systemów okrętowych”*, Gdańsk, 2008.
- [5] Rudnicki J., *Quantitative Assessment of Operation of Ship Main Diesel Engine*, International Conference on Computational Methods in Marine Engineering, MARINE 2011 CIMNE, Lisbona 2011.
- [6] Rudnicki J., *Analysis and Evaluation of the Working Cycle of the Diesel Engine*, Journal of Polish CIMAC, Vol. 6, No 1, Gdańsk 2011.



MODEL OF SEAWATER POLLUTED BY OIL-IN-WATER EMULSION AS A RESPONSE TO THE INCREASING SHIPPING ACTIVITIES

Kamila Rudz

Gdynia Maritime University
ul. Morska 81-87, 81-225 Gdynia
tel.: +48 58 6901504, fax: +48 58 6901399
e-mail: kamilar@am.gdynia.pl

Abstract

Intensive shipping affects marine environment in an extent degree, increasing seawater pollution by hazardous substances, including fuel oil and crude oil. Bilge water from ship power plants usually contains a mixture of dispersed oils, which form spherical droplets of diameter ranging from 0.01 to 10 μm . Present methods for detection of dispersed oil require taking a water sample or putting a measuring device into seawater, which allows only to gather point data from limited locations. In order to meet the demand of remote monitoring of endangered zones, a study of optical properties of oil-in-water emulsions was conducted. Presented model of seawater polluted by oil-in-water emulsion can potentially enable remote optical detection of oil-in-water emulsion in visible bands. It is based on the fact that oil droplets become additional absorbents and attenuators in water body. Optical analyses consist of calculations of spectral absorption and scattering coefficients and scattering phase functions for oil emulsions on the basis of Lorentz-Mie theory including measurements of refractive index and determination of oil droplets size distribution. The radiative transfer theory is applied to simulate the contribution of oil emulsion to the remote sensing reflectance. Presented system for radiative transfer simulation is based on Monte Carlo code and it involves optical tracing of virtual photons.

Keywords: oil pollution, oil-in-water emulsion, bilge water, remote sensing reflectance, seawater model

1. Introduction

Pollution of marine waters with hazardous oil products has turned into a fundamental ecological problem in the last decades, since shipping technologies and industry became to develop rapidly. It has been therefore a subject of numerous research projects, including detection and identification of oil using optical methods [4,5,20,22]. The main source of seawater pollution are crude oils and petroleum products, in most cases descending from ship discharges and flowing in with the rivers. As an example, ship-related operational discharges of oil include the discharge of bilge water from machinery spaces, fuel oil sludge, and oily ballast water from fuel tanks. Most of oil pollution studies are focused on remote detection of extensive surface films with airborne and onboard satellite microwave radars and lidars. However, oil spill detection is focused on incidental accidents and does not deal with everyday pollution originating from shipping and maritime activities (e.g. routine shipboard operations such as cleaning of cargo tanks) and with the rivers from the land-based sources (e.g. agriculture and industrial activities, powerboat racing). The most significant amount of oil pollution enters the seas with river inflows containing industrial and agricultural runoff, or as a result of daily shipping activities and crude oil exploitation, or from

natural seeps (GESAMP, 1993; GPA, 2002). Oil from this sources dissolves in a minor degree (0.2 – 0.7%) and is mostly found in the form of oil droplets dispersed in seawater (oil-in water emulsion). Oil emulsion amounts to over 80% of the total oil pollution in Baltic Sea estimated for 76 thousand tons per year (HELCOM, 1993). Among other sources, riverine input of oil products was estimated for 14-25 thousand tons yearly; sewage waters contribute for 4-14 thousand tons a year [4]. As the small-scale oil pollution is caused by human interference in marine environment, it should be also monitored on regular basis.

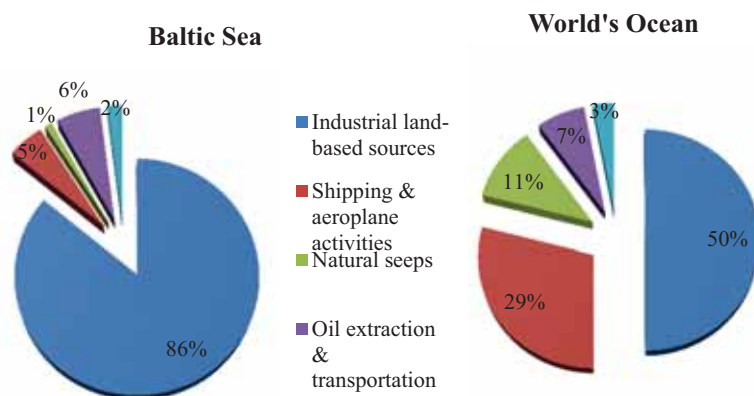


Fig. 1. Typical distribution of sources of oil pollution loads to the marine environment.
(Source: Global Marine Oil Pollution Information Gateway, 2011)

There are currently no methods for remote detection of petroleum derivatives dispersed in seawater in the form of emulsion. Oil products can considerably modify optical properties of seawater surface layer, with accounts to the most exposed regions, like coastal zones, estuaries, marine transportation routes or oil fields. Oil droplets become additional light absorbents and scattering centres influencing the process of radiative transfer in seawater [11,14]. Their presence changes the inherent optical properties (IOPs) of seawater, and in consequence it influences the upwelling light stream (i.e. water-leaving radiance), which is the basis of algorithms for deriving ocean parameters from remote sensing, including satellite remote sensing. The range of changes of seawater apparent optical properties (AOPs) can be predicted by solving the radiative transfer equation (RTE) using numerical methods/models [8].

2. Optical properties of oil-in-water emulsions

The average concentration of dispersed oil droplets in seawater was estimated to the range from 10^9 m^{-3} in oceanic water to over 10^{13} m^{-3} in coastal waters, e.g. Pomeranian Bay (Baltic Sea) [3]. The most probable concentration of total hydrocarbons is 5-20 $\mu\text{g/kg}$ (0.005 – 0.02 ppm) in the coastal part of the Gulf of Gdansk and 1-2 $\mu\text{g/kg}$ (0.001 – 0.002 ppm) in the open Baltic Sea, but it can vary from immeasurable values to several ppm in the estuary and harbour zones [22]. According to the MARPOL convention, ship discharge waters may legally contain up to 15 ppm of oil. In some regions the limits are more restricted (e.g. up to 5 ppm in Canadian inland waters).

Preliminary analyzes on the possible influence of oil emulsion on upwelling light field showed that Lorentz-Mie theory can be applied to calculate inherent optical properties of oil-in-water emulsions [13]. Lorentz-Mie theory is a complete solution to Maxwell's equation for scattering of electromagnetic waves by a homogeneous, spherical particle embedded in a nonabsorbing medium. It was also extended and applied for particles dispersed in absorbing media, such as seawater [1]. Oil dispersed in seawater was proved to form spherical droplets [6] and to fit the

single scattering model [23]. According to Lorentz-Mie theory, the IOPs of oil-in-water emulsion can be computed on the basis of complex spectral refractive index of particles matter and particle droplets size distribution. Complex refractive indices of several oil products were given by Kaniewski et al. [5], by Otremba [12] in spectral (350-700 nm) and temperature (0-40°C) dependence, and by Rudz (Fig. 2).

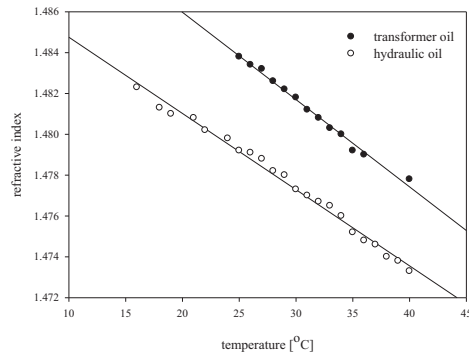


Fig. 2. Exemplary temperature dependence of refractive index for two types of oil

Exemplary oil droplets size distributions of two types of crude oil (*Petrobaltic* and *Romashkino*) were measured using an analogue microscope by Otremba and Krol [12,13]. They were also parameterized in relation to ageing time on water surface by a log-normal function. The study revealed that the majority of crude oil droplets dispersed in water had radius less than 2.5 μm . At the same time only a few droplets were larger than 5 μm in radius. It was shown that the maximum of size distribution function can shift from 0.4 μm to 0.05 μm in the period of two weeks causing a change in emulsion's optical properties. Lorentz-Mie theory was then applied to calculate light attenuation specific cross sections, spectral absorption and scattering coefficients [7]. Phase functions for oil-in-water emulsions of *Petrobaltic* and *Romashkino* crude oils were calculated by Otremba and Piskozub [15].

3. Radiative transfer model of seawater polluted by oil-in-water emulsion

Radiative transfer process in water body is described by equations linking the radiance, which was at first easier to measure, with inherent optical properties of seawater characterizing absorptive and scattering properties by its constituents (Eq. 1). Numerical radiative transfer simulations are used to predict the upwelling light stream using given seawater inherent optical properties. They compute the light propagation in seawater under specified conditions and allow evaluating the influence of each factor on remote sensing reflectance separately.

The model of marine environment consists of three elements:

- (1) pure water – with spectral absorption coefficient given by Pope and Fry (1997) and spectral scattering coefficient given by Smith and Baker (1981);
- (2) natural components of unpolluted seawater – with spectral absorption and attenuation coefficients measured in Baltic Sea using in-situ spectrophotometer AC-9 (WET Labs Inc.) during the ship cruises of Oceania r/v conducted by the Institute of Oceanology of Polish Academy of Sciences [21], and phase functions adapted from Petzold (1972), Mobley et al. [9] and Freda [2];
- (3) oil droplets – with optical characteristics described above.

The time-independent Radiative Transfer Equation (RTE) for horizontally homogenous water,

widely used in oceanography, is expressed by the following formula:

$$\cos \theta \frac{dL(z, \theta, \varphi, \lambda)}{dz} = -c(z, \lambda)L(z, \theta, \varphi, \lambda) + \int_{4\pi} L(z, \theta', \varphi', \lambda) \beta(z, \psi, \lambda) d\Omega' + S(z, \theta, \varphi, \lambda) \quad (1)$$

where:

$c(z, \lambda)$ – total light beam attenuation coefficient equal to the sum of absorption coefficient and scattering coefficient: $c(z, \lambda) = a(z, \lambda) + b(z, \lambda)$,

$\beta(z, \psi, \lambda)$ – volume scattering function (describing angular distribution of scattering process),

ψ – scattering angle between the direction of incident light (θ, φ) and the direction of scattered light (θ', φ'),

$S(z, \theta, \varphi, \lambda)$ – source function describing emission and inelastic scattering into the beam (such as fluorescence or bioluminescence).

The above mentioned inherent optical properties of oil-in-water emulsions have been implemented into a system of radiative transfer simulation based on Monte Carlo code in order to estimate their influence on remote sensing reflectance [17,18]. Its general scheme is presented in the Fig. 3. The boundary conditions for radiative transfer simulations are the incident light zenith angle (modeling the sun height), statistics of sea surface waves parameterized by the wind speed (Cox and Munk distribution) and the sea bottom reflectance (which can be neglected by setting 1000 m depth). Simulations were conducted in the visible bands.

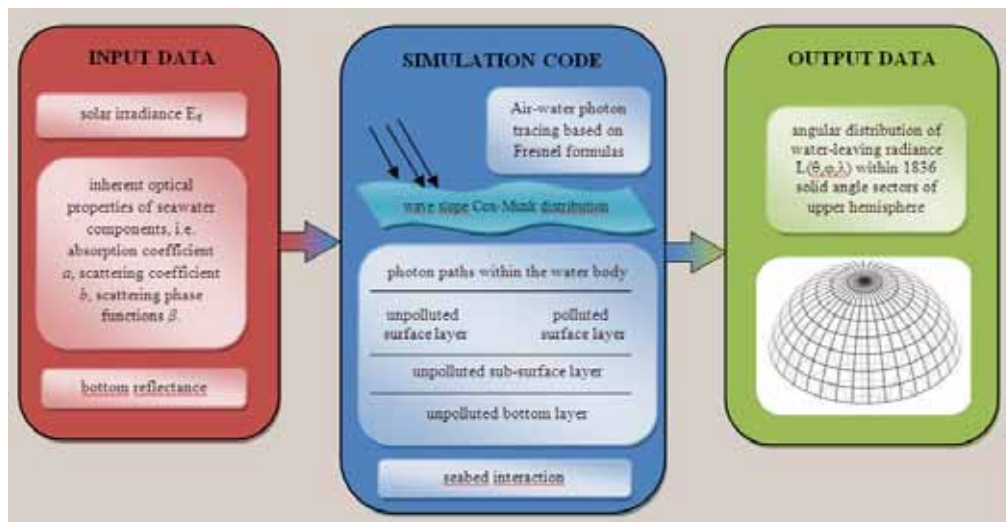


Fig. 3. General operational scheme of Monte Carlo radiative transfer simulation

Monte Carlo methods, developed during the second world war, are now widely used for radiative transfer modelling [8,10,11]. Monte Carlo methods effectively account for multiple scattering if the photon packets are followed until they contain a negligible amount of energy. In the presents study a model created by Piskozub (1992-2003) and developed by Otremba and Krol [12,13] and by Otremba and Rudz [16,19,20] was used. The Monte Carlo code involves optical tracing of photons within a given solid sector of upper hemisphere, on the basis of probability of visible light absorption and scattering by seawater constituents, including oil droplets. It allows conducting single-wavelength simulations limited to the wavelengths of which the seawater IOPs are known. It does not include inelastic scattering, which means that simulation results may differ

from field measurements, especially in the spectral range of chlorophyll fluorescence (650-700 nm).

The code consists of a three-step interaction:

- Air – water interaction - probability of surface reflection is calculated from the refraction index of seawater according to Fresnel formulas.
- Absorption and elastic scattering within the water body. Probabilities are calculated respectively as follows:

$$p_a = 1 - e^{-a}, \quad p_b = 1 - e^{-b} \quad (2)$$

- Interaction with the seabed (bottom reflectance coefficient).

4. Input data for radiative transfer simulation

Input data for Monte Carlo radiative transfer simulations are the inherent optical properties of all seawater components, i.e. spectral absorption coefficient $a(\lambda)$, spectral scattering coefficient $b(\lambda)$ and phase functions $p(\lambda, \theta)$ of the volume scattering function; and the boundary conditions, i.e. the zenith angle of incident light (modelling the sun height), statistics of sea surface waves parameterized by the wind speed (Cox and Munk distribution) and the sea bottom reflectance (neglected by setting 1000 m depth).

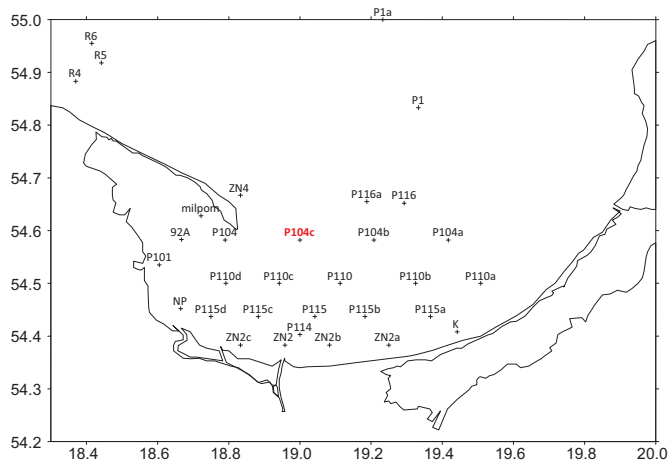


Fig. 4. Station P104c (54°35.0 N, 018°59.9 E) in the Gulf of Gdansk

The data for natural components of Baltic Sea were measured using *in-situ* spectrophotometer AC-9 (WET Labs Inc.) in the Gulf of Gdansk (station P104c) during the ship cruise of Oceania conducted by the Institute of Oceanology of Polish Academy of Sciences in April 2009 (Fig. 4). A three-layer seawater model were created in order to discretize continuous values for the purpose of radiative transfer numerical model. Only the surface layer (0-8 m) was then virtually polluted by 1 ppm of *Petrobaltic* and *Romashkino* crude oil separately (Fig. 3). Spectral dependences of absorption and scattering coefficients are shown in Fig. 5.

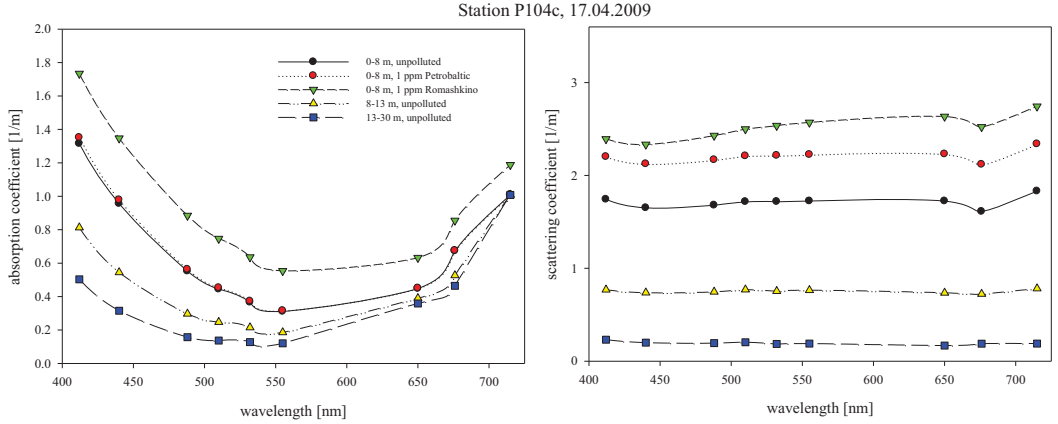


Fig. 5. Spectral distributions of absorption and scattering coefficients for a three-layer seawater model built on the basis of measurements in Baltic Sea at the stations 92A and P104c

5. Results and discussion

The water-leaving radiance L_w was calculated within the half angle of 7° , which corresponds to the Ramses Trios hyperspectral radiometers field of view. Remote sensing reflectance R_{rs} was calculated as the ratio of the water-leaving radiance to the downward sky irradiance E_d :

$$R_{rs} = \frac{L_w}{E_d}. \quad (3)$$

Simulations were conducted for a flat sea surface and for the sea surface characterized by the wind speed of 5 m/s. The wind speed measured at the station P104c was 6.7 m/s and the sun elevation was 44° (i.e. zenith angle set as a direction of incident photons). The output data is the spectral distributions of the upward radiance $L(\theta, \phi, \lambda)$ within 1836 solid angle sectors.

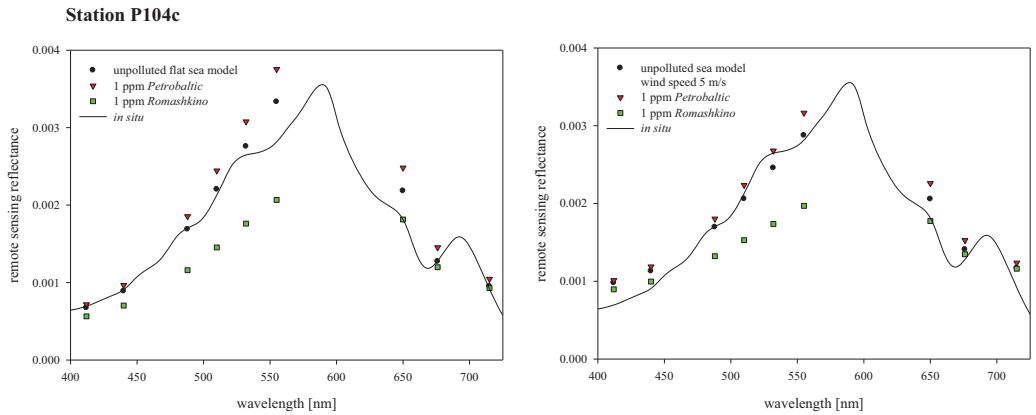


Fig. 6. Remote sensing reflectance from in situ measurements (solid line) in Baltic Sea and simulated results (points) for unpolluted seawater and for seawater polluted by 1 ppm of Petrobaltic and Romashkino crude oil emulsion, with the assumption of a flat sea surface (left graph) or for the sea surface parameterized by the wind speed of 5 m/s. (right graph).

The addition of *Petrobaltic* crude oil caused less than 2% increase of the total absorption coefficient of the surface seawater layer in the entire considered spectral range, and a significant increase (almost 30% for central wavelengths) of the total scattering coefficient. *Romashkino* emulsion significantly increased the total absorption coefficient for 60-74% and gave over 40% contribution to the scattering coefficient, in both cases slightly increasing with the wavelength (see Tab. 1).

Stronger absorption of *Romashkino* implies a decrease of the remote sensing reflectance. The impact of scattering coefficient depends on the angular distribution of the volume scattering function. High scattering in forward directions would drop the upward light stream and the advantage of backscattering would result in the increase of the water-leaving radiance. Addition of *Petrobaltic* emulsion barely affects seawater absorption coefficient, therefore the influence of scattering on remote sensing reflectance is more remarkable. Relatively high backscattering ratio can be explained by the domination of small oil droplets. The drop of R_{rs} caused by *Romashkino* emulsion together with its high absorption and high scattering coefficients suggest the stronger impact of absorption on the upwelling light stream. This could be a result of the advantage of forward scattering over backscattering caused usually by larger particles.

Tab. 1. Percentage increase of absorption and scattering coefficients in the surface 8 m layer caused by addition of 1 ppm of oil emulsion.

| P104c wavelength [nm] | Petrobaltic | | Romashkino | |
|--------------------------|-----------------------|-----------------------|-----------------------|-----------------------|
| | a [m^{-1}] | b [m^{-1}] | a [m^{-1}] | b [m^{-1}] |
| 488 | 1.9 | 29.1 | 60.2 | 44.7 |
| 510 | 1.8 | 28.8 | 68.1 | 45.6 |
| 532 | 1.8 | 28.9 | 74.0 | 47.6 |

Tab. 2. Percentage increase or decrease (signed with “-”) of remote sensing reflectance caused by addition of oil emulsion to the model of marine environment.

| P104c wavelength [nm] | Petrobaltic | | Romashkino | | Model accuracy | |
|--------------------------|-------------|-------|------------|-------|----------------|-------|
| | Flat sea | 5 m/s | Flat sea | 5 m/s | Flat sea | 5 m/s |
| 488 | 9.9 | 6.4 | -31.2 | -22.0 | -1.1 | -0.6 |
| 510 | 11.0 | 8.7 | -34.0 | -25.8 | 1.2 | -5.4 |
| 532 | 11.6 | 9.1 | -36.1 | -29.3 | 4.3 | -7.1 |

Simulated R_{rs} for unpolluted seawater was compared with *in situ* measurements in the Baltic Sea. The best model accuracy was achieved for central wavelengths of 488, 510 and 532 nm and it was 1-7%. The results shown in the Fig. 6 reveal that in considered spectral range the light *Petrobaltic* crude oil caused 9-11% increase of R_{rs} while the heavy *Romashkino* reduced R_{rs} for 22-36% (Tab. 2).

6. Summary

Radiative transfer process is the physical basis for all ocean colour remote sensing and must be fully understood when evaluating the performance of any particular sensor and retrieved products. There is therefore a need of comprehensive datasets containing all the information necessary for a complete radiative transfer calculation, which is especially important in optically complex waters. Interpretation of reflectance spectra requires a simultaneous multi-parameter analysis of light propagation in seawater. The influence of each IOP parameter on remote sensing reflectance is non-linear and highly variable. However, it can be studied separately in terms of a numerical radiative transfer simulation. The introduced study begins a supplement of the missing knowledge about optical properties of oil-in-water emulsions and their contribution to the upwelling light field

measured with remote sensing methods. The presence of high-absorptive and low-backscattering crude oil emulsions can be easily remarked on any marine water background, as they would cause a significant decrease of remote sensing reflectance. Those features usually imply large-sized droplets which scatter in forward directions. On the other hand, high backscatter fraction observed for small-sized particles should strengthen the water-leaving radiance, but that effect may be shadowed by high absorption. It seems that absorption spectrum of oil emulsion decides of its potential detectability in turbid waters. In clean ocean waters the backscatter fraction seems to be more significant. A separate study should be performed in order to determine the IOPs for more commonly used crude oils and their mixtures. Further study would also enable successive investigations on seawater affected by oil emulsion. As an example, the radiative transfer model can contribute to the improvement of satellite algorithms accuracy for determination of water parameters derived from the water-leaving radiance, regarding coastal zones, estuaries, main marine transportation routes and oil extraction areas. It will also improve the accuracy of shipboard and offshore measurements, which are used for calibration of satellite data and for other seawater optical observation and monitoring. It is also possible that it will enable the remote detection of oil-in-water emulsion.

Acknowledgements

I would like to thank M. Darecki and S. Sagan (IOPAS) for making their data available for this study. My thanks also go to J. Piskozub (IOPAS) for making the code for Monte Carlo radiative transfer simulation available. I also thank H. Toczek (GMU) for technical support.

References

- [1] Babin, M., Morel, A., Fell, V. F.-S. F., Stramski, D., *Light scattering properties of marine particles in coastal and open ocean waters as related to the particle mass concentration*, Limnology and Oceanography, 48 (2), pp. 843-859, 2003.
- [2] Freda W., *Parameterization of light scattering phase function in the marine environment*, Ph. D. thesis (in Polish), Inst. Oceanol. PAS, Sopot 2011.
- [3] Gurgul H., Staroń W., *The oil substances concentration of the River Świna*, Proc. 19th Conf. Of the Baltic Oceanographers, pp. 638-647, Sopot 1994.
- [4] Hagerhaal B., *Where does the oil come from?* WWF Baltic Bulletin, pp. 2-9, 1995.
- [5] Kaniewski, E., Otremba, Z., Stelmaszewski, A., Targowski, W., *Spectral relationships of the complex refractive index of selected kinds of oil*, Proc. XIX Conf. Baltic Oceanogr., pp. 158-165, Sopot 1994.
- [6] Krol T., *A computed model of the Mie coefficients for spherical absorbing and scattering particles*, Stud. Mater. Oceanol. ((in Polish), 49, pp. 43-62, 1985.
- [7] Król, T., Stelmaszewski, A., Freda, W., *Variability In the optical properties of a crude oil – seawater emulsion*, Oceanologia, 48 (S), pp. 203-211, 2006.
- [8] Leathers, R. A., Downes, T. V., Davis, C. O., Mobley, C. D., *Monte Carlo Radiative Transfer. Simulations for Ocean Optics: A Practical Guide*, Naval Research Laboratory, Washington, DC, 2004.
- [9] Mobley C. D., Sundman L. K., Boss E., *Phase function effects on oceanic light fields*, Appl. Opt. 41(6), pp. 1035–1050, 2002.
- [10] Mobley, C. D., *Estimation of the remote-sensing reflectance from above-surface measurements*, Appl. Optics 38(36), pp. 7442-7455, 1999.
- [11] Mobley, C. D., *Light and Water: Radiative Transfer in Natural Waters*, Academic Press, 1994.

- [12] Otremba Z., Król T., *Modelling of the crude oil suspension impact on inherent optical parameters of the coastal seawater*, Pol. J. Environ. Stud., 11(4), pp. 407-411, 2002.
- [13] Otremba, Z., Krol, T., *Light attenuation parameters of polydisperse oil-in-water emulsions*, Optica Applicata, XXXI (3), pp. 600-609, 2001.
- [14] Otremba, Z., *Oil droplets as light absorbents in seawater*, Opt. Express 15 (14), pp. 8592-8597, 2007.
- [15] Otremba, Z., Piskozub, J., *Phase functions of oil-in-water emulsions*, Optica Appl.. XXXIV (1), pp. 93-99, 2004.
- [16] Otremba, Z., Rudz, K., *Ocean optics in application to remote detection of an oil-in-water emulsion originating from the engine room*, Journal of KONES Powertrain and Transport, 17 (3), Warsaw 2010.
- [17] Rudz, K., Baszanowska, E., Rohde, P., Zielinski, O., *Fluorescence Methods and Monte Carlo Radiative Transfer Simulation Applied to Oil Detection in Baltic Sea*, Joint Proceedings, 24, pp. 52-59, Bremerhaven 2011.
- [18] Rudz, K., Darecki, M., Toczek, H., *Modelling of seawater polluted by light and heavy crude oil droplets*, Journal of KONES Powertrain and Transport, 19 (2), pp. 473-480, Warsaw 2012.
- [19] Rudz, K., *Emulsified Fuels of Machine Origin in Seawater – a Contribute to Remote Detection*, Journal of KONES Powertrain and Transport, 18 (3), pp. 375-382, Warsaw 2011.
- [20] Rudz, K., *Skutki zrzutu olejowego w polu światła w morzu*, Zeszyty Naukowe Akademii Morskiej w Gdyni, nr 64, pp. 99-108, Gdynia 2010
- [21] Sagan, S., *Rzeczywiste właściwości optyczne wód Bałtyku*, Polska Akademia Nauk, Rozprawy i monografie 21/2008.
- [22] Stelmaszewski, A., *Determination Of Petroleum Pollutants In Coastal Waters Of The Gulf Of Gdańsk*, Oceanologia, 51(1), pp. 85–92, 2009.
- [23] Stelmaszewski, A., Król, T., Toczek, H., *Light scattering in Baltic crude oil - seawater emulsion*, Oceanologia, 51(3), pp. 405-414, 2009.



ANALYSIS OF RING PRESSURE DISTRIBUTION ON A DEFORMED CYLINDER FACE

Wojciech Serdecki

*Institute of Combustion Engines and Transport
Poznań University of Technology
3, Piotrowo St., 60-965 Poznań
tel. +48 665 2243, fax: +48
e-mail: wojciech.serdecki@put.poznan.pl*

Abstract

Elastic properties of correctly designed piston compression ring should provide full contact of ring face and the cylinder surface. Actually, because of various phenomena and processes experienced during engine assembly and operation an initially cylindrical liner is being subjected to wear and deformations which eventually affects that contact and cause formation of slots distributed along the cylinder circumference.

Following paper describes the most often met deformations of cylinder and presents an evaluation of their influence on the process of compression ring collaboration with the surface of misshaped cylinder. Mathematical relations that allow to calculate the change of ring cylinder pressure and location of areas where blow-by can occur have been presented as well. The presented analyses were supplemented with charts illustrating changeability of certain quantities characteristic for ring and liner construction, using a marine engine ring as an example. The relations established during investigation will be used for a construction of mathematical model of phenomena accompanying the operation of piston-cylinder assembly elements, in the subject of blow-by in particular.

Keywords: *marine combustion engine, piston ring, ring elastic pressure*

1. Introduction

Guarantee of combustion chamber tightness is considered the most important among other tasks fulfilled by the engine labyrinth sealing. Although during engine run there always happen charge losses, but they could be minor ones when the collaboration of ring and liner is correct one. The mathematical models are constructed in order to properly design and monitor the operation of the labyrinth sealing, but authenticity of results acquired using such models depends on correctness of input data. Values of some of them are difficult to calculate or even to estimate. Geometry of slots along the cylinder circumference that cause the blow-by belong to this group. Information how to draw such leakiness can be found in literature. For example, for determination of the slot area S_{sz} between operating surfaces of ring and liner (assuming circular shape of ring) following expression could be used [3]:

$$S_{sz} = \frac{2 \cdot a \cdot h}{3} + \frac{3 \cdot H^2 \cdot h}{2 \cdot a} - \frac{3 \cdot H \cdot h^2}{2 \cdot a} + \frac{h^3}{2 \cdot a}, \quad (1)$$

where, according to Fig. 1:

a – chord where is no contact,

h – maximum height of slot between ring and cylinder,

H – maximum distance between liner and chord connecting slot ends.

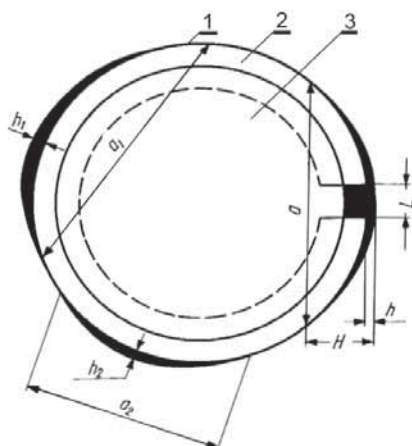


Fig. 1. Schematic of new ring contact with a worn cylinder (visible slots); 1 – cylinder face, 2 – compression ring, 3 – piston [3]

The total area of slots will equal the sum of individual slot areas distributed along the cylinder circumference and the area of ring gap.

The presented way of slot area calculations could be questionable because it does not take into consideration a number of influencing factors that change themselves during engine run. Ring elasticity which extorts its adjustment to a deformed surface of cylinder liner could be classified within this group of factors. This problem was chosen by the Author as the main subject of investigations.

The surface of a new cylinder liner could be compared to an ideal cylinder but the measurements show that even for a new liner its circumferential line differs from ideal circuit (it is a line resulting from a cut of a cylinder with a plane perpendicular to its axis). Among basic causes of these differences one should mention deformations created during liner assembly into cylinder block or those caused by fixing of cylinder head. Moreover, differentiation of cylinder shape could be observed even within a single engine which is a result of various, often difficult to recognize causes such as different thermal and mechanical loads, faulty operation of injection system, etc. Considerable cylinder deformations could be found along the cylinder generatrix. Their maximal values most often emerge within the area of collaboration of the first compression ring with the cylinder face when piston stays in the TDC. This phenomenon is being explained with a shortage in oil supply and absence of conditions favorable for formation of a continuous oil film. Because this problem was described in detail in earlier studies of the author [4,7], a proposed mathematical description of cylinder will be presented here. It should be noted that the presented studies could be treated as an introduction to further research and it is why several factors relative to engine run have been omitted as for example the oil film over cylinder surface or an effect of gas forces. It is very probable that taking into account influence of these factors the conclusions concerning possibilities of slot formation will change considerably.

2. Mathematical description of cylinder circumferential line

Mathematical notation of cylinder shape should contain a description of its circumferential line course and of a profile line. Deformation of cylinder face, relative to chosen plane of cylinder

cross-section can be expressed as the difference between actual value of cylinder radius $r(\varphi)$ and the radius of new cylinder r_o (see Fig. 2):

$$\Delta r(\varphi) = r(\varphi) - r_o. \quad (2)$$

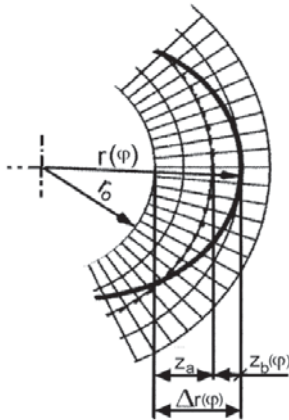


Fig. 2. Course of cylinder circumferential line with explanation of characteristic dimensions

Deformation of the circumferential line $\Delta r(\varphi)$ can be expressed as a sum of following components: z_a and $z_b(\varphi)$:

$$\Delta r(\varphi) = z_a + z_b(\varphi), \quad (3)$$

where the z_a component will be further called the cylinder constant deformation (or even wear of cylinder face) whereas the $z_b(\varphi)$ component will be called cylinder deformation.

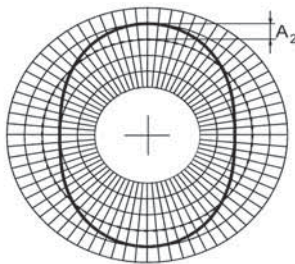
For a mathematic description of cylinder deformation one can use the Fourier harmonic series:

$$z_b(\varphi) = \sum_{h=1}^n A_h \cos(h\varphi + \delta_h), \quad (4)$$

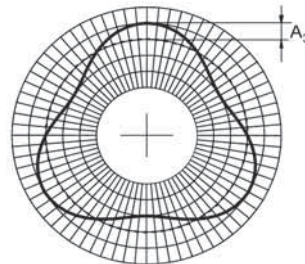
where A_h and δ_h are amplitude and phase shift of consecutive harmonics, respectively. Though a high number of harmonics is required for a precise description of circumferential line course, practically only dominant harmonics are taken into account, those of highest amplitudes (research proves that these are second and fourth harmonics [2]). Exemplary courses of the cylinder circumferential line specified with just one harmonic have been presented in Fig. 3.

As a result of the change in cylinder shape the ring pressure undergoes adjustment from initially constant ($p(\varphi) = p_z = \text{const.}$) to the one changing along the cylinder circumference. Definition of a circumferential variability of ring pressure requires a mathematical specification of cylinder curvature and the course of so called neutral line of a free ring. It is so because after ring installation in cylinder the curvature of its neutral layer changes itself from the one corresponding to the free form $v_p(\varphi)$ to another one corresponding to the curvature of cylinder $v_c(\varphi)$ (assuming full contact of ring and liner).

a)



b)



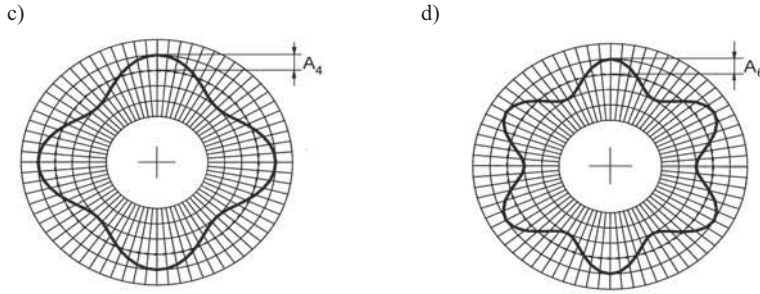


Fig. 3. Course of cylinder circumferential line relative to selected harmonics of the Fourier series: $h = 2$ (a), $h = 3$ (b), $h = 4$ (c), $h = 6$ (d), for $\delta_h = 0$

The cylinder curvature radius can be written in following form as it has been proved in [6]:

$$v_c(\varphi) = \frac{1}{r(\varphi)} \left(1 - \frac{z_b''(\varphi)}{r(\varphi)} \right), \quad (5)$$

while the curvature of free ring neutral layer is given as:

$$v_p(\varphi) = \frac{1 - K(1 + \cos \varphi)}{r_m}, \quad (6)$$

where K is a ring characteristic parameter (the way of its determination was presented in [4]). The value of bending moment loading the ring is given in the form:

$$M_g(\varphi) = E \cdot I \cdot [v_c(\varphi) - v_p(\varphi)], \quad (7)$$

where E denominates the modulus of elasticity of a rod (the ring is equate to a rod), while I means an inertia moment of its cross-section. Using the earlier presented relations the formulas have been established that allow calculations of bending moment value $M_g(\varphi)$ and ring pressure $p_m(\varphi)$ at the point of ring neutral layer corresponding to the φ angle (the way of formulation of these equations was given in [6])

$$M_g(\varphi) = \frac{E \cdot I}{r_m^2} \cdot [K \cdot r_m \cdot (1 + \cos \varphi) - z_a - z_b(\varphi) - z_b''(\varphi)], \quad (8)$$

$$p_m(\varphi) = \frac{E \cdot I}{h_p \cdot r_m^4} [K \cdot r_m - (z_a + z_b(\varphi) + 2z_b''(\varphi) + z_b^{(4)}(\varphi))]. \quad (9)$$

Using the presented formulas one could try to determine a changeability of ring pressure against the deformed liner.

3. Determination of ring pressure on deformed liner

As mentioned before the cylinder circumferential line undergoes various changes due to numerous causes. In order to simplify further analyses this study deals only with cases where the

cylinder deformation can be described with just one harmonic and the value of even deformation has been assumed as zero, i.e. $z_a = 0$.

With these assumptions it can be proved that relations describing changes in bending moment and ring pressure take on the following form (similar dependences were given in [1]):

$$M_g(\varphi) = \frac{E \cdot I}{r_m^2} \left[K \cdot r_m \cdot (1 + \cos \varphi) + A_h \cdot (h^2 - 1) \cdot \cos(h\varphi + \delta_h) \right], \quad (10)$$

$$p_m(\varphi) = \frac{E \cdot I}{h \cdot r_m^4} \left[K \cdot r_m - A_h \cdot (h^2 - 1)^2 \cdot \cos(h\varphi + \delta_h) \right]. \quad (11)$$

Depending on the size of deformation amplitude A_h the ring pressure will change. When the amplitude does not exceed a certain value (called critical) the ring will contact along the entire circumference to the deformed cylinder (Fig. 4).

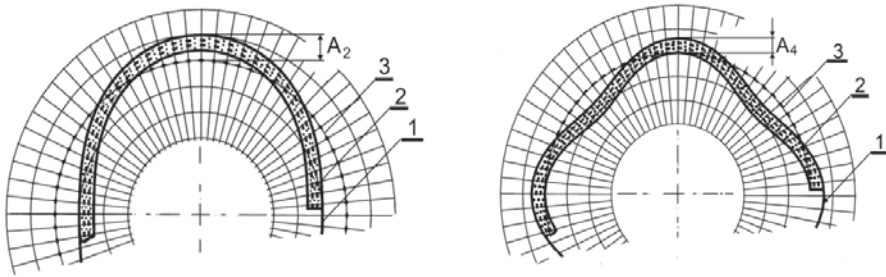


Fig. 4. A sketch of ring section touching the face of deformed liner: 1 – actual circumferential line of a deformed liner, 2 – ring section, 3 – circumferential line of a new ring (there is no proportion between size of elements and deformation in this figure)

Until after exceeding the critical value of amplitude A_{kr} areas where the pressure resulting from ring own elasticity is insufficient to push the ring against the liner (i.e. areas where ring pressure is naught or negative) will appear. An assumption has been adopted that due to this phenomenon slots between ring and liner will occur where blow by can take place.

According to (11) the $p_m(\varphi)$ pressure is equal to zero when following condition is fulfilled:

$$\cos(h \cdot \varphi) = \frac{K \cdot r_m}{A_h \cdot (h^2 - 1)^2}. \quad (12)$$

Taking into consideration that the value of $\cos(x)$ does not exceed 1 critical values of deformation amplitude for selected harmonics could be determined by the transformation of above formula:

$$A_{kr,h} = \frac{K \cdot r_m}{(h^2 - 1)^2} \quad (13)$$

Which means that the critical amplitude values of individual harmonics are:

$$A_{kr,2} = \frac{K \cdot r_m}{9}; \quad A_{kr,3} = \frac{K \cdot r_m}{64}; \quad A_{kr,4} = \frac{K \cdot r_m}{225}; \quad \text{and so on.}$$

Higher the number of harmonic used for description of cylinder deformation lower the value of critical amplitude. For example, for the harmonic $h = 2$ the critical amplitude is about 25 times higher than the amplitude for harmonic $h = 4$.

In turn, the minimum value of the φ angle that define the slot limits can be calculated using following formula

$$\varphi_o = \frac{\arccos\left(\frac{K \cdot r_m}{A_h(h^2 - 1)^2}\right) - \delta_h}{h} = \frac{\arccos\left(\frac{A_{kr,h}}{A_h}\right) - \delta_h}{h}. \quad (14)$$

This formula can be used only when the condition of $A_h \geq A_{kr,h}$ is fulfilled.

Values of the $\varphi_{o,i}$ angle (where i are the consecutive natural numbers) that determine the slot limits (areas where is no ring pressure) can be determined using a general formula:

$$\varphi_{o,i} = \frac{\pi \cdot (i+1)}{h} - \varphi_o \quad - \text{for odd values of } i,$$

$$\varphi_{o,i} = \frac{\pi \cdot i}{h} + \varphi_o \quad - \text{for even values of } i.$$

Presented below exemplary calculations were performed for a compression ring of marine engine (such ring was earlier a subject of investigation reported in [4]). Basic technical data are summarized in Table 1.

Table 1

| Technical data of exemplary IC engine compression rings | | |
|---|--------------------|-------------------------|
| Quantity | | Ring (marine engine) |
| cylinder diameter d | [m] | 0.480 |
| ring neutral radius r_m | [m] | 0.232 |
| axial height h_p | [m] | 0.015 |
| radial thickness g_p | [m] | 0.016 |
| gap clearance m | [mm] | 49.0 |
| Young modulus E | [Pa] | $105 \cdot 10^9$ |
| mean pressure p_o | [MPa] | 0.063 |
| tangential force F_t | [N] | 219 |
| stiffness EI | [Nm ²] | 537.6 |
| parameter K | [-] | 0.0220 |

The effect of cylinder deformation size on a course of bending moment variations and ring pressure was evaluated in a course of calculations. Two cases of cylinder deformations were analyzed, namely when the cylinder circumferential line was described with harmonics of the 2nd and 4th order. The obtained results for selected values of cylinder deformation amplitude have been presented on graphs in Figs. 5 and 6.

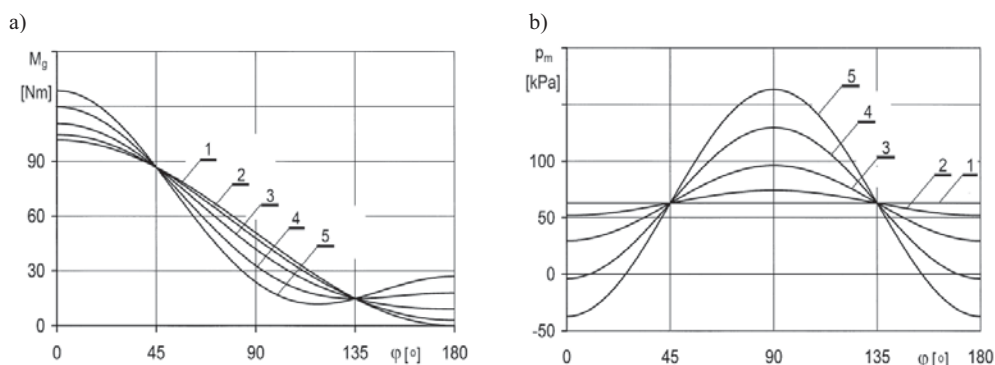


Fig. 5. Courses of bending moment M_g (a) and ring pressure p_m (b) defined along its circumference for selected values of deformation amplitudes A_2 : 1 – 0 μm , 2 – 100 μm , 3 – 300 μm , 4 – 600 μm , 5 – 900 μm

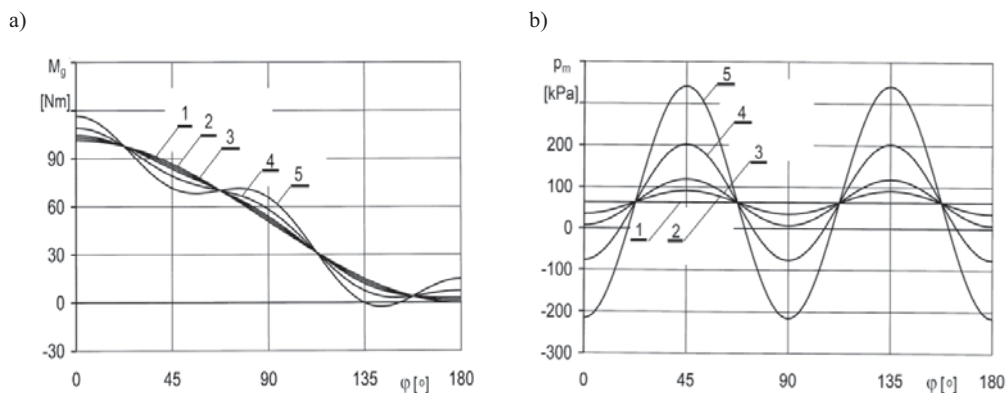


Fig. 6. Courses of bending moment M_g (a) and ring pressure p_m (b) defined along its circumference for selected values of deformation amplitudes A_4 : 1 – 0 μm , 2 – 10 μm , 3 – 20 μm , 4 – 50 μm , 5 – 100 μm

The curves course shows that within regions where the increase in amplitude leads to lesser cylinder diameter the ring pressure increases while for bigger diameter this pressure decreases. There is a critical value of deformation amplitude for which the ring is not pushed against the liner by its own elasticity though it still touches the cylinder face (value of these amplitudes calculated according to Eq. (13) are summarized in Table 2.

Table 2

| Values of $\varphi_{0,i}$ angle for selected values of 2 nd and 4 th harmonics | | | | | | | |
|--|--------------|--------------|---------------------------------------|--------------|-------------|--------------|--------------|
| h = 2 $A_{kr,2} = 567 \mu\text{m}$ | | | h = 4 $A_{kr,4} = 22,7 \mu\text{m}$ | | | | |
| $\varphi_{0,i} [\text{rad}]/[^\circ]$ | | | $\varphi_{0,i} [\text{rad}]/[^\circ]$ | | | | |
| $A_i [\mu\text{m}]$ | i = 0 | i = 1 | $A_i [\mu\text{m}]$ | i = 0 | i = 1 | i = 2 | i = 3 |
| 300 | – | – | 20 | – | – | – | – |
| 600 | 0.166 / 9.50 | 2.97 / 170.5 | 50 | 0.275 / 15.7 | 1.29 / 74.3 | 1.85 / 105.7 | 2.86 / 164.3 |
| 900 | 0.445 / 25.4 | 2.69 / 154.5 | 100 | 0.335 / 19.2 | 1.23 / 70.8 | 1.91 / 109.2 | 2.81 / 160.8 |

An increase of the amplitude value over its critical value leads to an increase in area of ring contact absence described with angles $\varphi_{0,i}$ (14). These values of angle (only for a section of ring) are presented in Table 2 and in Fig. 7 (only selected ones).

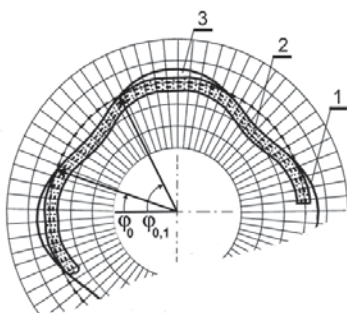


Fig. 7. Sketch of ring section in deformed cylinder:
1 – actual circumferential line of deformed cylinder,
2 – section of ring, 3 – slot hypothetical location ;
 $\varphi_{0,i}$ – angles defining boundary points of ring to deformed cylinder face contact

Within the areas of ring-liner contact so called light slots appear. Their geometry depends on the course of ring neutral line. Definition of course of that line, consequently the area of slots, is a complicated problem which will be discussed in further papers.

References

- [1] Bardzimashvili T., Kell j., Romelashvili E., Distortion inside a piston bore. Michigan State University MTH 844, 2004.
- [2] Iskra A., Studium konstrukcji i funkcjonalności pierścieni w grupie tłokowo-cylindrowej. Wydawnictwo PP, Poznań 1996.
- [3] Kozaczewski W., Konstrukcja grupy tłokowo-cylindrowej silników spalinowych. WKŁ, Warszawa 2004.
- [4] Serdecki W., Analysis of relations between the compression ring characteristic parameters. Journal of POLISH CIMAC. Energetic aspects, Gdańsk 2011, Vol. 6, No. 1.
- [5] Serdecki W., Krzymień P., How the wear of cylinder liner affects the cooperation of piston-cylinder assembly of ic engine. Materiały konferencji Kones 2012.
- [6] Serdecki W., Krzymień P., The Effect of changes in cylinder liner geometry on the operation of piston compression ring. Materiały konferencji KONMOT 2012.
- [7] Serdecki W., Badania współpracy elementów układu tłokowo-cylindrowego silnika spalinowego. Wydawnictwo Politechniki Poznańskiej, Poznań 2002.



INCREASING SHIP PROPULSION EFFICIENCY AS AN ALTERNATIVE TO HELP REDUCE FUEL CONSUMPTION AND CO₂ EMISSION

Part I

Energy Efficiency Design Index (EEDI) as a new criterion in ship design

Tadeusz Szelangiewicz, Katarzyna Żelazny

*Westpomeranian of Technology in Szczecin, Faculty of Maritime Technology and Transport,
Piastów 41, 71-065 Szczecin, Poland*

tel. +48 91 449 41 26, fax: +48 91 449 46 95

e-mail: tadeusz.szelangiewicz@zut.edu.pl, katarzyna.zelazny@zut.edu.pl

Abstract

From 2013 onwards EEDI for newly built ships will become mandatory. Ships meeting the CO₂ emission standards will be granted energy certificate for needed for exploitation. The article presents the EEDI in the current form, energy certification procedure as well as reduction of CO₂ emission planned for coming years (Part I). The majority of ships built at present, meets the CO₂ emission standards for 2013, yet their further decrease in subsequent years will consequently necessitate further actions as well. One of them is ship hull design of smaller resistance values and higher propulsion efficiency. The article (Part II) presents calculation results of the numerical analyses (CFD) performed for an actually built ship, aiming at decreasing propulsion power and therefore the EEDI value as well.

Key words: *Energy Efficiency Design Index, International Energy Efficiency Certificate for the ship, ship hull geometry, propeller efficiency, streamline rudder, computation fluid dynamics (CFD)*

1. Introduction

Aiming at the so called greenhouse gas reduction (including CO₂) has resulted in the introduction of new criteria and standards, in combustion engine design or entire means of transport. IMO has drawn up Energy Efficiency Design Index (EEDI) for newly built and designed ships, mandatory since 2013, which is defined as follows:

$$EEDI = \frac{CO_2 \text{ emission}}{\text{transport work}} \quad (1)$$

and expressed in CO₂ grammes/1 tonne·mile of transported cargo.

Introduction of such criterion is to enforce such ship design and exploitation (together with its propulsion) as to decrease CO₂ emission (CO₂ emission will be gradually reduced in subsequent years).

Although the main aim of the EEDI is CO₂ reduction, still the very structure of this index allows it to be used as yet another design criterion as well as some kind of transport efficiency

measure. Proper application of EEDI in ship design can therefore reduce CO₂ emission on the one hand, and lead to optimal choice of technical and service parameters on the other, which in turn maximise economic performance for a shipowner.

2. Energy Efficiency Design Index

Research into EEDI has been carried out for years now. As a basis laid the assumption that sea transport of cargo is also associated with CO₂ emission, which has been defined as, [5]:

$$\text{Attained design CO}_2 \text{ index} = \frac{C_F \cdot SFC \cdot P}{\text{Capacity} \cdot V_{ref}}, \quad (2)$$

where:

- C_F – conversion factor between fuel consumption and CO₂ emission,
- SFC – specific fuel consumption,
- P – 75% of the rated installed power (MCR),
- Capacity – deadweight for all types of carriers and gross tonnage for passenger ships,
- V_{ref} – the ship speed at specified at calm sea (no wind, no waves).

The formula (2) was initially a complex one with additional coefficients. There have been over a dozen of corrections and amendments in total, proposed mainly by Denmark, Japan, and the USA. The current version, subject to further research and analysis, recommended for ship design is presented below [2]:

$$\frac{\left(\prod_{j=1}^M f_j \right) \left(\sum_{i=1}^{nME} P_{ME(i)} C_{FME(i)} SFC_{ME(i)} \right) + (P_{AE} C_{FAE} SFC_{AE}) + \left(\prod_{j=1}^M f_j \left(\sum_{i=1}^{nPTI} P_{PTI(i)} - \sum_{i=1}^{neff} f_{eff(i)} P_{AEeff(i)} \right) C_{FAE} SFC_{AE} \right)}{f_i \cdot \text{Capacity} \cdot V_{ref} \cdot f_w} - \frac{\left(\sum_{i=1}^{neff} f_{eff(i)} P_{eff(i)} C_{FME} SFC_{ME} \right)}{f_i \cdot \text{Capacity} \cdot V_{ref} \cdot f_w}, \quad (3)$$

where:

- $C_{FME(i)}$ – a non-dimensional conversion factor between fuel consumption (in grams) and CO₂ emission (also in grams) on the basis of carbon content, Table 1,
- $SFC_{ME(i)}$ – specific fuel consumption (main engine),
- $P_{ME(i)}$ – 75% ships' total installed main power (MCR),
- C_{FAE} – a non-dimensional conversion factor (like $C_{FME(i)}$) for auxiliary engines,
- SFC_{AE} – specific fuel consumption (auxiliary engines),
- P_{AE} – power of auxiliary engines, IMO MEPC define it according to MCR for ships power below and above 10 000 kW,
- $P_{PTI(i)}$ – 75% shaft motor power,
- $P_{AEeff(i)}$ – auxiliary power reduction due to innovative electrical energy efficient technology measured at $P_{ME(i)}$,
- $f_{eff(i)}$ – availability factor of innovative energy efficiency (if used),
- $P_{eff(i)}$ – output of innovative mechanical energy efficient technology,
- V_{ref} – is the ship speed, measured in nautical miles per hour (knot), on deepwater in the condition of maximum allowed summer load draught as provided in confirmed stability information,
- f_i – the capacity factor for any technical/regulatory limitation on Capacity ,

- f_w – a non-dimensional coefficient indicating the decrease of speed in representative sea conditions of wave height, wave frequency and wind speed,
- f_j – a correction factor to account for ship specific design elements.

Table 1. Non-dimensional factor C_F for different type of fuel [2]

| Type of Fuel | Reference | Carbon content | C_F (t-CO ₂ /t-Fuel) |
|----------------------------------|---------------------------------|----------------|--------------------------------------|
| 1. Diesel/Gas Oil | ISO 8217 Grades DMX through DMC | 0.875 | 3.206000 |
| 2. Light Fuel Oil (LFO) | ISO 8217 Grades RMA through RMD | 0.86 | 3.151040 |
| 3. Heavy Fuel Oil (HFO) | ISO 8217 Grades RME through RMK | 0.85 | 3.114400 |
| 4. Liquified Petroleum Gas (LPG) | Propane | 0.819 | 3.000000 |
| | Butane | 0.827 | 3.030000 |
| 5. Liquified Natural Gas (LPG) | | 0.75 | 2.750000 |

The EEDI formula has been drawn up mainly for conventional propulsion systems (combustion engine) and does not have to be used in other propulsion systems such as: diesel-electric, turbine or hybrid propulsion types.

The EDDI formula is quite a complex one, where two basic groups of parameters can be distinguished:

- the first group, pertaining to the marine power plant, that is main and auxillary engine(s) power, specific fuel consumption, conversion factors between fuel consumption and CO₂ emission, power of waste heat generators, as well as parameters defining the application and use of innovative technology – given in the formula numerator (3),
- the first group, pertaining to ship exploitation, that is, the capacity, the ship speed on calm sea, the decrease of a ship speed in real-life weather conditions, which can be found in the formula denominator as well as a nominator parameter defining type and specific work conditions eg. sailing through ice.

Currently binding EEDI version is by no means final, although it will be mandatory since 2013. It has been widely discussed, with numerous changes proposed eg. on values or the calculation methods of some parameters (power, speed, capacity) or their coefficients (eg. decrease in ship speed on rough sea).

3. Reference line

In order to establish the expected CO₂ emission a reference line has been drawn up for various types of ships of different sizes. It will be enforced since 2013. EEDI calculation will be performed for each newly built ship and compared against the appropriate reference line (for the ship type and size). If the EEDI value will be equal or smaller than that on the reference line, the ship will be granted International Energy Certificate and fit for exploitation. Examples of reference lines in 2013 are given in Fig. 1÷3.

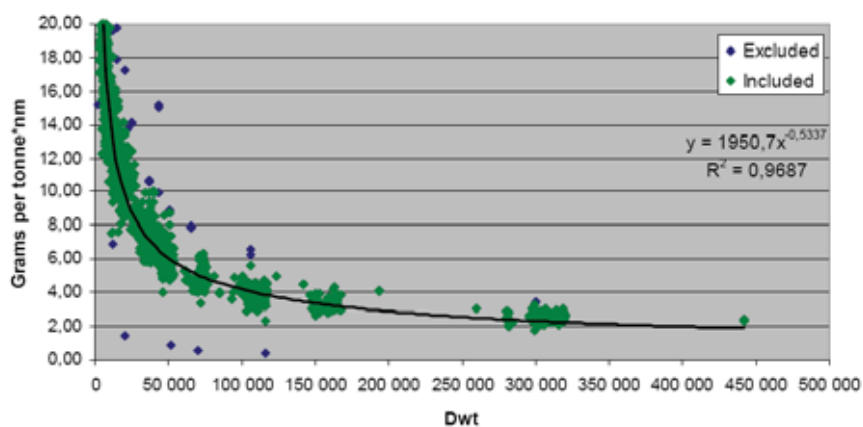


Fig. 1. Reference line for tanker ships, [1]

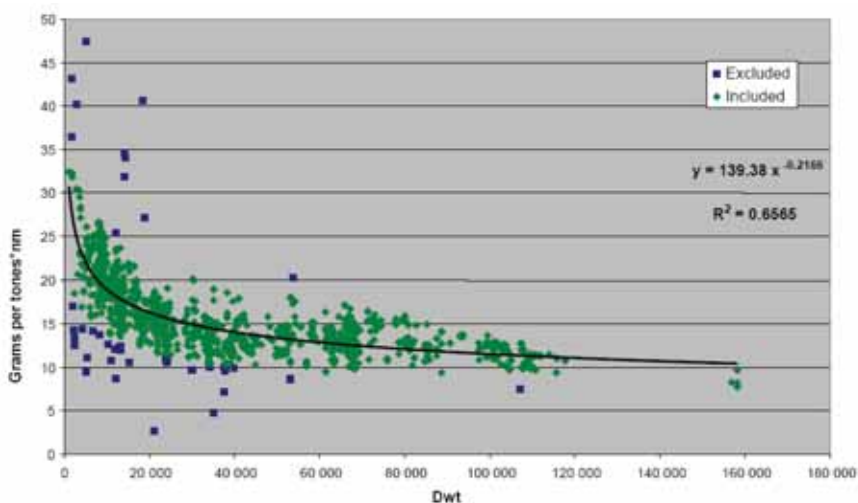


Fig. 2. Reference line for containerships, [1]

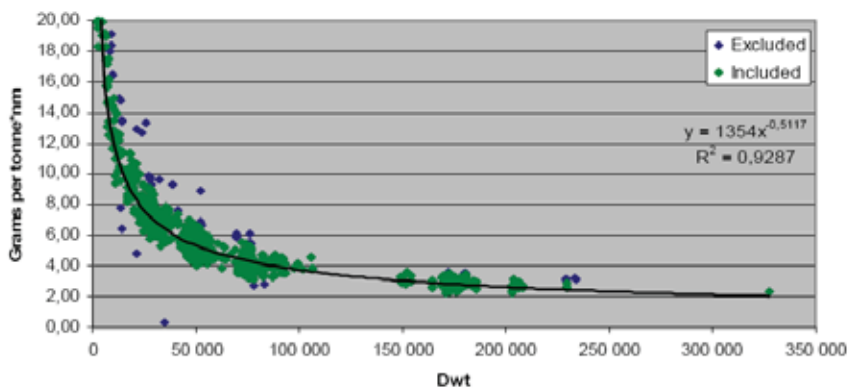


Fig. 3. Reference line for bulk carriers ships, [1]

Methodology for defining the reference line was first proposed by Denmark. In order to determine the reference line (base line) Lloyd's Register Fairplay (LRFP) data on existing, already built ships was used. Such data is incomplete, therefore some simplifications had to be made, or some missing data completed using similar ships with regression relationship. For all the ships used, a constant specific fuel consumption (SPF) was assumed, independently from the actual engine of a ship. The calculations do not include potential shaft generators, although they might have been present on some of the ships.. Therefore, the EDDI values as seen on Fig.1÷3 are above the reference line, which is not necessarily true. Thus further research has been undergoing in order to adjust the reference line as needed, especially for some types of large capacity ships.

In order to facilitate EEDI estimation for a newly built ship and establish whether it meets the CO₂ emission criteria, the reference line has been approximated as follows [3]:

$$L_{ref} = a \cdot b^{(-c)} \quad (4)$$

where a, b, c are parameters, whose values for each ship type are presented in the Table 2 below.

Table 2. Parameters for determination of reference values for the different ship types [3]

| Ship type defined in regulation 2 | a | b | c |
|-----------------------------------|---------|-----------------|--------|
| 2,25 Dry bulk carrier | 1354,0 | DWT of the ship | 0,5117 |
| 2,26 Gas carrier | 1252,60 | DWT of the ship | 0,4597 |
| 2,27 Tanker | 1950,70 | DWT of the ship | 0,5337 |
| 2,28 Container ship | 139,38 | DWT of the ship | 0,2166 |
| 2,29 General cargo ship | 290,28 | DWT of the ship | 0,3300 |
| 2,30 Refrigerated cargo carrier | 227,01 | DWT of the ship | 0,244 |
| 2,31 Combination carrier | 1219,00 | DWT of the ship | 0,488 |

Since further reduction in CO₂ emission is planned for subsequent years, then the reference line will be changing accordingly. Prognostic values of CO₂ (expressed as a percent in relation to the basal values of reference line in 2013) are given in Table 3.

Tabela 3. Reduction factors (in percentage) for the EEDI relative to the EEDI Reference line [3]

| Ship Type | Size | Phase 0 1 Jan 2013 – 31 Dec 2014 | Phase 1 1 Jan 2015 – 31 Dec 2019 | Phase 2 1 Jan 2020 – 31 Dec 2024 | Phase 3 1 Jan 2025 – and onwards |
|----------------|-------------------------|--|--|--|--|
| Bulk carrier | 20,000 DWT and above | 0 | 10 | 20 | 30 |
| | 10,000 – 20,000 DWT | n/a | 0-10* | 0-20* | 0-30* |
| Gas carrier | 10,000 DWT and above | 0 | 10 | 20 | 30 |
| | 2,000 – 10,000 DWT | n/a | 0-10* | 0-20* | 0-30* |
| Tanker | 20,000 DWT and above | 0 | 10 | 20 | 30 |
| | 4,000 – 20,000 DWT | n/a | 0-10* | 0-20* | 0-30* |
| Container ship | 15,000 DWT and above | 0 | 10 | 20 | 30 |
| | 10,000 – 15,000 DWT | n/a | 0-10* | 0-20* | 0-30* |

| | | | | | |
|----------------------------|----------------------|-----|-------|-------|-------|
| General cargo ship | 15,000 DWT and above | 0 | 10 | 20 | 30 |
| | 3,000 – 15,000 DWT | n/a | 0-10* | 0-20* | 0-30* |
| Refrigerated cargo carrier | 5,000 DWT and above | 0 | 10 | 20 | 30 |
| | 3,000 – 5,000 DWT | n/a | 0-10* | 0-20* | 0-30* |
| Combination carrier | 20,000 DWT and above | 0 | 10 | 20 | 30 |
| | 4,000 – 20,000 DWT | n/a | 0-10* | 0-20* | 0-30* |

* Reduction factor to be linear interpolated between the two values dependent upon vessel size.

4. International Energy Certificate of a Ship

EEDI value calculation and International Energy Certificate for a new ship will be issued by the state Marine Administration on the basis of approved ship design documentation. It means that the subsequent ship exploitation together with changeable sailing conditions (shipping routes, weather) will have no influence on the EEDI value.

The EEDI certificate is therefore valid throughout the life of the ship [3], unless the ship undergoes a major conversion so as it is regarded as a new ship. The certificate loses its validity when the ship is withdrawn from the service or transferred to the flag of another state (sold, hired). It is possible however, that the marine administration of both contracting states, reach the agreement and transmit the certificate together with the copies of the relevant survey reports to the new ship's operator within a three-month period. Subject to specified conditions the certificate is deemed valid.

In some documents and publications it is emphasized that in order to reduce CO₂ emission, the shipping routes must be optimised, the service speed of the ship decreased or higher quality fuel used. According to the currently binding criteria, such activities – although environmentally friendly – will not affect the already calculated EEDI value, and hence be decisive in meeting the required standards for the international energy certificate.

5. EEDI guidelines in ship design

Reference lines shown on Fig. 1-3 are the product of statistical analysis of EEDI values for various ship sizes (capacity) of the existing vessels of the same time, built in different years.

Although the reference lines result from approximate EEDI calculation values, still however even with the exact EEDI calculation value there will be some ships, whose EEDI will be above the reference line. As the Table 3 shows, the reduction factor of CO₂ emission from newly built ships with combustion engines will be steadily increasing. Therefore, even at present the significant potential for decreasing EEDI values (and at the same time improving the ship energy efficiency) is indicated as follows:

- improved hull design aiming at higher propulsion efficiency,
- more efficient propulsion engine – lower specific fuel consumption,
- higher fuel quality,
- development of new technologies, better waste heat recovery system,
- larger ship construction (bigger capacity),
- decreasing the ship's speed,
- optimisation of the shipping route.

While some of the above suggestions do not play any major role now, since eg. EEDI value together with certificate is determined for a newly built ship and its future service together with

shipping route optimisation is not taken into account; there are still other – pertaining to the propulsion engine, new technologies or fuel quality, which can be worked upon bearing in mind that our experience in these fields so far suggests that further improvements will not be revolutionary.

Low-speed engines, in turn, use the lowest quality fuel, which makes them economical to use. Building larger ships, suggested above, is not always profitable for the ship operator and the distribution of the ports large enough for them must be taken into account as well. Decrease in service speed of a ship is possible, but necessarily within a safety limit. Even now, the IMO has published guidelines, suggesting that decrease in service speed in order to lower the EEDI value of a ship, must not impede ship safety, i.e. manoeuvrability of the ship under adverse conditions or safe sailing against the opposite or oblique waves.

The remaining solution, could possibly be found in the optimisation of the hull and propeller design so as to minimise the propulsion power and – at the same time - decrease ship fuel consumption and CO₂ emission.

The above considerations for improvement in hull design seem very attractive, however they could possibly be used for an unfounded suggestion, that the EEDI value of a new ship is lower than the actual. What is more, as already stated in some projects, it is possible to estimate the EEDI value in a dishonest way taking advantage of a possible lack of precision in regulations.

Bibliography

- [1] GHG-WG 2/2/7 – *Consideration of the energy efficiency design index for new ships*, 2010.
- [2] MEPC.1/Circ.681 (2009) – *Interim Guidelines on the Method of Calculation of the Energy Efficiency Design Index for New Ship's*.
- [3] MEPC 62/24/Add. 1, Annex 19, Resolution MEPC.203(62), 2011.
- [4] Study on tests and trials of the Energy Efficiency Design Index as developed by the IMO, Report for project 6543, deltamarin Ltd, Finland 2011.
- [5] Yoshi Ozaki, John Larkin, Kirsi Tikka, Keith Michel, *An Evaluation of the Energy Efficiency Design Index (EEDI) Baseline for Tankers, Containership, and LNG Carriers*, ABS 2010.



INCREASING SHIP PROPULSION EFFICIENCY AS AN ALTERNATIVE TO HELP REDUCE FUEL CONSUMPTION AND CO₂ EMISSION

Part II

Research on hull and propeller design optimisation in order to decrease the EEDI value

Tadeusz Szelangiewicz, Katarzyna Żelazny

*Westpomeranian of Technology in Szczecin, Faculty of Maritime Technology and Transport,
Piaśtów 41, 71-065 Szczecin, Poland*

tel. +48 91 449 41 26, fax: +48 91 449 46 95

e-mail: tadeusz.szelangiewicz@zut.edu.pl, katarzyna.zelazny@zut.edu.pl

Abstract

From 2013 onwards EEDI for newly built ships will become mandatory. Ships meeting the CO₂ emission standards will be granted energy certificate for needed for exploitation. The article presents the EEDI in the current form, energy certification procedure as well as reduction of CO₂ emission planned for coming years (Part I). The majority of ships built at present, meets the CO₂ emission standards for 2013, yet their further decrease in subsequent years will consequently necessitate further actions as well. One of them is ship hull design of smaller resistance values and higher propulsion efficiency. The article (Part II) presents calculation results of the numerical analyses (CFD) performed for an actually built ship, aiming at decreasing propulsion power and therefore the EEDI value as well.

Key words: Energy Efficiency Design Index, International Energy Efficiency Certificate for the ship, ship hull geometry, propeller efficiency, streamline rudder, computational fluid dynamics (CFD)

1. Introduction

The first part of the article presents a few ways of decreasing CO₂ emission in new ship design and construction.

Optimisation of hull and propeller design aimed at reduction of propulsion efficiency and thus resulting decrease in fuel consumption and CO₂ emission, is one of the methods which make it possible to meet the IMO standards of EEDI values for newly designed and built transport ships, in force since 2013. Such research in design is also indispensable bearing in mind that CO₂ reduction standards will become stricter in subsequent years from 2015 onwards according to a schedule presented in (Table 3 [2]).

Optimisation of ship hull and screw propeller design should be carried out in the following stages:

- global optimisation of the main design parameters of a ship, aimed at maximum reduction of resistance (and thus propulsion power) for a given service speed and ship capacity, taking account of other necessary parameters, e.g. technical;

- local optimisation, which means local modification of hull design geometry, e.g. at the stern in order to facilitate propeller contact with water (wake current field);
- optimisation of propeller efficiency for a modified stern design of a ship;
- optimisation of geometrical parameters of spade rudder located behind the propeller in order to increase their efficiency.

All the above actions together should result in a simultaneous reduction of a ship's resistance and an overall increase of propulsion efficiency hull-propeller – spade rudder.

There are several ways to achieve the above goal :

- optimisation based on approximate methods (formulas resulting from systematic model testing); such formulas, however, do not contain a number of specific geometrical parameters, hence their application for the above goal is severely limited or – as in case of local optimisation – even impossible;
- optimal hull design resulting from model testing – such method calls for a number of hull design models, which generates high costs and is therefore not used in practice;
- using CFD method and tools which have a full potential to succeed in such design project.

This part of the article presents the initial results numerical analysis aimed at decreasing ship resistance of a real, built ship and increasing its propulsion efficiency so as to reduce propulsion power at the same time reducing the EEDI value as well.

2. Modified ship and the scope of calculations

Hull modification and subsequent numerical analyses were performed for a B 573 ship (Table 4) built in Szczecin shipyard with a complete design documentation, basin model test and sea trials.

Table 4. Main parameters of B 573 ship in various loading conditions

| | | |
|-------------------------------|----------|----------------------|
| Length between perpendiculars | L_{pp} | 172 m |
| Waterline length | L_{WL} | 176.41 m |
| Hull breadth | B | 32.2 m |
| Draught | T | 11.0 m |
| Deadweight | P_N | 45000 t |
| Speed | V | 14.5 w |
| Volumetric displacement | ∇ | 50500 m ³ |
| Wetted surface area | S | 8200 m ² |
| Block coefficient | C_B | 0.807 |

Body lines, rudder location and dimensions of a real ship (shown in Fig. 4 and 5) were treated as input values for further modification in the ship geometry.

The scope of research covered:

- modification of hull geometry in order to determine the influence of such modification on:
 - resistance of a ship's hull model,
 - distribution of the wake current field velocity,
- propeller efficiency calculation for new wake currents field,
- propeller geometry was modified for the working conditions (behind the ship's hull)
- geometry of the spade rudder was modified in order to:

- increase steering efficiency,
- increase propeller efficiency by its relations to spade rudder.

Hull modification was performed in such a way as to maintain ship constant displacement, deadweight tonnage, length and breadth. Changing given parameters within these particular groups, the remaining values were left stable.

Their scope covered the following (Table 5):

- change of the ship's hull block coefficient C_B ,
- change of the ship's hull prismatic coefficient C_p
- change of location of the longitudinal centre of buoyancy LCB,
- manual change of the entire ship's hull form or its stern part only.

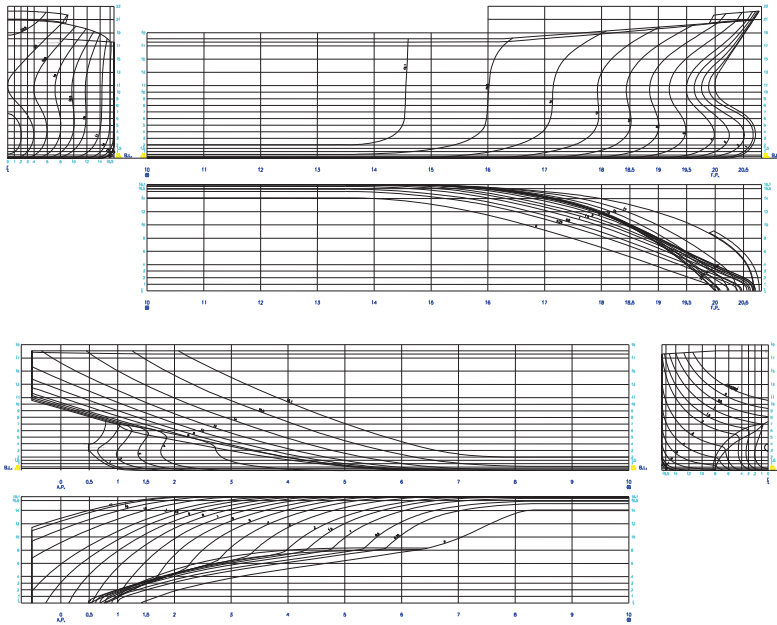


Fig. 4. Body lines of the analyzed hull form of B 573 ship

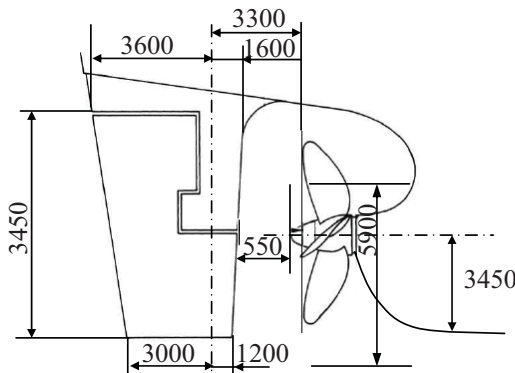


Fig. 5. The semi-spade rudder behind the screw propeller of B 573 ship [8].

Table 5. Range of changes of B573 ship hull form

| Number of variant | | Change of parameter | Parameter |
|-------------------|--|---------------------|-----------|
| 1. | Change of the block coefficient C_B ; its initial value $C_B = 0,800$ | -0,01 | 0,79 |
| 2. | | -0,005 | 0,795 |
| 3. | | -0,015 | 0,785 |
| 4. | | +0,01 | 0,81 |
| 5. | | +0,005 | 0,805 |
| 6. | | +0,015 | 0,815 |
| 7. | Change of the the prismatic coefficient C_P ; its initial value $C_P = 0,790$ | -0,01 | 0,78 |
| 8. | | -0,02 | 0,77 |
| 9. | | -0,03 | 0,76 |
| 10. | | +0,01 | 0,8 |
| 11. | | +0,02 | 0,81 |
| 12. | Change of longitudinal location of the centre of buoyancy LCB. its initial location: equal to 48% Lwl measured aft from FP | -1% shift fore | 47% |
| 13. | | -2% shift fore | 46% |
| 14. | | -3% shift fore | 45% |
| 15. | | +1% shift aft | 49% |
| 16. | | +2% shift aft | 50% |
| 17. | | +3% shift aft | 51% |
| 18. | Manual hull form modification of its stern part only – symmetric hull form | - | - |
| 19. | Manual hull form modification of its stern part only – asymmetric hull form | - | - |

For each of the hull versions new body lines and next numerical computational grids were prepared, and finally calculations of resistance and wake distribution were performed. Example frame sections of modified hull form variants are shown in Fig. 6 ÷ 8.

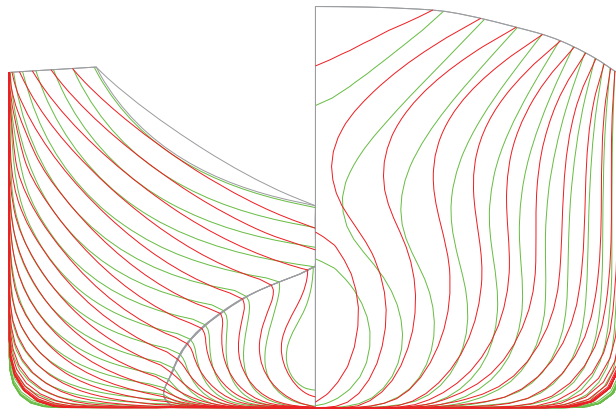


Fig. 6. Variant no.1 – original hull form - marked green; modified hull form – marked red

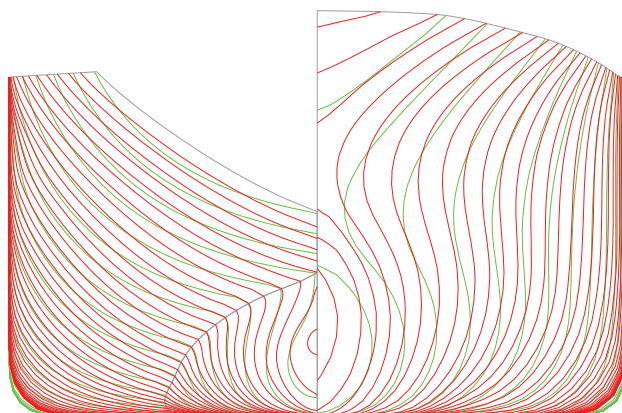


Fig. 7. Variant no.2 – original hull form - marked green; modified hull form – marked red

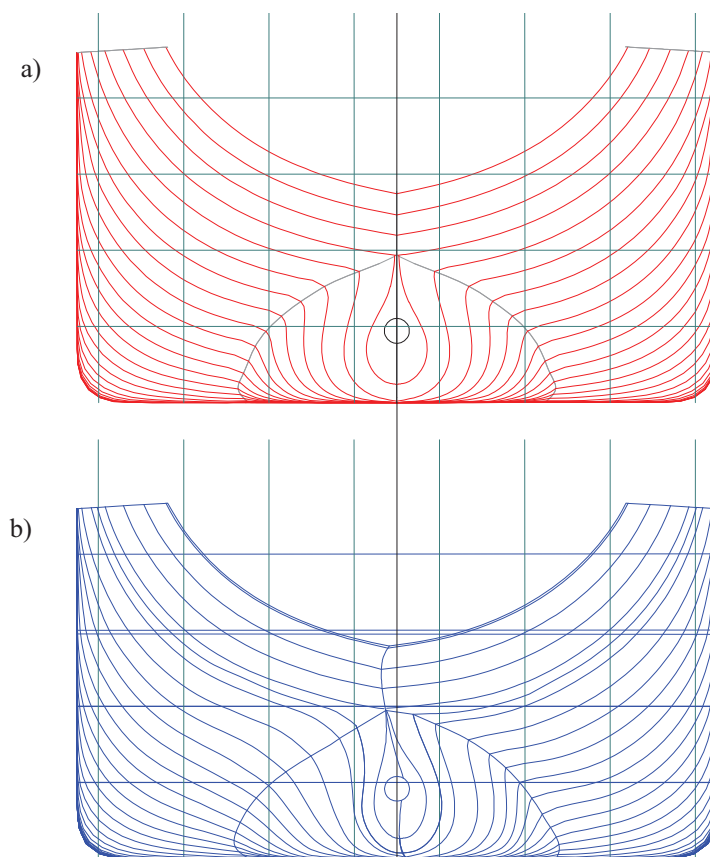


Fig. 8. Variant no.19 – body lines of stern part of B 573 ship hull: a) before modification (symmetric stern), b) after modification (asymmetric stern)

3. Numerical analysis of the ship body, screw propeller and spade rudder

All the numerical analyses have been performed using computer cluster NEPTUN (owned by the Chair of Ocean Technology and Marine System Design, Faculty of Marine Technology and Transport, West Pomeranian University of Technology, Szczecin) with the help of FLUENT software.

Numerical analysis has been performed for the ship in the same model scale, as for the model tests (scale ratio 1:25).

For the ship model have been defined and a numerical computational grid of non-structural type with prismatic elements in boundary layer (Fig. 9) has been created, in order to subsequently convert it into polyhedron-type elements (Fig. 10). Non-structural grid was created using the Gambit system, with FLUENT software used for conversion.

Conversion of non-structural grids into the polyhedron-type makes it possible to reduce the number of grid elements 3 up to 5 times as well as to improve grid parameters, - especiall the element skewness parameter. Ultimately, the total number of all elements used in calculations for individual ship movements fell within the range of 650.000 – 750.000.

For each calculation, the convergence of iteration for residual values of all calculations and ship's body coefficient forces has been controlled.

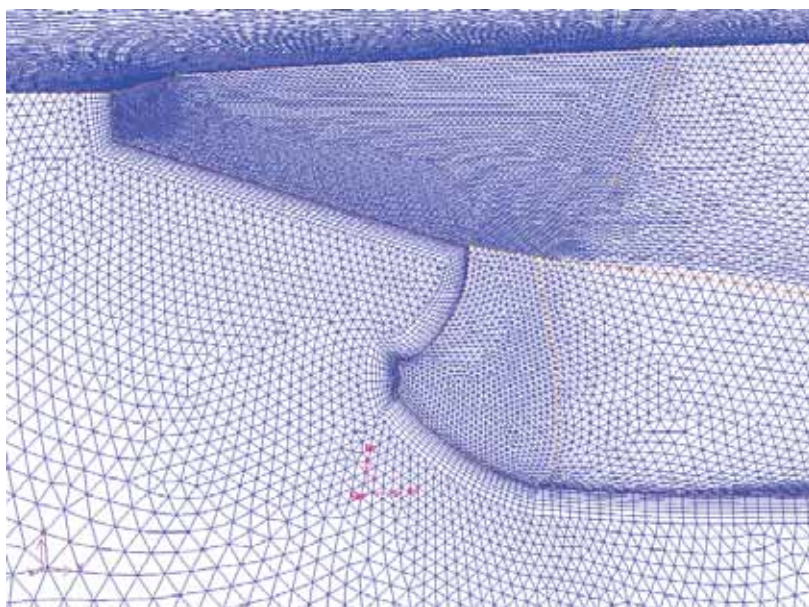


Fig. 9. Non-structured tetrahedral grid of the ship's stern section before the conversion

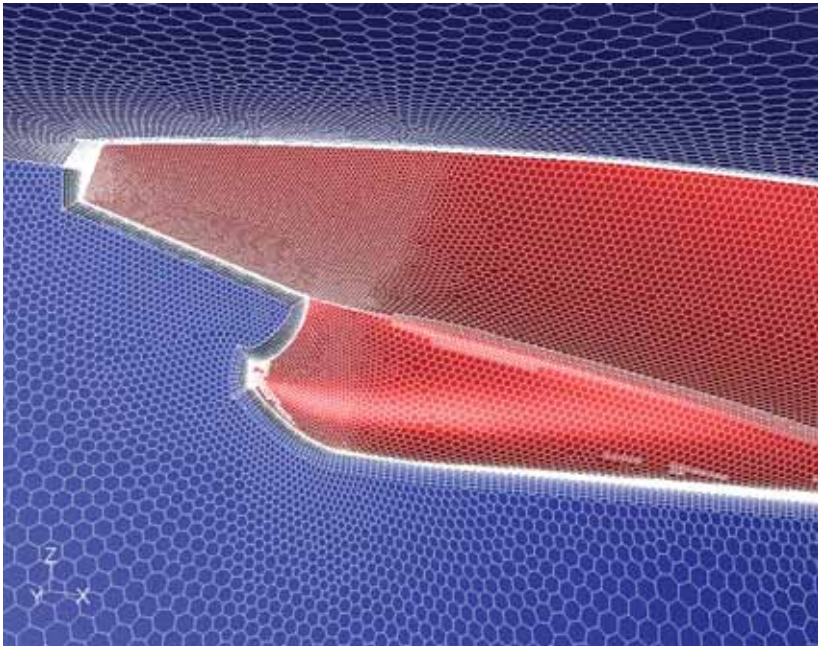


Fig. 10. Polyhedral grid obtained from a conversion of non-structured tetrahedral one

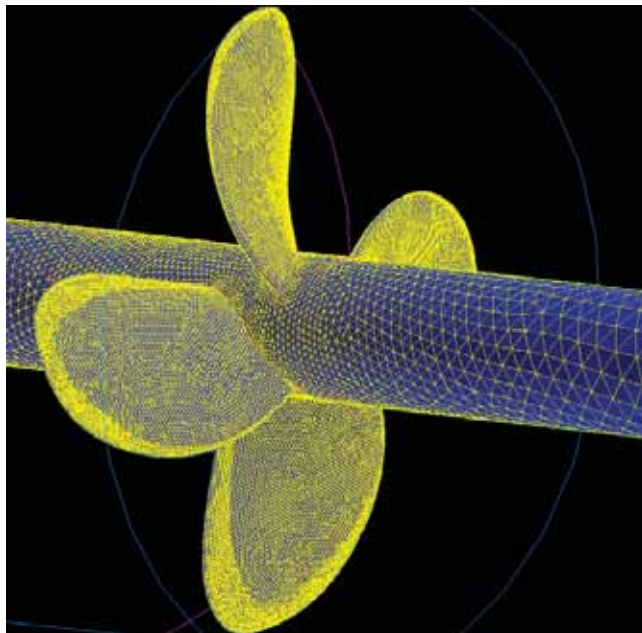


Fig.11. Non-structural grid of a propeller installed in the B 573 ship before conversion

Prior to numerical analyses proper, several other tests have been performed:

- comparison of resistance calculation results for the analysed ship form (Fig. 4) and model test results [1] using CFD methods,

- comparison of calculations of the actual propeller and rudder hydrodynamical characteristics against the model ones.

The test results can be found in a separate report [3].

4. Calculation results

In numerical analyses of the hull-screw propeller-rudder system the following parameters have been studied:

- 19 versions of the B 573 hull design (the final – 19th version with an asymmetric stern design),
- 2 versions of a screw propeller,
- 5 versions of the spade rudder.

Ship resistance for a modified hull versions (Table 5) has been calculated from the general formula in the form below:

$$\vec{R} = \int_S \vec{p}_n dS, \quad (5)$$

where \vec{p}_n is a resultant elemental stress on dS element of wetted hull surface area (in Fluent calculations \vec{p}_n , stresses made up from normal stresses \vec{p} and stresses tangent (viscous stresses) $\vec{\tau}$ to elemental surfaces, which have been replaced by finite surfaces ΔS resulting from a created numerical grid – Fig. 10).

Screw propeller efficiency has been calculated as a mean value of a propeller working in a non-homogenous wake currents field, calculated for each version of a ship's hull individually:

$$\bar{\eta} = \frac{\int_{d/2}^D dT \cdot V_s}{\int_{d/2}^D dQ \cdot \omega}, \quad (6)$$

where D – screw diameter, d – hub diameter, dT, dQ – local elemental thrust and moment calculated on propeller surface element (Fig. 11), V_s – local speed of water influx to a screw propeller element surface, ω – screw propeller angular speed.

Selected calculation results have been presented in [5]÷[10] with a more detailed account in [3]. Propeller efficiency results calculated for wake currents in all 19 versions of hull design (Fig. 12) seem most interesting in this respect, since some variants of the modified hull design resulted in lower propeller efficiency, with the majority of the modifications, however, resulting in higher propeller efficiency.

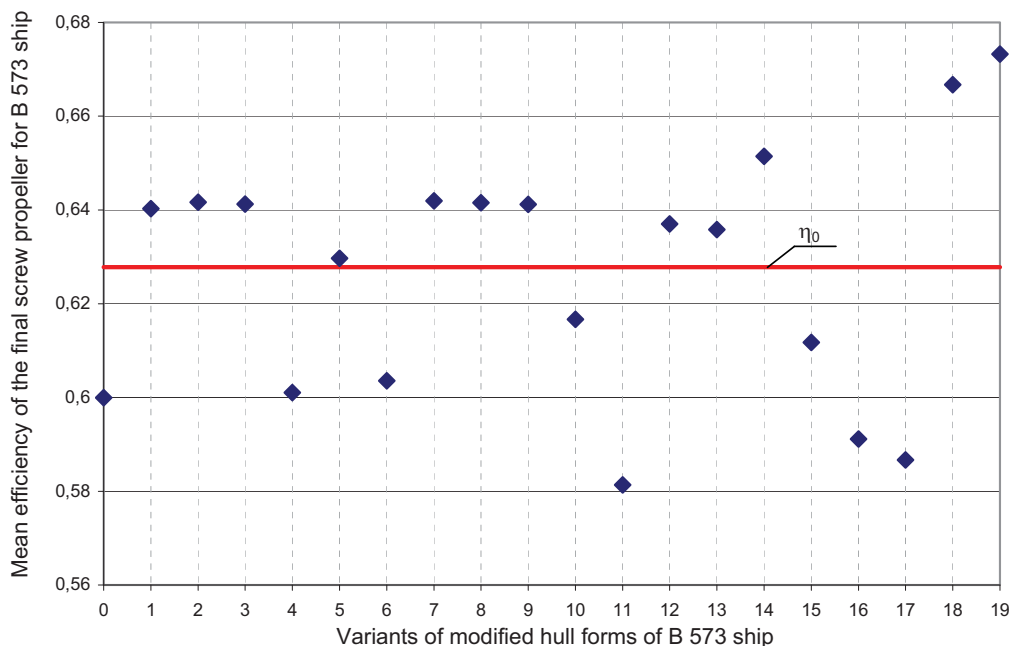


Fig. 12. Mean efficiency of B 573 ship's screw propeller operating in nonhomogenous wake current field, where:

η_0 - maximum efficiency of the final screw propeller in homogenous flow velocity field,
variant 0 – original hull form (without modification) in wake current velocity field measured during model tests,
variant 18 – the manually modified stern part of ship's hull – symmetric hull form
variant 19 – the manually modified stern part of ship's hull – asymmetric hull form

Finally, having analysed all the calculation variants, the results thus obtained present as follows:

- 2% decrease in ship's hull resistance,
- 4.5% increase of screw propeller efficiency (by more optimal wake current field),
- additional increase of 2% in screw propeller efficiency resulting from streamlining the profile as well as rudder location in relation to the propeller.

Subsequently, the influence on EEDI value of the optimal results of numerical analyses against the EEDI value of the actual ships have been compared:

- the EEDI value for B 573 ship prior to modifications EEDI = 5,6308
- with the modifications: EEDI_{max} = 5,1803 (to reduce 8 %).

5. Conclusions

- EEDI although mandatory from 2013 onwards, seems to need some further discussion in order to ensure that the International Energy Certificate is awarded without impeding the ship safety and in full transparency as to avoid dishonest practices (i.e. possible taking advantage of some lack of precision in current regulations).
- Meeting the standards for CO₂ emission required for the International Energy Certificate for the ships built and designed at present is by no means difficult.

- Meeting such standards (CO₂ emission) in the coming years will require more effort resulting in an improved ship design (resistance-propulsion relationship, propulsion system, overall ship energy consumption).
- Ship body modelling together with the analysis of the hull- propeller- rudder system working together has a wide potential of reducing ship propulsion efficiency thus reducing its EEDI value as well..
- The results of numerical analyses of the ship's hull, screw propeller and rudder design presented here by CFD results are preliminary and do not cover all possible relationships between the ship system parameters of the hull- screw propeller – rudder type. Since the results look promising, further research in this field has been continued.

Bibliography

- [1] Jaworski, S., Syrocki, W., *Ship B 573: Results of Model Tests-Resistance, Wake Measurements*, Technical Report No RH-95/T-041A, Ship Design and Research Centre, Gdańsk, 1995.
- [2] MEPC 62/24/Add. 1, Annex19, Resolution MEPC.203(62), 2011.
- [3] Raport końcowy z projektu badawczego rozwojowego nr 0430/R/2/T02/06/01: *Numeryczne badania współdziałania steru, śruby i rufy statku zmierzające do poprawy właściwości napędowych i manewrowych statku transportowego*, kierownik projektu: prof. dr hab. inż. Tadeusz Szelangiewicz, Szczecin 2009.
- [4] Syrocki, W., *Ship B 573 Results of the Model Tests*, Ship Design and Research Centre, Technical Report No. RH-96/T-023A, Gdańsk, 1995.
- [5] Szelangiewicz, T., Abramowski, T., *Numerical analysis of influence of ship hull form modification on ship resistance and propulsion characteristics*, Part I: *Influence of hull form modification on ship resistance characteristics*, Polish Maritime Research, No. 4(62), Vol. 16, Gdańsk 2009, pp. 3 ÷ 8.
- [6] Szelangiewicz, T., Abramowski, T., *Numerical analysis of influence of ship hull form modification on ship resistance and propulsion characteristics*, Part II: *Influence of hull form modification on wake current behind the ship*, Polish Maritime Research, No. 1(63), Vol. 17, Gdańsk 2010, pp. 3 ÷ 9.
- [7] Szelangiewicz, T., Abramowski, T., Żelazny, K., *Numerical analysis of influence of ship hull form modification on ship resistance and propulsion characteristics*, Part III: *Influence of modifications on screw propeller efficiency*, Polish Maritime Research, No. 1(63), Vol. 17, Gdańsk 2010, pp. 10 ÷ 13.
- [8] Szelangiewicz T., Abramowski T., Handke: *Numerical analysis influence of streamline rudder on screw propeller efficiency*, Polish Maritime Research, No. 2(65), Vol. 17, Gdańsk 2010, pp. 18 ÷ 22
- [9] Szelangiewicz, T., Abramowski, T. *Numerical analysis of influence of selected elements on effectiveness of streamline rudder*, Polish Maritime Research, No. 3(66), Vol. 17, Gdańsk 2010, pp. 3 ÷ 7.
- [10] Szelangiewicz, T., Abramowski, T., Żelazny, K., *Numerical analysis of effect of asymmetric stern of ship on its screw propeller efficiency*, Polish Maritime Research, No. 4(67), Vol. 17, Gdańsk 2010, pp. 13 ÷ 16.



INSTALLATION VESSELS OF OFFSHORE WIND FARMS AND THEIR TAKE-OFF SYSTEMS

Wiesław Tarelko

Gdynia Maritime University
ul. Morska 81-87, 81-225 Gdynia, Poland
tel.: +48 58 6901331
e-mail: tar@wm.am.gdynia.pl

Abstract

Polish shipbuilder Crist S.A. is to build a heavy lift jack-up vessel named Vidar for German construction giant Hochtief Solutions. Like Hochtief's other heavy-duty equipment, the new special-purpose jack-up vessel will also speed up installation and servicing times for the latest generation of offshore wind farms. According to principal characteristics, Vidar will have 148 meters length and 90 accommodation places. The evident uncertainties of the regulatory situation for specialized offshore vessels hamper the timely development of the offshore wind energy. These installation and servicing vessels can be adequately regulated by Guidelines defining the appropriate application of existing requirements from the Special Purpose Ships Code (SPS Code). Due to amounts of the accommodation places, there is interface with SOLAS regulations for passenger vessels. But they are no passenger vessels, therefore specific passenger vessel requirements such SOLAS safe return to port requirements should be not applied. This situation yielded the shipbuilder Crist initiative to investigate the regulatory obstacles at International Maritime Organization (IMO) forum. Therefore, they have asked Polish department for Subcommittee of Ship and Equipment Design of IMO to review the applicability of the existing IMO instruments. This paper is an outcome of the carried out study concerning some aspects of offshore wind farm installation and maintenance issues.

Keywords: power plant, heavy lift jack-up vessel, wind farm, installation and maintenance

1. Introduction

Wind power is one of the most important and promising forms of renewable energy being developed. It produces no emissions and is an excellent and alternative in environmental terms to conventional electricity production based on fossil fuels such as oil, coal. It is common knowledge that the world electricity production is based primarily on fossil fuels. Burning of fossil fuels increases amounts of carbon dioxide in atmosphere what, in turn, contributes to climate change.

Moreover, we can observe the following global market tendencies:

- shortage of oil and gas reserves and natural resources in politically stable countries[1],
- growth of the world population to 9 billion by 2030 according to high scenario [2],
- security of energy supply for developed countries necessary for their economic sustainability [3].

The EU directive [4] on renewable energy sets ambitious targets for all member states, such that the EU will reach a 20% share of energy from renewable sources by 2020. It also improves the legal framework for promoting renewable electricity, requires national action plans that establish pathways for the development of renewable energy sources, and creates cooperation mechanisms to help achieve the targets cost effectively.

Renewable energy is energy which comes from natural resources such as: sunlight, wind, rain, tides, and geothermal heat, which are renewable (naturally replenished).

Land-based and offshore wind power refers to the construction of wind farms to generate electricity from wind.

Better wind speeds are available offshore compared to on land, so offshore wind power contribution in terms of electricity supplied is higher. The advantage is that the wind is much stronger off the coasts, and unlike wind over the continent, offshore breezes can be strong in the afternoon, matching the time when people are using the most electricity. However, offshore wind farms are relatively expensive.

The Swedish offshore wind farm Lillgrund in the Øresund is built between Malmö and Copenhagen. The wind farm with a total installed capacity of 110 MW is operated by the Swedish utility Vattenfall and officially came on line in June 2008 and produces enough electricity to supply 60,000 Swedish households. As of February 2012, the Walney Wind Farm in United Kingdom is the largest offshore wind farm in the world at 367 MW, followed by Thanet Offshore Wind Project (300 MW), also in the UK. The London Array Wind Farm (630 MW) is the largest project under construction. This project will be dwarfed by subsequent wind farms that are in the pipeline, including Dogger Bank at 9,000 MW, Norfolk Bank (7,200 MW), and Irish Sea (4,200 MW). For comparison, the total installed capacity of the largest power plant in Russia and the world sixth-largest hydroelectric plant (Sayano-Shushenskaya DAM located on the Yenisei River) is 6,400 MW (Dogger Bank - 9,000 MW).

Development of offshore wind farms is an emerging market, especially Europe, with many initiatives by several governments supporting this part of the renewable energy sector. With increasing demand for offshore wind farms, their components need to be manufactured, transported, installed, and maintained. At present, only a limited capacity of dedicated installation units is available on the market, resulting in the development and construction of new installation units. Ships and offshore structures, such as Offshore Wind Farm Construction Vessels and Service Crafts, could be purpose build or converted. These designs might deviate from existing ship types currently employed in the offshore oil and gas sector, such as Mobil Offshore Drilling Units and Offshore Supply Vessels.

This paper describes the recent and predicted trends concerning installation and servicing vessels of offshore wind farms and their take-off systems. Factors influencing technical limitations of both the vessels and the take-off systems will be presented as well.

2. Offshore wind turbines and their limitations

Windmills were used in Persia as early as 200 B.C. The wind-wheel of Heron of Alexandria marks one of the first known instances of wind powering a machine in history. The concept of using wind energy for grinding grain spread rapidly through the Middle East and was widespread long before the first windmill appeared in Europe. According to [5], the first electricity generating wind turbine, was a battery charging machine installed in July 1887 by Scottish academic, James Blyth to light his holiday home in Marykirk, Scotland. Some months later, American inventor Charles F. Brush built the first automatically operated wind turbine for electricity production in Cleveland, Ohio. 1951 - first utility grid-connected wind turbine to operate in the U.K. was built by John Brown & Company in the Orkney Islands.

The wind turbine is actually rated at 6,15 MW [6] (wind company REpower and C- Power NV installed the wind turbine, the first of 48 for the Thornton Bank II wind farm, which is being constructed approximately 28km off the Belgian coast). The recent growth rate (size, power and cost) of offshore wind turbines is presented in Figure 1. The hub heights will be between 85m and 100m above sea level, and the total turbine height will not be greater than 175m. As a rule, the turbines have three blades because engineers have found that three blades is the most efficient and least troublesome way to harvest wind. Turbines with two blades are actually even more efficient

[7]. But because they are also lighter and tend to spin faster, they are also noisier. These designs also require a special tilting hub that acts as a sort of shock absorber, which is expensive. Having more than three blades raises other problems. For one thing, the extra material needed to build the blades raises the cost. And the more blades there are, the lighter and thinner they need to be. Relatively thin blades are more flexible, making them prone to bend and break. Three-bladed turbines are not perfect, but they avoid many of these problems.

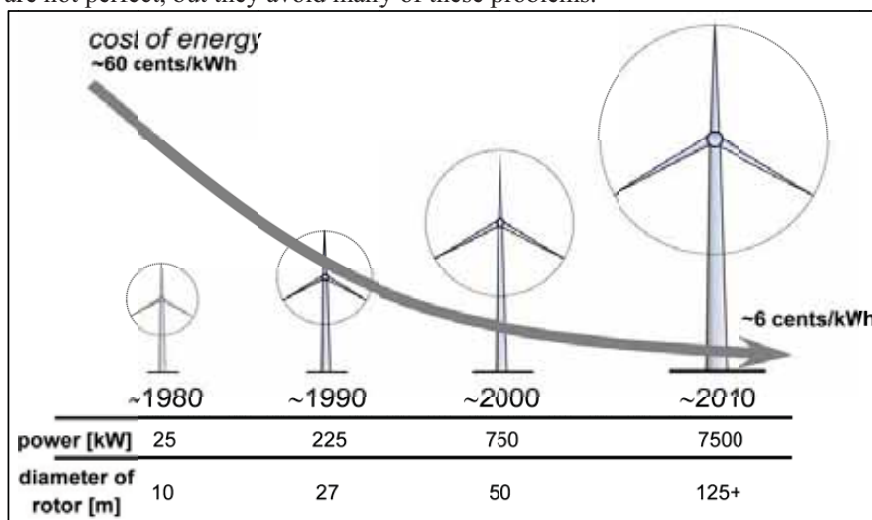


Fig. 1. Wind turbine growth: size, power and cost

Turbines typically begin generating electricity at a minimum wind speed of 3m/s, with full power being achieved from 13m/s. For safety reasons (Fig. 2) they will begin to shut down at wind speeds greater than 25m/s. Their typical rotation speeds varies between 5 to 20rpm.

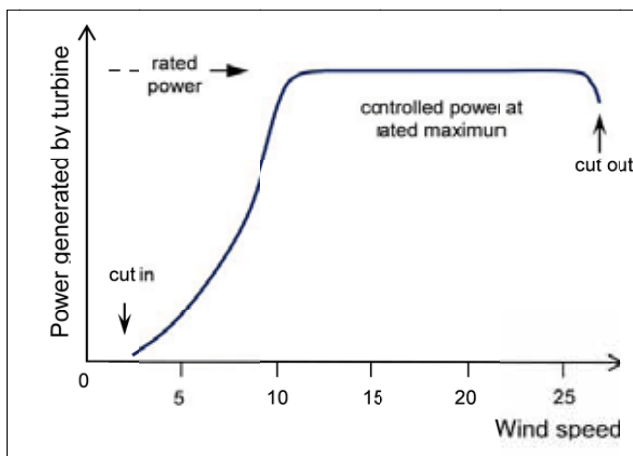


Fig. 2. Wind turbine power operating range

For large, commercial size horizontal-axis wind turbines, the generator is mounted in a nacelle at the top of a tower, behind the hub of the turbine rotor. Typically wind turbines generate electricity through asynchronous machines that are directly connected with the electricity grid. Usually the rotational speed of the wind turbine is slower than the equivalent rotation speed of the electrical network. Therefore, a gearbox is inserted between the rotor hub and the generator (750-3600 rpm). This also reduces the generator cost and weight.

Older style wind generators rotate at a constant speed, to match power line frequency, which allowed the use of less costly induction generators. Newer wind turbines often turn at whatever speed generates electricity most efficiently. This can be solved using multiple technologies such as doubly fed induction generators or full-effect converters where the variable frequency current produced is converted to DC and then back to AC, matching the line frequency and voltage. Although such alternatives require costly equipment and cause power loss, the turbine can capture a significantly larger fraction of the wind energy. In some cases, the DC energy is transmitted from the turbine to a central (onshore) inverter for connection to the grid.

The turbine represents just one third to one half of costs in offshore projects today, the rest comes from infrastructure, maintenance, and oversight [8].

Some of the environmental concerns that will need to be considered both in the planning process for individual farms, and as we move forward in general with offshore wind turbines are [9]: bird impacts, habitat disruption, fisheries impacts, potentially noise, and attitudes of people.

Generally birds are at risk from collision with the turbines. In addition, habitat use can be affected by construction and operation and maintenance. Birds can be displaced from ideal feeding or nesting grounds, or will avoid turbines during daily movement or migration. Lighting on wind towers might attract birds. The most of the habitat disruption will take place during turbine and transmission installation. When the trenches are being dug to bury the transmission cables, or during wind turbine installation, events known as frac-outs can occur (the condition where drilling mud is released through fractured bedrock into the surrounding rock and sand and travels toward the surface). Introduction of new artificial habitats with positive effects on fish communities after full development of artificial reef communities has been observed. No linkage between the strength of the electromagnetic field and the migration of selected fish species has been noticed. Noise from wind turbines will travel underwater and could disturb aquatic organisms. Studies from existing offshore turbines note that the noise is very low frequency, and many species are actually unable to hear it, whereas noise from construction activities could disrupt organisms in the short-term. According to Danish studies [9], more than 40% of investigated people stated that they preferred future wind farms to be moved out of sight.

3. Foundation of offshore wind power turbines

Several factors should be taken into account during installation of wind power turbines:

- water depths,
- seabed conditions,
- environmental conditions.

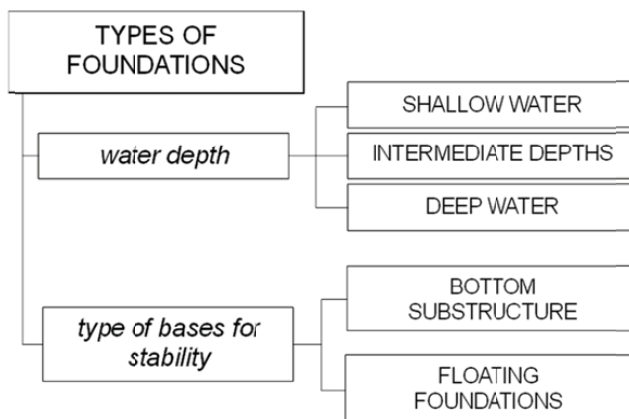


Fig. 3. Foundations of offshore wind power turbines

Foundation technology is designed according to site conditions. Water depth, maximum wind speed, wave heights currents, and surf properties affect the foundation type.

According to the water depth, we can distinguish shallow water, intermediate depths, and deep water types of the offshore wind turbine foundations, whereas their stability can be achieved by fixed bottom structures or floating foundations (Fig. 3).

We can distinguish the following fixed bottom substructures:

- a monopile (single column) base used in waters up to 30 meters deep,
- gravity base structures, for use at exposed sites in water 20-80 m deep,
- suction caisson structures, in water 20-80 meters deep,
- tripod piled structures, in water 20-80 meters deep,
 - conventional steel jacket structures, as used in the oil and gas industry, in water 20-80 meters deep.

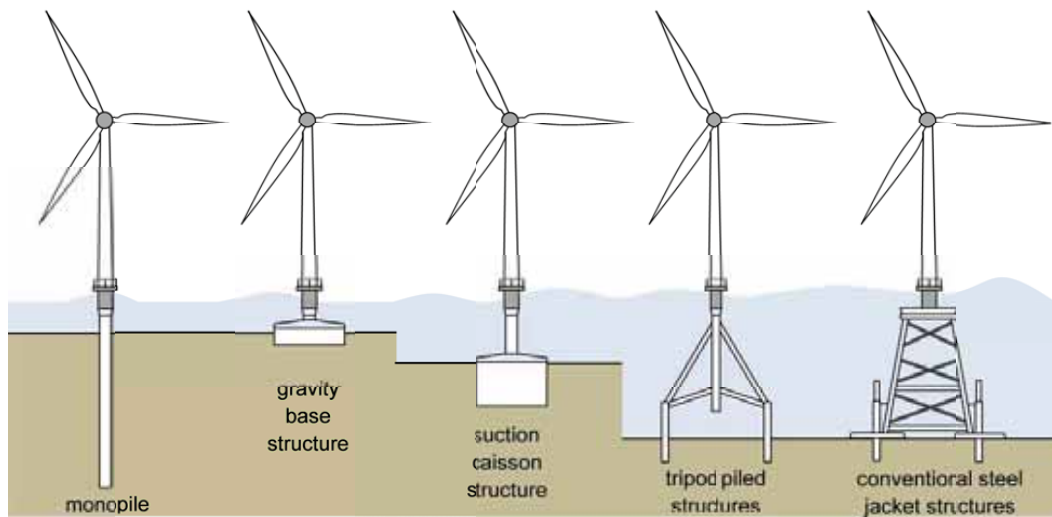


Fig. 4. Fixed bottom substructures of offshore wind power turbines

The monopile consists of a steel pile which is driven approximately 10 - 20 meters into the seabed. The foundation consists of a steel pile with a diameter of between 3.5 and 4.5 meters.

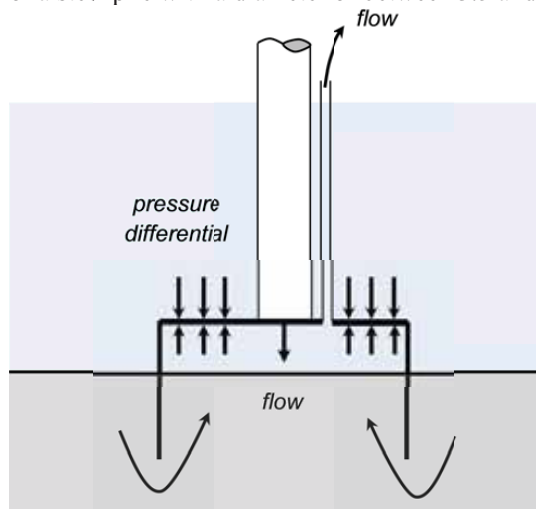


Fig. 5. Graphic representation of achieving hydrostatic pressure difference

The pile is driven some 10 to 20 meters into the seabed depending on the type of underground. The gravity foundation consists of a large base constructed from either concrete or steel which rests on the seabed. Steel is lighter and normally filled with granular material or concrete.

A suction caisson structure have tubular steel foundation installed by sealing the top of the steel bucket and creating a vacuum inside. Hydrostatic pressure difference and the dead weight of the structure cause the bucket to penetrate the soil (Fig. 5).

The tripod foundation structure based on technology used by the oil and gas industry. The piles on each end are typically driven 10 -20 meters into the seabed, depending on soil conditions. This technology is generally used at deeper depths.

The conventional steel jacket structure used a jacket foundation, similar to a lattice tower. The jacket foundations allow to install its turbines 10-15 miles offshore.

In the offshore oil and gas industry, the water depth limit for fixed platforms is about 450 m. In the offshore wind industry, the limit is likely to be less than 100 m because of economic conditions.

Floating structures consist of a floating platform and an anchoring system. There are several alternative designs for floating turbine foundations all of which are variations on the spar and tension-leg concepts in the oil and gas industry.

Floating turbine foundations can be (Fig. 6):

- barges,
- spar buoys,
- tension leg platforms (TLP).
- The barges achieves stability from the large water plane area-to-volume ratio that allows it to remain buoyant in water.

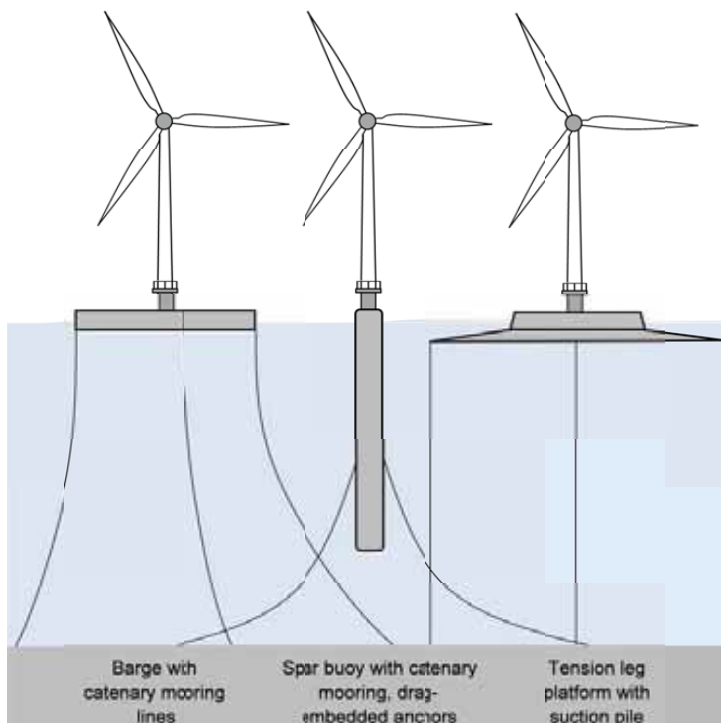


Fig. 6. Floating foundations of offshore wind power turbines

The spar buoys are designed for deeper waters of up to 300 meters. It incorporates an elongated cylindrical tank with a high aspect ratio, which holds ballast at the tank bottom. The ballast helps

to lower the center of gravity of the tank and make it more stable. In addition, the spar buoy is moored to the ocean bed with either taut or catenary lines to provide further stability. The tension leg platforms are examples of semi-submersibles, which are installed below the zone of major wave action so that they are essentially anchored in still water. They achieve stability through the use of vertical mooring lines that are attached to tank legs and tensioned by the reverse buoyancy of the tank. Only a slender member breaks the surface, which also reduces the wave loads.

4. Vessels and crafts servicing offshore wind power systems

Manufactured components of offshore wind farms need to be transported, installed, and maintained. At present, only a limited capacity of dedicated units is available on the market, resulting in the development and construction of new ones. Ships and offshore structures, such as offshore wind farm construction vessels and service crafts, could be purpose built or converted. These designs might deviate from existing ship types currently employed in the offshore oil and gas industry, such as Mobile Offshore Drilling Units (MODU) and Offshore Supply Vessels (OSV). Availability of offshore vessels and platforms is a prerequisite for the timely achieving of EU targets regarding the renewable energy. Only a minority of ships serving the construction and maintenance of offshore wind farms are purpose built. Among the existing service vessels some are only marginally converted or adapted to perform their new function in a very demanding environment.

Offshore wind farm units designed for transporting, installation and maintenance offshore turbines and their units can be two main types (Fig. 7):

- offshore wind farm construction vessels (OWFCV),
- offshore wind farm service crafts (OWSSC).

This terminology is accordance with practice used at IMO forum, what was presented by Germany delegation during 56 session of Design and Equipment Subcommittee of IMO [10].

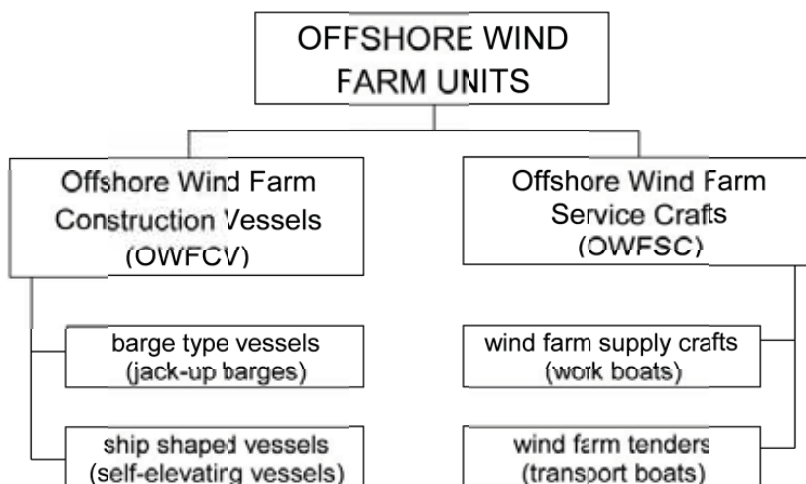


Fig. 7. Types of offshore wind farm units

Offshore Wind Farm Construction Vessels (OWFCV) are designed to carry out foundation work, tower and turbine installation as well as maintenance work during the operation phase. They can be either barge type or ship shaped and can be both self-propelled or without propulsion.



Fig. 8. Jack-up barge for installation of offshore wind farm

The jack-up barges are floating units that are capable elevating themselves at the construction site on their jack up legs (Fig. 8). They are not self-propelled units and they must be towed to the construction site. The service speed of the barges is dependent on the tug's power (a speed of 5 knots can be assumed). Jack-up barges do not have Dynamic Positioning Systems (DPS) that allows a unit to automatically maintain its position through the coordinated control of thrusters. Jack-up barge cargo capacity ranges from 900 to 2000 tons in terms of weight. Their operational water depth (max) is in the range of 18 to 50 meters and leg lengths are 40 to 82 meters whereas their jacking speed is generally in range of 0.15 to 0.8 meters/minutes.



Fig. 9. Ship shaped vessel for transportation and installation of offshore wind farm

Ship shaped vessels are self-propelled units that are specially designed in line with the industry demands. These purpose-built self-propelled transportation and installation vessels have jack up legs and cranes with big lifting capacities. Their maximum operational water depth ranges between

24 meters and 45 meters while the leg lengths are varying from 32 meters to 85 meters.

The service speed of the ship shaped vessels is in the range of 7.8 to 12.5 knots and the jacking speed is in the range of 0.35 to 0.8 meters/minute.

Ship shaped vessels have Dynamic Positioning Systems which enables them to stay constant at a certain point to be able to land their legs on the exact locations precisely.

The self-propelled vessels with dynamic-positioning system can easily cost 3-5 times as much as juck-up barges with the same crane capacity and jacking system [11]. A self-propelled vessel can achieve higher transit speeds than a towed barge and can work independently (without tug boats).

Offshore Wind Farm Service Crafts (OWFSC) are designed with the versatility to allow them to provide offshore support on offshore wind farms, for survey work, for remotely operated vehicles (ROV) and dive support. They can be used to transport service personnel, parts and tools offshore on the wind farm. Internally they have some places for seating or accommodation of service crew. Externally they have sufficient working deck aft and they can be fitted with a customized bow section designed for safe personnel transfer.

5. Take-off systems of vessels servicing offshore wind farms

Power plants of Offshore Wind Farm Construction Vessels can provide energy for various purposes, mainly for:

- jacking units out of the water,
- working of cranes,
- propulsion and dynamic-positioning of the vessel.

Diesel engines compose the majority of power sources on OWFCVs. They drive large electric generators, which produce electricity that is sent through cables to electric switch and control gear. The primary machinery requirements for OWFCVs are the jacking system and the crane. Since they do not operate simultaneously, a single power plant can be used to power both systems. Cranes capable of lifting turbine components require as much as a few thousands kilowatts of power supply. This amount of power should suffice for a jacking system that meets lifting capacity and jacking speed requirements for a vessel carrying three to four complete sets of turbine components. Heavier vessels with larger jacking system requirements will require more installed power.

The self-propelled vessels will require a separate plant providing approximately 20000 kW of power to the propulsion system, which can also be used to power a dynamic-positioning system. This power plant could also power the crane, but is unlikely to suffice for simultaneous operation of the DP system and the jacking system.

Depending on whether condition, OWFCVs can perform the necessary steps to jack up within approximately eight hours. The jacking process is the following:

- position the vessel at a target location,
- lower the legs,
- elevate the hull out of the water,
- pre-load the legs.

The purpose of pre-loading is to prove the soil's load-bearing capability. This can be achieved by pumping sea water ballast into the vessel hull or by selectively raising one leg at a time (on vessel with four or more legs) in order to transfer load to the lowered legs. To achieve even heel and trim prior to jacking operations, the OWFCVs require a relatively robust ballasting system.

OWFCVs are trending toward four-leg configurations of the jacking system. The oil and gas industry typically uses three-leg jack-ups. The reason for using four legs is to reduce the time required to pre-load the legs (i.e., test the soil). A three-legged rig requires sea water ballasting to achieve pre-load. With four legs, pre-loading can be achieved by lifting one leg at a time, thereby transferring loads to the other legs. A fourth leg also provides redundancy in the event of a single-leg failure. Nevertheless, there are six-leg configurations of the jacking system what decrease of its

power supply per leg. Leg profile cross-section can be tubular, rectangular or lattice. As a rule, the jack-up legs are to be fitted with spud cans. They consist of a plate or dish designed to spread the load and prevent over penetration of the leg into the sea bed. Spuds are circular, square or polygonal, and are usually small.

A continuous hydraulic jacking system or a rack and pinion system can be applied for vessel elevating. A jack-house contains and protects the jacking system. In the four jack houses, on two elevations, a set of hydraulic or electric sea fastening devices should be installed. These devices consist of plates and a hydraulic or electric device to fix the legs during transport.

Lifting out of the water induced larger loads on the legs, which in turn required the size to be increased. The increased leg size had a knock on effect, the winches had to be enlarged and the number of reeving's increased in order to achieve the required lifting capacity. The increased size of each of the components amplified the associated costs.

Currently the installation of offshore wind farms involves using heavy lift cranes. They should be best suited for transporting and handling the foundations for the latest generation of up to 6 MW offshore wind turbines, as well as the turbine towers, nacelles, rotors and blades. As a rule, cranes are operated in the elevated position, however there are OWFCVs specially designed for crane operations in the floating condition. The lifting performance in floating condition is established by means of ballasting. The heavy lift cranes should fulfill the following requirements:

- maximum weight to be lifted ('pick weights'),
- maximum height above sea surface,
- needed spatial clearance for objects being lifted.

Moreover, they should be large enough to lift anywhere on the vessel deck, this negates any requirements for skidding large sensitive equipment. The weight of the crane should be kept as small as possible to reduce unnecessary loads on the stabilization legs. As a rule the heavy lift cranes are fully integrated into the vessel hull. The heavy lift cranes can be hydraulic or electric driven. The crane requirements for installation of 3,6 MW and 5 MW offshore turbines and monopile foundations are presented in Table 1.

Table 1. Crane requirements for turbines and associated monopile foundations

| Parameters | Siemens 3.6 MW | REPower 5 MW | Monopiles |
|---------------------|-----------------------|---------------------|---------------------|
| Maximum pick weight | 138 tons | 320 tons | 200-500 tons |
| Maximum pick height | 80 meters | 85-90 meters | less than 30 meters |

Existing OWFCVs can operate their cranes in up to 18 knots wind speed at the deck level (approximately 25 knots at the crane tip) and can jack-up and down in seas as high as 1.5 to 3 meters (significant wave height).

In a case of OWFCVs, their power plants supply of energy necessary for propulsion and steering. They can be fitted with several azimuth thrusters for propulsion, maneuvering and dynamic positioning and few bow thrusters for maneuvering and dynamic positioning. As a rule, diesel electric propulsion is used for vessel's propelling. Electric power is generated by several diesel driven generators. The vessel with a clean hull, sailing on even keel in deep water with sea state not exceeding 2 and wind force not exceeding 2°B can achieve the speed up to 12 knots. The azimuth and tunnel thrusters have fixed pitch subject to dynamic positioning (DP) analysis.

OWFCVs are equipped with a dynamic positioning system. All wiring, arrangement and components are suitable for DP operation. The dynamic positioning system can operate as a minimum in the following modes:

- standby mode: the vessel's position is not actively controlled by the DP system,
- manual mode: the vessel's position can be controlled by the operator,
- auto mode: the system keeps the vessel at the given position and heading with high accuracy; the position is measured by the use of the position reference systems,
- mixed manual auto mode: the operator may select a combination of manual and automatic positioning, and can control one or more of the three axes (surge, sway and yaw) manually as

in the manual mode, while the remaining are controlled automatically by the system as in auto mode,

- auto track mode: the vessel is able to follow a predefined track of way-points,
- anchor control mode,
- auto pilot mode allowing the DP system to control the vessel heading,
- jacking mode.

The DP system can use the following systems as position reference:

- DGPS different satellite systems, which should be capable to read GPS and Glonass signals at the same time, as well the Galileo signal in the future,
- external DGPS input from mobile, mission based equipment,
- external reference systems (laser or radar based).

The DP system must be based on a mathematical model and control all thrusters in thrust and direction. Moreover, it should control the vessel thrusters in most optimum way, utilizing mathematical modeling of vessel behavior in order to provide the required positioning accuracy and reliability for the various modes of operation.

According to the technical specification of the offshore wind farm construction vessel VIDAR [12], electric power is generated by six diesel driven generators with rated power approximately 4000 kW and one 700 kW emergency generator. Diesel electric propulsion is used for vessel propelling and dynamic positioning by means of four azimuth thruster motors and three tunnel thruster motors with rated power 2 600 kW and 2 500 kW respectively.

The VIDAR power plant provides 20 000 kW total power, what guarantees the following operating parameters:

- service speed 10,2 knots with minimum three aft azimuth thrusters working at 85% power,
- lifting force 24 000 ton with lifting speed up to 1 m/min,

The VIDAR main features will be a 1 200 ton crane, a loading capacity of up to 6 500 tons, and the ability to work in water depths of up to 50 meters. These properties will make the VIDAR one of the most powerful lifting vessels in Northern Europe.

6. Conclusion

Wind power is one of the most important and promising forms of renewable energy being developed. The increasing demand to produce renewable energy from the offshore wind power forces developing the various structural designs of offshore units. Manufactured components of offshore wind farms need to be transported, installed, and maintained. These tasks are realized by ships and offshore structures, such as offshore wind farm construction vessels and service crafts. Their more and more complicated power plants have to provide energy for various purposes, mainly for: jacking units out of the water, working of cranes and, propulsion and dynamic-positioning of the vessel. Therefore their operation and maintenance requires preparing the appropriate qualified personnel. Such personnel should be educated and trained at faculties of technical and maritime universities, where offshore units are subjects of their interest.

Acknowledgment

The author is a chairperson of Polish department for Subcommittee of Ship and Equipment Design of International Maritime Organization from 1996.

References

- [1]. Laherrere J. Oil and gas: what future? Groningen annual Energy Convention. 2006
<http://oilcrisis.com/laherrere/groningen.pdf>

- [2]. World population to 2300. Department of Economic and Social Affairs. Population Division. United Nations. 2004 <http://www.un.org/esa/population/publications/>
- [3]. Chevalier J.M. Security of energy supply for the European Union. European Review of Energy Markets. Volume 1, Issue 3, November 2006.
- [4]. Directive 2009/28/EC of the European Parliament and of the Council of 23 April 2009 on the promotion of the use of energy from renewable sources and amending and subsequently repealing Directives 2001/77/EC and 2003/30/EC. Official Journal L 140, pp. 0016 – 0062.
- [5]. Green Syndications. Wind Turbine Timeline http://greensyndications.com/?page_id=2
- [6]. Thornton Bank: First six-megawatt turbine for offshore wind farm installed. C – Power http://www.repower.de/fileadmin/press_release/2012_03_21_Thornton_Bank_First_Turbine_e.pdf
- [7]. Wind Turbine Blade Aerodynamics. WE Handbook-Aerodynamics and Loads. www.gurit.com/files/.../2_aerodynamics.pdf
- [8]. Jacobson M. Z., Delucchi, M.A. A Path to Sustainable Energy by 2030". 2009 <http://www.stanford.edu/group/efmh/jacobson/Articles/I/sad1109Jaco5p.indd.pdf>
- [9]. Offshore Wind Farms and the Environment Danish Experiences from Horns Rev and Nysted. Danish Energy Authority. http://193.88.185.141/Graphics/Publikationer/Havvindmoeller/Offshore_wind_farms_nov06/pdf/havvindm_korr_16nov_UK.pdf
- [10]. Safe and Sustainable Exploitation of Renewable Energy - International Standards for Offshore Wind Farm Vessels. An introduction to DE 56/12. International Maritime Organization, 15 February 2012, DE 56, London
- [11]. Marine Vessels for Construction and Maintenance of Offshore Wind Farms. APPENDIX A. Tetra Tech EC, Inc. Boston Massachusetts, 2009, www.masscec.com/...
- [12]. Self Elevating Wind Turbine Installation Unit. Technical Specification. StoGda Ship Design & Engineering sp. z o.o. CRIST S.A., Gdansk 2011.



SIMULATION OF VIBRATIONS OF MACHINE ELEMENTS ON THE EXAMPLE OF VIBRATIONS OF MARINE DIESEL CYLINDER LINERS

Aleksander Valishin, Andrzej Adamkiewicz

Maritime University of Szczecin
str. Waly Chrobrego 1-2, 70-500 Szczecin, Poland
e-mail: kdirm@am.szczecin.pl

Abstract

The article presents new methods for studying mechanisms of vibrations by means of their simulation in the electronic environment "Electronics Workbench". 4CH 8,5/11 marine diesel cylinder liner was represented as a mechanical circuit of two-terminals – elements with mass, internal friction (dissipation), and stiffness. The use of electro-mechanical analogy of vibration systems has allowed the transition from mechanical chain to a chain of electrical circuits in the electronic environment «Electronics Workbench». The obtained values of the parameters of 4CH 8,5/11 diesel liner vibrations in the electronic environment (frequency, amplitude and vibration velocity) were in good reliance with the results of natural experiment.

Key words: Marine Diesel, cylinder, vibrations, simulation, modelling

1. Introduction

Corrosive and erosive destruction of the cooling surfaces of marine diesel engines, and in particular the surfaces of the cooling cylinder liners, significantly reduces their resource indicators. The research indicates that the resource of cylinder liners exposed to the erosion - corrosion attack, reduces up to 50% of its theoretical value. It is commonly assumed that these processes are generated by vibrations of liners which are caused by piston impulses coupled with transposition of connecting rod at the moment of overtravel. Impulses generated by cylinder liner vibrations are responsible for creating in the cooling water favorable environmental conditions for cavitation. For more active influence on the negative effects of vibration cavitation in the engines the benchmark trials are required as well as development of methods for calculating the durability of parts under the influence of cavitation erosion.

This problem can be solved by obtaining a reliable picture of the nature of cylinder liner vibrations at any alighting in a cylinder block considering influence of all force factors (the value of piston impulse, pulse of operating gas pressure in a cylinder). A visual model, one that reflects real conditions of liner vibrations or with some assumptions close to them, can be achieved by modelling of the process in computer virtual environment. The obtained parameters of vibration (frequency, amplitude and vibration acceleration) will simulate the characteristics of the damping device (stiffness, mass and dissemination property).

2. Assumptions to the mathematical model

This was done by introducing the mechanical system in the form of a combination of separate elements with different properties selecting active elements that can deliver energy into a mechanical system and stimulate its movement [1]. The mentioned mechanical chain will reproduce dynamic properties of the original mechanical system with an acceptable accuracy.

In the experiment two-terminals (elements with one input and one output) were used as components of the mechanical chain.

A mechanical chain with separate units of cylinder parts with the same wall thickness can be used as a model of liner with flanges and alighting zones.

In this way the entire liner is divided into separate rings and thin-walled cylinder with a constant wall thickness that corresponds to the middle of the liner between the alighting zones (Fig.1). Each unit in this mechanical chain is characterized by its mass, resilience, viscous friction, and consists of the following basic two-terminals: resilient element (stiffness), dissipative element (damper) and inertia element (mass).

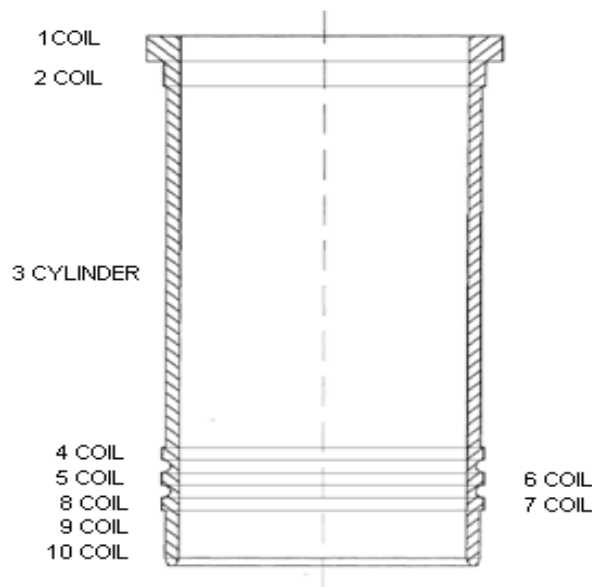


Fig. 1. An example of the 4CH 8,5/11 diesel engine liner division into units of mechanical chain

An equivalent scheme of a two-terminal connection into a mechanical chain of ten units representing a cylinder liner of the 4CH 8,5/11 type is shown in Fig.2. During the set up of this scheme the following rules were adopted:

- Elements of mass, stiffness and dampers are connected to a fixed bearing by one fastener. Thus, the displacement of one of the poles of each component in relation to the fixed bearing is zero, which simulates the installation conditions of liner edges inside the cylinder block;
- If all elements of the mechanical system move with equal speed, their two-terminals are connected in parallel, and if the same force is transmitted through all elements, two-terminals are connected sequentially.

Fig.2 shows two-terminals which characterize mass of the rings denoted by symbols M_1, M_2, \dots, M_9 ; two-terminals characterizing ring stiffness are denoted by the k_1, k_2, \dots, k_9 symbols; symbols B_1, B_2, \dots, B_9 - two-terminals, which characterize the dissipative properties of the rings, F – an active two-terminal of force determined by value of the force activating liner vibrations.

Thus, the task of determination of liner vibration frequency is brought to the determination of parameters of each element of the equivalent mechanical chain and solution of Kirchhoff's equations, performed for each node and contour of the chain.

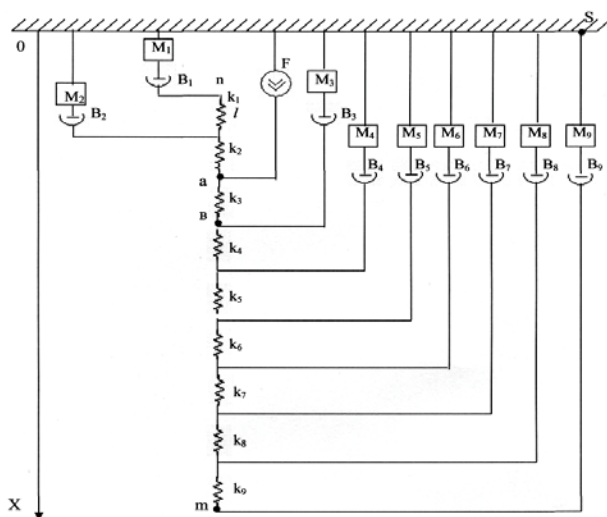


Fig. 2. Model of a mechanical chain of engine 4U8,5/11 cylinder liner (sleeve)

According to the decomposition of a simulated liner into separate sections (see Fig. 1), each of the units, except the third one, is a model of a ring and the third unit is a model of a smooth thin-walled cylindrical shell.

3. The mathematical model of cylinder shell vibrations

Each of the rings will generate asymmetric bending vibrations, during which the radial displacement (normal to median surface) of deformable elements of the ring is accompanied by a circumferential shift (tangent to the contour of cross-section). Radial pressure of elastic forces of the ring, resulting from deformation and referred to the center line, is expressed by the following equation [3]:

$$q = \frac{1}{r^2} \left(M + \frac{d^2 M}{d\varphi^2} \right), \quad (1)$$

where:

r – radius of curvature of the centerline of the ring,
 M – bending moment at any section of the ring,
 φ – angular coordinate of the considered section.

In its turn, bending moment is determined by dependence:

$$M = \frac{EJ}{r^2} \left(U + \frac{d^2 U}{d\varphi^2} \right), \quad (2)$$

where:

E – modulus of elasticity of the ring material,

J – centroidal moment of inertia of the ring section,

U – radial displacement of the points of the center line within the deformation of the ring.

Then, the formula for the elastic force pressure will take the following form:

$$q = \frac{EJ}{r^4} \left(w + 2 \frac{d^2 w}{d\varphi^2} + \frac{d^4 w}{d\varphi^4} \right). \quad (3)$$

The frequency of characteristic vibrations of the ring can be determined by the formula of S.P. Timoshenko [4]:

$$\omega^2 = \frac{EJ}{r^4 \rho \delta} \frac{n^2 (n^2 - 1)^2}{(n^2 + 1)}, \quad (4)$$

where:

ρ – density of the ring material,

δ – the cross-sectional area of the ring,

n – number of radial half waves in the cross section of the ring.

Note that the formula for the free vibration frequencies of the ring (4) can be obtained directly from the differential equations of the ring motion at a known formula for the elastic forces (3) and radial displacements given in the form:

$$w(t) = w_0 \cos n\varphi \sin \omega t. \quad (5)$$

An analysis of the obtained equations (3) and (4) suggests that the ring stiffness element as a link of the equivalent scheme, can be expressed as follows:

$$k_i = \frac{EJ_i}{r_i^4} \frac{n^2 (n^2 - 1)^2}{(n^2 + 1)}, \quad (6)$$

and mass element -

$$m_i = \rho \delta_i. \quad (7)$$

For the third unit of the equivalent mechanical chain modeling the smooth cylindrical shell with a wall thickness δ , the expression for the free vibration frequency is given by the formula:

$$\omega^2 = \frac{D_u}{R^4 \rho \delta} \frac{n^2 (n^2 - 1)^2}{(n^2 + 1)}, \quad (8)$$

Where the cylindrical stiffness of the shell is:

$$D_{uu} = \frac{E\delta^3}{12(1-\mu^2)}, \quad R - \text{radius of the cylinder.}$$

Comparing the natural frequencies of the ring and the cylinder (4) and (8) it is easy to see that they are the same, if we replace the bending stiffness D_{uu} by the normal stiffness EJ in formula (8), assuming δ cross-sectional area of the ring.

If $R/L \geq 0,1$, then the finite length of the cylinder must be taken into account and the following formula should be used:

$$\omega^2 = \frac{1}{\rho\delta} \frac{E\delta\left(\frac{\pi R}{L}\right)^4 + \frac{D_{uu}}{R^2}(n^2 - 1)^2 n^4}{R^2\left(\left(\frac{\pi R}{L}\right)^2 + (n^2 + 1)n^2\right)}. \quad (9)$$

Then, similarly to formulas (6) and (7) the value of stiffness and mass of the third unit of the chain for the case $R/L < 0,1$ would be:

$$k = \frac{D_{uu}}{r^4} \frac{n^2(n^2 - 1)^2}{(n^2 + 1)}, \quad (10)$$

and for the case $R/L \geq 0,1$

$$k = \frac{E\delta\left(\frac{\pi R}{L}\right)^4 + \frac{D_{uu}}{R^2}(n^2 - 1)^2 n^4}{R^2\left(\left(\frac{\pi R}{L}\right)^2 + (n^2 + 1)n^2\right)}, \quad (11)$$

$$m = \rho\delta. \quad (12)$$

4. Identification of model parameters

Parameters of damper elements of the mechanical chain can be defined on the basis of reference data on the logarithmic decrement for the liner material. Simultaneously it should be kept in mind that determination of the damping characteristics of the material in a methodological sense is a much more complicated problem than the experimental determination of any other mechanical characteristics of the material, since the definition of the dissipation energy of the material at its cyclic deformation within elastic limit requires sophisticated methods of experiment, that border with physical ones. Therefore, the question of methods for determining the damping characteristics of the material is extremely important and the reliability and validity of experimental data depend on how well the method has been chosen.

Lack of attention to the specific characteristics of methods for the determination of the dissipation energy in the materials cyclically deformed in the range of Hooke's law, has led to extensive evidence about a damping ability of the same materials, often contradicting each other.

As a result, it is necessary to select references on the damping ability of materials very carefully, taking into account a high sensitivity of damping rates to the experimental methods of their obtaining.

Certain reference data on damping properties of various brands of cast iron were obtained for the frequencies of cyclic deformation of samples in the range of 10-30 Hz. However the frequency of cyclic deformation plays an important role in determining the damping properties of a material only in ultrasonic range – 20000 Hz and more. Natural frequencies of cylinder liner vibrations are in the range of 1000-2000 Hz, so a cyclic deformation within this range would not be significant.

Within the heterogeneous states of stress observed in the vibrations of cylinder liner inflexibly fixed at the top collar, the damping decrement is an integral characteristic of damping properties of the entire material and is usually associated with the amplitude of maximum tension. Therefore, when determining damping properties of components of the chain, it is important to chose the value of the decrement corresponding to the maximum amplitude of liner vibration stresses.

The damper resistance coefficient b is related to the logarithmic decrement θ by the following equation:

$$b_i = \frac{1}{\pi} \theta \sqrt{m_i k_i}, \quad (13)$$

where:

m_i, k_i – parameters of the mass of the elements and the stiffness of a chain link.

Basing on these assumptions calculations of mechanical chain parameters of the simulation model of the 4Ч8,5/11 diesel liner have been made.

Parameters of mass elements of all links of the chain which model the liner of the 4Ч8,5/11 diesel engine were determined from formulas (7), (10). Mass elements in this case will have the dimension of linear density. Density of the liner material $\rho = 7840 \text{ kg/m}^3$.

Tab. 1. Elements of mass in mechanical chain of liner 4CH 8,5/11

| № chain link | $\delta_i, \text{ m}$ | $m_i = \rho \delta_i \text{ kg/m}$ |
|--------------|------------------------|------------------------------------|
| Ring1 | $2,985 \cdot 10^{-03}$ | 23,399 |
| Ring 2 | $1,414 \cdot 10^{-03}$ | 11,084 |
| Cylinder 3 | $4,000 \cdot 10^{-03}$ | 31,36 |
| Ring 4 | $1,414 \cdot 10^{-03}$ | 11,084 |
| Ring 5 | $6,872 \cdot 10^{-04}$ | 5,388 |
| Ring 6 | $1,414 \cdot 10^{-03}$ | 11,084 |
| Ring 7 | $6,872 \cdot 10^{-04}$ | 5,388 |
| Ring 8 | $1,414 \cdot 10^{-03}$ | 11,084 |
| Ring 9 | $1,118 \cdot 10^{-03}$ | 8,768 |
| Ring 10 | $8,388 \cdot 10^{-04}$ | 6,576 |

Stiffness parameters of the elements of the mechanical chain of the 4CH 8,5/11 diesel liner were determined from formula (6) for all units, except the third - simulating a smooth cylinder where formula (11) was used. According to these formulas stiffness per length unit is determined, so the dimension of the stiffness parameters is N/m^2 .

Parameters of damping elements were calculated from formula (13) and have in this case the dimension of mechanical resistance per unit of length.

Tab. 2. Elements of stiffness and dampers of the mechanical chain of the 4CH 8,5/11 liner

| № chain unit | $k_i, N/m^2$ | $b_i = \frac{1}{\pi} \theta \sqrt{m_i k_i}, \frac{kg}{s \cdot m}$ |
|--------------|-----------------------|---|
| Ring 1 | $6,741 \cdot 10^{11}$ | $3,641 \cdot 10^{04}$ |
| Ring 2 | $3,529 \cdot 10^{11}$ | $1,813 \cdot 10^{04}$ |
| Cylinder 3 | $1,462 \cdot 10^{09}$ | $6,013 \cdot 10^{03}$ |
| Ring 4 | $3,529 \cdot 10^{11}$ | $1,813 \cdot 10^{04}$ |
| Ring 5 | $1,811 \cdot 10^{11}$ | $9,055 \cdot 10^{03}$ |
| Ring 6 | $3,529 \cdot 10^{11}$ | $1,813 \cdot 10^{04}$ |
| Ring 7 | $1,811 \cdot 10^{11}$ | $9,055 \cdot 10^{03}$ |
| Ring 8 | $3,529 \cdot 10^{11}$ | $1,813 \cdot 10^{04}$ |
| Ring 9 | $2,852 \cdot 10^{11}$ | $1,450 \cdot 10^{04}$ |
| Ring 10 | $2,137 \cdot 10^{11}$ | $1,087 \cdot 10^{04}$ |

5. Methodology of problem solution

As presented above, a further analysis of the mechanical chain is connected with the solution of the system of Kirchhoff's equations, which must be performed for each node and contour of the chain. There are other ways of treating a chain consisting of individual units. In particular, the amplitude-frequency and phase-frequency characteristics of the system are determined by the inverse Laplace transform transfer function of the system, which in turn is the multiplication or the sum of the transfer functions of the individual units, depending on how they are connected with each other – in a sequential or parallel way.

Since the procedure of describing of the characteristics of individual units and their interconnections through the transfer functions is sufficiently formalized and there are plenty of studies on circuit calculations based on this technique, determination of the amplitude-frequency characteristics of the cylinder liner simulator is not complicated. However, a more vivid and interesting from the research point of view, is the method of virtual experiment. By changing the parameters of various elements of the chain in this experiment, it is possible, together with multivariable analysis of the mechanical system, to get its response to a variety of effects.

For the virtual experiment, the software for automotive design Electronics Workbench (EWB) [2], has been used.

As this software was developed for designing electrical circuits it was necessary to perform a transfer from a mechanical chain model to an electrical circuit one to work in the Electronics Workbench (EWB) environment. Such a transfer is made on the basis of physical analogies between mechanical and electrical vibration processes. Vibrations in different systems: vibrations of load under the force of elastic spring, electrical vibrations in the contours with inductivity and capacity, spread of sound waves have common mathematical formulation and expressed by the same differential equations. Thus the movement of load on an elastic spring in a viscous medium under the driving force is described by the equation

$$M \frac{d^2 x}{dt^2} + B \frac{dx}{dt} + k \cdot x = Q(t), \quad (14)$$

and a differential equation of electrical circuit with one pair of nodes would be:

$$C \frac{d^2 u}{dt^2} + \frac{1}{R} \frac{du}{dt} + \frac{1}{L} \cdot u = \frac{di}{dt}. \quad (15)$$

Comparing equations (14) and (15), we can establish the similarity between mechanical and electrical values. Dynamic equations for an n – contour electrical circuit consisting of a current source i_j , resistors R_{jk} , capacitors C_{jk} and inductors L_{jk} , are Lagrange equations of the second kind:

$$\frac{d}{dt} \left(\frac{dT_e}{d\dot{q}_j} \right) + \frac{dU_e}{dq_j} + \frac{dF_e}{d\dot{q}_j} = \frac{di_j}{dt}, \quad (j=1, 2, \dots, n), \quad (16)$$

where the energy of the electric field

$$T_e = \frac{1}{2} \sum_{j=1}^n \sum_{k=1}^n C_{jk} \cdot \dot{u}_j \cdot \dot{u}_k, \quad (17)$$

Energy of magnetic field

$$U_e = \frac{1}{2} \sum_{j=1}^n \sum_{k=1}^n \frac{1}{L_{jk}} u_j \cdot u_k, \quad (18)$$

dissipation function

$$F_e = \frac{1}{2} \sum_{j=1}^n \sum_{k=1}^n \frac{1}{R_{jk}} \cdot \dot{u}_j \cdot \dot{u}_k. \quad (19)$$

Equations (14), (15) and (16) result from the fact that kinetic energy of a mechanical system corresponds to the energy of electric field, potential energy – energy of the magnetic field, generalized forces – rate of current. Then, Lagrange equations of the second kind for an electrical system by the adopted analogy of “force – current” express the first law of Kirchhoff: algebraic sum of currents in the node is equal to zero [1].

The obtained under these rules equivalent electrical scheme for the solution of a system of equations describing the vibrations of a mechanical system (liner) was designed in the dialog box of Electronics Workbench (EWB) and is presented in Figure 3.

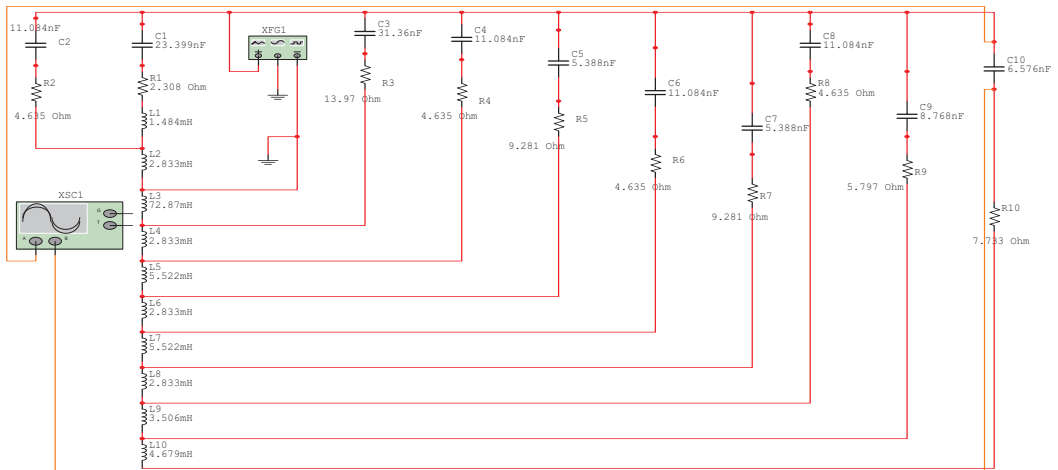


Fig. 3. An equivalent electrical circuit for the 4Ч8,5/11 liner

6. Programme and results of experiments

According to input analogies between mechanical and electrical values the parameters of elements of the electrical circuit were defined: mass elements of units

m_i , expressed in $\kappa\text{g}/\text{m}$, are compared to capacitance C_i , expressed in nanofarads; elements of stiffness k_i , expressed in pascals, compared to the inductance in H so that $1/L_i = k_i$, and coefficient of damper resistance b_i , expressed in $\kappa\text{g}/\text{m}\cdot\text{s}$, - electrical resistance R_i , defined as $R_i = 1/b_i$ and expressed in ohms.

The obtained parameters of the equivalent electrical circuit for the 4CH8,5/11 diesel liner are presented in Table 3.

Tab. 3. Parameters of the electrical circuit of a liner simulator

| № chain unit | Inductance L, mH | Capacitance C, nF | Resistance R, Om |
|--------------|---------------------|----------------------|---------------------|
| Ring 1 | 1,484 | 23,399 | 2,308 |
| Ring 2 | 2,833 | 11,084 | 4,635 |
| Cylinder 3 | 72,87 | 31,36 | 13,97 |
| Ring 4 | 2,833 | 11,084 | 4,635 |
| Ring 5 | 5,522 | 5,388 | 9,281 |
| Ring 6 | 2,833 | 11,084 | 4,635 |
| Ring 7 | 5,522 | 5,388 | 9,281 |
| Ring 8 | 2,833 | 11,084 | 4,635 |
| Ring 9 | 3,506 | 8,768 | 5,797 |
| Ring 10 | 4,679 | 6,576 | 7,733 |

Generation of unit vibrations in the simulating circuit was carried out by an impulse generator available at Electronics Workbench (EWB) library. An oscilloscope is included in the equivalent electrical scheme as a controller to register the frequency of vibrations.

The virtual experiment with an electrical scheme – simulating a model of the 4Ч8,5/1 diesel liner 1 in the EWB environment was held under the following parameters of the output impulse generator signal:

- signal waveform – rectangular,
- frequency of signal 200 Hz,
- impulse duration 1%, which is 0,05 ms.

Another operation mode with the signal frequency of 200 Hz and impulse duration of 2% was also applied in the experiment. Such frequency and duration of an impulse corresponds to the shock of the piston within a degree of turn of the crankshaft with rotating frequency equal to 1500 rpm. The resulting vibration oscillograms are shown in Figures 4 and 5.

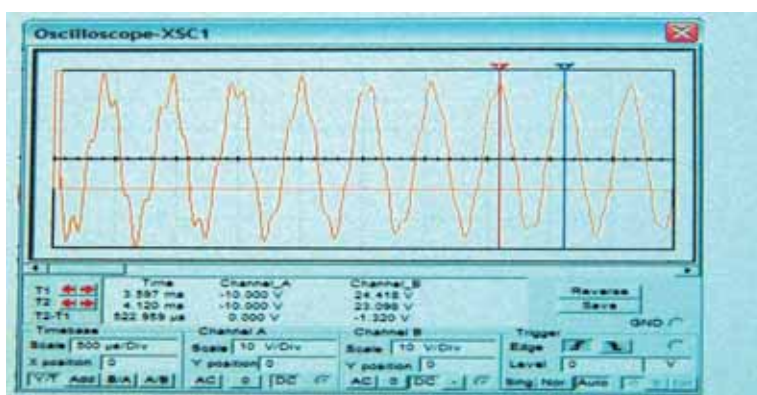


Fig. 4. An oscillogram of liner the 4CH 8,5/11 liner vibrations (a simulating model). Signal frequency 200 Hz, impulse duration 1%

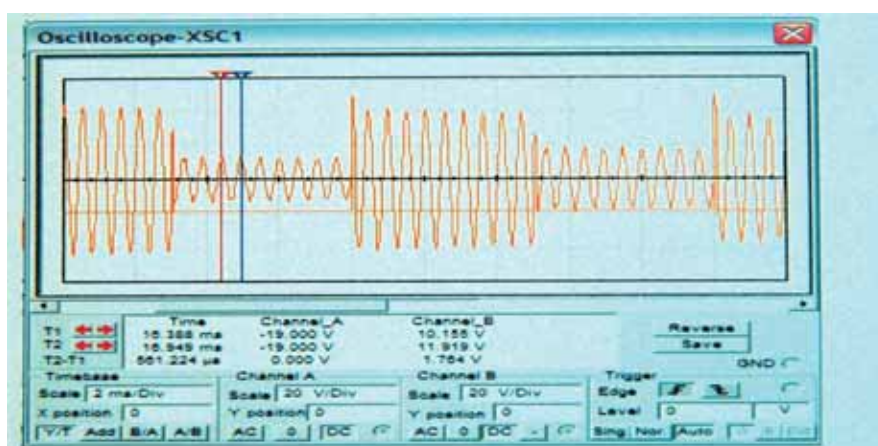


Fig. 5. An oscillogram of r the 4CH8,5/11 liner vibration (a simulating model). Signal frequency 200 Hz, impulse duration 2%

7. Final remarks

The nature of the obtained vibration oscillograms shows that impulse influence on the system generates vibrations of several harmonics at once, and in the time of approx. 3,5 ms, the higher harmonic is practically damped and vibrations occur with the frequency of the first harmonic. Table 4 shows the measurement results of first harmonic frequency.

Tab. 4. The frequencies of the first harmonic vibrations of the liner

| Signal frequency, Hz | Impulse duration, % | Vibration period ms | Vibration frequency f , Hz |
|----------------------|---------------------|---------------------|------------------------------|
| 200 | 1 | 522,959 | 1912,2 |
| 200 | 2 | 581,224 | 1720,5 |

Simultaneously parameters of 4Ч8,5/11 diesel cylinder liner vibrations were measured on a mechanical test bench where the frequency of the natural diesel liner vibration was $f = 1727 \pm 198 \text{ Hz}$. In this way, the results obtained in the virtual experiment match well with the results of the natural vibrations of the liner.

References

- [1] Genkin M. D. Editor: Measuring and Testing. Handbook, Vol. 6 Vibration in Engineering. Chief editor Chelomey V.N., Mashinostroenie, Moscow, 1981.
- [2] Karlaschuk V. I.: Electronic laboratory on IBM PC. Solon- Press, Moscow 2005.
- [3] Pogodaev L., Kuzmin A.A., Erosion of materials and shipping facilities in homogeneous liquids and gases. SPGUVK, St. Petersburg 2004.
- [4] Timoshenko S.P., Young D.H., Weaver W. Vibration in Engineering: Trans. From English, Mashinostroenie, Moscow 1985.



ANALYSE OF MARINE DIESEL ENGINE PERFORMANCE

Prof. Roman A. Varbanets, D.Sc.

Odessa National Maritime University

34, Mechnikova str., Odessa, Ukraine 65029, tel.: +380 48 7283119

e-mail: roman.varbanets@gmail.com

Assoc. Prof. Sergey A. Karianskiy, PhD

Odessa National Maritime Academy

8, Didrikhson str., Odessa, Ukraine 65029, tel./fax.: +380 48 733 44 29

e-mail: karik@imare.onma.edu.ua

Abstract

Ships safety and economic efficiency depends on the main and auxiliary diesel engines technical condition and technical operation. The probability of failure and a sudden stop of diesel at sea would be minimized if the routine monitoring of parameters is done and found defects removed on time. The purpose of this control is the even distribution of load between the cylinders under the condition of fuel equipment and main diesel systems normal state. The power plant capacity, fuel efficiency and compliance with MARPOL environmental restrictions depend on it. In this report we will discuss the survey methods of the ship's diesels working process, which improve their efficiency. Use of such methods will enrich the information capability and modeling quality of the PC based Engine Room simulators.

Keywords: *Engine Room simulators, turbocharger rpm, gas distribution mechanism, fuel injection and valves timing, monitoring*

1. Introduction

On low speed engines there are well known in seamanship mechanical drives for determining the basic parameters of the working process and indicator power of cylinders. They cannot be used for medium-and high-speed diesel engine because of mechanical drives inertia. For those of diesel engines, which make up the majority of the offshore and fishing fleet, only electronic control systems may be used.

Capabilities of most electronic systems are focused mainly on getting the indicator working process parameters such as maximum combustion pressure P_{max} , maximum compression pressure P_{comp} , mean indicated pressure MIP . However, besides these there are several other important diagnostic parameters of fuel injection equipment and gas distribution mechanism. Their control allows you to assess more accurately the technical condition and to adjust the marine diesel engines. First of all fuel injection timing and valve timing is included into such settings.

In the problem of determining the working process parameters, there is a problem of data synchronization, i.e. representation of them, depending on the phase rotation of the crankshaft, for example $p_{cyl}=f(\varphi)$. Traditionally, this problem is solved by means of sensors on the flywheel. Disadvantages of this method are that it is difficult to consider all the factors that

influence the phase error. Besides, setting the sync sensor requires preliminary diesel preparation and definite expenses.

Thus, there are two problems to be solved for the perfect modeling and condition monitoring of marine diesel in operation: 1) parallel determination of the indicator work process parameters and timing of fuel injection and gas distribution; 2) the solution of sync problem in terms of improving its accuracy and efficiency.

An important element of diagnosis of a diesel engine is a characterization of turbocharging. On the main engine turbines tachometer and charge air pressure gauges can be installed. On the turbines for auxiliary diesel engines, as a rule, there are no such devices. In this article we shall discuss how during the operation such important parameter, as the rotational speed of the turbocharger can be determined. The above problems are solved in the PC based system for diesel condition monitoring.



Fig. 1. Equipment of the diesel engine performance analyzing system

2. Diesel engine performance analyzing system

The purpose of the system is to diagnose main and auxiliary marine diesel engines see Fig. 1. Also it can be used on other mobile and stationary diesel power plants. Gas pressure sensor and vibro sensor are included into the standard version. The system measures and calculates the following: *RPM*, *Pmax*, *Pcomp*, *MIP*, *indicated power*, *fuel injection and valves timing*, *gas pressure*, *fuel injection and valves vibro diagrams*.

Fuel injection and valves timing as well as estimation of technical condition of separate units are determined by means of contact vibrosensor. It records high frequency signals that occur during the ascent and landing injector and valves timing during engine working cycle, see Fig. 2.

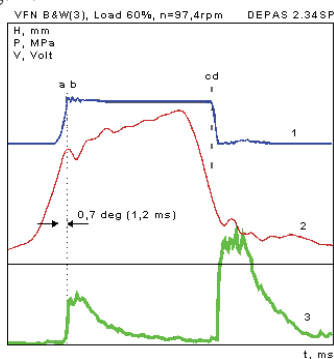


Fig. 2. Fuel injection timing with the help of vibrodiagram

Due to analyzing of fuel injection equipment and valve timing mechanism vibrodiagrams together with working process indicator diagram the spectrum of monitored parameters has been significantly widened. The engine cylinder technical condition diagnosis became possible not only by cylinder gas pressure but also by key data of fuel injection and valve timing.

3. Data synchronization method

The Top Dead Center (TDC) of a piston is calculated by analyzing diagrams of gas pressure in the working cylinder. Design algorithm of synchronization is based on the fact that in case of pure compression (without fuel injection and combustion) in the cylinder, the speed degree of increasing gas pressure is equal to zero: $dP/d\varphi=0$ at TDC position of the piston, see Fig. 3. On the referent diagram of pressure the site of pure compression before the beginning of combustion is allocated. Factors of non-linear mathematical model of a curve $dP/d\varphi$ are calculated by means of minimization method. Mathematical data synchronization method leads to precise calculation of *MIP* and indicated power.

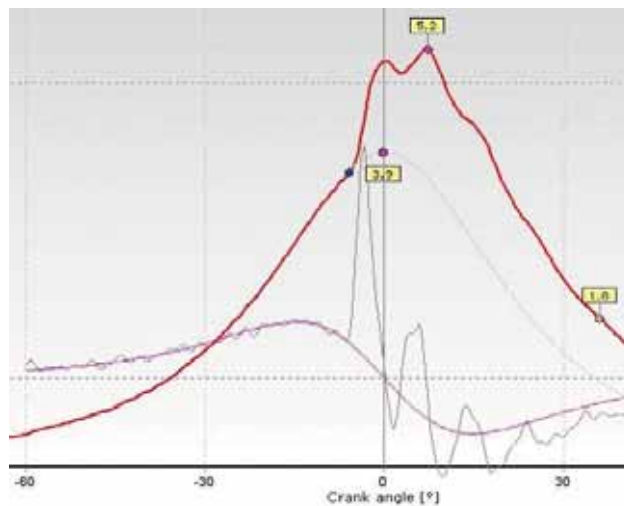


Fig. 3. TDC determination with the help of $dP/d\varphi$ mode

4. Example 1. Four-stroke engine

Diagnosing the working cylinder of a medium speed diesel engine is shown at Fig. 4.

Fig. 4A shows the indicator diagrams of work process and results of the work process basic parameters calculation: indicated power, *MIP*, the maximum compression and combustion pressure, the angle of the start of combustion, etc. Fig. 4B shows the vibrodiagrams of fuel injection and gas distribution which is recorded simultaneously with the indicator diagrams. It may be noted the normal operation of fuel equipment according to specified vibroimpulses (without distortion) of rising (15° bTDC) and setting (4° aTDC) needle.

The first to the left vibroimpulse characterizes the signal while closing the inlet valves. Fractional value of the vibroimpulse shows the fact that inlet valves do not close simultaneously. It is a defect of gas distribution mechanism.

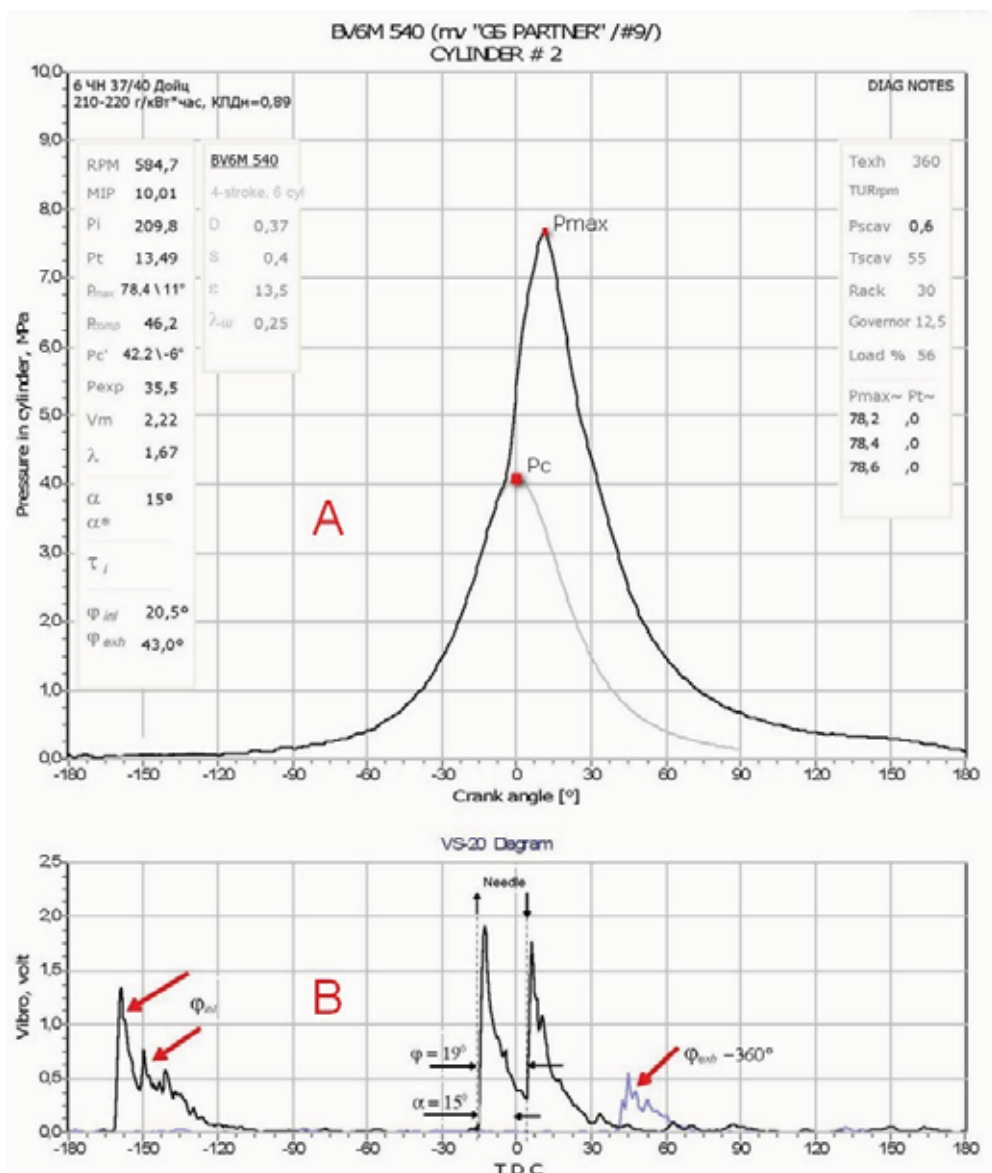


Fig. 4. Medium speed diesel engine working process

5. Example 2. Two-stroke engine

Another example of S60MC two-stroke low-speed main engine work process diagnosis shown on Fig. 5.

Reference points on diagrams:

1. Point on the indicator diagram which corresponds to a moment of the beginning of fuel self-ignition,
2. Geometrical advance angle of fuel feed by HPFP (a plunger is beginning to close the cut-off port),

3. Fuel feed cut off (the low edge of HPFP plunger is starting to open the cut-ff port),
4. Rising of injector circulation valve and termination of fuel circulation ($P \sim 1.0 \text{ MPa}$),
5. Rising of injector needle ($P = 25.0 \pm 2 \text{ MPa}$) – real angle of the fuel injection beginning,
6. Injector needle fit – real angle of the fuel injection termination,
7. Injector circulation valve fit – the beginning of fuel circulation,
8. Angle of complete closing of the exhaust valve – valve plate fit in its seat,
9. Angle of the beginning of damper action at the end of exhaust valve stroke,
10. Increase of a high-frequency noise level while opening the exhaust valve.

According to diagrams on Fig. 5 and obtained parameters, the condition of the cylinder, the high pressure fuel equipment and mechanism of gas distribution is normal.

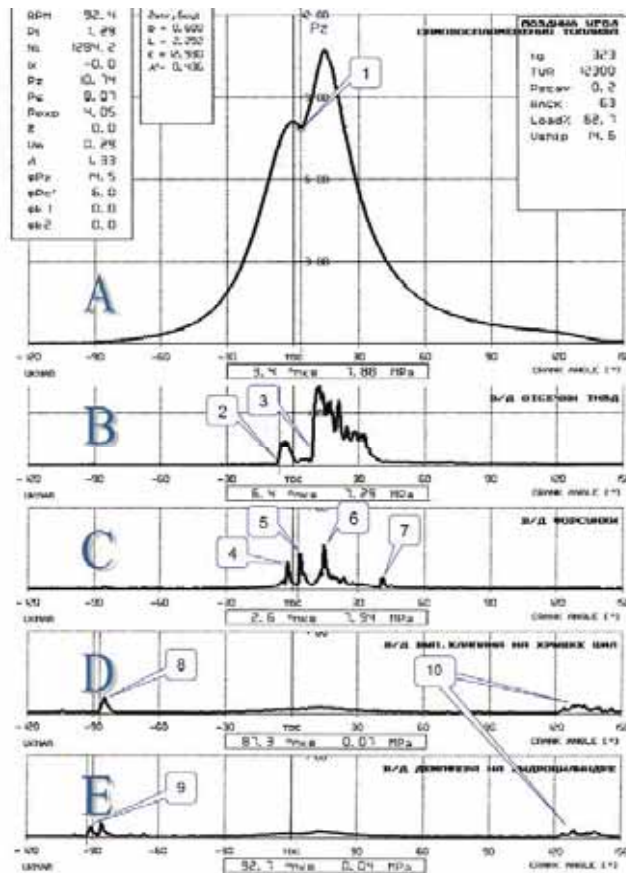


Fig. 5. Two-stroke low-speed main diesel engine working process

6. Determining the speed of TURBOCHARGER

Charge air pressure depends on the speed of turbocharger. In connection with this problem of its operational definition is especially important during the operation for all types of diesel engines. To determine the frequency of turbocharger rotation the amplitude spectrum of acoustic signal of an air compressor was used. The spectrum of the main engine turbocharger, see Fig. 6 and auxiliary engine turbocharger see Fig. 7.

The spectral analysis showed that the compressor side is generating audio signal with a frequency equal to the frequency of rotation multiplied by the number of blades.

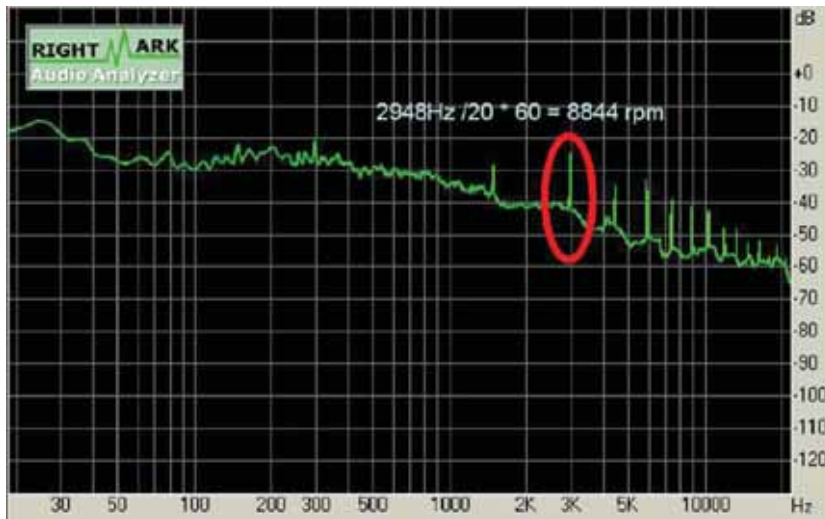


Fig. 6. Caption: Spectrum of the main engine turbocharger



Fig. 7. Spectrum of the auxiliary diesel engine turbocharger

For diesel 6L80MCE with type TURBOCHARGER VTR 564-31 (20 of compressor blades) the expected frequency is equal to:

$$F_q = 9000 \text{ rpm} / 60 * 20 = 3 \text{ kHz.}$$

The minimum and maximum possible speed of TURBOCHARGER and, accordingly, the frequency of signals can be taken as follows:

$$\begin{aligned} \text{MAX: } & 6000 \text{ rpm} / 60 * 20 = 2 \text{ kHz,} \\ \text{MIN: } & 20000 \text{ rpm} / 60 * 20 = 6667 \text{ Hz.} \end{aligned}$$

In this range there is only one distinct maximum, see Fig. 6. The corresponding frequency is:

$$TURrpm = 2948 \text{ Hz} / 20 * 60 = 8844 \text{ rpm.}$$

It is interesting to note that in the medium-auxiliary diesel Daihatsu 6PL 24 with a turbo-generator VTR 201, the number of compressor blades also turned to be 20. Using similar arguments we calculate the speed of the turbine rotor diesel mode at 380 kW:

$$TURrpm = 6557 \text{ Hz} / 20 * 60 = 19671 \text{ rpm.}$$

7. Conclusions

Diagrams and data shown in Fig. 4-7 are greatly valuable for engineers as they illustrate technical condition of working cylinder, its high pressure fuel equipment and auxiliary systems.

This method of working process monitoring can be very useful in practice. Besides, the received from ship's diesel data will help to create more real models in PC based Engine Room simulators.



ENHANCING HEAT EXCHANGE IN FORCED CONVECTION WITH VARIABLE AIR FLOW DIRECTION

Sylwester Wawrzyniak

University of Technology and Life Sciences in Bydgoszcz
Av. Prof. S. Kaliskiego 7, 85-789 Bydgoszcz
tel.: +48 52 3408288, fax: +48 52 3408245
email: sylwester.wawrzyniak@utp.edu.pl

Abstract

In this article there are presented tests results of the process of heat exchange between a flat plate placed vertically behind a stream element being a mono-stable jet nozzle with two states of the air outflow. Depending on the state of the air outflow, the air stream flows round a part of the wall in a different direction. In this work there are presented results of measurements recorded for selected parameters of the air outflow.

Keywords: heat transfer, airflow control, impinging jets, air nozzle.

1. Introduction

In the processes of heat exchange (heating, cooling) the thermal efficiency of a device is of great importance as well as the temperature distribution on the heated or cooled element. This article deals with the problems connected with the heat exchange process, involving heated air, being the heat carrier, flowing out of the nozzle thus enabling occurrence of two characteristic states of the air stream. As regards intensity of the heat exchange between a solid body and a liquid flowing around it, this is the fluctuation of its speed and direction, while flowing around the obstacle, that really matters. Properly matched parameters of the stream flow should inhibit formation of a boundary layer considered to be the main thermal resistance during heat exchange between a solid body and an air stream flowing around it.

One of the ways of heating by hot air is directing the stream perpendicularly to the heated body. The flow of hot air hits the wall (flat, stiff wall) and, flowing into direction radial to the axis of the nozzle, heats it (fig. 1).

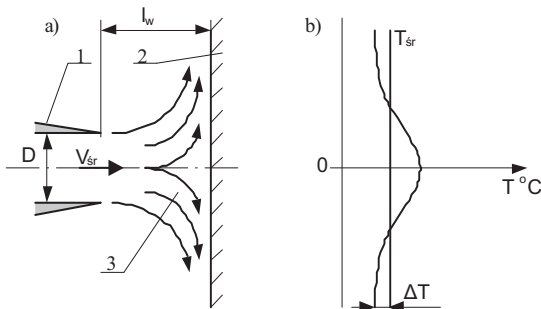


Fig. 1. Flow around flat wall; a) diagram of airflow, b) temperature distribution on the wall; 1-nozzle, 2-wall, 3- lines of airflow direction

The mean value of temperature T_{sr} and the degree of its non uniformity δ_T depend on the conditions of the heat inflow within a given area. Thus, the task involves providing proper conditions for the inflowing air. It is possible through using a controlled stream element with pulsing exhaust jet. A direction change of the speed vector of air, flowing round the studied flat surface, is a distinctive feature of the produced air stream.

Improving the efficiency of the heat exchange process will make it possible to reach a higher value of temperature for the heated element, in the same time. Analyzing the amount of thermal energy taken over by the element from the air flowing round it will make it possible to reach the same value in a shorter time. Shortening of the heating process time is also connected with a reduction of energy used in this process. Attempts to find a way to reduce the amount of energy have been made in many works on the subject of micro-pneumatics in which stream micro-valves find application. Reduction in energy consumption is connected with environment protection. Ecological aspects play a more and more important role in construction, utilization and recycling and are being focused on by more and more researchers [2].

2. Test stand

The test stand is presented in figure 2. The designed and constructed control systems make it possible to control the main stream (flowing out of the nozzle) following parameters [1.3]:

- main stream volume rate Q_{vm} ;
- control stream volume rate Q_{vc} ;
- temperature of stream T ;
- frequency of stream oscillation f_c ;
- space filling of signal PWM (refers to the time of the flow duration in its particular states).

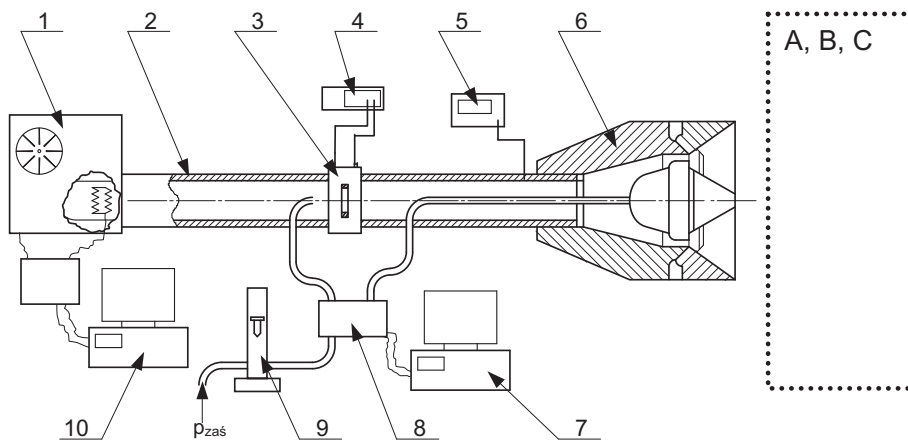


Fig. 2. Scheme of a test stand: 1 – supply and heating systems for the main stream, 2 – the main pipe, 3 – orifice, 4 – digital micro-manometer CMR 10A, 5 – system for measurement and recording temperature of the flow flowing into the nozzle, 6 – the tested axial-metric nozzle with internal core, 7 – computer PC with measurement card producing control signals f_c and PWM, 8 – electro-pneumatic throw-over valve of the control flow, 9 – rotameter (measurement of the control flow rate), 10 – computer PC with measurement card for control of the flow rate and the main flow temperature, p_{zas} -source of control flow A,B,C – measurement systems of the heated wall, speed distribution of air flowing out of the nozzle and visualization of the air flow behind the nozzle

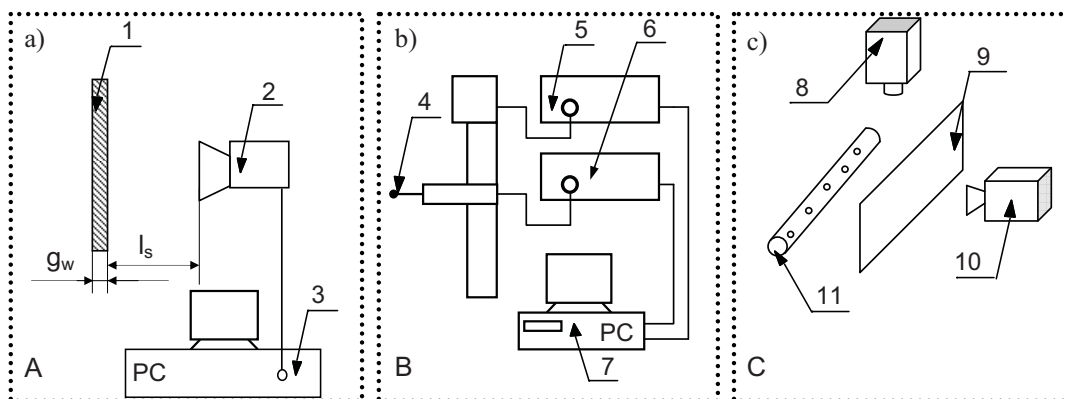


Fig. 3. Schemes of measurement systems used in tests (to fig.2): a) measurement of the heated wall temperature, b) measurement of speed of the air flowing out of the nozzle, c) visualization of the air outflow from the nozzle and its flowing round the resistance wall; 1-heated element (resistant wall) by the air flowing out from the nozzle, 2-thermographic video camera, 3-PC computer recording data from the thermographic video camera 4-single-fiber measurement probe 55P11, 5-uniaxial system of traversion Dantec Light Weight Traverse, 6-thermal anemometer StreamLine with one channel module CTA90C10, 7- computer PC with software for control of the traversion system, 8-digital video camera recording the visualized air flow, 9- transparent resistant wall, 10-lighting system with regulation of the light beam width, 11-system of paraffin vapor generation visualizing the air flow

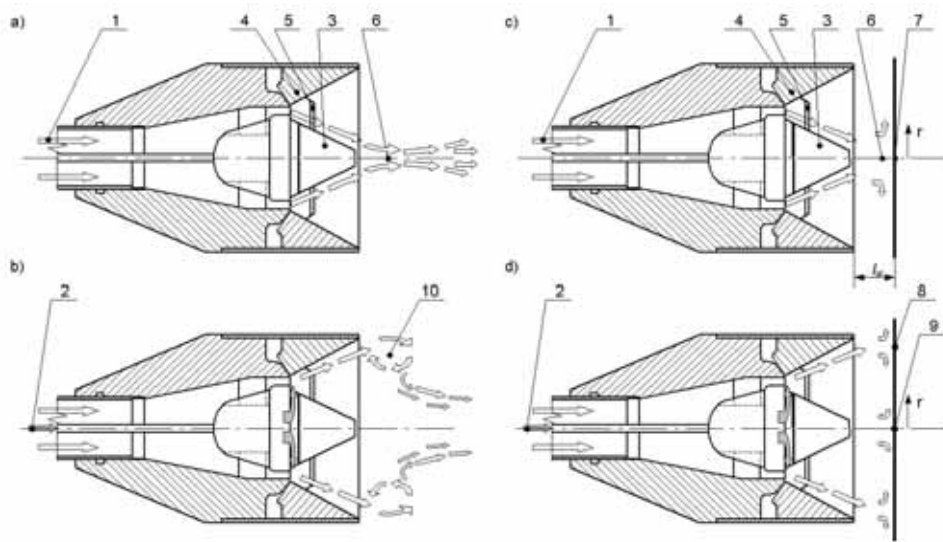


Fig. 4. Scheme of the nozzle operation, air flow through the nozzle and its flowing round the wall; a) first steady state – free outflow, b) second steady state – free outflow, c) the first steady state – outflow onto a flat perpendicular wall, d) the second steady state – outflow onto a flat perpendicular state, 1-main stream, 2-control stream, 3-the nozzle inner core, 4- the nozzle male cone, 5-spoiler, 6-point of the stream connection, 7-stagnation point, 8-stagnation circle, 9- the reverse stream stagnation point, 10-tridodal whirl formed in the second fixed state with a free flow

The measuring equipment shown in Figure 3 allows to perform the following measurements:

- measurement of the heated wall temperature
- measurements of the average velocity of air stream flowing from the nozzle;
- visualization of air flow behind the nozzle (flow without and with the wall)..

Measuring devices are placed behind the nozzle as shown schematically in fig. 2.

The analyzed nozzle is a monostable stream element whose distinctive feature is the internal core to which a stream controlling the outflow of the main stream is supplied. This element is monostable with two steady states of the main stream outflow. In the first steady state (while the control stream is switched off) the air flows out along the inner cone (core). In the second steady state (while the control stream is switched on) the air flows out along the outer cone. These states are characterized by different concentrations of the stream. In order to equalize rates of the flow volume of the air flowing out of the nozzle for both fixed states, the control stream is not only turned on and off but also switched within valve 8 in fig.2. A scheme of the nozzle operation has been shown in figure 4 [4.5.6].

As the flow control, which allows you to change the steady state flow can be used a synthetic jet with adequate power. Research of such a synthetic jet generated by the speaker were carried out among others in Institute of Thermomechanics of the Academy of Sciences of the Czech Republic [1.2].

3. Experimental tests

Thermographic tests were conducted for a definite range of input parameters. Values of particular quantities within the accepted ranges were measurable and controllable [1]. The values of particular input variables were:

- the stream oscillation frequency $f_c=0,5; 0,8; 0,9; 1,0; 1,1; 1,2; 1,3; 1,5; 2,0$ Hz;
- space filling of signal PWM=20; 50; 80 %;
- distance of the wall from the end of nozzle $l_w=70; 80; 90; 100$ mm.

The direction of the flow round the wall in the first and second state underwent a distinct change within the range of accepted distances of the wall from the nozzle end in the first and second state [2,3].

Before measurements the nozzle was initially heated in order to decrease heat losses from the stream through raising the temperature of the housing during the resistant wall heating process. Initial heating involved 30 min. flow of air through a nozzle, the air was heated to temperature $T=50$ °C. Thermographic measurements were started at the time when the environment mean temperature was $T_o=24\pm0,5$ °C.

Thermographic video camera of VIGO S.A. was used for the wall temperature measurements. Actually this was a thermographic scanner with resolution 240x240 points. The time of measurements was fixed and equal to 8 min. and 20 seconds for fixed values of input parameters. This was a time necessary to carry out 20 measurements, that is, runs of the video camera head [7].

4. Results of thermographic tests

The results of temperature measurements of the wall flowed round by air can be presented:

- in the form of thermographic image;
- in the form of a table with temperature values.

Different temperature distributions have been obtained for the air flow with different values of input variables. In figure 5 there are selected results of these measurements. The amount of heat taken over by the wall from the heating air was calculated for the wall unit volumes provided by the thermographic video camera resolution and the difference in temperatures recorded at the beginning and at the end of the heating process.

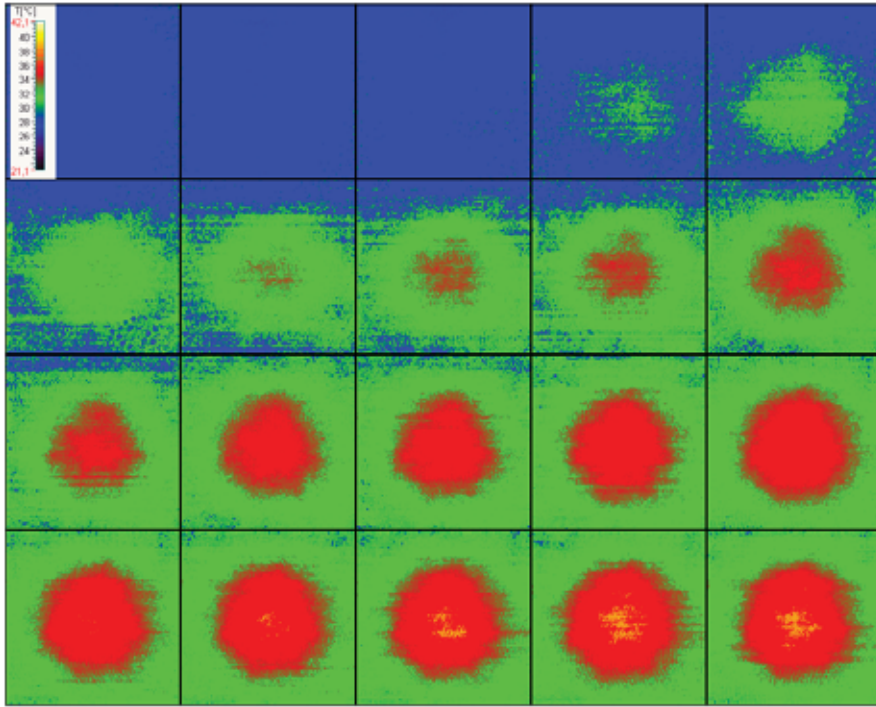


Fig. 5. The results of thermographic measurements for the flow, in the first steady state, when the wall distance from the nozzle is $l_w=70\text{mm}$. The figure shows 20 successive measurements, in the first image there is a scale of temperatures

In order to compare and analyze the influence of the air stream flow oscillation on the process of heat transfer, dimensionless indicators have been determined for different values of input parameters.

a) indicator of the heat exchange process

$$w_Q = \frac{Q_{uz}}{Q_{nom}}, \quad (1)$$

where:

Q_{uz} - amount of heat taken over by the wall for a flow with defined parameters,

Q_{nom} - amount of heat obtained from the flow in the steady state one.

b) indicator of the wall distance from the nozzle l_w / D_{zd}

where:

l_w - distance of the wall from the nozzle,

D_{zd} - external diameter of the nozzle.

c) coefficient of the temperature distribution non-uniformity

$$\delta_T = (T_{\max} - T_{\min}) / T_{sr}, \quad (2)$$

where:

T_{\max} - maximum temperature of the wall,

T_{\min} - minimum temperature of the wall,

T_{sr} - mean temperature of the wall.

Selected results of measurements of wall temperature for different flow parameters are shown in fig. 6. The values of the coefficients w_q and dT will determine the impact of the air flow parameters for the transfer of heat by the wall from the air flowing from the nozzle. Figures 7, 8 and 9 shows the values of these coefficients calculated for the flow of air with different values of the parameters f_c , PWM, l_w .

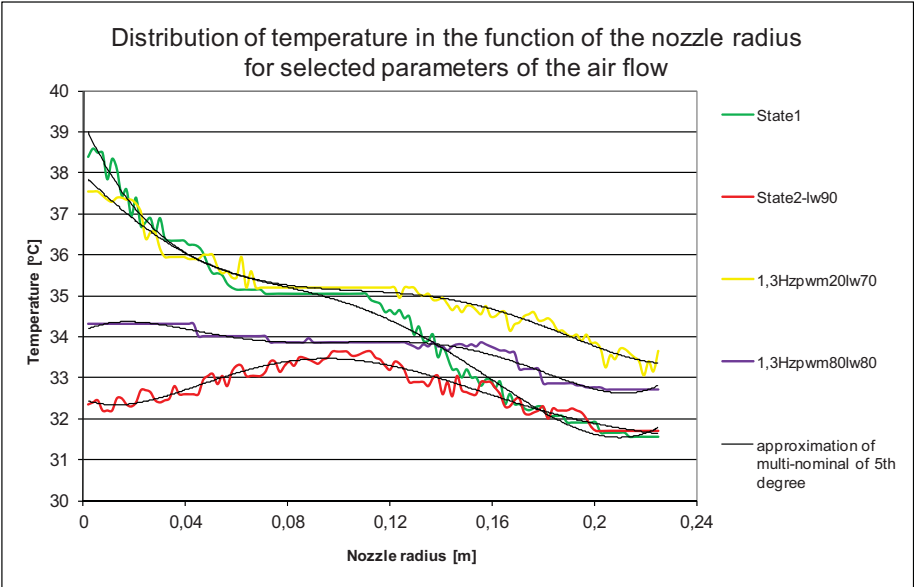


Fig. 6. Selected temperature measurement results of the wall flowed round by heated air, obtained for different parameters including approximation of multi-nominal of 5th degree

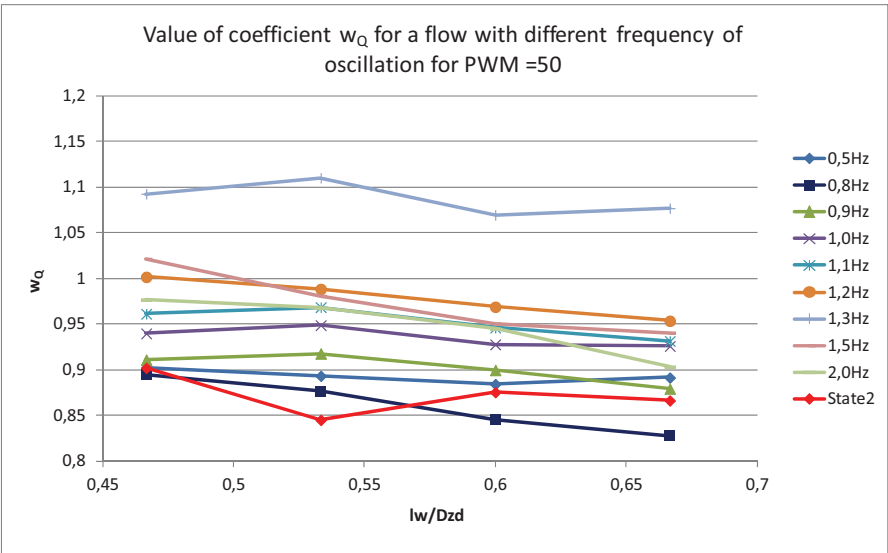


Fig. 7. Value of indicator w_q , for PWM =50, for different values of frequencies of the control signal in function l_w/Dzd

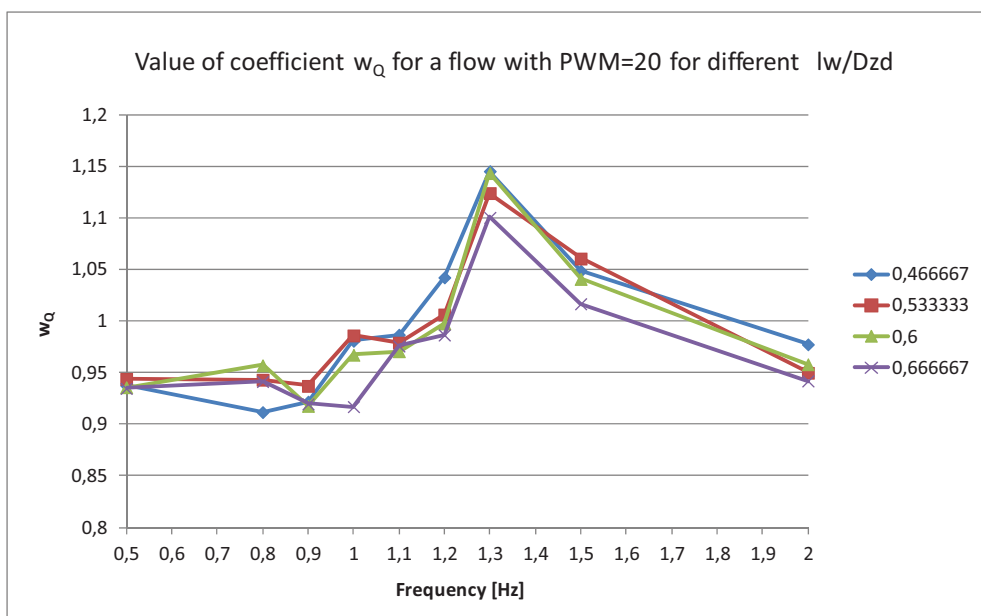


Fig. 8. Values of coefficient w_Q for l_w/D_{zd} in function of frequencies of the control signal f_c

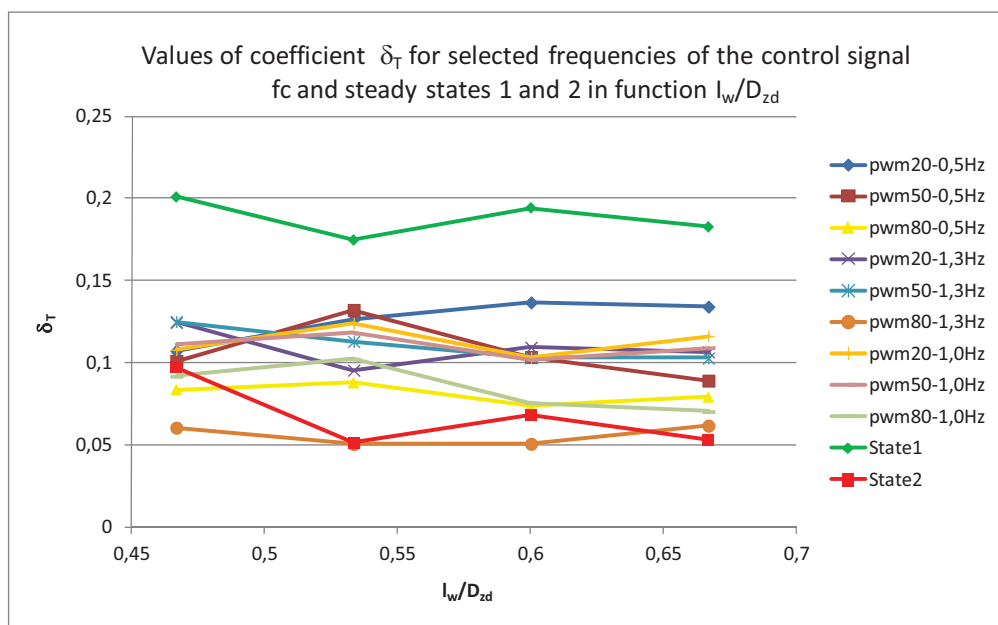


Fig. 9. Values of coefficient δ_T for selected frequencies of the control signal f_c and steady states 1 and 2 in function l_w/D_{zd}

5. Discussion and conclusion

In effect of changing parameters of the air stream flowing out of a nozzle there have been obtained different values of indexes describing the heat exchange process.

Form the point of view of the heat exchange process intensification (heating), the most important parameter affecting the process course is the frequency of change of the flowing out air stream steady state (parameter f_c). For the accepted range of low frequencies the obtained results definitely indicate that the frequency with value $f_c = 1.3\text{Hz}$ increases the amount of heat taken over by the wall from the air flowing around it. For the remaining six out of nine values of the control stream frequency there have been obtained values of index w_q smaller than 1, which indicates a reduction of the heat amount taken over by the wall. The influence of f_c frequency is particularly well seen in figure 8.

From the point of view the temperature distribution on the examined element the most important thing is the filling space of PWM signal (fig.9). On the basis of conducted tests it can be found that the most uniform temperature distributions on the heated element can be obtained for high values of PWM. The highest value of the temperature non-uniformity coefficient was reached for the flow in the first steady state. However, the highest values of the heated wall have been reached for this state.

Application of a controlled stream element and an appropriate match of the air stream outflow parameters enables enhancing the heat exchange process and shaping the temperature distribution on the heated element (flat wall).

References

- [1] Trávníček, Z., Tesař, V., Kordík, J., *Performance of synthetic jet actuators based on hybrid and double-acting principles*, Journal of Visualization 11 (3) 221–229 (2008).
- [2] Broučková, Z., Kordík, J., Trávníček, Z., *Aktivní řízení anulárního proudu radiálním syntetizovaným proudem*, Praha, Ústav termomechaniky AVČR v. v. i, 56 s, 2009.
- [3] Wawrzyniak, S., *Shaping of working parameters of monostable power fluidics element in order of heat transfer* (in Polish: Kształtowanie parametrów roboczych monostabilnego elementu strumieniowego dużej mocy w aspekcie jakości procesu wymiany ciepła), PhD thesis, University of Technology and Life Sciences in Bydgoszcz, 2008.
- [4] Wawrzyniak, S., *Position for research of influence of air flow oscillations on temperature of electronic components*, 14 International Conference on Developments in Machinery Design and Control 2010, Gliczarów Górny 07-10.09-2010.
- [5] Wawrzyniak, S., *Stanowisko do badania właściwości przepływowych dyszy osiowosymetrycznej*, Pneumatyka – przemysłowe systemy sprężonego powietrza, str. 25-28, nr 3/68/2008.
- [6] Wawrzyniak, S., *Axi-symmetric nozzle research methodology*, 12 International Conference on Developments in Machinery Design and Control 2008, Nowogród 09-12.09-2008.
- [7] Wawrzyniak, S., Nowicki, K., *Analiza numeryczna rzeczywistego przepływu powietrza za dyszą osiowosymetryczną*, PNEUMA 2004, Bydgoszcz – Wiktrowo, artykuł w Pneumatyka 4(47) 2004, str.34-36.
- [8] Wawrzyniak, S., Peszyński, K., *Continuous visualization of flow in power fluidic elements and basic analysis*, National Conference with International Participation ENGINEERING MECHANICS 2003, Svratka, Czech Republic, pp. 248-249.
- [9] Wawrzyniak, S., Peszyński, K., *Preliminary study into thermal properties of controlled axi-symmetric nozzle*, INŽENÝRSKÁ MECHANIKA 2005 Svratka, Česká republika, 9-12.05.2005.



INFLUENCE OF BASIC TURBOFAN ENGINE PARAMETERS ON MULTIPURPOSE AIRCRAFT MANEUVERS INDEXES

Piotr Wygonik

Rzeszow University of Technology
al. Powstańców Warszawy 12, 35-959 Rzeszów, Poland
tel. +48 17 865 12 41, fax: +48 17 865 19 42
e-mail: piowyg@prz.edu.pl

Abstract

The problem described in the paper concerns the choice strategy of so-called design point of the flow engine in a multi-role aircraft at the initial stage of aircraft and engine design as the aviation system. The design point is defined by the height and speed of flight and engine parameters of heat flow which allows in particular to determine the mass and dimensions of the engine. The following analysis represents an attempt to seek other than the classic (based on a maximum within unitary thrust, specific fuel consumption) criteria for calculation point for the multi-role aircraft. Multipurpose aircraft, during every mission, very often must perform many tasks and at the same time must use the energy source for the maneuvers. The mathematical model of the chosen tasks of an aircraft has been presented, which due to the energetic requirements do not allow to build the uniform optimization criteria. The models of such flight stages have been presented: take off, climbing with the maximum velocity and the maximum angle of climb, horizontal flight both sub-and supersonic, turn determined. In order to make the considerations easier the engine model was reduced to two parameters: non-dimensional loading coefficient and the coefficient of relative engine measure. During the conducted calculations the values of the non-dimensional coefficients were determined allowing to optimize the tasks performed by the aircraft during the mission. By making comparisons of the determined characteristics the acceptable values of the non-dimensional engine coefficients were shown and the assessment criteria of the aircraft manoeuvre properties vital for the realization of the entirety of its mission were presented.

Keywords: multipurpose aircraft, airplane engine integration, turbofan engines, engine thrust

1. Introduction

In the process of aircraft designing the right strategy of the aircraft and engine characteristics is of the great importance in order to get the system capable of performing certain air tasks with the smallest energetic expenditure. The energetic possibilities of an aircraft depend on the parameters and characteristics of the power unit. The power unit should ensure required by an aircraft performance properties at all stages of air task i.e. during the take off, climbing, overshoot and during the complex combat maneuver (turning, pull up, loop). The energetic requirements of an aircraft are fixed limitations for the engine designer. They determine the range of the possible changes in thermo-gas-dynamical parameters of the engine comparative cycle, its size, mass and the way of control. It is assumed that the characteristics of an aircraft for which the power unit is chosen are known. There are no publications in which the problem of the selection of engine parameters and determinations of its optimum characteristics for multi-purpose engine is described. These problems are partially described in [1,3], but the analyses concern the issues

connected with the optimization of the constructional scheme of an engine, not the physical aspects of the selection of engine parameters for an aircraft. The statistics of the chosen parameters of the engine comparative cycle [5] in operation, and the analyses results in [3] show that there is not a physical law, quality criterion, rule in an empirical sense, which constructors would take into account while choosing the engine parameters [1,3,5]. Even at the same temperature level T_3^* , some of the values π_s^* and α for the aircraft engines with the same purpose can differ, even twice. It shows that while choosing the engine parameters in many cases backs out of the analytical, optimum for the engine values. It is noticeable that there is no general tendency in the relation between parameters. There are known the following parameters: aircraft aerodynamic characteristics (polar), aircraft mass parameters and performed by an aircraft tasks – determined by the flight parameters such as flight velocity and flight height. The aim is to find the energetic engine parameters which will enable to determine (for the assumed criteria and limitations) the optimum adjustment of engine and aircraft characteristics for the realization of the required air task. For the models building the general non-dimensional parameters [5-7] were used. The parametrical analysis, conducted on the basis of the non-dimensional parameters, enables the main directions of optimum research of an engine and the aircraft as a whole to be found. In order to get to know the physical aspects connected with the choice of optimum thermal-flow parameters of the turbine engine and their influence on the aircraft characteristics we should:

- Show the assessment criterion of the aircraft performance and decide on their relation with the engine parameters,
- choose the design point for an engine (work range, flight conditions),
- choose engine parameters which would be subjected to optimization.

In the optimization tasks usually the simplified analytical models are used both for the aircraft and the engine. The required degree of simplifications is determined by the necessity and retaining the physical and qualitative compatibility of the analytical model with the researched model. One of the way to solve the task is the use, while model constructing, the general parameters of a non-dimensional form. It enables to decrease the number of variables in the task, and to decrease the dimension of the problem and avoid difficulties connected with recalculating a lot of solutions.

2.Mathematical model of aircraft and power unit

The aircraft movement in co-ordinate system connected with aircraft velocity has been presented in [1,2]. The aircraft movement equations introduced bellow have been written in a form which takes into account the dimensional character of variables. For the needs of the presented article the non-dimensional analysis was presented. The way of movement equations derivation considering the non-dimensional variables has been shown in [4,5]. For further considerations the basic relations have been reminded (presented in [5,6,7]). Non-dimensional coefficient S_{ZN} (called the geometrical parameter of engine adjustment to an aircraft), determining the relative engine dimension [4,5,6]:

$$S_{ZN} = \frac{iF_{Sil}}{F_{sk}}, \quad (1)$$

where:

F_{Sil} - engine cross- sectional area,

F_{SK} – aircraft wing area,

i – number of engines.

Aircraft range is one of the most important criteria of the assessment of aircraft performance properties. The calculations of the aircraft range depending on the flight conditions have been

presented in [1,2]. For the needs of the research the model of range determination has been chosen for the constant flight and the constant coefficient of aerodynamic lift (i.e. the height of flight changes). The dependence which describes the range for the above limitations is known as the Breguet formula [3]:

$$x = \frac{EaM_a}{gc_j} \ln \frac{1}{1 - \bar{m}_{pal}}, \quad (2)$$

where:

E- aircraft lift/drag ratio,

M_a - Mach number,

a- sound speed,

c_j - unitary fuel usage,

m_{pal} - relative mass of the burnt fuel

$$\bar{m}_{pal} = \frac{\Delta m}{m_s},$$

Δm - mass of the burnt fuel during the flight,

m_s – primary aircraft mass.

In fig. 1 there have been presented the differences in the range of subsonic and supersonic flight and the influence of the geometric parameter of an engine, i.e. the S_{ZN} value on the maximum value of the range [6]. The theoretical range of an aircraft during the subsonic flight achieves its maximum for the low values of S_{ZN} (almost half lower than the required values of parameter for the supersonic flights). During the supersonic flight the range decreases significantly and its extreme, as a S_{ZN} function shifts towards higher values of S_{ZN} . Very important information which results from the conducted calculations is the fact that the range expressed by the equation (2) has its extreme as for S_{ZN} .

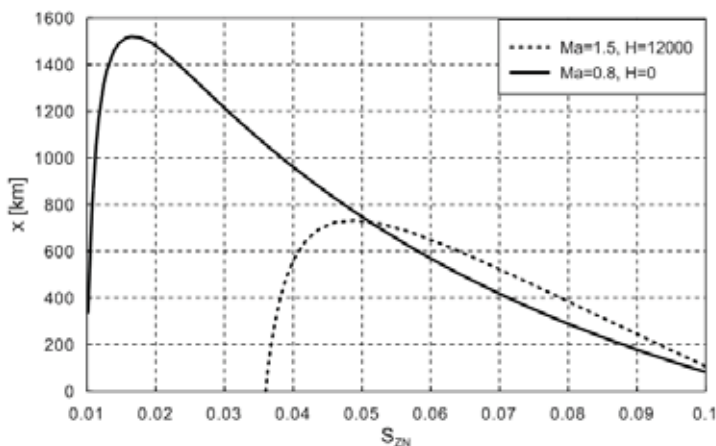


Fig. 1. Influence of the parameter of engine adjustment to the aircraft S_{ZN} on the theoretical range for the subsonic flight (full line) and supersonic flight (dashed line)

In [5] definition of non-dimensional coefficient of aircraft wings loading was presented:

$$\Psi_s = \frac{m_s g}{p_H F_{SK}}, \quad (3)$$

where:

m_s - aircraft mass,
 p_H – static pressure,

and non-dimensional coefficient of thrust loading [5]:

$$\nu = \frac{K_{sil} S_{ZN}}{\Psi_s}, \quad (4)$$

In equations(1-4) the parameters of engine K_{sil} (non-dimensional engine thrust [5]) depend on the engine characteristics. The formulas (1,3,5) which present the dimensionless parameters have the same properties as the physical parameters of the form "dimensioned" (related to) for a certain amount and speed of an aircraft. The author carried out statistical analysis (based on available catalogue information) that modern multirole aircraft such as the F-16, Gripen Jas 39 have at the start the coefficient $\nu \approx 1.2$ and $\psi_s = (0.028-0.042)$, while the heavier aircrafts such as the MiG 29, F-14 $\nu \approx 1.2-1.4$ and $\psi_s = (0.038-0.048)$.

3. Method of selection of engine and aircraft parameters

While selecting the power unit for the multipurpose aircraft it is necessary to show such parameters and criteria of engine assessment which ensure the realization of air tasks at the required energetic expenditure. The selection of engine parameters should be done on the basis of energetic criteria. The use of non-dimensional parameters, which later will be treated as "adjustment" parameters of engine to an aircraft enable to build the analytical model of the energetic system of the power unit-aircraft-air task. It makes possible further assessment of the influence of the accepted parameters of engine on the indexes of aircraft efficiency assessment. Taking into account the non-dimensional parameters as in (1-4), the equation of the aircraft movement (the way of its derivation) has been shown in detail in w [4,5,6]) and has the form of:

$$\nu = \frac{a}{g} \frac{dM_a}{dt} + \left(1 + \frac{a}{g} M_a^2 \frac{da}{dH} \right) \sin \Theta + \frac{1}{2} \frac{kc_x M_a^2}{\Psi_s}, \quad (5)$$

It is the formula, which for the assumed parameters of air task (M_a , H , ψ_s), allows to determine indispensable for flight value of ν coefficient. It is then assumed that the ν value determined on the basis of the aircraft flight conditions will be marked by the „N”- ν_N index. The first term of (5) equation means the value of the thrust loading coefficient for the case of horizontal acceleration, whereas the second one for the climbing with the constant velocity at the angle Θ , and the last term in (5) equation means the value of ν_N coefficient for the horizontal flight with constant velocity. On the other hand, the ν value can be determined for the power unit. This value, as a disposable value for the engine is marked by "R" index:

$$\nu_R = \frac{K_{sil} S_{ZN}}{\Psi_s}, \quad (6)$$

The above dependence enables to determine non-dimensional thrust loading coefficient and the relative fuel usage only when it is known the flight plan; that is the height change H and flight velocity Ma during the mission and there are known the engine characteristics.

4. Criteria of aircraft maneuvering

The significant criterion of maneuvering assessment of multipurpose aircraft is climbing. Following [2] and assuming that the total aerodynamic lift is on the aircraft plane and the vectors of thrust force are directed along the flight path of an aircraft, then the angle of the fastest climbing γ_{PWmax} will be determined from the following formula:

$$\sin \gamma_{PW \max} = \frac{\nu E_{PW \max}^2 - \sqrt{1 + E_{PW \max}^2 (1 - \nu^2)}}{1 + E_{PW \max}^2}, \quad (7)$$

where:

Lift/Drag ratio of the fastest climbing

$$E_{PW \max}^2 = \frac{6}{\nu \Gamma \left(1 + \frac{36 K c_{D0}}{\nu^2 \Gamma^2} \right)}$$

coefficient

$$\Gamma = 1 + \sqrt{1 + \frac{12 K c_{D0}}{\nu^2}}$$

c_{D0} – parasitic drag,

K – coefficient of aircraft polar.

The data for calculating the aircraft polar was taken from [1] for F-16 airplane. In fig. 2 there has been presented the dependence of the angle $\gamma_{PW \max}$ from ν coefficient in the borders (ν_{\min}, ν_{\max}).

The next characteristic flight stage is the right turn of an aircraft (without the sideslip). The right turning can be performed only when the bank angle of an aircraft Φ is bigger than zero [2]. The bank angle is determined by the G-load coefficient n :

$$n = \frac{1}{\cos \Theta}, \quad (8)$$

Substituting into equation (5) the expression (8), and assuming that the speed of the turn is constant, after the simple transformation (5) it was determined non-dimensional thrust loading coefficient ν for the right turn:

$$\nu = \frac{k M_a^2}{2} \left(\frac{c_{D0}}{\Psi_s} + \frac{4 \Psi_s K n^2}{(k M_a^2)^2} \right), \quad (9)$$

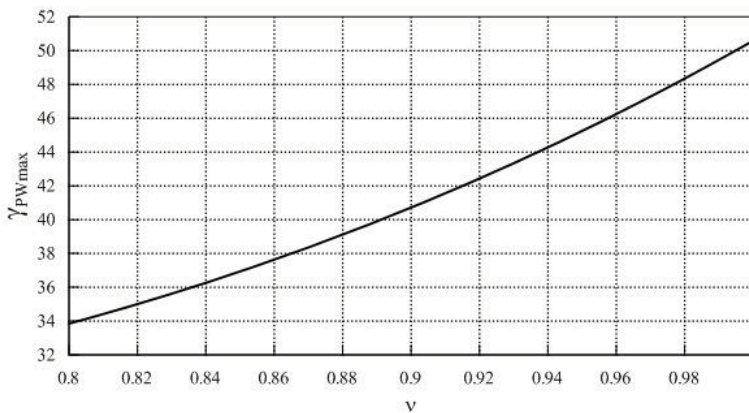


Fig. 2 Dependence of angle of fastest climbing $\gamma_{PW \max}$ from ν parameter

Formula (9) allows to determine the indispensable value of the ν coefficient depending on the n G-load coefficient and non-dimensional wing loading coefficient ψ_s , in which is “hidden” the

aircraft mass. On the G-load coefficient in turn there are imposed limitations which concern the situation when the aircraft mass is partially decreased by the mass of the used during the flight fuel and armament (so-called combat mass) and it is assumed that the coefficient $n=9$. On the other hand for the maximum take off mass the assumed value of the n G-load coefficient in turn is smaller and is $n=7$ [2].

The most important part of the aircraft mission is its take off. In the procedure calculations of aircraft take off it is better to assume the length of the take-off run L_S and determine for it the indispensable value of the thrust loading coefficient at the take off [5]:

$$v_S = \mu_S + \frac{\frac{k_S \zeta_S}{c_{Z_{\max}}}}{1 - e^{-\tau L_S}} , \quad (10)$$

where:

coefficients: $k_S = \frac{M_0}{M_S}$, $\tau = \frac{g k \zeta_S}{a^2 \psi_S}$,

M_S – stalling speed,

ζ_S - reduced coefficient of aircraft total resistance during takeoff [3,5,6],

$C_{Z_{\max}}$ – value of coefficient of aerodynamic lift in the conditions of take off.

5. Calculation example

To find limitations the calculations for exemplary aircraft data have been conducted. It was assumed that the take off mass of aircraft $m_s=10500$ [kg], the atmosphere parameters are according to the standards of International Standard Atmosphere [1]. At this stage of calculations there are not known the characteristics of engine that is why to simplify the considerations the calculations have been conducted for some values of ψ_S coefficient. It was assumed that this coefficient is the function of wing loading coefficient at the start ψ_{S0} according to the formula:

$$\Psi_S = k_m \Psi_{S0} , \quad (11)$$

Coefficient k_m determines the change of aircraft mass during the air mission, caused by the fuel usage and armament ($k_m=1$ – for takeoff mass, $k_m=0.55$ – aircraft without fuel and armament).

The change in value of coefficient ψ_S in function of H height has been presented in fig.3.

The decline in pressure connected with the growth in flight height causes the increase in the value of ψ_S coefficient. The lines which limit the graph show the border of the changes in values of the coefficient ψ_S for an aircraft depending on the flight height. During the take off the value of the coefficient in the accepted example is $\psi_{S0}=0.04$. In fig. 4 it has been presented the influence of values of ψ_S coefficient and the length of the run on the indispensable value of v coefficient.

Multipurpose aircraft can perform a number of tasks at various subsonic and supersonic velocities. The calculations on the influence of the ψ_S coefficient and flight velocity on the v coefficient during the horizontal flight with constant velocity were conducted and the results have been presented as graphs in fig. 5. The fulfillment of the requirement, obtaining the minimum value of the thrust indispensable during the turn performed at the given value of n G-load coefficient is important from the point of view of aircraft maneuvering has been presented in fig.6.

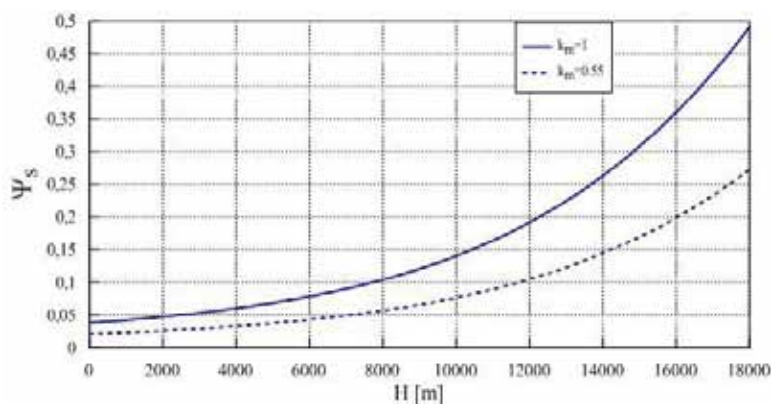


Fig.3 Change of values of coefficient ψ_s together with the growth of flight height for two values of coefficient k_m . ($k_m=1$ – for takeoff mass, $k_m=0.55$ – aircraft without fuel and armament)

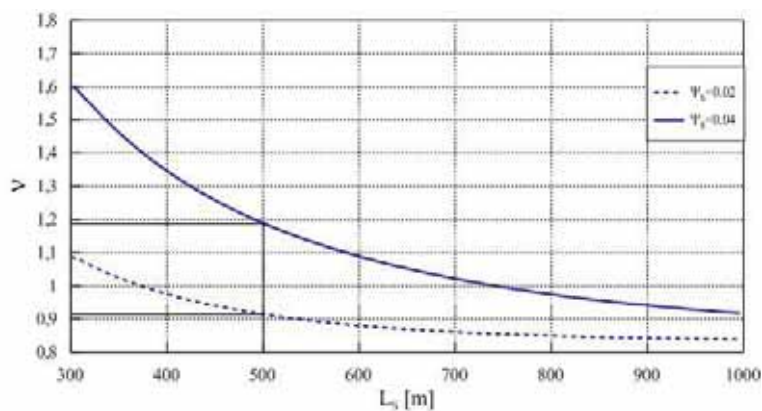


Fig. 4 Influence of run way L_s and ψ_s coefficient on the value during the take off. The calculations for two values $\psi_s = \psi_{s0} = 0.04$, and $\psi_s = 0.02$ (for $k_m = 0.55$)

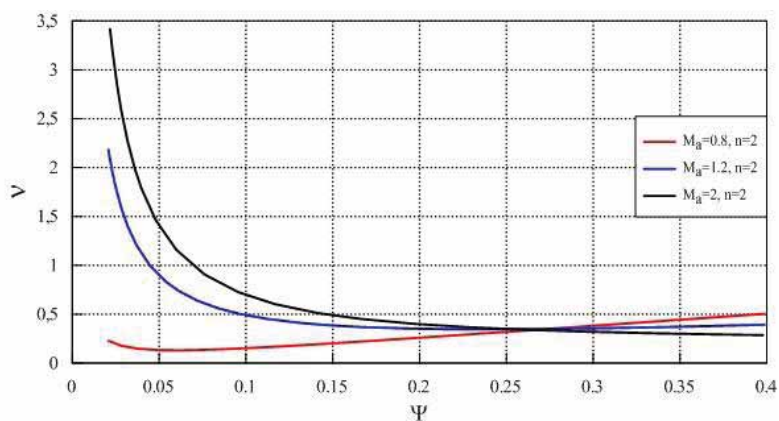


Fig.5 The influence of flight velocity and changes of ψ_s coefficient on the value coefficient v during the steady horizontal flight

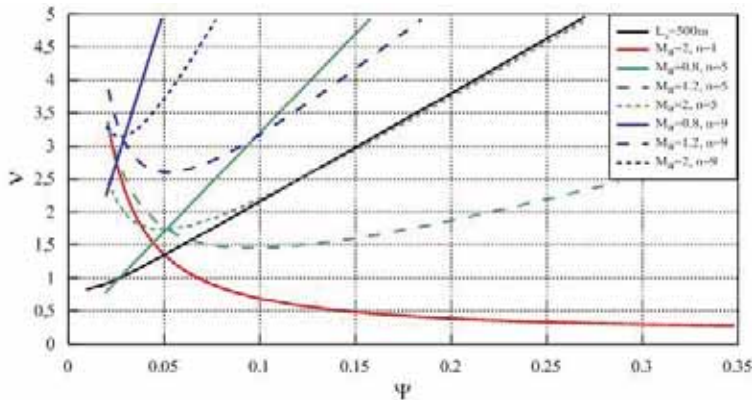


Fig.6 Influence of some chosen aircraft flight conditions and changes of wing loading coefficient ψ_s on indispensable for flying value of wing loading coefficient ν

In fig. 6 there have been presented the requirements for the ν coefficient, critical with regard to v stages of flight. From the graph in fig. 6 one can assume that in order to perform the turn with the high values of n G-load coefficient the flights with high wing loading (big aircraft mass) require the big values of the indispensable thrust, which exceeds the requirements for the take off.

In fig. 6 there have been presented the requirements for the ν coefficient, critical with regard to v stages of flight.

6. Conclusions

Each curve presented in fig. 5, 6 is the borderline value for ν , at the given flight velocity and ψ_s (aircraft mass). The biggest requirements because of the ν value concern the turn (in figures $n=1$) at small flight velocities as the growth gradient ν together with the growth of the flight height (grows ψ_s) is the biggest among all the presented curves. The requirement of the horizontal flight with the constant supersonic velocity is not a limitation at big heights. The consequence of the maneuver choice which determines the loading ν during the aircraft flight is to determine the values of the indispensable coefficient, non-dimensional thrust loading which must be counterbalanced by the power unit and the thrust depended on the thermo-gas-dynamical parameters. An analysis of the graphs of Figure (1-6) provides information about the limitations for the propelling set (by ν parameter) of the plane depending on the mission (subsonic, supersonic, mixed). The study shows that supersonic, maneuvering flight is a criterion for the selection of the engine (not even the take off of the airplane). The application of dimensionless parameters to the analysis of the aircraft powerplant can significantly simplify the analysis, and allows the testing of the influence of the engine characteristics directly on the mission done. This results directly from the definition adopted by the parameters in their current form because they involve the engine, aircraft and mission. They are therefore a higher level parameters of performance compared to a conventionally used in the literature of the unitary and specific fuel consumption. All the presented in the analysis dimensionless parameters are sensitive to changes in flight conditions and characteristics of the engine and can be considered as criteria for assessing the quality and quantity of air engine system - airplane - air mission. There are conducted further simulations to examine the influence of engine thermal-gas parameters (static pressure, temperature before the turbine, the by-pass degree) on the value of the parameter ν , S_{zn} , ψ .

References

- [1] Filippone A., *Flight performance of fixe and rotary wing aircraft*; Elsevier Ltd. 1998
- [2] Goraj Z., *Dynamika i aerodynamika samolotów manewrowych z elementami obliczeń*. Biblioteka Naukowa Instytutu Lotnictwa, Warszawa 2001.
- [3] Orkisz M., *Podstawy doboru turbinowych silników odrzutowych do płatowca*. Biblioteka Naukowa Instytutu Lotnictwa, Warszawa 2002.
- [4] Rumiancev S.W., Sgilevskij W.A., *Sistemnoe projektirovanie awiacionnovo dwigatela.*, Izdatelstwo MAI, Moskva 1991 (in russian)
- [5] Wygonik P., *Kryteria doboru parametrów silnika turbinowego do samolotu wielozadaniowego*. Silniki Spalinowe, 4/2006.
- [6] Wygonik P., *The influence of on-design bypass turbine engine parameters on multipurpose aircraft mission energy-consuming*, Journal of KONES Powertrain and Transport, Vol.17, No.1/2010.
- [7] Wygonik P., *Determining of the optimum size of turbo fan engine for obtaining the maximum range of multipurpose-airplane*, Journal of KONES Powertrain and Transport, Vol.17, No. 2/2010.



THE USAGE OF MULTI-EQUATION MODELS IN THE ANALYSIS OF DYNAMIC PROCESS IN MARINE DIESEL ENGINE RESEARCH

Ryszard Zadrag

*Polish Naval Academy
Faculty of Mechanical and Electrical Engineering
ul. Śmidowicza 69, 81-103 Gdynia, Poland
r.zadrag@amw.gdynia.pl*

Marek Zellma

*Polish Naval Academy
Faculty of Mechanical and Electrical Engineering
ul. Śmidowicza 69, 81-103 Gdynia, Poland
m.zellma@amw.gdynia.pl*

Abstract

Contemporary empirical researches on the object, which is combustion engine, are processed basing on the theory of experiment. Available software applications to analyze the experimental data commonly use the multiple regression models, which enables studying effects and interactions between input values of the model and single output variable. Using multi-equation models gives free hand at analyzing measurement results because it enables analysis of effects and interaction of many output variables. It also allows analysis of the measurement results during dynamic process. In this paper author presents advantages of using the multidimensional regression model on example of researches conducted on engine test stand.

Keywords: *diagnostic, theory of experiments, marine diesel engine, exhaust gas toxicity, multi-equation models*

1. Introduction

During the working process of the engine, its structure parameters are changing. It doesn't affect its performance, described by a set of output parameters. The reciprocal relationship between the parameters of the structure and parameters of the motor output allows under certain conditions to treat the symptoms of the output parameters as engine condition, measured without dismantling, because the physicochemical processes occurring during the working process and figures describing them can generally be observed and measured from the outside. These figures include the value of the emission of exhaust components.

This simple combination is of interest to writers and aims to analyze the suitability and performance indicators to evaluate the emission parameters of the engine structure. At this point however, a comment is in place, as in the classical sense, output parameter can be regarded as diagnostic only while meeting the characteristics, that is: uniqueness, of sufficient width of the

change field and availability. Thus, should the indicators and emission characteristics be considered a diagnostic parameter?

Given the complicated measure, the cost of equipment, and the ambiguity of (the presence of extremes), and the characteristics of toxic compounds, a negative answer comes to mind. Nevertheless, the rapid development of measurement methods, progressively more advanced analyzers with increasing measurement power, ie: speed and capacity of archiving items, which make the signal of changes in emissions of toxic compounds more useful, carrying more and more information useful for subsequent analysis.

The above approach goes as far as to impose a need to use the theory in empirical research experiment. The primary objective of this research work is to demonstrate the relationship between the input signals (introduced by the investigator), and the output signals (seen by him). The ultimate goal of statistical analysis of measurement results is to define a function of the test object and an empirical model of a functional engine. Very extensive calculations using probability theory, stochastic processes, and calculus that are associated with this task are very labor intensive and without the use of computer technology and specialized software, it is impracticable. In the process of solving problems of inter-linkages and complementary aspects of approximation, the correlation statistics, assessment of the relevance and measurement uncertainty as well as the adequacy of test object's functions, including questions of mathematical and graphical determination of singular points, available computer programs are used, including the package STATISTICA PL.

It should be emphasized that the statistical computer analysis can involve a number of models that do not include interaction and do not take into account the interactions of varying degrees of involvement adopted to describe the model input variables. At the same time there is a possibility in the statistical analysis to reject (ignore) both freely chosen input variables describing the object of research as well as the various types of interactions. This means that choosing the right (most appropriate) model depends on the operator, and their expertise and specialized knowledge of the theoretical basis of the discussed issue.

While assuming a less accurate representation of reality, practically determining the nature of change (trend) output quantities, there is the possibility of significant simplification of approximating polynomials by considering only the input variables and their only statistically significant interactions. The complexity of the model and the degree of entanglement of the basic volumes are also strongly determined by the degree of approximating polynomials. Hence it is reasonable to seek to create models of a possibly simple form, and most preferably linear models. It is assumed that due to the possibility of errors, it is better to describe the studied problem of non-linear nature with small linear segments than a non-linear description of a complex whole.

The software commonly used in the field of experimental design and subsequent analysis does not provide the freedom to analyze the collected material, and uses ready analysis diagrams described above. Thus, interfering with the program (software package) itself is not possible. The recently observed development of the social sciences, medicine and economics has caused rapid progress in the application of statistical methods, securing planning of the experiment [1,2,3,5,6]. In this area, econometrics in particular has some great achievements, and the new approach to statistical analysis used there can be successfully implemented in technical studies [1,2]. Among other things, the use of multi-equation models (models with interdependent equations) makes it possible to study not only the correlation between the input and output, but also take into account the feedback between output variables and thereby give the possibility of direct analysis. This assumption, as opposed to the commonly used multiple linear regression, is closer to reality even while taking into account the dilemma of diesel, that is the relationship between the concentration of CO, HC and NO_x concentration.

This approach was presented by the authors including the earlier works, where the results of research on the engine fuel supply system (fuel injection) and charge exchange system (with

particular emphasis on TPC) were presented using a divalent fractional plan and a multi-equation model [7, 8, 9, 10, 11].

The multi-equation model relations between input signals and output signals can be described by a system of linear equations

$$\begin{aligned}
y_1 &= b_{12}y_2 + b_{13}y_3 + b_{14}y_4 + \cdots + b_{1M}y_M + a_{10} + a_{11}x_1 + a_{12}x_2 + \cdots + a_{1N}x_N + \xi_1 \\
y_2 &= b_{21}y_1 + b_{23}y_3 + b_{24}y_4 + \cdots + b_{2M}y_M + a_{20} + a_{21}x_1 + a_{22}x_2 + \cdots + a_{2N}x_N + \xi_2 \\
y_3 &= b_{31}y_1 + b_{32}y_2 + b_{34}y_4 + \cdots + b_{3M}y_M + a_{30} + a_{31}x_1 + a_{32}x_2 + \cdots + a_{3N}x_N + \xi_3 \\
&\vdots \\
y_M &= b_{M1}y_1 + b_{M2}y_2 + \cdots + b_{MM-1}y_{M-1} + a_{M0} + a_{M1}x_1 + a_{M2}x_2 + \cdots + a_{MN}x_N + \xi_M
\end{aligned} \tag{1}$$

where:

$y_i, i = 1, 2, \dots, M$ - explained variable (output),

$x_j, j = 1, 2, \dots, N$, - the explanatory variables (input),

b_{ij} – is a factor present in the i -th equation with j -th being the explained variable (output),
 $i, j = 1, 2, \dots, M$

a_{ij} - is a factor present in the i -th equation with j -th being the explanatory variable (input),
 $i = 1, 2, \dots, N, \quad j = 0, 1, \dots, N,$

ξ_i - is a non-observable random component in the i -th equation.

The solution of the equation (1) is reduced to its matrix form

$$\mathbf{BY} = \mathbf{AX} + \boldsymbol{\xi} \quad (2)$$

where A, B, ξ – matrix of coefficients,

and the selection of the coefficients in the equations (1) with the values of the input signals known from measurements on the real object. The next step is to bring the equation (2) to the reduced form

$$\mathbf{Y} = \mathbf{P}\mathbf{X} + \boldsymbol{\eta} \quad (3)$$

where: $\Pi := B^{-1}A$, $\eta := B^{-1}\xi$.

As a result, after verifying the significance of coefficients and, consequently, the rejection of insignificant values, correlations between equations describing the output variables, both the input variables and the remaining output variables, are obtained.

Multi-equation models, as demonstrated by the earlier works of the authors, show a significant adjustment to the value obtained in the experiment [7,8,9,10,11]. However, they describe the changes in the output parameters (indicators of toxic compounds) in steady states of the engine, when the influence of structural parameters is not the greatest. Hence the problem with the wide variety of changes in the output parameter. The situation changes when we do an analysis of the changes in output parameters during transient processes. In the course of its duration, due to, among other things, imperfections of control systems, there is a chance of a repeated, though usually short-term instances when the parameter values are exceeded in comparison to the set

Using these somewhat detrimental to the engine operating states, it was decided to implement tested in steady-state multi-equation models for analysis of dynamic processes.

Assuming that the process of changing the exhaust emissions occurs over time, which means it is dynamic, the multi-equation model can be described with a system of linear differential equations. Since the measurement of the concentration of toxic compounds is a discrete measurement, the time-discrete signal (time sequence) is a function whose domain is the congregation of integers. Thus, a discrete-time signal is a sequence of numbers. This kind of sequences will continue to be recorded in the functional notation.

The relations between the input signals $x_1[k], x_2[k], \dots, x_n[k]$, and output signals $y_1[k], y_2[k], \dots, y_m[k]$, $k = 0, 1, 2, \dots$, will be described by a system of linear differential equations.

[illegible]

$y_i[k], i = 1, 2, \dots, m$ - output signal values at k,

a_{ij} – is a coefficient found in i -th equation with j -th output signal, $i, j = 1, 2, \dots, m$

b_{ji} - is a coefficient found in i -th equation with j -th input signal, $i = 1, 2, \dots, m$, $j = 0, 1, \dots, n$,

ξ_i - is a non-observable random component in i -th equation.

$$\mathbf{y}[k+1] = \mathbf{A}\mathbf{y}[\mathbf{k}] + \mathbf{B}\mathbf{x}[\mathbf{k}] + \xi \quad (5)$$
$$\mathbf{B} = \begin{bmatrix} b_{11} & b_{12} & \cdots & b_{1m} \\ b_{21} & b_{22} & \cdots & b_{2m} \\ \cdots & \cdots & \cdots & \cdots \\ b_{m1} & b_{m2} & \cdots & b_{mm} \end{bmatrix}, \quad \mathbf{A} = \begin{bmatrix} a_{11} & a_{12} & \cdots & a_{1n} \\ a_{21} & a_{22} & \cdots & a_{2n} \\ \cdots & \cdots & \cdots & \cdots \\ a_{m1} & a_{m1} & \cdots & a_{mn} \end{bmatrix},$$

$$\mathbf{y}[k] = \begin{bmatrix} y_1[k] \\ y_2[k] \\ \dots \\ y_m[k] \end{bmatrix}, \quad \mathbf{y}[k+1] = \begin{bmatrix} y_1[k+1] \\ y_2[k+1] \\ \dots \\ y_m[k+1] \end{bmatrix}, \quad \mathbf{x}[\mathbf{k}] = \begin{bmatrix} x_1[k] \\ x_2[k] \\ \dots \\ x_n[k] \end{bmatrix}, \quad \boldsymbol{\xi} = \begin{bmatrix} \xi_1 \\ \xi_2 \\ \dots \\ \xi_m \end{bmatrix}.$$

Later denoting:

$$\mathbf{C} = \begin{bmatrix} c_{11} & c_{12} & \dots & c_{1m} & c_{1m+1} & c_{1m+2} & \dots & c_{1m+n} \\ c_{21} & c_{22} & \dots & c_{2m} & c_{2m+1} & c_{2m+2} & \dots & c_{2m+n} \\ \vdots & \vdots & \ddots & \vdots & \vdots & \vdots & \ddots & \vdots \\ c_{m1} & c_{m1} & \dots & c_{mn} & c_{mn} & c_{mn+1} & \dots & c_{mn+n} \end{bmatrix}, \quad \boldsymbol{\eta} = \begin{bmatrix} \eta_1 \\ \eta_2 \\ \vdots \\ \eta_m \end{bmatrix},$$

$$c_{iv}[k] = b_{iv}[k], \text{ dla } v = 1, 2, \dots, m, \quad c_{iv}[k] = a_{iv}[k], \quad \text{ dla } v = m+1, m+2, \dots, m+n, \quad (6)$$

$$\mathbf{z}[k] = \begin{bmatrix} z_1[k] \\ \vdots \\ z_m[k] \\ z_{m+1}[k] \\ \vdots \\ z_{m+n}[k] \end{bmatrix},$$

$$z_v[k] = y_v[k], \text{ dla } v = 1, 2, \dots, m, \quad z_v[k] = x_{v-m}[k], \quad \text{ dla } v = m+1, m+2, \dots, m+n,$$

system of equations (4) and functionals (6) are shown in reduced form

$$\mathbf{y}[k+1] = \mathbf{C} \mathbf{z}[k] + \boldsymbol{\eta}. \quad (7)$$

By identifying the system of equations (1), (4) we get to understand a problem of selecting coefficients using the values determined by real property measurements

$$\tilde{x}_1[k], \tilde{x}_2[k], \dots, \tilde{x}_n[k], \quad k = 0, 1, 2, \dots, N \text{ input signals } x_1, x_2, \dots, x_n$$

and values

$$\tilde{y}_1[k], \tilde{y}_2[k], \dots, \tilde{y}_m[k], \quad k = 0, 1, 2, \dots, N+1 \text{ input signals } y_1, y_2, \dots, y_m,$$

in $t_k = kT$ instants.

Measured values can be written in matrix form (8):

$$\tilde{\mathbf{X}} = [e_1 | e_2 | \dots | e_m | e_{m+1} | e_{m+2} | \dots | e_{m+n}] = \begin{bmatrix} \tilde{y}_1[0] & \tilde{y}_2[0] & \dots & \tilde{y}_m[0] & \tilde{x}_1[0] & \dots & \tilde{x}_n[0] \\ \tilde{y}_1[1] & \tilde{y}_2[1] & \dots & \tilde{y}_m[1] & \tilde{x}_1[1] & \dots & \tilde{x}_n[1] \\ \vdots & \vdots & \vdots & \vdots & \vdots & \vdots & \vdots \\ \tilde{y}_1[N] & \tilde{y}_2[N] & \dots & \tilde{y}_m[N] & \tilde{x}_1[N] & \dots & \tilde{x}_n[N] \end{bmatrix}$$

Coefficients $b_{i1}, \dots, b_{im}, a_{im+1}, \dots, a_{im+n}$, $i = 1, 2, \dots, m$, of the above system of equations are chosen specifically so functional (9)

$$J_i(b_{i1}, \dots, b_{im}, a_{i(m+1)}, \dots, a_{i(m+n)}) = \sqrt{\sum_{k=1}^N (a_{i1}\tilde{y}_1[k] + \dots + a_{im}\tilde{y}_m[k] + b_{i(m+1)}\tilde{x}_1[k] + \dots + b_{i(m+n)}\tilde{x}_n[k] - \tilde{y}_i[k+1])^2},$$

reaches a minimum for $i = 1, 2, \dots, m$.

In the denotations adopted above (6), functionals (9) can be written as (10)

$$J_i(c_{i1}, c_{i2}, \dots, c_{i(m+n)}) = \sqrt{\sum_{k=0}^N (c_{i1}\tilde{z}_1[k] + \dots + c_{im}\tilde{z}_m[k] + c_{i(m+1)}\tilde{z}_{m+1}[k] + \dots + c_{i(m+n)}\tilde{z}_{m+n}[k] - \tilde{y}_i[k+1])^2},$$

$$i = 1, 2, \dots, m, \quad \tilde{z}_\nu[k] = \tilde{y}_\nu[k], \text{ dla } \nu = 1, 2, \dots, m, \quad \tilde{z}_\nu[k] = \tilde{x}_{\nu-m}[k], \text{ dla } \nu = m+1, m+2, \dots, m+n.$$

Matrix (8) is essentially a system of linearly independent vectors in Hilbert space

$$\mathbf{e}_1 = \begin{bmatrix} \tilde{y}_1[0] \\ \tilde{y}_1[1] \\ \vdots \\ \tilde{y}_1[N] \end{bmatrix}, \mathbf{e}_2 = \begin{bmatrix} \tilde{y}_2[0] \\ \tilde{y}_2[1] \\ \vdots \\ \tilde{y}_2[N] \end{bmatrix}, \dots, \mathbf{e}_m = \begin{bmatrix} \tilde{y}_m[0] \\ \tilde{y}_m[1] \\ \vdots \\ \tilde{y}_m[N] \end{bmatrix}, \mathbf{e}_{m+1} = \begin{bmatrix} \tilde{x}_1[0] \\ \tilde{x}_1[1] \\ \vdots \\ \tilde{x}_1[N] \end{bmatrix}, \dots, \mathbf{e}_{m+n} = \begin{bmatrix} \tilde{x}_n[0] \\ \tilde{x}_n[1] \\ \vdots \\ \tilde{x}_n[N] \end{bmatrix}.$$

The issue of choosing the best model out of the class of equations (11) in the sense of minimizing the quality coefficient of identification was solved using the orthogonal projection theorem [3,6]. Given the vastness of the issue, the shift leading to the equation in matrix form was omitted

$$\mathbf{G}(\mathbf{C}_i^0)^T = \mathbf{W}_i, \quad (12)$$

where:

$$G = \begin{bmatrix} \sum_{k=0}^N \tilde{y}_1[k]\tilde{y}_1[k] & \dots & \sum_{k=0}^N \tilde{y}_m[k]\tilde{y}_1[k] & \sum_{k=0}^N \tilde{x}_1[k]\tilde{y}_1[k] & \dots & \sum_{k=0}^N \tilde{x}_n[k]\tilde{y}_1[k] \\ \dots & \dots & \dots & \dots & \dots & \dots \\ \sum_{k=0}^N \tilde{y}_1[k]\tilde{y}_m[k] & \dots & \sum_{k=0}^N \tilde{y}_m[k]\tilde{y}_m[k] & \sum_{k=0}^N \tilde{x}_1[k]\tilde{y}_m[k] & \dots & \sum_{k=0}^N \tilde{x}_n[k]\tilde{y}_m[k] \\ \dots & \dots & \dots & \dots & \dots & \dots \\ \sum_{k=0}^N \tilde{y}_1[k]\tilde{x}_1[k] & \dots & \sum_{k=0}^N \tilde{y}_m[k]\tilde{x}_1[k] & \sum_{k=0}^N \tilde{x}_1[k]\tilde{x}_1[k] & \dots & \sum_{k=0}^N \tilde{x}_1[k]\tilde{x}_n[k] \\ \dots & \dots & \dots & \dots & \dots & \dots \\ \sum_{k=0}^N \tilde{y}_1[k]\tilde{x}_n[k] & \dots & \sum_{k=0}^N \tilde{y}_m[k]\tilde{x}_n[k] & \sum_{k=0}^N \tilde{x}_1[k]\tilde{x}_n[k] & \dots & \sum_{k=0}^N \tilde{x}_n[k]\tilde{x}_n[k] \end{bmatrix} = \tilde{\mathbf{X}}^T \tilde{\mathbf{X}}$$

$$(\mathbf{C}_i^0)^T = \begin{bmatrix} c_{i1}^0 \\ \vdots \\ c_{im}^0 \\ c_{im+1}^0 \\ \vdots \\ c_{im+n}^0 \end{bmatrix}, \quad \mathbf{W}_i = \begin{bmatrix} \sum_{k=0}^N \tilde{y}_i[k+1] \tilde{y}_1[k] \\ \vdots \\ \sum_{k=0}^N \tilde{y}_i[k+1] \tilde{y}_n[k] \\ \sum_{k=0}^N \tilde{y}_i[k+1] \tilde{x}_1[k] \\ \vdots \\ \sum_{k=0}^N \tilde{y}_i[k+1] \tilde{x}_n[k] \end{bmatrix} = \tilde{\mathbf{X}}^T \tilde{\mathbf{y}}_i[k+1]$$

Thus, the matrix equation (12) can be expressed as

$$(\tilde{\mathbf{X}}^T \tilde{\mathbf{X}})(\mathbf{C}_i^0)^T = \tilde{\mathbf{X}}^T \tilde{\mathbf{y}}_i[k+1] \quad (13)$$

Which gives

$$(\mathbf{C}_i^0)^T = (\tilde{\mathbf{X}}^T \tilde{\mathbf{X}})^{-1} \tilde{\mathbf{X}}^T \tilde{\mathbf{y}}_i[k+1], \quad i = 1, 2, \dots, m \quad (14)$$

Thus, the optimal coefficients

$$c_{ij}^0, \quad i = 1, 2, \dots, m, \quad j = 1, \dots, m, m+1, \dots, m+n.$$

of the reduced model form (10) can be determined from the equation

$$(\mathbf{C}^0)^T = (\tilde{\mathbf{X}}^T \tilde{\mathbf{X}})^{-1} \tilde{\mathbf{X}}^T \tilde{\mathbf{Y}}[k+1] \quad (15)$$

$\tilde{\mathbf{X}}_{(N+1) \times (m+n)}$ - matrix of measured values of signals $y_1, y_2, \dots, y_n, x_1, x_2, \dots, x_m$,

$\tilde{\mathbf{X}}_{(m+n) \times (N+1)}^T$ - transposed matrix to the matrix of measured values of input signals,

$(\tilde{\mathbf{X}}^T \tilde{\mathbf{X}})_{(N+1) \times (N+1)}^{-1}$ - inverse to the Gram matrix $\mathbf{G}_{(N+1) \times (N+1)}$,

$\tilde{\mathbf{Y}}_{(N+1) \times m}[k+1]$ - matrix of measured values of output signals y_1, y_2, \dots, y_m ,

$\tilde{\mathbf{Y}}_{m \times (N+1)}^T$ - transposed matrix to the matrix of measured values of output signals,

N - number of measurements, n - number of input signals, m - number of output signals.

3. The study of dynamic process in engine fuel supply system through multi-equation models

The object of this research was the engine fuel supply system (fuel injection) of a single-cylinder test engine 1-SB installed in the Laboratory of the Exploitation of Marine Power Plants at the Naval Academy (10). The experimental material was collected by a bivalent fractional plan. The implementation of specific measuring systems (measuring points) of the above experiment design were performed using a programmable controller, which allowed a high repeatability of dynamic processes. The period between an onset of the clipping of injection system components and the re-stabilization of output quantities was adopted as the duration of the dynamic process. This period was chosen through a series of experiments, and it averaged to about 320 seconds.

In order to identify the impact of the technical condition of the fuel supply system on the parameters of the engine power during dynamic processes, sets of input quantities (preset parameters) and output quantities (observed parameters) were defined. For the purpose of this study a set of input quantities X was limited to three elements, that is: x_1 - engine speed n [r/min]; x_2 - engine torque T_{iq} [N·m]; x_3 - coking of the spray nozzle S_k [μm^2].

Similar treatment was applied to the set Y of output quantities, limiting the number of its elements to only the primary toxic compounds in exhaust manifold: y_1 - concentration of carbon monoxide

in the exhaust manifold $C_{CO(k)}$ [ppm]; y_2 – concentration of hydrocarbons in the exhaust manifold $C_{HC(k)}$ [ppm]; y_3 – concentration of nitrogen oxides in the exhaust manifold $C_{NOx(k)}$ [ppm]. Changes of the input and output quantities during the dynamic process are shown in Fig. 1.

Statistical identification was made using GRETL [2]. Estimation of the equation coefficients for specific output variables was performed using the least-squares method and it had to verify the significance of its parameters and, consequently, the rejection of insignificant values, which consequently led to a significant simplification of the models. Equations describing the changes in concentration of hydrocarbons (y_2) and the concentration of nitrogen oxides (y_3) have undergone the greatest simplification. (Table 2, 3). In the case of the equation describing the change of hydrocarbons in a way that they depend significantly on the structure parameter, which represents coking of the spray nozzle (x_3). The case of a model describing changes in carbon monoxide (y_1) is similar.

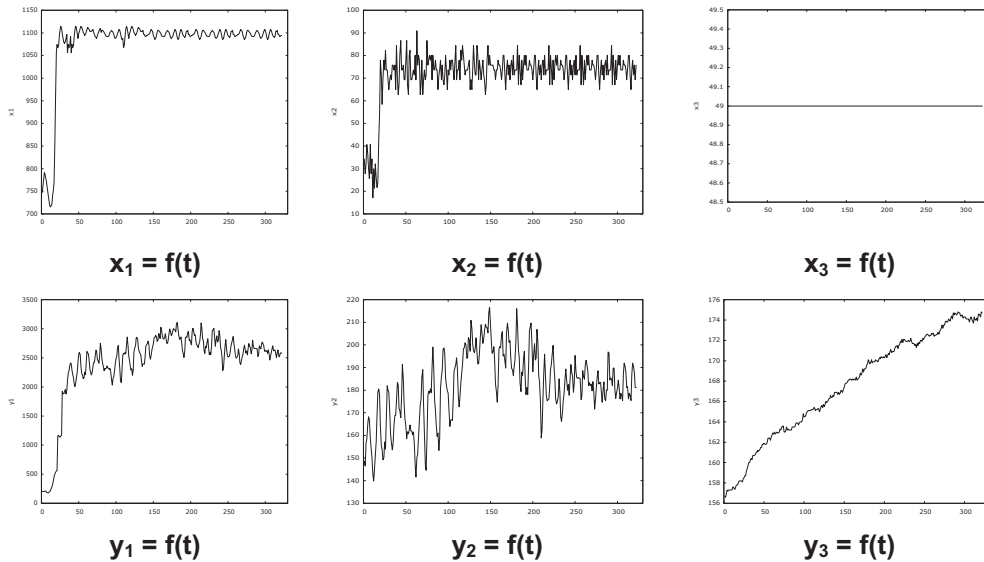


Fig. 1. Changes of the input and output quantities during the dynamic process
where: x_1 – engine speed n [r/min]; x_2 – engine torque T_{lq} [N·m]; x_3 – coking of the spray nozzle S_k [μm^2]; y_1 – concentration of carbon monoxide in the exhaust manifold $C_{CO(k)}$ [ppm]; y_2 – concentration of hydrocarbons in the exhaust manifold $C_{HC(k)}$ [ppm]; y_3 – concentration of nitrogen oxides in the exhaust manifold $C_{NOx(k)}$ [ppm]; t – duration of the process [s]

Table 1. Least-squares estimation of the dependent variable y_1

| | Coefficient | Mean error | Student t | p value | |
|------|-------------|------------|-------------|-----------|-----|
| y3 1 | 2,91309 | 1,43271 | 2,0333 | 0,04286 | ** |
| x1 1 | 0,644317 | 0,130189 | 4,9491 | <0,00001 | *** |
| x3 1 | -18,2606 | 5,31195 | -3,4376 | 0,00067 | *** |
| y1 1 | 0,884015 | 0,0193211 | 45,7538 | <0,00001 | *** |

Table 2. Least-squares estimation of the dependent variable y_2

| | Coefficient | Mean error | Student t | p value | |
|------|-------------|------------|-------------|-----------|---|
| y1 1 | 0,00120044 | 0,00067661 | 1,7742 | 0,07699 | * |

| | | | | | |
|------|----------|-----------|---------|----------|-----|
| x3_1 | 0,412034 | 0,0899356 | 4,5814 | <0,00001 | *** |
| y2_1 | 0,873606 | 0,0279092 | 31,3017 | <0,00001 | *** |

Table 3. Least-squares estimation of the dependent variable y_3

| | Coefficient | Mean error | Student t | p value | |
|------|--------------|-------------|-------------|-----------|-----|
| y1_1 | -5,65987e-05 | 2,41816e-05 | -2,3406 | 0,01987 | ** |
| x1_1 | 0,000396798 | 0,000206581 | 1,9208 | 0,05565 | * |
| y3_1 | 0,998597 | 0,00112836 | 884,9995 | <0,00001 | *** |

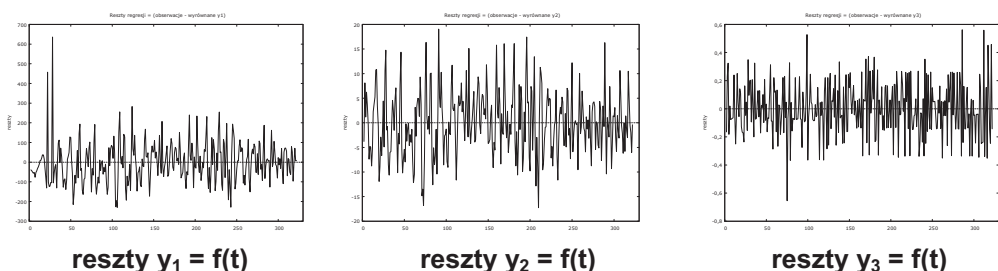


Fig. 2. Graph of the regression residuals for output variables

where: y_1 - concentration of carbon monoxide in the exhaust manifold $C_{CO(k)}$ [ppm]; y_2 - concentration of hydrocarbons in the exhaust manifold $C_{HC(k)}$ [ppm]; y_3 - concentration of nitrogen oxides in the exhaust manifold $C_{NOx(k)}$ [ppm]; t - duration of the process [s]

An even distribution of residuals from the regression of mean values may be indicative of being a good fit model to the values obtained from an experiment on the engine.

4. Summary

Presented description of the active experiment space by the multidimensional models gives great possibilities in analysis of measurement data and scientific conclusions. Furthermore, assuming that coefficients' matrix $(C^0)^T$ is orthogonal, there is a possibility of fulfilling reverse task, that is assessing, with complex relevance at known input variables, which describe work point i.e. engine rotational speed n and torque load T_{iq} , the other input quantities. In the nearest future authors will work on this issue.

References

- [1] Koško M., Osińska M., Stępińska J.: *Ekonometria współczesna*. TONiK, Toruń 2007.
- [2] Kufel T.: *Ekonometria. Rozwiązywanie problemów z wykorzystywaniem programu GRETL*, Wydawnictwo Naukowe PWN, Warszawa. 2007.
- [3] Kukielka L.: *Podstawy badań inżynierskich*, Wydawnictwo Naukowe PWN, Warszawa 2002.
- [4] Piaseczny L. Zadrag R.: *The influence of selected damages of engine SI type on the changes of emission of exhaust gas components*. Silniki Spalinowe, Opole 2009.
- [5] Polański Z.: *Planowanie doświadczeń w technice*, PWN, Warszawa 1984.
- [6] Robertson J., Robertson S.: *Pełna analiza systemowa*, Wydawnictwa Naukowo-Techniczne, Warszawa 1999.

- [7] Zadrag R.: *Kryteria doboru parametru diagnostycznego na potrzeby diagnostyki okrętowego silnika spalinowego*, LOGISYKA Nr 4/2010, ISSN 1231-5478, Poznań 2010.
- [8] Zadrag R.: *Modele wielorównaniowe szczelności układu wymiany ładunku silnika okrętowego*, Monografia „SLNIKI GAZOWE – wybrane zagadnienia pod redakcją naukową Adama Dużyńskiego, seria Monografie nr 183, Wydawnictwo Politechniki Częstochowskiej, ISBN 978-83-7193-461-2, ISSN 0860-501., Częstochowa 2010.
- [9] Zadrag R.: *The multi-equational models in the analysis of results of marine diesel engines research*, Międzynarodowa Konferencja Eksploziesel& Gas Turbine'2009, Międzyzdroje-Kopenhaga 2009.
- [10] Zadrag R. i inni: *Modele identyfikacji stanu technicznego silnika na podstawie oceny emisji składników spalin*, Sprawozdanie z projektu badawczego nr 4T12D 055 29, AMW, Gdynia 2008.
- [11] Zadrag R., Zellma M.: *Analiza wyników badań silników spalinowych przy wykorzystaniu modeli wielowymiarowych*, Sympozjum Siłowni Okrętowych Symso'2009, Gdynia 2009.



THE SELECTED METHODS OF UTILISING THE WIND POWER AS THE AUXILIARY SOURCE OF ENERGY ON DIESEL ENGINE POWERED SHIPS

Wojciech Zeńczak

West Pomeranian University of Technology in Szczecin
41 Piastów Ave, PL 71-065 Szczecin, Poland
tel.: +48 91 4494431, fax: +48 91 449 4737
e-mail: wojciech.zenczak@zut.edu.pl

Abstract

In the article there are presented some selected methods of the wind power conversion for the purposes of supplementing the ship's main propulsion or supporting the electric energy production which provide the opportunities to improve the ship's energy effectiveness ratio. The wind energy has been characterised in terms of its application on ships. A proposal has been made to apply the arrangement including the wind turbine with horizontal axis for the electric energy production and the fuel savings have been estimated during its operation. A concept has been discussed involving a special kind of thruster [towing kite] in the form of the towing kite connected by means of a rope with the ship and supporting her main propulsion. Also the arrangements such as Flettner rotors and turbine with vertical axis have been referred to.

Key words: environment protection, renewable energy sources, ship's power plant, energetic effectiveness

1. Introduction

The ships are considered as belonging to the most effective transport means in terms of the CO₂ emissions calculated per unit of the cargo transported at the distance of 1 km. Despite this fact as well as despite the fact that the ships participation in the anthropogenic emission of this gas worldwide at present amounts to as little as approximately 3%, this sector is nevertheless required to implement actions to reduce the emissions of the greenhouse gases [6]. The issues related with the limitation of the greenhouse gas emissions by the ships, after a couple of years of discussions, have become reflected in the regulations stipulated by the International Maritime Organisation (IMO). The decision taken in July 2011 about the introduction of the new chapter 4, regulating the ship's energy effectiveness, to the Annex VI of the MARPOL Convention has been a significant step. Thus since 1 January 2013 the determination of the Energy Efficiency Design Index (EEDI) shall apply to all the newly built ships larger than 400 GRT whereas all the ships, ie the newbuildings and the existing ones built prior to this date shall be covered by the Ship Energy Efficiency Management Plan (SEEMP) that allows the ship optimum operation [13].

It is possible to achieve the small value of EEDI, which is, to put it simply, defined as the total CO₂ emissions from the fuel combustion in main and auxiliary engines and in the boilers in

reference to the transport work, in the effect of all the undertakings favourable to the reduction of the ship's fuel consumption. The transport work is here determined as the product of the ship's design deadweight (DWT) and the design speed measured for the ship's maximum loading with 75% of the nominal power on the shaft [13]. The basic actions to reduce EEDI include eg the utilisation of the exhaust gas waste heat. The application of the wind power or solar energy also helps to diminish this value.

The selected manners of the utilisation of these energy sources on the ships have been presented *inter alia* in the author's works [10, 11]. On account of the new situation resulting from the EEDI implementation the issue of utilising the wind and solar energy on the ships gets more meaningful and it is reflected by the appearance of the new or modernised arrangements of the wind utilisation on the ships. In the further course of the paper the selected methods of wind utilisation as the supplementary energy source for the purposes of aiding the main propulsion or generation of the electric energy will be presented.

2. General Characteristics of the Wind Energy

The wind power is the energy coming from the solar radiation. The temperature differences which appear due to unequal heating of the earth and atmosphere cause the appearance of the air motions which, carrying the heat, tend to equalise the temperatures. The Earth spherical shape causes that the biggest difference in the energetic potential is formed in between the equatorial zone and the poles. Two basic air circulations are thus created, one in the zone between the tropics and the other between the tropics and the poles. The heated air from the equator areas rises upwards and flows towards the poles of both hemispheres. In the areas of the tropics the air masses start to drop down which leads to the formation of the tropical high-pressure areas. From these areas the air flows closer to the earth surface, partly towards the poles and partly back towards the equator. In the effect of the Coriolis force action, which is the effect of the Earth rotation, and also due to the friction force at the Earth surface, the direction of these currents is not compatible with the direction of the pressure horizontal gradient. Thus the horizontal air currents moving nearby the Earth surface towards the equator, called trade winds, have the north-easterly direction on the northern hemisphere and south-easterly on the southern one. The velocities of the trade winds at the earth surface amount to 5-8 m/s on the average. In the moderate zone the air masses circulation is not as orderly as that due to the existence of many moving high and low-pressure areas causing that the wind may practically blow from any direction. However, on the northern hemisphere the south-westerly and west winds prevail whereas on the southern hemisphere the north-westerly and west winds prevail [4]. Besides this global circulation the monsoons or the season winds should be mentioned that change the direction twice a year and which are caused by the differences in the heating of the lands and oceans. In the summer they blow from over the ocean towards the land (the summer monsoon – oceanic), and in the winter from the land towards the ocean (the winter monsoon – continental one).

The air circulation in the poles area is of no practical meaning for the ocean trade and therefore it will not be discussed. The local winds being the effect of the local differences in the temperatures are independent of the global circulation and overlap it. For the offshore trade the breezes as having the daily cycle and the nature similar to that of the monsoons, although in a small scale may be significant as well as the boras blowing from over the low mountain ridges towards the warm sea.

In the wind power engineering the major significance has the annual average wind velocity on a given area at the specified height over the earth surface in terms of the available wind energy for the use by the wind power plant. The increase of the height over the earth surface is generally accompanied by the wind average velocity.

The wind velocity profile or in other words the graph showing the average velocity of the wind blowing from a given direction as a function of height over the earth or water area, is strongly dependent on the area shaping and surface roughness as well as time of velocity averaging. The research shows that the friction effect on the air horizontal movements is significant in the air layer in direct contact with the earth, of the thickness around 1 km [4]. According to all the classifications of the surface roughness the water surface, as the open sea, belongs to the areas of the lowest roughness values. The velocity profile with the large averaging times are presently recommended to be defined by use of the logarithmic formula while earlier it was the power formula. The logarithmic formula (1) gives the results closer to the reality in the earth adjacent layer up to 200 m:

$$\frac{\bar{v}_2(z_2)}{\bar{v}_1(z_1)} = \frac{\ln\left(\frac{z_2 - z_0}{s_0}\right)}{\ln\left(\frac{z_1 - z_0}{s_0}\right)} \quad (1)$$

where:

z_1, z_2 , – the heights where the average 10 minutes velocities are measured (determined),

z_0 – parameter characteristic for the wall-adjacent layer related to the surface roughness,

s_0 – Earth surface roughness measure (determines the height where the wind velocity gets down to zero,

\bar{v}_1 , – average 10 minutes velocity measured (assumed) at the height $z_1=10$ m,

\bar{v}_2 – average 10 minutes velocity determined for the height z_2 [2, 4].

In case of the surface like the sea $z_0=0$ m, and $s_0=0,0002$ m [2]. The velocity profiles calculated basing on the relation (1) for the various average velocities \bar{v}_1 , assumed as those measured at the height of 10 m above the sea level are shown in figure 1.

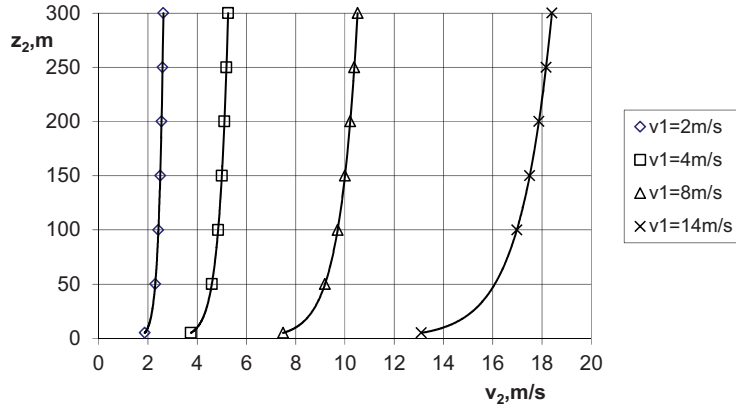


Fig 1. Vertical profiles of the wind calculated on the basis of the velocity value \bar{v}_1 , at the height of 10 m

For the surfaces of bigger roughness the bigger velocity gradients would occur along given height. This is of large significance in the land wind power engineering for the selection of the location of the wind power plant. In case of the offshore wind farms this is a useful information for the establishing of the tower heights and wind force at a given height. The power of the wind stream \dot{m}_A flowing through the surface A perpendicular to its direction depends on the velocity in 3rd power and can be determined from the relation:

$$N = \frac{1}{2} \dot{m}_A v^2 = \frac{1}{2} \rho v^3 A \quad (2)$$

where:

N – wind power,

A – surface area where the wind flows,

\dot{m}_A – wind mass stream flowing through the surface,

ρ – air density,

v – wind velocity.

Thus the arrangements enabling the utilisation of the winds blowing at big heights should be preferred.

In case of ships using the wind energy the knowledge of the wind velocity profile is also of big importance for the application of some technologies.

3. Wind as the Energy Source on Ships

3.1. Introduction

The energy of wind, besides the heat from wood burning, has been the renewable energy used by the humans as the earliest. The history of the application of the wind has begun from the sail boats and goes back as far as approximately 8,000 years. The Egyptians used the wind force for

the propulsion of the boats by means of the simple square sail; the boats having been used to transport people and goods on the Nile [8].

Nowadays there are different shape sails still in use either in sports and recreation boats. In a minor scale they have also been used as the supporting propulsion means on the motor ships. During the fuel crises the interest in such ideas has been growing. The primary deficiency of the sail propulsion is the necessity to tack if the wind direction is not as desired. Therefore on account of the very much stable wind direction and its velocities the trade winds would be most preferably utilised by the sailors.

There have been the attempts made to eliminate the inconvenience of the sails by the application of the other arrangements such as eg Flettner rotors utilising the Magnus effect or even wind turbines which were mechanically coupled with the propeller [8].

Recently the interest in the wind energy results from the reasons presented in the introduction. Apart from the improvement of the earlier solutions such as Flettner rotors [5] or wind turbines, in Germany there has been developed the concept originating in the beginnings of the XIX century where the kite was applied for the boat propulsion. The contemporary towing kite is constructed as a kite connected to the ship by means of a rope, the kite bearing the structural resemblance to paraglider. This solution utilises the bigger wind velocities blowing at the heights within 100 and 500 m above the sea level which has been presented in figure 1.

Besides supporting the main propulsion the wind energy may also be successfully utilised to drive the electric energy generators. For this purpose the most useful seem to be the horizontal axis turbines. Still a solution applied in 2011 by Stena Lines is also worth mentioning – that consisting in placing on the fore deck of the ferry Stena Jutlandica of the two wind turbines with the vertical four metres Darrieus' type axis of the total power of 8 kW. Within a year they generate 23 MWh of the electric energy which is used for the lighting of the vehicle deck. The most significant merit of the applied turbines is not so much the generation of the electric energy, but rather the reduction of the front air resistance to allow the fuel savings of approximately 80 to 90 Mg by main engines in a year [9].

3.2. The Application of the Wind Turbine with the Horizontal Axis on Ship

The wind turbine power P can be represented by the relation (3).

$$P = C_p \frac{\pi D^2}{4} \cdot \frac{\rho \cdot v_0^3}{2} \quad (3)$$

where:

D – turbine rotor diameter,

C_p – wind power utilisation coefficient (theoretical maximum value amounts to 0,59),

v_0 – wind velocity before rotor.

Since the power increases together with the square value of the rotor diameter, the largest possible diameters should be aimed at. In Europe the biggest diameter, 127 m, is that of the turbine type Enercon E126 with the 7.58 MW power. The height of the tower is 135 m [14]. The dimensions of the turbines on board the ship must be however significantly smaller in view of the ship's stability. If several turbines are installed, the distance to be kept in between them shall be not less than 4 diameters of the rotor in order to prevent the mutual interfering of the wind jet

which means the necessity of the selection of the rotor diameters adapted to the ship's main dimensions. Thus it is purposeful to install the wind turbines on large vessels allowing to select the turbines with rotors of bigger diameters.

One of the biggest ships built at one time in Stocznia Szczecińska was the product tanker B573 of the length overall 183 m and breadth 32.2 m. While complying with the aforesaid criteria and assuming the installation of the wind turbines in the most favourable area, ie on the superstructure it would be possible to apply eg 2 turbines with the 8 m diameters rotors. The example of the arrangement of two turbines is shown in figure 1.

To determine the turbine power in relation to the wind force the formula (1) has been used. For the calculations there has been assumed the power coefficient that characterises the most efficient turbines with the special blade profiles $C_p = 0,5$. The diagram representing the relation of the power of the single turbine and the wind velocity is presented in figure 3.

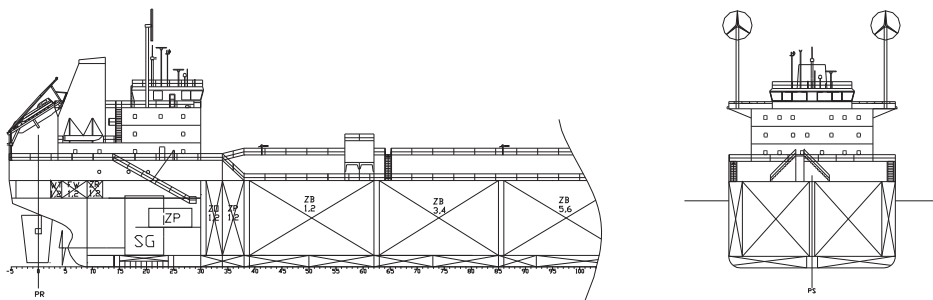


Fig 2. A possible location of the wind turbines on the product tanker

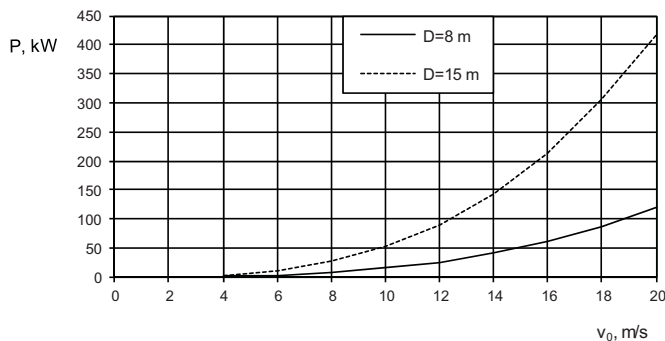


Fig 3. The power outputs achieved from one turbine for various diameters as the function of the wind velocity

As shown in the diagram with the assumed rotor diameter of 8 m the power outputs obtained are not any large ones. From the two turbines and with the wind force corresponding to 6 to 7 Beaufort scale (ca 16 m/s) the power output to be obtained is approximately 120 kW. This consists ca 30% of the electric energy demand during the ship's stay on the roads. Therefore it is possible to achieve a certain relief for Diesel generating set and the savings at the level of 20 kg of Diesel oil within an hour. However, these are not any meaningful values. As shown in the

diagram only the application of the rotor of diameter ca 15 m would offer with the same wind force the power output of ca 210 kW from one turbine. With two turbines then the full demand would have been satisfied. Such diameter for the rotor is still acceptable, however it would be necessary to locate the turbines at the bigger distance from each other, eg one in the aft and one in the fore. It is also possible to use bigger number of the turbines, but with smaller diameters that would give similar benefits.

3.3. Towing Kite

A new arrangement is the proposal of using the kite as the auxiliary ship's propulsion consisting in joining it with the ship by means of the towrope of 100 – 500 m length. Should the wind blow favourably from the stern or backstay, the rope with the kite attached at its end is uncoiled from the compartment in the fore, passing through a roller located at the top of a not too tall mast of the height varying by pulling up or down. The most advanced and well tested system is that of Messrs Sky Sails. Here the kite resembles the two-layer inflatable paraglider. Owing to the adequate profile at the kite, similarly as on the aeroplane wing, there appears the carrying force facilitating it rising. Inside the towrope there is the cable supplying the pod placed underneath the kite and incorporating the electronic operating system. While the kite is kept in constant motion doing the figure of eight in the air the carrying force increases and then a large towing force is developed. The entire operation is surveyed by computer [1].

The first attempts with the application of the kite the Sky Sails conducted in 2002 on a small boat weighing 360 kg which has developed the speed of 7.4 km/h. The positive experiences with the other boats made the company conduct the tests on a ship. The first one was 55 m long motor ship Beaufort and the kite mounted thereon, operated still manually, had the surface area of 160 m².

The first cargo ship worldwide with the fully automatically operated kite was that launched in 2007 – 475 TEU containership, MS Beluga Sky Sails. The ship developed the speed of 15.5 knots with the main engine power output of 3,840 kW. According to the manufacturer's assurances with the kite surface area equal to 160 m² it is possible to achieve the ca 15-20% savings in the fuel consumption, and for the kite of double the surface area operating at the height up to 420 m provided for the bulk carrier of 25,000 DWT, even up to 35% [12].

The kite is an attractive propulsion appliance because the force with which it acts on the ship generates directly the towing power without any additional energy losses resulting from its conversion. While assuming the average value of the Diesel engine powered ship propulsion efficiency, defined according to [7] as the ratio of the towing power to the power carried to the tail-end, equal to ca 0.5, then the equivalent engine power output for the transfer of the same speed to the ship must be twice as big as the kite power output. Pursuant to [3] the kite of surface area 320 m² can "replace" 20 MW of the main engine power output.

The precise determination of the kite towing force is a complex issue on account of its movements with the variable speed and the dependence on many construction parameters. A good approximate of the measurement values is provided in the model presented in [1].

The force exerted by the wind on the kite surface can be determined from the relation (2) for the wind power through the relation:

$$N = \vec{F} \vec{v} = \frac{1}{2} \rho v^3 S_w \quad (3)$$

where:

\vec{F} – wind force vector,
 \vec{v} – wind velocity vector,
 S_w – kite usable surface area swept over by the wind.

The kite usable area S_w , in the result of its movements, is swept over in a variable manner by the wind, ie the same fragment of its surface is swept over every certain specific time. For this reason the wind utilisation coefficient is introduced ε_k and thus the kite usable power P_k can be presented by the following relation:

$$P_k = \varepsilon_k N = \varepsilon_k \frac{1}{2} \rho v^3 S_w = \frac{1}{2} \rho v^3 S_k \quad (4)$$

where:

S_k – conventional surface area where the wind acts on the kite.

The surface S_k for the kite doing the figures of eight in the air is equal approximately to the surface of the path covered by the kite so to the product of the kite way along the figure eight and the width of the kite. Practically the value S_k depends inter alia on such parameters as the surface, shape coefficients, positioning angle towards the wind direction, the shape of the “eight” and kite speed in the movements along the “eight”. Knowing power P_k from the relation (5) there can be determined force F_k acting on the kite and whose vector is parallel to the wind velocity vector:

$$P_k = F_k v = \varepsilon_k N = \varepsilon_k \vec{F} \vec{v} = \varepsilon_k F v = \frac{1}{2} \rho v^3 S_k, \quad (5)$$

therefore

$$F_k = \varepsilon_k F v = \frac{1}{2} \rho v^2 S_k. \quad (6)$$

In fact for the ship what is important is the value of the force in the rope perpendicular to the surface S_k . and the towing force. The force in the rope F_L can be presented in the form of the relation (7)

$$F_L = F_k \cos \alpha \cos \beta = \frac{1}{2} \rho v^2 S_k \cos \alpha \cos \beta \quad (7)$$

where:

α – angle between the rope and wind direction in the horizontal plane,
 β – angle between the rope and wind direction in the vertical plane.

Since the surface S_k depends on many parameters and can be determined only experimentally, then it is stated as follows

$$F_L = v^p A \cos \alpha \cos \beta \quad (8)$$

where:

p, a – experimentally established constants.

Eventually the towing force is determined from the relation:

$$F_h = F_L \cos \alpha_A \cos \beta_H \quad (9)$$

where:

α_A – instantaneous angle between the rope and the ship's motion direction in the vertical plane,
 β_H – instantaneous angle between the rope and the ship's motion direction in the horizontal plane.

Thus in case of the towing force of relatively minor value eg 20 kN reached by the kite of the surface area 80 m² and the ship's speed of 14 knots (7.2 m/s) there is 144 kW towing power generated. Assuming the efficiency of the motor ship's propulsion system equal to $\eta_n=0,5$, this corresponds to the saved main engine power equal to 288 kW. For example for the B186 containership built in Stocznia Szczecińska with the engine developing the contractual power of 12,180 kW and the specific fuel consumption of 0.171 kg/kWh, the application of the kite under such assumptions would produce the savings of ca 50 kg/h of the fuel.

4. Summary

The two methods of the utilisation of the wind blowing at different heights above the water surface offer some insight into the benefits possible to be achieved and resulting from the application of the wind energy on the motor ships. From the considerations made it results that the turbines with the horizontal axis and dimensions of the rotor diameter exceeding 15 m would provide the notable and measurable benefits in the amount of the fuel saved by the generating sets during the ship's stay. Therefore such arrangements could be taken into account on large ships, eg tankers. Also another location of the turbines could be considered as well as the application of another number of the turbines, eg 4 turbines – in the fore and aft and at the superstructure sides, offering the undisturbed operation and larger total power.

Also the application of the towing kite as the propulsion appliance is beneficial as it utilises the strong and permanent winds blowing at the significant heights above the water level and supports the main propulsion. In this case in relation to the kite surface area and the meteorological conditions it is possible to reduce considerably the main engine power output in comparison to the ship driven by the engine alone and to achieve the limitation of the fuel consumption.

References

- [1] Aschenbeck S., Eisber R., Lrngr T., Szczesny W., Kreutzer R., Schlaak M.: *Testergebnisse des SkySails-Systems*, Schiff und Hafen, Januar 2009, pp. 36-40.
- [2] Chmielniak T.: *Technologie energetyczne*, WNT, Warszawa, 2008.
- [3] Erhard M., Strauch H.: *Control of Towing Kites for Seagoing Vessels*, <http://arxiv.org>., dostęp z dnia 12.07.2012
- [4] Flaga A.: *Inżynieria wiatrowa*, Arkady Sp z o.o. Warszawa 2008.
- [5] *Innovatives Spezialschiff mit kombiniertem Antriebssystem*, Schiff und Hafen, Januar 2011, pp. 28-33.
- [6] Mundt T., Köpke M.: *MEPC 62: Energy Efficiency Design Index verabschiedet*, Schiff & Hafen, 9/2011, pp 12-15.
- [7] Staliński J.: *Teoria okrętu*, Wydawnictwo Morskie, Gdańsk 1969.
- [8] Urbański P., *Pędniki okrętowe, historia i rozwój*, Okrętownictwo i Żegluga sp. z o.o., Gdańsk 2001.
- [9] *Wind turbine power „world first” for ferry*, Motorship July/August, 2011, pp.10.

- [10] Zeńczak W., *Stand und Perspektiven der Anwendung der Solarenergie auf Schiffen*, XIV Symposium Nutzung Regenerativer Energiequellen und Wasserstofftechnik, 8-10 November, Stralsund 2007, pp. 154-158.
- [11] Zeńczak W., *The Possibility of Renewable Energy Use on Ships*, eds. J. Mikielwicz, W. Nowak, Wydawnictwo Uczelniane Politechniki Szczecińskiej, Szczecin 2004, pp.317-324.
- [12] *Zugdrachen für Bulker*, Schiff und Hafen, April 2011. pp.9.
- [13] www.imo.org – (update: 04.07.2012).
- [14] www.enercon.de – (update: 11.07.2012).



THE ETHANOL THE SUPPLEMENTARY FUEL OF THE COMBUSTION ENGINE

Bogdan Żółtowski, Piotr Stanowski

*Faculty of Mechanical Engineering
University of Technology and Life Sciences in Bydgoszcz
e-mail: bogzol@utp.edu.pl, tel. 52 340 82 83*

Summary

The key issue of this paper is the acquisition of information in the field of percentage composition of the mixture of unleaded petrol Pb-95 and non-dehydrated distilled ethanol and modifying additions (ignition initiator, water emulsifier, combustion stabilizer, corrosion inhibitor) for the supply of modern spark ignition engine, without the need to introduce any changes of constructional nature or in the settings of the controller of engine's ignition structure.

Keywords: *internal-combustion engines, alternative fuel, ethanol, part load, environment*

1. Introduction

The development of motorization and gradually decreasing raw materials of oil-derivative fuels induces to search for fuel substitutes (commonly referred to as alternative fuels), as well as to decrease the consumption of the non-renewable energetic raw material. Moreover, European law limiting the emission of toxic components of exhaust fumes accompany the limitations in fuel consumption and at the same time increase the requirements in the field of efficiency range of modern drive units of motor vehicles.

One of the solutions is looking for new ecological fuels, among which fuels of vegetable origin play a dominant role. Vegetable oils in their pure form practically are not suitable for spark ignition engines due to high viscosity and density, low octane number and insufficient resistance to low temperatures. Chemically processed vegetable oils known as methyl esters are devoid of the aforementioned disadvantages.

Fuel substitutes (alternative fuels), including ethanol, can be applied in a broad range of equipment and vehicles with four-stroke spark ignition engines, which constitutes 73% of car participation in Poland and 62% in Europe. Presently these fuels are not produced on a commercial scale in Poland. Ethanol increases the octane number, and, as an oxidant, causes smaller emission of toxic combustion products such as carbon oxide, nitrogen oxides and dusts. Fuel mixtures with a considerable amount of ethanol require, however, additives improving tribological characteristics of fuel and decreasing its volatility.

Ethanol can be produced of many raw materials containing simple carbohydrates (molasses, whey) or polysaccharides (starch, cellulose). In Poland, the main raw materials used for the production of ethanol are rye and corn. In perspective, cellulose is a promising raw material for ethanol production, with the hydrolysis of cellulose, however, being too expensive at this point.

The range of presented research was focused on the suitability of engines operating in cars in town traffic. The research was supported by the measurements of the parameters of operating

engine quality (external characteristics, fuel consumption, cooling liquid temperature, the temperature of fumes, toxic composition of fumes) appearing during the realization of the planned stationary experiment on an engine test bench). The results of the research are useful for the assessment of operation effectiveness of a spark ignition engine supplied with the fuel proposed herein (power, torque, fuel consumption).

2. Research methodology

Cars equipped with internal-combustion spark ignition engines are an important group of vehicles operating in economy of various types. The research was focused on stationary experiments – on engine test bench, limiting its range to partial power research, with parameters determined through the analysis of the most frequently used power and torque in such conditions. Having analyzed town traffic conditions (motivated below), a decision was made to conduct a partial power research for the following parameters:

- power 22,82kW at 2000min⁻¹, which reflects 32% of the nominal power,
- torque 109Nm, which 59% of the maximal torque at the rotary speed of 2000min⁻¹.

The key target of the research was to check experimentally the possibilities of application of non-dehydrated distilled ethyl alcohol in connection with base fuel Pb-95 in specific proportions and special additives as refiners. Moreover, the influence of tested fuel on the performance a spark ignition engine was tested, marking out engine's external characteristics with partial power (operating parameters similar to the ones of town traffic), researching at the same time the emission of toxic substances. Stationary measurements that verify the assumptions of this paper also aim at introducing into field tests a long-term test conditioning the implementation of developed fuel.

2.1. Tested items

The tests were conducted on an engine of X20SED (2.0i DOHC) type – Fig.1, supplied with the proposed fuel and its mixtures in specific proportions with petrol Pb95.



Fig.1. A general view of the tested engine and a sample mixture of fuel

For the supply of the tested internal-combustion engine on which the usefulness of the fuel proposed herein was verified the following components were used:

- commercial unleaded petrol Pb 95 with the following proportions: C(carbon) – 85%, H(hydrogen) – 15%,
- ethanol fuel (90% non-dehydrated distilled ethanol, 10% modifying additives, including: 1,5-3,2% ignition initiator, 3-6% water emulsifier, 0,4-0,6% combustion stabilizer, 0,1-0,2% corrosion inhibitor),
- and respective mixtures of the aforementioned fuels in the proposed proportions:
 - 80 % Pb95 – 20 % Ethanol,
 - 70 % Pb95 – 30 % E,

- 60 % Pb95 – 40 % E,
- 50 % Pb95 – 50 % E,

The fuel used for the purposed outlined in this paper is an innovative proposal of new patent pending ethanol fuel – patent application number **P 383859**.

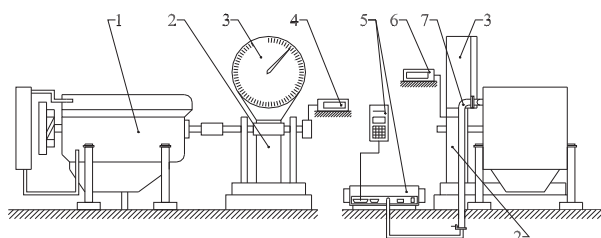
For the assessment of the influence and possibility of applying the innovative fuel a new engine was used – of X20SED (2.0i DOHC) applied as a drive of such cars as Daewoo Leganza, Nubira, as well as Chevrolet Rezzo and Evanda:

- spark ignition engine,
- number of cylinders - 4,
- cylinder diameter - 86,0 mm,
- piston stroke - 86,0 mm,
- engine cubic capacity - 1 998 cm³,
- compression degree - 9,6±0,2,
- nominal power - 98 kW at 6000 1/min,
- maximal torque - 184 Nm at 4400 1/min.

The tested internal-combustion engine belongs to one of the groups of the most frequently applied types of spark ignition engines in midrange and luxury cars, considering capacity, performance and technological advancement.

2.2. Test station

Stationary tests were conducted in a laboratory of internal-combustion engines. The test station of a well-equipped engine test bench with a hydraulic brake was presented in Fig.2.



Description: 1 - engine, 2 - HWZ hydraulic brake, 3 - dynamometer, 4 - tachometer 5 - probe for the measurement of exhaust fume composition, 6 - fume temperature gauge, 7 - exhaust system.

Fig.2. Test station scheme

The test station enables the realization of the following measurements:

- engine torque,
- rotary speed of engine craftshaft,
- engine oil temperature,
- cooling liquid temperature,
- fume temperature,
- temperature of water flowing out of the brake.

From the point of view of engine construction durability while supplying with the proposed fuel, it was extremely important to monitor the temperature of flue gases. This measurement was registered with the help of thermocouple placed at the level of lambda probe in the outlet levelling device.

2.3. Test conditions

Measurements for the purpose of compiling engine characteristics while testing each type of fuel were conducted in the following conditions:

- the temperature of sucked air and surrounding pressure are similar to normal values as per PN-78/S-02005;
- burdening force, rotary speed, temperature of engine cooling liquid or oil are constant for approximately 1 minute;
- rotary speed of the crankshaft can fluctuate up to ± 10 1/min from the assumed value;
- measurements of the rotary speed and fuel consumption last approximately 30 seconds in the case of manually-controlled measurement;
- measurements of torque and fuel consumption are conducted at the very same time;
- the number of measuring points sufficient to obtain the characteristics of proper shape and character of performance (as per BN-70/1374-01) – the minimum of 6;
- measuring points are condensed near the extremum and other characteristic points on the curves.

An engine test bench, where the tests were conducted, enables to prepare:

- external characteristics of the engine (known as full power characteristics);
- partial power characteristics;
- load characteristics.

In the tests, experiment conditions and the way of determining the characteristics of internal-combustion engines were specified as per the branch norm BN-70/1374-03.

Engine tests were conducted on unleaded petrol Pb95 as a base fuel, and it was a point of reference while supplying the engine with mixtures of Pb95 and ethanol fuel, simply called ethanol. A significant element of the research was also an attempt to determine the influence of tested fuel on the degradation of natural environment, as well as the durability and construction reliability of the engine.

3. The analysis of test results

The results of the research presented in this paper concern outlining engine external characteristics on partial powers – without the need to introduce any changes to engine construction and while supplying the engine with innovative ethanol fuel.

Fuel – [Pb95 petrol]

Tests results for Pb95 were presented in Fig.3 and 4.

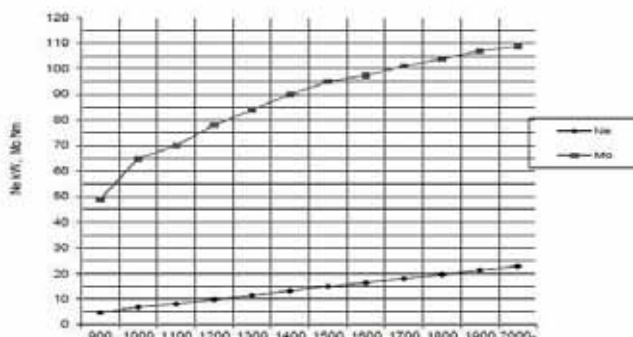


Fig.3. The course of the rotary moment M_o and power N_e of the tested engine

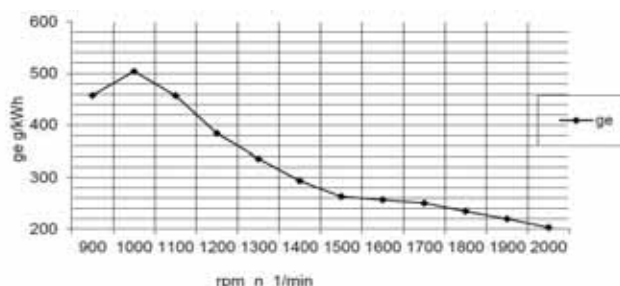


Fig.4. The course of unit fuel consumption of the tested engine

Unit fuel consumption with reference to rotary speeds, apart from neutral gear rotations (900 to 1500 1/min), does not exceed the limits assumed for this type of engine. At the rotary speed of 2000 1/min is a low value; however, it should be noted that it concerns the characteristics of partial powers. As a result of the test on 30 spark ignition engines, an average value of unit fuel consumption 345 g/kWh was obtained for the rotary speed of 2000 1/min.

Fuel – [Pb95 petrol 80% + ethanol 20%]

Test results for fuel mixture [80x20] were presented in Fig.5 and 6.

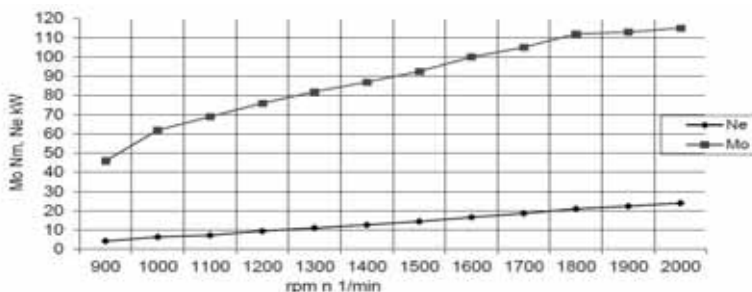


Fig.5. The course of the rotary moment and power of the tested engine

As shown in Fig.5, the tested engine supplied with the mixture achieved 9,4% higher power, which proves better preparation of the inflammable mixture, as well as course of the combustion process and greater portion of fuel injected into the cylinder. This is a consequence of 9,9% greater density of fuel. The course of unit fuel consumption is similar to the previous case; however, at the rotary speed of 2000 1/min it is 6,4% lower, which is definitely influenced by the better course of the combustion process. Engine supplied with a mixture of 80% Pb95 and 20% ethanol in the range of 900 to 1700 1/min of rotary speeds had minimally lower rotary moment values than when supplied with the base fuel. At rotary speed higher than 1700 1/min these values exceeded the values of the base curve, reaching 5,5% higher than the curve at the speed of 2000 1/min.

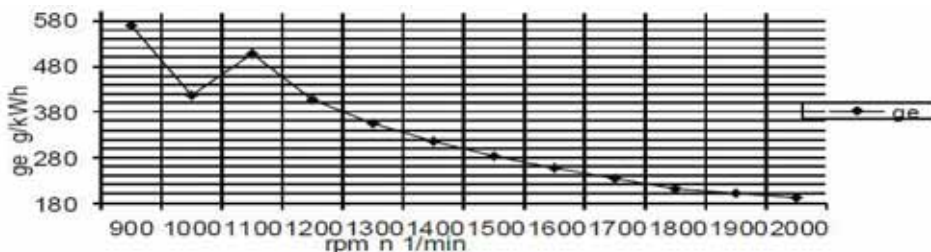


Fig.6. The course of unit fuel consumption of the tested engine

Similarly to the supply with Pb95 only, unit fuel consumption was small and equalled from 190 to 280 g/kWh in the rotary speed range of 1500 – 2000 1/min, which is comparable to the consumption in the case of Pb95 only.

• Engine torque

Engine torque presents possibilities of performing a given operation. Basic characteristics with petrol Pb95, fuel consisting in 80% of Pb95 and in 20% of ethanol, as well as fuel 50% Pb95 – 50% ethanol were selected for analysis. An engine supplied with the last fuel achieved satisfactory results. The comparison of the torque of the tested engine for three types of fuel mentioned was presented in Fig.7.

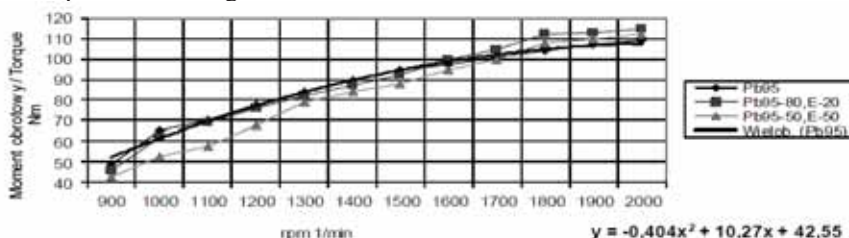


Fig.7. The comparison of the torque value of the tested engine

Since the curve of engine torque supplied with petrol Pb95 was adopted as a basis for comparison, its theoretical course was assumed, also referred to as a trend curve for this fuel. This is a polynomial curve described with an equation shown in the corner of Fig.7. The degree of the compliance of test results with this curve was investigated.

The variance of y feature equals: $s^2 = 348,066$ and $\phi^2 = \Delta^2 / n s^2$
 where: n – the number of measurement

hence: $\phi^2 = 19,25 / 12 \times 348,066 = 19,25 : 4176,792 = 0,0046$

This means that actual and theoretical values are incompatible only in 0,46%. In other words, they are compatible in 99,54%. This enabled to determine the coefficient of compliance between two curves, and at the same time to check the reliability of the research.

An engine supplied with a mixture of 80% Pb95 and 20% ethanol with reference to rotary speeds from 900 to 1700 1/min achieved torque values minimally smaller than in the case of base fuel only. Above the rotary speed of 1700 1/min these values exceeded the reference values, reaching 5,5% above the curve at the speed of 2000 1/min.

For the mixture of 50% Pb95 and 50% ethanol, with reference to rotary speeds from 900 to 1800 1/min the tested engine achieved torque values considerably smaller (25% smaller) than when supplied with base fuel. Above the rotary speed of 1800 1/min these values exceeded the base curve values, reaching 2,7% above the curve at the speed of 2000 1/min.

The comparison of the trend lines for two remaining curves of the torque in Fig.8 does not bring in any new information due to the fact that the trend lines, similarly to the torque curve of the supply with Pb95, are polynomial curves of the second degree and the comparison of equations describing them is as follows:

$$Pb\ 95 \quad y_i = -0,404x^2 + 10,274x + 42,557$$

$$Pb\ 95-80\ \%,\ E-20\ \% \quad y_i = -0,3063x^2 + 10,008x + 39,83$$

$$Pb\ 95-50\ \%,\ E-50\ \% \quad y_i = -0,2818x^2 + 10,096x + 32,852$$

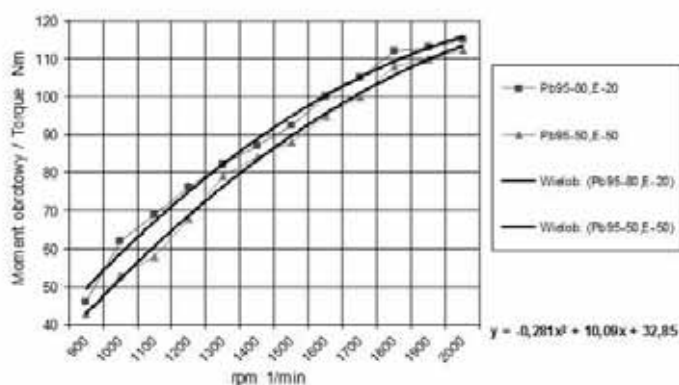


Fig.8. The comparison of the torque trend lines of the tested engine

The analysis of Fig.8 shows that the coefficient of conformity in the case of mixtures will be similar to petrol Pb95, with a smaller value, however, for the mixture of Pb-80%, E-20 %. The trend curves in the form of second degree equation reflect the nature of test results obtained on engine test bench well.

• Engine power

With reference to engine power, the situation is not so favourable, which is shown in Fig. 9. Power differences of the tested engine for partial loads of the tested mixtures of fuel are minima; hence, the curves of the torque, being clearer and more diversified, were adopted for analysis.

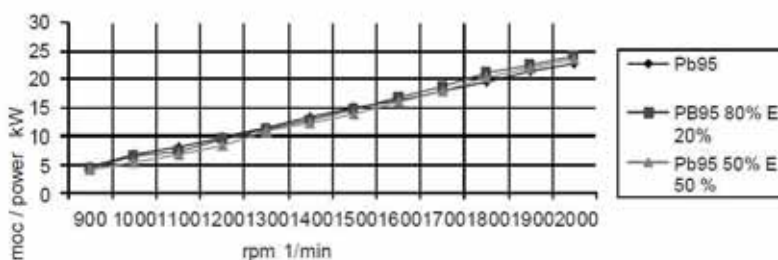


Fig.9. The characteristics of partial powers of the tested engine

For fuel mixtures 30% Pb95 – 70% E, 20% Pb95 – 80% E there was no stable engine performance in the whole range of rotary speeds included in the test; thus, no characteristics were made in this case. The analysis of power curves shows that the mixtures of commercial fuel with ethanol can be successfully applied for the supply of spark ignition engines, with the borderline proportion in the composition of mixture being 50% Pb95-50%E (not more than this) due to engine performance stability.

• Unit fuel consumption

Unit fuel consumption for the rotary speed of 2000 1/min oscillated between 190,3 and 217 g/kWh and did not exceed the limits adopted for this type of engine operating on partial powers. The curves obtained in the tests for all percentage relations of fuels show huge consumption with reference to neutral gear, which is normally omitted in producers' characteristics. That is why the proper analysis was conducted for the range 1500÷2000 1/min of rotary speed. Fig.10 shows the courses of unit fuel consumption for the three compositions of mixtures mentioned above.

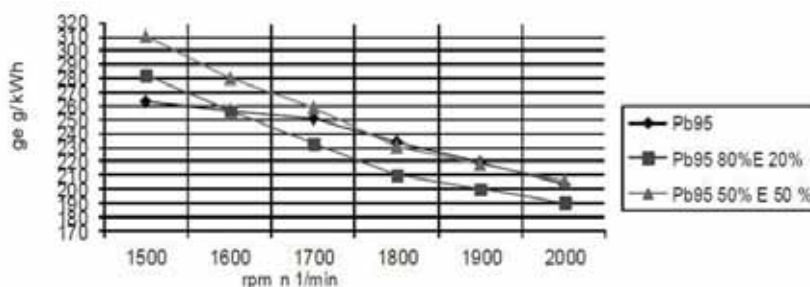


Fig.10. Unit fuel consumption of the tested engine

The analysis of Fig.10 proves that the courses of unit fuel consumption are similar in character in the case of petrol and ethanol mixtures. The mixture Pb95 80% - E 20% definitely has the best results – at the rotary speed of 2000 1/min, fuel consumption is 6,3% smaller than for pure petrol and mixture Pb95 50% - E 50%.

4. The assessment of the tested engine state degradation

In the research the change in engine durability during tests with different mixtures of fuels was short-term, and the assessment of construction state changes was almost impossible. Taking care of the repetitiveness of testing conditions, keeping recommended engine temperatures and measuring gas temperature and its composition, in reference to normal performance conditions with base petrol Pb95, determined the indirect, very approximate assessment of tested engine degradation.

The obtained test results offer the following conclusions:

1. during the research, the engine was not subject to a long-term test and operated on partial powers; during the test no engine failure or damage took place;
2. the temperature of media included in the statistical elaboration of test results, such as: cooling liquid on engine input and output, fumes and fume emission components prove a stabilized area of engine performance;
3. the results obtained for various mixtures of fuel in relation to the base fuel did not exceed allowed parameter values prognosing the accelerated process of wear and tear of parts or the whole engine;
4. organoleptic and technical assessment of the engine after the test did not disclose any damage in the engine seal and no engine oil consumption was found.

Fume temperature

In the course of painting out engine external characteristic, fume temperature was measured, taking into account the assessment of construction tension while supplying the engine with various fuel mixtures. The tested engine fulfilled the requirements also in the case of modified fuel - Fig.11.

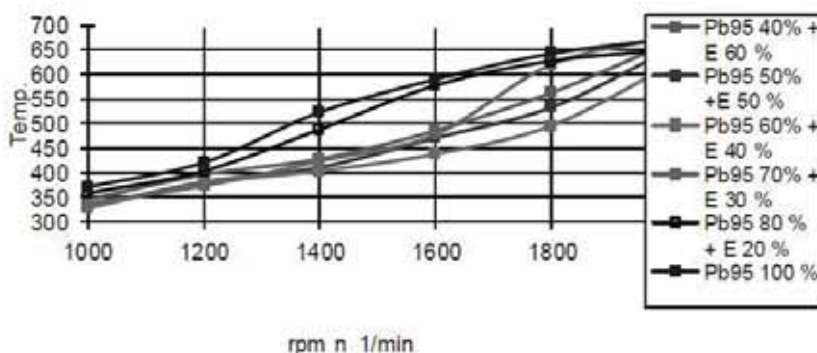


Fig.11. Fume temperature for various fuels

Fig.11 presents two clusters of curves. The first one refers to fume temperature for petrol Pb 95 and mixture Pb 95–80% plus ethanol 20%, where fume temperatures in the range from 1200 1/min to 2000 1/min of rotary speed were significantly higher (on average approximately 100°C higher). The second cluster of curves referring to other mixtures represents lower combustion temperatures in the whole rotary speed range apart from the speed of 2000 1/min, at which all the curves approach the value of petrol Pb95. Only the mixture with the proportions 70% Pb 95 - 30% ethanol has a different course of combustion temperature, which for the rotary speed of 1800 1/min has similar values to petrol supply only. Undoubtedly, a considerable amount of petrol in the mixture is responsible for this phenomenon.

• Engine cooling liquid temperature

In the obtained test results the temperature of the cooling liquid on the input and output was taken also into account. The measurement of this liquid's temperature, reaching 70°C on the input and not exceeding 95°C on the output, confirms proper thermostat operation and efficient engine cooling system.

The values of cooling liquid temperature for different ethanol fuels did not differ from the temperatures of liquids obtained during the test on base fuel.

Analysing the course of the conducted test, the lack of threats on the part of proposed ethanol fuel to the efficiency, reliability and durability of engine construction can be stated. It would be, however, too hasty to stop at this knowledge stage, without enriching them with future durability tests.

5. Conclusions

Along with an increase in the requirements that fuels have to face, an increasing number of cars worldwide, a perspective of running out of fuel resources, an interest in alternative energy sources rises, particularly fuels of vegetable origin. Currently works on complex and proper solution and ordering of the whole range of issues related to the realization of pro-ecological initiatives in vehicle maintenance for the protection of natural environment are conducted.

As proved in this paper, ethanol can be used as an additive to petrol or constitute the main component of fuels. The reason for applying ethanol as fuel is an increase in the independence of the local fuel market and a decrease in the costs of fuel import, as well as the possibility of fair contamination reduction and limitation of the influence of fuel combustion on the climate.

The production of ethanol for fuel industry is perfectly justified in Poland. Current production enables to apply ethanol addition as a substitute for approximately 2% of fuels.

Considerable resources (waste, by-products from processing industry, surplus of crops) May contribute to increase current ethanol production a few times and obtain ethanol's 12% participation in fuels. Experienced staff and proper production resources enable to cross possible technical barriers while developing distilleries' production powers, mainly through building modern, complex installations.

The realization of tests and obtained results confirm the possibility of using the energetic material of organic origin in question (bioethanol), whose acquisition and production can take place in Poland, at the same time giving the option of making use of the agricultural potential and ensuring the development of distilling industry.

The results of the presented research can constitute a basis for starting the next stage with an extended scope of maintenance tests and, finally, the production of substitute fuel by Polish petrochemical industry.

Literature

- [1] Stanowski P.: The influence of the admixture of ethanol on the parameters of the work engine with the ignition the sparkle. The doctor's trial, WIM, UTP, Bydgoszcz 2012.
- [2] Tylicki H.: The exploitation of combustion engines in vehicles. PWSZ, Pila 2005.
- [3] Żółtowski B.: Investigation of combustion engines. ATR, Bydgoszcz 1996 (s.140).
- [4] Żółtowski B., Tylicki H.: Chosen problems of exploitation in machine engines. PWSZ, Pila 2004.